HD-H'ph cpd

QUANTUM OPTOELECTRONICS

COSPONSORED BY
OPTICAL SOCIETY OF AMERICA
IEEE/LASERS AND ELECTRO-OPTICS SOCIETY
IN COOPERATION WITH
JAPAN SOCIETY OF APPLIED PHYSICS

1991 TECHNICAL DIGEST
SERIES VOLUME 7

MARCH 11-13, 1991
SALT LAKE CITY, UTAH

POSTDEADLINE PAPERS

COMPONENT PART NOTICE

THIS PAPER IS A COMPONENT PART OF THE FOLLOWING COMPILATION REPORT:

TITLE: 'Proceedings of the Optical Society of America Photonic Science Topical Meeting Series. Volume 7. Quantum Optoelectronics Held in Salt Lake City, Utah on 11-13 March 1991,'

TO ORDER THE COMPLETE COMPILATION REPORT, USE AD-A 253 823.

THE COMPONENT PART IS PROVIDED HERE TO ALLOW USERS ACCESS TO INDIVIDUALLY AUTHORED SECTIONS OF PROCEEDING, ANNALS, SYMPOSIA, ETC. HOWEVER, THE COMPONENT SHOULD BE CONSIDERED WITHIN THE CONTEXT OF THE OVERALL COMPILATION REPORT AND NOT AS A STAND-ALONE TECHNICAL REPORT.

THE FOLLOWING COMPONENT PART NUMBERS COMPRISE THE COMPILATION REPORT:

AD#: P007 819 THUR AD#: P007 889

AD#: AD#:

AD#: AD#:

DTIC ELECTE AUG 18 1992 S B D

Accession For	
NTIS GRA&I	☑
DTIC TAB	☐
Unannounced	☐
Justification	
By	
Distribution/	
Availability Codes	
Dist	Avail and/or Special
A-1	

DISTRIBUTION STATEMENT A
Approved for public release;
Distribution Unlimited

DTIC FORM 463 MAR 85

OPI: DTIC-TID

TABLE OF CONTENTS
POSTDEADLINE PAPERS

PDP1 **Strong photo-optic effects in periodically δ-doped InGaAs/GaAs multiple quantum well structures,** A. Larsson and J. Marserjian.....295

PDP2 **Normally-on and normally-off asymmetric Fabry-Perot reflection modulators produced by impurity free disordering,** M. Ghisoni, G. Parry, M. Pate, G. Hill, and J. S. Roberts.....299

PDP3 **Lasing in sub-micron wide vertical cavity microlasers by picosecond optical pumping,** J. L. Jewell, A. Scherer, B. Van der Gaag, S. L. McCall, J. P. Harbison, L. T. Florez, and L. M. Schiavone.....303

PDP4 **Fast escape of photocreated carriers out of shallow quantum wells,** J. Feldmann, K. W. Goossen, D. A. B. Miller, A. M. Fox, J. E. Cunningham, and W. Y. Jan.....307

PDP5 **Femtosecond time-resolved studies of high field parallel transport in GaAs quantum wells,** W. Sha, T. B. Norris, W. J. Schaff, and K. E. Meyer.....311

Key to Postdeadline Papers.....315

spectra are governed by the collective excitations of the quantum wires.[2] The dominant feature is a strongly anisotropic dispersion of the plasmons with respect to the wire direction which reflects the free propagation of plasmons along the wires and their confinement perpendicular to the wires.

[1] M. Kohl, D. Heitmann, P Grambow, and K. Ploog, PRL 63,2124(1989) [2] T. Egeler, G. Abstreiter, G. Weimann, T. Demel, D. Heitmann, P Grambow, and W. Schlapp, PRL 65,1804(1990)

Room Temperature Exciton Absorption, Excitonic Nonlinearities, and Exciton-Phonon Interaction in (Zn,Cd)Se/ZnSe Quantum Wells

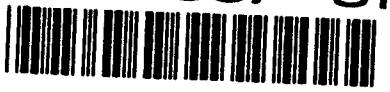
N. Pelekanos, J. Ding, and A.V. Nurmikko

Division of Engineering and Department of Physics

Brown University, Providence, RI 02912

(401)863-2869

AD-P007 819



H. Luo, N. Samarth, and J. Furdyna

Department of Physics

University of Notre Dame, Notre Dame, IN 46556

Summary

Wide-bandgap II-VI compound semiconductor heterostructures are presently being researched for their potential optoelectronic applications at short visible wavelengths, especially in the blue region of the spectrum. In terms of prospective modulator use, a particular difficulty has been the absence so far of the distinct exciton resonances which have been widely exploited e.g. for electro-absorptive purposes in III-V semiconductor quantum wells. In case of ZnSe and related alloys, the problem is fundamental due to the very large exciton-LO phonon coupling: the Fröhlich interaction strength for bulk ZnSe is six to eight times larger than that for GaAs. One the other hand, since the bulk exciton binding energy for ZnSe is $E_x \approx 17$ meV and that for

92-22348



the LO-phonon $\hbar\omega_{LO}$=31 meV, one might hope to increase the exciton binding by quantum well confinement so as to obtain $E_x \geq \hbar\omega_{LO}$ for reducing the exciton-LO-phonon scattering (dissociation) rate. Efforts to achieve have been thwarted so far, in part because of the lack of appropriate electron-hole confinement in ZnSe-based heterostructures. Here we report on the succesful observation and characterization of quasi-two dimensional excitons in (Zn,Cd)Se/ZnSe quantum wells [1]. We note that room temperature excitons have been recently observed in (Zn,Cd)Te/ZnTe quantum wells at red wavelengths [2]. ZnTe, however, is considerably less polar than ZnSe so that the circumstances there are more akin to GaAs.

Figure 1 shows a comparison between the absorption spectra of two $Zn_{1-x}Cd_xSe$/ZnSe multiple quantum well samples ($x \approx 0.24$) of $Zn_{1-x}Cd_xSe$ well thicknesses L_w=200 Å and L_w=35 Å, respectively. The 1S heavy-hole exciton absorption peak is clearly present at room temperature (and beyond) for the narrow well sample while almost disappeared for the wider well sample at 200 K. The exciton Bohr radius in bulk ZnSe is approximately 40 Å so that the latter corresponds to a nearly 3-D case. We also see in Fig. 1 an enhancement in the exciton oscillator strength for the quasi-2D case. By integrating over the 1S absorption line, the narrow sample has an enhancement of about a factor of six in its oscillator strength (note the broader linewidth). Because of the large absorption coefficients present in our heterostructures, the excitonic resonances are readily seen also in **single** quantum well samples. **Figure 2** shows the absoprtion spectrum at several temperatures for a $Zn_{1-x}Cd_xSe$/ZnSe structure which consisted of three single quantum well sections of different thickness (30, 60, and 180 Å, respectively). The temperature dependence of the transmission spectrum in this sample shows clearly how only the quasi-2D

exciton survives to room temperature.

Analysis of the temperature dependence of the linewidth of the exciton absorption for samples in the quasi-2D case shows clearly how the exciton-LO scattering rate is reduced by more than a factor of two when compared with bulk ZnSe. This indicates that the condition $E_x \geq h\omega_{LO}$ is probably satisfied so that exciton scattering to the electron-hole continuum states is no longer energetically favored. Note that this is a circumstance not encountered (or needed) in the III-V semiconductor quantum wells (or with ZnTe [2]), where the Fröhlich interaction is much weaker to begin with.

We have performed initial experiments to study nonlinear exciton absorption in the (Zn,Cd)Se/ZnSe quantum wells. Dye laser pulses ($\tau_p \approx 5$ psec) whose duration was much shorter than the exciton lifetime at this temperature were employed in a single beam configuration. **Figure 3** shows the absorption coefficient as s function of the incident pulse energy for the MQW sample of $L_w = 35$ Å at T=10 K, recorded at the peak of the n=1 HH absorption. The solid line shows the fit to a simple saturation model where the intensity dependence of the absorption coefficient is expressed as $\alpha(n) = \alpha_o/[1+n/n_s] + \alpha_s$, where n_s is the exciton saturation density and α_s accounts for other linear losses such as scattering. From the model and the experiment we deduce a saturation exciton density $n_s \approx 3\times10^{12}$ cm^{-2} in our experimental conditions. This value is in good agreement with a phase-space filling model [3] if a quasi-2D exciton Bohr radius of approximately 20 Å is used in this rough estimate. At higher high temperatures, where nonlinear exciton absorption is also observed, the quantitative interpretation

is more complex due to a larger number of scattering and relaxation channels which determine the details of the exciton distribution function.

Finally, we have investigated the quasi-2D excitons in the (Zn,Cd)Se/ZnSe quantum wells in magnetic fields up to 23 Tesla. The observed diamagnetic shifts as well as some excited exciton state structure is at least qualitatively consistent with the estimated enhancement to the binding energy (E_x~30 meV) by the confinement effects. We have also observed strong increase in the 1-LO phonon sidebands in luminescence from these structures in high magnetic fields.

The research at Brown University and the University of Notre Dame was supported by the Defense Advanced Projects Agency, under the University Research Initiative program (N00014-90-J-1582). The work at Brown and Notre Dame was also supported by the National Science Foundation (at Brown ECS-8916026; at Notre Dame DMR-89-13706).

References:

[1] some of our initial results appear in Appl. Phys. Lett., December 1990.

[2] D. Lee, J.E. Zucker, A.M. Johnson, R.D. Feldman, and R.F. Austin, Appl. Phys. Lett. 57, 1132 (1990)

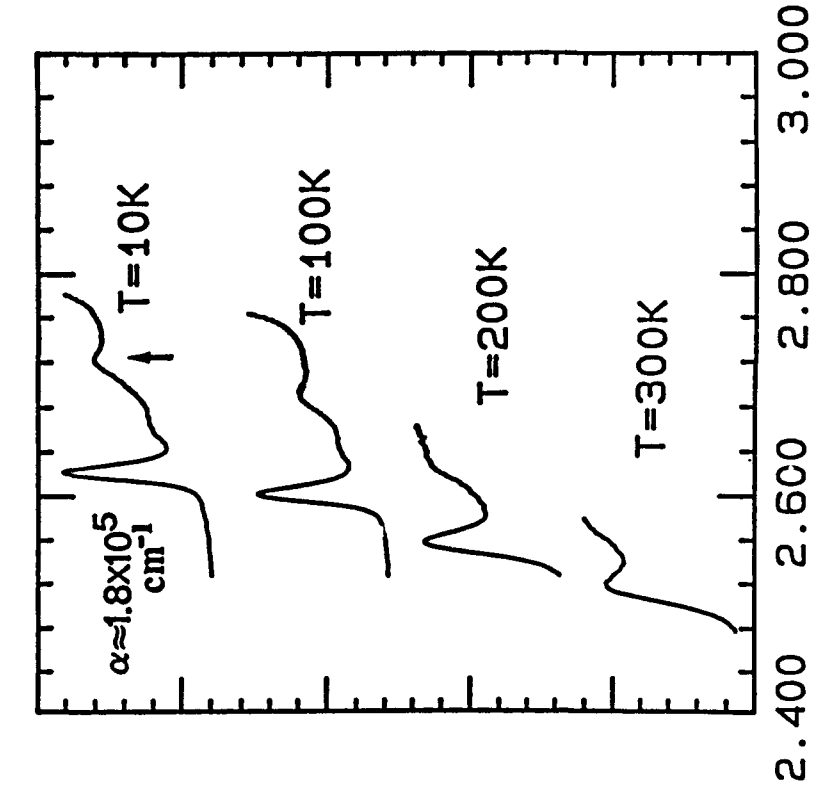
[3] D.S. Chemla, D.A.B. Miller, P.W. Smith, A.C. Gossard, and W. Wiegmann, IEEE J. Quant. Electr. QE-20, 265 (1984)

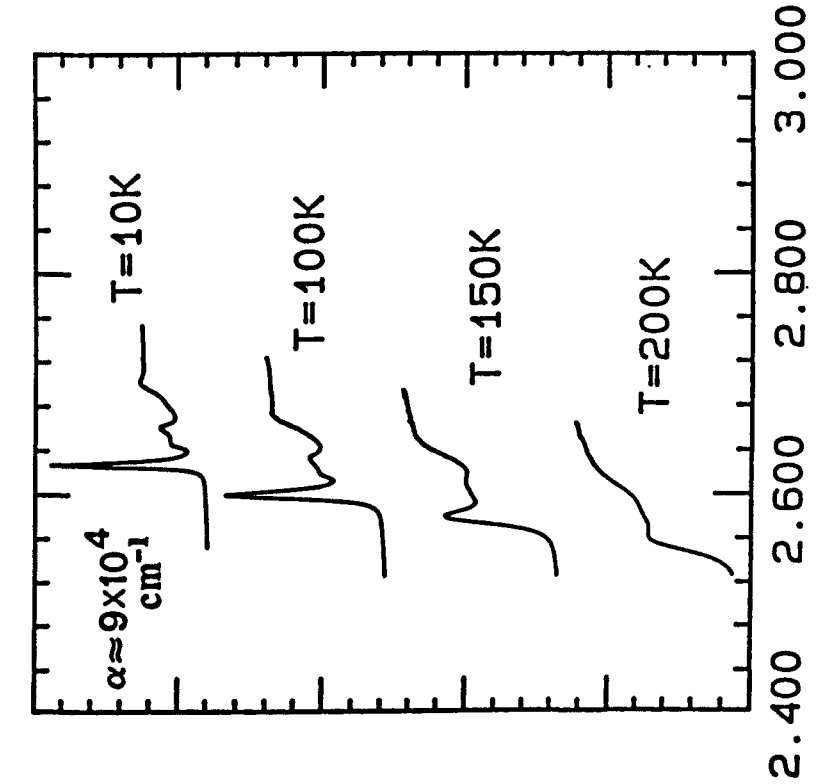
Figure Captions:

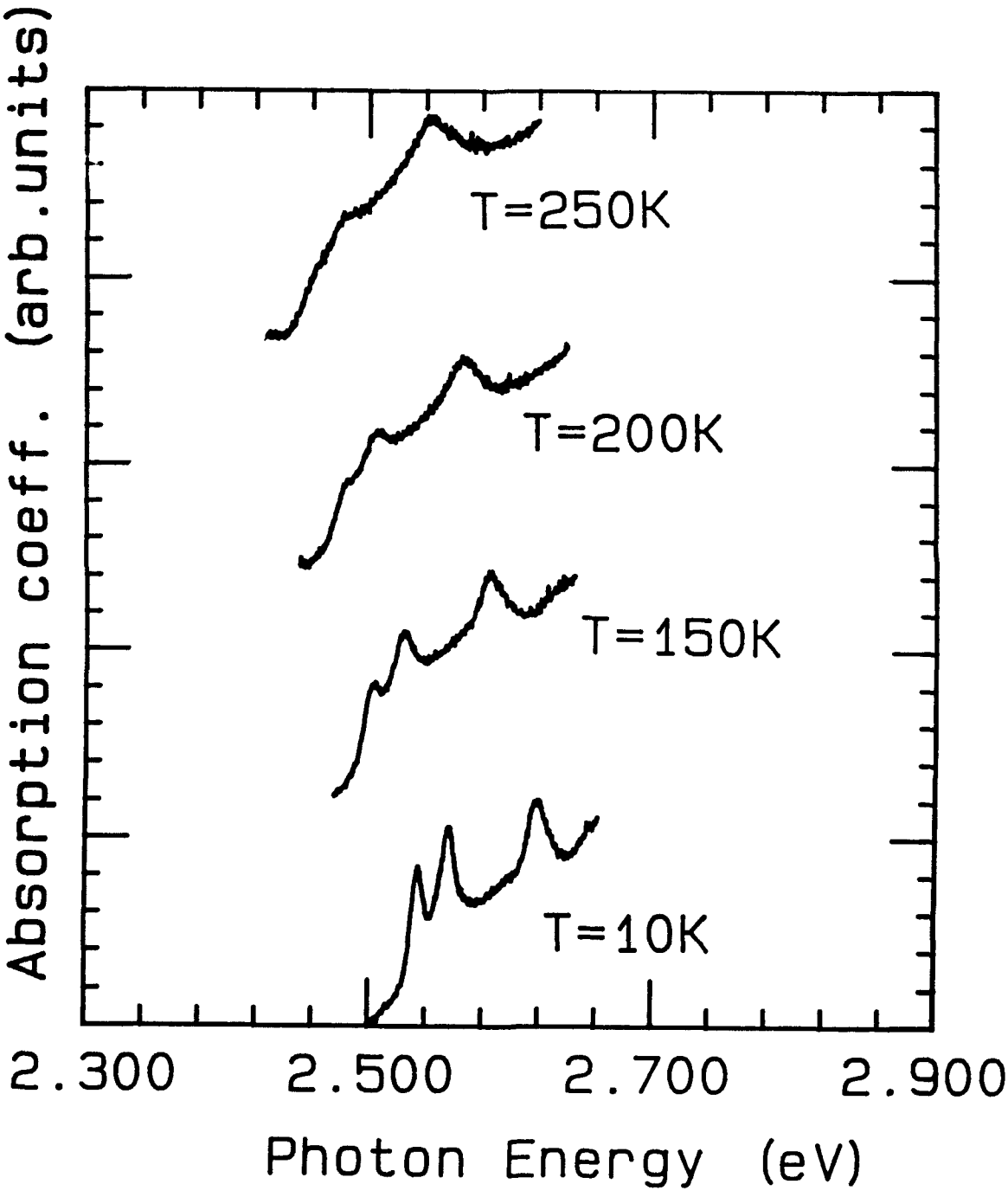
Figure 1: Absorption coefficient of a (Zn,Cd)Se/ZnSe MQW samples with well thicknesses L_w= 200 Å (left) and 35 Å (right) as a function of temperature. The peak value of the absorption coefficient is also indicated. The arrow marks the LH exciton transition.

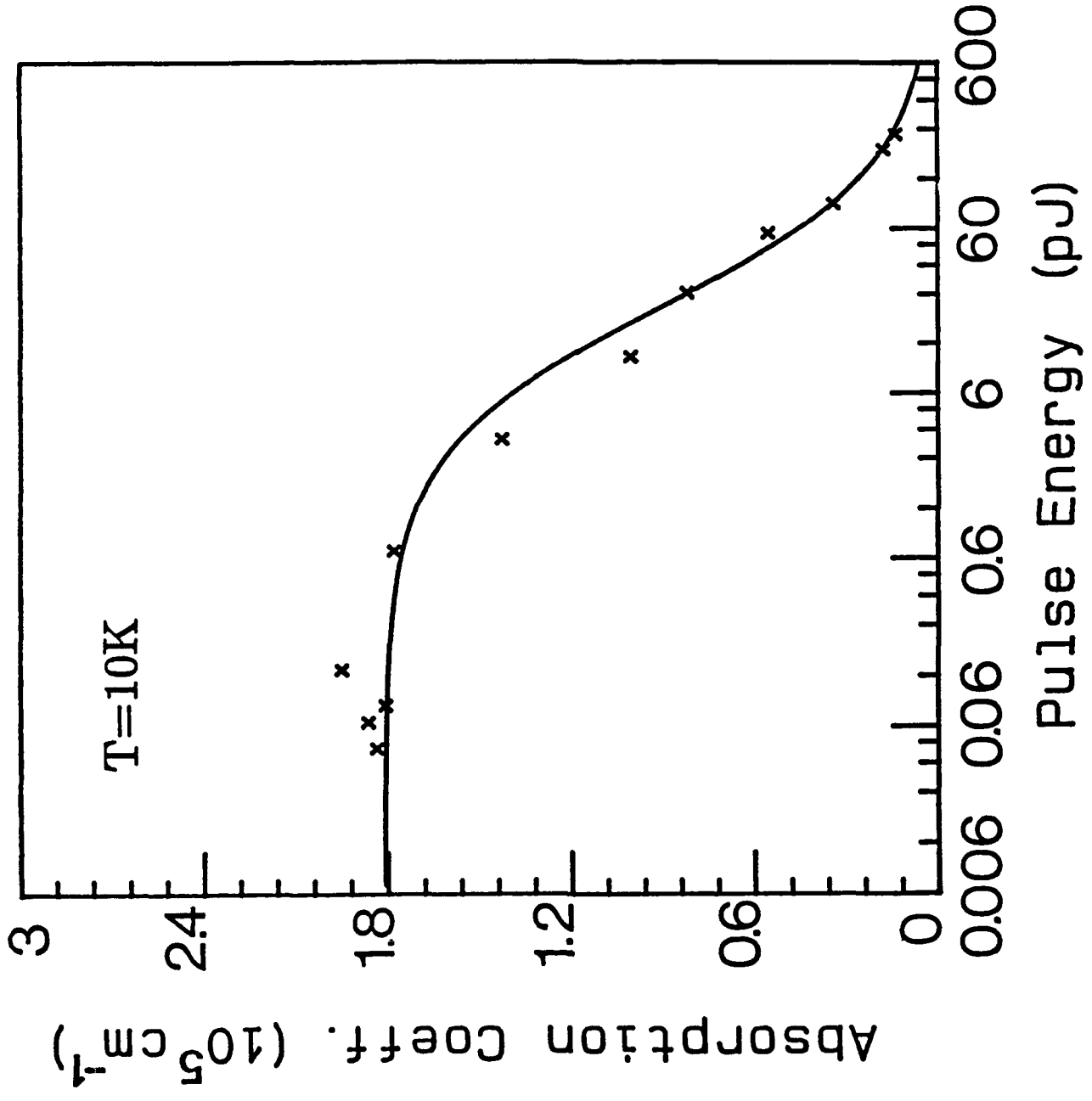
Figure 2: Temperature dependence of absorption coefficient obtained from three single quantum wells of thicknesses L_w= 30 Å, 60 Å, and 180 Å, respectively.

Figure 3: Nonlinear absorption at T= 10K of the narrow well MQW sample at the peak of the n=1 HH absorption. Crosses are data points and the solid line is a calculated fit.


Absorption coeff. (arb.units)
2.400
2.600
2.800
3.000
Photon Energy (eV)
α≈1.8x10^5 cm^-1
T=10K
T=100K
T=200K
T=300K


Absorption coeff. (arb.units)
2.400
2.600
2.800
3.000
Photon Energy (eV)
α≈9x10^4 cm^-1
T=10K
T=100K
T=150K
T=200K


Absorption coeff. (arb.units)
T=250K
T=200K
T=150K
T=10K
2.300
2.500
2.700
2.900
Photon Energy (eV)


T=10K
Absorption Coeff. (10^5 cm^{-1})
3
2.4
1.8
1.2
0.6
0
0.006
0.06
0.6
6
60
600
Pulse Energy (pJ)

Analysis and Assessment of Tilted Superlattices for Quantum Wire Laser Applications

AD-P007 820

Jong Chang Yi, Nadir Dagli and Larry Coldren

Electrical and Computer Engineering Department
University of California
Santa Barbara, CA 93106

Ultrafine submonolayer epitaxy on vicinal substrates [1] by molecular beam epitaxy MBE [2] or matalorganic chemical vapor deposition [3], [4] has been recently studied and developed extensively. By using this deposition mode, periodic lateral structures named tilted superlattices (TSL) have been successfully demonstrated [2], [3]. Figure 1(a) and (b) show the cross sectional TEM and schematic profiles of a TSL. A TSL is directly grown on an off axis or vicinal GaAs substrate by alternating deposition of two materials of different compositions. The end result is an array of quantum well wires (QWW) with a period T, which is determined by the tilt angle, α of the substrate. For example when α is 2° T is 80 Å and when α is 1° T is 160 Å. Such QWW are considered to be superior to bulk and quantum well structures. First of all as the dimensionality decreases, the density of states (DOS) becomes well localized and sharply peaked. Consequently, by using such a one dimensional system in the active region of a semiconductor laser, one can obtain a larger temperature coefficient, larger relaxation frequency, and smaller threshold current. Secondly, the QWW array has an anisotropic band structure, so it exhibits enhanced gain along particular directions. Thirdly, since the quantum confinement is tighter, the exciton binding energy is higher and high performance optical modulators are possible. However, there are several criteria that needs to be met for true quantum wire lasing. First of all the spacing between the first and the second subbands in the conduction band should be sufficiently larger than the thermal energy to prevent the distribution of the carriers over several subbands and the creation of a very broad gain curve. This subband spacing should also be sufficiently larger than the broadening of the energy levels due to unavoidable imperfections or defects in the structure. The large subband spacing also helps to create a large separation between the Fermi level and the second subband to suppress the second gain peak. Furthermore, the first subband level should be sufficiently lower than the potential energy of the cladding material. Otherwise, carriers can be excited to the cladding regions and demonstrate bulk like behavior. Other than these requirements for good electronic confinement, one needs to consider the optical confinement. A good optical confinement requires a low average Al content in the quantum wire region and the cladding regions. In all these respects, the TLS has several significant advantages in comparison with the arrays of QWW fabricated with the fine line lithography techniques. The lateral dimensions are in the low nanometer range which is suitable for obtaining sufficient quantum size effect, the structure is obtained processing free, hence is free from processing damage. Although the efforts on TSL growth resulted in structures that demonstrated lasing [5] and polarization dependent optical properties [6], a detailed theoretical analysis and assessment of TSL are still lacking. In this paper such a study is undertaken and and TSL is assessed including the effects of unavoidable imperfections on the optical properties.

In the analysis two different methods are employed. One method reduces a single QWW into a modular electrical equivalent circuit by using a mode expansion in the solution of Schrodinger equation. Modularity of the equivalent circuit allows one to cascade the basic circuit to model an array of QWW. This approach allows one to analyze an array with different wires, hence the effects of imperfections, such as wire width fluctuations. The other method utilizes the finite element method (FEM) to solve the Schrodinger equation using periodic boundary conditions. So this method can analyze an infinite array of QWW and create the E-k diagram from which the density of state function can be directly obtained.

92-22349

The parameters that are available to engineer the structure are shown in Figure 1(b). The overall thickness of the TSL, h_1, is chosen to be 100 Å, which is an optimum value for both strong quantum confinement and the good interface quality. The wire material is GaAs and the barrier material between wires, and the cladding material above and below TSL, have Al contents of x_b and x_c respectively. The outer well thickness, h_2, is varied from 0 Å to 100 Å. When h_2 is 100 Å, there are no barriers between the wires and the TSL is identical to a slightly perturbed quantum well due to the tilt of the substrate. As h_2 decreases confinement increases, and for h_2=0 it becomes the strongest. T is a parameter which can be changed by changing the substrate misorientation. The width and the separation of the wires, W and S, are kept to be equal, hence they are half of T. x_c is another parameter which is confined between 0.25 and 0.4. Below 0.25 the quantum confinement becomes weak, and above 0.40, the optical confinement becomes poor. x_b can be optimized in the range from 0.25 to 0.1. Below 0.25, again the quantum confinement becomes weak. On the other hand, the overall Al content in the barrier region is not so important for the optical confinement, since the overall thickness of the TSL is 100 Å, which is very small compared to the overall extent of the optical wave. Figure 1(c) shows two examples of conduction band wave functions at two different barrier thicknesses. When h_2 is 0 confinement is very strong and the electron wave function is well localized. However, in a practical structure wire widths fluctuate due to unavoidable imperfections during the growth. Obviously the wavefunction, hence the energy eigenvalues are very sensitive to such fluctuations. In the second case, the barrier partially extends into the superlattice and the wavefunction is extended indicating strong coupling between the wires. In that case, the wavefunction hence the energy eigenvalues are less sensitive to wire width fluctuations, but due to strong coupling between the wires energy eigenvalues are broadened into minibands. This negates the expected benefit due to reduced dimensionality. This argument indicates that, in principle it should be possible to find an optimum structure that results in minimal energy broadening due to either coupling or wire width fluctuations by controlling the degree of coupling between the wires. Figure 2 shows the DOS of the conduction band of a TSL on 2 ° vicinal GaAs substrate, i.e., when W=S=40 Å, as h_2 is varied from 0 Å to 100 Å. The wire material is GaAs and x_b and x_c are both 0.25. When h_2 is 100 Å, there are no barriers between wires and the TSL is identical to a slightly perturbed quantum well and a steplike DOS profile is observed. As h_2 decreases, DOS becomes more and more localized. However, even when h_2 is 0 Å, the DOS is far from the ideal DOS of a quantum wire, where sharp and well localized peaks are observed. Those broad DOS profiles are due to the relatively low potential height in the barrier material. This in turn results in excessive coupling between the wires and energy levels are broadened due to miniband formation. The lowest miniband width is about 30 meV. The first reported TSL quantum wire laser [5] had this structure with h_2=50 Å. Even though the evidence of two dimensional confinement is apparent from the emission wavelength (λ=8277Å), which agrees well with the calculations, and the polarization dependence of the optical properties, which is due to the modulation of the electronic wavefunction, the DOS does not show the strongly peaked features desired for optimal laser characteristics as shown in figure 2, which is due to non optimum nature of the structure.

If the barrier material is changed to pure AlAs, the energy broadening due to excessive coupling, hence miniband formation can be eliminated. This also raises the confined energy values and necessitates an increase in the Al content of the cladding material to obtain a larger energy margin between the lowest miniband level and the cladding energy level. The DOS of a TSL for which x_b and x_c are 1 and 0.4 respectively are plotted in figure 3. Here, very sharp and well localized DOS peaks are observed when h_2 is less than 20 Å. The lowest miniband width is as small as 7 meV. But for higher h_2 values wire to wire coupling becomes dominant due to small wire to wire separation and the DOS is not much different than the previous case. The spacing between the first and second miniband is as wide as 80 meV, which is much larger than the thermal energy at room temperature, hence it could be possible to observe quantum effect at room temperature.

In practice, however, a TSL is far from being ideal as figure 1(a) indicates. The interfaces between wires and barriers are subject to fluctuate due to the growth rate fluctuations [2]. Furthermore, the growth interface may tilt if the growth rate does not have the correct nominal value. Both of these effects create energy broadening and smearing of the DOS. The effect of interface, or wire and barrier width fluctuations around a nominal value, which results in perpendicular growth interface, were studied both by varying W and S values of an ensemble of ten wires using the equivalent circuit approach, and using a stochastic approach combined with the FEM analysis. Both approaches yield very similar results. The miniband broadening due to random wire width fluctuation with an average of 3 Å is plotted in figure 4. This approximately corresponds to a 1% fluctuation in the growth rate. The minimal miniband width occurred at non-zero h_2 value, in this case, at h_2=20 Å. So if the energy broadening due to wire width fluctuation is considered, the non-zero h_2 value would be more desirable.

The effect of the interface tilt can be considered by introducing the tilt parameter p, which is directly proportional to the growth rate [2]. If m and n are defined as the fractions of GaAs and AlAs monolayers over a step of width T, then p is defined as m+n. If p is 1, then the width of newly deposited monolayer width is exactly same as that of the previously deposited monolayer, and the interface would grow vertically. However, if p is slightly different from 1, then the width of newly deposited monolayer is different from that of the previously deposited monolayer. Then the interface becomes tilted. The tilt angle is very sensitive to p values. For example, 1 % variation in p value results in a 20 ° tilt of interface. In figure 5, the miniband variation vs tilt parameter, p, is plotted. As the tilt angle is very sensitive to p value, so is the miniband. As p deviates from 1, the miniband minima shifts to higher energies and the miniband width becomes wider, especially when h_2 is small.

In summary, for the TSL structures, large miniband spacings and large energy margins between the first miniband and cladding energy can be obtained if the coupling between wires is suppressed. This can be achieved by increasing the Al content in the barrier and the cladding, by reducing h_2, and also by reducing α, which results in increased barrier width. However, the miniband broadening due to interface fluctuation and misorientation is large at smaller h_2 values. Therefore non-zero outer well thickness around 20 Å is the optimum geometry for minimal miniband width for α=2°. Further results on the gain and absorption characteristics and at various tilt angles will be reported at the conference.

References:

1. P. M. Petroff, A. C. Gossard, and W. Wiegmann, *Appl. Phys. Letters* 45 620 (1984).
2. J. M. Gaines, P. M. Petroff, H. Kroemer, R. J. Simes, R. S. Geels, and J. H. English, *J. Vac. Sci.Technol.* B 6 1378 (1988).
3. T. Fukui and H. Saito, *Appl. Phys. Letters* 50 824 (1987).
4. T. Fukui and H. Saito, *J. Vac. Sci.Technol.* B 6 1373 (1988).
5. M. Tsuchiya, L. A. Coldren, and P. M. Petroff, *Seventh International Conference on Integrated Optics and Optical Fiber Communication, Paper 19C1-1*, Kobe , Japan (1989)
6. M. Tsuchiya, J. M. Gaines, R. H. Yan, R. J. Simes, P. O. Holtz, L. A. Coldren, and P. M. Petroff, *Phys. Rev. Lett.*, 62,446 (1989).

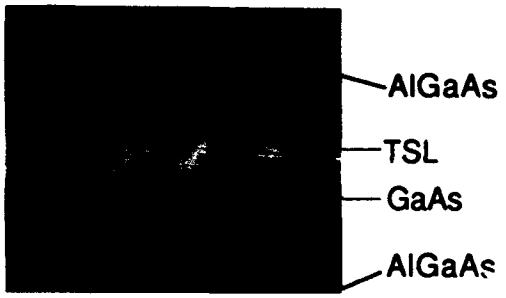


Fig.1.(a) Cross sectional TEM profile of a TSL.

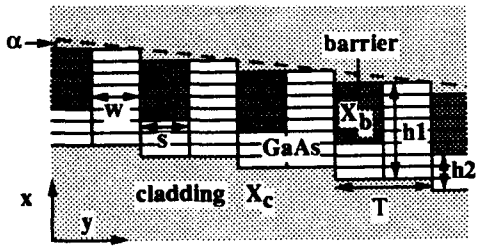


Fig.1.(b) Schematic cross sectional profile of a TSL.

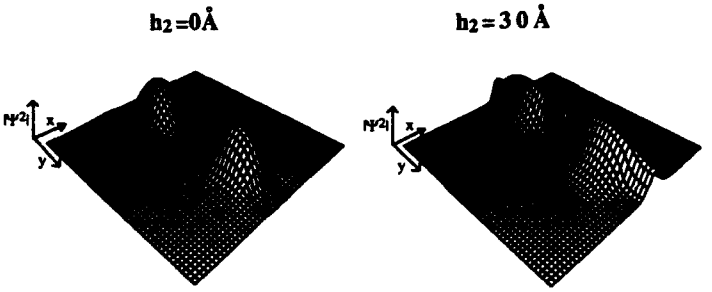


Fig.1.(c) Conduction band electronic wavefunctions for two different confinement levels.

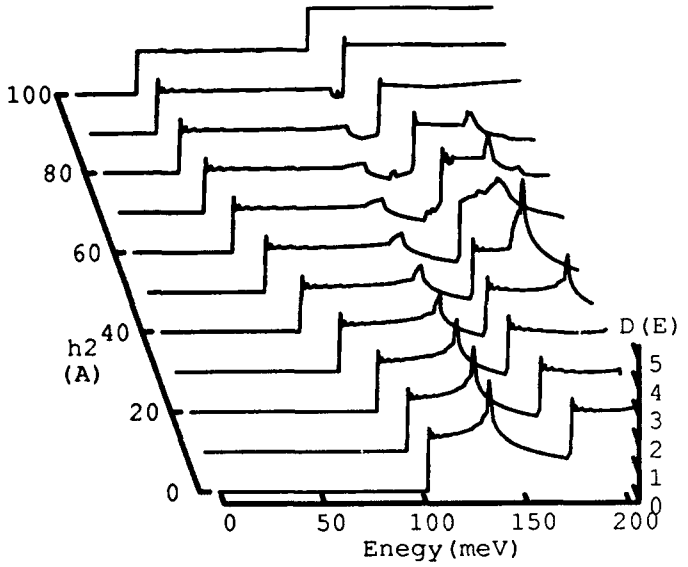


Fig.2. Conduction band density of states (10^9/eV•cm) of a TSL with x_b=0.25, x_c=0.25, W=S=40Å, h_1=100Å.

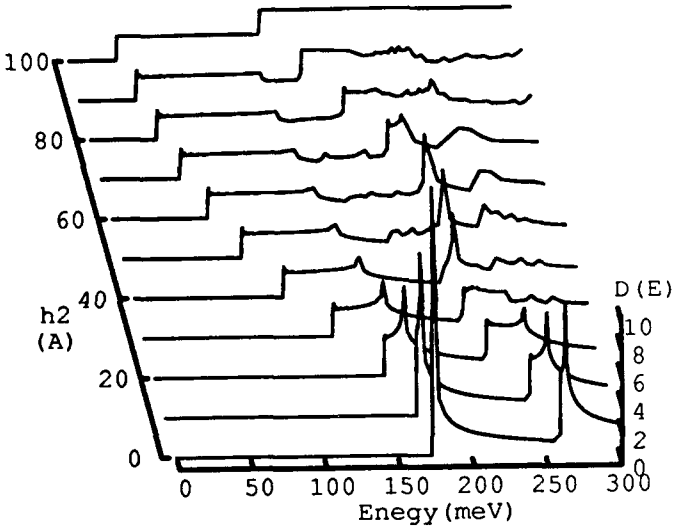


Fig.3. Conduction band density of states (10^9/eV•cm) of a TSL with x_b=1.0 , x_c=0.40, W=S=40Å, h_1=100Å.

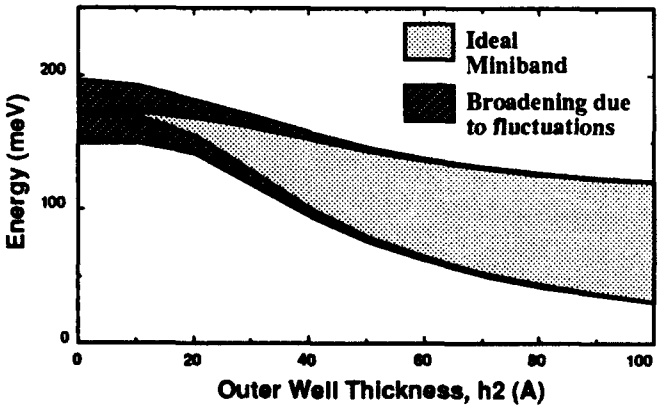


Fig.4. Miniband broadening of the lowest conduction band subband due to random wire width variations with an average of 3 Å.

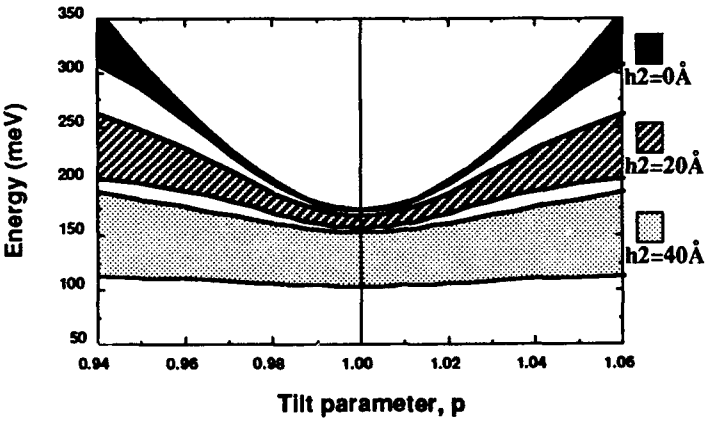


Fig.5. Miniband variation of the lowest conduction band subband vs tilt parameter p.

Luminescence Anomaly of Two-Dimensional Excitons in GaAs Coupled Quantum Wells

AD-P007 821

T. Fukuzawa
IBM Research, Tokyo Research Laboratory
5-19 Sanban-cho, Chiyoda-ku, Tokyo 102, Japan
Phone 3- 288-8366, FAX 3-265-4251

92-22350

The possibility of a phase transition into an ordered state in a two-dimensional (2D) system of spatially separated electron-hole pairs has been suggested by Lozovik and Yudson [1] and Shevchenko [2] independently. Their proposal has recently been extended by Fukuzawa et al. to a system formed by two GaAs/AlGaAs coupled quantum wells subject to an electric field [3,4]. The long exciton lifetimes that can be achieved in such a semiconductor heterostructure, as well as the small Coulomb screening due to the interaction between oriented dipoles, make it particularly suitable for the study of phase transitions, be it like the one proposed by Lozovik and Yudson, and Shevchenko, or a Kosterliz-Thouless transition of a neutral Coulomb gas [5].

The photoluminescence (PL) of GaAs-$Ga_{0.7}Al_{0.3}As$ structures consisting of two 50Å quantum wells separated by a 40Å barrier has shown a dramatic temperature dependence when an electric field is applied perpendicular to the well interfaces. The polarization of carriers and the energy shifts induced by the field lead to a PL spectrum consisting of two distinct peaks, one of which is associated with spatially "direct" interband transitions and another, much more intense, that involves spatially-separated electrons and holes ("type-II" exciton).

At 25K the full width at half maximum (FWHM) of the "type-II" exciton PL peak was ≃5.5meV, which is typical for narrow wells prepared by molecular beam epitaxy without any growth interruption. As the temperature decreased, the FWHM increased significantly to a value that depended on the excitation power (from 0.02 to 0.58W/cm^2), but at ≃10K it decreased abruptly and at 6K saturated to a value as low as 3.4meV [6]. This behavior was not observed for the "direct" transition or when the field was not present; in both cases, the PL linewidth increased gradually with decreasing temperature.

Time-dependence measurements of the PL spectra at 2K yielded the field-enhanced lifetime of the type-II excitons, which at 28kV/cm was more than two orders of magnitude longer than in the absence of the field [7], in good agreement with theoretical predictions [3,4]. Time-resolved spectra of the "type-II" exciton PL at different temperatures showed thermalization of excitons within their lifetime, down to at least 12K, at which a monotonic increase in linewidth with time was most apparent. In contrast, at 6K the linewidth decreased in the first nanoseconds after excitation and then gradually returned to its initial value.

The original results from CW experiments were tentatively interpreted in terms of a phase transition of excitons, by which a coherent excitonic state was possibly responsible for a drastic reduction in inhomogeneous line broadening. Recent time-resolved experiments have shed more light on the physical mechanisms of linewidth reduction, which has been explained by a model with Fermion-like statistics resulting from inhomogeneous broadening and repulsion between the excitons [8].

References

[1] Y.E. Lozovik and V.I. Yudson, Sov. Phys. JETP Lett. **22**, 274 (1975).

[2] S.I. Shevchenko, Sov. J. Low Temp. Phys. **2**, 251 (1976).

[3] T. Fukuzawa, S.S. Kano, T.K. Gustafson and T. Ogawa, Proceed. of 4th Int. Conf. on Modulated Semiconductor Structures, Michigan, July 1989, page 747; Surface Science **228**, 482 (1990).

[4] T. Fukuzawa, T.K. Gustafson and E. Yamada, IEEE J. Quantum Electron. Lett. **26**, 811 (1990)

[5] For a review, see, e.g., P.Minnhagen, Rev. Mod. Phys. **59**, 1001 (1987)

[6] T. Fukuzawa, E.E. Mendez and J.M. Hong, Phys. Rev. Lett. **64**, 3066 (1990)

[7] A. Alexandrou, J.A. Kash, E.E. Mendez, M. Zachau, J.M. Hong, T. Fukuzawa and Y. Hase, Phys. Rev. B **42**, 9225 (1990)

[8] J.A. Kash, M. Zachau, E.E. Mendez, J.M. Hong and T. Fukuzawa (unpublished)

Modulators: I

MB 11:00am–12:30pm
Salon F

Emilio Mendez, *Presider*
IBM T. J. Watson Research Center

AD-P007 822

High-contrast Fabry-Perot Electroabsorption Modulators

Ran-Hong Yan*, Robert J. Simes**, and Larry A. Coldren

Department of Electrical and Computer Engineering,
University of California, Santa Barbara, CA 93106. Tel: (805) 893-4486

In the search for practical optical modulators for optical switching, communications, and interconnections, various device parameters need to be optimized, and the optimization should depend on the applications. For large array applications, surface-normal modulators are preferred. Because of the enhanced optoelectronic interaction length available in resonators without actually increasing the active region thickness, and the cavity balance provided by the resonance, devices with Fabry-Perot structures have both low operating voltage and high-contrast advantages.

Figure 1 briefly summarizes the contrast ratio between on and off states of various optical modulators, and the required voltage swing as well as reflectivity change for this contrast ratio. Basic structures are schematically shown in the inset. Dashed lines represent normalized transfer functions, defined as the percentage modulation of the input light per unit driving voltage.

More than 10 dB contrasts are relatively easy to obtain with Fabry-Perot structures with unequal mirrors, i.e. asymmetric Fabry-Perot structures. With low cavity loss, the overall reflectivity is quite high with a ~ 97 % bottom mirror reflectivity in most of these structures. With applied fields, the increased cavity loss reduces the effective reflectivity from the bottom mirror at the top surface, and the overall reflectivity can be made zero when the effective reflectivity from the bottom has an equal magnitude to the top mirror reflectivity, yielding the off state.

The device [4] with a ~ 80 % top mirror and an active region of 24 quantum wells (100 Å GaAs/100 Å $Al_{0.2}Ga_{0.8}As$) illustrates a reflectivity change of more than 40 % for an operating voltage swing of only 2 volts, i.e. > 20 %/V. This is the highest modulation efficiency ever reported in a surface-normal device. A sensitivity analysis shows that tolerances of 2 nm in operating wavelength, 0.5 volts in operating voltage, 0.3 % in layer thickness or 10 °C in temperature variation can be expected from such a device with a *finesse* of ~ 10.

[1] T. H. Wood, *J. Lightwave Tech.* **6**, 743 (1988).
[2] M. Whitehead and G. Parry, *Electron. Lett.* **25**, 566 (1989).
[3] R. H. Yan, R. J. Simes, and L. A. Coldren, IEEE *Photon. Tech. Lett.* **1**, 273 (1989).
[4] R. H. Yan, R. J. Simes, L. A. Coldren, and A. C. Gossard, *Appl. Phys. Lett.* **56**, 1126 (1990).
[5] R. J. Simes, R. H. Yan, R. S. Geels, L. A. Coldren, J. H. English, A. C. Gossard, and D. G. Lishan, *Appl. Phys. Lett.* **53**, 637 (1988).
[6] T. Y. Hsu, W. Y. Wu, and U. Efron, *Electron. Lett.* **24**, 603 (1988).
[7] G. D. Boyd, D. A. B. Miller, D. S. Chemla, S. L. McCall, A. C. Gossard, and J. H. English, *Appl. Phys. Lett.* **50**, 1119 (1987).
[8] R. B. Bailey, R. Sahai, and C. Lastufka, Optical Society of America, *Topic Meeting on Quantum Wells for Optics and Optoelectronics*, 1989, Paper PD-1.
[9] B. Pezeshki, D. Thomas, and J. S. Harris, Jr, *Appl. Phys. Lett.* **57**, 1491 (1990).
[10] M. Whitehead, A. Rivers, G. Parry, J. S. Roberts, and C. Button, *Electron. Lett.* **26** (1990).

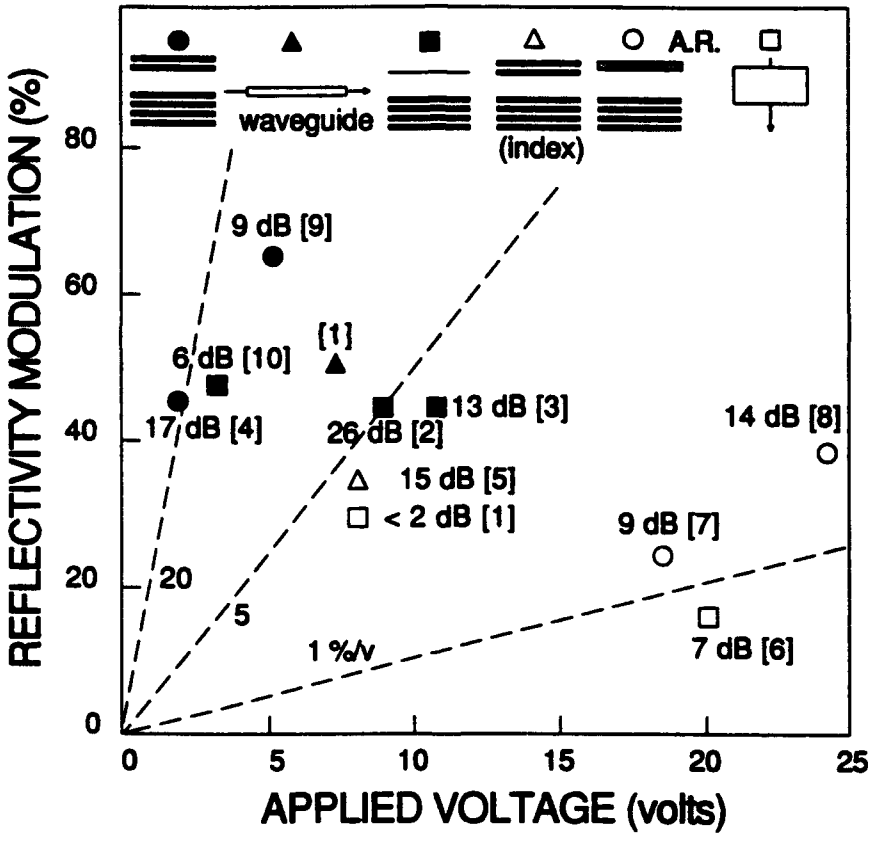


Figure 1 A performance comparison of various surface-normal optical modulators. The dash lines represent different normalized transfer functions of 1, 5 and 20 %/V. The numbers are the contrast ratios [references].

*Present address: AT&T Bell Labs, Holmdel, NJ 07733.
**Present address: Division Composants Optoélectroniques, Laboratories de Marcoussis, 91460 Marcoussis, France.

AD-P007 823

HIGH CONTRAST PHOTONIC GATE ARRAYS CONSISTING OF VERTICALLY INTEGRATED MULTIPLE-QUANTUM-WELL REFLECTION MODULATORS AND PHOTOTRANSISTORS

Chikara Amano, Shinji Matsuo, and Takashi Kurokawa

NTT Opto-electronics Laboratories
3-1, Morinosato Wakamiya, Atsugi 243-01, Japan

1. INTRODUCTION

Given their extremely high-speed capability, optical logic gates based on the quantum confined Stark effect (QCSE)[1] of multiple-quantum-well (MQW) structures are highly promising as basic devices for photonic signal processing. Although a number of schemes have been demonstrated including Symmetric Self Electro-optic Effect Devices (S-SEED)[2], the contrast ratios usually obtained are insufficient due to the short modulation path.

We have developed novel photonic gate arrays consisting of vertically integrated GaAs/AlGaAs MQW reflection modulators and GaAs/AlGaAs heterojunction phototransistors (HPT). They operate as NOR gates with high contrast ratio and optical gain.

2. DEVICE DESCRIPTIONS

As shown in Fig.1, the proposed photonic gate arrays consist of vertically integrated MQW reflection modulators and phototransistors, which are optically isolated and electrically connected in series by a distributed Bragg reflector (DBR). A bias voltage is applied to the MQW modulators through phototransistors. When input and bias lights are incident on the phototransistor and modulator, respectively, output is obtained as reflection light from the modulator. Each pixel can be driven independently.

The photonic gates exhibit NOR-gate functions as follows:
(1) When the input light is off, the MQW pin modulator is at zero-biased condition. The modulator is thus in transmission state when the input light wavelength is at the absorption edge.
(2) When the input light is on, the phototransistor switches to an on-state, so the modulator is fully reverse-biased. The output is suddenly changed from a high- to a low-level because the modulator switches to an absorption state.

The photonic gates provide the following three key advantages:
(1) Contrast ratio is high because a long modulation path can

92-22352

be obtained by introducing an alternating quarter-wavelength mirror and increasing the thickness of the intrinsic MQW layer.
(2) Low insertion loss and wide bandwidth are obtained because the driving wavelengths are at the absorption edge.
(3) The gates exhibit optical gain and can be driven even by input light with the same wavelength as the output light.

3. EXPERIMENT

The following two components were stacked in order on a Si-doped GaAs substrate by molecular beam epitaxy:
(1) A GaAs/AlGaAs heterojunction phototransistor consisting of an n-GaAs collector, a p-GaAs base, and an n-$Al_{0.3}Ga_{0.7}As$ emitter layer.
(2) A GaAs/AlGaAs MQW reflection modulator consisting of an n-DBR (25 pairs of AlAs(715Å)/$Al_{0.3}Ga_{0.7}As$(629Å)), an i-MQW(220 pairs of GaAs well(100Å) and $Al_{0.3}Ga_{0.7}As$(80Å) barrier), a p-$Al_{0.3}Ga_{0.7}As$ clad, and a p-GaAs cap layer.
The total thickness of the epitaxial layers is 14 μm. Be and Si were used as p- and n-type dopants.

p- and n-type ohmic contact metals were evaporated on the front and back surfaces, respectively. After mesa-etching was performed, spaces between the pixels were filled with polyimide. The GaAs substrate was cleaved to a thickness of 100 μm, and backside windows for input lights were formed by selective etching. Anti-reflection(AR) coatings were evaporated on the surfaces of the modulators. The residual surface reflectivity of GaAs wafers with the AR coating is less than 0.1% at 850-870 nm. The pixel area is a dot with a diameter of 100 μm.

A semiconductor laser beam with a wavelength of 860 nm was used as input. Wavelength-tunable Ti-doped sapphire laser was used as the bias light source, where the standard wavelength was set at 860 nm. Output light was separated from bias using a polarizing beam splitter and a quarter-wavelength plate. Bias voltage was set at a constant value of 30 V. In our measurement system, reflectivities of less than 0.1% were detectable, which is almost equivalent to the background reflectivity of the AR-coating.

4. RESULTS AND DISCUSSION

Input/output characteristics of the photonic gate arrays are shown in Fig.2. When the input power was increased more than -15 dBm, the output power fell abruptly from -4 to -20 dBm. This result indicates that the devices operate as a NOR gate with a critical threshold.

The contrast ratio and insertion loss as a function of bias wavelength are indicated in Fig. 3. When the bias wavelengths are 856-860 nm, extremely high contrast ratios of more than 20

dB were obtained with low insertion loss. These contrast values are the highest ever reported for QCSE-based optical logic devices and are attained by (1) increasing the MQW layer thickness to 4 μm by high-purity molecular beam epitaxial growth, and (2) introducing a high-reflectivity AlAs-$Al_{0.3}Ga_{0.7}As$ quarter-wavelength mirror[3].

As shown in Fig.3, the bandwidth of the contrast ratio more than 15 dB is about 8 nm. These values are about three times those recently reported for an MQW asymmetric Fabry-Perot modulator[4].

From the input/output characteristics shown in Fig.2, a large output power of -4 dBm is switched by a small input power of -10 dBm, so the optical gain is 6 dB.

Switching time when input power is 1 mW is 20 ns, which is limited by total capacitances of gates, bias voltage, and responsivities of phototransistors and modulators[2].

5. SUMMARY

We have proposed and successfully fabricated novel photonic gate arrays consisting of vertically integrated GaAs/AlGaAs MQW reflection modulators and GaAs/AlGaAs heterojunction phototransistors. They operate as NOR gates with high contrast ratio and optical gain. Higher contrast ratios and faster switching times are expected by precisely designing the layer structures and pixel sizes.

ACKNOWLEDGMENT

The authors would like to thank Drs. T. Ikegami and T. Sugeta for helpful discussions and encouragement throughout this work.

REFERENCES

[1] D.A.B. Miller, D.S. Chemla, T.C. Damen, A.C. Gossard, W. Wiegmann, T.H. Wood, and C.A. Burrus, Phys. Rev. B32, 1043 (1985).

[2] A.L. Lentine, H.S. Hinton, D.A.B. Miller, J.E. Henry, J.E. Cunningham, and L.M.F. Chirovsky, IEEE J. Quantum Electron. QE 25, 1928 (1989).

[3] C. Amano, S. Matsuo, T. Kurokawa, and H. Iwamura, Appl. Phys. Lett., to be submitted.

[4] M. Whitehead, A. Rivers, G. Parry, J.S. Roberts, and C. Button, Electron. Lett. 25, 984 (1989).

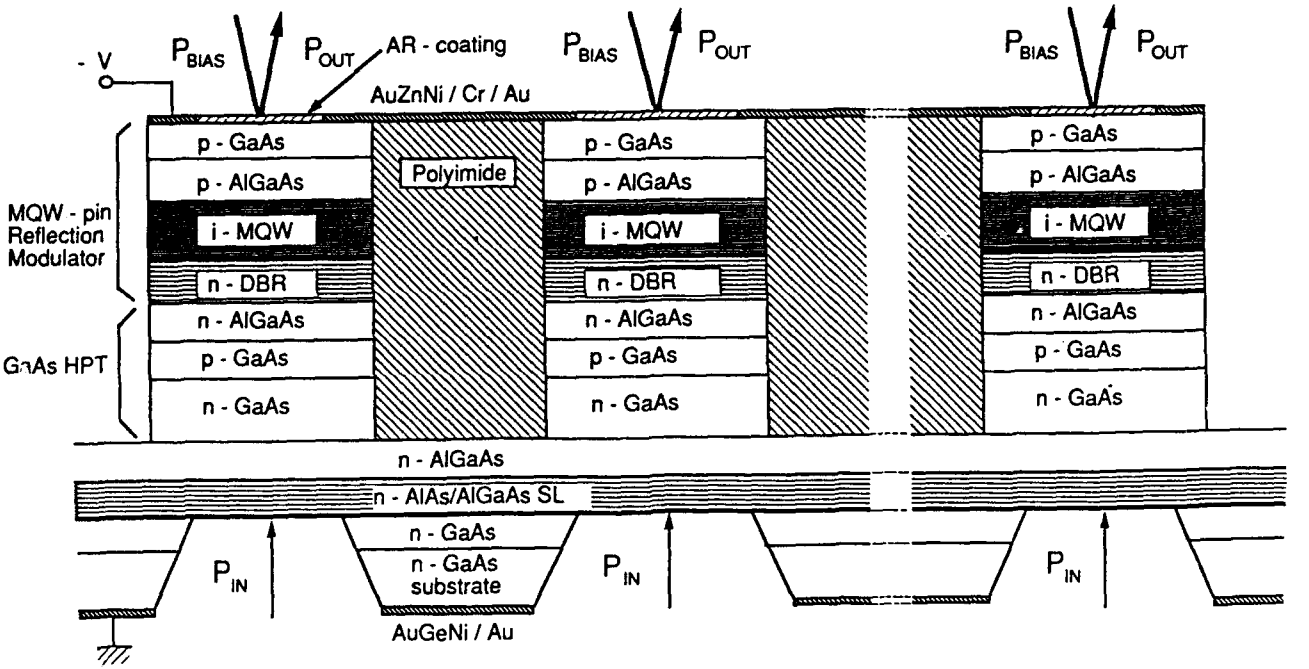


Fig.1. Cross-sectional view of photonic gate arrays.

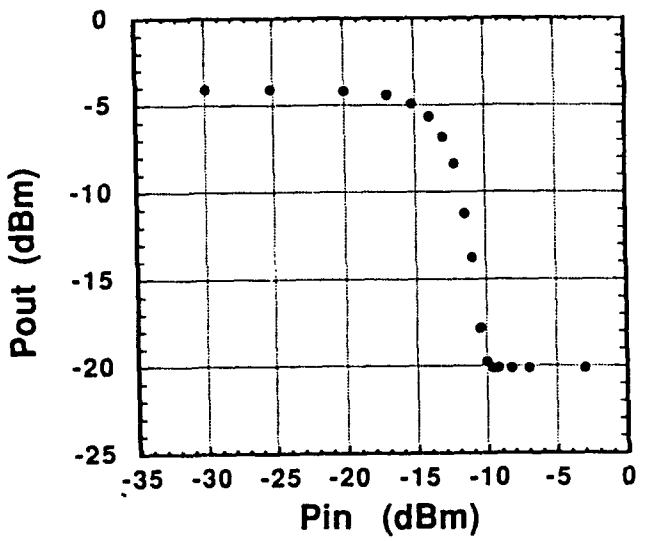


Fig.2.
Input/output characteristics of photonic gate arrays.
Bias light power is 0 dBm.

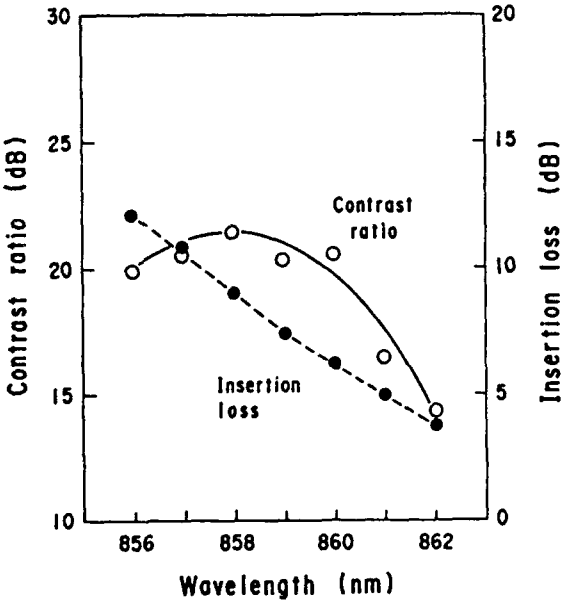


Fig.3.
Contrast ratio and insertion loss as a function of bias wavelength for photonic gate arrays.

LOW FIELD ELECTROABSORPTION AND SELF-BIASED SELF-ELECTROOPTIC EFFECT DEVICE USING SLIGHTLY ASYMMETRIC COUPLED QUANTUM WELLS

K. W. Goossen, J. E. Cunningham, D. A. B. Miller, W. Y. Jan,
A. L. Lentine*, A. M. Fox, and N. K. Ailawadi

AT&T Bell Laboratories,
Holmdel, NJ 07733,
USA

*AT&T Bell Laboratories,
Naperville, IL 60566,
USA

AD-P007 824

92-22353

Quantum wells and related layered semiconductor structures show strong electroabsorption that can be applied to make optical switches and modulators [1]. Many different structures are possible, each with different electroabsorption characteristics. In addition to conventional rectangular wells, structures investigated include coupled wells, both symmetric [2] and asymmetric [3], graded wells [4], low-barrier wells [5], and superlattices [6]. The optimum structure depends to some extent on the application. Here we describe a novel, slightly asymmetric coupled well structure designed to operate at very low fields. The resulting operating fields are so low that we can make a self-biased symmetric self-electrooptic effect device(S-SEED); this is an opto-electronic switching device without a power supply [7], and this is the first demonstration of such a device suitable for use in two-dimensional arrays.

For S-SEED operation, we want to use the lowest possible electric field so that we can minimize the switching energies [8]. The optical switching energy is directly proportional to the field change required in switching; this is because all of the charge involved in charging and discharging the internal capacitance, C, of the device is photogenerated by absorption of the incoming light. The charge required per unit area (and hence the required absorbed optical energy per unit area) is proportional to the field in the device. In addition, it is obviously important to minimize the operating voltage swing, V, to reduce the electrical energy, since this energy is about $(1/2)CV^2$ for electrically driven modulators.

One problem with trying to design a modulator that is very sensitive to field is that, in the usual p-i-n structure, even in moderate forward bias we never get to zero field (flat-band) in the structure. In operation of the S-SEED, and in operating a modulator without incurring a large forward current, the device will only typically be forward biased to about 1V. This leaves about 5000 V/cm field across the quantum wells for a 1 μm thick intrinsic region and a 1.5 eV bandgap energy (as in GaAs). If we design a symmetric structure such as a superlattice or coupled quantum well to be very sensitive at low field, we may not be able to take advantage of this because in operation we cannot reduce the field sufficiently.

The solution we attempt here is to make a slightly asymmetric structure. In this case we can use the asymmetry effectively to prebias the structure to try to compensate for the unavoidable minimum field. At zero or very low fields, the lowest electron state is predominantly in the thicker well (see Fig. 1). Beyond some field, this electron becomes predominantly in the thinner well. The basic operation is then otherwise similar to that of a coupled well [2]. The overlap of electron and hole in the lowest states is strongly reduced with field because the electron and hole are pulled into opposite wells; this is sometimes referred to as an effective "blue shift" because the oscillator strength lost from the lowest transition is largely transferred to higher energy transitions. We can also view the slightly asymmetric coupled well in terms of resonant coupling. Below a certain critical field, the lowest electron state is substantially in the left well. At a finite field, the left well and right well states resonantly couple. Beyond this field, the lowest electron state is substantially in the right well. Such behavior, including excitonic effects, has recently been

explained in detail [9]. Asymmetrizing the structure serves to move this critical field away from zero to the desired finite value. These two descriptions are equivalent.

In Fig. 2, we show experimental results for a structure with 63 angstrom and 58 angstrom wells separated by a 14 angstrom barrier, with each such period separated by a 35 angstrom barrier. An intrinsic ("i") region approximately 1 μm thick containing these coupled wells is contained in a p-i-n structure as usual. The spectra clearly show the effective blue shift or loss of overlap of the lowest transition. The structure is clearly useful for voltages between 1V forward bias and 1-4 V reverse bias. Note in particular that there is a substantial change in absorption between +1 V and -1 V. This is quite exceptional compared to conventional quantum wells. This design therefore has given us a modulator that is indeed very effective at low fields. (In contrast to the conventional quantum well, however, there is little further improvement in contrast with further increase in voltage past 4 V.)

By connecting two such p-i-n diodes in series, as shown in Fig. 3, we can make a S-SEED without an electrical power supply. This device behaves like any other S-SEED, showing optical bistability in the ratio of the two light beam powers shining on the diodes. (The bistability arises from the decrease in photocurrent with increasing reverse bias, a negative differential conductivity.) In the present case, there is, however, no need for a voltage supply. The stable states correspond to one diode in forward bias (about +1 V) and the other in reverse bias (about -1 V). Because the device shows considerable change in absorption between +1 and -1 V, there is no need for any other supply voltage. The optical input/output characteristic is also shown in Fig. 3 for a wavelength of about 835 nm.

The ability to make two-dimensional arrays of self-biased devices should enable us (i) to avoid the space taken by power supply rails, (ii) to avoid having to define the position and size of the array until after fabrication, potentially increasing the yield of usable arrays, (iii) to eliminate any electrical crosstalk between devices, and (iv) to avoid one failed device from shorting the rest of the array.

In principle, this structure should also have an enhanced exciton near flat band. When the electron and hole are substantially in the same well, the exciton should be relatively strongly bound because they are close. This should lead to a smaller exciton, with correspondingly strong absorption. As the electron is pulled into the opposite well by the field, the exciton should get weaker and larger, further reducing the absorption. It is not clear in practice, however, whether we are yet getting any significant benefit from this in the actual device.

In conclusion, we have demonstrated that slightly asymmetric coupled quantum wells allow us to make modulators that can operate at very low fields and voltages while still allowing us to handle the finite field always present in the diode structure. This should allow low-energy optical modulators and switches, and has enabled us to demonstrate a self-biased S-SEED suitable for parallel arrays without an electrical power supply.

References

[1] D. A. B. Miller, Int. J. High Speed Electronics, **1**, 19 (1990)

[2] M. N. Islam, R. L. Hillman, D. A. B. Miller, D. S. Chemla, A. C. Gossard, and J. H. English, Appl. Phys. Lett. **50**, 1098 (1987)

[3] H. Q. Le, J. J. Zayhowski, and W. D. Goodhue, Appl. Phys. Lett. **50**, 1518 (1987)

[4] G. D. Sanders and K. K. Bajaj, J. Vac. Sci. Technol. B, **5**, 1295 (1987)

[5] K. W. Goossen, J. E. Cunningham, and W. Y. Jan, Appl. Phys. Lett. (to be published)

[6] J. Bleuse, P. Voisin, M. Allovon, and M. Quillec, Appl. Phys. Lett. **53**, 2632 (1988); I. Bar-Joseph, K. W. Goossen, J. M. Kuo, R. F. Kopf, D. A. B. Miller, and D. S. Chemla, Appl. Phys. Lett. **55**, 340 (1989)

[7] J. S. Weiner, A. C. Gossard, J. H. English, D. A. B. Miller, D. S. Chemla, and C. A. Burrus, Electronics Lett. 23, 75 (1987)

[8] D. A. B. Miller, Opt. Quantum Electron. 22, S61 (1990)

[9] A. M. Fox, D. A. B. Miller, G. Livescu, J. E. Cunningham, J. E. Henry, and W. Y. Jan, Phys. Rev. B, 42, 1841 (1990)

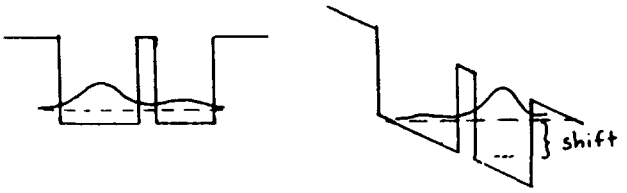


Fig. 1. Electron in a slightly asymmetric coupled quantum well without and with field.

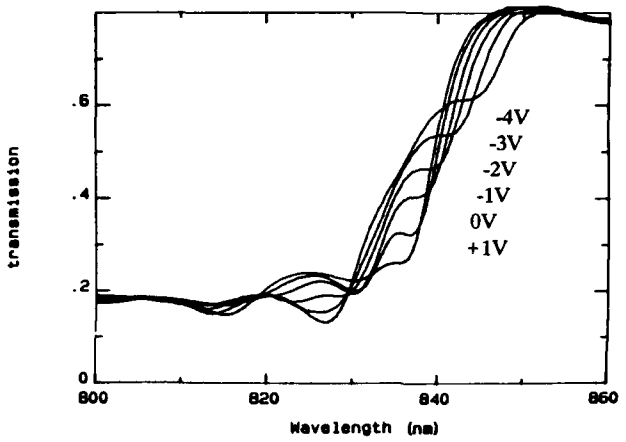


Fig. 2. Electroabsorption in the slightly asymmetric coupled quantum well sample.

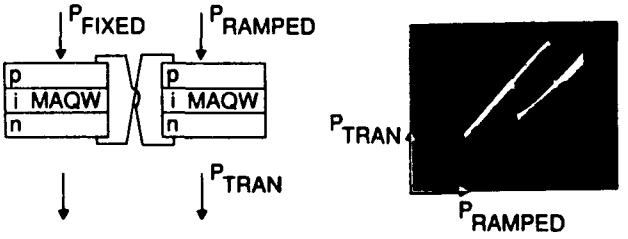


Fig. 3. Schematic and optical input/output characteristic for the self-biased SEED.

Reflection Electro-Absorption Modulator with High Reflectivity Change in a Novel Normally-Off Configuration

D. Thomas, B. Pezeshki, and J. S. Harris Jr.
Solid State Laboratories, Stanford University, Stanford CA 94305

AD-P007 825



INTRODUCTION:

Vertical optical modulators utilizing the large absorption changes in quantum wells are promising for optical computing and optical interconnect technologies. While normally-on devices can be applied to interconnect technologies, normally-off reflection or transmission modulators presenting negative differential conductivity are required for producing bistability, in various Self Electo-optic Effect Device (SEED)[1-2] configurations.

Reflection Electro-Absorption Modulators (REAMs) that use a Fabry-Perot (F-P) cavity have demonstrated high contrast and low insertion loss[3] for normally-on devices. The highest performance devices so far have used the Quantum Confined Stark Effect (QCSE) to increase the optical absorption and consequently change the reflectivity of the device with voltage. The F-P mode of the cavity is usually designed to be below the exciton energy, and the front mirror reflectivity is kept low. These devices use the large absorption change of QCSE and have very low residual absorption since they work below the absorption edge, but are of normally-on type, the higher reflectivity occurring at zero bias.

Normally-off transmission or reflection modulators, so far, have always exploited a decrease in absorption at the operating wavelength. They can operate at the exciton wavelength at zero voltage and shift the exciton with bias, utilizing the QCSE[1,2,4]. This method, however, leads to lower absorption ratios due to transitions into the quantum well continuum. These tend to lower performance, generally increasing the insertion loss in the on-state. Utilizing a blue shift of the absorption edge reduces the residual absorption. Various reflection or transmission SEEDs have been constructed using different mechanisms inducing blue shift[5-7]. These blue-shift methods, however, all perform more poorly than the QCSE in terms of absorption changes.

Here we present a novel method where an increase in absorption can lead to an increase in device reflectivity and a consequent negative differential photoconductivity, thus enabling us to use the larger absorption change and maximum to minimum absorption ratio (X) of the QCSE to fabricate normally-off modulators and SEEDs.

THEORY OF OPERATION:

The total reflectivity of a Fabry-Perot cavity at the Fabry-Perot mode, R_T, depends on the front mirror reflectivity, R_f, and the effective back mirror reflectivity, $R_{b'}$, where $R_{b'}$ includes the attenuation of the cavity $R_{b'} = R_b e^{-2\alpha L}$. L is the length and α is the absorption coefficient of the cavity material.

$$R_T = \left[\frac{\sqrt{R_f} - \sqrt{R_{b'}}}{1 - \sqrt{R_f R_{b'}}}\right]^2 \qquad (1)$$

R_T is plotted on Fig. 1 as a function of $R_{b'}$ for various front mirror reflectivities. R_T goes to zero when the matching condition $R_f = R_{b'}$ is satisfied. In normally-off devices the matching condition is satisfied at zero bias. The operation of various reflective devices can be understood from the figure. Conventionally, the front mirror reflectivity is kept low (solid curve), and a reduction in absorption (i.e. moving to the right of the diagram while staying on the same R_f curve)is required

92-22354



to increase the reflectivity, using either red[4], or blue shift[7]. Our device, however, has a higher front mirror reflectivity (dotted curve) and operates to the left of the matching condition, which causes *increased* reflectivity as absorption *increases*.

Although we require a higher front mirror reflectivity to operate a device in this way, we do not suffer a penalty in terms of insertion loss and modulation ratio. For a given cavity size and absorption, the trade-off between the modulation ratio and insertion loss turns out to be the same as for the normally-on device[3] and depends only on X. Using the QCSE to increase the absorption gives us a higher X, thus superior performance in the trade-off between modulation ratio and insertion loss. On the other hand, the higher front mirror reflectivity required for the same degree of performance does decrease the optical bandwidth and increase the sensitivity to temperature.

RESULTS:

To demonstrate this concept, we optically coated the front surface of a previously fabricated REAM[3] by adding three periods of SiO_2 / TiO_2 quarter-wave layers, increasing the front mirror reflectivity from 50.3% to an estimated value of 93%. This value was chosen to approximately match the effective back mirror reflectivity R_b' at zero bias. The reflectivity was measured, using a white light source and a 1/2 meter spectrometer.

Fig. 2 shows the total device reflectivity as a function of wavelength for various applied biases. In accordance with the previously discussed theory, we see the reflectivity at the bottom of the F-P dip first increases in value as absorption increases with voltage, and then decreases as the excitonic resonance moves beyond the F-P wavelength. The F-P dip also broadens, reaching a maximum width between 4 and 5 Volt, when the absorption is the greatest and the cavity finesse is being reduced by the absorption. At 11 Volt bias, the finesse is partially recovered as the exciton resonance is now at the low energy side of the F-P dip, and severely reduced in strength by the high field. One also observes a shift of the F-P minimum from side to side. This swing results from refractive index variations accompanying the absorption change, according to the Kramers-Kronig relation.

Fig. 3 shows the normalized reflectivity as a function of voltage at three different wavelengths. We see that at 8264 Å we obtain an increase in reflection of 47%, the highest reported to date, and a measured contrast ratio of 15. This value might be limited by our setup.

In order to examine the latching capabilities of our device, we then measured the photocurrent under monochromatic illumination generated by passing the white light through the monochromator. Fig. 4 shows the photocurrent generated under illumination at 8264 Å. The initial increase in photocurrent with field is due to the larger collection efficiency of the photo-generated carriers. However, the photocurrent rapidly decreases as the device reflectivity increases. Overall, there is more than a 30% reduction in photocurrent as the device becomes more reflective. The minimum in reflectivity corresponds to the maximum in the photocurrent, thus allowing high contrast ratios in bistable circuits.

Although our device is far from being optimized, since it is a modification of a previously existing REAM, we have obtained very high performance in terms of insertion loss and modulation ratio. Fig 5 summarizes the performances of reported normally-off electro-absorption modulators. Our device has the lowest insertion loss with a very reasonable modulation ratio. The only significant disadvantage to our cavity design is the narrow optical bandwidth. Since the sharpness of the Fabry-Perot dip in our device is dominated by the phase changes caused by the multi-layer mirrors[8], we can increase the bandwidth by going to a larger cavity, or perhaps using a semitransparent Au mirror.

CONCLUSION:

We present a high performance normally-off modulator which works by increasing the optical absorption coefficient with bias. Using this method with the QCSE, we report the largest reflectivity change in such a modulator. The novel cavity design allows an increase in the absorption coefficient to reduce the total absorption and leads to a pronounced negative differential photoconductivity.

[1] D. A. B. Miller, D. S. Chemla, T. C. Damen, A. C. Gossard, W. Wiegmann, T. H. Wood, and C. A. Burrus, Appl. Phys. Lett. **45**, 13 (1984).
[2] A. L. Lentine, H. S. Hinton, D. A. B. Miller, J. E. Henry, J. E. Cunningham, and L. M. F. Chirovsky, Appl. Phys. Lett. **52**, 1419 (1988).
[3] B. Pezeshki, D. Thomas, and J. S. Harris, Jr., Appl. Phys. Lett. **57**, 1491 (1990), references therein.
[4] M. Whitehead, A. Rivers, G. Parry, and J. S. Roberts, Electron. Lett. **26**, 1589 (1990).
[5] I. Bar-Joseph, K. W. Goossen, J. M. Kuo, R. F. Kopf, D. A. B. Miller, and D. S. Chemla, Appl. Phys. Lett. **55**, 340 (1989).
[6] K-K. Law, R. H. Yan, J. L. Merz, and L. A. Coldren, Appl. Phys. Lett. **56**, 1888 (1990).
[7] K-K. Law, R. H. Yan, L. A. Coldren, and J. L. Merz,, Appl. Phys. Lett. **57**, 1345 (1990).
[8] B. Pezeshki, D. Thomas, J. S. Harris Jr, Paper presented at the SPIE conference, Aachen (Nov. 90).

The authors would like to acknowledge support of ONR/DARPA through contract N00014-84-K-0077 and ONR/SDIO through contract N00014-89-K-0067.

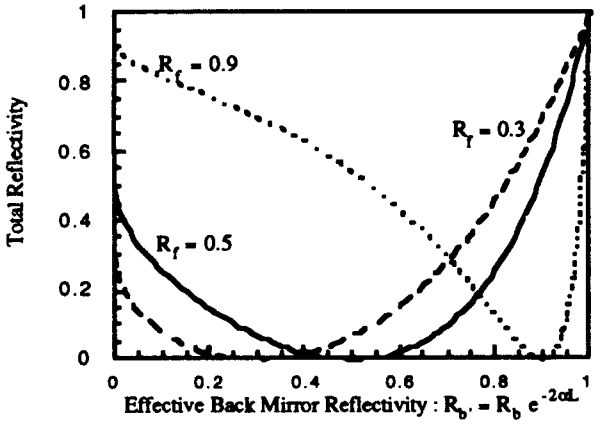


FIG. 1. Calculated total device reflectivity as a function of the effective cavity reflection for various front mirror reflectivities. Note: Rb'=1 corresponds to zero loss, while Rb'=0 corresponds to infinite absorption.

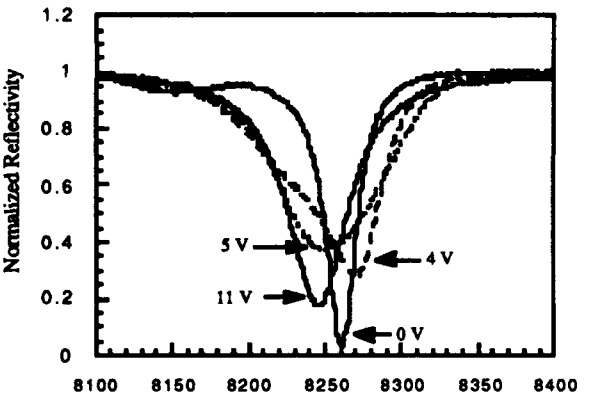


FIG 2. Normalized reflection versus wavelength at various reverse bias voltages.

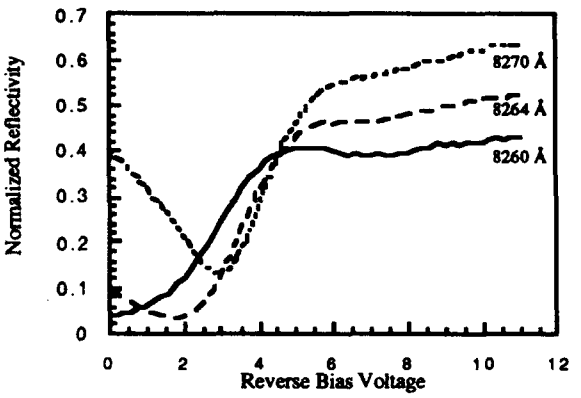


FIG. 3. Measured normalized reflectivity as a function of reverse bias voltage at 3 different wavelengths.

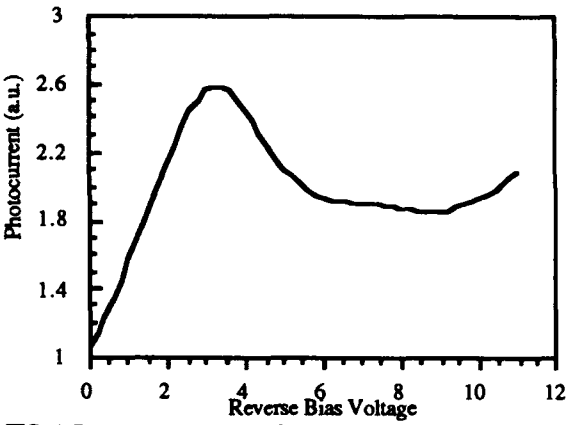


FIG. 4. Photocurrent resulting from the illumination of the modulator under 8264 Å light as a function of reverse bias voltage. The large negative photoconductivity causes bistability in SEED configurations.

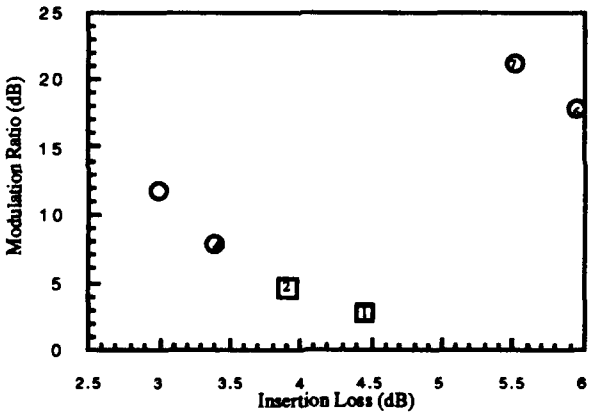


Fig. 5 Modulation ratio vs. insertion loss for previously reported normally-off reflection (circles) and transmission (squares) modulators. The numbers correspond to references. Our device is the open circle.

High Power Extremely Shallow Quantum Well Modulators

K.W. Goossen, J.E. Cunningham, and W.Y. Jan
AT&T Bell Laboratories
Holmdel, NJ 07733

AD-P007 826

L.M.F. Chirovsky and R.A. Morgan
AT&T Bell Laboratories
SSTC

Light modulators based on electroabsorption in quantum wells (QW's) [1] have been extensively studied in recent years. Their operation relies on the fact that at room temperature a strong exciton can exist due to confinement in the quantum wells,[2] which results in a strong absorption feature which can be manipulated with an applied electric field. Applications include optical interconnection of integrated circuits,[3,4] lightwave applications,[5] and optical computing. For the latter there exists self electro-optic effect devices (SEED's) which comprise of a QW p-i-n modulator in series with a battery and a load which may be another QW modulator.[6] This circuit is bistable because of the negative resistance of the reverse biased QW modulator when illuminated at the QW exciton peak. This results from the fact that the exciton red-shifts with increasing electric field, causing the absorption, and hence the photocurrent, to decrease with increasing reverse bias. Switching of the SEED is induced by changing the light intensity incident relative to the load's current-voltage characteristic . Since the transmission of the QW modulator depends on field it also switches, resulting in optical control of light transmission.

SEED switching speeds increase as the operating light intensities increase, since the reverse-biased QW modulator is essentially a capacitor and therefore its charging rate is linearly proportional to the photocurrent. However, build-up of photo-induced carriers in the QW's caused by finite escape time limits the intensity. This is because the exciton saturates at a certain carrier level, so that the electroabsorption degrades. It has been found that carrier escape is facilitated by making the barriers of the QW's lower or thinner.[7] In this paper we study the limiting behavior of lowering the barrier to zero. We report the remarkable observation of a room temperature exciton for GaAs-$Al_xGa_{1-x}As$ QW's for x as low as 0.02. This corresponds to a total band offset of 25 meV, so that the barriers are lower than the thermal energy (kT). The exciton ionizes under small fields, resulting in a change in reflection from 12 % to 47 % upon changing the bias of our p-i(multi-QW)-n/dielectric mirror device from 0V to -10V. Upon raising the intensity of the device to 1mW in a 3 μm diameter spot the device still has a change in reflection from 13 % to 39 %.

92-22355

We report on both transmission and reflection samples (i.e., with an integral dielectric mirror) with various QW barrier heights and widths including "standard" QW's with x=0.3 barriers. All were grown by gas-source molecular beam epitaxy (GS-MBE). In all the samples the width of the intrinsic region was about 1 μm. The structure of the transmission samples consisted of a 1.5 μm n $Al_{0.3}Ga_{0.7}As$ layer grown atop a n^+ GaAs substrate, followed by an intrinsic region consisting of the multi-QW. We also report measurements on a sample with a bulk GaAs intrinsic region. Finally a 0.6 μm p $Al_{0.3}Ga_{0.7}As$ layer was grown, followed by a 50 angstrom p^+ GaAs cap. The shallow QW's were grown at 600 C. The reflection sample was grown on an undoped substrate. First an undoped mirror consisting of quarter wave layers of AlAs and $Al_{0.1}Ga_{0.9}As$ was grown, followed by a 500 angstrom thick n^+ contact layer and a 300 angstrom thick n^- thick spacer layer, both $Al_{0.1}Ga_{0.9}As$. This was followed by an undoped 60 period multi-QW consisting of 100 angstrom wells clad on both sides by 60 angstrom barriers with 100 angstrom spacers on both edges of the MQW. Finally a p layer was grown as before. We etched 200 × 200 μm mesas and made gold top contacts. For the reflection sample the mesa was etched to the n contact layer and Au/Ge contact made, and an anti-reflection coating applied. For the transmission measurements the sample was mounted upside-down with epoxy on a sapphire disk. The substrate was then etched down to the $Al_{0.3}Ga_{0.7}As$ stop-etch layer, and an anti-reflection coating deposited.

In Fig. 1 we show photocurrent measurements for four of the samples with well/barrier widths of 100/100 angstrom and barrier heights ranging from 0 to x=0.06. The intrisic width of each sample is 1 μm. Measurements for applied biases of 0, -2, and -4 volts are shown. All measurements in this paper are at room temperature.

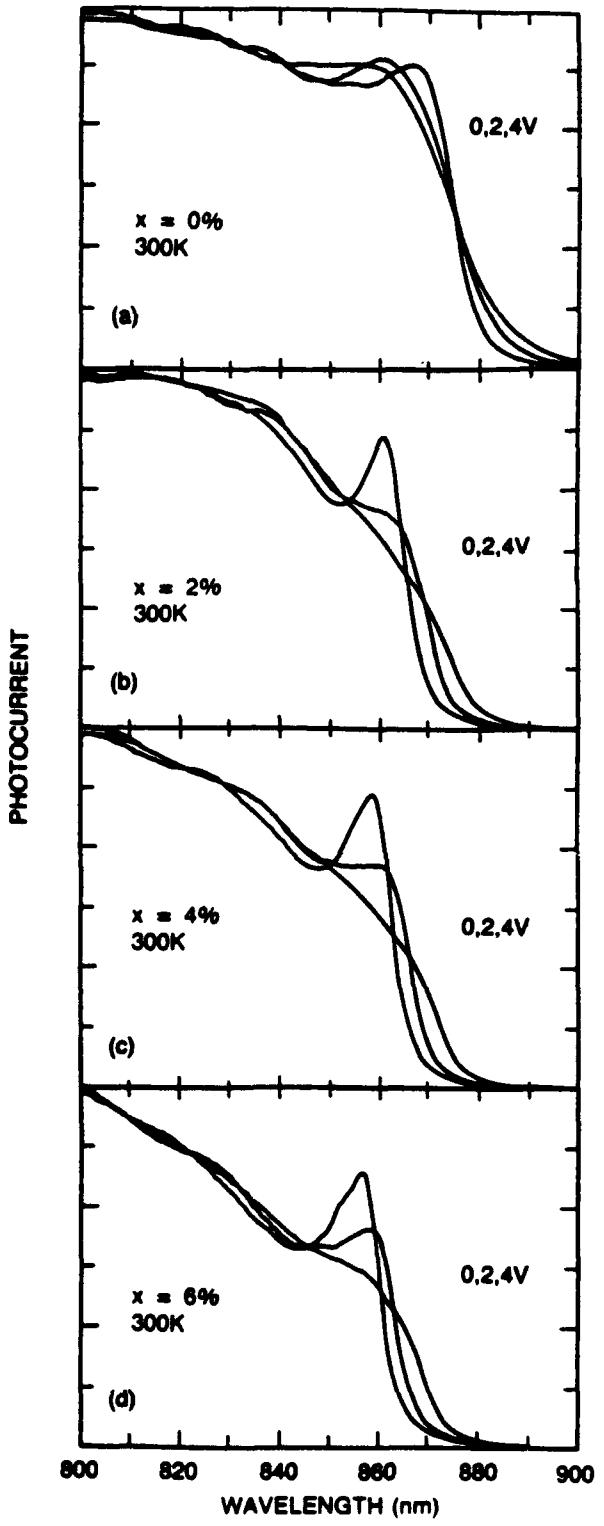


Fig. 1: Photocurrent measurements of samples with quantum well barrier height ranging to zero, showing that only an infinitesimal barrier is needed to retain an exciton at room temperature.

For the bulk sample a small exciton-like feature is seen that simply broadens with field. However, for the x=0.02 sample we see that only a slight barrier results in a strong exciton at 0V. The exciton rapidly ionizes under field and also red shifts as is commonly observed in the quantum confined stark effect.[8] We will show that the exciton ionization leads to enhanced electroabsorption (EA) for the shallowest QW's at low fields. As the barrier height is raised the ionization is not so strong. This causes the low-field EA to be weaker, but we will show that the high-field EA becomes stronger as x is raised. This can be explained by a sum-rule argument: since the exciton "holds together" better for deeper wells as the field increases, it carries oscillator strength with it as it red-shifts, resulting in less oscillator strength at the zero-bias exciton position.

Transmission measurements of the x=0.02 sample are shown in Fig. 2 for biases from +1V to -5V in steps of 1V. The exciton produces strong absorption under no field. The rapid ionization of the exciton as the field is applied leads to a change

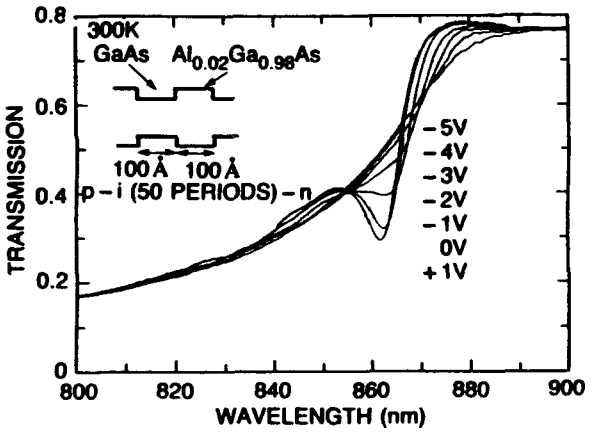


Fig. 2: Transmission of x=0.02 sample.

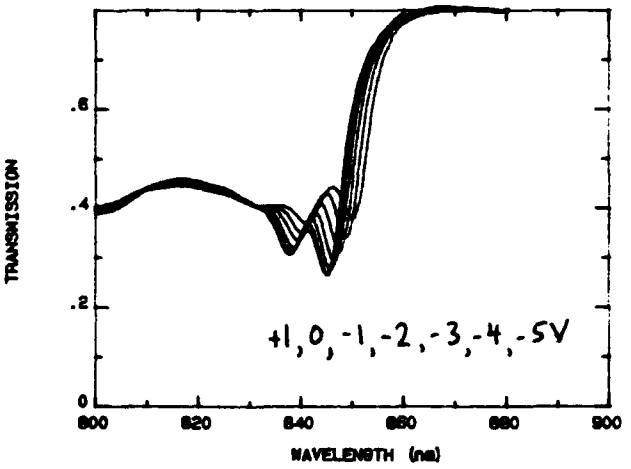


Fig. 3: Transmission of x=0.3 sample.

of transmission from 29 % to 47 % for a +1V to -3V swing. (Recall that the intrinsic region of all the samples is 1 μm so a reverse bias of 3V corresponds roughly to a field of 4.5 V/μm, assuming that the fermi-level is pinned near the band edges in the p and n regions.) Under higher fields the transmission changes are slight. This is because the exciton has already ionized almost completely so that further bias has little effect.

For comparison the transmission of a "standard" quantum well sample with well/barrier widths of 95/45 angstrom and x=0.3 barriers is shown in Fig. 3. Note that since this device relies on a shift of the exciton which is quadratic with voltage its low-field modulation is much worse than the shallow QW sample. In Fig. 4 the contrast ratio (i.e., the transmission normalized to the transmission at +1V) on the exciton peak of bulk, shallow (x=0.02) and standard QW samples is shown as a function of bias. It is clear that the shallow well sample has the best performance over this range of bias. The standard QW sample's contrast is hampered by the movement of the light hole into the operation wavelength near -7V, while the shallow QW sample has a monotonic increase. However, above 10V/μm the standard QW's contrast will continue to increase while that of the shallow will not. As discussed above, this results from the fact that for deeper wells the exciton holds together better under high fields, so that by a sum-rule argument the exciton continues to take oscillator strength with it under high biases, thus removing oscillator strength from the zero-bias exciton wavelength. Therefore if one is willing to employ such large voltages, one should use standard QW's. Note however that the optical switching energy of SEEDs increases linearly with the voltage and we show below that standard QW's have substantially lower saturation intensities.

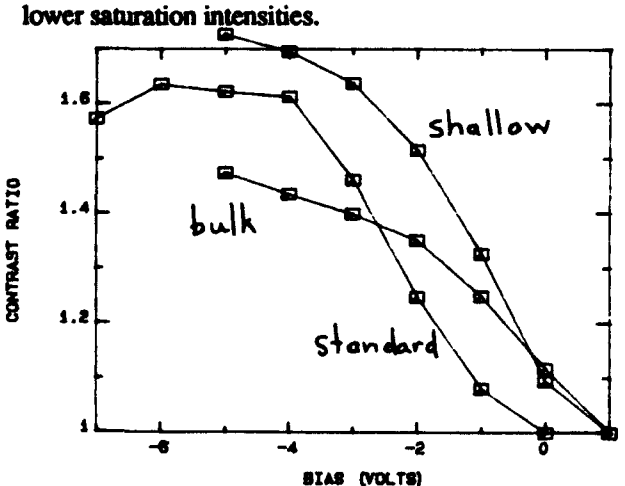


Fig. 4: Contrast ratio of bulk, shallow QW, and standard QW transmission modulators.

We must point out, though, that in non-SEED applications, where bistability is not a requirement (i.e., optical interconnect applications), one may operate with a wavelength below the band-gap, so that the absorption increases with bias. In this case it is clear from Figs. 2,3 that the standard QW's are preferable because the exciton remains intact, causing the transmission to drop sharply. While this mode of operation tends to produce less contrast, it results in larger changes in transmission.

In Fig. 5 we show measurements on our reflection device. The center position of the dielectric mirror is at the exciton peak. Again, there is a strong exciton which ionizes rapidly with field, resulting in a change in reflection from 12 % to 47 % for 0 to 10V operation. It is interesting to note that in this sample the heavy and light holes can be distinguished and are shifted slightly compared with the transmission sample shown in Fig. 2. We believe that strain existed in the transmission samples causing the slight shift, which has little affect on performance.

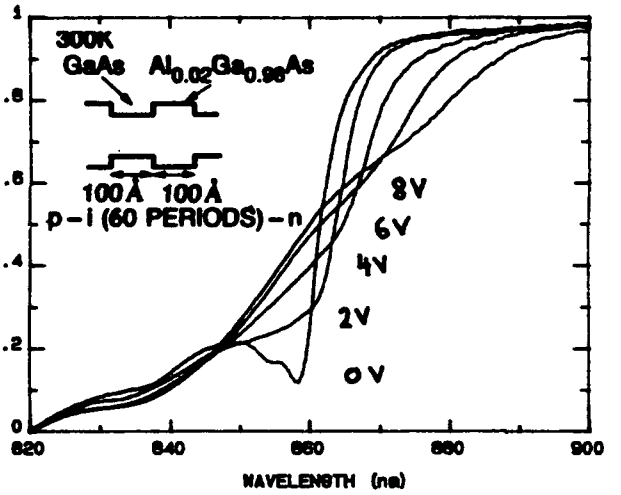


Fig. 5: Reflection of x=0.02 sample with integral mirror.

All the previous transmission measurements were made with a lamp and monchrometer. We then employed a Ti:Sapphire laser tuned to the exciton peak and performed measurements of reflection vs. voltage for different intensities. The laser was focussed to a gaussian spot with a diameter of approximately 3.25 μm (distance between the $1/e^2$ points). Heating effects have been studied using other samples by using low-duty cycle chopping, and were found to be slight. It may be that heat builds up faster than the time scale of our acousto-optic modulator (several MHz), and this is under study. Note that heating could only cause a degradation of the results so that in a real system even better performance may be expected. In Fig. 6

measurements are shown for intensities of 0.01, 0.4, 1, 2 and 3 mW power. At 1 mW we still obtain a change in reflectivity from 13 % to 39 %. Even at 3 mW a contrast ratio of 1.9 exists between -1 and -9V.

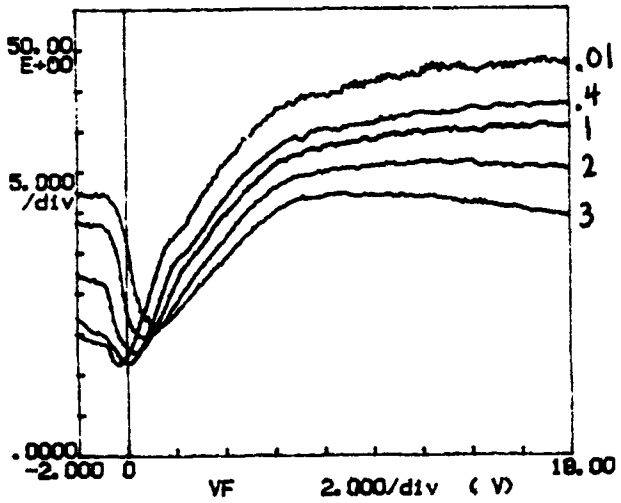


Fig. 6: Refectivity vs. voltage for 0.01, 0.4, 1, 2, 3 mW (3 μm spot) for the x=0.02 sample.

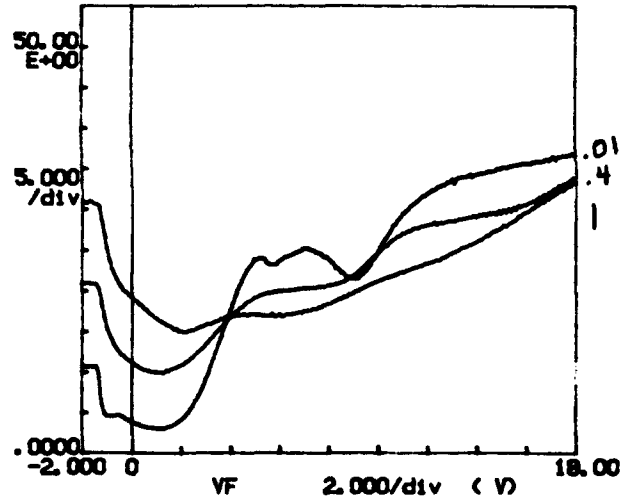


Fig. 7: Reflectivity vs. voltage for 0.01, 0.4 and 1 mW for a x=0.3 sample with 35 angstrom barriers. This sample has more periods resulting in higher contrast but larger insertion loss.

However, note that at this power in forward bias the absorption has saturated. This is because only a small field exists to sweep the carriers out. In the standard arrangenment of SEED devices the modulators are driven into forward bias. Therefore without more complicated circuitry to prevent the modulator from going into forward bias no contrast would be acheived at this power. At 1mW there is still a contrast of about 2 between forward (+0.8V) and reverse bias. Note that for our best previous sample [9] with thin barriers (x=0.3, 35 angstrom), contrast between forward and reverse bias dissappears by 0.4 mW for 8V operation and by 1 mW for 18V operation (Fig. 7).

In conclusion, we report that for GaAs-$Al_xGa_{1-x}As$ QW's with x as low as 0.02, a strong exciton exists at room temperature, resulting in electroabsorption that is actually stronger at low fields compared to standard QW's for operation on the exciton peak, due to ionization of the exciton. We report a change in reflection from 12 % to 47 % for 0-10V operation for a shallow QW modulator with an integral mirror. Such a low barrier results in higher saturation intensities since it is easier for photogenerated carriers to escape the QW. With a 3 μm diameter spot, we retain 13 % to 39 % reflection changes for 1 mW operation and contrast ratio of 2 for normal SEED operation.

References

[1] T.H. Wood, C.A. Burrus, D.A.B. Miller, D.S. Chemla, T.C. Damen, A.C. Gossard, W. Weigmann, Appl. Phys. Lett. 44, 16 (1984)

[2] D.A.B. Miller, D.S. Chemla, T.C. Damen, A.C. Gossard, W. Weigmann, T.H. Wood, C.A. Burrus, Phys. Rev. Lett. 53, 2173 (1984).

[3] G.D. Boyd, D.A.B. Miller, D.S. Chemla, S.L. McCall, A.C. Gossard and J.H. English, Appl. Phys. Lett. 50, 1119 (1987).

[4] K.W. Goossen, G.D. Boyd, J.E. Cunningham, W.Y. Jan, D.A.B. Miller, D.S. Chemla, and R.M. Lum, IEEE Phot. Tech. Lett. 1, 305 (1989).

[5] J.E. Zucker, T.L. Hendrikson, and C.A. Burrus, Appl. Phys. Lett. 52, 945 (1988).

[6] D.A.B. Miller, D.S. Chemla, T.C. Damen, T.H. Wood, C.A. Burrus, A.C. Gossard and W. Wiegmann, IEEE Jour. Quan. Elec. QE-21, 1462 (1985);
D.A.B. Miller, Opt. and Quantum Electron., to be published (Nov. 1990).

[7] A.M. Fox, D.A.B. Miller, G. Livescu, J.E. Cunningham, J.E. Henry, and W.Y. Jan, Phys. Rev. B 42, (July 15, 1990).

[8] D.A.B. Miller, D.S. Chemla, T.C. Damen, A.C. Gossard, W. Weigmann, T.H. Wood and C.A. Burrus, Phys. Rev. B 32, 1043 (1985); J.E. Zucker, I. Bar-Joseph, C.H. Joyner, A. Dentai, M.D. Divino, D.S. Chemla, Elec. Lett. 25, 973 (1989).

[9] R.A. Morgan, J.M. Freund, L.M.F. Chirovsky, L.A. D'Asaro, R.F. Kopf and J.M. Kuo, Proc. IEEE LEOS meet. Nov. 1990.

AD-P007 827

Coherent Nonlinear Laser Spectroscopy Studies of Exciton Relaxation, Dephasing and Energy Transport in GaAs Quantum Wells

D.G. Steel, S.T. Cundiff, M. Jiang, Hailin Wang, M.D. Webb

Randall Laboratory of Physics, University of Michigan, Ann Arbor, MI 48109

Optical resonant excitation of excitons with nearly monochromatic light of energy E leads to an optically induced polarization (coherence) and a population of excitons within ΔE of E where $\Delta E \sim \hbar\gamma_h$ (γ_h is the homogeneous linewidth of the exciton). The decay of this excitation must be characterized by the decay rate of the polarization (called the dephasing or transverse relaxation rate, $\gamma_t=\gamma_h$) as well as the decay rate of the population about energy E (called longitudinal the relaxation rate, γ_l). In a simple ideal quantum well, quasi two dimensional excitons are described by a Bloch type wave function and are free to move in the well plane. At low exciton density, decay of the excitation is then expected to be predominantly due to exciton-phonon scattering along with exciton recombination. In practice, however, nonideal growth processes result in interface roughness and corresponding disorder, leading to localization of lowest energy excitons and inhomogeneous broadening of the exciton absorption spectrum. Higher energy excitons remain quasi-delocalized or extended and the transition region, identified as the middle of the absorption resonance, is designated the exciton mobility edge.[1] Extended excitons are expected to dephase quickly (~ps) due to phonon and defect scattering whereas scattering processes for localized excitons are characterized by longer time scales (~100ps).

Localized excitons are in a local minimum in energy, and at very low temperature, decay of the localized exciton at energy E is expected to be dominated by migration between localization sites. The migration is accompanied by absorption or emission of acoustic phonons to compensate for the energy difference. While the migration is due to the overlap of the exciton wave functions between different sites for small intersite distances, the intersite dipole-dipole interaction mediates the migration process when the intersite distance is much greater than the localization length. It is estimated that the typical magnitude of participating phonon wave vectors is within a few times of the inverse of the localization length,[2] which indicates the energy of participating phonons is on the order of 0.01 to 0.1 meV. Such behavior has been reported in InGaAs/InP structures where all excitons appear to be localized.[3] At higher temperatures (>10K), thermal activation of localized excitons to delocalized states becomes important. This process is associated with phonon absorption, and has been observed in earlier work in GaAs MQW structures.[3,4] The measured activation energy indicates that the onset of delocalized excitons is near the absorption line center.

In this work we combine the results of frequency domain four-wave mixing (FDFWM) with transient FWM (TFWM) to provide a more complete picture of the relaxation of the lowest energy heavy hole exciton in GaAs/AlGaAs multiple quantum well structures. In these experiments, two nearly collinear co-polarized fields interact in the medium to create an excitation proportional to $E_1E_2^*$. A coherent signal is produced through scattering of an orthogonally polarized field, E_3. The signal is proportional to $\chi^{(3)}E_1E_2E_3$ where $\chi^{(3)}$ is the third order susceptibility. In FDFWM, information is obtained by measuring the signal as a function of the detuning of the different input frequencies. For example, tuning ω_2 gives a linewidth determined by excitation relaxation (the width and shape contains information about the different γ_l). Tuning ω_3 eliminates inhomogeneous broadening and provides information on γ_t. It also provides a measure of the quasi-equilibrium exciton distribution in the presence of spectral diffusion due to scattering from energy E to E'. In transient FWM, inhomogeneous broadening of the resonance leads to a delay in the signal emission with respect to the third pulse. The coherent emission is called a stimulated photon echo (SPE). If the system is homogeneously broadened, the signal is prompt with respect to the third pulse and the emission is called a free polarization decay (FPD). Relaxation rates are determined by measuring the signal amplitude as a function of t_2-t_1 (measures γ_t) or t_3-t_2 (measures γ_l).

Samples consist of 65 periods of 96 Å GaAs wells and 98 Å $Al_{0.3}Ga_{0.7}As$ barriers, mounted on a sapphire disk with the substrate removed. The data presented in this paper were obtained on samples characterized by a typical absorption linewidth of order 2 meV for the HH1 exciton, and a Stokes shift of 1-1.5 meV between the HH1 exciton absorption and emission.

92-22356

Figure 1a shows the FWM line shape obtained by tuning ω_2 for excitation 0.6 meV below absorption line center where excitons are expected to be localized. The line shape shows two components characterizing γ_l. The broad component corresponds to a relaxation time of 30 ps while the narrow component corresponds to 1.2 ns. The fast relaxation time is believed to be due to phonon assisted migration between localization sites and thermal activation to quasi-delocalized states. The resultant scattering establishes a quasi-equilibrium distribution of localized excitons which decays more slowly due to recombination. This longer lived component of the excitation is the origin of the 1.2 ns structure in the data. Confirmation of the presence of spectrally diffused excitons is seen in Fig. 1b where we show the FWM line shape obtained by tuning ω_3. The sharp resonance corresponds to the homogeneous line shape of the exciton while the low energy tail reflects the quasi-equilibrium distribution of excitons. A simple calculation assuming a strong redistribution model shows a similar line shape as seen by the solid line. While the FWM response enables the measurement of the redistribution of excitons, this low energy tail complicates the measurement of the true homogeneous linewidth. We will return to this in TFWM.

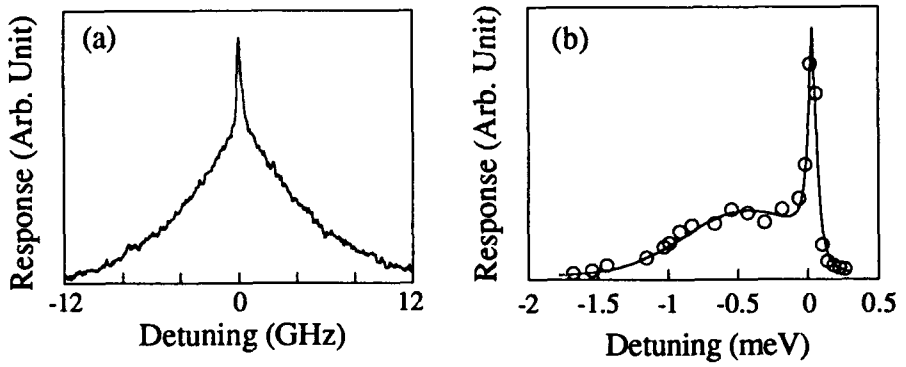


Figure 1. (a) The FDFWM response leading to a line shape determined by decay of the excitation (tuning ω_2). Two components are observed at 10K due to recombination (the narrow component) and spectral diffusion (the fast component). (b) The FDFWM line shape obtained by tuning ω_3 corresponding to the homogeneous line shape (the sharp resonance) and a low energy tail due to spectral diffusion. Zero detuning in (b) corresponds to $\omega_3=\omega_1$, ω_1 and ω_2 1.5 meV below absorption line center. The line shape is obtained at 5K.

It is significant to compare the above results with line shapes obtained above line center. Figure 2a

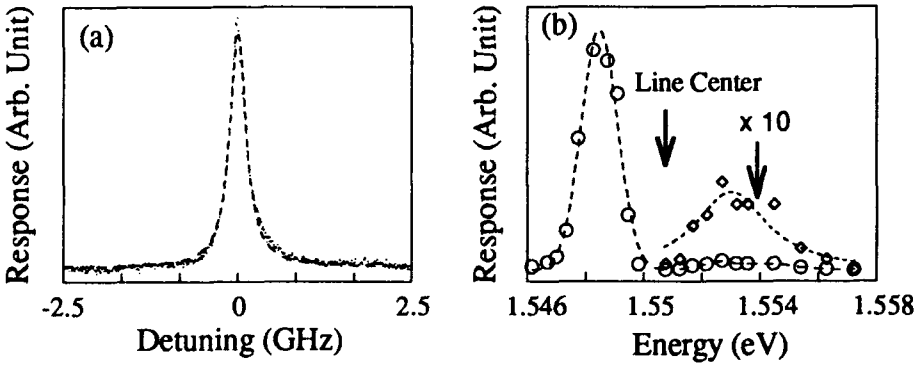


Figure 2. The FDFWM response obtained 2 meV above absorption line center. (a) Tuning ω_2 shows a single resonance due to recombination. (b) Tuning ω_3, we see two resonances. The upper resonance is the homogeneously broanded resonance from delocalized excitons. The lower resonance is due to excitons which have localized. The energy of the lower resonance corresponds to the luminescence maximum.

shows the FWM line shape as a function of ω_2. Here, a single component is observed corresponding to a lifetime of 1.2 ns. Above line center, excitons are expected to be delocalized. Phonon scattering along the 2D exciton dispersion curve leads to a rapid decay of the excitation on a time scale of 1ps.[5] This time scale leads to a very broad structure not clearly observable in FWM. However, the resultant quasi-equilibrium decays due to recombination giving rise to the 1.2 ns structure in the figure. The line shape corresponding to the homogeneous profile, obtained by tuning ω_3, is shown in Figure 2b. This structure is notable for the presence of a double resonance. We believe the higher resonance corresponds to the homogeneous line shape of the free exciton. Scattering along the 2D dispersion curve is of course a form of spectral diffusion. However, this contribution is not observable in optical measurements since the k-selection rule results in weak optical transitions away from k=0 of the exciton. Hence, the lineshape reflects the homogeneous shape of the exciton. The low energy resonance is due to free excitons which have localized by emission of acoustic phonons.

In the study of FDFWM response of the localized excitons, spectral diffusion complicates the determination of the homogeneous line shape. In the particular, the low energy tail as well as part of the sharp resonance seen in Figure 1b is the result of spectral diffusion. TFWM does not provide information on the details of the redistribution, but can provide a direct measure of the dephasing time of this inhomogeneously broadened resonance. Moreover, the SPE provides a means to determine the longitudinal and transverse relaxation time in the same measurement. Figure 3 shows a plot of the measured times as function of temperature and wavelength. The inset in Fig. 3a show typical decay curves which are purely single exponential (on this time scale) for both relaxation rates.

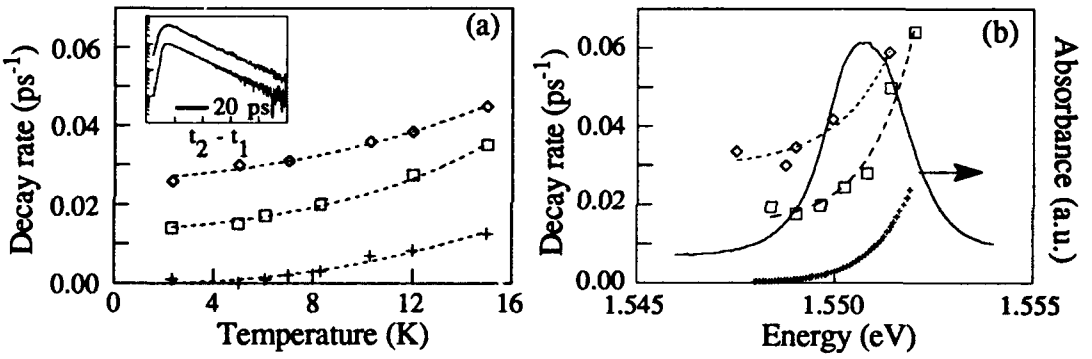


Figure 3. The TFWM response. γ_l (diamonds), γ_t (squares), and γ_{ph} (crosses) as function of temperature (a) and excitation energy (b). Inset: Upper curve is decay time integrated signal due to longitudinal relaxation as a function of $\tau=t_3-t_2$. Lower curve is decay due to dephasing as a function of $\tau=t_2-t_1$. The decay rate for $\gamma_t(\gamma_l)$ is 4 (2) times the measured time-integrated decay of the signal.

We first note that at low temperature (Fig. 3a) and large tuning below resonance (Fig. 3b), we have the interesting result that $\gamma_t=\gamma_l/2$. In simple two level systems if there is no ground state scattering, it is well known that $\gamma_t=\gamma_l/2+\gamma_{ph}$, where γ_{ph} is the so-called extra dephasing that results from scattering processes that change the phase of the coherence, but do not change the state. Hence, at low temperature or energy, we see that $\gamma_{ph}=0$. However, as the temperature or excitation energy increases, γ_t increases faster than γ_l, suggesting that if the simple relationship holds between γ_t and γ_l, then the exciton is experiencing extra dephasing, i.e., scattering which changes the phase of the exciton, but not the state. It is important to note that this effect has been observed in other samples, though in at least one sample, we found $\gamma_t=\gamma_l/2$, independent of temperature or energy. This result suggests the extra dephasing is due to phonon-defect scattering.

The temperature and energy dependence of the longitudinal relaxation rate are qualitatively explained by recent theoretical work describing scattering of localized excitons. In this model at the lowest temperatures, excitons absorb and emit acoustic phonons and migrate between localization sites by long range dipole-dipole interactions. The phonon assisted migration rate has the form given by $\exp(BT^{\alpha})$. In this expression, B is positive and independent of temperature but is expected to increase with the exciton

energy and depends on the details of interface roughness; α is estimated to be between 1.6 and 1.7. The predicted temperature dependence is quite different from that of variable range hopping used by Mott to interpret electronic conduction in the localized regime[6], and is attributed to the role of the long-range dipole-dipole interaction involved in the migration of the localized exciton and the fact that variable range hopping only accounts for the absorption of phonons. At higher temperatures, thermal activation to delocalized states, varying as $\exp(-E_a/kT)$, is expected to dominate the behavior. The solid curve in Fig. 3a shows the model, where in the lower temperature region the dependence follows the phonon assisted migration model, and for T>10K, the form is Arrhenius where E_a=0.8±0.1 meV. Given that the measurement was made 0.8meV below line center, the value for E_a suggests that the transition region is located at line center, as expected. (Note: In the fitting the data to the model, the form $\exp(BT^{\alpha})$ fits up to 15K while the form $\exp(-E_a/kT)$ fits down to 10K.) Very similar results for γ_l have been obtained in FDFWM[7] where a clear temperature evolution of the quasi-equilibrium exciton distribution was obtained.

The above TFWM measurements were made at 5×10^7excitons/cm^2-layer. At densities above 5×10^9, the decay dynamics observed in the time integrated signal become increasing complex. However, time resolving the coherent emission showed two pulses in the emission, the delayed signal corresponding to the SPE in the above measurements and a prompt signal, the FPD. Figure 4a shows the time resolved emission. The decay rates associated with the FPD are quite different from the SPE emission and are shown in Fig. 4b. The immediate conclusion from this measurement is that the complex decay dynamics observed at higher excitation density is due to the presence of both a homogeneously broadened resonance, giving rise to the FPD signal, and an inhomogeneously broadened resonance, giving rise to the SPE emission. In addition, measurements show that both signals exhibit a similar spectral dependence located near the luminescence peak.

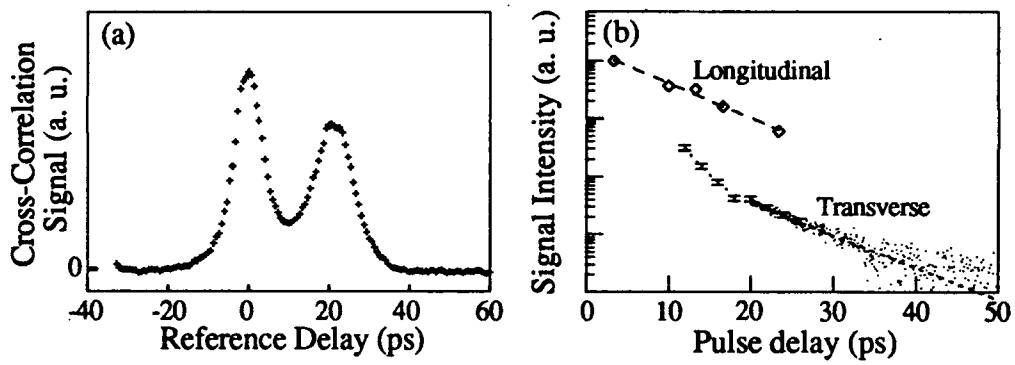


Figure 4. (a) Time resolved emission showing the presence of both a FPD signal (at delay time =0) and a SPE signal (at delay time =20ps). (b). Measurement of γ_l and γ_t for the FPD emission.

This work was supported by the Air Force Office of Scientific Research and the U.S. Army Research Office. MBE samples were provided by P.K. Bhattacharya.

REFERENCES

1. J. Hegarty, L. Goldner, M. D. Sturge, Phys. Rev. **B30**, 7346 (1984).
2. T. Takagahara, J. Lumin. **44**, 347 (1989); Phys. Rev. **B32**, 7013 (1985).
3. J. Hegarty, K. Tai and W.T. Tsang, Phys. Rev. **B38**, 7843 (1988).
4. J.E. Zucker, A. Pinczuk, D.S. Chemla, and A.C. Gossard, Phys. Rev. **B35**, 2892 (1987).
5. L. Schultheis, A. Honold, J. Kuhl, K. Kohler, C.W. Tu, Phys. Rev. **B34**, 9027 (1986).
6. N.F. Mott, and E.A. Davis, *Electronic Processes in Noncrystalline Materials*, 2nd ed.
7. H. Wang, M. Jiang, D.G. Steel, Phys. Rev. Lett. **65**, 12565 (1990).

AD-P007 828

Temporal oscillations of the excitonic absorption in a magnetic field

I. Bar-Joseph and S. Bar-Ad

Department of Physics, Weizmann Institute of Science, Rehovot 76100, Israel

Optical experiments in semiconductor heterostructures have been widely applied during the last few years to investigate the steady state behavior of 2-D systems in magnetic fields.[1] The dynamics of these systems in the very short time scales received only little interest until very recently, when Stark et al have looked at the nonlinear dynamics of magneto-excitons in GaAs/AlGaAs multiple quantum wells (MQW).[2] In this paper we report the observation of a transient oscillatory behavior of the magneto-exciton absorption. We show that these oscillations are *absorption quantum beats*, caused by a coherent superposition between two excited spin polarized excitons. This coherent state persists as long as the excitons exist, for a few 10's of picoseconds! To our knowledge this is the first observation of absorption quantum beats in solids. We show that we can measure by these technique the Lande g factor of the electron and holes in semiconductors.

The experiments were conducted at liquid helium temperature in a split coil 5 Tesla magnet, using a standard pump-probe configuration with a time resolution of $\sim$ 0.5ps. The 4 windows of the cryostat allowed optical access in two orientations of the sample - normal ($B_\perp$) or parallel ($B_{||}$) to the magnetic field. We have studied two GaAs/AlGaAs samples: a MQW sample with a pronounced hh exciton peak at 769 nm, and a short period superlattice (30/30 A) with a weaker exciton peak at 736 nm. The substrate of the samples was removed to allow transmission measurements.

Figure 1 shows the relative change in transmission $\Delta T/T = -\Delta\alpha l$ at B=0 and B=4T, for the MQW sample pumped and probed at the hh exciton, slightly below the absorption peak. The sample was mounted in the $B_\perp$ orientation, almost perpendicular to the light beams. Figure 1a is measured at B=0 with *orthogonal* pump and probe polarizations. The slow decay of the signal is due to the finite life time of the exciton.[3,4] The solid curve in Fig. 1b was taken at B=4T at the same wavelength and pump and probe polarizations. Very deep oscillations are clearly visible, which are being damped

92-22357

with the same decay time as in the B=0 case. Up to 6 oscillations were observed with a period time of 8 ps. The dashed curve in Fig. 1b was measured with *parallel* pump and probe polarizations, also at B=4T. The pronounced oscillatory behavior is still present, but this time in an anti-phase to the oscillations of the orthogonal polarizations case!

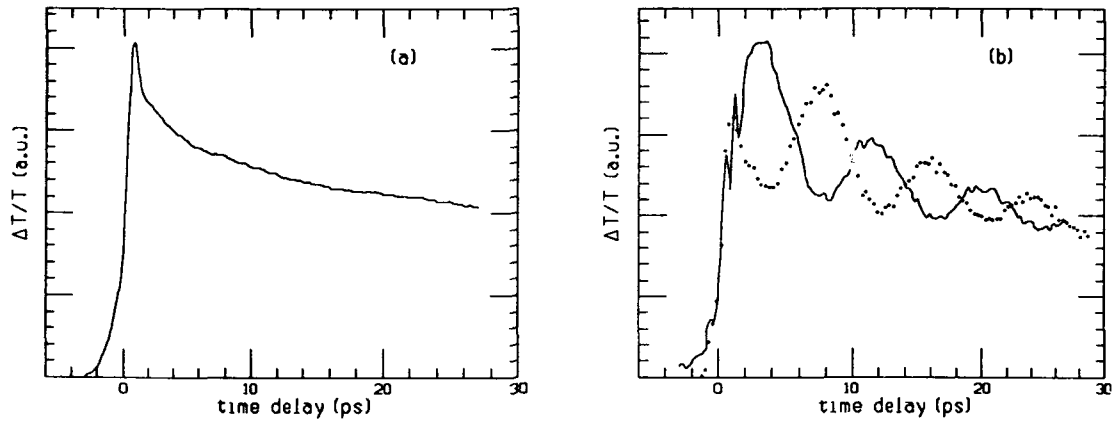


Fig. 1: *Absorption change of the hh exciton for (a) B=0 and (b) B=4T. The solid line curves were measured at orthogonal pump-probe polarizations, and the dotted at parallel polarizations.*

Figure 2 shows the dependence of the oscillations on the magnetic field strength. The two traces were measured at 2T and 4T, at orthogonal polarizations configuration. It can be seen that the oscillation period is inversely proportional to the magnetic field strength.

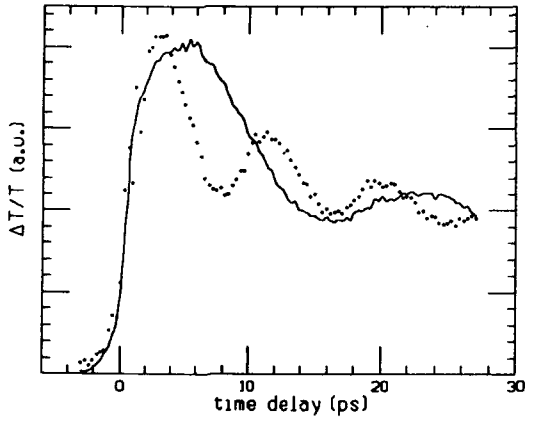
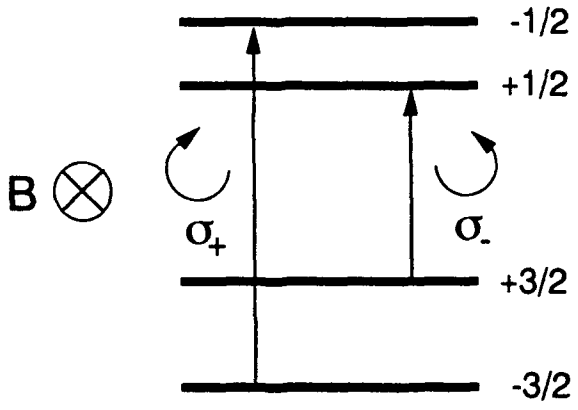


Fig. 2: *Pump-probe signal at 2T (solid) and 4T (dotted).*

The situation is changed dramatically when circular polarizations are used. When-

ever the pump or the probe polarization is circular the oscillations disappear, and we obtain a simple decay as in the B=0 case. In the particular case of counter-rotating circular polarizations the pump-probe signal vanishes almost entirely for very long probe delays, except for some weak signal which we attribute to residual ellipticity in the circular polarizations. It indicates that there is no measurable spin flip for very long times (> 1ns). Finally, we repeated the experiment with the cryostat rotated by 90 degrees, such that the magnetic field was in the plan of the layers and the light beams were normal to them. No oscillations were observed in none of the polarizations. The same general behavior, slightly less pronounced, was observed with the superlattice sample.



To understand the origin of these oscillations we should recall the nature of the transitions involved. Figure 3 shows the electron and hh energy levels in a magnetic field. The degeneracy of the two electron spin states is removed and the separation between them is $2\mu g_e B$, where g_e is the Lande factor for electrons in GaAs.

Fig. 3: *Electron and heavy hole levels in B field*

Note that g_e is believed to be negative, thereby causing the $J = 1/2$ state to be lower in energy.[5] Similarly, the degeneracy of the $J = 3/2$ and $J = -3/2$ hh states is removed, this time with a positive hh Lande factor. The two allowed transitions, $\Delta J = \pm 1$, are marked in the figure, and correspond to *circularly* polarized light in opposite directions. A linearly polarized pump, therefore, excites the two transitions coherently. During the pump pulse duration in the sample the system behaves as a driven oscillator, and the polarizability of the medium consists of two counter-rotating vectors, whose sum is in the direction of the exciting pulse polarization. However, as the pump pulse exits the sample the two polarizability vectors rotate at two different eigenfrequencies, ω_+ and ω_-, and there is a net polarizability in both the x and y directions, which beats at the difference frequency, $(\omega_+ - \omega_-)$. A linearly polarized probe interacts

with this net polarizability and its transmission is modulated by this beat frequency. A circularly polarized pump or probe, on the other hand, interacts only with one of the oscillators and the beating phenomenon disappears. It should be noticed that these quantum beats are different in nature from the ones reported in Ref. (6), where it is a simple interference of two radiating dipoles. In our case the energy dissipation in the sample oscillates at the beating frequency! The mechanism which damps the oscillations is the exciton ionization which destroys the coherence of the prepared state.

Let us finally remark that we can obtain from the measured oscillation period the sum of the Lande g factors of the electron and the hh. Repeating this experiment for the light holes and in bulk material, where other combinations of spin polarized excitons can be excited should enable us to accurately separate the g factors for the electrons and for the heavy and light holes.

References:

1. W. Chen, M. Fritze, A.V. Nurmikko, D. Ackley, C. Colvard, and H. Lee, Phys. Rev. Lett., **64**, 2434 (1990).

2. J.B.Stark, W.H. Knox, D.S. Chemla, XVII Int. Quant. Electron. Conference (IQEC) 1990, paper QTUI4.

3. W.H. Knox, R.L. Fork, M.C. Downer, D.A.B. Miller, D.S. Chemla, C.V. Shank, A.C. Gossard, and W. Wiegmann, Phys. Rev. Lett., **54**, 1306 (1985).

4. M. Wegener, I. Bar-Joseph, G. Sucha, M.N. Islam, N. Sauer, T.Y. Chang and D.S. Chemla, Phys. Rev. **B39**, 12794 (1989).

5. A.M. White, I. Hinchliffe, P.J. Dean, Solid State Commun. **10**, 497 (1972).

6. E.O Gobel, K. Leo, T.C. Damen, J. Shah, S. Schmitt-Rink, W. Schafer, J.F. Muller, and K. Kohler Phys. Rev. Lett., **64**, 1801 (1990).

AD-P007 829

OPTICAL PROPERTIES OF QUANTUM WELLS COMPOSED OF ALL-BINARY InAs/GaAs SHORT-PERIOD SUPERLATTICES

Martin D. Dawson, X.R. Huang, D.S. McCallum, Thomas F. Boggess
Arthur L. Smirl and T.C. Hasenberg[1]

Center for Laser Science and Engineering, University of Iowa,
124 AMRF Oakdale Campus, Iowa City, IA 52242
[1]Hughes Research Laboratories, 3011 Malibu Canyon Road, Malibu, CA 90265

Strained alloy InGaAs/GaAs multiple quantum well structures (MQWs), on GaAs substrates, are being investigated[1] for use in optical modulators, low-threshold diode lasers, photodetectors and other opto-electronic devices operating near 1 μm. Attempts are being made to cover the 0.9-1.1 μm spectral range by varying well-widths and/or alloy mole-fraction and by growing such structures on superlattice or alloy buffer layers[2]. Special problems, however, are posed in growing these strained ternary alloy quantum wells with high quality by epitaxial techniques. Alloy concentration is difficult to reproduce, and alloy-disorder introduces an additional line-broadening contribution and non-uniformity into the materials. The critical thickness parameter[3] places an upper limit on the indium mole-fraction (and thereby the strain) for growth directly on GaAs, restricting the flexibility in varying the well width for increased spectral coverage. Typically[3], this mole-fraction must be less than 0.2, and the lattice-parameter mismatch below 2%, for well-widths ~10 nm.

Here, we focus on structures in which each quantum well consists of an ordered InAs/GaAs short-period superlattice as an attractive alternative to the random InGaAs alloy structures. These all-binary MQWs are highly-strained (7% lattice parameter mismatch) and can accomodate high average indium mole-fraction (30-40%) in wide wells (10-20 nm) without evidence of strain relaxation due to misfit dislocation formation. They are grown directly on GaAs, and are anticipated to be able to cover the 0.95-1.07 μm spectral range for device applications without requiring complex buffer layers. Preliminary evidence indicates that sample reproducibility may be improved in these materials, relative to the alloy, due to the control of composition and layer thickness possible during growth with all-binary constituents. In addition, alloy-disorder scattering, and its associated line-broadening contribution, should be much-reduced or eliminated. In the following, we present data on the optical properties of a variety of InAs/GaAs superlattice quantum well structures of this type, covering the spectral range from 965-1030 nm. Clearly-resolved excitonic absorption peaks have been observed at room temperature in all the structures. In optimized samples at 15 K, photoluminescence and excitonic absorption linewidths are below 10 meV, with the photoluminescence Stokes-shifted by less than 1 meV. We discuss these results and their implications for opto-electronic devices, and also briefly review our recent measurements of the magnitudes of the nonlinear coefficients associated with excitonic absorption bleaching in these structures.

Fig.1 shows the room temperature absorbance of five of the samples, designated 2x5x6, 2x5x8, 2x4x4, 2x4x6 and 2x4x10. This notation denotes the composition of each quantum well in a particular sample: an $(InAs)_2(GaAs)_5$ or $(InAs)_2(GaAs)_4$ superlattice, where the subscripts refer to the thickness in monolayers of each binary constituent. The number of repetitions of the InAs bi-layers in each superlattice of a given structure is given by the third number, which in effect specifies the well width. Thus, in the 2x5x6 case, for example, each well consists of six $(InAs)_2$ layers interleaved with five $(GaAs)_5$ layers. It should be noted in this context that 2 monolayers of InAs is below the critical thickness for growth on GaAs[4]. These superlattice wells are separated from their neighbors by 20-nm-thick GaAs barrier layers, which provide the quantum

92-22358

confinement. Each sample contains fifty equivalent wells. The migration-enhanced epitaxial growth and optimization of these structures, on GaAs substrates, has been described in more detail elsewhere[4].

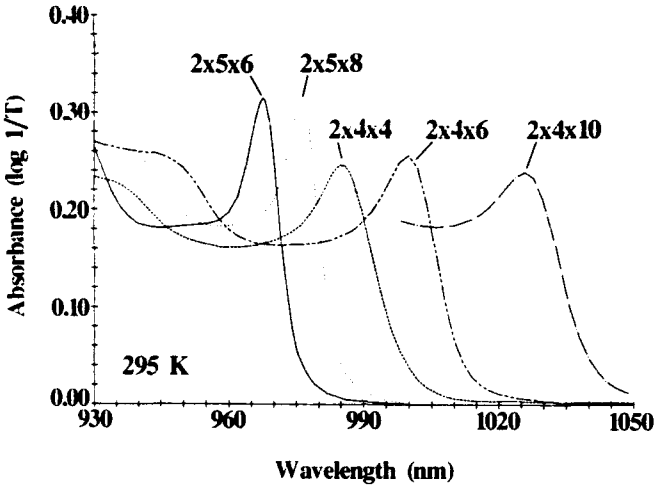


Fig.1 Room temperature absorbance of the InAs/GaAs superlattice MQW samples.

The primary features of note in Fig.1 are the strong, clearly-resolved absorption peaks in the 960-1030 nm range. We associate these peaks with the n=1 heavy-hole (hh) exciton. Note that we are able to vary the spectral position of the peak for a given superlattice composition by adjusting the well width, i.e. the overall length of the superlattice. In going from the 2x5x6 to the 2x5x8 case, for example, the well width varies from 10.7 to 14.8 nm and the peak wavelength shifts from 967 to 976 nm. This is consistent with each of these wells functioning as a 2-d structure. We focus for most of what follows on the $(InAs)_2(GaAs)_5$ structures, for which the growth has been optimized and the majority of the data taken.

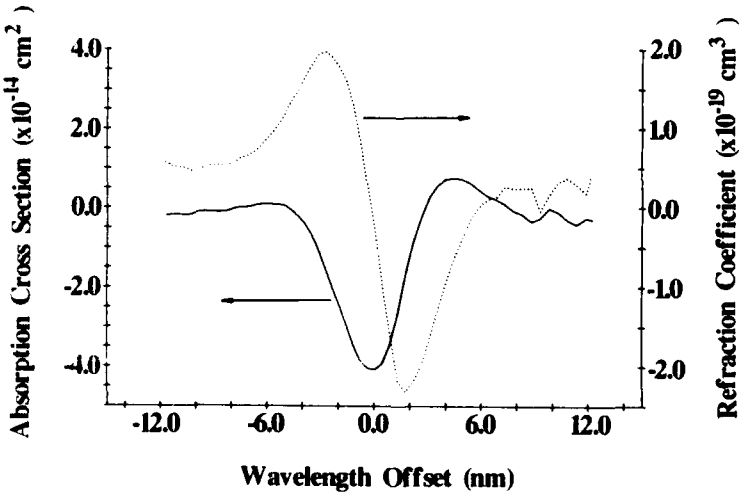


Fig.2 Spectral dependence of nonlinear optical coefficients for 2x5x8 sample.

The room-temperature n=1 hh excitonic linewidth has been determined using the Gaussian lineshape fitting technique of Chemla et al[5]. In the 2x5x6 case, for example, the full-width half maximum (FWHM) linewidth obtained in this manner is 13 meV, which we emphasise is for a fifty period sample, indicating the high-quality of the material. Picosecond pump-probe differential transmission and transient grating techniques have been used to determine the magnitudes of the nonlinear optical coefficients associated with bleaching of this excitonic absorption in the samples. Maximum values for the nonlinear refraction coefficient, n_{eh}, and the absorption cross-section per photo-generated electron-hole pair, σ_{eh}, were 2.5×10^{-19} cm^3 and 4.3×10^{-14} cm^2, respectively. This is illustrated in Fig.2, which shows the spectral dependence of n_{eh} and σ_{eh} as a function of wavelength offset from the excitonic absorption peak for the 2x5x8 sample. The values are comparable to those obtained previously[5] for GaAs/AlGaAs and unstrained InGaAs/InP MQWs, indicating promise for the materials in nonlinear optical switching and modulator applications.

Further evidence of the material quality has been obtained by measurements performed at low temperature. At 15 K the n=1 hh excitonic absorption peaks are much more clearly resolved, and the maximum absorption strength increased, due to elimination of LO-phonon scattering. For the 2x5x6 and 2x5x8 samples, the FWHM absorption linewidths have been determined to be 5.5 and 6.1 meV, respectively, which we again emphasise are for fifty-period structures. These narrow linewidths may give a first indication of reduction of the alloy-disorder line-broadening contribution, although they do not provide conclusive proof of this. They do, however, provide strong evidence of the uniformity, quality and reproducibility of the well material. Additional evidence for reproducibility has been obtained by the close correspondence of spectral features for repeated growth runs of structures of the same type[4]. Efficient photoluminescence, occurring in the vicinity of the n=1 absorption peak and attributed to excitonic recombination, has been observed in all cases. The photoluminescence linewidths (FWHM) vary from ~7.5 to ~8.0 meV in going from the 2x5x6 to 2x5x8 samples, which are, to our knowledge, the narrowest yet reported for the binary superlattice structures.

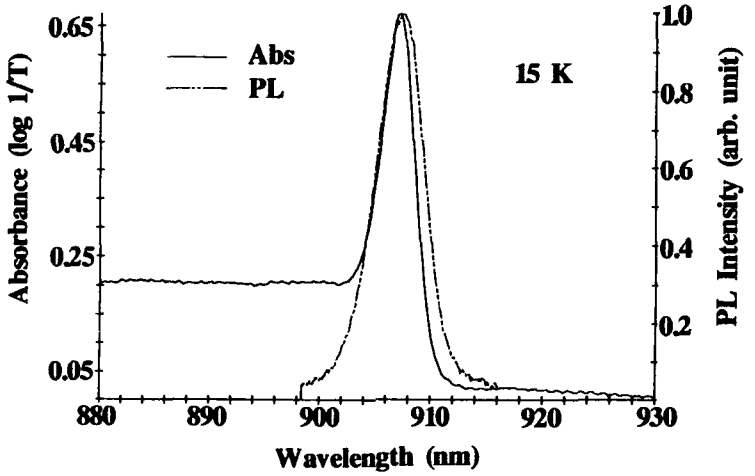


Fig.3 Excitonic absorbance and photoluminescence at 15 K for 2x5x6 sample.

An example of the 15 K absorption and photoluminescence results, taken for the 2x5x6 sample, is shown in Fig. 3. A remarkable feature of the data is the close correspondence between the absorption and photoluminescence peaks (to ~0.5 meV). A similar correspondence was

observed for other samples. Red-shifts of the emission relative to the n=1 hh excitonic absorption of several meV have been common at low temperature for all but the very highest quality MQWs and have been attributed to excitonic localization due to material imperfections within the wells. This shift has been particularly difficult to reduce in the case of ternary alloy wells because of the additional localization mechanism due to alloy disorder. The absence of a significant red-shift in the data is consistent with the elimination of the alloy disorder contribution in all-binary samples and is indicative of high interface quality, although it is possible that the exciton is thermally delocalized at 15 K.

We have also performed time-resolved studies of the photoluminescence. At 15 K, the photoluminescence decays were determined to be near exponential, consistent with monomolecular exciton-dominated recombination, with time-constants of 1800 and 1650 ps for the 2x5x6 and 2x5x8 samples, respectively. These long lifetimes provide further evidence of the high material quality.

In addition to varying the well-width, extension of the spectral coverage using structures of this type can be obtained by varying the thickness of the GaAs spacer layers in the superlattice. Referring again to Fig.1, for example, we see room temperature absorbance data for our first attempt at growth of 50-period 2x4x4, 2x4x6 and 2x4x10 samples. Although the growth is not yet optimized, the excitonic absorption features are strong and clearly-resolved, and cover the range 980 to 1030 nm. It should be noted that the average indium mole-fraction in these structures is nearly **40%**, much higher than that which can be achieved with quality InGaAs alloy wells of the same overall thickness, grown directly on GaAs. We believe that this may be due to the GaAs layers in the superlattice acting as stress-relief layers; as long as the InAs layers themselves are below the critical thickness, the GaAs layers provide a measure of isolation between adjacent strained layers. Thus it is not appropriate to simply consider the overall energy stored in each well, compared to that required for misfit dislocation formation, in determining limiting indium mole-fraction for a given well width, as it is in the case of a uniformly-strained alloy well.

In conclusion, we have measured the optical properties of a variety of structures containing quantum wells composed of all-binary InAs/GaAs short-period superlattices. These measurements have indicated the high quality of the material and provide preliminary evidence for some of the distinct properties expected for these structures, including reproducibility and narrow optical linewidths, indicating that they hold promise for opto-electronic device applications. When all combinations of well-width and GaAs spacer-layer thickness have been examined (including, for example $(InAs)_2(GaAs)_3$ superlattices) we anticipate full spectral coverage of at least the 950 to 1070 nm range in discrete intervals of ~5 nm, grown directly on GaAs substrates. These materials should be useful as active layers in strained-layer lasers, detectors and nonlinear optical switching and modulating devices for this wavelength range.

The work at the University of Iowa was supported by the U.S. Office of Naval Research.

[1] E.P. O'Reilly, Semicond. Sci. Technol. **4**, 121 (1989).
[2] T.K. Woodward, T.Sizer II, D.L. Sivco, and A.Y. Cho, Appl. Phys. Lett. **57**, 548 (1990).
[3] S.L. Weng, J. Appl. Phys. **66**, 2217 (1989).
[4] T.C. Hasenberg, D.S. McCallum, X.R. Huang, A.L. Smirl, M.D. Dawson, and T.F. Boggess, J. Cryst. Growth (accepted for publication).
[5] S. Schmitt-Rink, D.S. Chemla, and D.A.B. Miller, Adv. in Phys. **38**, 89 (1989).

AD-P007 830

92-22359

Room Temperature Excitons in II-VI CdZnTe/ZnTe Multiple Quantum Wells

D. Lee, A.M. Johnson, J.E. Zucker, R.D. Feldman, and R. F. Austin

AT&T Bell Laboratories, HO 4D-321, Holmdel, NJ 07733

Recent room temperature observations of lasing[1,2], excitonic absorption peaks[3,4], and blue LEDs[5,6] in wide-gap II-VI semi conductor multiple quantum wells (MQWs) provide great promise for unique device applications. A good understanding of the physical mechanisms necessary to account for these recent observations could be extremely important for future device applications.

The present CdZnTe/ZnTe system has intriguing properties -- alloy quantum wells and strained layers. Nevertheless, excellent sample quality is indicated by a very small Stokes shifts of the photoluminescence (PL) with respect to the PL excitation spectrum (PLE) and narrow absorption linewidths. Furthermore, well-defined room temperature absoption peaks are observed for a wide range of Cd concentrations and well-widths. This offers large flexibility in the choice and composition of materials for better bandgap engineering.

The $Cd_xZn_{1-x}Te$/ZnTe MQWs were grown by molecular beam epitaxy on GaAs substrates. A $Cd_yZn_{1-y}Te$ alloy buffer layer was grown to reduce the strain in the QW and enhance the critical thickness of the total MQW stack. Samples grown in this fashion give very bright PL and very small Stokes shift between PL and PLE peaks (~ 1meV for sample A with x=0.33,Lw=67A and ~ 0.5meV for sample C with x=0.10,Lw=40A) at 6K as shown in figure 1. Raman scattering experiments also confirm the coherent growth of these structures.

The low temperature absorption linewidth reflects the degree of inhomogeneous broadening. The linewidths shown in Fig. 2a) and c) are close to and smaller than the estimated inhomogeneous contribution from both alloy fluctuations and monolayer well-width fluctuations. The large absorption coefficient, especially for sample C, is notable, reaching $\alpha(\text{wells})=3.3\times10^5\text{cm}^{-1}$ at 6K. This value is much larger than that of GaAs MQWs, reflecting the inherently stronger oscillator strength of wide-gap II-VI semiconductors.

Figure 2b) and d) show well-defined room temperature excitonic absorption peaks. At this temperature the dominant line broadening mechanism is the thermal broadening due to exciton-LO phonon scattering, which is particularly strong in wide gap II-VI semiconductors. Figure 3 shows the temperature dependence of absorption linewidth (HWHM) for three samples with different Cd concentrations (x=0.33,0.25,0.10). A fit yields homogeneous broadening coefficients Γ_{LO}'s[7] from 11.5 meV for x=0.33 to 16 meV for x=0.10. The important resultant trend, smaller Γ_{LO} with higher alloy content in

the QW, enables us to observe sharper room temperature excitonic peaks in the samples with higher alloy concentration even though the low-temperature absorption linewidths are broader.

We have also measured optical saturation intensities at the excitonic absorption peaks for samples with x=0.25,Lw=50A and 100A. The absorption coefficient and the fitted line for Lw=100A is shown in Figure 4. The measured saturation intensities were 15 kW/cm^2 for the 100A well and $32kW/cm^2$ for the 50A well samples. This saturation intensity is more than one order of magnitude higher than those for III-V MQWs[7]. This high saturation intensity is mostly due to the smaller Bohr radius a_χ of a wide gap II-VI semiconductor (a_χ ~ 60A in bulk ZnTe, ~ 160A for bulk GaAs). A high saturation intensity coupled with a well-defined absorption peak is favorable for high power room temperature operation of electro- absorptive modulators and SEEDs.

References

[1] A.M. Glass, K. Tai, R.B. Bylsma, R.D. Feldman, D.H. Olson, and R.F. Austin, Appl. Phys. Lett. 53, 834 (1988)

[2] J. Ding, H. Jeon, A.V. Nurmikko, H. Luo, N. Samarth, and J.K. Furdyna, Appl. Phys. Lett. December (1990)

[3] D. Lee, J.E. Zucker, A.M. Johnson, R.D. Feldman, and R.F. Austin, Appl. Phys. Lett. 57, 1132 (1990); D. Lee, A.M. Johnson, J.E. Zucker, R.D. Feldman, and R.F. Austin, IQEC' 1990 post deadline paper QPDP-18 (1990)

[4] J. Ding, N. Pelekanos, A.V. Nurmikko, H. Luo, N. Samarth, and J.K. Furdyna, Appl. Phys. Lett. December (1990)

[5] M. A. Haase, H. Cheng, J. M. Depuydt, and J. E. Potts, J. Appl. Phys. 67, 448 (1990)

[6] J. Ren, K. A. Bowers, B. Sneed, D. L. Dreifus, J. W. Cook,Jr., J. F. Schetzina, and R. M. Kolbas, Appl. Phys. Lett. 57, 1901 (1990)

[7] D.S. Chemla, D.A.B. Miller, P.W. Smith, A.C. Gossard, and W. Wiegmann, IEEE, J.Quan. Elect. QE-20, 265 (1984)

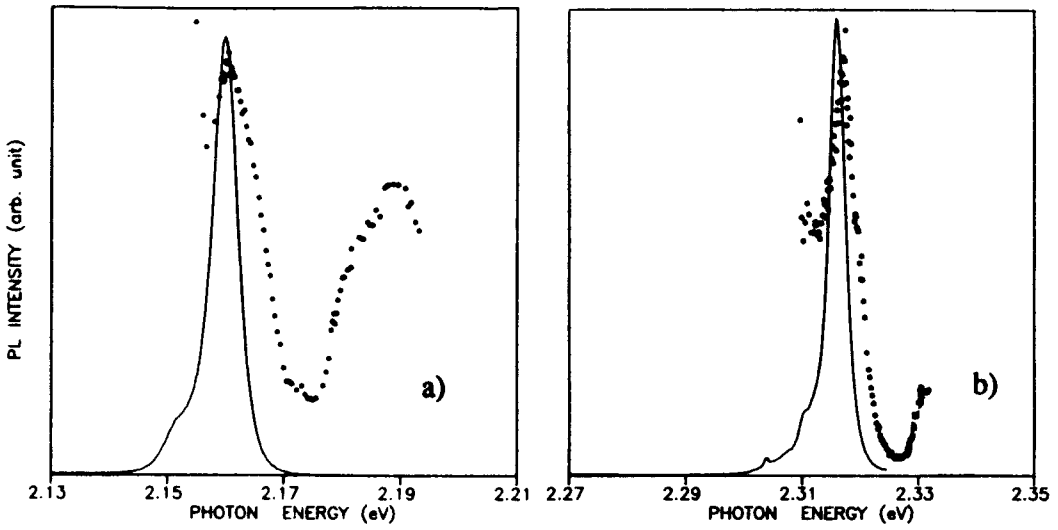


Fig. 1 PL and PLE spectra at 6K for a) sample A (x=0.33,Lw= 67A) b) sample C (x=0.10,Lw=40A). Solid curves are for PL and filled circles are for PLE

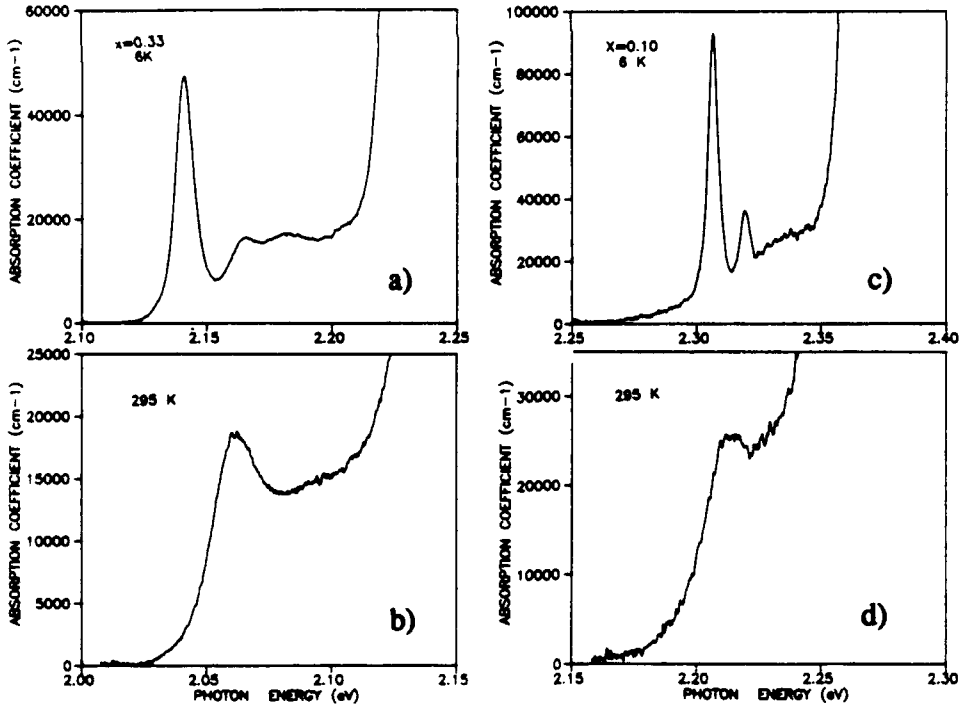


Fig. 2 Absorption spectrum of sample A (C) showing well-resolved n=1 hh excitonic feature at a)(c) 6K and b)(d) 295K. Absorption coefficients refer to the total thickness of CdZnTe wells plus ZnTe barriers.

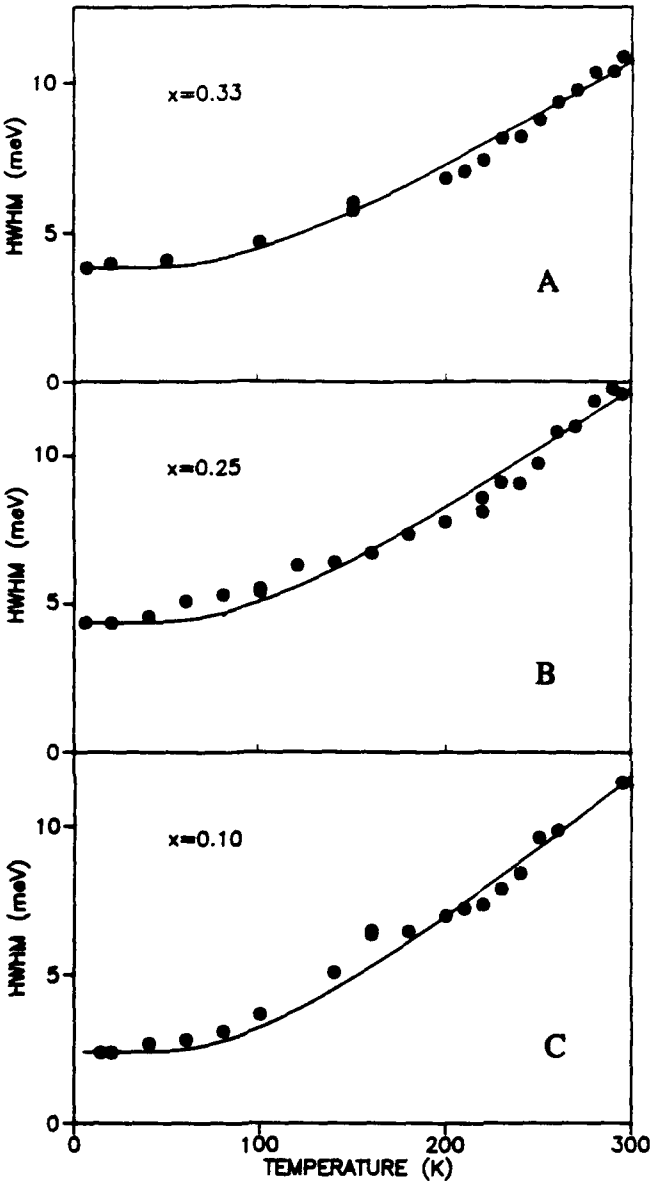


Fig. 3 Ground state absorption linewidth (HWHM) as a function of temperature for samples A, B (x=0.25, Lw=50A), C. The points are measured and the solid lines are fits : $\Gamma(T)=\Gamma_{6K}+\Gamma_{LO}(e^{\hbar\omega_{LO}/kT}-1)^{-1}$

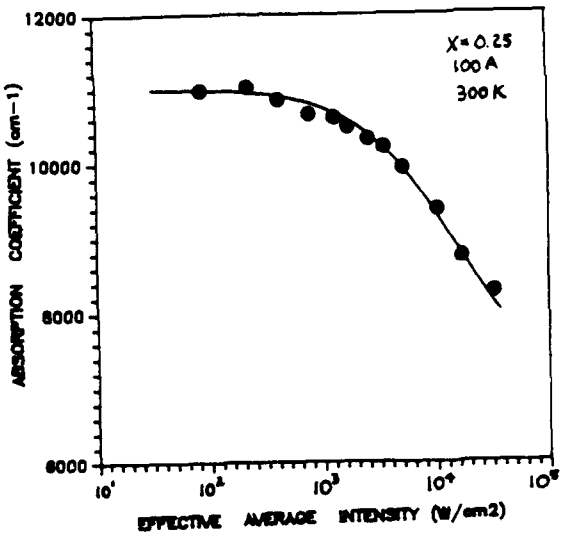


Fig. 4. Room temperature absorption coefficient as a function of optical intensity for sample with x=0.25, Lw=100A. Filled circles are experimental data. Solid line is a fit with excitonic saturation intensity I_{SAT}=15kW/cm^2 : $\alpha(I)=\alpha_0+\alpha_1/(1+I/I_{SAT})$

Modulators: II

MD 4:00pm–5:30pm
Salon F

Larry Coldren, *Presider*
University of California, Santa Barbara



Low Driving Voltage and Low Chirp InGaAs/InAlAs MQW Electro-absorption Modulator

Hirohisa Sano, Hiroaki Inoue, Shigehisa Tanaka, Shoichi Hanatani and Koji Ishida

Central Research Laboratory
Hitachi Ltd.
Kokubunji Tokyo 185 Japan

AD-P007 831

With the progress of the ultra high-bit rate optical transmission system, there has been much interest in the InGaAs/InAlAs MQW electro-absorption (EA) modulators because of their wide bandwidth[1] and high modulation efficiency around 1.55μm wavelength[2]. However, the modulator should be not only high-speed and low-driving voltage but low loss and low chirp for the practical use.[3]

In this paper, we analyze the absorption layer thickness dependence of the modulation characteristics for the InGaAs/InAlAs MQW EA modulators. From the analysis, the new device structure and experimental results of low driving voltage and low chirp MQW EA modulator for 10Gb/s transmission are demonstrated.

The modulation characteristics of MQW EA modulators has a strong dependence on the MQW absorption layer thickness. The thinner the layer thickness, the stronger the electric field but the smaller the Γ factor (optical confinement factor). This may give us an optimum layer thickness for low driving voltage and low loss characteristics. The Γ factor of the thin layer enables to operate the modulator near the exciton absorption wavelength. Around the absorption peak, the phase modulation characteristics becomes smaller and/or changes its sign due to the anomalous dispersion. Therefore, low chirp modulation characteristics would be attained with low driving voltage operation. In order to evaluate these quantities experimentally, we prepared several modulators having different thicknesses of the InGaAs/InAlAs MQW absorption layer. Figure 1 shows the schematic view of the modulator. The MQW consists of the 70Å InGaAs wells separated by 70Å InAlAs barriers to match the 1.55μm wavelength operation. The MQW is sandwiched by the p and n doped InAlAs cladding layers so that an electric field can be applied only to the MQW layer by reverse bias. The 3~4μm width and 2.3μm height ridge waveguides were processed by the RIBE, and embedded by thick PIQ passivation to reduce the bonding pad capacitances for high speed operation. The waveguides were cleaved into 200μm length, and both facets were AR coated.

92-22360

Figure 2 shows the driving voltage giving 15dB extinction ratio as a function of the MQW absorption layer thickness, the additional phase shift accompanied by EA modulation is also shown by the dashed line. The upper horizontal axis denotes the Γ factor in the MQW absorption layer calculated by the BPM analysis[4]. A wavelength tunable LD(1.50~1.60μm) was used for the input light source with TE polarization. The incident light was coupled to the

modulator with a 12μm radius tapered fiber and the output light was monitored by the power meter with a coupling lense. The phase shift with 15dB extinction was measured with Mach-Zehnder interferometer technique. Each sample has a different value of the Γ factor according to the absorption layer thickness. Therefore, in order to maintain the total internal absorption loss constant, the incident light wavelength for each sample was tuned to the wavelength where the additional loss compared to the 1.60μm wavelength (where the MQW has negligible absorption loss) became 1dB at 0V bias.

Experimental results in Fig.2 show both the driving voltage and the phase shift decrease as the absorption layer thickness. However, further reducing the absorption layer thickness deteriorates guiding property and may cause waveguide cut-off. Therefore, we introduced the new waveguide structure into the MQW EA modulator. The schematic cross-section of the device is shown in Fig.3. The waveguide layers consisted of short period MQWs (p- and n-doped) were inserted to both sides of the undoped MQW absorption layer to assist the light propagation. The 35Å/35Å InGaAs/InAlAs short period MQW layers, whose absorption wavelength is 1.30μm , were designed to show the negligible absorption coefficient at 1.55μm wavelength and the same refractive index with that of the MQW absorption layer.

The thicknesses of absorption layer and p- and n- doped waveguide layers were 0.07μm, 0.06μm and 0.06μm respectively. The device length were designed to 150μm to reduce the junction capacitance. The total device capacitance was 0.5pF. The bandwidth calculated from CR time constant was 12GHz, which was enough for 10Gb/s transmission. The Γ factor of the MQW absorption layer was estimated to be 6~7% by the numerical calculation. The modulation characteristics of the device for various incident wavelengthes is shown in Fig.4. The driving voltage at 1.54μm is 1.5V. The maximum extinction ratio is 20~25dB, which restricted by the maximum absorption coefficient of exciton absorption.

The additional phase shift accompanied by EA modulation at 1.54μm wavelength is shown in Fig.5. The phase shift was measured with Fabry-Perot technique using the device without AR coating. As shown in the figure, phase shift efficiency decreases with applied voltage due to the anomalous dispersion and QCSE as we expected. Since the EA modulation efficiency increase exponentially with applied voltage, α-parameter, ratio of efficiency of phase and intensity modulation, varies and decreases with applied voltage. Applying voltage of 1.5V accompanies 0.45π of the total phase shift, corresponding to 0.8 of α-parameter. However, the α-parameter can be reduced further by introducing the DC bias, for example applying 0.5V of DC bias reduces the total phase shift to 0.30π, corresponding to 0.5 of α-parameter only with 2dB of absorption loss increase. The measured 3-dB bandwidth was 9GHz which was smaller than the calculated value from CR time constant. This degradation is due to the series resistance enhanced by the decrease of device size.

The driving voltage and the additional phase shift of this improved modulator were also plotted in Fig.2. These data coincide with the lines obtained by the conventional modulators.

So that one may expect that the further reducing the absorption layer thickness improves these quantities. However, the increased device capacitance and the decreased Γ factor deteriorates high speed response and the maximum extinction ratio. We believe that, though the obtained 0.5 of α-parameter is lowest so far, an optimization of the device structural parameters is still possible to achieve lower chirp performance of the InGaAs/InAlAs MQW EA modulator.

We revealed that the thin absorption layer of the InGaAs/InAlAs MQW EA modulator improved driving voltage and chirping characteristics. The new structure which assist the light propagation in spite of extremely thin absorption layer was proposed. The fabricated modulator showed the 1.5V of driving voltage and 0.5-0.8 of α-parameter under 15dB extinction ratio and 9GHz bandwidth.

References

1) K.Wakita, I.Kotaka, O.Mitomi, Y.Kawamura and O.Mikami, IOOC'89, paper 19C2-2, Kobe Japan (1989)
2) H.Sano, J.Glinski, H.Inoue, H.Nakamura, Y.Sasaki and K.Ishida, ibid. paper 20B1-17
3) F.Koyama and K.Iga, J. Lightwave Technol. LT-6, pp 87-93 (1988)
4) D.Yevick and G.Hermansson, Electron.Lett., 63, pp 479-483 (1985)

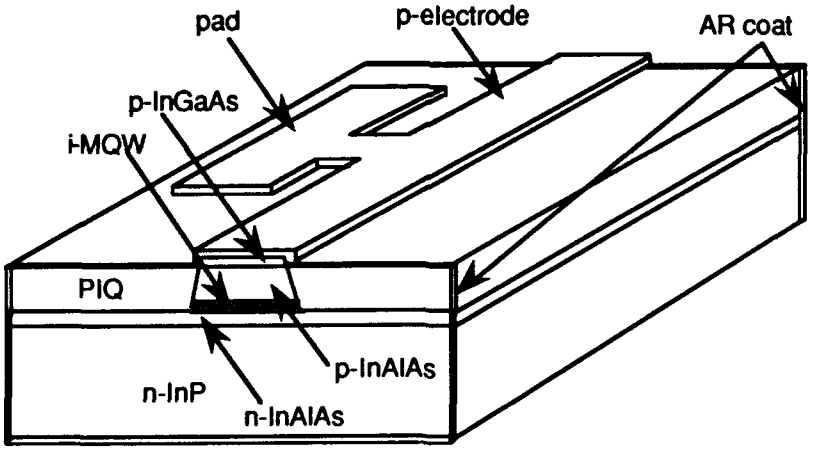


Fig.1 Schematic view of the InGaAs/InAlAs MQW EA modulator.

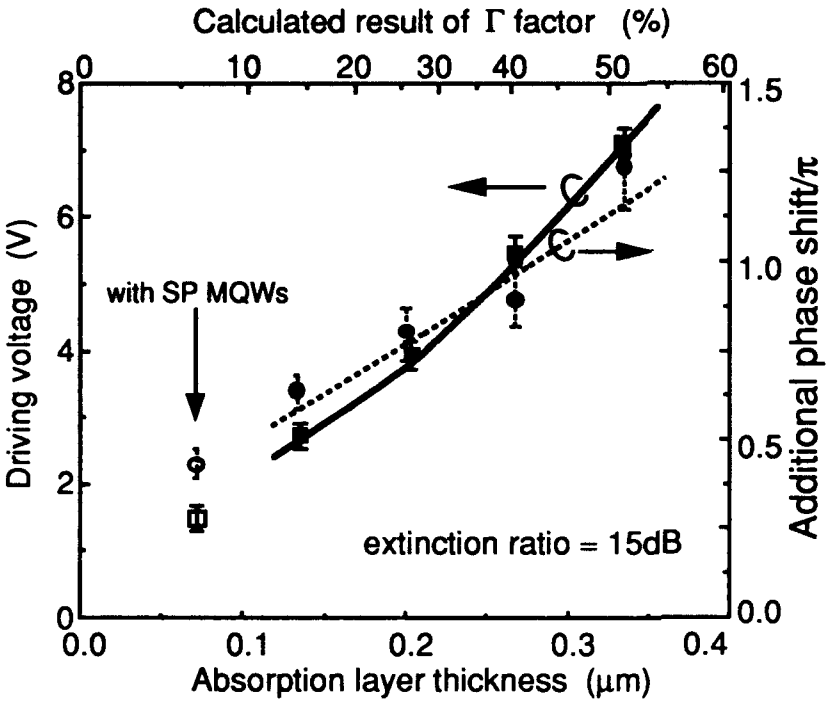


Fig.2 The driving voltage and the additional phase shift as a function of absorption layer thickness.
SP MQWs denote the short period MQWs.

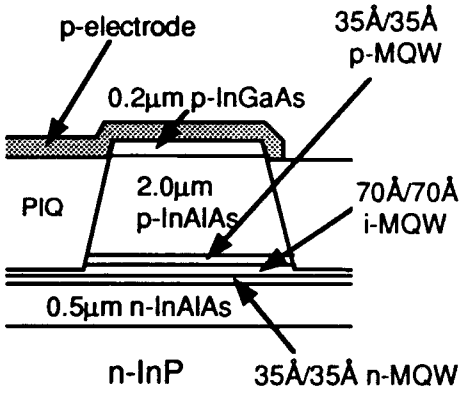


Fig.3 The cross section of the modulator with SP MQWs.

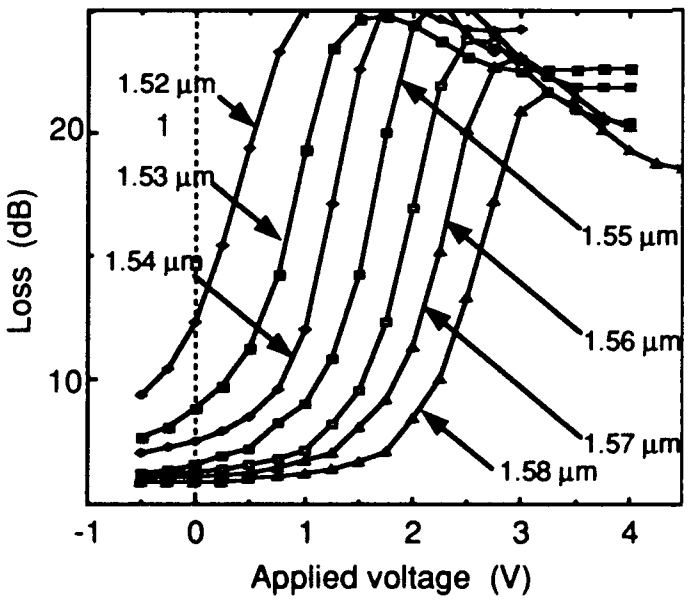


Fig.4 The modulation characteristics for several wavelengthes.

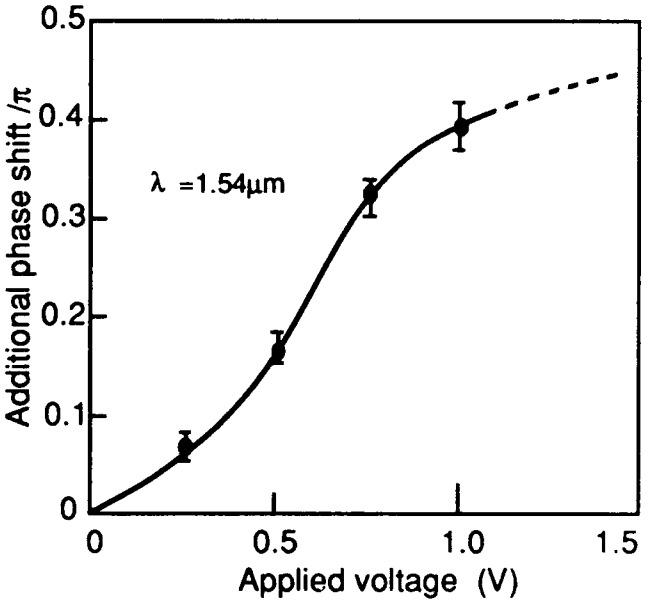


Fig.5 Phase modulation characteristics of the modulator.

A New Optical Waveguide Switch/Modulator using the Heterostructure Field Effect Transistor.

T. Vang, G.W. Taylor, S. Sargood, P. Cooke, P. Claisse
AT&T Bell Laboratories
Room 4F-432
Crawfords Corner Road
Holmdel, NJ 07733

AD-P007 832



An optical waveguide switch/modulator is an important element for photonic switching systems. It is very important for these devices to be compatible with other electronic and optical components. In particular, it is desirable to have them monolithically integrated with lasers, transistors, and detectors. Implementation of a modulator is typically done using the Quantum Confined Stark Effect(QCSE) in a reverse biased PIN structure or using free carrier effects, both electrons and holes, in a forward biased PN structure. It has also been demonstrated that control of only electrons in a single quantum well via a gate electrode in an FET configuration can dramatically affect the optical absorption[1]. A detailed analysis of the physical mechanisms controlling the changes in absorption due to the channel charge has also been given[2]. Modulators using gate control of a channel charge benefit from both the high contrast available due to free carriers as well as high speed due to FET action. Recently the Heterostructure Field Effect Transistor (HFET) was reported[3] as an ideal transistor for optoelectronic integration because of its unique waveguiding properties. We report here the operation of the HFET as an optical absorption modulator using its waveguiding capability.

The HFET structure was grown by MBE using a single quantum well separate confinement heterostructure, where the GaAs well acts as the channel for the transistor. An 80Å n-doped (5E18 cm-3) charge sheet is located at the heterointerface. A schematic of the HFET modulator is shown in Figure 1, along with the testing arrangement in Figure 2. Light was coupled into a cleaved 300μm long HFET with a 5μm wide rib which acts as the gate contact. Transmission spectra were taken for the two charge states of the device as shown in Figure 3. Below threshold (Vg=-1.50V) the channel is empty of charge and the quantum well absorption is maximum. Above threshold (Vg=+1.0V) the channel is full of charge (1.2E12 cm-2) and the quantum well absorption is greatly reduced via the 2-D Moss-Burstein effect.

92-22361



A blue shift of 20meV is observed at the fundamental absorption edge and an increase in transmission by a factor of 9.4 is observed for a voltage change of 2.5V. Figure 4 shows the transmission of the modulator (10x300μm), and the corresponding transconductance and gate leakage (8μm gate length HFET) as a function of gate voltage. The transmission of the modulator closely follows the transconductance of the device showing that the charge introduced into the channel dramatically increases the transmission. The gate leakage is less than 10μA for both measured gate voltages. The differential transmission peak occurs approximately 15meV below the lasing energy of the device when operated as a laser[3]. Therefore this device is suitable to operate as an absorption modulator or as an electrorefractive optical switch when coupled with a laser in an integrated technology. The 4μm gate length HFET had a threshold of 0.1V and a g_m of 33mS/mm. The corresponding BICFET[4] (single source) had a current gain of 33. The speed of the modulator will be determined by the HFET which is expected to be the same as the HEMT (15GHz for a 1μm gate length in GaAs/AlGaAs). The compatibility of the modulator, HFET, BICFET, and laser indicates the feasibility of an integrated opto-electronic technology.

REFERENCES

[1] D. S. Chemla, I. Bar-Joseph, C. Klingshirn, D. A. B. Miller, J. M. Kuo, Applied Physics Letters 50(10) p585, 1987.

[2] D. S. Chemla, I. Bar-Joseph, J. M. Kuo, T. Y. Chang, C. Klingshirn, Gabriela Livescu, D. A. B. Miller, IEEE Journal of Quantum Electronics, vol 24, no 8 p 1664, 1988.

[3] G. W. Taylor, P. A. Kiely, IEEE Transactions on Electron Devices, to be published.

[4] P. R. Claisse, G. W. Taylor, P. Cooke, D. P. Docter, LEOS Annual Meeting 1990, paper SDL8.7

[5] G. W. Taylor, P. A. Kiely, A. Izabelle, D. L. Crawford, M. S. Lebby, T. Y. Chang, B. Tell, K. Brown-Goebler, J. G. Simmons, IEEE Electron Device Letters, vol. 10, No. 2, p. 2652, 1989.

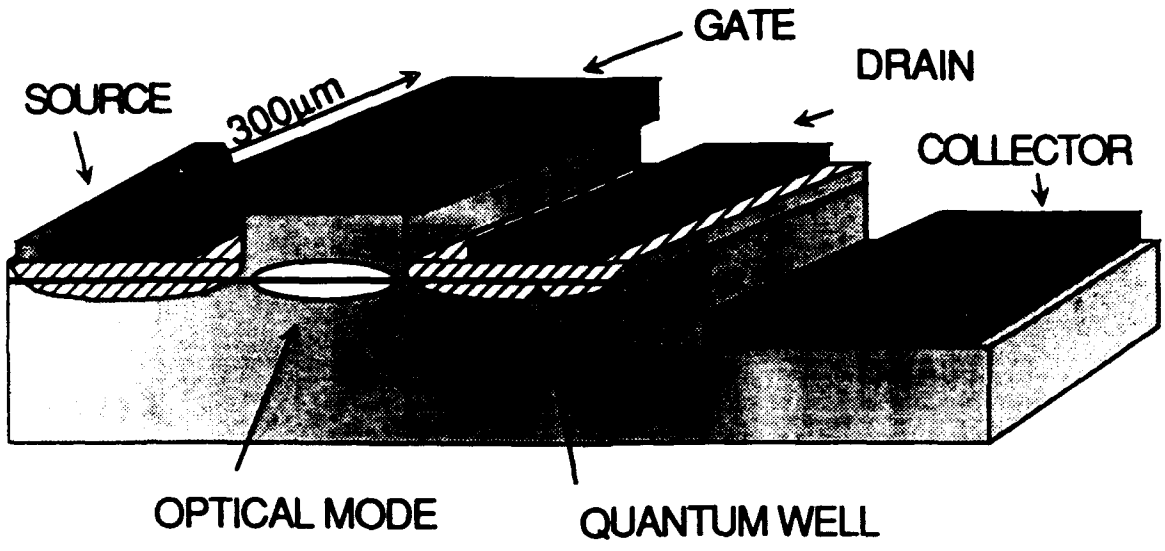


Figure 1 Schematic of the HFET optical modulator.

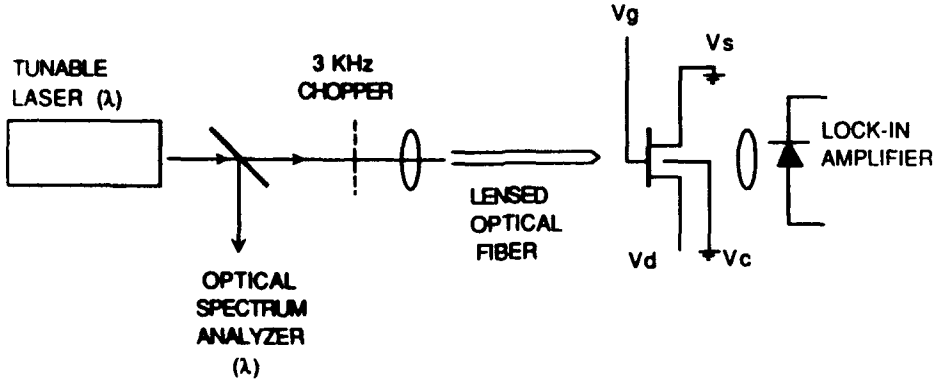


Figure 2 Transmission testing arrangement.

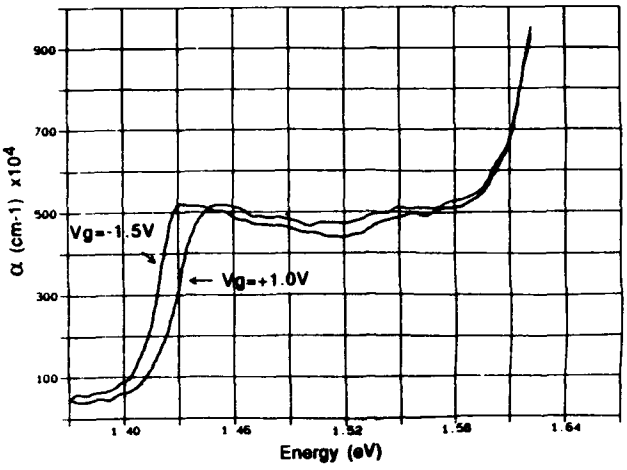


Figure 3 Absorption spectra for the two charge states of the device.

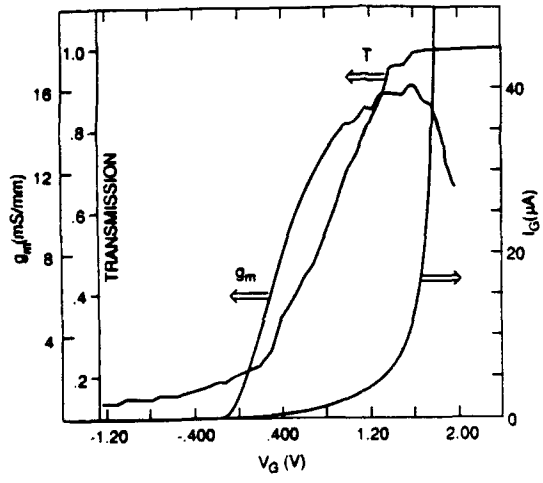
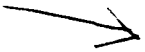


Figure 4 Transmission, transconductance, and gate leakage as a function of gate voltage.

AD-P007 833



Multiple Quantum Well Optical Modulators for Solid State Lasers

T. K. Woodward[1], Theodore Sizer, II.[1], T. H. Chiu[1], D. L. Sivco[2], A. Y. Cho[2]
[1] AT&T Bell Laboratories, Holmdel NJ 07733
[2] AT&T Bell Laboratories, Murray Hill, NJ 07974

Realization of multiple quantum well (MQW) optical modulators that operate at wavelengths in the 1 μm range is desirable, because of the ready availability of high-power, reliable solid state lasers at these wavelengths.[1] Recent advances in diode pumping of solid state laser media such as Neodymium doped Yttrium Aluminum Garnet (Nd:YAG) and Yttrium Lithium Fluoride (Nd:YLF) has made them efficient and reliable sources of coherent radiation. Such devices might find application in potential optical computing and communication architectures. Production of MQW materials with bandgaps in the 1 μm range is complicated by a lack of lattice-matched substrates and a lattice mismatch between potential quantum barrier and well materials. We describe recent efforts we have made to realize MQW modulators that operate in the 1 μm range and summarize some of our results.

We consider both GaAs and InP-based materials. MQW modulators require about 1 μm of absorbing material for useful normal incidence absorption modulation. This is in excess of most critical thickness estimates, requiring strain relaxation issues to be addressed.[2] Consider for example the most attractive GaAs-based materials system for 1 μm range MQW applications, $In_xGa_{1-x}As$ / $Al_xGa_{1-x}As$.[1,3,4,5] $In_{0.25}Ga_{0.75}As$, near the appropriate composition for 1 μm modulators, has about a 1.8 percent lattice mismatch to GaAs. Since there are no compound semiconductors with bandgaps smaller than GaAs that also possess a lattice constant smaller than GaAs, lattice mismatch of this sort must always be considered. Nevertheless, working MQW modulators can be realized.

The primary advantages of InP-based materials are a decreased lattice mismatch to InP substrates and a wider range of available materials as compared to GaAs-based MQW systems. Indeed, there are a number of InP-lattice matched quarternary materials that can be engineered to the 1.06 micron wavelength range.[6] However, quarternary materials can be difficult to grow and possess a high level of alloy disorder in the quantum well material. Thus, strained ternary InP-based compounds may also be reasonable alternatives for 1 μm modulators. Thus, we have initially considered $InAs_yP_{1-y}$, a special case of the quarternary $In_xGa_{1-x}As_yP_{1-y}$. $InAs_yP_{1-y}$ possesses both a smaller lattice mismatch to InP and a lower level of alloy disorder as compared to $In_xGa_{1-x}As$ / GaAs. Neglecting quantum size effects and strain, the appropriate composition for a bandgap of 1.165 eV(1.065 μm) is $y \simeq 0.15$. The lattice mismatch to InP at this composition is about 0.5 percent. Strain and quantum size effects can both be expected to increase this As mole fraction. [1,3] $InAs_yP_{1-y}$, which has not been widely investigated with modern crystal growth techniques, has the additional interesting property of being one of relatively few III-V ternary materials produced by mixing the group V element.

92-22362



$In_xGa_{1-x}As$ / GaAs materials were produced by solid source molecular beam epitaxy (MBE), whereas $InAs_yP_{1-y}$ materials were grown by chemical beam epitaxy (CBE). In all cases, conventional photolithographic techniques were used to produce mesa devices that have good electrical properties.

The major finding of our $In_xGa_{1-x}As$ / GaAs sample studies is that sharp exciton features and pronouced quantum confined stark effect (QCSE) can be obtained at 1.06 μm wavelengths, even at high strain levels.[7] Additionally, we have found that the buffer layer plays a role in determining the quality of the resulting film. We have grown a number of samples, both directly on GaAs, as well as on strain relief buffer layers having lattice constants intermediate between GaAs and the $In_xGa_{1-x}As$ well material. We observe that the bandgap of the MQW overlayer depends on whether the sample is grown directly on GaAs or on the strain relief buffer layer. We note that samples demonstrate a trend toward improved performance when grown on strain relief buffer layers. We represent our results with Fig. 1, which illustrates data from one of the samples studied. Absorption data are shown in Fig. 1(a), scaled to the total thickness of the undoped layer (1.5 μm), for various reverse biases. In Fig. 1(b), we present $\Delta T/T$ $(T(V) - T(0)/T(0))$ data for various modulation voltages. Transmission contrast ratio at the exciton peak is 1.6. It should be emphasized that these data are obtained in a single pass transmission geometry, the GaAs substrate being transparent at the wavelengths of interest. Thus, contrast levels may be doubled by operating in a reflective geometry, and might be increased further with various resonator concepts.[8,9] Symmetric self electro-optic effect devices (SEEDs) of various types can be realized in this sample with Nd:YAG and Nd:YLF lasers as their power source.

In Fig. 1(a), we present 300 K absorption spectra for a representative $InAs_yP_{1-y}$ / InP sample, obtained at various reverse biases. Normalization is to the total thickness of the MQW material, 1 μm in this case. A well developed exciton feature is present, which also shifts to longer wavelength with voltage. However, a rapid broadening of the exciton is also evidenced. This broadening has also been observed to a lesser degree in the $In_xGa_{1-x}As$ samples, and can be explained by field ionization effects. This effect is quite pronounced and is manifest by the rapid broadening of the exciton with field such that there is virtually no evidence of it at 10 V (1×10^5 V/cm). Ionization is facilitated by the small difference in bandgap between the quantum well and the InP barrier regions. The total band gap difference is only 170 meV, which is divided between the conduction and valence band. In Fig. 1(b) $\Delta T/T$ spectra are presented. The contrast ratio is roughly 1.4 at the exciton peak and is obtained with only 50 periods, in comparison to the 1.6 obtained in $In_xGa_{1-x}As$ with 100 periods. Note further that maximum contrast is obtained with relatively low voltage, due to the rapid ionization of the exciton. Again, Nd:YAG and Nd:YLF driven SEED devices can be realized with this sample.

In Fig. 3, were present a comparison of the zero bias absorption spectra of the previously illustrated $InAs_yP_{1-y}$ sample with that of an $In_xGa_{1-x}As$ /GaAs MQW modulator (Sample

B of Ref [1]) also having 50 periods of 100 Å barriers and 100 Å QWs. Since the two samples have nominally the same barrier and well thicknesses and the same number of periods, the relative scaling of the two samples is not dependent on the normalization, which in this case is to the total thickness of absorbing material (5000 Å in both cases). Note the more sharply defined exciton in the $InAs_yP_{1-y}$ sample as compared to the $In_xGa_{1-x}As$. Note further that the absolute absorption strength of the $InAs_yP_{1-y}$ is 25 percent larger than that of the $In_xGa_{1-x}As$. These two factors may make $InAs_yP_{1-y}$ preferable to $In_xGa_{1-x}As$ for 1 μm MQW modulator operation.

We believe that the increased exciton peak sharpness derives mainly from the decreased lattice mismatch in the $InAs_yP_{1-y}$ / InP system. Nonuniform strain accomodation across the surface of the modulator can contribute to shifts in the bandedge that tend to broaden the apparent exciton profile and decrease its height.[1] Using an areal mapping technique, we have been able to observe this strain non-uniformity and verify that indeed there is much greater strain uniformity in the $InAs_yP_{1-y}$ samples as compared to conventionally grown $In_xGa_{1-x}As$ samples. To do this, we utilize the fact that the $\Delta T/T$ signal is very sensitive to the bandedge location (see Figs. 1(b) and 2(b)). Since the bandedge depends on the strain, an image of $\Delta T/T$ across the surface of the mesa obtained at a wavelength near the band edge can reveal the strain variations.

In summary, we have demonstrated the capabilities of two materials systems to produce MQW modulators that operate in the 1 μm wavelength range compatible with solid state lasers, and explained some of the advantages and problems associated with each. Additionally, we have developed a strain imaging technique that allows strain uniformity to be gauged in the devices.

References

[1] T. K. Woodward, Theodore Sizer II, D. L. Sivco, A. Y. Cho, *Appl. Phys. Lett.* **57**, 548 (1990).

[2] G. Allen Vawter, D. R. Meyers, *J. Appl. Phys.* **65**, 4769 (1989).

[3] S. Niki, C. L. Lin, W. S. C. Chang, and H. H. Wieder, *Appl. Phys. Lett.* **55**, 1339 (1989).

[4] W. Dobbelaere, D. Huang, S. Kalem, H. Morkoç, *Electron. Lett.* **24**, 1239 (1988).

[5] I. J. Fritz, T. M. Brennan, J. R. Wendt, D. S. Ginley, *Appl. Phys. Lett.* **57**, 1245 (1990).

[6] J. E. Zucker, I. Bar-Joseph, C. H. Joyner, A. Dentai, M. D. Divino, D. S. Chemla, *Electronics Lett.* **25**, 973 (1989).

[7] D. A. B. Miller, *Optical and Quantum Electronics* **22**, S61 (1990).

[8] A. K. Tipping, G. Parry, A. J. Moseley, *Semicond. Sci. Technol* **5**, 525 (1990).

[9] R. H. Yan, R. J. Simes, L. A. Coldren, *Appl. Phys. Lett.* **55**, 1946 (1989).

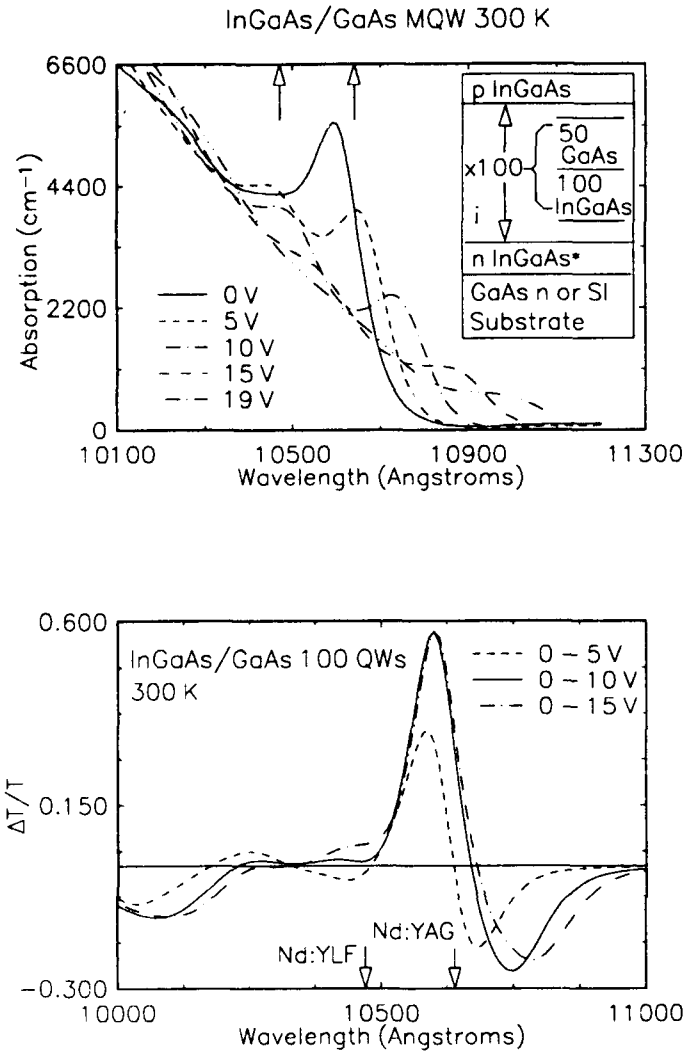


FIG. 1. $In_xGa_{1-x}As$ / GaAs absorption spectra and $\Delta T/T$ data at 300 K.

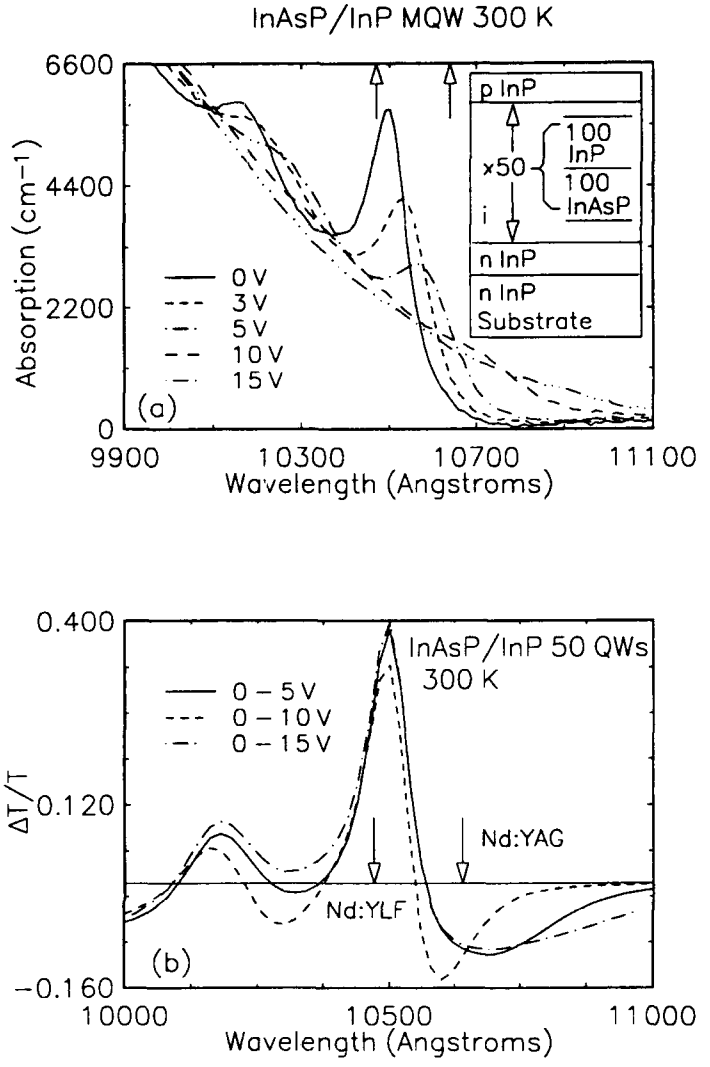


FIG. 2. $InAs_yP_{1-y}$ / InP absorption spectra and $\Delta T/T$ data at 300 K.

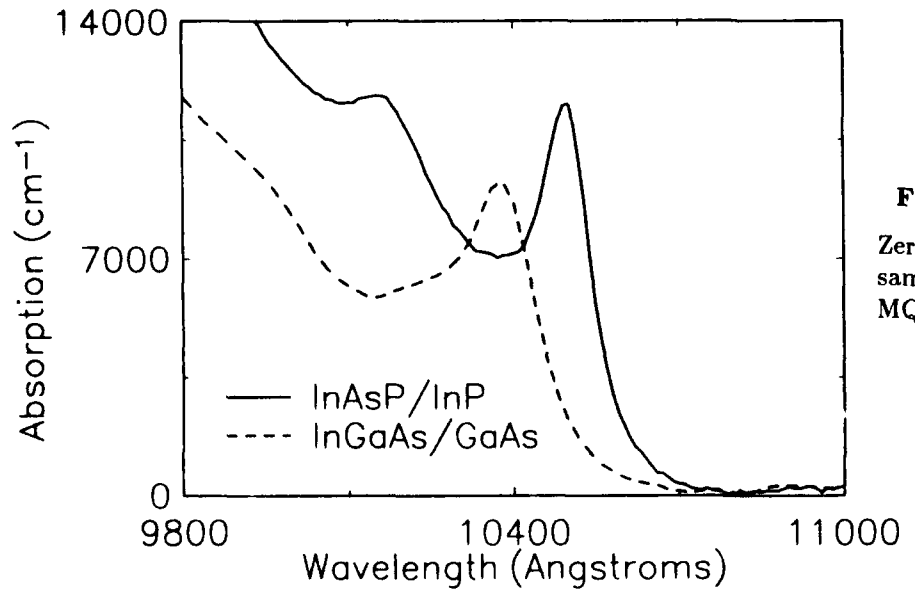


FIG. 3.

Zero bias absorption for the $InAs_yP_{1-y}$ sample (solid), compared to an $In_xGa_{1-x}As$ MQW sample having similar geometry (dashed).

Increased Optical Saturation Intensities in GaInAs Multiple Quantum Wells(MQWs) with AlGaInAs Barriers

Thomas H. Wood, John Z. Pastalan, Charles A. Burrus, Jr.,
Tao Y. Chang, Nicholas J. Sauer, and Bart C. Johnson

AD-P007 834

AT&T Bell Laboratories
Crawford Hill and Holmdel Laboratories
Holmdel, NJ 07733

Electroabsorptive devices made with quantum wells and bulk III-V semiconductors are proving to be useful for both optical modulation and optical logic elements. For many applications, the saturation of this electroabsorption at high optical intensities is a serious problem. For example, both external modulators[1] [2] and SEEDs[3] [4] display contrast saturation at high power. A decrease in bandwidth at high power has also been observed.[2][5] Although phase-space filling is believed to be the dominant mechanism of absorption saturation in the absence of a field in MQWs, Cavicchi *et al.*[7] demonstrated that large photogenerated hole populations could screen fields applied to MQWs. This effect was shown to be the dominant cause of electroabsorption saturation in GaInAs/InP MQWs at room temperature.[2] In order to increase absorption saturation intensities, it is necessary to design the structure to increase the emission rate for holes. It was recently shown that decreasing the barrier height and thickness can increase saturation intensities in GaAs/AlGaAs MQWs.[3] In this paper, we show that, by changing the barrier material from InP to AlGaInAs, the saturation intensities are increased by roughly a factor of 30. In addition, we demonstrate that the use of quaternary AlGaInAs barriers, instead of ternary AlInAs, produces good material quality with low trap density, and that this material displays a strong quantum-confined Stark effect(QCSE).

The sample was similar to that used previously for measurements in the GaInAs/InP system. A set of fifteen quantum wells, each 80 Å wide, made of GaInAs, were grown with 120 Å wide barriers, made of AlGaInAs. The sample was grown by Molecular Beam Epitaxy(MBE) at a substrate temperature of 500 C. The AlGaInAs had a photoluminescence wavelength of approximately 1.17 μm. These wells were in the 0.65 μm-thick undoped region of a *pin* diode. A transverse modulator approximately 64 μm in diameter was fabricated for electroabsorption measurements.

Quantum wells with barriers made from quaternary AlGaInAs should have advantages over wells with ternary AlInAs barriers due to the lower aluminum content of the quaternary. MBE grown $Al_xGa_yIn_{1-x-y}As$ has been shown to contain electron and hole traps whose density and capture cross-section both increase with the x value.[8] The photoluminescence linewidth also exhibits the same trend. Consistent with these facts, broad-area lasers using MBE GaInAs/AlGaInAs MQWs[9] have been shown recently to offer a much reduced threshold current density compared to those using MBE GaInAs/AlInAs MQWs, even though the latter ones used higher growth temperatures to improve the photo-

92-22363

luminescence efficiency.[10] Since effective manifestation of the QCSE in an MQW *pin* diode requires a low trap density in the *i*-region, barriers of AlGaInAs clearly offer an important advantage over those of AlInAs in this respect. Although $x = 0.03$ $Al_xGa_yIn_{1-x-y}As$ quantum wells with AlInAs barriers have been previously reported,[11] we believe this is the first report of the use of AlGaInAs as a barrier material.

Fig. 1 shows a measurement of the photocurrent spectra of this wafer at 5 different biases. Clear excitonic resonances are observed at low-field, along with a shift of those resonances to longer wavelength as the field is increased. These results are superior to those we have obtained with ternary AlInAs barriers, and we believe this is due to a lower trap density in the quaternary barrier, which contains less aluminum than the ternary.

To measure the electroabsorption saturation, we illuminated the device with cw light from an F-center laser and applied a 2 *ns* electrical pulse.[2] The amount of modulation was measured by a fast detector. Fig. 2 shows the electrical signal applied to the modulator, along with generated optical pulses at two intensities. Unlike the results obtained with InP barriers,[2] the optical pulses are fast under all conditions. This indicates that, within our time resolution of ~350 *ps*, there is no degradation in the speed of response of this modulator.

The measured electroabsorption magnitude as a function of incident optical intensity for the AlGaInAs-barrier modulator is shown in Fig. 3. Also shown, for comparison, are data for a GaInAs MQW modulator with 150 Å InP barriers.[2] Both devices were measured at 2 and 8 V bias. The figure shows that each of the devices displays a higher saturation intensity when the bias is increased. We believe this is due to faster sweepout of photogenerated carriers at higher bias. In addition, the device with AlGaInAs barriers shows a saturation intensity approximately 30 times higher than the similar device with InP barriers. We believe this increase in saturation intensity is due to fact that the GaInAs/AlGaInAs material system has approximately 28% of the band discontinuity in the valence band,[12] [13] whereas in the GaInAs/InP material system the valence band contains approximately 58% of this offset.[14] This smaller valence-band offset in the GaInAs/AlGaInAs material system increases the emission rate for holes from the wells, and thus decreases electric field screening by the photogenerated holes. This is confirmed by preliminary measurements of the photocurrent response to a short optical pulse,[2] which indicate a hole sweepout time approximately 15 times faster in the AlGaInAs sample than in the InP sample.

In summary, we have shown that quaternary AlGaInAs is an excellent material for barriers for long-wavelength quantum wells. In addition to being relatively easily grown by MBE, it has a low trap density, which produces a good QCSE response. It has a lower valence band discontinuity, which we believe provides for dramatically increased optical saturation intensities. This may explain the absence of any effect of high optical powers in previous measurements in AlGaInAs/AlInAs MQWs.[11]

REFERENCES

1. M. Suzuki, H. Tanaka, and S. Akiba, Electron. Lett. **25**, 88(1989).

2. Thomas H. Wood, John Z. Pastalan, Charles A. Burrus, Jr., Bart C. Johnson, Barry I. Miller, Jose L. deMiguel, Uziel Koren, and Martin G. Young, Appl. Phys. Lett. **57**, 1081(1990).

3. A. M. Fox, D. A. B. Miller, G. Livescu, J. E. Cunningham, J. E. Henry, and W. Y. Jan, Appl. Phys. Lett(in press).

4. K. Obata, M. Yamanishi, Y. Yamaoka, Y. Kan, J. Hayashi, and I. Suemune, Appl. Phys. Lett. **57**, 419(1990).

5. U. Koren, B. I. Miller, T. L. Koch, G. Eisenstein, R. S. Tucker, I. Bar-Joseph, and D. S. Chemla, Appl. Phys. Lett. **51**, 1132(1987).

6. M. Suzuki, H. Tanaka, and S. Akiba, Electron. Lett. **24**, 1272(1988).

7. R. E. Cavicchi, D. V. Lang, D. Gershoni, A. M. Sergent, H. Temkin, and M. B. Panish, Phys. Rev. B **38**, 13474(1988).

8. D. Biswas, Y. Chin, J. Pamulapati, and P. Bhattacharya, J. Appl. Phys. **67**, 2450(1990).

9. M. Quillec, M. Allovon, F. Brillouet, A. Gloukhian, J. P. Praseuth, and B. Sermage, Electron. Lett. **25**, 1731(1989).

10. H. Temkin, K. Alavi, W. R. Wagner, T. P. Pearsall, and A. Y. Cho, Appl. Phys. Lett. **42**, 845(1983).

11. K. Wakita, I. Kotaka, H. Asai, S. Nojima, O. Mikami, Electron. Lett. **24**, 1324(1988).

12. R. People, K. W. Wecht, K. Alavi, and A. Y. Cho, Appl. Phys. Lett. **43**, 118(1983).

13. A. Sandhu, Y. Nakata, S. Sasa, K. Kodama, and S. Hiyamizu, Jpn. J. Appl. Phys. **26**, 1709(1987).

14. D. V. Lang, M. B. Panish, F. Capasso, J. Allam, R. A. Hamm, A. M Sergent, and W. T. Tsang, Appl. Phys. Lett. **50**, 736(1987).

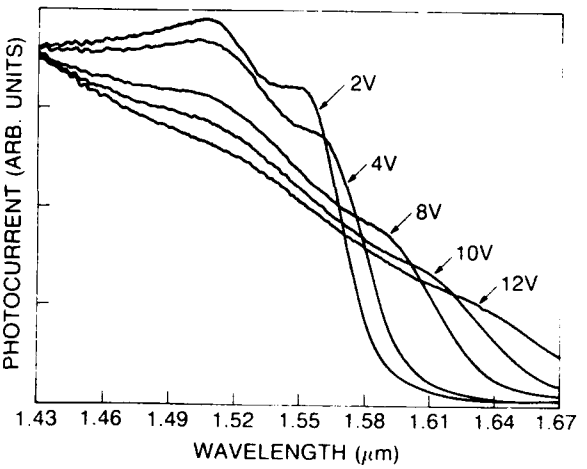


Figure 1: Photocurrent spectra of sample with 80 Å GaInAs quantum wells and 120 Å AlGaInAs barriers.

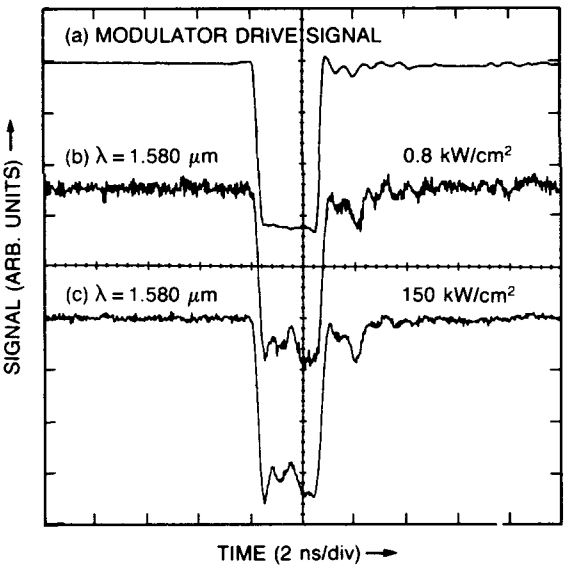


Figure 2: Sampling oscilloscope traces. Trace (a) shows the electrical pulse applied to the modulator, while traces (b) and (c) show the generated optical response at low and high optical intensities. Note that fast response is seen at both low and high intensity.

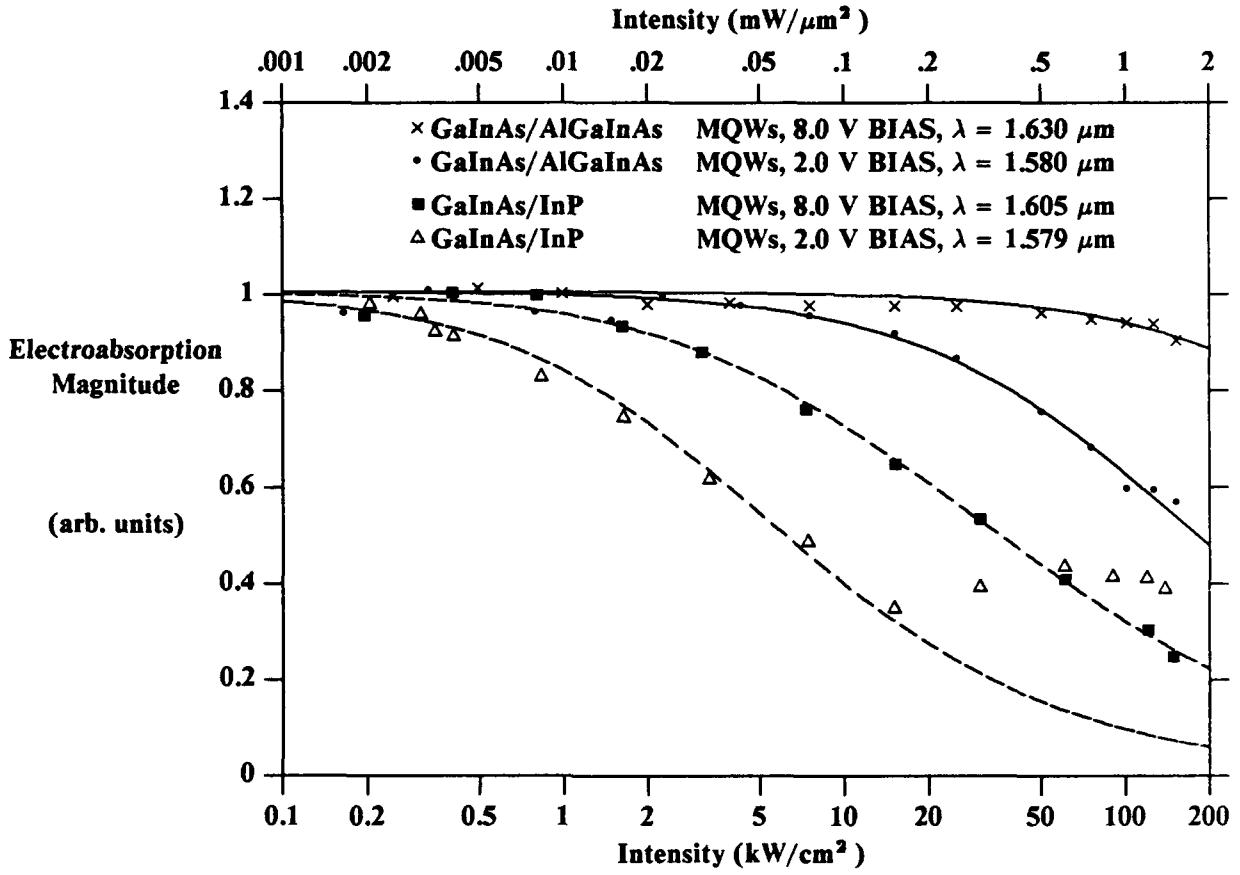


Figure 3: Electroabsorption saturation of GaInAs quantum well samples. The figure shows that samples with AlGaInAs barriers have approximately 30 times higher saturation intensities than similar samples with InP barriers.

OPTICAL BISTABILITY WITH SUBPICOSECOND SWITCHING TIME

Jérôme PAYE and Danièle HULIN
Laboratoire d'Optique Appliquée
ENSTA-Ecole Polytechnique
Centre de l'Yvette
91120 Palaiseau FRANCE

AD-P007 835

Optical bistability is one of the most promising ways toward optical dynamic memories [1]. To overcome the fundamental limitations of electronics concerning speed and parallelism, optical logic elements have been demonstrated with fast response times and/or parallel architectures. Concerning speed, the subpicosecond time scale has been reached for all-optical gates [2]. Since computation requires a means to store transient data, there is a need to demonstrate an optical memory element with a switching time that can match the subpicosecond response time of all-optical gates.

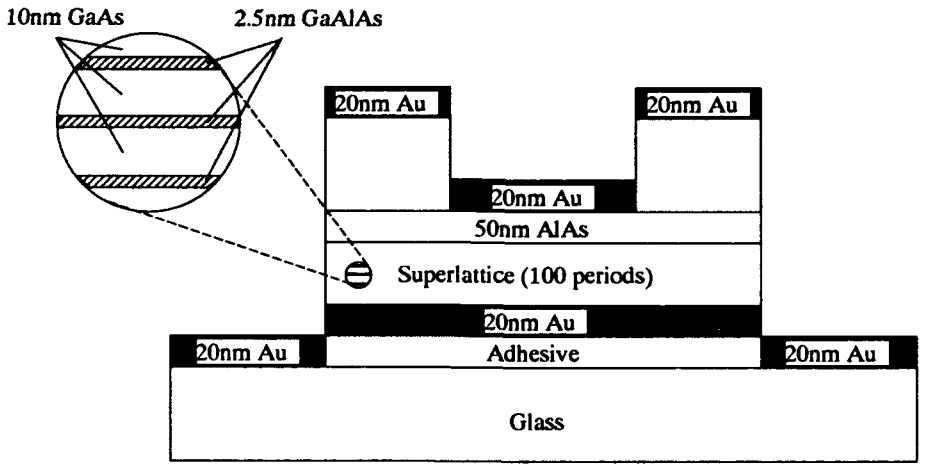


Figure 1: Sample

It is well known that the nonlinear Fabry-Pérot etalon (NLFP) can be used as a bistable device with switching times in the millisecond to nanosecond domains. Our work shows that the NLFP can exhibit a bistable behavior on an ultrashort time scale. For the sake of possible integration in a parallel architecture, we chose the nonlinear medium as a semiconductor because matrices of such elements are technologically feasible [3]. Since ultrafast behavior

92-22364

of the NLFP requires ultrafast response and recovery times of the nonlinear medium, we took advantage of the optical Stark effect (OSE) [4]. This causes an instantaneous shift of the exciton lines during the light pulses and thus changes the refractive index. The interesting feature of the OSE is that it occurs with light pulses having a photon energy smaller than the energy gap, in the transparency region. Thus we use the NLFP in a purely dispersive configuration.

In Fig. 1 we show the sample. The nonlinear medium is GaAs/GaAlAs multiple-quantum wells and gold layers act as mirrors for the Fabry-Pérot etalon. All experiments were performed at 20 K.

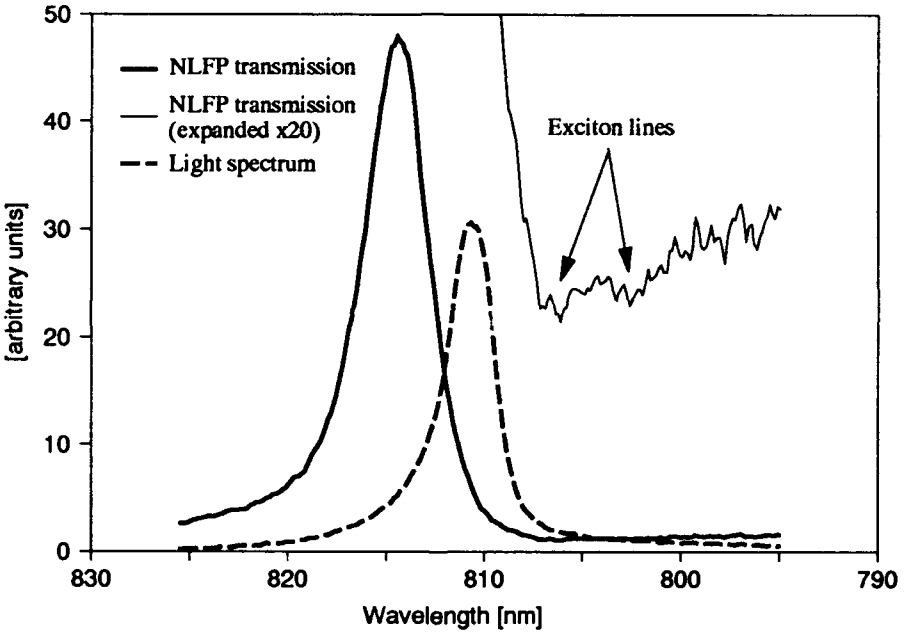


Figure 2: Transmission of the NLFP (thick solid line), expansion of this curve (thin solid line), spectrum of the light pulses (dashed line).

Since the optical Stark shift decreases when the detuning between the laser and the exciton line increases, we designed the sample in order to set a transmission peak of the etalon very close to the absorption edge (Fig. 2). The light pulses originated from a 620 nm colliding-pulse mode-locked femtosecond laser with subsequent amplification, continuum generation, spectral selection and reamplification of the near infrared pulses. In order to obtain optical bistability it is necessary to have the wavelength of the light on the high-energy side

of the NLFP transmission peak and the spectrum of the light has to be narrower than the NLFP peak (cf Fig. 2). Such a spectrum for the laser sets the duration (FWHM) of the pulses to 350 fs.

Pump-probe experiments have been performed to verify that the wavelength of the transmission peak shifts and recovers within the duration of the pulse. To monitor the temporal shape of the transmitted pulse we formed the cross-correlation between the IR pulse and a 90 fs pulse at 620 nm, using sum-frequency generation in a KDP crystal.

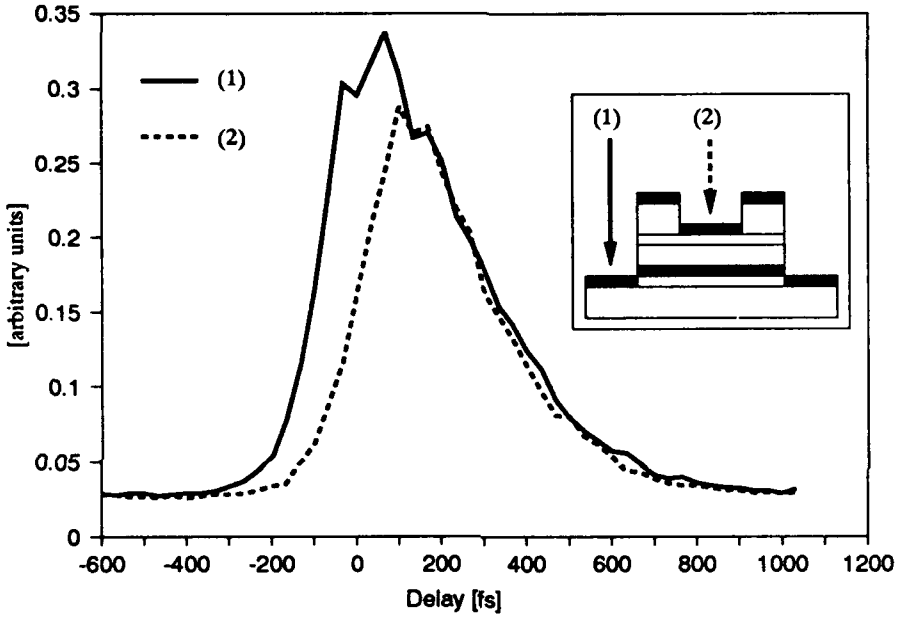


Figure 3: Temporal profile of the input light (solid line) and of the output light (dashed line). The inset shows how the measurement is performed (cf text).

In Fig. 3 we show the temporal profile of the outcoming pulse. The solid line (1) corresponds to the situation where the light pulse passes only through the gold layer. This measures the instantaneous intensity of the pulse incident on the NLFP, with the absorption of gold taken into account. The dashed curve (2) represents the temporal profile of the light pulse transmitted through the whole NLFP. Theoretical calculations of the transmission of ultrashort pulses in a linear Fabry-Pérot show that the temporal shift between the two curves is due to the linear response time of the Fabry-Pérot. After cancelling this linear effect we plotted in Fig. 4 the instantaneous output intensity versus the instantaneous input intensity. When the integrated intensity of the incident pulse is high enough (about 200 GW/cm^2) an hysteresis cycle is clearly shown which is consistent with a bistable behavior.

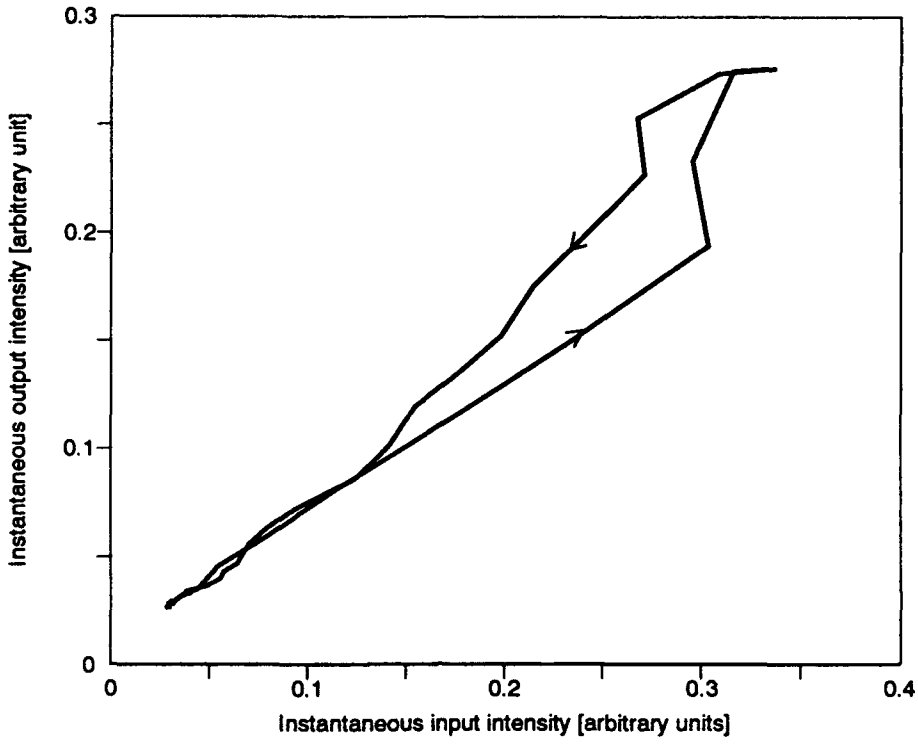


Figure 4:Instantaneous input intensity versus instantaneous output intensity. The output is previously shifted by 56 fs to cancel the linear NLFP response time.

This experimental result shows that the hysteresis loop is traversed in about 350 fs. From this we can estimate a switching time of less than 100 fs. To our knowledge, this is the fastest device with memory ever reported.

REFERENCES:

[1] H.M. GIBBS, "Optical Bistability, Controlling Light With Light", Academic Press, New York (1985).

[2] D. HULIN, A. MYSYROWICZ, A. ANTONETTI, A. MIGUS, W. T. MASSELINK, H. MORKOC, H. M. GIBBS, N. PEYGHAMBARIAN; Appl. Phys. Lett. 49, 749 (1986).

[3] J.L. OUDAR, B. SFEZ, R. KUSZELEWICZ, J. C. MICHEL, R. AZOULAY; Phys. Stat. Sol. B 159, 181 (1990).

[4] A. MYSYROWICZ, D. HULIN, A. ANTONETTI, A. MIGUS, W. T. MASSELINK, H. MORKOC; Phys. Rev. Lett. 56, 2748 (1986).

AD-P007 836

Large excitonic blue-shift and nonlinearity in narrow asymmetric coupled quantum wells

Y. J. Ding, C. L. Guo, S. Li, J. B. Khurgin, K.-K. Law[1], *J. Stellato*[2], *C. T. Law, A. E. Kaplan, and L. A. Coldren*[1]
Department of Electrical and Computer Engineering,
The Johns Hopkins University, Baltimore, MD 21218
[1]Department of Electrical and Computer Engineering,
University of California, Santa Barbara, Santa Barbara, CA 93106
[2]Harry Diamond Laboratories, Adelphi, MD 20783

Conventional self-electrooptic effect device (SEED) [1] is based on the so-called quantum-confined Stark effect (QCSE), which results in the red-shift of the effective bandgap. Thus, it has significant residual absorption and requires high operational voltage. In the attempt to overcome these disadvantages, the so-called blue-shifting SEED schemes were proposed [2]. Blue-shifting SEED can be based on QCSE in strained <111> structures [3] and Wannier-Stark localization [4]. Here, we report our observation of blue-shift of heavy-hole excitonic transition and third-order optical nonlinearity in narrow $GaAs/Al_xGa_{1-x}As$ asymmetric coupled quantum wells (ACQW's) based on the anticrossing of strongly coupled *heavy-hole* (not electron as in [5]) levels in two narrow ACQW's for the first time.

Our structure differs from other ACQW structures used to observe third-order nonlinearity [6] and nonlinear photoluminescence [7] in two major aspects:

(1) Our ACQW's are nearly three times narrower than those used in [5-7] and other works.

(2) The geometry of our ACQW's is such that the thicker well is closer to the n-type doped region (Fig. 1(a)), so the *hole* (rather than electron as in [5-7] and Fig. 1(b)) resonance between two coupled wells can occur.

The ACQW sample was grown by molecular beam epitaxy on Si-doped (100) n^+ GaAs substrate. It has 25 ACQW periods, each of which consists of two GaAs QW's with thicknesses of 18 Å and 32 Å separated by 15 Å $Al_{0.4}Ga_{0.6}As$ barrier. Thicker 100 Å barrier separated the coupled QW's from each other. The 3000 Å undoped $Al_{0.45}Ga_{0.55}As$ has been incorporated into the structure designed for the waveguiding experiments. The entire undoped multiple ACQW structure was sandwiched between n^+ and p^+ $Al_{0.45}Ga_{0.55}As$ layers. The whole structure thus represented a *pin* photodiode, with intrinsic layer (its thickness $\sim$0.72 μm) being a multiple ACQW structure. Arrays of small photodiodes, 250 μm in diameter were fabricated on mesa structures. Argon-pumped Dye laser was used as a tunable source. Photo-current spectra were measured using lock-in amplifier at 78 K.

In our low-power photocurrent measurements, the blue shift of the heavy-hole excitonic transition has been observed within the reverse bias range, 2 - 2.35 V, see Fig. 2. The sharp increase in the oscillator strength of the heavy-hole excitonic transition was observed at - 2.25 V, at a relatively low laser intensity, 9.2 mW/cm^2. According to our calculations, this voltage almost exactly corresponds to the reverse bias voltage at which anticrossing of heavy-hole levels occurs (Fig. 1(*a*)). We have also observed a very interesting phenomenon - an increase of the magnitude of blue-shift with the increase of laser intensity. The maximum blue-shift of heavy-hole excitonic

92-22365

transition observed in our experiment, was ~ 10 mev at the laser intensity, ~ 270 mW/cm^2, see Fig. 2. The external reverse bias at which the anticrossing occurs increase as the the laser intensity increases.

At the fixed reverse bias ~ -3 V, the photocurrent spectra were measured for different laser intensities, (Fig. 3(a)). At low laser intensities, the excitonic transition peaks were hardly distinguishable. Since when the device is overbiased, the exciton is easy to be ionized and its energy becomes very sensitive to the QW width variations [8], the transition appears washed-out. When the intensity was increased, heavy-hole and light-hole excitonic transitions have appeared. As the intensity was further increased, the peaks first narrowed and then broadened again. Lower energy peak moves toward the lower energies and the higher energy peak toward the higher ones. The diverging trend of these transitions has indicated the existence of the intrinsic feedback resistance inside the *pin* structure. The downshift of heavy-hole excitonic transition peak up to 4.9 meV was observed. Due to proximity of the effective masses of the light hole and the electron, the light-hole excitonic transition always shows only the red shift, maximum of which ~ 1.7 meV was observed. Similar to the intrinsic feedback mechanism described in Ref. [9], the effect observed in our experiment can be regarded as a self-electrooptic effect where the load resistance is provided by the tunneling of carriers through the barriers. Our preliminary simulation results (the broken lines in Fig. 3(b)) confirm the existence of the intrinsic resistance with the magnitude ~ 100 KΩ for heavy-hole and ~ 320 KΩ for light-hole. Using external resistance to provide additional feedback, optical bistability has been observed at the laser wavelength corresponding to the heavy-hole excitonic transition as shown in Fig. 4.

This research is supported by the AFOSR and NSF.

[1] D. A. B. Miller *et al.*, *IEEE J. Quant. Electr. QE-21,* 1462 (1985).

[2] J. Khurgin, *Appl. Phys. Lett. 53,* 779 (1988); D. A. B. Miller, *Appl. Phys. Lett. 55,* 202 (1989).

[3] K. W. Goosen *et al.*, *Appl. Phys. Lett. 56,* 715 (1990).

[4] P. Voisin *et al.*, *Phys. Rev. Lett. 61,* 1637 (1988); G. R. Olbright, *et al.*, in *1990 Technical Digest Series,* Vol. 7 (OSA, Washington, DC 1990), pp. 13-14.

[5] H. Q. Le, J. J. Zayhowski, and W. D. Goodhue, *Appl. Phys. Lett. 50,* 1518 (1987); J. W. Little and R. P. Leavitt, *Phys. Rev. B39,* 1365 (1989); Y. Tokuda, K. Kanamoto, and N. Tsukada, *Appl. Phys. Lett. 56,* 2166 (1990).

[6] J. W. Little *et al.*, *Appl. Phys. Lett. 51,* 1786 (1987).

[7] Y. Tokuda *et al.*, *J. Appl. Phys. 65,* 2168 (1989).

[8] See e.g. W. S. Fu *et al.*, *Appl. Phys. Lett. 57,* 1404 (1990).

[9] K. Obata *et al.*, *Appl. Phys. Lett. 57,* 419 (1990).

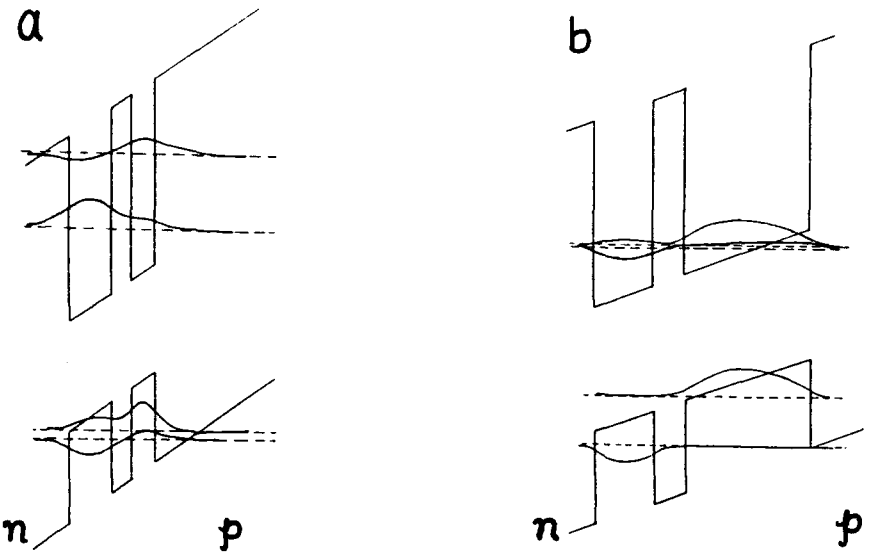


Fig. 1 (*a*) reverse-biased ACQW structure with wider well closer to the n-type region, which was designed and used for this experiment. (*b*) reverse-biased ACQW structure with wider well closer to the p-type region.

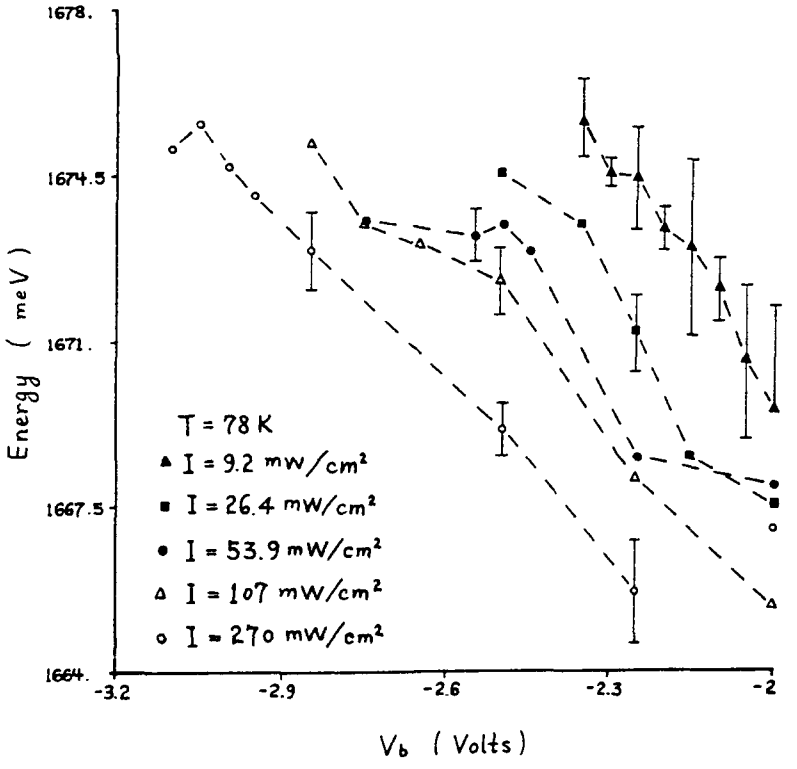


Fig. 2 The energy in the photo-current spectra at which the heavy holes in two coupled wells undergo resonance vs. reverse bias for different laser intensities.

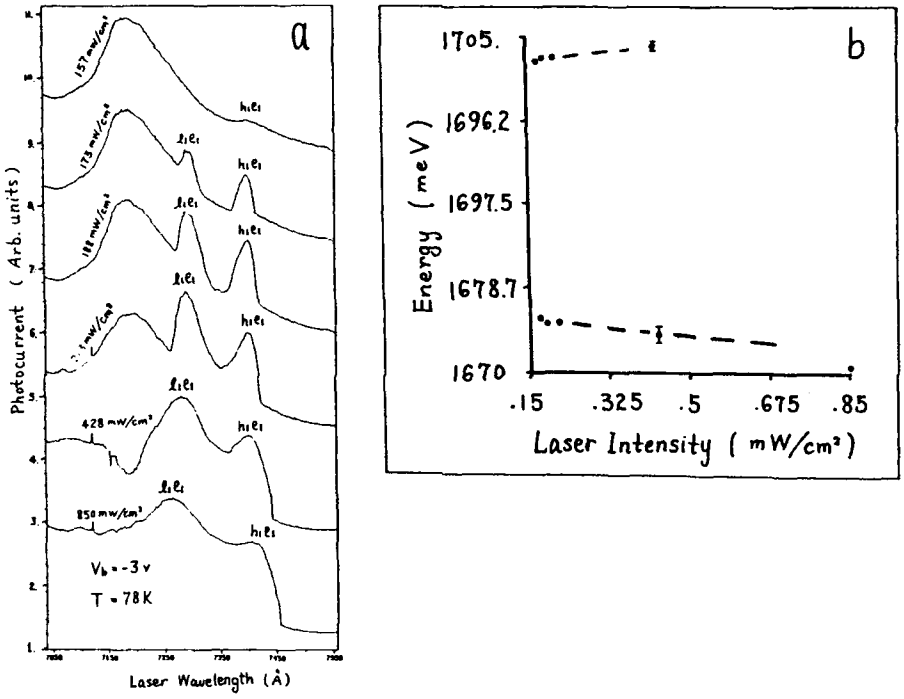


Fig. 3 (*a*) measurement of photocurrent spectra is shown at the constant reverse bias ($V_b \sim -3$ V) for different laser intensities. (*b*) at $V_b \sim -3$ V, the energies of heavy-hole and light-hole excitonic resonance transitions are plotted vs. laser intensity for dots: experimental data and broken lines: theoretical simulations.

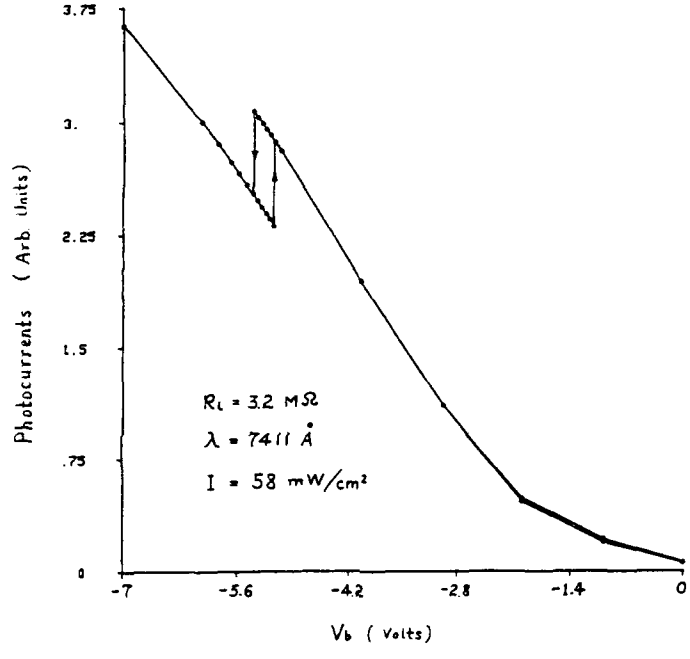


Fig. 4 Optical bistability is observed at the laser intensity ~ 58 mW/cm^2, external resistance ~ 3.2 MΩ, and laser wavelength ~ 7411 Å (heavy-hole excitonic transition).

Quantum Effects in Microcavity Lasers

TuA 8:30am–10:00am
Salon F

Duncan Steel, *Presider*
University of Michigan



Cavity Quantum Electrodynamics in Semiconductor Lasers

Y. Yamamoto, R. Horowicz, S. Machida, G. Björk* and W. H. Richardson**

NTT Basic Research Laboratories
Musashino-Shi, Tokyo 180, Japan

* Department of Microwave Electronics, The Royal Institute of Technology
Stockholm, Sweden

* Jet Propulsion Laboratories
Pasadena, CA 91109, U.S.A.

92-22366

AD-P007 837

A one-dimension (planar) microcavity structure shown in Fig. 1(a) can increase the coupling efficiency β of spontaneous emission into a single cavity resonant mode, if the spontaneous emission spectral width $\Delta\omega_e$ is smaller than the microcavity resonance width $\Delta\omega_c$ and if the refractive-index difference Δn is fairy large.[1] The loss of spontaneous emission into spurious modes, 1-β, are due to the two (degenerate) orthogonal polarization modes and the leaky guided modes propagating in a plane of the microcavity. A three-dimensional (waveguide) microcavity structure shown in Fig. 1(b) features several advantages over the one-dimensional structure. The increase in β is realized without requiring $\Delta\omega_e < \Delta\omega_c$ and large Δn. The degeneracy of the two orthogonal polarization modes can be lifted and the leaky guided modes can be made cut-off by the waveguide structure. Therefore, the spurious spontaneous emission into these modes can be suppressed. The spontaneous emission lifetime τ_s can be also decreased in the three-dimensional microcavity. On the other hand, the one-dimensional microcavity cannot decrease τ_s but can only increase τ_s.

One application of such a microcavity structure is a light emitting diode (LED) with high quantum efficiency and broad modulation bandwidth. A conventional LED suffers from small quantum efficiency due to isotropic spontaneous radiation patterns and narrow modulation bandwidth limited by a natural spontaneous lifetime. As shown in Fig. 2, the nearly 100% quantum efficiency is realized in a microcavity structure with $\beta \simeq 1$ without asking the stimulated emission by a strong lasing field. The increase in modulation bandwidth is realized either by a decreased τ_s or by a β-modulation scheme. The coupling

efficiency β of spontaneous emission is modulated by shifting the emission wavelength with respect to the cavity resonant wavelength as shown in Fig. 3. If the spontaneous emission lifetime can be kept constant for β-modulation, the modulation bandwidth is not limited by the spontaneous emission lifetime τ_s but is determined only by the photon lifetime τ_{ph}. This is because the total spontaneous emission intensity and so the carrier density are kept constant and only the radiation pattern is modulated.

The other application of such a microcavity structure is a single photon laser and single photon/single atom laser. Even though the quantum efficiency of a microcavity laser with $\beta = 1$ is the same at below and above the oscillation threshold as show in Fig. 2, the photon is mainly produced by spontaneous emission at below the oscillation threshold and is mainly produced by stimulated emission at above the oscillation threshold. The average photon number at the oscillation threshold is one if the population inversion is complete ($n_{sp} = 1$), where the probabilities of spontaneous emission and stimulated emission are equal. The average number of electron-hole pairs is given by τ_s/τ_{ph}, which is typically on the order of $10^2 \sim 10^3$. However, if τ_s is decreased by two or three orders of magnitude by a three-dimensional microcavity and is made equal to τ_{ph}, both the average photon number and the average electron-hole pair are equal to one at the oscillation threshold.

Since a microcavity structure can suppress the random coupling noise of spontaneous emission by increasing β, the quantum noise properties of a semiconductor laser can be improved. A conventional constant-current-driven semiconductor laser with $\beta \ll 1$ features the intensity noise squeezing only at the pump rate well above the threshold.[2] On the other hand, a microcavity semiconductor laser with $\beta \simeq 1$ features the intensity noise squeezing at all pump rates including below, near, and above the threshold. The quantum nondemolition measurement of photon number can be realized also at the pump rate well above the threshold by utilizing the quantum correlation between the photon number and the junction voltage.[3] A microcavity semiconductor laser with $\beta \simeq 1$ features the strong quantum correlation between the photon number and the junction voltage at all pump rates and so realize the QND measurement of photon number at any pump rate regions.

References

[1] Y. Yamamoto, S. Machida, K. Igeta and Y. Horikoshi, in Coherence and Quantum Optics VI, ed. L. Mandel, E. Wolf and J. H. Eberly (Plenum, 1990)

[2] Y. Yamamoto, S. Machida and O. Nilsson, Phys. Rev. A34, 4025 (1986); S. Machida, Y. Yamamoto and Y. Itaya, Phys. Rev. Lett. 58, 1000 (1987)

[3] W. H. Richardson and Y. Yamamoto, "Quantum correlation between the photon number and the junction voltage in semiconductor lasers," to be published.

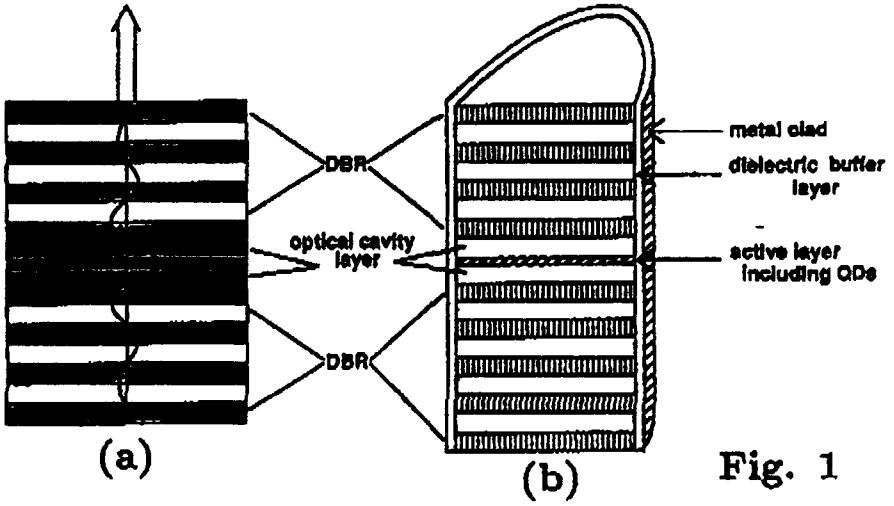


Fig. 1

Fig. 1 (a) A planar microcavity structure for modifying the radiation pattern. (b) A metal clad waveguide microcavity structure for modifying the radiation pattern.

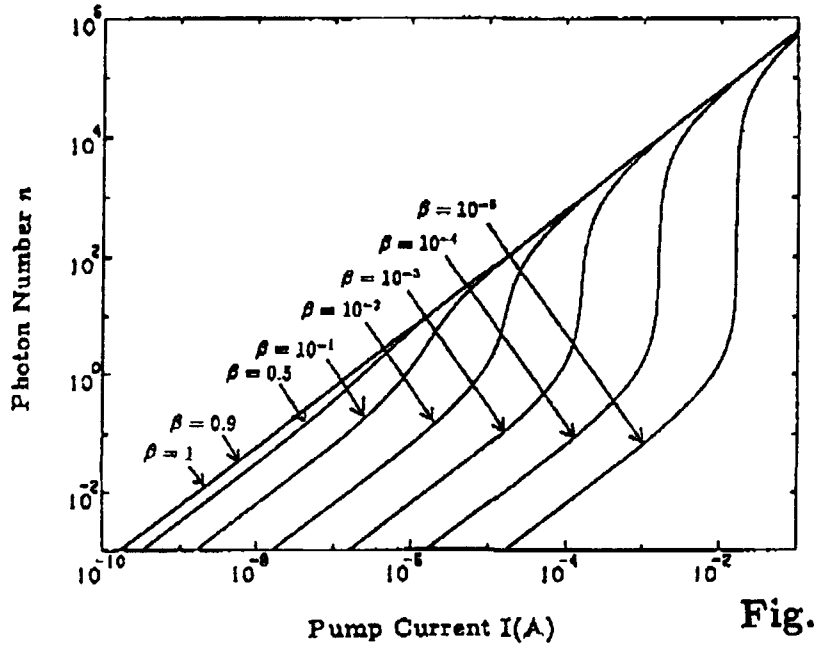


Fig. 2

Fig. 2 Internal photon number n_0 vs. pump current I as a function of spontaneous emission ccefficient β. $n_{sp} = 1$ and $\gamma = 10^{12}$ s^{-1}

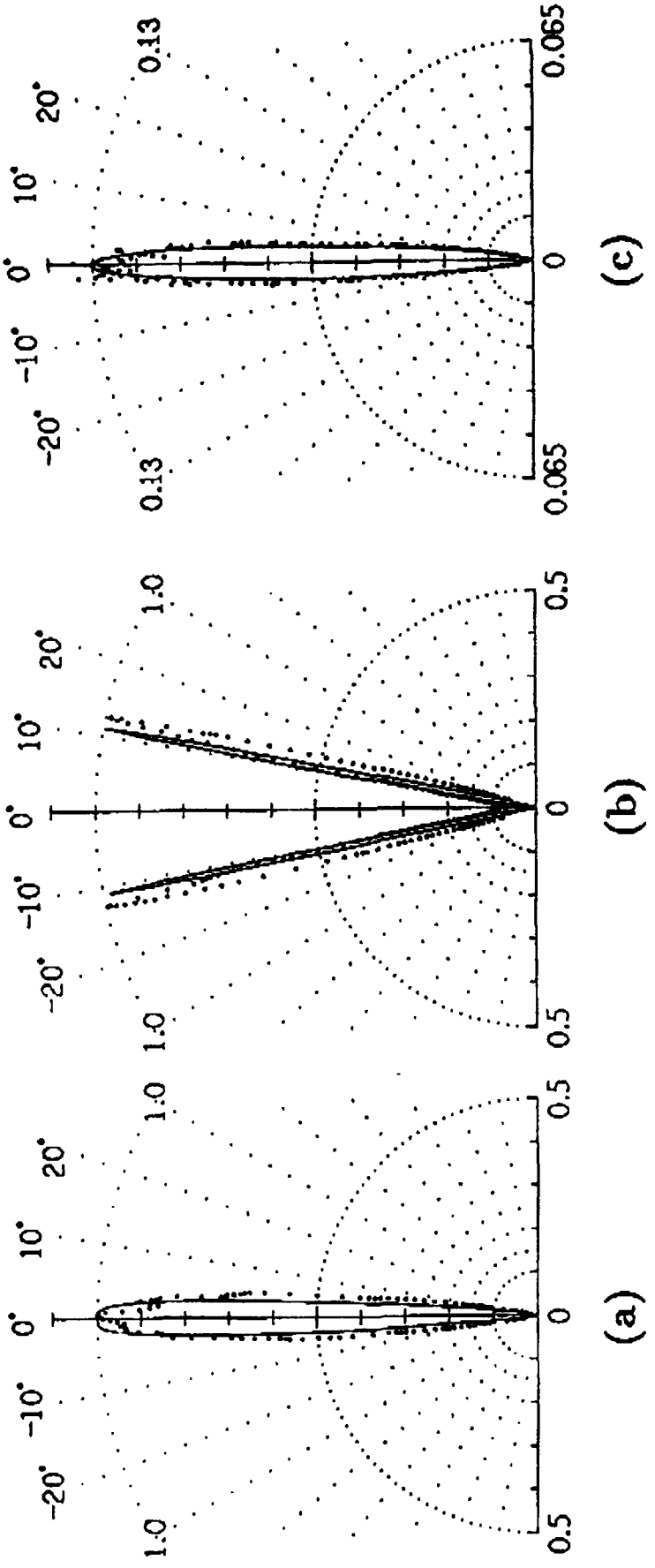


Fig. 3

Fig. 3 Experimental and theoretical radiation patterns from GaAs quantum well in a one-wavelength microcavity. (a) $\lambda_e = \lambda_0 = 800$ nm. (b) $\lambda_e = 800$ nm and $\lambda_0 = 815$ nm (c) $\lambda_e = 800$ nm and $\lambda_0 = 790$ nm.

AD-P007 838

Enhanced and Inhibited Spontaneous Emission in Vertical Microcavity Structures with Two Kinds of GaAs/AlGaAs Quantum Wells

Y. Arakawa, T. Yamauchi, and M. Nishioka
Research Center for Advanced Science and Technology, University of Tokyo
4-6-1 Komaba, Meguro-ku, Tokyo 153 Japan
Phone: 81-3-481-4463, FAX: 81-3-485-5135

92-22367

Spontaneous emission is not an immutable interaction between a material and the vacuum field[1-6]. In fact, enhancement and inhibition of spontaneous emission rates through change in the cavity have been observed in the fluorescence of dye molecules deposited in the all part of the Fabry-Perot resonator. When the cavity length is smaller than the half wavelength of the fluorescence ($\lambda/2$), the spontaneous emission is inhibited. Otherwise it is enhanced. Thus the cavity effects can control the interaction between atoms and vacuum fields to the resonant mode, changing the emission rate into the resonator modes dramatically by tuning the resonator. Moreover, the difference in the mode densities between the enhancement and the inhibition also affects the change in the spontaneous emission lifetime. On the other hand, these enhancement and inhibition of the spontaneous emission have been also investigated in the semiconductor lasers, as suggested by Yablonovitch[7]. Recently, Yamamoto *et al.* demonstrated such enhancement and inhibition of the spontaneous emission by preparing both λ- and $\lambda/2$- vertical cavity lasers which are epitaxially grown on two different wafers[8].

In this paper, we measured intensity and lifetime of photoluminescence from 76Å quantum wells (QWs) and 114Å QWs which are respectively placed at the maximum and the nodes of the standing wave formed by a vertical λ-microcavity structures. The results indicate that, when the λ-microcavity mode is tuned to the bandgap energy of the 76Å QWs (enhanced condition), the spontaneous emission rate into the resonator modes is enhanced by a factor of 40 compared with the case that the cavity mode is tuned to the bandgap energy of the 114Å QWs (inhibited condition). In addition, increase of the spontaneous emission lifetime is successfully observed with the inhibited condition. These results demonstrate existence of enhanced and inhibited spontaneous emission effects in the microcavity structures.

The vertical microcavity structures were grown by our low pressure MOCVD growth system. Nonuniformity of the epitaxial growth rate is utilized so that the wavelength of the cavity mode can be varied by choosing locations on the wafer. Figure 1 shows a schematic band diagram of the λ-cavity structures. Bottom and top grating mirrors are composed of 22+1/2 pairs of AlAs and $Al_{0.4}Ga_{0.6}As$ layers whose thicknesses are $\lambda/4$. An appropriate point can be chosen on the wafer so that the highly reflective zone covers the wavelength of the luminescence from the QWs at T=80K with a peak DBR reflectivity coefficient of about 95%. The λ-microcavity region is composed of GaAs QWs and $Al_{0.4}Ga_{0.6}As$ barrier regions. The λ-cavity has two kinds of QWs

whose thicknesses are 76Å and 114Å. The three 76Å QWs, whose barrier thickness is 50Å, are placed at the center of this cavity (i.e., at the maximum of the one wavelength standing wave). Therefore, the spontaneous emission of electron-hole pairs in the 76Å QWs are enhanced, because the transition matrix element is proportional to the field intensity $|E(z)|^2$. On the other hand, the 114Å QWs are placed at the two nodes of the standing wave in the cavity. Though the vacuum fields are interacting with the emission of electron-hole pairs in the 114Å QWs, the spontaneous emission in these QWs is inhibited because this luminescence cannot couple to the nodes of the standing wave. Thus we can control the coupling effects between the luminescence and the cavity mode by changing the position of the QWs. Here the total GaAs thickness of each kind of wells is the same.

The λ-microcavity structures were optically-pumped through the top mirror by a synchronously pumped mode-locked dye laser. The pulse duration from the dye laser is about 20 picoseconds with a wavelength of 7120Å. The incident pumping light is not reflected by the top DBR mirror, because the reflective zone is away from the wavelength of the incident light. The temperature of the sample was 80K. Since the photon energy of the pumping light (7120Å) is lower than the $Al_{0.4}Ga_{0.6}As$ bandgap energy, the incident light is pumping only the GaAs QW region without being absorbed by the $Al_{0.4}Ga_{0.6}As$ spacers and the barrier layers. Under this excitation condition, the total number of the excited carriers in 76Å QWs is the same as that in 114Å QWs because the total GaAs thickness of each kind of QWs has the same thickness.

Figure 2 shows the PL spectra from the λ-microcavity structures, when both the wavelength of the cavity mode and the DBR high reflectivity coefficient band are completely away from the wavelength of the emission of the QWs (i.e., there is no cavity effect). As shown in this figure, the PL intensity of each kind of QWs is almost the same with a full width half maximum (FWHM) of 60Å, which indicates that the spontaneous emission rate is almost the same in the two kinds of QWs. The excited carrier concentration, N_C, is about $2\times10^{17}(cm^{-3})$. Under this excitation, the spontaneous emission is still dominant compared with the stimulated emission.

Figure 3 (a) shows the PL spectra when the wavelength of the cavity mode coincides with the quantized bandgap energy of the 76Å QWs (7950Å) placed at the maximum of the optical standing wave. In this case, the spontaneous emission at this wavelength is enhanced, while the spontaneous emission from the 114Å QWs is almost completely suppressed. As a result, only one PL peak from the 76Å QWs is observed. On the other hand, when the cavity mode coincides with the quantized bandgap energy of the 114Å QWs (8085Å) placed at the nodes of the optical wave, the PL peak appears at 8085Å as shown in Figure 3(b). However, the peak intensity of the PL peak in the figure is 40 times smaller than the PL at 7950Å in Figure 3(a). These results suggest existence of the inhibition effect in the spontaneous emission from the 114 Å QWs.

To confirm the difference between enhancement and inhibition of the spontaneous emission, the carrier lifetime is measured. In an experiment in which the interaction between a Rydberg atom and dye molecules in the resonator was observed, a remarkable difference between the enhanced

spontaneous lifetime and the inhibited one was observed[5,6]. In contrast, in semiconductor structures, the nonradiative emission component makes it difficult to observe the change in the carrier lifetime and the change might be hidden by dependence of the sample qualities. However, in our microcavity structures, both the enhanced and the inhibited spontaneous emission can be measured in the same wafer by utilizing nonuniformity of the growth rate. Therefore, we can observe even the small change without being disturbed by the dependence of wafer quality on samples. Our result is the first report on the carrier lifetime with enhanced and inhibited spontaneous emission.

Figure 4 shows the lifetime of the PL with the inhibited (closed circle) and enhanced (open circle) spontaneous emission, plotted as a function of the carrier density excited in the QWs. The results indicate that the lifetime with the cavity mode which is resonant on the 114Å QWs (Figure 3(b)) is longer than the lifetime with the cavity mode which is resonant on the 76Å QWs (Figure 3(a)). These results experimentally demonstrate the difference between the inhibited and enhanced spontaneous emission effects. Note that the lifetime of the PL from the 76Å QWs is almost the same as that from 114Å QWs when the cavity mode on resonance is tuned away from the PL emission wavelength. Therefore, we can exclude the possibility that the nonradiative emission rates in the two kinds of QWs causes the difference in the carrier lifetimes between the inhibited and the enhanced cases. The observed change in the lifetime is as small as about 16 per-cent, which is due to the fact that the spectral linewidth of the spontaneous emission in the QWs is larger than the linewidth of the microcavity resonator. In fact, with the increase of the excited carrier density, the difference is smaller because the spontaneous emission linewidth becomes larger.

In conclusion, we successfully demonstrated the existence of the enhanced and inhibited spontaneous emission effects in the λ-microcavity structures with two kinds of QWs whose thickness are 76Å QWs and 114Å QWs, through the measurement of both PL intensity and carrier lifetime. The results indicate that, when the λ-microcavity mode is tuned to the photon energy of the 76Å QWs (enhanced condition), the spontaneous emission rate into the resonator modes is enhanced by a factor of 40 compared with the case that the cavity mode is tuned to the photon energy of the 114Å QWs (inhibited condition). In addition, an increase of the spontaneous emission lifetime is observed in the inhibited condition.

References

[1] D. Kleppner, Phys. Rev. Lett. **47**, 233 (1981)
[2] P. Goy, J. M. Raimond, M. Gross, and S. Haroche, Phys. Rev. Lett. **50**, 1903 (1983)
[3] G. Gabrielse and H. Dehmelt, Phys. Rev. Lett. **55**, 67 (1985)
[4] D. J. Heinzen, J. J. Childs, J. E. Thomas, and M. S. Feld, Phys. Rev. Lett. **58**, 1320 (1987)
[5] F. De Martini, G. Innocenti, G. R. Jacobovitz, and P. Mataloni, Phys. Rev. Lett. **59**, 2955 (1987)
[6] R. G. Hulet, E. S. Hilfer, and D. Kleppner, Phys. Rev. Lett. **55**, 2137 (1985)
[7] Eli Yablonovitch, Phys. Rev. Lett. **58**, 2059 (1987)
[8] Y. Yamamoto, S. Machida, W. Richardson, K. Igeta, and G. Bjork, International Quantum Electronics Conference (Anaheim, California, 1990) p138

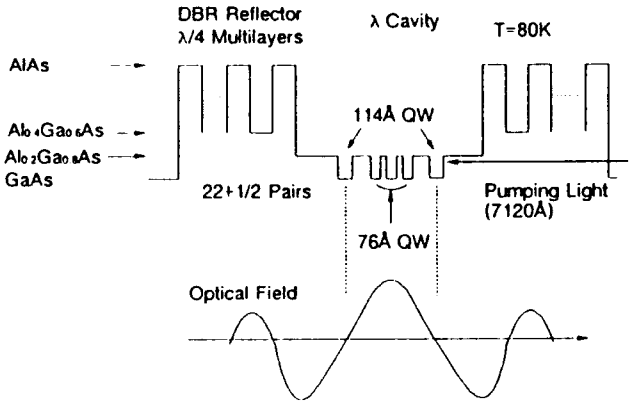


Figure 1: A schematic illustration of the band diagram of the λ-microcavity structures.

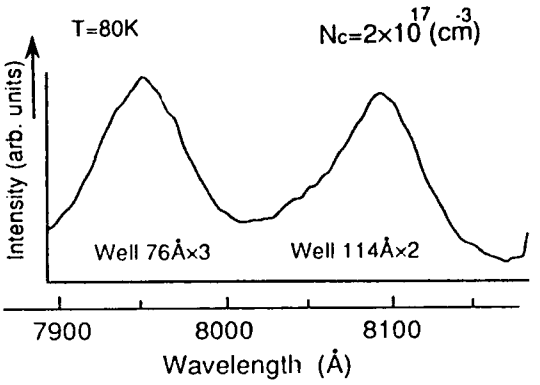


Figure 2: Photoluminescence spectra from the λ-micro cavity structures with two kinds of QWs when both the wavelength of the cavity mode and the band of the DBR high reflectivity are completely away from the wavelength of the emission of the wells.(i.e., there is no cavity effect)

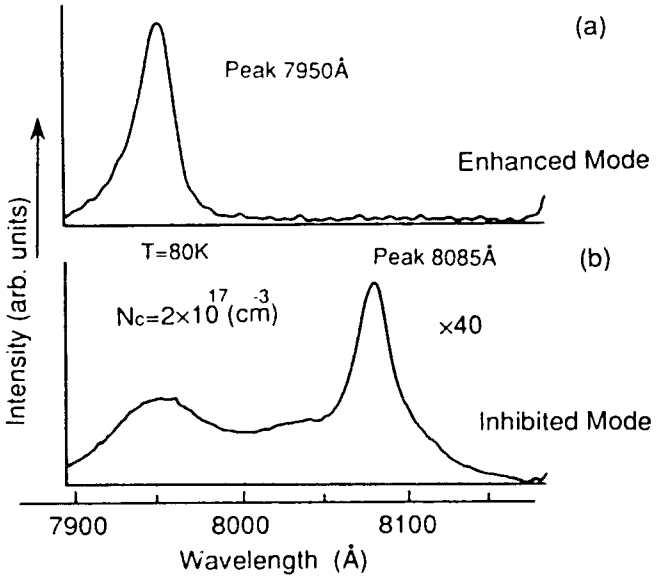


Figure 3: (a) Photoluminescence spectra when the cavity mode coincides with the peak of the 76Å QWs (7950Å) placed at the maximum of the optical wave. (b) Photoluminescence spectra when the cavity mode coincides with the peak of the 114Å QWs (8085Å) placed at the nodes of the optical wave.

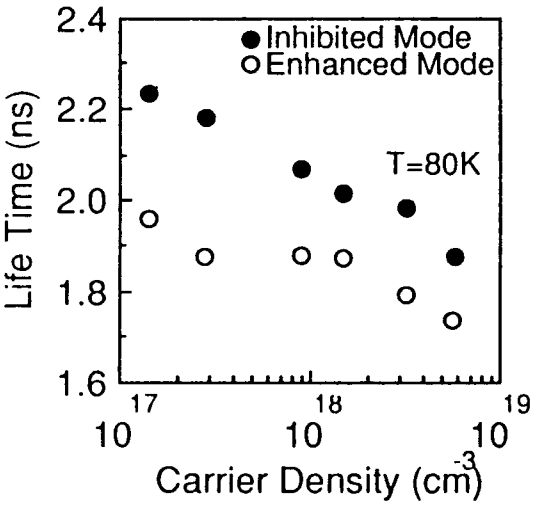


Figure 4: Lifetime of the photoluminescence with the inhibited and enhanced spontaneous emission, plotted as a function of the carrier density injected in each kind of QWs.

AD-P007 839

AN ULTIMATELY LOW-THRESHOLD SEMICONDUCTOR LASER WITH SEPARATE QUANTUM CONFINEMENTS FOR SINGLE ELECTRON-HOLE PAIR AND SINGLE PHOTON FIELD

92-22368

Masamichi Yamanishi and Yoshihisa Yamamoto*

Department of Physical Electronics, Hiroshima University, Saijocho, Higashihiroshima 724, Japan

*NTT Basic Research Laboratories, 3-9-11, Midori-cho, Musashino-shi, Tokyo 180, Japan

The threshold pump rate P_{th} of a laser is determined by three factors: coupling efficiency β of spontaneous emission into a lasing mode, a population inversion parameter n_{sp} for a given pump rate, and photon decay rate γ (or a photon lifetime $\tau_p=1/\gamma$), i.e., $P_{th}=\gamma n_{sp}/\beta$. The population inversion parameter n_{sp} is given by $n_{sp}=E_{cv}/(E_{cv}-E_{vc})$ where E_{cv} and E_{vc} are stimulated emission and absorption rates for one photon in a lasing mode, respectively. The value of β is on the order of 10^{-4} to 10^{-5} for a conventional semiconductor laser. To decrease the threshold pump rate P_{th}, we can increase β close to one by using a single-mode cavity. We can also decrease γ by increasing the cavity Q value. However, the population inversion parameter depends on the minority carrier density N_e, which is determined by the pump rate P, the spontaneous lifetime τ_{sp}, and the active volume V. Thus, $N_e=P\tau_{sp}/V$. In bulk GaAs or quantum-well GaAs at room temperature, a minority carrier density greater than $10^{18}cm^{-3}$ is required to exceed the transparency point ($E_{cv}=E_{vc}$) and create a population inversion ($n_{sp}>0$). With typical numerical parameters for a GaAs edge-emitting laser and a GaAs single-QW surface-emitting laser, such as $V=10^{-10}cm^3$ (0.1-μm-thickness, 3-μm-width, and 300-μm-length) and $V=3\times10^{-14}cm^3$ (10-nm-QW-thickness and 2-μm-diameter), the pump rates required to exceed the transparency point are $P=3\times10^{16}s^{-1}$ and $P=10^{13}s^{-1}$. Here $\tau_{sp}=3ns$ is assumed. These correspond to the pump currents of 5.0mA and 1.6μA, respectively. In other words, the population inversion may set the lower limit of the threshold currents of existing semiconductor lasers.

If the population inversion ($n_{sp}>0$) is realized for an arbitrarily small carrier number and if the population inversion parameter can always take the lowest positive value, $n_{sp}=1$ ($E_{vc}=0$), we can expect to break through the above-mentioned limitation on the lowest threshold current. For an ideal semiconductor laser with $\gamma=10^{11}s^{-1}$ (or $\tau_p=10ps$), $n_{sp}=1$ (or $E_{vc}=0$), and $\beta=1$, the threshold pump rate is as small as $P_{th}=10^{11}s^{-1}$. This corresponds to an ultimately low threshold pump current I_{th} of 16nA. At a microwave frequency, such a single-mode-

cavity maser was experimentally demonstrated by injecting excited Rydberg atoms into a high-Q super-conducting cavity [1]. Maser oscillation was observed at an extremely low pump rate, for which the average number of excited Rydberg atoms inside a cavity was less than 0.1.

In this paper, we propose a new semiconductor surface-emitting laser configuration. The quasi-single-mode microcavity structure proposed here can increase β close to one, and a dc-biased QD also proposed here can decrease E_{vc} close to zero and equivalently achieve $n_{sp} \cong 1$ for an arbitrarily small pump rate and for an arbitrarily large number of QDs. Therefore, an extremely small threshold current, close to the ultimate value, 16nA, would be realized, independently of the volume of the active region.

Let us consider a QD, with the dimensions of ~10nm cube, in which both electron and hole are confined in all directions. The electron and the hole have discrete energies, so that the emission and absorption lines of such a QD resemble those of a two-level atom. In the case of the Rydberg atom maser [1], only an excited atom can be injected into the cavity to interact with the field. In the semiconductor QD laser, however, there are a fixed number of QDs in the active volume. Some of these are unexcited and work as "absorptive atoms". This problem can be overcome by appling a dc electric field across the QDs.

Suppose that the dc electric field is applied to the GaAs QD by electrodes close to the QD. In Fig.1, these electrodes are heavily-doped n^+ and p^+-$Al_xGa_{1-x}As$ layers [2]. The QD is embedded in lightly-doped $Al_xGa_{1-x}As$ layers with thickness comparable to the size of the QD. It is assumed that the CR time constant of the bias circuit is much shorter than the electron-hole pair recombination time τ_{sp}. When the forward bias voltage of about 1.7V (slightly smaller than the built-in potential of the $Al_xGa_{1-x}As$ pn junctions) is applied to the junction, an electron and a hole can be injected by tunneling through the thin barrier layer. Nevertheless, the remained voltage drop across the pn junction, ~0.3V, results in an internal electric field, ~100kV/cm. Here it is assumed that the built-in potential of $Al_xGa_{1-x}As$ pn junction is 2V for x=0.45. Once an electron-hole pair is injected into the ground states of the QD, the junction voltage is dropped and the internal field E_{in} inside the QD is decreased by screening as shown in Fig.1(b). However, the initial voltage across the electrodes of about 0.3V is quickly (on the time scale of ~CR) restored to the original value by the "image" charges induced on the electrodes. This is accomplished before the electron-hole pair is recombined to emit a photon. The "image" charges on the electrodes not only restore the intial voltage but also increase the electric field E_{out} in the i-$Al_xGa_{1-x}As$ layers, which the electron-hole

pair feels, as shown in Fig.1(b). This may result in a red-shift of the emission line from the absorption line due to the quantum confined Stark effect, E_{1A}-E_{1E} as shown in Fig.1(c) [2]. The quantum confined Stark effect is thus modulated by the presence of the image charges on the electrodes. It is worthwhile to note that the carrier injection into the QD can take place even in the presence of the electric field in the proposed mesoscopic diode structure.

The red shift for the emission of the first electron-hole pair was estimated as a function of the original bias field E_0 in a GaAs QD with sizes, L_x=L_y=100Å and L_z=150Å. The difference between the emission line and the absorption line is 2-6meV, depending on the size of the QD, the thickness of the barrier layers, and the strength of applied field [2]. If the homogeneous and inhomogeneous broadening of the emission and absorption lines in GaAs can be made smaller than 2-6meV, the emission can be made free from the absorption by unexcited QDs. The absorption line of an excited QD; i.e., the excitation line of the second electron-hole pair, is about 10meV higher than the absorption line of an unexcited QD, E_{2A}-E_{1A} as shown in Fig.1(c) [2]. Therefore, the emitted light is also free from absorption by an excited QD. In this way, the population inversion parameter n_{sp} can be made close to one no matter how small the pump current.

The radiation pattern of the spontaneous emission can be concentrated on a single lasing mode by the microcavity structures shown in Fig.2. The microcavities with optical cavity layers of half-wavelength thickness shown in Fig.2 are cladded by the distributed Bragg reflectors [3]. A distributed Bragg reflector can have a reflection coefficient higher than 0.999 for a normally propagating cavity resonant mode, so the photon decay rate can be decreased to 10^{11}~10^{12}s^{-1} even though the cavity length is only a half-wavelength. Moreover, if the emission linewidth is much narrower than the cavity-resonant bandwidth and the dipole moment is oriented within the plane of the microcavity structure, the coupling efficiency β of spontaneous emission into the cavity resonant mode can be increased to more than 0.95 by using DBR materials with very different refractive indices [3]. The narrow optical lines and in-plane dipole moment are easily realized by the three dimensional confined structures (QDs) subjected to dc electric fields. Another advantage of the proposed laser is extremely fast switching capability. An extremely wide band modulation by switchings of the electric field in the QDs ($f_c \geq 10^{11}$Hz) would be possible even at low pump currents, ≤100nA. This will be presented at the meeting.

In conclusion, we have theoretically demonstrated that the new semiconductor surface-emitting laser, with the dc-biased QD for discrete

emission free from absorption and with the microcavity controlling the radiation pattern of spontaneous emission, can attain an ultra-low threshold pump current below 100nA. Such a micro-semiconductor laser with separate quantum confinements for the electron-hole pair and the photon field may find application to new fields such as optical communication inside digital processors.

REFERENCES

[1] D. Meschede, H. Walther and G. Muller, Phys. Rev. Lett. **54**, 551 (1985).
[2] M. Yamanishi, Y. Osaka and M. Kurosaki, Jpn. J. Appl. Phys. **29**, L308 (1990).
[3] Y. Yamamoto, S. Machida, K. Igeta and Y. Horikoshi, in Coherence and Quantum Optics VI, ed. by L. Mandel, E. Wolf and J. H. Eberly (Plenum, 1990).

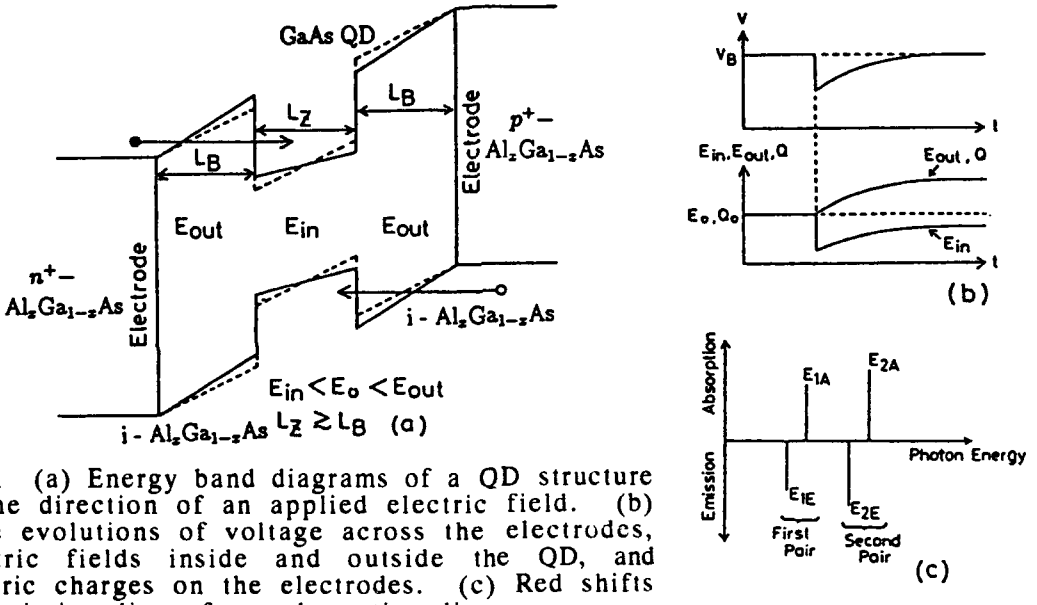


Fig.1 (a) Energy band diagrams of a QD structure in the direction of an applied electric field. (b) Time evolutions of voltage across the electrodes, electric fields inside and outside the QD, and electric charges on the electrodes. (c) Red shifts of emission lines from absorption lines.

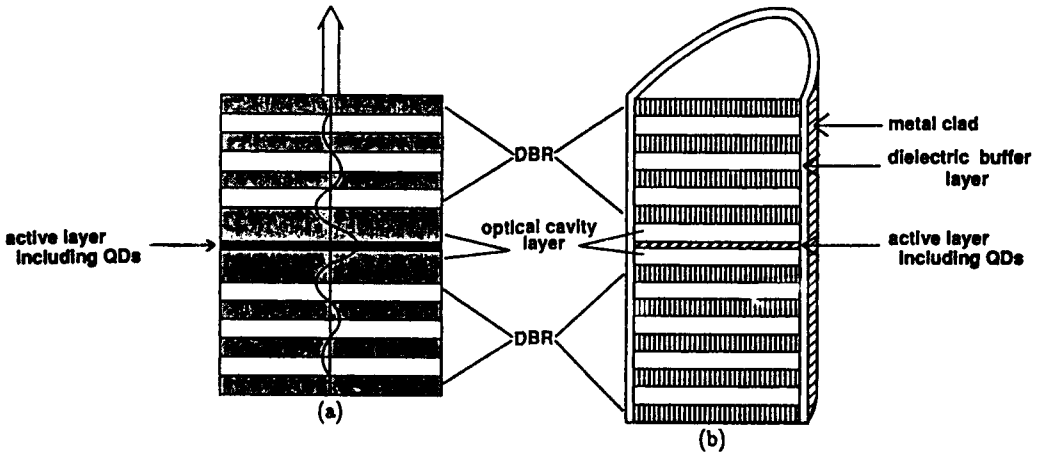


Fig.2 (a) A planar microcavity structure for modifying the radiation pattern. (b) A metal clad waveguide microcavity structure for modifying the radiation pattern.

AD-P007 840

Surface-Emitting-Laser Operation and Optical Switching Characteristics in Vertical to Surface Transmission Electro-Photonic Devices with a Vertical Cavity (VC-VSTEP)

I. Ogura, T. Numai, H. Kosaka, M. Sugimoto, and K. Kasahara

Opto-Electronics Research Labs., NEC Corporation
34 Miyukigaoka, Tsukuba, Ibaraki 305 JAPAN
Telephone: 0298-50-1172, FAX: 0298-56-6140

1. Introduction

The advantage of optical interconnections over electronic interconnections is that they are free of mutual interference and require no capacitive charging. The development of low power consumption optical functional devices has led to the possibility of 2-D optical functional interconnections. One of these devices, which can serve as an optical switch, an optical memory and an optical logic device, is the AlGaAs/GaAs based Vertical to Surface Transmission Electro-Photonic Device (VSTEP)[1],[2]. Although these devices can be in either light-emitting-diode form and edge-emitting laser diode form, they cannot satisfy both high conversion efficiency and compact configuration found in the VCSELs[3]-[5]. Another problem is the non-transparency of the substrate which causes light input and output to be directed only from the top.

In this paper, we report on the first surface emitting laser operation in VSTEPs with a vertical cavity (VC-VSTEPs) and on its optical switching characteristics with strained quantum well thin(100Å) InGaAs active layers used as absorption layers when off. Significantly shorter optical write-in time than that of the LED-mode VSTEP has been achieved. One resultant problem is that the thin absorption layers may cause reduced absorption efficiency. This could be solved through absorption enhancement using multiple reflection mirrors[6] for lasing.

2. Device structure and characteristics

Figure 1 shows the structure of the fabricated VC-VSTEP. A wafer was grown on an n-GaAs substrate by molecular beam epitaxy. This device has a pnpn

92-22369

structure with three inserted undoped InGaAs strained quantum wells. Two distributed Bragg reflector (DBR) mirrors with alternating λ/4 AlAs/GaAs layers are formed at both ends. The distance between two DBRs was 3λ. InGaAs active layers were placed at the position by λ far from the lower DBR, so that active layers which serve as gain/absorption media in the electrically ON/OFF state coincide with the antinode of the standing wave in the cavity. Lower reflector mirror(24.5 pair) is Si-doped with a carrier concentration of $2x10^{18}cm^{-3}$. Upper reflector mirror (15 pair) is Be-doped with a carrier concentration of $3x10^{18}cm^{-3}$. Pseudo-graded structure was introduced between the p-AlAs and p-GaAs layers to reduce resistance from abrupt interfaces[7]. InGaAs active layers were separated by undoped $Al_{0.25}Ga_{0.75}As$ barrier layers[2]. 10 μm, 20μm, and 30μm-square mesas were formed by etching epi-layers to the n-GaAs layer surface within the lower DBR, on which ohmic contact for the n-side was formed. Non-alloyed Cr/Au, which also increases reflectivity at the upper mirror, was evaporated on the mesa top.

Figure 2 shows current vs. light output characteristics, inset with current vs. voltage characteristics. The switching voltage is 5V, and the holding voltage is 2.5V. The threshold current (Ith) was around 2.5mA for a 10 μm-square device, because the band structure when on effectively confines carriers. The oscillation wavelength was 955nm. Importantly, all 100 VC-VSTEPs extracted from a grown wafer emitted laser light. Furthermore, oscillation wavelength deviation within the 2.3mm space was only 2.2Å (Fig. 3). 1k-bit LED mode VSTEPs were made within about a 1mmx1mm area[8]. Both results suggest the oscillation wavelengths of VC-VSTEPs made within a 1mmx1mm area can coincide.

3. Experimental results and discussion

Using two 30μm-square VC-VSTEPs (Ith:18mA), one for a laser light source and the other for an optical switch, cascadability was examined. VC-VSTEPs were adhered on thin glass plates and the light input/output were from the substrate (bottom) surface. The light was coupled in and out with 20 magnification lens. Figure 4 shows the resultant pulse response when light from one VC-VSTEP was injected to the other. The injected light pulse (20ns) from one VC-VSTEP (upper trace in Fig.4) successfully switched on the other VC-VSTEP (lower trace). Optical switching as fast as 10 ns has been confirmed. This is two to three orders of magnitude improvement over the experiments with a LED mode VSTEP being used as a light source. Operating speed was limited by set-up and low speed electric

driver. As shown in the lower trace in Fig.4, after the light was removed the VC-VSTEP as an optical switch remained in the ON state, and could emit light with current injection. The result successfully shows the VC-VSTEP can be cascaded.

In this experiment, the absorption efficiency was low which caused a high switching energy of several tens of pJ. This absorption efficiency is expected to be increased with a properly structured cavity. Figure 5 shows the calculated absorptivity for the light injected from the substrate when the pairs number for the lower mirror is changed. The absorption peak is determined by InGaAs layer's absorption coefficient α and pairs numbers of reflectors. If the resonant wavelength of the DBRs is shorter than the exiciton peak, α is around 3,000cm^{-1}[9]. This calculation suggests that the resultant high switching energy was due to the low absorptivity of about 2% with 24.5 pairs lower reflector and also suggests the effective absorptivity increase with the pairs number decrease, which will result in much lower switching energy and shorter optical write-in time. The 15.5 pairs lower reflector may result in significant absorptibity increase without remarkable threshold gain increase.

4. Summary

The first vertical cavity surface emitting laser type VSTEPs with low threshold current and the feasibility of high-speed cascadability have been successfully demonstrated. Even with very thin active layers as absorption layers, multi-reflection effect increases the absorptivity during write-in. Optimal design for the pairs numbers of the upper and lower reflectors will allow shorter write-in time through increased light absorption from the substrate.

References

[1] K. Kasahara et al., Appl. Phys. Lett., **52**, p.679, (1988).
[2] Y. Tashiro et al., Appl. Phys. Lett., **54**, p.329, (1989).
[3] K. Iga et al., J. Quantum Electron., **QE-24**, p.1845 (1988).
[4] J. L. Jewell et al., Electron. Lett., **25**, p.1123 (1989).
[5] R. S. Geels et al., Appl. Phys. Lett., **57**, p.1605 (1990).
[6] M. S. Ünlü et al., Appl. Phys. Lett., **57**, p.750 (1990).
[7] R. S. Geels et al., Photonics Tech. Lett., **2**, p.234 (1990).
[8] K. Kasahara et al., Tech. Dig. 7th Int. Conf. Integrated Optics and Optical Fiber Communication, Vol. 3. Kobe, 1989, p.158.
[9] T. E. Van Eck et al., Appl. Phys. Lett., **49**, p.135 (1986).

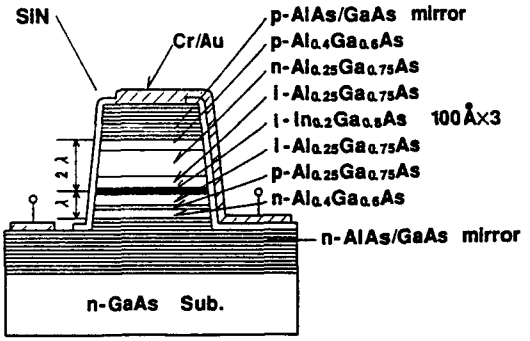


Fig.1 Device structure

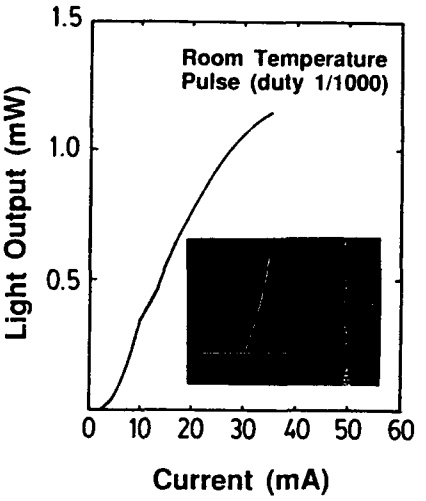


Fig.2 Current-light output/ current-voltage(inset) characteristics

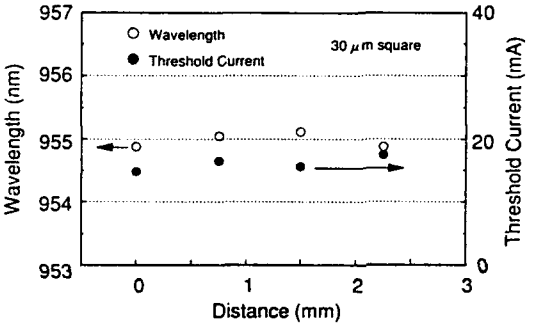


Fig.3 Wavelength and threshold current dependence on position



Fig.4 Result of cascadability experiment
(horiz. 50ns/div)
upper : driving current of one VC-VSTEP as a light source (40mA/div)
middle/lower: bias voltage for/current response of the other VC-VSTEP as an optical switch (middle 3V,lower 8mA/div)

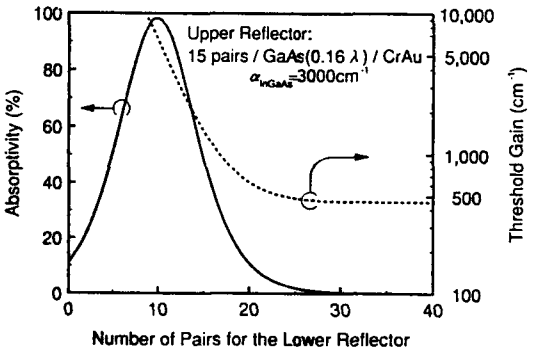


Fig.5 Calculated absorptivity and threshold gain

AD-P007 841

ELECTRIC FIELD-INDUCED ENHANCEMENT AND INHIBITION OF EXCITONIC SPONTANEOUS EMISSION IN GaAs QUANTUM WELLS EMBEDDED IN QUANTUM MICRO-CAVITIES

N. Ochi, Y. Honda, M. Yamanishi, T. Shiotani, and I. Suemune

Department of Physical Electronics, Hiroshima University, Saijocho, Higashihiroshima 724, Japan

Spontaneous emission of an atom is not an immutable property of an atom but can be controlled by modification of the vacuum field fluctuations surrounding the atom[1]. In fact, inhibition and enhancement of spontaneous emission of atoms both at microwave and optical frequencies have been demonstrated experimentally [2]-[5]. It has, also, been demonstrated that spontaneous emission from GaAs quantum wells (QWs) is altered by embedding the QWs between AlAs/AlGaAs distributed Bragg reflectors (DBRs) [6]-[8]. Such an artificial modification of the spontaneous emission in semiconductor micro-structures is very important, particularly from device use point of view. We may, also expect enhancement and inhibition of spontaneous emission induced by tuning of emission wavelength of atoms or active materials embedded in fixed micro-cavities, instead of variation of micro-cavity structures. In this paper, we demonstrate, for the first time, controllable enhancement and inhibition of excitonic spontaneous emission by *dc* electric fields applied to a GaAs QW embedded in a pair of AlAs/AlGaAs DBRs.

The schematic structure of the device tested in our experiment is shown in Fig.1. An undoped GaAs QW with a thickness of 10nm is located at the center of an undoped AlAs optical cavity with half-wavelength (~134nm) thickness. The optical cavity is sandwiched between a pair of p^+- and n^+- doped DBRs consisting of twenty alternative quarter-wavelength layers of $Al_{0.2}Ga_{0.8}As$ and AlAs. The AlAs barrier was adopted to prevent, as much as possible, carrier-escaping from the GaAs QW produced by an intense electric field (~100kV/cm). As a result, we constructed the half-wavelength cavity since the index of refraction of the AlAs barriers adjacent to the GaAs QW is smaller than those of the first

92-22370

layers of the DBRs ($Al_{0.2}Ga_{0.8}As$). Each layer of the structure was sequentially grown in a Riber 32 R&D molecular beam epitaxy system. The GaAs QW is localized at an anti-node position of the standing wave zero-point fluctuation in the $\lambda/2$-cavity so that the spontaneous emission into a normal direction is expected to be enhanced or inhibited in the $\lambda/2$-cavity when the excitonic emission wavelength in the QW is tuned or detuned to the resonant wavelength of the micro-cavity λ_r, respectively. The measured reflection coefficient R at the top surface of the micro-cavity for normally incident light is plotted as a function of wavelength. The clear dip in the reflection coefficient R, centered at the stop-band of the coupled DBR cavity indicates the formation of standing wave of the light at the resonant wavelength λ_r inside the cavity.

As for photoluminescence measurement, the GaAs QW was pumped selectively by a dye laser beam with a photon energy of 1.72eV, smaller than the band gap of $Al_{0.2}Ga_{0.8}As$ (~1.84eV at T=50K). Also, the photon energy of the dye laser beam, 1.72eV was chosen to be sufficiently higher than the band gap of the GaAs QW. Thus, the rate of carrier generation by the photon-pumping is expected to be independent of electric fields in the QW. The *p-i-n* diode including the GaAs QW and the micro-cavity was biased by the *dc* voltage V, as shown in Fig.1. The internal electric field perpendicular to the QW plane can be controlled by the applied bias voltage. The spectra of the spontaneous emission from the GaAs QW and of the reflection coefficient R at low temperature ~50K are shown in Fig.3 for different bias voltages V (different applied fields, E=35~174kV/cm). The emission spectrum associated with $1e$-$1hh$ shifts toward red with the decreasing voltage (increasing electric field) while the reflection spectrum is essentially insensitive to the change in the voltage. Spontaneous emission from the GaAs QW was much stronger than that around λ~830nm from the GaAs substrate. In the low field regime ($E \leq 69$kV/cm), the emission intensity increases sharply with the increasing field. When the peak emission wavelength due to the $1e$-$1hh$ excitonic transition is tuned to the resonant wavelength of the cavity by the applied field, the spontaneous emission intensity is maximized as shown in Fig.3, indicating enhancement of spontaneous emission. This is in marked contrast to the usual quantum confined Stark effect taking place without well-designed

micro-cavities in which the emission intensity decreases monotonically with the increasing electric field as shown in Fig.4. The measured reflection spectrum of the device shown in Fig.4 was essentially structure-less, as was expected. In the case of the well-designed micro-cavity (Fig.3), a further increase in the electric field ($E \geq 69 kV/cm$) results in much stronger suppression (inhibition) of the emission intensity, compared to the case of Fig.4.

In conclusion, with a combination of quantum confined Stark effect with modification of vacuum field fluctuation, we have, for the first time, demonstrated the controllable enhancement and inhibition of excitonic spontaneous emission by *dc* electric fields applied to a GaAs QW located at the center of a fixed DBR micro-cavity. The phenomenon observed here is very useful for making new devices. For instance, an incorporation of the quantum micro-cavities into field effect light emitters [9] may promise us a remarkable improvement of the external efficiency for light output of the devices, $\eta_{ex} \geq 10\%$ [10]. Also, it is very interesting to clarify dynamics of the field-induced switchings of the spontaneous emission from the micro-cavity and field-dependence of recombination life time of the excitons interacting with the modified vacuum field fluctuations. The study on the dynamics and exciton life time is now proceeding.

The authors express their thanks to Dr. Y. Yamamoto, NTT Basic Research Labs. and Dr. A. Shimizu, Sakaki Quantum Wave Project for fruitful discussions.

REFERENCES

[1] E. M. Purcell, Phys. Rev. **69**, 681 (1946).
[2] P. Goy, J. M. Raimond, M. Gross and S. Haroche, Phys. Rev. Lett. **50**, 1903 (1983).
[3] G. Gabrielse and H. Dehmelt, Phys. Rev. Lett. **55**, 67 (1985).
[4] R. G. Hulet, E. S. Hilfer and D. Kleppner, Phys. Rev. Lett. **55**, 2137 (1985).
[5] D. J. Heinzen, J. J. Chils, J. E. Thomas, and M. S. Feld, Phys. Rev. Lett. **58**, 1320 (1987).
[6] Y. Yamamoto, S. Machida, K. Igeta, and Y. Horikoshi, talk presented at XVI Int. Conf. Quantum Electron. WB-2 (Tokyo, July 1988).
[7] H. Yokoyama, K. Nishi, T. Anan and H. Yamada, talk presented at OSA Topical Meeting on Quantum Wells for Optics and Optoelectronics (Salt Lake City, March 1989).
[8] Y. Yamamoto, S. Machida, K. Igeta and Y. Horikoshi, in Coherence and Quantum Optics VI, ed. by L. Mandel, E. Wolf and J. H. Eberly (Plenum, 1990).
[9] Y. Kan, M. Okuda, M. Yamanishi, T. Ohnishi, K. Mukaiyama and I. Suemune, Appl. Phys. Lett. **56** 2059 (1990).
[10] A similar idea was independently considered by A. Shimizu and M. Okuda.

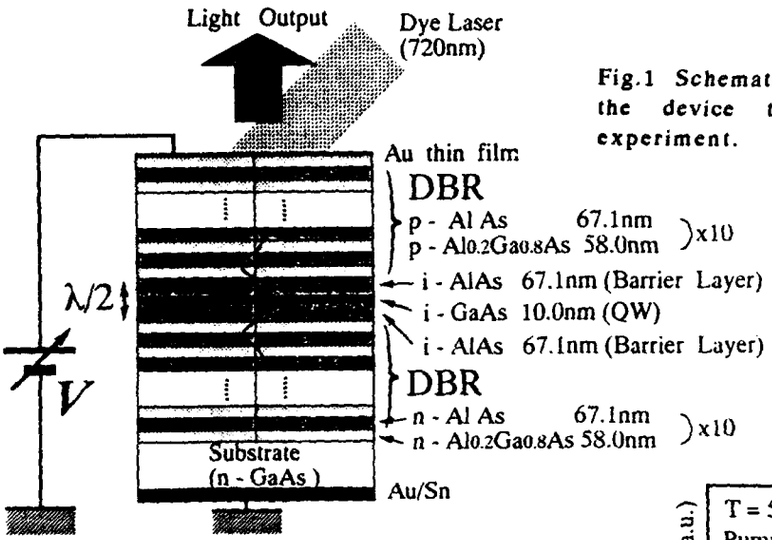


Fig.1 Schematic structure of the device tested in the experiment.

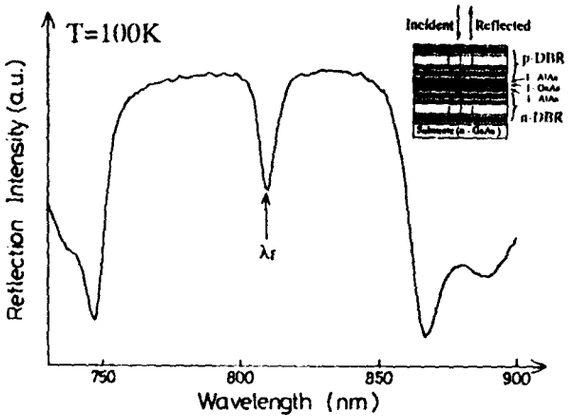
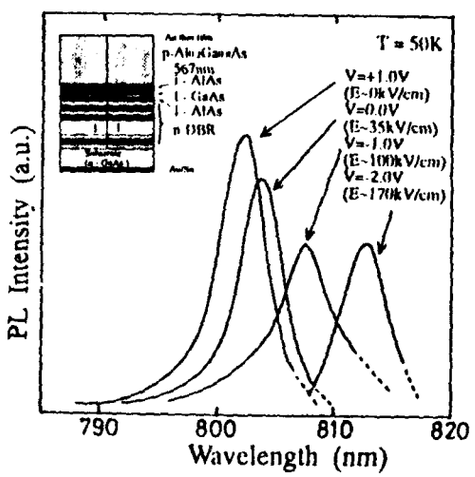


Fig.2 Experimental reflection coefficient R of a λ/2-cavity as a function of probe wavelength at T~100K.



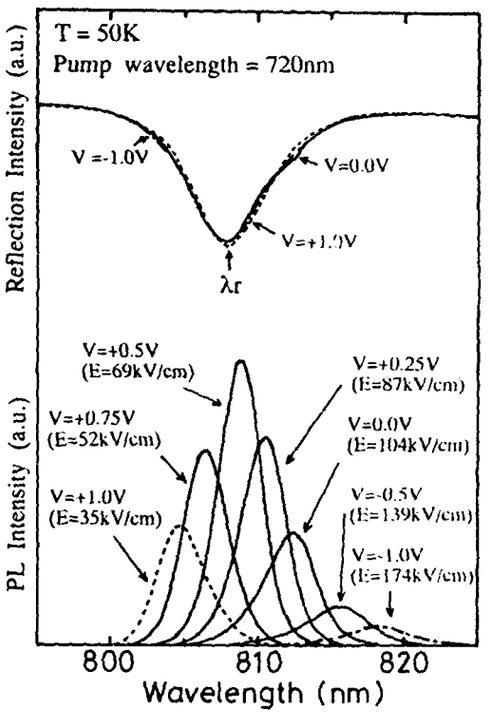


Fig.3 The spontaneous emission and reflection spectra for different voltages (different electric fields) in the (λ/2)-cavity diode at T~50K.

Fig.4 The spontaneous emission spectra for different voltages in a diode without well-designed cavity at T~50K. Emission spectra from the GaAs substrate was subtracted from the original data to obtain the emission spectra from the GaAs QW shown in the figure.

Magnetic and Collective Phenomena

TuB 10:30am–12:00m
Salon F

M. Yamanishi, *Presider*
Hiroshima University, Japan



AD-P007 842

Excitonic Phenomena in the Quantum Hall Effect Regime

W. Chen, M. Fritze, and A.V. Nurmikko
Division of Engineering and Department of Physics
Brown University, Providence RI 02912
(401)863-2869

92-22371

Summary

The use of optical spectroscopic probes show exciting new possibilities and avenues in the investigation of 2-dimensional (2D) and lower dimensional electron systems in high magnetic fields, e.g. in studies of the Quantum Hall effect and (possible) Wigner crystallization. Both spectral shifts [1] and pronounced amplitude changes [2] have been observed in luminescence and absorption from modulation-doped heterojunctions, which are to varying degrees commensurate with integer and/or fractional filling factors. A key question concerns the physical meachnism behind the interaction of the optically active probe with the 2D gas, and whether the probe acts as a weak or strong perturbation. We have investigated these issues in asymmetric, n-type (Al,Ga)As/(In,Ga)As/GaAs and (Al,Ga)As/GaAs/(Al,Ga)As single quantum wells through steady state and picosecond photoluminescence experiments. The SQW's were designed with two principal criteria: (i) to optimize the electron-hole spatial separation and confinement so that weak but finite excitonic effects exist, and (ii) that the Fermi level of the 2D electron gas lies near an otherwise unoccupied conduction band (e.g. the n=2 subband). We find in the (In,Ga)As and GaAs SQW's that the recombination of the 2D electrons with a low density of photoholes ($\sim 10^6$ cm^{-2}) is dominated by a spectrally sharp many-body exciton. This 'edge singularity' involves multiple Coulomb scattering [3] at E_F, making its formation a sensitive indicator of the 2D gas, especially in a magnetic field. We observe very large amplitude oscillations, over three orders of magnitude, in the luminescence of the edge singularity with magnetic field. These variations are correlated to particular filling factors from simultaneous transport measurements,

suggesting a direct link to the QHE.

We would like to acknowledge our valued collaboration with M. Hong and L.L. Chang (IBM T.J. Watson Laboratory), and D. Ackley (Motorola Inc.).

Supported by NSF and an IBM Materials Award

References:

[1] B.B. Goldberg et al, Phys. Rev. Lett. **65**, 641 (1990), H. Buhmann et al, Phys. Rev. Lett. **65**, 641 (1990)

[2] W. Chen et al Phys. Rev. Lett. **64**, 2434 (1990); A.J. Turberfield et al, Phys. Rev. Lett. **65**, 637 (1990)

[3] J.F. Mueller et al Mod. Phys. Lett.; Phys. Rev. B, December 15, 1990

AD-P007 843

92-22372

Collective recombination of two-dimensional electron gas with bound holes and density dependent band-gap renormalization in GaInAs/AlInAs single quantum wells

Y.H. Zhang[a], M. Potemski[b], R. Cingolani[a], K. Kern[a], J.C. Maan[b], and K. Ploog[a]

[a] *Max-Planck-Institut für Festkörperforschung, D-7000 Stuttgart 80, Federal Republic of Germany*

[b] *Hochfeld-Magnetlabor des Max-Planck-Instituts für Festköperforschung, F-38042 Grenoble, France*

Due to the k-conservation restriction the intrinsic luminescence from the two-dimensional electron gas (2DEG) in modulation-doped (MD) quantum wells (QWs) of high structural perfection consists of a sharp peak centered around the band gap instead of a step-like emission band extending up to the Fermi edge as expected[1-3]. Therefore, in such QWs it is not possible to study the density of states as well as the optical processes involving electrons near the Fermi edge directly by means of photoluminescence (PL) experiments. In order to observe the luminescence involving all occupied electron states below the Fermi edge in the 2DEG, some mechanism has to be introduced to localize photogenerated holes and relax the k-conserving law. Alloy fluctuations may localize the holes in ternary MD QW[4], but the random character of this localization potential causes some difficulty for reproducible studies.

In this work we present the observation of the collective radiative recombination of all two-dimensional electrons with bound holes in a series of symmetrically (both side) MD $Ga_{0.47}In_{0.53}As/Al_{0.48}In_{0.52}As$ single quantum wells (SQWs). By taking advantage of a charge-transfer effect, the electron density dependent band-gap renormalization of MD SQWs with different well widths has also been obtained. Our findings demonstrate a direct way to study the density of states, the Fermi energy and the density dependent band-gap renormalization of 2DEG systems.

The samples of the present investigation were grown lattice-matched on semi-insulating Fe-doped InP substrates by molecular beam epitaxy (MBE). After growing an $Al_{0.48}In_{0.52}As$ buffer layer, the n-type symmetrically MD SQW, which consists of 20nm spacer layers and 33nm Si-doped $Al_{0.48}In_{0.52}As$ barrier layers at each side of the well, was deposited with a well width of $10.5nm$ for samples a, c and $13.0nm$ for sample b. In the center of the $Ga_{0.47}In_{0.53}As$ well a 6.3nm wide region was doped with Be at a level of $3*10^{16}cm^{-2}$. It is very important to choose a suitable doping level of acceptors to provide an effective hole localization mechanism without strong degradation of the 2DEG mobility. This is

particularly required to avoid the broadening of Landau levels in magnetoluminescence experiments.

The PL spectra at low temperature of three typical samples with different electron sheet concentration are shown in Fig. 1. The excitation intensity was kept rather low in order to avoid heating of the electrons as well as a change of their concentration. The spectra in Fig. 1 have been shifted in energy for better comparison. The Shubnikov-de Haas oscillations of magnetoresistance measurements under illumination reveal electron sheet concentrations of $1.2*10^{12}cm^{-2}$, $1.7*10^{12}cm^{-2}$ and $2.8*10^{12}cm^{-2}$ for sample *a*, *b* and *c*, respectively. Using these results, we find that the energy bandwidths of the luminescence spectra increase linearly with the 2DEG concentrations. Inspection of the spectra of Fig. 1 reveal that the luminescence intensity increases rapidly at the low energy side. After reaching a certain value, it remains almost constant towards higher energy. This behavior reflects the 2D constant density of states. At the high energy side a sharp cut-off corresponding to the Fermi edge appears. These findings simply indicate that the radiative recombination involves all the electrons of different k with localized holes. Since the center region of the well is intentionally doped with Be, the localization is probably caused by the ionized Be acceptors. The PL spectrum obtained from a MD SQW without Be doping in the well usually centres asymmetrically around the band-gap edge and has a long tail extending to the Fermi edge (as schematically shown by the dashed line in Fig. 1) instead of a step-like emission band.

The magnetoluminescence spectra of sample *c* taken at different fields are shown in Fig. 2. Distinct Landau levels can be observed above 4 *Tesla*. At 10 *Tesla* just 6 Landau levels are fully occupied, giving an electron sheet concentration of $2.9*10^{12}cm^{-2}$. This result is in good agreement with the value determined by magnetotransport measurements, indicating that the luminescence really results from the recombination involving all the electrons in the 2DEG. The data of Fig. 2 also imply the conclusion that the selection rule of Landau levels is relaxed. Our results demonstrate that in these sampls the photogenerated holes are localized as expected. We therefore attribute the luminescence bands to the recombination of all 2D electrons with different k-states up to the Fermi edge with holes bound to the Be acceptors in the well. Considering that the luminescence can reveal the band gap and Fermi energy simultaneously, our findings provide a very convenient and reproducible way to directly measure the change of the band gap upon variation of the 2D electron density.

By exploiting the charge-transfer effect in these MD SQWs[5-7], we can even *reduce* the 2DEG concentration in the well simply by *increasing* the photoexcitation intensity. In Fig. 3 we show the excitation dependent photoluminescence spectra of sample *a*. The change of the luminescence energy bandwidth (the Fermi energy) is a direct measure for

the variation of the electron sheet concentration. Monitoring the band-gap energy and the Fermi energy simultaneously, the band-gap renormalization of the one-component electron plasma can be derived as a function of the electron density. Together with the theoretical calculation of Ref. 8 the density dependent band-gap renormalizations of samples *a* and *b* are plotted in Fig. 4. The results show that the band-gap renormalization of the wider QW is less density dependent than that of the narrow one. The discrepancy between our measured data and the calculation arises from the fact that the 2DEG in MD SQW is not ideally two dimensional.

In summary, a series n-type MD $Ga_{0.47}In_{0.53}As/Al_{0.48}In_{0.52}As$ SQW with Be doping in the central region of the well has been grown by MBE without dramatic degradation of the electron mobility at low temperature. In these samples luminescence of all electrons in the 2DEG up to the Fermi edge with photogenerated holes bound to Be acceptors has been observed. The energy bandwidth of the luminescence spectra agree well with the Fermi energies of the 2DEG in different samples. Magnetoluminescence experiments have confirmed that the photogenerated holes are localized in the well. By exploiting the charge-transfer effect, the electron-density dependency of band-gap renormalization has been also quantitatively measured.

Reference

1. A. Pinczuk, Jagdeep Shah, R.C. Miller, A.C. Gossard and W. Wiegmann, *Solid State Commun.* 50, 735(1984).

2. A.F.S. Penna, Jagdeep Shah, A. Pinczuk, D. Sivco, and A.Y. Cho, *Appl. Phys. Lett.* 46,184(1985)

3. R. Cingolani, W. Stolz, and K. Ploog, *Phys. Rev.* B40, 2950(1989); R. Cingolani, W. Stolz, Y.H. Zhang and K. Ploog, *J. Lumin.* 46, 147(1990).

4. M.S. Skolnick, J.M. Rorison, K.J. Nash, D.J. Mowbray, P.R. Tapster, S.J. Bass, and A.D. Pitt, *Phys. Rev. Lett.* 58, 2130(1987).

5. A.S. Chaves, A.F.S. Penna, J.M. Worlock, G. Weimann, and W. Schlapp: *Surface Sci.* 170, 618(1986).

6. I.V. Kukushkin, K.von Klitzing, K. Ploog, V.E. Kirpichev, and B.N. Shepel: *Phys. Rev.* B40, 4179(1989).

7. Y.H. Zhang, R. Cingolani, K. Ploog:(unpublished results)

8. S.Das Sarma, R. Jalabert, and S.-R Eric Yang: *Phys. Rev.* B41, 8288(1990).

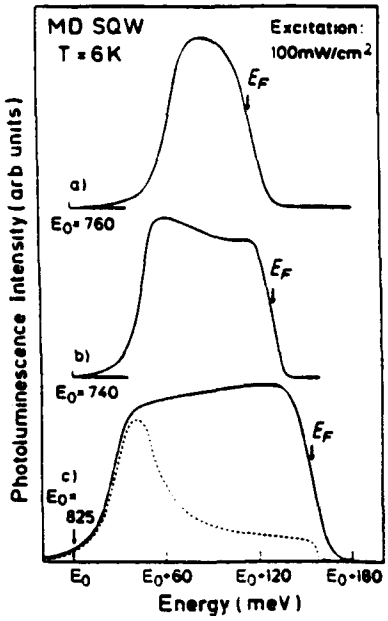


Fig. 1. Photoluminescence spectra of $Ga_{0.47}In_{0.53}As/Al_{0.48}In_{0.52}As$ MD SQWs with different electron sheet concentrations under low excitation at 6K. The energy bandwidths are 52.2 *meV*, 85.0 *meV* and 129 *meV* for samples *a*, *b* and *c*, respectively. The dashed line shows schematically the luminescence line-shape of MD SQWs without Be doping in the well.

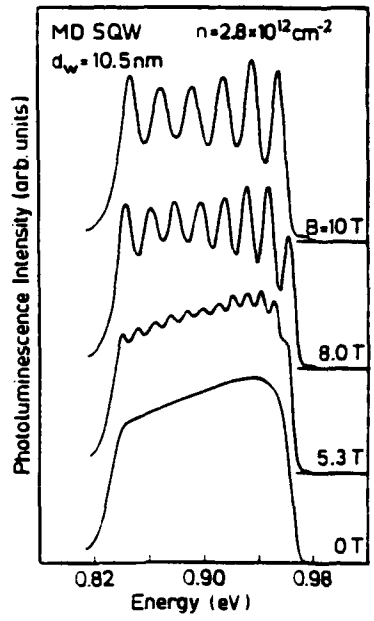


Fig. 2. Magnetoluminescence spectra of sample *c* of different magnetic fields, showing that the electrons at different occupied Landau levels recombine with localized holes.

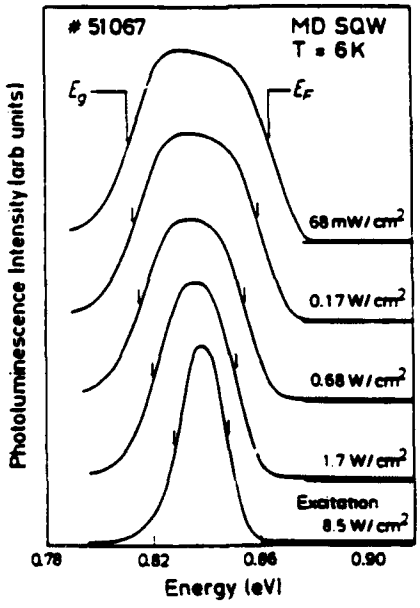


Fig. 3. Excitation dependent photoluminescence spectra of sample *a* with a well width of 10.5*nm*. The band gap and Fermi edge are given by the middle points of the high- and low-energy edges, respectively.

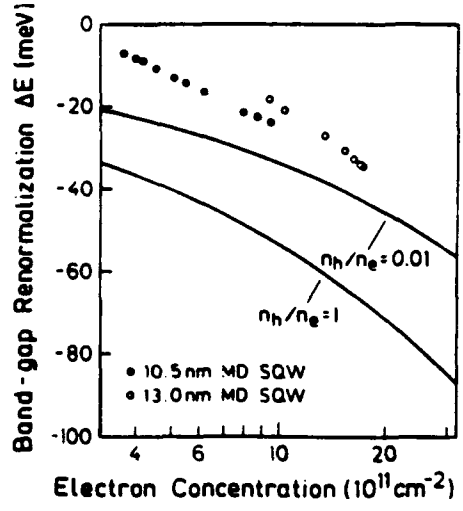


Fig. 4. Band-gap renormalization (ΔE) as a function of the 2D electron concentration. The "•" and "○" represent the data of sample *a* with 10.5*nm* well width and of *b* with 13.0*nm* well width, respectively. The n_h/n_e represent the ratio of concentrations of holes and electrons used in the calculation.

AD-P007 844

Ultrafast Dynamics of Magnetically Confined Excitons in GaAs Quantum Wells

J. B. Stark, W. H. Knox, D. S. Chemla
Room 4B-427, (201) 949-7317, Fax: (201) 949-6010
AT&T Bell Laboratories, Holmdel, New Jersey 07733

S. Schmitt-Rink
AT&T Bell Laboratories, Murray Hill, New Jersey 07974

Spatial confinement along one dimension, using the methods of epitaxial crystal growth, has demonstrated that linear and nonlinear optical properties depend strongly on dimensionality[1]. Confinement along the remaining directions, however, continues to present formidable technological obstacles. Difficulties in the control of the surface properties and size distribution of quantum dots and semiconductor microcrystallites results in materials with unsatisfactory optical quality. Confinement along all three dimensions can be achieved, in materials of excellent optical quality, by placing a quantum well material in a perpendicular magnetic field. As the field is increased, the extension of the resulting electronic orbitals decreases, so that the dimensionality of the states may be tuned from two to zero dimensions. Using femtosecond excite-and-probe optical techniques in fields as large as 12 Tesla, we measure the time resolved dynamics of zero dimensional magneto-excitons. Because the magneto-exciton resonances are well resolved and separated, we excite at energies below and coincident with the first resonance, as well as coincident with the second, and between the first and second resonances. Our results indicate that confinement to zero dimensions results in strong modifications to linear and nonlinear optical properties, and eliminates the majority of scattering channels available for the relaxation of excess energy.

The samples studied include quantum well and *p-i-n* structures, with well thicknesses of approximately 7.5 nm. All are grown by molecular beam epitaxy (MBE), with substrates removed by chemical etching, and antireflection coatings applied to eliminate Fabry-Perrot interference fringes. The quantum wells are located in regions of intrinsic material, so that no electron or hole gas is present. The linear absorption spectrum of a quantum well, in a *p-i-n* structure at 4.2 K, is shown (Fig. 1) as a function of magnetic field, for both circular polarizations of the incident light. At zero field, the 1s heavy hole (hh) and 1s light hole (lh) exciton are well resolved below the light hole bandedge. At higher energies, nominally forbidden transitions appear as weak structures. At still higher energy, optical transitions to the second electronic subband are observed. As the magnetic field increases, the continuum of states above the heavy and light hole bandedges evolves into a complex structure of individual peaks. These are the magneto-exciton states. The complexity of the valence band structure is apparent in the strong anticrossing behavior seen among the higher lying magneto-exciton states.

Amplified pulses at 805 nm with 1μJ energies and 8 kHz repetition rate[2] are focused into a jet of ethylene glycol, to produce broadband continuum pulses of ~100 fs duration. These pulses pass through a four prism dispersion compensator, so that all pulse fronts arrive at the sample at the same time, over the range of wavelengths measured. The continuum is split into pump and probe, with the pump passing through a narrow-band interference filter, for selection of the excitation spectrum, and a variable delay stage, to establish the relative delay between pump and probe. Each beam then passes through a separate polarizer and $\lambda/4$ plate pair, to establish the polarization of each beam independently. Lens pairs focus the beams onto the sample, in the center of a 12 Tesla magnet, with the probe beam collected into an optical fiber, and delivered to an optical multichannel analyzer for parallel detection. A shutter is used to chop the pump beam, as spectra are collected alternately for the excited and unexcited sample.

92-22313

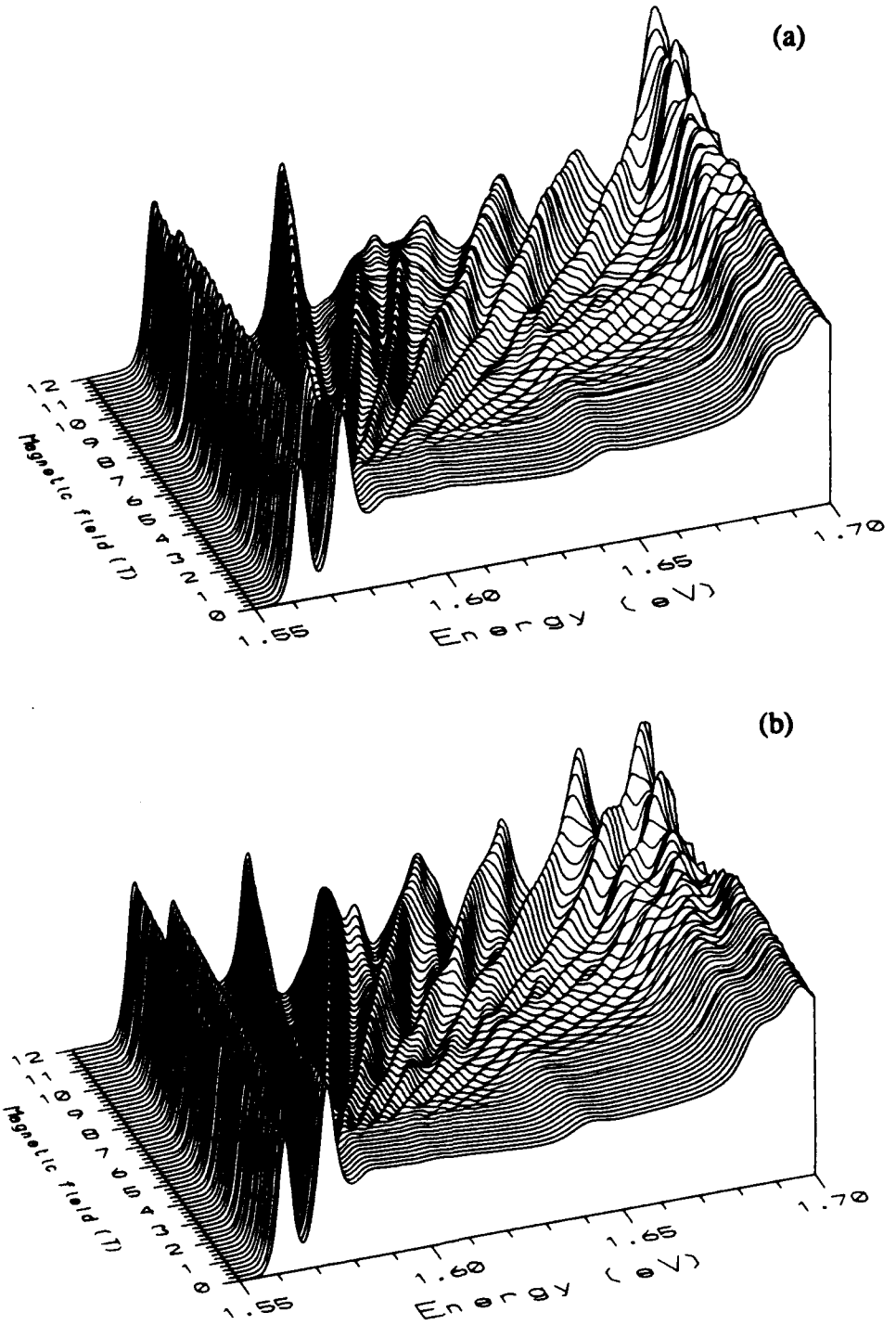


Figure 1 Linear absorption spectra for (a) σ_- and (b) σ_+ circularly polarized light.

At zero field, a linearly polarized pump beam was used to create a population of 1shh excitons. The absorption spectrum (Fig. 2a), shows the optical density of the sample before the arrival of the pump (dotted area). Figure 2b shows the differential absorption signal after the pump arrives, and, in the inset, the changes made to the linear spectrum. Creating a population of 1shh excitons causes that resonance to lose strength due to phase space filling of the states needed to create the resonance.

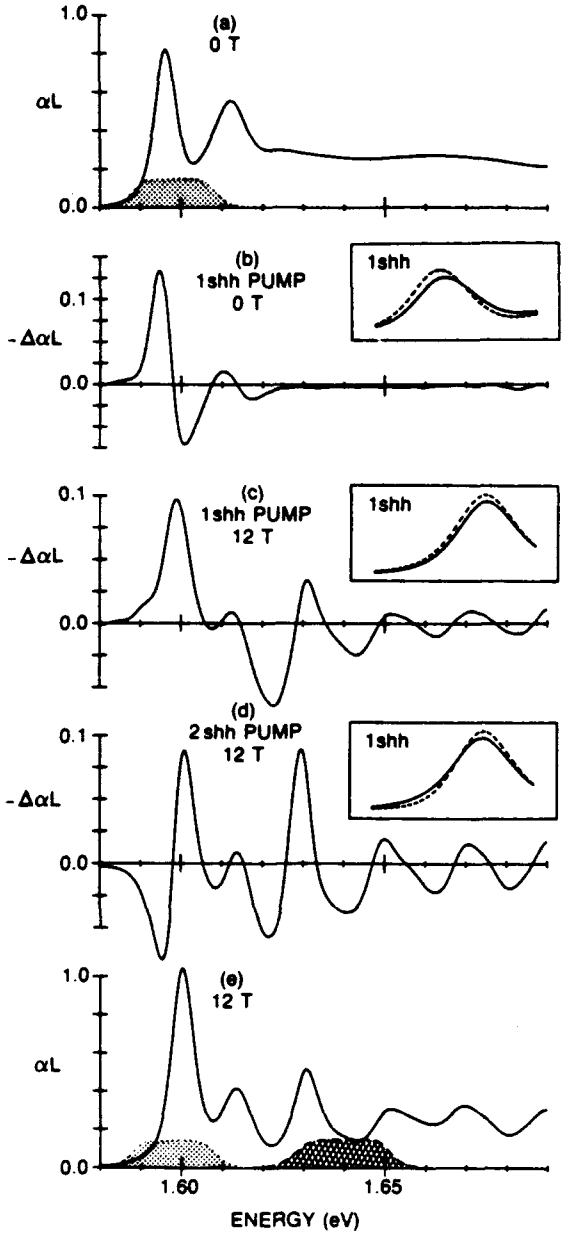


Figure 2 Linear absorption at 0 T (a) and 12 T (e). Dotted and hatched areas indicate the pump spectra for 1s and 2s hh exciton pumping, respectively. Differnetial transmission for 1s hh exciton pumping at 0 T (b) and 12 T (c), and for 2s hh exciton pumping at 12 T (d), all for probe 600 fs after pump. Insets show the ocrresponding 1s hh exciton absorption 600 fs before (dashed) and 600 fs after (solid) the arrival of the pump.

The 1shh also shifts to the blue. This shift can be understood as the response to the short range repulsive potential of hard core particles[3], or as the net result of a bandgap renormalization and reduction of the exciton binding energy[4].

At 12 T, 1shh magneto-excitons are created in the analogous experiment (Fig. 2e, pump is dotted area). The differential absorption spectrum (Fig. 2c) again exhibits the loss of oscillator strength due to phase space filling. At 12 T, however, the blue shift has been quenched (Fig. 2c, inset). This indicates that the 1shh magneto-excitons have been confined sufficiently to cease interacting, demonstrating that at 12 T, confinement of the magneto-excitons from two to zero dimensions has been achieved. The charge density created in the magneto-exciton state renormalizes the bandgap, so that the 2shh state shifts to the red. Direct excitation of a population into the 2shh state (Fig. 2e, hatched pump) yields a differential spectrum (Fig. 2d, and inset) which demonstrates that, in general, the occupation of a magneto-exciton state at high field causes a loss of oscillator strength of that state, with no shift, together with a red shift of unpopulated states.

Resonant creation of a population in an excited magneto-exciton state permits a measurement of the relaxation dynamics by which a nonthermal distribution thermalizes and cools. Because the zero dimensional density of states is discrete, all low energy scattering channels are eliminated, resulting in longer relaxation times. Furthermore, creation of a virtual population by nonresonant excitation provides a means to measure the effect of confinement on the coherent exciton-exciton and exciton-photon interactions. In an optical Stark effect experiment (Fig. 3), the quantum well is excited 40 meV below the lowest magneto-exciton. The differential absorption demonstrates a transient blue shift of the 1shh state, as well as the transient nonlinear response of the higher lying magneto-excitons. Remarkably, the discrete density of states of the magneto-excitons affords an opportunity, unique in semiconductor physics, to apply an ultrafast excitation between a pair of states, where the absorption is essentially zero. In this manner, the optical Stark effect has been measured for excitations even above the lowest

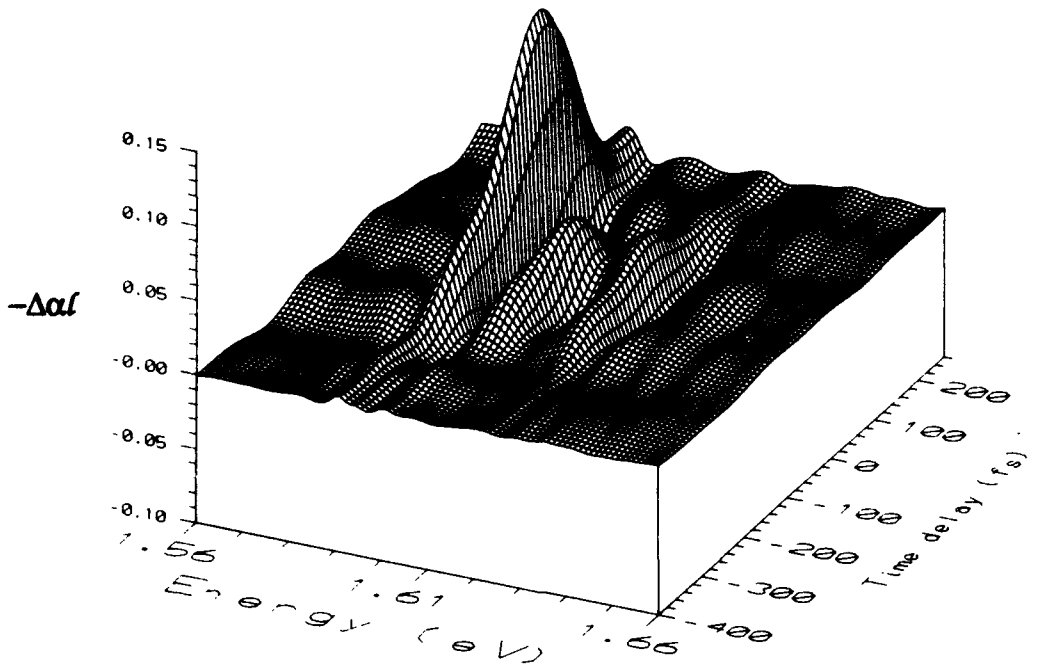


Figure 3 Differential transmission from the optical Stark effect of 12 T magneto-excitons. Energy shifts are seen at the 1shh, 1slh and 2shh resonances. Three points are interpolated between each pair of data points to make the surface profile clear.

resonance. The result is a red shift of those resonances below the excitation, in accordance with theory[5].

A qualitative understanding of the nonlinear optical properties of the magneto-exciton may be obtained from the density matrix equations for interacting two dimensional electron-hole pairs in a perpendicular magnetic field, in the presence of pump and probe optical fields[5]. These calculations determine the energies and oscillator strengths of the various magneto-exciton states as a function of excitation conditions. The calculational and experiental results compare favorably, in general, and provide a framework within which the physics of the magneto-exciton system may be understood.

We have measured the femtosecond time resolved dynamics of zero dimensional magneto-excitons, under resonant and nonresonant excitation. The nonlinear optical properties and relaxation dynamics are seen to be strongly modified by confinement along all three dimensions. The exceptional optical quality afforded by MBE grown quantum well materials, together with the uniform confinement provided by a large perpendicular magnetic field, affords a unique opportunity to investigate the optical and electronic processes governing the behavior of semiconductor systems as they are confined to zero dimensions. While the experiments reported here demonstrate the response of the energies of the magneto-exciton states to transiently created populations, continuing studies exploit the selective coupling of the circularly polarized light to the spin split states to measure the dependence of spin relaxation rates on the dimensionality of the states.

We gratefully acknowledge the expert assistance of G. E. Doran and J. E. Henry for preparation of the samples, and C. W. Tu and W. Wiegmann for sample growth.

[1] S. Schmitt-Rink, D. S. Chemla, and D. A. B Miller, Adv. Phys. **38**, 89 (1989).
[2] W. H. Knox, J. Opt. Soc. Am. B **4**, 1771 (1987).
[3] N. Peyghambarian, et al, Phys. Rev. Lett. **53**, 2433 (1984).
[4] S. Schmitt-Rink, D. S. Chemla, and H. Haug, Phys. Rev. B **37**, 941 (1988).
[5] C. Stafford, S. Schmitt-Rink, and W. Schäfer, Phys. Rev. B **41**, 10000 (1990).

BAND GAP RENORMALIZATION IN QUANTUM CONFINED SEMICONDUCTOR SYSTEMS

AD-P007 845

R. Zimmermann

Zentralinstitut für Elektronenphysik
Hausvogteiplatz 5-7, D-1086 Berlin, FRG
FAX: 30-314 22064

The band gap renormalization (BGR) at high carrier densities is a many-body effect which has been studied intensively in the past for bulk semiconductor materials. The renewed interest in the BGR issue is stimulated by measurements on systems of reduced dimensionality like quantum wells or inversion layers. A careful lineshape analysis of optical experiments is needed to extract reasonable BGR values. Interestingly enough these studies have revealed that the different sublevels do not shift at the same amount. This can be traced back to the well-documented non-rigid shift of the energy bands in the bulk since increasing sublevel numbers refer to increasing momentum in the growth direction.

First theoretical investigations of the BGR in quantum wells [1] have assumed a purely two-dimensional behaviour and derived the $N^{1/3}$ law at zero temperature. (N is the sheet carrier density in cm^{-2}). Finite well width and finite barrier height have been included in [2]. Whereas local density approximation (LDA) or the plasmon-pole approximation have been widely used, full dynamical RPA calculations have been published only recently [3,4]. Here we present results of an RPA calculation with finite temperatures, non-diagonal screening, and finite-barrier Coulomb form factors.

The self-energy due to exchange and correlation changes the band dispersion by essentially lowering the energy gap. In our investigation of finite temperature effects on the BGR in confined systems (quantum wells and quantum wires) we prefer to use a summation over Matsubara frequencies [4] instead of frequency integrals [3]. The RPA self energy is expressed by the screened potential and Fermi occupation functions. Due to the

92-22374

confinement, the three-dimensional momentum is not longer a good quantum number, and the screened potential follows from a matrix equation with respect to a sublevel pair index. Ingredients are the polarization function including intersublevel transitions and the Coulomb potential form factors. For the latter we use the confinement wave functions valid for finite barriers. Even in this case the form factors can be given in analytical form. As we are focussing on a situation where more than one sublevel is filled with carriers there is no reason to reduce the matrix problem to a simple equation as done e.g. in [5]. The diagonal coupling in the sublevel pair index is dominant, but nondiagonal terms are important especially when investigating the difference between filled and unfilled sublevels, as first stressed in [3].

As an example, we show in Fig.1 the BGR of a typical quantum well in a density region where the second sublevel starts to be filled. For the n-doped case (dashed curves) the onset of filling gives rise to a kink in the BGR of the second sublevel. We interprete this as an exchange effect acting more effectively within the same sublevel. In contrast, the correlation (Coulomb hole) is predominantly due to all carriers irrespective of their distribution over the sublevels. The much smaller BGR difference for a two-component plasma (full curves in Fig.1) can now be explained as a reduced importance of exchange since more sublevels (electron e, heavy hole HH, light hole LH) are filled.

In the LDA, the sublevel dependence of the shift is underestimated (numerical results not shown here). There is only the non-perfect spatial matching of the density distribution - compared with the "probing" confinement wave function of the sublevel under study - which gives rise to different shifts. Exchange arguments are completely outside the LDA. When casting the self energy into a real-space potential it is just its nonlocal nature which accounts for the sublevel dependence of the BGR.

From the vast experimental material on the BGR in quantum wells [6,7,8] we display rather new results fom Lach and coworkers [9] as symbols in Fig.2. Using a lateral confinement of the electron-hole plasma by mesa etching extremely high and

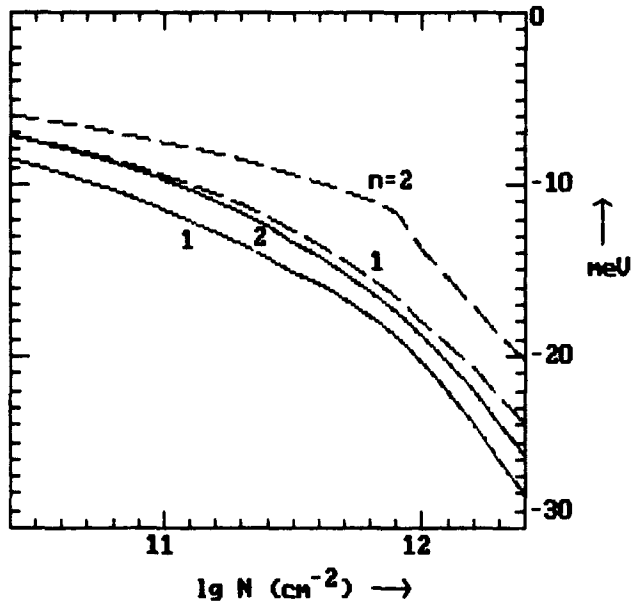


Fig.1 Calculated band gap renormalization of the first (e1-HH1) and second (e2-HH2) sublevel transition in an AlGaAs/GaAs single quantum well (L_z = 20 nm, x = 0.30) at a temperature of 10K. Full curves - optical excitation, dashed - n-doping.

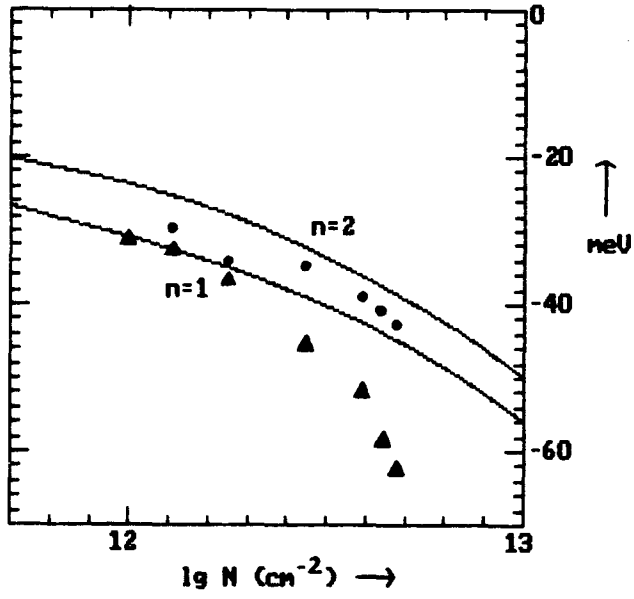


Fig.2 Density dependence of the BGR for the first (e1-HH1, triangles) and second (e2-HH2, dots) sublevel transition. Full curves - dynamical self-energy calculation, symbols - experimental data from [9] (L_z= 10.3 nm, x = 0.37, T = 300K).

uniform plasma densities have been obtained. Due to the large BGR values found, technical problems as the e.g. correct lineshape fit or the proper choice of the unexcited sublevel position give only a small error. The striking result of a smaller BGR shift for the second sublevel transition is explained correctly by the calculation, but the quantitative agreement is not sufficient. With increasing density, the theory gives always a diminishing shift difference, in contrast to the experiment. Further investigations are needed to resolve this puzzle.

References

[1] S. Schmitt-Rink, C. Ell, S.W. Koch, H.E. Schmidt, and H. Haug, Solid State Comm. 52, 123 (1984)

[2] G.E.W. Bauer and T. Ando, J. Phys. C 19, 1537 (1986)

[3] G. Bongiovanni, J.L. Staehli, A. Bosacchi, and S. Franchi, 5th Internat. Conf. on Superlattices and Microstructures, Berlin 1990

[4] R. Zimmermann, E.H. Böttcher, N. Kirstaedter, and D. Bimberg, 5th. Internat. Conf. on Microstructures and Microdevices, Heraklion (Crete) 1990

[5] C. Ell and H. Haug, phys. stat. sol. (b) 149, 117 (1990)

[6] C. Weber, C. Klingshirn, D.S. Chemla, D.A.B. Miller, J.E. Cunningham, and C. Ell, Phys. Rev. B38, 12748 (1988)

[7] G. Bongiovanni and J.L. Staehli, Phys. Rev. B39, 8359 (1989)

[8] K. Bohnert, H. Kalt, A.L. Smirl, D.P. Norwood, T.F. Boggess, and I.J. D'Haenens, Phys. Rev. Lett. 60, 37 (1988)

[9] E. Lach, A. Forchel, D.A. Broido, T.L. Reinecke, G. Weimann, and W. Schlapp, Phys. Rev. B42, 5395 (1990)

AD-P007 846

TRANSIENT OPTICAL PROPERTIES OF THE QUASI-TWO-DIMENSIONAL ELECTRON-HOLE PLASMA

92-22375

R.Cingolani, H.Kalt, and K. Ploog

Max-Planck-Institut für Festkörperforschung , D-7000 Stuttgart 80, FRG

M.Potemski, and J.C.Maan

Max-Planck-Institut für Festkörperforschung, Hochfeld Magnetlabor, 38042 Grenoble, France

We investigate the time evolution of the luminescence emitted by a high density 2D electron-hole plasma (EHP) and its optical properties in magnetic fields up to 20 T in GaAs/Al_xGa_{1-x}As multiple quantum wells (MQW). Under these conditions lifetime effects due to many body interactions as well as magnetic quantization of the density of states must be taken into account.

The heterostructures consist of 25 periods of GaAs/$Al_{0.36}Ga_{0.64}$As with well and barrier widths of 10 and 15 nm, respectively. Sample a) is grown directly on the GaAs substrate while sample b) is grown on a 1 μm thick $Al_{0.36}Ga_{0.64}$As cladding layer acting as optical confiner for the luminescence. Fig.1 shows the totally different emission spectra obtained from the two heterostructures [1]. MQW samples with low optical confinement (sample a) exhibit broad emission bands due to the progressive filling of the higher quantized states as the photogeneration rate is increased. On the contrary, MQW heterostructures grown on optically confining AlGaAs cladding layers (sample b) show a sharp stimulated emission (S-band) evolving on the low energy side of the fundamental n=1 heavy-hole transition. No band filling emission is observed indicating saturation of the spontaneous emission [1] and shortening

of the radiative lifetime [2]. From the line-shape fit of the electron-hole plasma luminescence [3] we estimate a total photogenerated carrier density of about 1.5 $\cdot 10^{13} cm^{-2}$ (corresponding to a partial filling of the n=2 light-hole subband) and a band gap renormalization of the order of 60 meV.

Above the threshold for stimulated emission the carrier lifetime decreases down to several tens of picoseconds with increasing photogeneration rate (Fig.2) The decay time of the EHP luminescence emitted by the higher energy states in the well of sample a) is $\tau_a \simeq 500$ ps. After this transient the broad band filling luminescence disappears and the luminescence arises from a thermalized electron-hole plasma at the n=1 subband. In sample b) the stimulated emission rises following the time evolution of the exciting pulse, and decays with a time constant τ_b=31 ps. This extremely efficient decay channel reduces the effective photogenerated carrier density by a factor τ_b/τ_a and prevents the observation of a spontaneous radiative decay from higher energy states. For longer times, the emission spectrum shows again the broad spontaneous EHP emission around the energy of the fundamental interband transition.

The spectral position of the S-band indicates the energy position of the renormalized band gap edge. The measured transient band gap renormalization is depicted in Fig.3. The band gap shrinkage is maximum at the end of the exciting pulse , then it decreases and vanishes in about 100 ps, following the time evolution of the carrier density.

In light of these results we now discuss the magnetooptic spectra of samples a) and b) under the same excitation as in Fig.1. Above 8 T the EHP luminescence spectra of sample a) exhibit sharp peaks related to inter-Landau level transitions superimposed to the band filling luminescence [4]. The Landau level structures blue-shift linearly with increasing field and 14 inter-Landau levels transitions can be observed at 18 T. From the slope of the fan-chart plots (1.37 meV/T) a 20 % many-body enhancement of the electron mass is deduced [5]. The extrapolation of the fan

curves at zero field crosses the energy axis at a lower energy than the unperturbed band gap of the investigated MQW , indicating a band gap renormalization of 18 meV, independent of the photogeneration rate , as first reported in Ref.[5]. Lifetime effects dominate the radiative recombination processes in sample b). The electron-hole population rapidly decays through the stimulated emission channel from the lowest Landau level and the magneto-luminescence spectra only exhibit one strong peak, whose field dependence is shown in Fig.5. The most striking result is that, in constrast to sample a), the renormalized band gap obtained from the zero field extrapolation of the fan-chart diagram clearly depends on the excitation intensity. The absolute BGR value of 32 meV obtained at the maximum excitation intensity (I_o curve in Fig.5) corresponds to a carrier density of 1.1 $\cdot 10^{11} cm^{-2}$, in agreement with the carrier density reduction estimated in sample b).

These results suggest that two different phases can form in the MQW in the presence of high magnetic fields: a long living highly-correlated particle system, analogous to a condensed exciton or electron gas at the equilibrium density, which does not show any spectral shift of the luminescence with increasing excitation intensity, and a short-living free-carrier population, which exhibits the usual electron-hole plasma behavior with density dependent band gap renormalization.

References

1 - R.Cingolani, K.Ploog, A.Cingolani, C.Moro and M.Ferrara, Phys. Rev.**B42**, 2893 (1990)

2 - R.Cingolani, M.Ferara, M.Lugara', Y.Chen, F.Bassani, J.Massies and F.Turco, Europhys. Lett. **7**, 751 (1988)

3 - R.Cingolani, H.Kalt, and K.Ploog, Phys. Rev. **B42**, (1990) in press

4 - R.Cingolani, G.C.La Rocca, H.Kalt, K.Ploog, M.Potemski, and J.C.Maan, to appear in Phys. Rev. B. (1991)

5 - M.Potemski, J.C.Maan, K.Ploog, and G.Weimann, Proc. ICPS19, ed. E.Zawadzki, IPPAS Warsaw 1988, p.119 ; ibid, Solid State Commun. **75**, 185 (1990); ibid, Surf.Sci. **229**, 380 (1990)

Fig.1 - Low-temperature high-excitation intensity PL spectra of samples a) and b) (I_o = $2MWcm^{-2}$).

Fig.2 - Time-resolved high-excitation intensity Pl spectra of samples a) and b). The temperature is 2K.

Fig.3 - Transient band gap renormalization in sample b) under different excitation intensities.

Fig.4 - Magnetic field dependence of the inter-Landau level transition energies from sample a).

Fig.5 - The same as in Fig.4 but for sample b) under different excitation intensites.

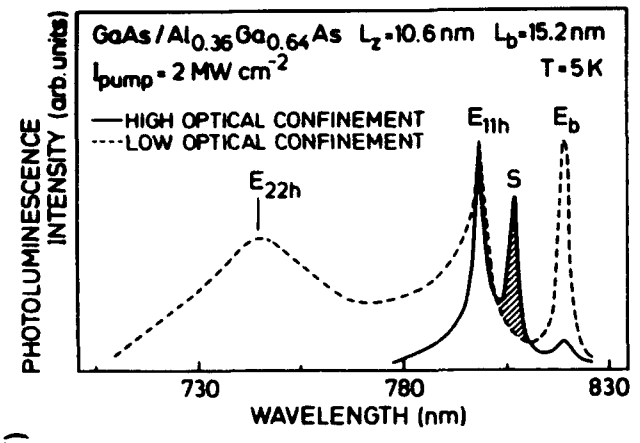


Fig.1

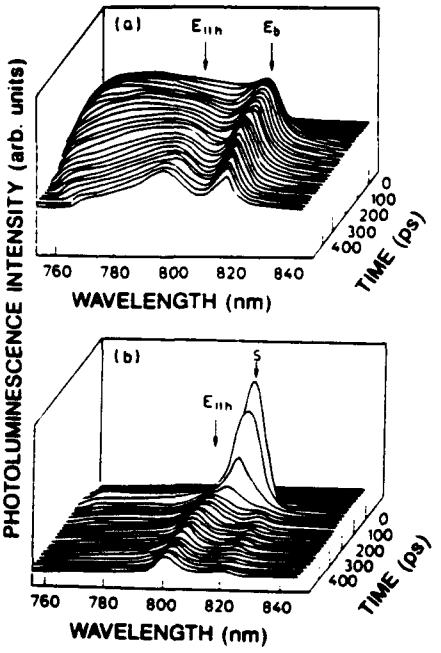


Fig.3

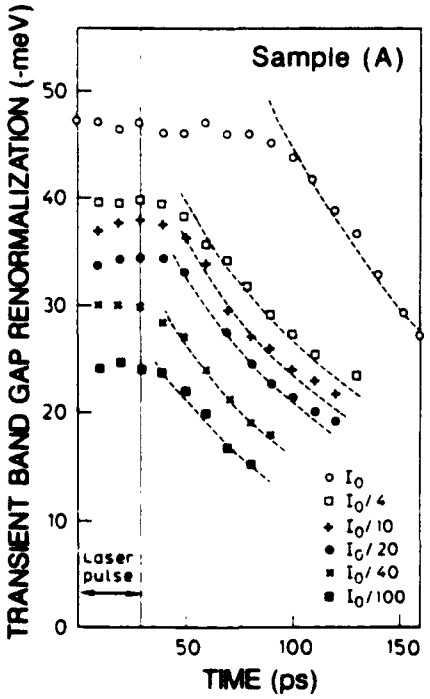


Fig.2

Fig.4

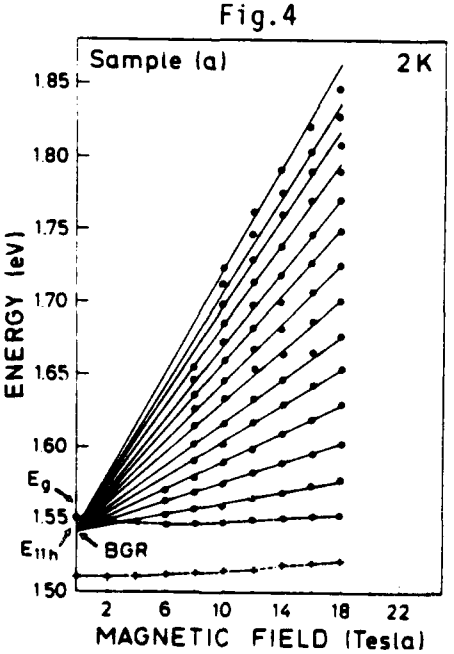
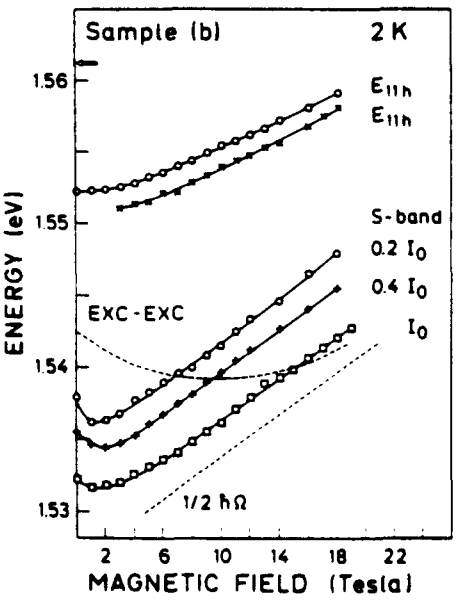


Fig.5



Quantum-Well Lasers and Amplifiers

TuC 1:30pm–3:00pm
Salon F

Y. Arakawa, *Presider*
University of Tokyo, Japan



Growth and performance of GaInP/AlGaInP visible light emitting laser-diodes.

AD-P007 847

Ad Valster and Gerard A. Acket

Philips Research Labs.

PO Box 80000, 5600 JA Eindhoven, The Netherlands

The quaternary alloy Al(x)Ga(1-x-y)In(y)P has the largest direct bandgap next to the nitrides among all III-V compound semiconductors (1). This alloy can be grown lattice matched to a GaAs substrate ($y \sim 0.5$) and spans at room temperature a direct bandgap ranging from 1.85 eV (for x=0) to about 2.25 eV (for x=0.3) at the Γ - X cross over.

To date the organometallic vapour phase epitaxy (OMVPE) technique has been demonstrated to be the most suitable growth technique for the AlGaInP alloy (2). High quality GaInP and AlGaInP bulk layers have been produced using low pressure OMVPE.

GaInP/AlGaInP double heterostructure lasers emitting in the spectral region of 660-680 nm are attractive for optical recording and as a replacement for He-Ne gas lasers in for instance laser printers and bar-code scanners. The simplest

92-22376

visible laser is a double heterostructure laser consisting of a GaInP active layer sandwiched between two AlGaInP cladding layers for optical and electrical confinement (3). Typical data are a threshold current at room temperature of 65 mA, an optical output power of 5 mW and a measured lifetime at 50 °C of more than 8000 hours, see figure 1.

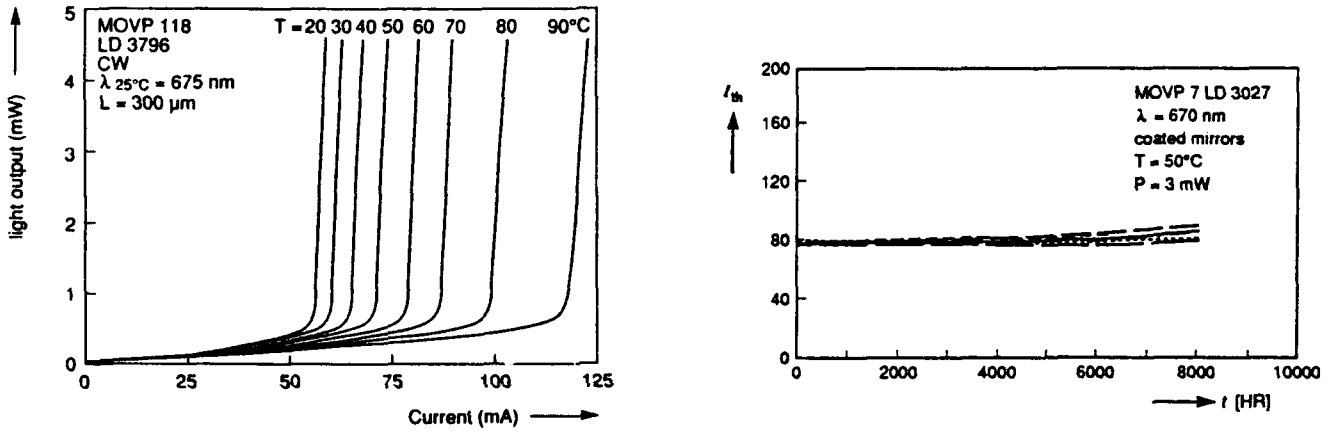


Fig. 1 Typical CW light-output vs current characteristics and APC lifetime performance of 670 nm visible lasers.

The lasing wavelength is 675 nm. A further reduction of the wavelength is attractive because of the increased sensitivity of the human eye towards shorter wavelengths. For replacement of He-Ne gas lasers it is espacially important to design laser diodes with a wavelength of 633 nm. One way to shorten the lasing wavelength is substitution

of gallium by aluminum resulting in a higher band gap quaternary active layer (4). Another way of shortening the wavelength is the use of quantum well active layers (5). These reported devices have rather high threshold currents because the band gap energy difference between the active layer and both cladding layers is reduced resulting in carrier overflow and increased threshold current (6).

An interesting and challenging phenomenon is the possibility of band gap increase over the entire AlGaInP alloy by changing the OMVPE growth conditions such as growth temperature and growth rate and the GaAs substrate misorientation (7). Optimizing above mentioned conditions the natural tendency for the formation of long range ordering in the crystal is blocked and the band gap for AlGaInP crystals is increased by an additional 100 meV.

Using this technique we reported for the the first time continuous wave operation of 633 nm light emitting laser diodes (8). The threshold current at room temperature is 80 mA and the laser diodes are CW lasing up to 45 °C. Lasers have been tested at a constant output power of 2 mW at 40 °C for more than 1000 hours showing no significant degradation. The active layer consists of GaInP wells of 50 Å separated by 40 A AlGaInP barriers.

Reducing the GaInP quantum well width to 14 Å and cooling down the laser diode to 77 K, CW laser emission at a record

low wavelength of 555 nm is demonstrated (9). This is close to the lower limit for the lasing wavelength in this alloy. In summary, this survey of the performance of visible light emitting GaInP/AlGaInP laser diodes grown by the OMVPE technique shows the still rapid improvement of research results in this field in combination with the appearance of mature diode laser device applications.

REFERENCES

1) H.C. Casey Jr. and M.B. Panish, Heterostructure lasers Part B, Academic Press, New York, 1978, 43-45

2) A. Valster, EWMOVPE III, Montpellier, France, 1989, paper IP-9.

3) A. Valster et al.,Philips J. of Research vol. 45 nos 3/4, 1990, 267-277.

4) S. Kawata et al., Electron.Lett, 23, 1987, 1327.

5) A. Valster et al., CLEO/IQEC, Anaheim, USA, 1990, paper CMC-3.

6) S.H. Hagen et al., Appl.Phys.Lett. 57,2291,1990.

7) A. Valster et al., J. Crystal Growth, to be published.

8) A. Valster et al., 12th IEEE laser conference, Davos, Switzerland,1990,paper C.1.

9) A. Valster et al., ibid,paper PD-12.

AD-P007 848

BEHAVIOUR OF A QUANTUM WELL LASER UNDER HIGH OPTICAL EXCITATION

B. DEVEAUD, F. CLEROT, S. MORIN,
Centre National d'Etudes des Télécommunications (LAB/OCM)
Route de Trégastel, 22300 LANNION FRANCE

K.FUJIWARA*,
Mitsubishi Electric Corporation, Amagasaki, Hyogo 661 JAPAN

92-22311

We have used luminescence spectroscopy with subpicosecond resolution in order to study comparatively the behaviour of quantum well (QW) laser structures with different confinement layer (CL) geometries: SCH (Separate confinement heterostructure), P- or L-GRINSCH (Parabolically or Linearly graded Index SCH). The three structures consist of a 50 Å QW with a CL of 2000 Å on each side. 600 fs long pulses at 2.04 eV, generated by an hybrid dye laser synchronously pumped by the doubled output of an YAG:Nd laser, are used to excite the sample and to detect luminescence, with a resolution equivalent to the pulse width, by upconversion in a $LiIO_3$ non linear crystal [1].

This technique allows the characterization of two processes of great interest for the behaviour of QW lasers. First the trapping dynamics of carriers into the QW which will obviously limit the high frequency operation of such devices. Second, the radiative properties of these structures under high excitation conditions (where laser action is possible provided enough feedback is put into the system).

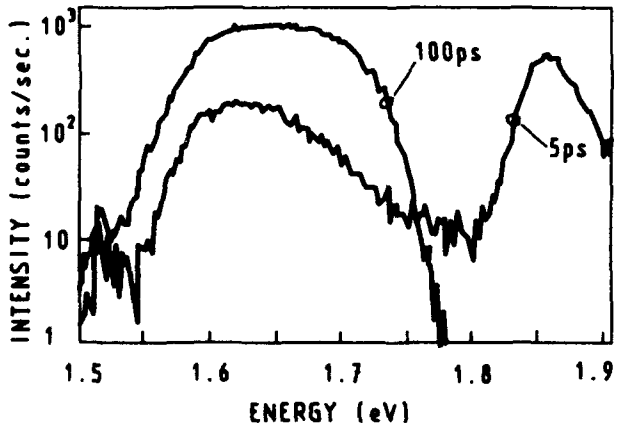


Fig.1: Luminescence spectra of a P-GRINSCH at different time delays: 5 and 100 ps.

We show on Figure 1 the luminescence spectra, obtained with subpicosecond time resolution of a P-GRINSCH (Parabolic graded Index separate confinement heterostructure structure) at two characteristic time delays (5 ps and 200 ps) after the excitation with a .01 nJ pulse. Such spectra evidence 3 luminescence bands: the first one at 1.85 eV corresponds to the luminescence of the confinement layers, the second, between 1.6 and 1.75 eV, corresponds to the 50 Å quantum well, and the third one at 1.52 eV is the luminescence of the GaAs buffer layer.

Information on the capture process of the photoexcited carriers is obtained by the study of the decay-time of the 1.85 eV band. This decay-time is very different in graded structures and in conventional SCH structures (Separate confinement heterostructures) : in the SCH the observed times range between 20 ps at 80 K and 14 ps at 190 K. As a result of the quasi-field drifting the carriers in the case of the GRINSCH structures, the observed decay times are much shorter : 2 ps at 20 K up to 9 ps at room temperature [2].

We have modelled the observed luminescence decays using a semiclassical drift-diffusion model. Our basic assumption is that the mean free path of the limiting species (holes are slower than electrons) is much shorter than the width of the CL layer, so a conventional model can be used there. Obviously, in the case of the GRINSCH structures, the observed times could not be fitted by such a description and we had to take into account a finite "quantum mechanical" trapping time at the edge of the well [3]. Capture in a quantum well is supposed to be mainly mediated by optical phonons and there have been predictions of strong resonances in the capture time [4,5,6]. The theoretically estimated trapping times would oscillate from 1 ps to 200 ps, as a function of the well width L_z. Recent experiments on multiple quantum well structures show that the capture time ranges between 650 fs and 1.2 ps [7]. We use a simple description where the carriers within 200 Å of the well are captured with a characteristic time of 1 ps [8].

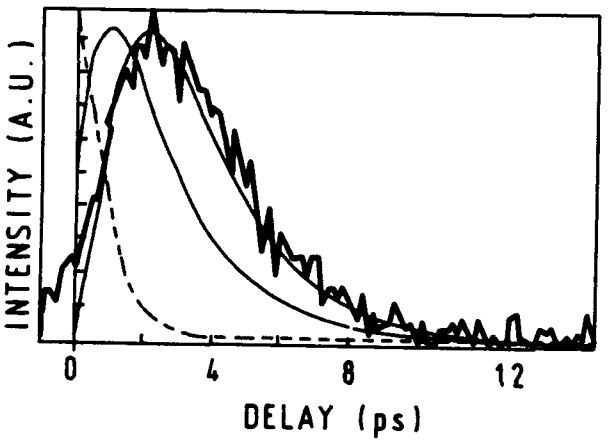


Fig.2: Decay time of the CL luminescence in a L-GRINSCH structure, together with different fits: (- -) instantaneous capture by the well, (–·–) 1 ps capture time, (—) same with intervalley scattering.

A characteristic result of such a calculation is presented on Fig. 2. Without the introduction of a finite capture time, the decay of the CL luminescence is obviously too short (dashed curve). With the 1 ps capture time, the decay time is quite well reproduced, but the curve is shifted towards the origin by about 1 ps. One of the advantages of the upconversion technique being the very precise determination of the zero time delay (within less than 100 fs [1]), such a discrepancy cannot be accepted. The only way to overcome this difficulty is to take into account the fact that we inject electrons at an energy where they transfer first to the L valley before coming back to the c valley [9]. This gives the full curve of Fig.2.

As excitation conditions in the GRINSCHs and in the SCH are not equivalent (the width excited at the laser energy being different), we have used our model to compare theoretically the two structures. If we inject a delta distribution of carriers at the edge of the CL, at room temperature, the time taken by 90 % of the carriers to get trapped in the well is 4 times longer in a SCH than in a GRINSCH (70 ps against 17.5 ps). This difference might allow GRINSCH structures to run faster than SCHs.

After capture into the well, the electrons and the hole form a very high density plasma : at an average power of 3 mW, we inject about 6×10^{12} cm^{-2} carriers into the well. This allows to study the properties of a plasma in a single QW, with a rather cold temperature. Difficulties raised by the usual procedure of luminescence lineshape fitting have been pointed out by Maan et al. [10]. The advantages of our system are the following:

i) we are able to obtain a very high density plasma (up to 5×10^{12} cm^{-2}), at a quite cold temperature (of the order of 50 K).

ii) This plasma has a well defined density as we only have one quantum well, our spectra are not time averaged, the time resolution is short compared to the radiative recombination rate even at the highest density, and we only probe the central part (about 5 µm in diameter) of the excited spot (about 30 µm in diameter).

iii) Reabsorption effects as well as stimulated emission [11] can be neglected in our configuration. We are not sure that diffusion effects can be neglected, but they have a negligible contribution over our time window of less than 1 ps.

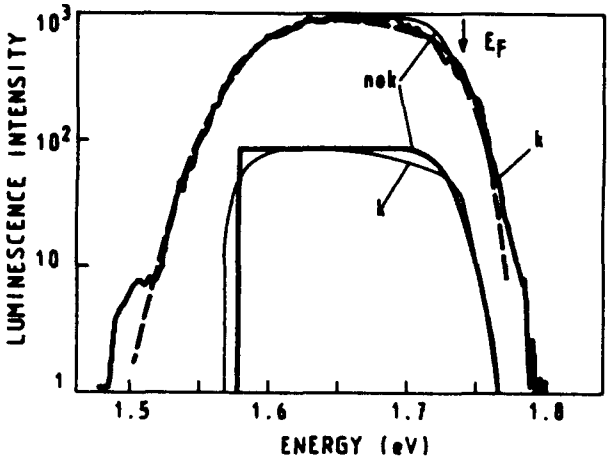


Fig.3: Luminescence spectrum of a 4.2×10^{12} cm^{-2} plasma. Fits assuming or not conservation of the k selection rule are shown. The corresponding unbroadened spectra are displaced by one decade.

The spectra that we observe are characteristic of the two dimensional density of states of the QW (the width of 50 Å only allows for one confined level). As expected, we obtain a rather rectangular shape with a broadened high energy side due to temperature effects. We also observe a very strong broadening on the low energy side of the spectrum, which has been observed by many teams [12], and attributed to the very short lifetime of the carriers [13]. Including such a broadening in the calculation, it is quite easy to obtain a reasonable fit of the observed spectra as shown on Fig. 3. The semilog plot evidences that this broadening is Gaussian and not Lorenzian.

We shall only detail here a few consequences of our observations. First, due to the small effective mass of light holes and to their smaller transition matrix element, their contribution in the spectra is not resolved. Our description will then only take into account the electron-heavy hole transitions. As is evidenced on Fig.3, the shape of the curve with or without relaxation of the k-selection rule is not very different. As a matter of fact, the strong lifetime broadening washes out the differences one would expect in the case of unbroadened spectra (see the lower part of Fig.3).

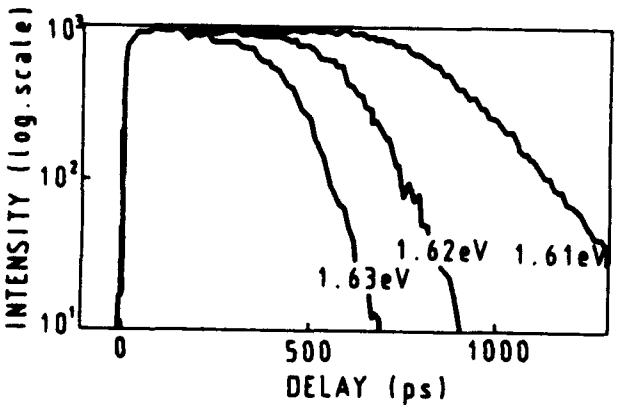


Fig.4: Decay curves of the QW luminescence at different energies above the band edge. The constancy of the signal is a direct demonstration of k-selection rule.

We are however able to state that k-selection rule is conserved up to the highest density used in our experiments. The argument is quite simple: Fig.4 shows the time behaviour of the luminescence intensity at a given energy above the bottom of the band. In the case of k- selection rule, the intensity should be constant for a degenerate plasma at low temperature (as is indeed observed). If the selection rule is lifted, the number of possible transition at a given energy is proportional to the plasma density. This should give rise to a decrease of about 30% over 100 ps, contrary to the experimental observations.

As far as the Band Gap Renormalization (BGR) is concerned, the situation is quite complex. The simple fitting procedure used by most authors includes a Lorenzian broadening. It is very clear from our semilog plot that the low energy tail is very different

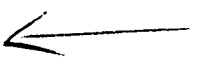
from a Lorenzian and would be closer to a Gaussian shape. This has already been pointed out by different authors [14,15]. As the value of the BGR is very dependant from the precise fit of the low energy edge of the spectrum, we have decided to use a Gaussian enlargement which gives a much better fit to this low energy edge. The result of our fitting procedure is that, between $5x10^{11}$ and $5x10^{12}$ cm^{-2} plasma density, we do not obtain a sizeable BGR (we estimate our experimental precision at about $\pm$ 5 meV. This does not tell us that BGR does not exist because, our fitting procedure is obviously too simple. However, it is obvious from these result that only a complete many body calculation can give a reasonable answer to this problem. In particular, such a calculation has to explain why should the low energy edge be Gaussian rather than Lorenzian. Although an approach to the answer has been proposed by Asada [14], his broadening factors are still unable to fit our spectra.

Aknowledgments:

The authors are indebted to A. Chomette, B. Lambert and A. Regreny for useful discussions, M. Otha and K. Mitsunaga for their growing the samples. We would also like to thank P.Georges and F.Salin for their invaluable help in setting up the laser system, and Coherent for the loan of the double jet dye laser.

References :

[1] J. Shah, T.C. Damen, B. Deveaud, D. Block, *Appl. Phys. Lett.*, **50**, 1307 (1987)
[2] B. Deveaud, F. Clérot, A. Regreny, K. Fujiwara, K. Mitsunaga, J. Ohta, *Appl. Phys. Lett.*, **55**, 2646 (1989)
[3] B. Deveaud, T.C. Damen, J. Shah, W.T. Tsang, *Appl. Phys. Lett.*, **52**, 1886 (1988)
[4] J.A. Brum and G. Bastard, *Phys. Rev.*, **B33**,1420 (1986).
[5] J.A. Brum, T. Weil, J. Nagle, B. Vinter, *Phys. Rev.*, **B34**, 2381 (1986)
[6] M. Babiker and B.K. Ridley, *Superlatt. Microstruct.*, **2**, 287 (1986)
[7] B. Deveaud, *20th Int. Conf. on the Physics of Semiconductors*, Thessaloniki (1990) to be published
[8] S. Morin, B. Deveaud, F. Clérot, K. Fujiwara, submitted to IEEE J-QE
[9] J.Shah, B.Deveaud, T.C.Damen, W.T.Tsang, A.C.Gossard, P.Lugli, *Phys. Rev. Lett.*, **59**, 2222(1987).
[10] J.C. Maan, M. Potemski, K. Ploog, G. Weimann, Proc. 6th Winterschool on Semiconductor Physics, Ed. G. Bauer, F. Kuchar, H. Heinrich, Springer Series on Solid State Sciences, to be published.
[11] R. Cingolani, K. Ploog, A. Cingolani, C. Moro, M. Ferrara, *Phys. Rev.* B42, 2893 (1990)
[12] See for example: G. Tränkle, H. Leier, A. Forchel, H. Haug, C. Ell, G. Weimann, *Phys. Rev. Lett.*, 58, 419 (1987); G. Tränkle et al *Phys. Rev.* B36, 6712 (1987)
[13] P.T. Landsberg, D.J. Robbins, *Solid State Electron.*, 28, 137 (1985)
[14] Asada, *IEEE Quantum Electron.*, QE29, (1989)
[15] G. Bongiovanni, J.L. Staehli, D. Martin, *Phys. Stat. Sol.* B150, 685 (1988)



Excitonic Gain, Laser Action, and the Role of Many-Body Effects in ZnSe-based Quantum Wells

J. Ding, H. Jeon, T. Ishihara*, and A.V. Nurmikko
Division of Engineering and Department of Physics
Brown University, Providence, RI 02912
(401)863-2869

AD-P007 849



H. Luo, N. Samarth, and J. Furdyna
Department of Physics
University of Notre Dame, Notre Dame, IN 46556

Summary

Among potential applications of wide-gap II-VI compound semiconductor quantum wells (QW) and superlattices at short visible wavelengths are lasers and nonlinear optical devices. Substantial progress has been recently made with ZnSe-based heterostructures; in particular (Zn,Cd)Se/ZnSe QW's have shown pulsed room temperature laser action in optical pumping experiments in both multiple and single well structures [1],[2]. At the same time, these QW's have also been found to display strong excitonic absorption features ($\alpha > 10^5$ cm^{-1}), which are well preserved up to room temperature [3] and beyond. This raises the question about the origin of the gain for lasers, that is, the role of Coulomb effects when compared to the usual inversion from an electron-hole plasma encountered e.g. in GaAs quantum well lasers. Here we show initial results of pump-probe experiments and laser studies which indicate the presence of excitonic gain up to temperatures at least as high as 200 K. Moreover, with increasing pair density, the gain evolves directly from saturation of the excitonic gain in the (Zn,Cd)Se/ZnSe quantum wells.

The upper portion of **Figure 1** shows the low temperature exciton absorption coefficient of a $Zn_{1-x}Cd_xSe$/ZnSe MQW ($x \approx 0.24$) sample which contained six wells of 35 Å thickness. In

92-22378



this part of our experiments, the transmission of a continuum dye laser probe through the MQW is measured under steady-state conditions (nsec pulses) under different pump excitation levels. The pump photon energy is above the bandgap of the ZnSe barrier layers. For laser experiments we also prepared cleaved structures, for which lasing through the end facets occurred at rather low pumping intensities in the low temeparture regime ($< 1 kW/cm^2$).

In the absence of the pump excitation (topmost trace in Fig. 1), the probe spectrum displays the characteristic excitonic absorption of (Zn,Cd)Se/ZnSe quantum wells (the n=1 heavy-hole 1S). The exciton Bohr radius in bulk ZnSe is approximately 40 Å so that this sample approximates a 2-D case. With increasing excitation level, the absorption saturates at about 30 kW/cm^2, followed by the appearance of a relatively narrow gain spectrum at the 1S exciton energy. This is shown in Fig. 1 by the amplified spontaneous emission (ASE) spectrum. The ASE effects turn on readily in uncleaved samples even for lateral gain lengths less than 100 μm. The gain as well asl the lasing in cleaved structures occurs, however, at a well defined resonance approximately 25 meV below the n=1 exciton peak (and remains unshifted over at least one order of magnitude in excitation intensity). Furthermore, the gain is preceded an induced absorption feature in this spectral range.

Figure 2 shows the relationship between the spectral position of the n=1 HH exciton absorption (unexcited MQW sample) and laser emission (photopumped, cleaved MQW sample) at several different temperatures. The stimulated emission (and gain in pump-probe experiments) occurs consistently below the exciton absorption edge as at T= 10K, and turns on following the saturation of this absorption. Only near room temperature does the stimulated emission spectrum approach that of the exciton absorption.

We have also found gain and stimulated emission effects which are closely tied to exciton absorption and its saturation in **single** quantum well structures. There are instances where gain at the n=1 HH exciton position is also avaialable for stimulated emission.

One possible interpretation of the behavior in Figures 1 and 2 is the presence of excitonic

molecules in these quasi-2D circumstances. In this interpretation, the development of significant gain at the expense of the saturating exciton shows that the electron-hole system retains a strongly Coulombic character at excess pair densities which are well below the plasma transition, unlike the case in most semiconductor quantum well systems studied to date. The stability of an excitonic molecule with a binding energy of the order of 20 meV is not wholly unexpected near the 2D limit; what is surprising, however, is the persistence of the effects at higher temperatures. The saturation of absorption occurs by phase space filling, hence reducing the absorption losses. Finally, the estimated pair density at the onset of gain (saturation of absorption) is approximately $3x10^{12}$ cm^{-2}, below the insulator-metal transition.

The research at Brown University and the University of Notre Dame was supported by the Defense Advanced Projects Agency, under the University Research Initiative program (N00014-90-J-1582). The work at Brown and Notre Dame was also supported by the National Science Foundation (at Brown ECS-8916026; at Notre Dame DMR-89-13706).

*On leave from Tohoku University, Sendai, Japan

References:

[1] H. Jeon, J. Ding, A.V. Nurmikko, H. Luo, N. Samarth, and J. Furdyna, Appl. Phys. Lett. Dec 17, 1990

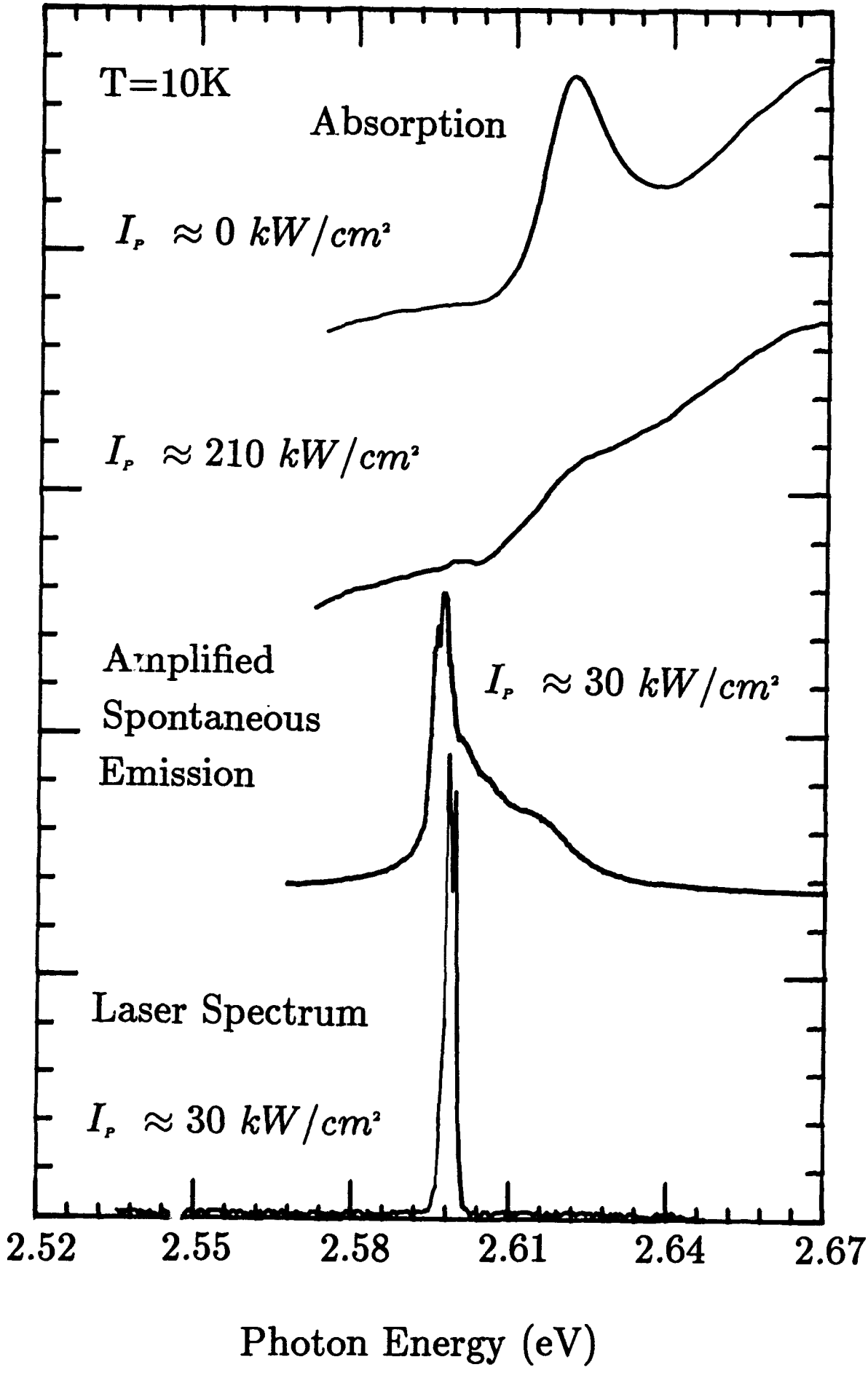
[2] J. Ding, H. Jeon, A.V. Nurmikko, H. Luo, N. Samarth, and J. Furdyna, Appl. Phys. Lett. Dec 24, 1990

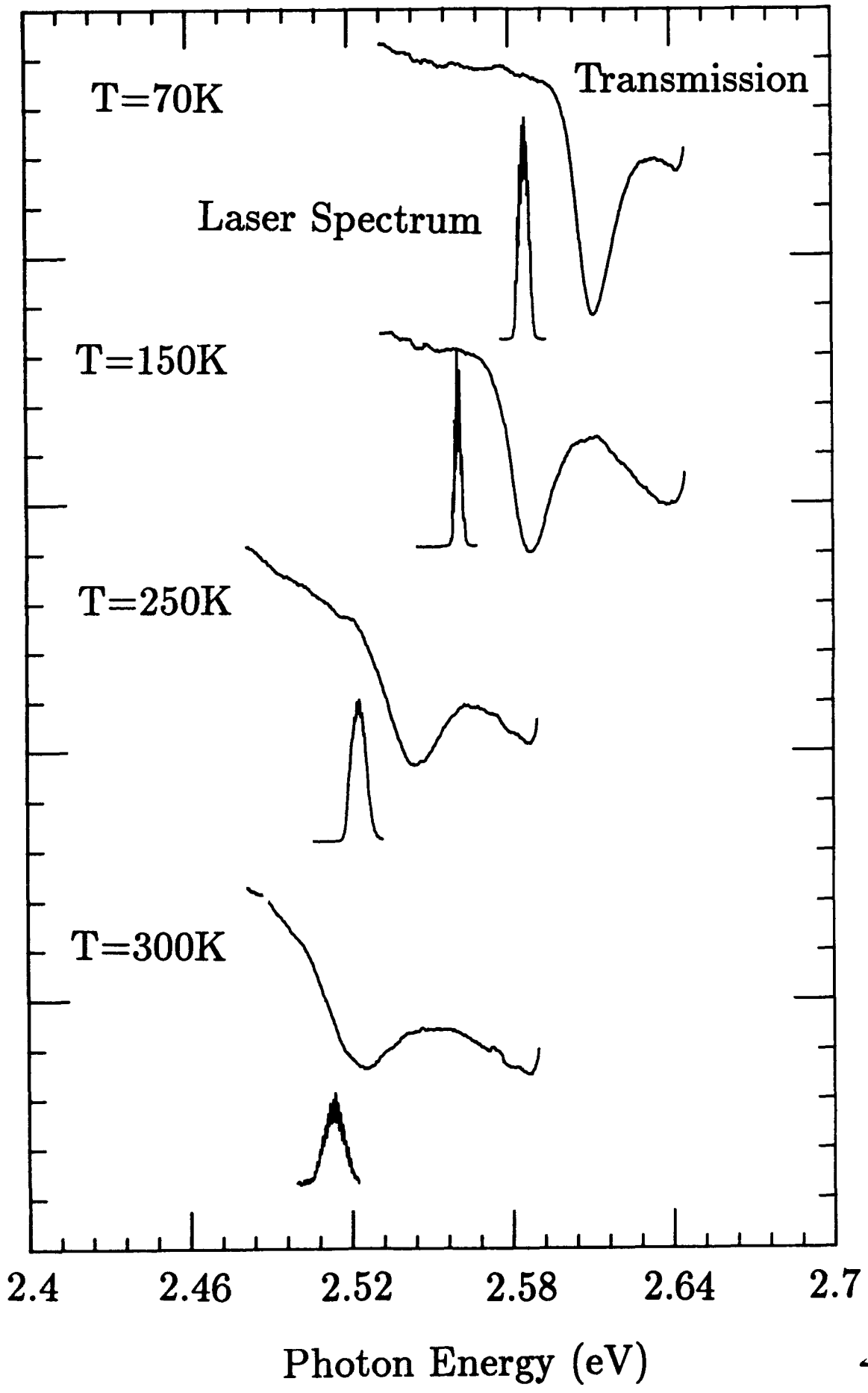
[3] J. Ding, N. Pelekanos, A.V. Nurmikko, H. Luo, N. Samarth, and J. Furdyna, Appl. Phys. Lett. Dec 31, 1990

Figure Captions:

Figure 1: Absorption coefficient of a (Zn,Cd)Se/ZnSe MQW structure composed of six 35 Å wide wells at T=10K, in the absence and presence of pump excitation (uper traces). The lower traces show the gain (in form of amplified spontaneous emission) and laser spectra.

Figure 2: Comparison of exciton absorption (shown as transmission spectrum) of unexcited MQW and the laser spectra in optically pumped MQW sample at four different temperatures.


T=10K
Absorption
$I_p \approx 0\ kW/cm^2$
$I_p \approx 210\ kW/cm^2$
Amplified
Spontaneous
Emission
$I_p \approx 30\ kW/cm^2$
Laser Spectrum
$I_p \approx 30\ kW/cm^2$
2.52
2.55
2.58
2.61
2.64
2.67
Photon Energy (eV)


T=70K
Transmission
Laser Spectrum
T=150K
T=250K
T=300K
2.4
2.46
2.52
2.58
2.64
2.7
Photon Energy (eV)

AD-P007 850

Pulsewidth-Dependent Self Phase Modulation in Semiconductor Traveling Wave Amplifiers

P. J. Delfyett[1], Y. Silberberg[1], G. Alphonse[2].

1) Bellcore, 331 Newman Springs Rd., Red Bank, N.J. 07701
2) David Sarnoff Research Center, Princeton, N.J., 08543

Introduction

In this work, we show a pulsewidth dependent self-phase modulation (SPM) of optical pulses in semiconductor traveling wave amplifiers due to nonlinear gain depletion and hot carrier thermalization, termed as the dynamic carrier cooling effect {1}. The dynamic carrier cooling effect can be observed as a fast (~ 1 psec) partial recovery of the gain of a semiconductor traveling wave amplifier when a femtosecond optical pulse propagates through the device. While SPM due to gain depletion has been observed before {2}, this is the first observation of SPM due to the dynamic carrier cooling effect.

Experimental Method

The optical pulses employed in the experiment were obtained from a hybrid mode locked external cavity semiconductor laser system {3}. The system is composed of 3 main components: a low power master oscillator, a high power single pass semiconductor traveling wave amplifier, and a dual grating compressor, which compensates for optical chirp impressed upon the oscillator pulse during the mode locking process. The laser system produces optical pulses which can be varied from 460 fsec to several picoseconds. The average output power, repetition rate and emission wavelength are 10 mW, 302 MHz, and 830 nm, respectively. The average power from the laser system translates to over 70 watts of peak power for the shortest pulses, which makes the pulses produced from this system both the shortest and most intense ever produced from an all semiconductor laser system.

Two types of experiments were performed to observe and verify the pulsewidth dependent optical nonlinearity induced by the carrier cooling effect. The first type employs single beams in which the optical pulsewidth could be varied from 460 fsec to 5 psec. These pulses were then injected into a semiconductor traveling wave amplifier operating in the gain regime. The corresponding amplified pulse spectra were then measured with weak and strong optical injection into the traveling wave amplifier. The second type of experiment employs dual beams in a standard time resolved pump-probe geometry, where time-resolved gain dynamics and time-resolved spectra could be measured.

Experimental Results

The experimental results of the single pulse experiments are summarized in Fig. 1. In Fig. 1(a), the input optical pulse spectra is shown. With low optical injection (< 1mW), the amplified optical spectrum replicates the input spectrum independent of input pulse duration. With high optical injection, the amplified pulse spectrum is severely distorted. In Fig. 1(b), the output amplified optical pulse spectrum is shown for the case of an input pulse duration of 460 fsec and an input average power of 5 mW. There are clearly two distinct spectral peaks which occur on both the high and low energy sides of the amplified pulse spectrum.

In Fig. 1(c), the output amplified optical pulse spectrum is shown for the case when the input optical pulse duration is 2 psec with an average power of 5 mW. This spectra shows a distinct peak on the low energy side of the spectrum, while the high energy side is completely absent of any spectral peak. Summarizing the single beam experiments we see that under high injection power, the amplified optical pulse spectrum is severely distorted, where the spectral distortion is highly pulsewidth dependent. The two regimes can be classified as spectral distortion which occurs when the input pulse duration is less 1 psec, and spectral distortion which occurs when the input pulse duration is greater than 1 psec.

92-22379

In order to obtain a clearer understanding of the pulsewidth dependent spectral distortion process, the time resolved gain dynamics were measured with short pulses (~ 560 fsec) and then with long pulses (~ 2 psec). The results of these experiments are summarized in Fig. 2(a,b). In Fig. 2(a), a plot of the gain of the probe pulse is plotted with respect to the time delay of the pump pulse for the case of an input pulse duration of 0.56 psec. The salient features of the gain dynamics in this case are the rapid depletion of the probe gain near $t = 0$, the fast (~ 1.5 psec) partial recovery of the gain, and then the slow gain recovery. The fast partial recovery is due to the dynamic carrier cooling effect, while the slow recovery is the normal carrier recovery. The gain dynamics in this case sharply contrast the results which are obtained when the input pulse duration is 2 psec. In Fig. 2(b), the gain dynamics of the traveling wave amplifier are shown for the case when the input optical pulse duration is 2 psec. The salient feature of the gain dynamics in this case is the step-like response of the probe gain, which is the normal gain depletion and carrier recovery. The dynamic carrier cooling effect does not play a major role in the gain dynamics for pulses longer than 2 psec.

Discussion

The gain dynamics play an important role in the pulse width dependent spectral distortion of optical pulses in traveling wave amplifiers. The results shown here can be explained in terms of self phase modulation occurring during the gain depletion and partial recovery. The experimental data points to the fact that gain depletion removes carriers due to stimulated emission. This causes a raise in the refractive index due to the plasma effect, and causes a red shift in the spectrum due to self phase modulation. Dynamic carrier cooling replenishes the gain, thus reducing the refractive index and causes a blue shift. In order to confirm these results, experiments were performed to time-resolve the spectral distortion of a probe pulse. The setup is identical to the setup employed for the pump probe gain dynamics, except that instead of the light being directed into a power detector, the light was directed into a spectrometer with a diode array readout. With this configuration, the spectrum of the probe pulse can be observed at various time delays between the pump and probe pulses.

In Fig. 3(a,b), plot of the time resolved probe spectra are shown for the short pulse and long pulse regimes, respectively. In Fig. 3(b), a definite red shift is observed in the peak of the amplified probe pulse spectra. At maximum gain depletion, the center frequency has returned to the original wavelength. In Fig. 3(a), one observes a red shift at early times with a simultaneous reduction of the intensity of the probe spectra. At maximum gain depletion, the peak of the probe spectra returns to the original carrier position, which immediately shifts towards the high energy side of the spectrum. This blue peak is then observed to increase in intensity as the gain recovers, and the peak is also seen to return back to the original carrier frequency. The data shown in Fig. 3(a,b) confirm the physical mechanisms responsible for the spectral distortions obtained in both the short and long pulse regimes.

Summary

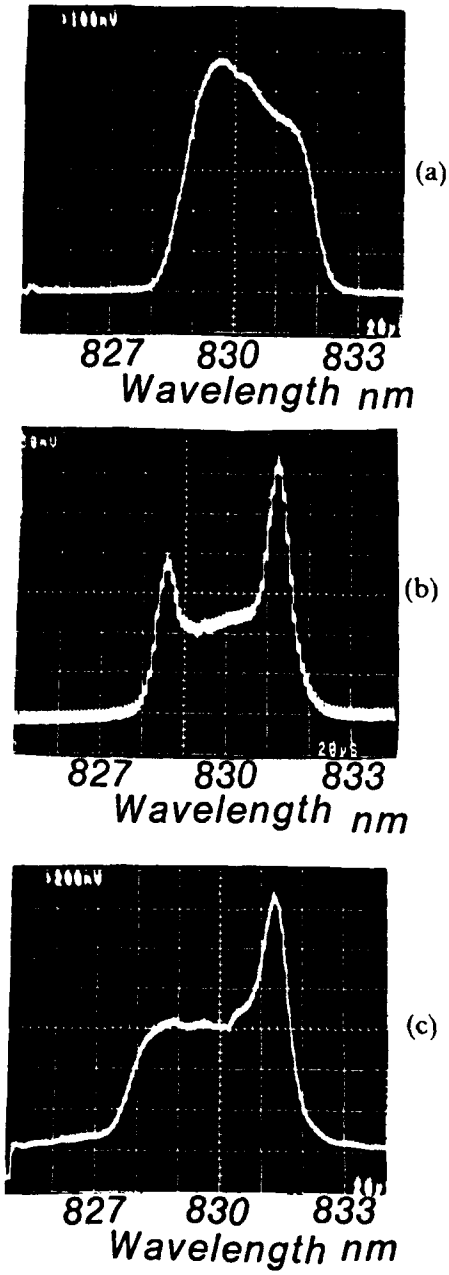
Pulsewidth dependent spectral distortion of picosecond and sub-picosecond optical pulses in traveling wave amplifiers was obtained with high injection intensity. The physical mechanisms responsible for the spectral distortion are both gain depletion, and hot carrier thermalization, which leads to self phase modulation of the optical pulse. The experimental results shown here are the first to our knowledge which show the effect of hot carrier thermalization on the self phase modulation of femtosecond optical pulses in semiconductor traveling wave amplifiers. Time-resolved spectra of the ultrafast gain dynamics were measured to support the experimental findings.

References

{1} K.L. Hall, J. Mark, E.P. Ippen, and G. Eisenstein, Appl. Phys. Lett., vol 56, pg. 1740, (1990)

{2} N.A. Olssen and G.P. Agrawal, Appl. Phys. Lett., vol 55, pg 13, (1989)

{3} P.J. Delfyett, C.-H. Lee, L. Florez, N. Stoffel, T. Gmitter, N. Andreadakis, G. Alphonse, and J. Connolly, (accepted for publication in Optics Letters)



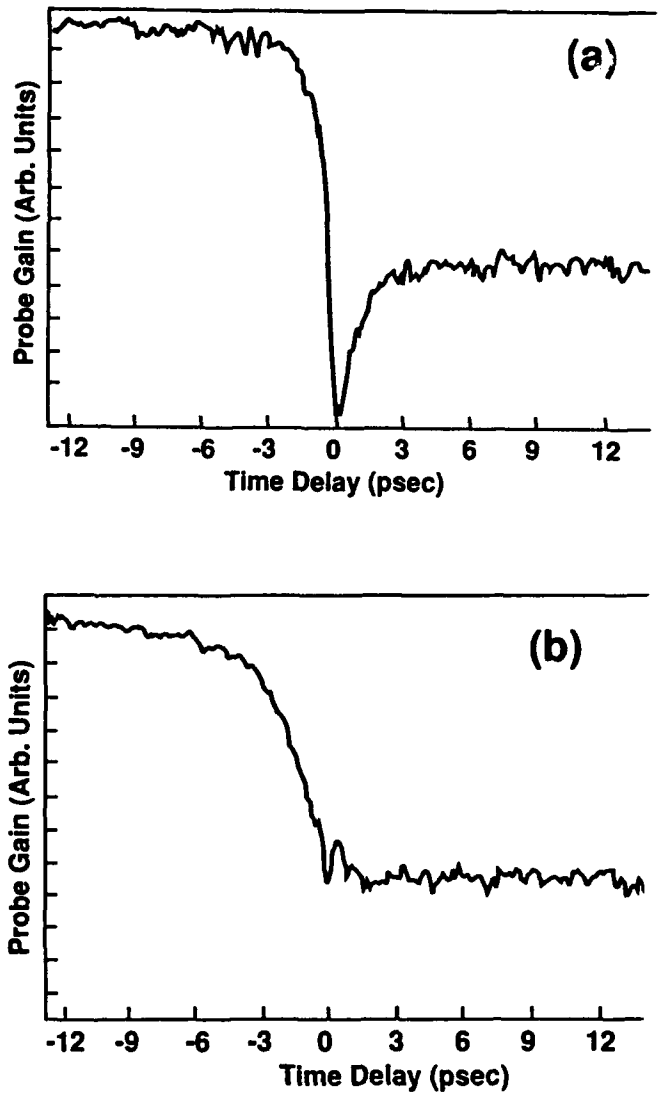


Fig.{2}Gain dynamics obtained from time resolved pump probe measurements for (a) input pulse widths of 560 fsec, and (b) input pulse widths of 2 psec.

Fig.{1}From top to bottom:
(a) Input optical spectrum to the traveling wave amplifier
(b) Output optical spectrum from the TWA with a 460 fsec input pulse.
(c) Output optical pulse spectrum from the TWA with a 2 psec input pulse.

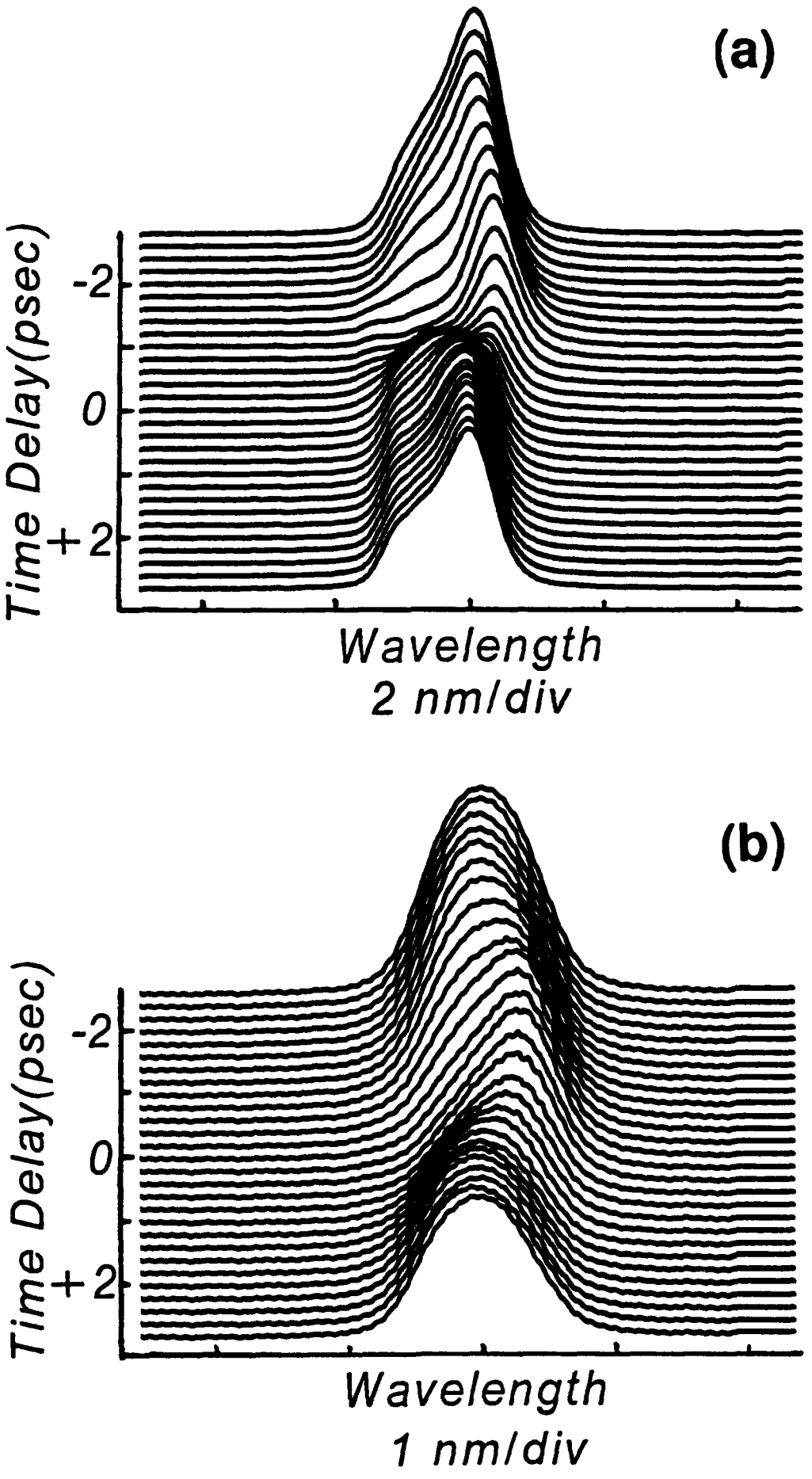


Fig.{3}Time resolved spectra of the probe pulse for (a) input pulses of 560 fsec, and (b) input pulses of 2 psec.

AD-P007 851

Femtosecond Gain Dynamics in Semiconductors

W. S. Fu,[a] G. E. Poirier, R. P. Bryan, J. F. Klem, and G. R. Olbright

Sandia National Laboratories,[b] *Albuquerque, New Mexico 87185*

92-22380

A. Paul, R. Binder and S. W. Koch

Optical Sciences Center and Physics Department, University of Arizona, Tucson, AZ 85721

J. S. Harris Jr.

Solid State Electronics Laboratory, Department of Electrical Engineering

Stanford University, Stanford, CA 94305

The fundamental study of semiconductor gain dynamics is crucial to the understanding of electron-hole-pair excitation dynamics and semiconductor lasers. While there have been numerous experimental and theoretical investigations of absorption dynamics, relatively few dynamical gain studies have been reported. One of the first time-resolved gain measurements examined focused primarily on hot-carrier relaxation in wide GaAs quantum wells (QWs).[1] In this paper we describe the complete temporal evolution of gain in narrow GaAs/$Al_{0.45}Ga_{0.55}As$ quantum wells. Using femtosecond pump/probe spectroscopy we have measured the development and subsequent decay (recovery) of gain (absorption). We present a detailed investigation of the exciton bleaching followed by gain buildup and decay. These optical nonlinearities are discussed in terms of phase-space filling, screening and thermalization of carriers. The observed ultrafast (< 400 fs) gain decay is explained in terms of plasma-expansion.

We performed femtosecond pump/probe absorption spectroscopy on a 55-period GaAs(23 Å)/$Al_{0.45}Ga_{0.55}As$(100 Å) quantum-well structure grown by molecular beam epitaxy. Pump pulses 100-fs in duration at an energy of 1.96 eV and a time-correlated white-light continuum probe were used to collect time-resolved nonlinear absorption spectra. We present these spectra in Fig .1 (the linear spectrum is labeled -1.0 ps and reveals the heavy-hole (HH) and light-hole (LH) excitons). Immediately following excitation we observe a spectral hole in the vicinity of the pump (see Fig. 1a; spectrum labeled +0.3 ps) due to phase-space filling followed by thermalization of the carriers and which eventually leads to gain. Dramatic changes are observed in the spectra: for example, in the spectra labeled +0.9 ps and +1.5 ps, the time-dependent buildup of the population inversion and the reduction of the bandgap are clearly resolved. These effects can be seen by comparing the onset of absorption at 1.699 eV and 1.758 eV for the +0.9 ps and -1.0 ps curves, respectively, and the crossover from gain to absorption at 1.764 eV for the +1.5 ps spectrum (this gain bandwidth of 65 meV corresponds to a carrier density of $N \simeq 3 \times 10^{12}$ cm^{-2}).

In Fig. 1b we present spectra which show the full temporal evolution of gain decay. In these spectra we observe an ultrafast gain decay which occurs from 1.5 ps to 3.0 ps followed by substantially slower gain decay components. We analyzed the gain decay more carefully using single-wavelength detection at the peak of the gain as a function of pump/probe delay. In Fig. 2a we present a single-wavelength (1.746 eV) time scan which shows the initial rapid decay of the gain and the much slower decay component. The slow time component shows $\simeq$ 10 ps exponential decay and has been attributed to stimulated emission in GaAs/AlGaAs QWs.[2] The expanded time scan shown in

Fig. 2b (heavy-solid line) isolates the ultrafast decay component. We also observe a transient increase in the absorption which occurs ~+0.8 ps after excitation and persists for only ~100 fs which most likely arises from competition between gain and bandgap renormalization. The density-dependence of this ultrafast gain decay is also shown in Fig. 2b. We observe an increase in the ultrafast decay time and a delayed onset of gain decay with decreasing carrier density. The power-dependent ultrafast gain decay might be evidence of high-density plasma expansion. Calculations of ambipolar transport for high-density electron and hole plasmas predict ultrafast plasma expansion with supersonic velocities.[3] Plasma expansion can lead to fast plasma cooling, reduction of the quasi-chemical potential energy and a density-dependent ambipolar diffusion coefficient. Furthermore we examined the effects of spatial plasma confinement by repeating the experiments on 100-μm-diameter mesas. We used reactive-ion etching to define mesas, and then removed the underlying GaAs substrate leaving mesas attached to a sapphire substrate. We repeated the above experiments on mesas and at even four-times-higher excitation power, we observed a decrease in the decay time and an increase in the gain threshold. These results indicate an ultrafast surface-recombination velocity again consistent with ultrafast plasma expansion.

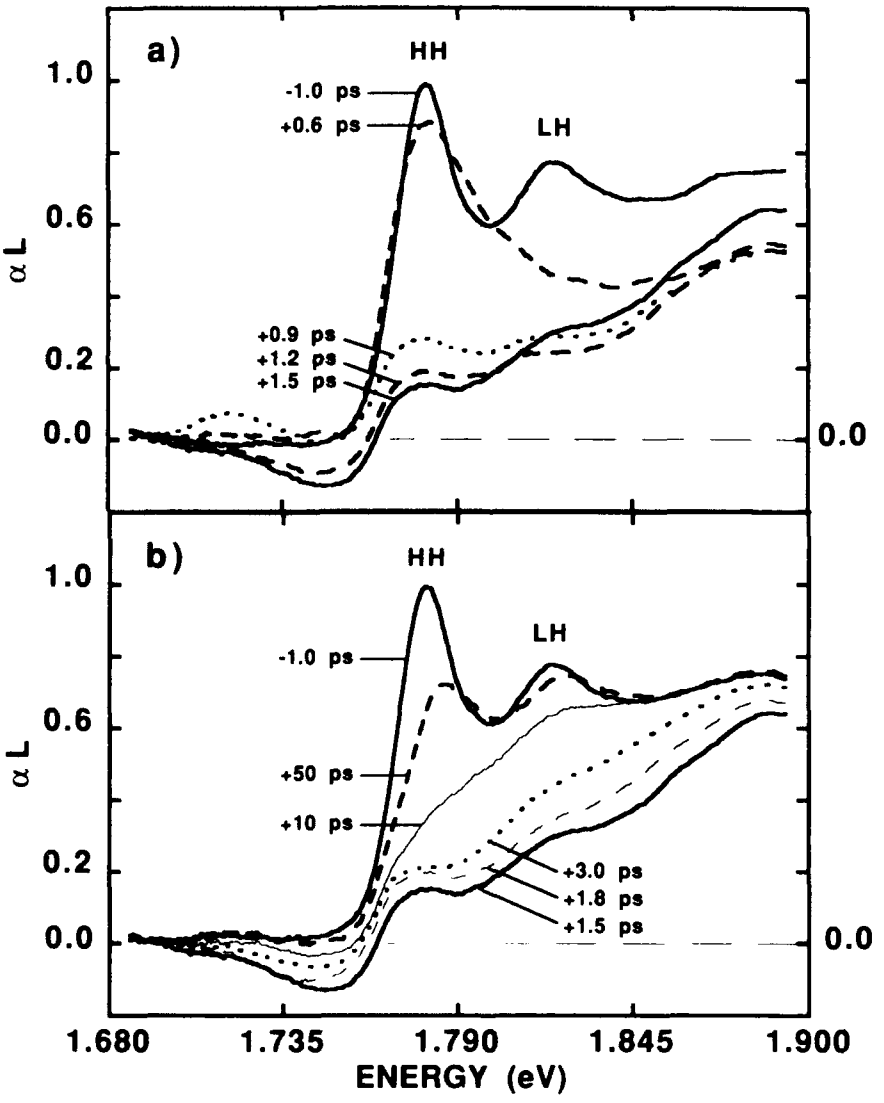


Figure 1. Time-dependent nonlinear absorption/gain spectra for pump/probe delays (a) $\leq$ 1.5 ps and (b) > 1.5 ps (E_{exc} = 1.96 eV, P_{exc} = 180 μW, pump diameter = 120 μm, f = 8.2 kHz, T = 15 K).

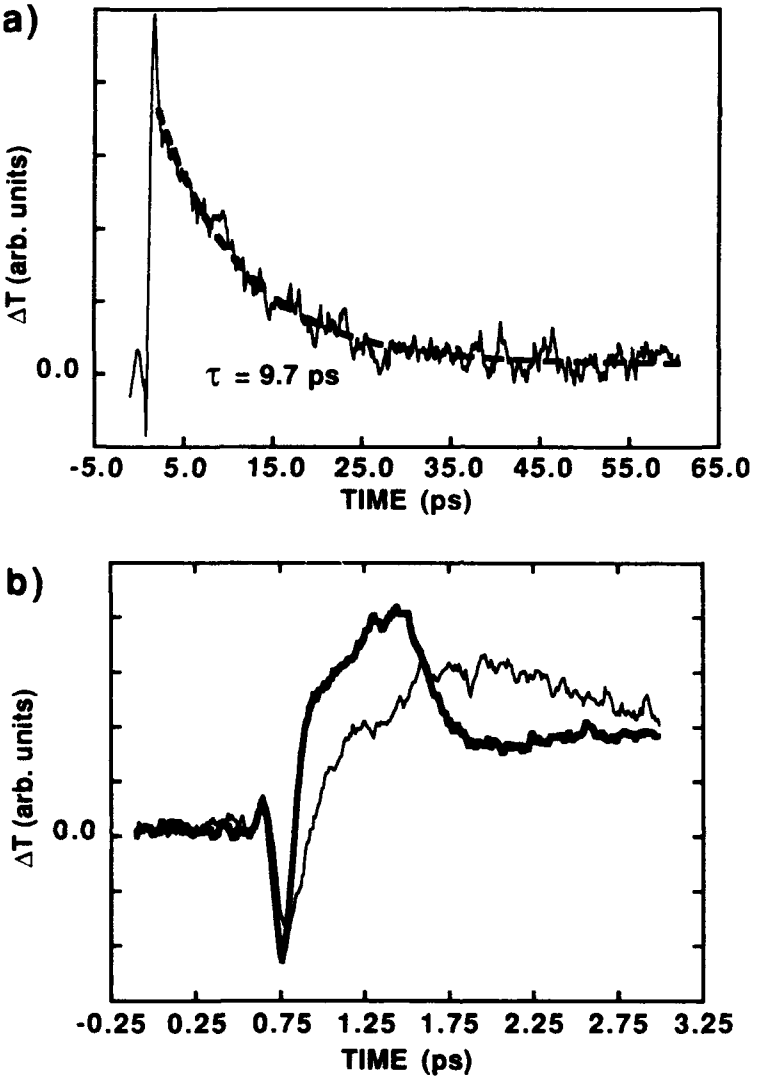


Figure 2. Single-wavelength time scans of the differential transmission ΔT a) 65 ps scan at P =180 μW, b) normalized 3.25 ps scan at P_{exc} = 110 μW (light solid) and P_{exc} = 180 μW (heavy solid). Detection energy = 1.746 eV, other experimental parameters same as in Fig. 1.

To theoretically analyze ultrafast gain dynamics in semiconductors, we numerically solved the semiconductor Bloch equations and included the relevant exchange and dynamic screening effects.[5] Fig. 3 shows examples of our computed absorption spectra for parameters corresponding to bulk GaAs under femtosecond excitation at 10 E_R above the unrenormalized bandgap (E_R = 4.2 meV is the exciton binding energy). The different curves in Fig. 3 show the probe absorption spectra for pump-probe overlap (0 fs delay), as well as for +500 fs, +1.0 ps and +2.0 ps probe delay, respectively. For pump-probe overlap one sees the spectral hole burned around the pump frequency, the bleaching of the exciton resonance, as well as bandgap renormalization leading to increasing absorption in the spectral region below the unrenormalized gap. This increasing absorption vanishes for positive time delays as the carrier populations relax down to the band minima. In the vicinity of +1.0 ps after excitation, one clearly sees the development of optical gain. Our calculations of the gain spectra for bulk GaAs show qualitative agreement with the experimental gain data for GaAs quantum wells, indicating that quantum-confinement effects do not have a large influence on the gain dynamics.

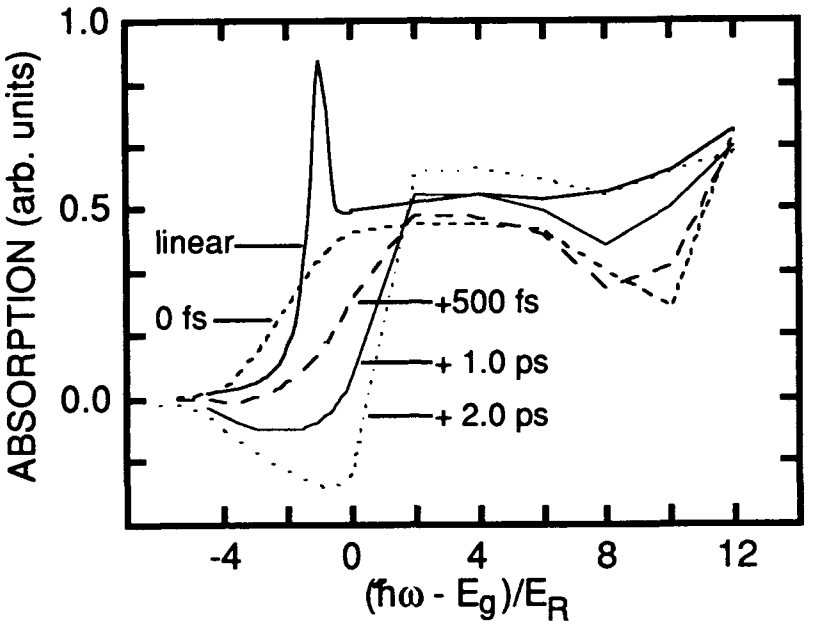


Figure 3. Calculated carrier-density-dependent absorption spectra computed for bulk GaAs at various pump probe delays. (injected density $2x10^{18}$ cm^{-3}, T= 15 K).

In summary we investigated the full temporal evolution of gain/absorption spectra in GaAs. We observed the development of absorption saturation and its recovery as well as gain and its decay. We also observed an ultrafast femtosecond gain decay consistent with ultrafast plasma expansion effects.

The Arizona group acknowledges support from NSF, SNL, JSOP, OCC and the Pittsburgh Supercomputer Center.

[a] Solid State Electronics Laboratories, Stanford University, Stanford, CA 94305.

[b] SNL research supported by DOE contract No. DE-ACO4-76DP00789.

References

1. C. V. Shank, R. L. Fork, R. Yen, J. Shah, B. I. Greene, A. C. Gossard and W. Weisbuch, Solid State Commun. 47 981 (1983).
2. W. Z. Lin, L. G. Fujimoto, E. P. Ippen, and R. A. Logan, Appl. Phys. Lett. 50, 124 (1987).
3. J. Dubard, J. L. Oudar, F. Alexandre, D. Hulin and A. Orszag, Appl. Phys. Lett. 50, 821 (1987).
4. G. Mahler and A. Fourikis, J. of Lumin. 30, 18 (1985).
5. S. Schmitt-Rink and D. S. Chemla, Phys. Rev. Lett. 57, 2752 (1986); W. Schäfer et al., phys. stat. sol. (b) **150**, 407 (1988); M. Lindberg and S. W. Koch, Phys. Rev. **B38**, 3342 (1988).

Poster Session

TuD 3:00pm–4:30pm
Salon D



Thermal emission of carriers in strained $In_xGa_{1-x}As/GaAs$ quantum wells due to a fast interface scattering

D-P007 852

G. Bacher, H. Schweizer, J. Kovac
4.Physikalisches Institut, Universität Stuttgart
Pfaffenwaldring 57, D-7000 Stuttgart 80, FRG
H.Nickel, W.Schlapp, R.Lösch
DBP-Telecom, Research Institute, P.O.Box 10030, D-6100 Darmstadt, FRG

92-22381

Strained $In_xGa_{1-x}As/GaAs$ heterostructures are recently used for the development of excellent semiconductor lasers[1]. Among other things, the efficiency as well as the high frequency properties of quantum well lasers are strongly influenced by the dynamics of the carrier capture into the quantum well. Especially threshold can be increased drastically by carrier leakage above the barriers. The capture time in laser structures is determined by both, the carrier transport to the quantum well and the scattering from the barrier states into the quantum well at the interface.
The time constants found in typical time-integrated[2] or time-resolved[3,4] experiments are mainly determined by the transport in the barrier, whereas the dynamics of the scattering process at the interface still remains unexplained.
To study this scattering process in strained $In_xGa_{1-x}As/GaAs$ quantum wells, we have varied the well width L_z and the In-content x systematically. As a result, we demonstrate by means of time-integrated and time-resolved photoluminescence (PL) a thermal emission of optically excited excitons out of the quantum well into the barrier already at low temperatures. Due to this thermal emission, a transfer of carriers between wells of different widths across the GaAs barrier can be observed. A quantitative description using a system of rate equations gives evidence of a scattering time below 100 fs between the quantum well and the barrier states at the interface.

The samples consist of several $In_xGa_{1-x}As$ layers cladded by 200 nm GaAs barriers. Each sample has a different In-content (x = 0.06, 0.12 or 0.2) and contains four quantum wells with L_z = 2 nm, 5 nm, 10 nm and 30 nm (except for x = 0.2), respectively. For the excitation, we used a cw-ml Ar^+-laser followed by a synchronously pumped dye laser (pulse width 10 ps, λ = 650 nm, P_{Peak} = 4 kW/cm^2). The PL signal was detected by a fast S1 microchannel-plate with an overall time resolution of about 50 ps. As an example, the low temperature PL spectra of the $In_{0.06}Ga_{0.94}As/GaAs$ sample is

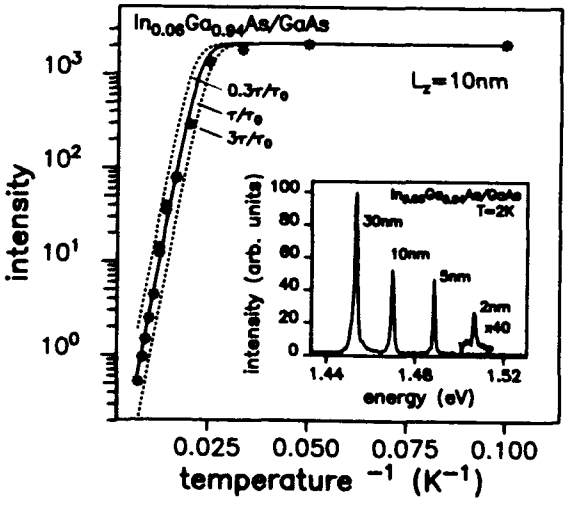


Fig.1 *PL intensity versus T (x=0.06; L_z=10nm) Fits are drawn in as described in the text. The inset show the low temperature (T=2K) spectrum of a sample with x=0.06*

shown in the inset of Fig. 1. Linewidths down to 0.35 meV, obtained in high resolution experiments, give evidence of an excellent sample quality[5]. In the main part of Fig. 1, the PL intensity of the quantum well with L_z = 10 nm is depicted versus temperature in an Arrhenius plot. At a characteristic temperature, a distinct drop of PL intensity is observed. At T > 50 K, the slope of log(I) versus T^{-1} is given by a characteristic activation energy E_A. A comparison between the confinement energy ΔE, in this paper defined as the difference between quantum well and barrier luminescence, and the experimentally found activation energy E_A show an excellent agreement. Therefore, we assume, that the thermal activation is determined by the total confinement of the excitons in the quantum well.
Based on this results, we use the following rate equation for a quantitative description

$$\frac{\partial c}{\partial t} = - \frac{c}{\tau} - \frac{c \cdot e^{-E_A/kT}}{\tau_0} + g \qquad (1)$$

with c = exciton concentration, τ = excitonic lifetime in the quantum well and g = generation rate by the laser excitation. Due to the thermal distribution of the carriers in the quantum well, a certain part of the excitons ($c \cdot \exp(-E_A/kT)$) is scattered into the GaAs barrier, reducing the PL intensity of the quantum well. τ_0 describes the effective scattering time from the high energy tail of the exciton distribution in the quantum well into the barrier states and is obtained by curve fitting.
Equation (1) is solved for steady state conditions ($\partial c/\partial t = 0$; $g = c_0/\tau$) and we obtain

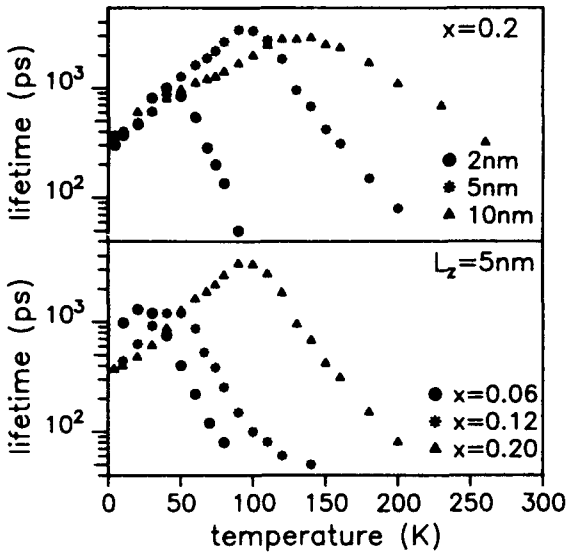
$$c(T) = \frac{c_0}{1 + \frac{\tau}{\tau_0} \cdot e^{-E_A/kT}} \qquad (2)$$

In a first approximation, we neglect the temperature dependence of τ/τ_0 with respect to the strong temperature dependence of $\exp(-E_A/kT)$. The solid line in Fig. 1 gives the fit using $E_A = \Delta E$ = 45 meV and τ/τ_0 = 145000, yielding a distinct decrease of PL intensity at temperatures $T \ll \Delta E/k$. The dotted lines, using 0.3 τ/τ_0 and 3 τ/τ_0, respectively, demonstrate the sensitivity of our model. In all the samples investigated, the excitonic lifetimes are in the range of several ns and therefore, we can give an estimation of the scattering time τ_0 between 10 fs and 100 fs.
Solving equation (1) with a carrier generation by a δ-function like laser pulse and the initial condition $c(t=0) = c_0$, we get for the effective lifetime in an $In_xGa_{1-x}As/GaAs$ quantum well

$$\tau_{eff} = \frac{\tau}{1 + \frac{\tau}{\tau_0} \cdot e^{-E_A/kT}} \qquad (3)$$

Therefore, similar to the reduction of PL intensity with increasing temperature, a drop of PL lifetime at a characteristic temperature is expected.

In Fig. 2, we have plotted the temperature dependence of the lifetime τ_{eff} for different well widths (x = 0.2; top) and for different In-contents (L_z = 5 nm; bottom), respectively.



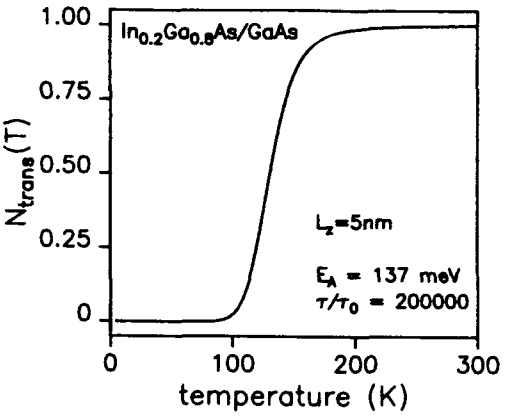


Fig.3 *Part of the excitons emitted into the barrier versus T for a quantum well with x=0.2 and L_z=5nm*

Fig.2 *PL lifetime versus temperature for different well widths L_z (x=0.2; top) and for different In-contents x (L_z=5nm; bottom)*

At low temperatures, τ_{eff} increases with increasing temperature, as expected for free excitonic emission in quantum wells[6]. At higher temperatures, dependent on the confinement energy ΔE, i. e. L_z and x, the thermal emission of the excitons into the barrier reduces τ_{eff} drastically, in agreement with equation (3). As an example, we have calculated the part of the thermally emitted carriers as a function of temperature for a quantum well with L_z = 5 nm and x = 0.2 (Fig. 3). In the calculation, we have used the experimentally determined parameters E_A and τ/τ_0. At T < 100 K, no thermal emission occurs and the recombination takes place in the quantum well. For temperatures larger than 150 K, the main part of the carriers is emitted into the barrier and we observe a strong reduction of the lifetime (see Fig. 2).

As the samples consist of several quantum wells with different L_z, we are able to observe a transfer of the excitons out of the narrow quantum wells into the wider ones across the barrier. This is demonstrated by the results plotted in Fig. 4. The intensity of two quantum wells with different well widths (L_z = 5 nm and 10 nm, respectively) is depicted as a function of time. τ_{eff} of the narrow well is already reduced by the thermal emission, whereas the lifetime in the thicker well is only determined by excitonic recombination (see also Fig. 2). Additionally, we observe a delayed onset in the PL intensity of the quantum well with L_z = 10 nm due to the carrier transfer between the quantum wells.

For a theoretical study, we consider two neighboring quantum wells with different L_z, separated by a GaAs barrier. The exciton concentration in the narrow quantum well is given by c_1, whereas c_2 describes the concentration in the wider one.

We thus obtain

$$\frac{\partial c_1}{\partial t} = - \frac{c_1}{\tau_1} - \frac{c_1 \cdot e^{-E_{A1}/kT}}{\tau_{01}} \qquad (4)$$

$$\frac{\partial c_2}{\partial t} = - \frac{c_2}{\tau_2} - \frac{c_2 \cdot e^{-E_{A2}/kT}}{\tau_{02}} + \alpha \cdot \frac{c_1 \cdot e^{-E_{A1}/kT}}{\tau_{01}} \qquad (5)$$

The carrier concentration in each quantum well is reduced by both, excitonic lifetime in the quantum well and exciton transfer out of the quantum well into the barrier. A part α of the thermally excited carriers out of the narrow quantum well is captured by the thicker one. The carrier capture and the relaxation into the ground state of the quantum well as well as the transfer between the quantum wells across the barrier are very fast and can be neglected in the time scale of our experiment[4].

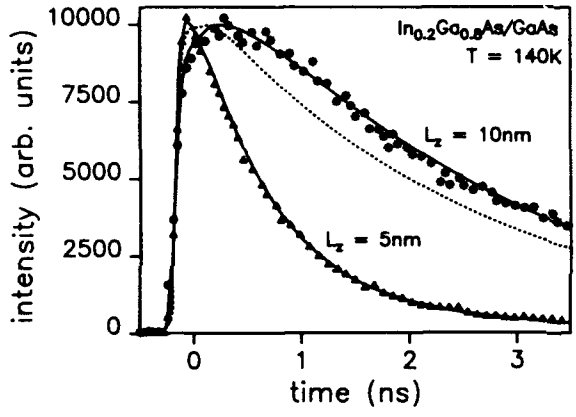


Fig.4 *Time-resolved PL of $In_{0.2}Ga_{0.8}As/GaAs$ quantum wells (L_z=5nm and L_z=10nm). Fits are included as described in the text*

Solving the equations (4) and (5), we can fit our measurements using α = 0.7 and E_{Ai} and τ/τ_{0i} as obtained by the time-integrated experiments (solid lines). Not all of the thermally excited carriers are captured by the wider quantum well, because a part of them can reach the substrate or the surface and therefore, we expect $\alpha < 1$. Additionally, we have drawn in a fit neglecting the transfer (dotted line). It is obvious, that the transfer between the quantum wells influence the carrier dynamics significantly.

We would like to thank M.H.Pilkuhn and A.Forchel for stimulating discussions. The financial support of this work by the Deutsche Forschungsgemeinschaft (SFB 329) is gratefully acknowledged.

References

(1) T.Ijichi, M.Ohkubo, N.Matsumoto and H.Okamoto
Conference Digest 12th Int. Sc. Laserconf., Davos, 44 (1990)

(2) E.H.Reihlen, A.Persson, T.Y.Wang, K.L.Fry and G.B.Stringfellow
J.Appl.Phys. 66, 5554 (1989)

(3) B.Deveaud, F.Clérot, A.Regreny, K.Fujiwara, K.Mitsunaga and J.Ohta
Appl. Phys. Lett. 55, 2646 (1989)

(4) D.Y.Oberli, J.Shah. J.L.Jewell, T.C.Damen and N.Chand
Appl. Phys. Lett. 54, 1028 (1989)

(5) H.Nickel, R.Lösch, W.Schlapp, H.Leier and A.Forchel,
Surface Science 228, 340 (1990)

(6) J.Feldmann, G.Peter, E.O.Göbel, P.Dawson, K.Moore, C.Foxon and R.J.Elliott
Phys. Rev. Lett. 59, 2037 (1987)

AD-P007 853

Time Resolved Spectroscopy of Coherent Switching in GaAs/AlGaAs Coupled Double Quantum Wells

G. Mayer, G. Lehr, H. Schweizer
4. Physikalisches Institut, Universität Stuttgart,
Pfaffenwaldring 57, D-7000 Stuttgart 80, F.R.Germany
Phone: 49-711-685-4961, FAX: 49-711-685-3500

H.P. Meier
IBM-Research Center, Rüschlikon, Switzerland

In the past several theoretical and experimental approaches for the design of optical computing devices have been given. Common to that devices is that they are at least bistable, so that they can be switched by a light pulse from one state into an other with or without an additional external electric field. Mahler et al.[1)] have proposed a device consisting of quantum dots with slightly detuned quantization energies, representing two eigen states that can be coherently switched by a laser pulse of appropriate energy and duration. Although technology is not so far to produce these structures with the high accuracy necessary, some of the basic features can in principal also be studied in 2-dimensional systems.

The realization of the switching device consists of two coherently coupled quantum wells (coupled double quantum well, CDQW). Because the eigen states have to be distinguishable, the two wells must be slightly different, which can be accomplished either by composition or by well width. Figure 1 shows the calculated eigen values (upper part of figure) and envelope functions (lower

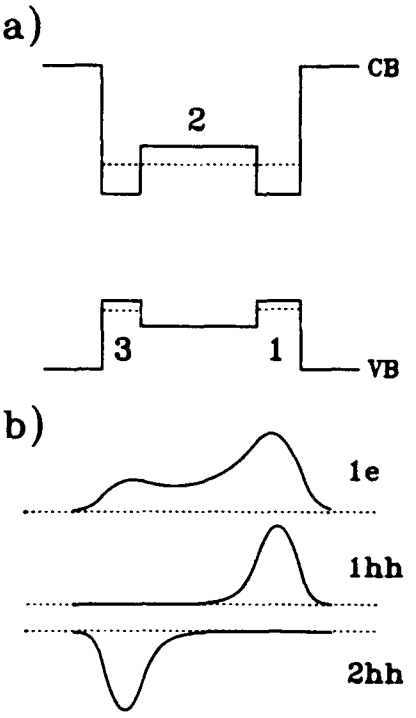


Fig. 1: Eigen states (a) and wave functions (b) of a coupled double quantum well system with slightly different wells.

92-22382

part) of the lowest electron and heavy hole subbands with geometrical data as used in our experiments. By optimizing the well widths, the barrier height and width, it can be achieved that the hole wave functions are strongly localized in the corresponding wells, while there is a high probability to find the electrons in both wells. Normally the system will be in its ground state 1. By a short resonant laser pulse it will be excited into the intermediate state 2, from where it will recombine both to state 1 and state 3: the system has been switched state 1 to state 3 with a certain probability.

The main part of our structure consists of two GaAs quantum wells with widths of 40Å and 45Å respectively, coupled through a 120Å wide barrier of $Al_{0.15}Ga_{0.85}As$. The cladding layers also consist of AlGaAs with an Al-content of 45%. The whole structure was grown with MBE on a p-type substrate and covered with p-type AlGaAs and GaAs layers of 300Å and 200Å, respectively. For reference purposes we also included a 70Å single quantum well (SQW), separated 1000Å from the CDQW. To apply an external electric field to the structure a semi-transparent Schottky-contact (Al, 10nm, transmittance ~33%) was evaporated.

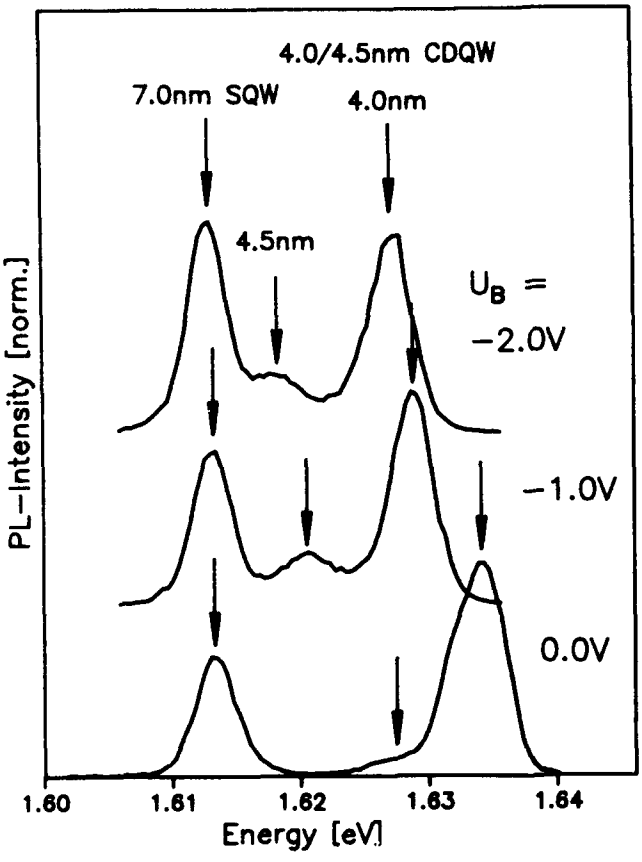


Fig. 2: Low temperature PL-spectra of a CDQW-structure at different reverse voltages V.

In the experiments charge carriers were generated directly in the CDQW-structure using a synchronously mode locked dye laser (DCM, λ= 640nm, FWHM ~12ps). To avoid line broadening effects due to band filling the laser intensity was kept below 100W/cm^{-2}. The photoluminescence (PL) was spectrally dispersed in a 32cm spectrometer and detected with a fast photon counting system. The time resolution of our delayed coincidence arrange-

ment is ~70ps, which can be further improved to 20-30ps using a deconvolution technique. All the experiments were carried out at 2K.

In Fig. 2 PL-spectra taken at different electric fields are shown. The spectra are dominated by the emission of the 40Å QW and the 70Å SQW. Due to the built-in electric field the transmission probability of the 45Å QW, which is closest to the Schottky-contact, is reduced and therefore the PL-intensity of the 45Å well is smaller by a factor of ~5 compared to the 40Å well. For the same reason the 45Å QW exhibits the strongest Stark shift (as denoted by the arrows). At the location of the 70Å SQW the electric field has completely decayed, so the 70Å SQW experiences no Stark shift at all. The coupling of the 40Å and 45Å wells can be demonstrated by evaluating the PL-intensity ratio as a function of the electric field, which is done in Fig. 3. For small voltages the intensity ratio is about 1:10 while for higher voltages the ratio approaches 1:3, clearly indicating the strong coupling of the wells over the delocalized electron state.

To get more information on the coherent nature of the coupling of the two wells we have performed time resolved experiments. Figure 4 shows the emission of the 40Å (squares) and the 45Å well (diamonds) for an external voltage of -2.0V. The decay is mono exponential over 4 decades, which displays the excitonic recombination character. Also included in the figure are fits to the experimental data with lifetimes of 338ps and 335ps for the 40Å and 45Å well, respectively (undistinguishable in the figure). Within the experimental error these values are equal. From the well width dependence of the lifetime[2] in zero field we derive lifetimes that should

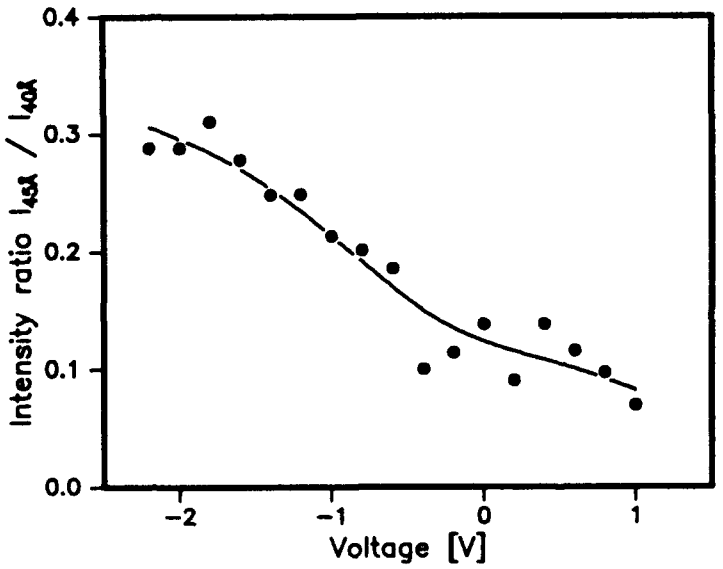


Fig. 3: Ratio of the PL-intensity of the 45Å-well and the 40Å-well as a function of the applied voltage.

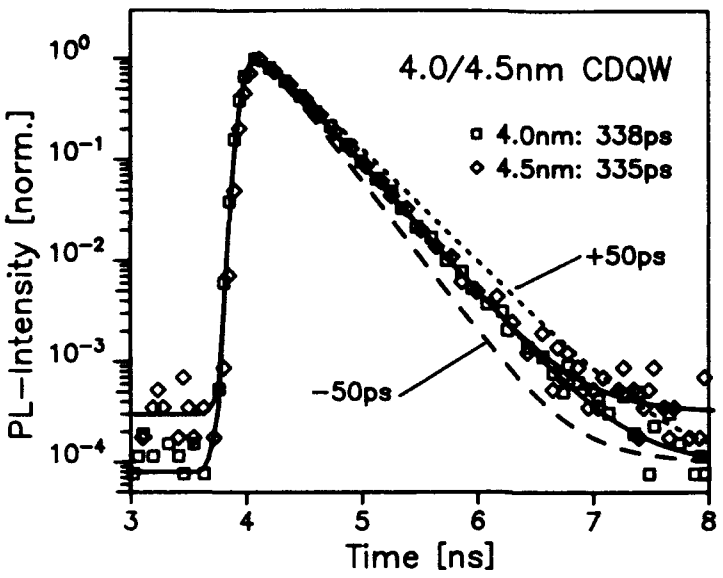


Fig. 4: Time resolved PL from the two components of the CDQW at an applied voltage of -2.0V. Squares: 40Å-well, diamonds: 45Å-well, solid lines: fits to the experimental data (almost undistinguishable in the figure). Also shown: calculated decay with τ=388ps (dots) and τ=288ps (dashed).

differ by about 50ps. This could be easily resolved in the experiment, as the dotted (τ=388ps) and dashed (τ=288ps) lines in figure 4 demonstrate. Furthermore, this difference should be more pronounced in the presence of an electric field[3]. The absence of any difference in the time behavior clearly demonstrates the strong coherent coupling in the CDQW-system.

In conclusion, we have shown first results of a coherent switching device. Resonant excitation experiments of the two quantum wells, which will give more insight into the coherent nature of the coupling, are underway and will be presented at the conference.

References:

1) K. Obermayer, G. Mahler, H. Haken, Phys. Rev. Lett. **58**, 1792 (1987)

2) J. Feldmann, G. Peter, E.O. Göbel, P. Dawson, K. Moore, C. Foxon, R.J. Elliott, Phys. Rev. Lett. **59**, 2337 (1987)

3) H.-J. Polland, L. Schultheis, J. Kuhl, E.O. Göbel, C.W. Tu, Phys. Rev. Lett. **55**, 2610, (1985)

Valence Band Structures of A Strained Quantum Well and Applications to Semiconductor Lasers

D-P007 854

Shun-Lien Chuang and Calvin Y.P. Chao
University of Illinois at Urbana-Champaign
Department of Electrical and Computer Engineering
1406 West Green Street
Urbana, Illinois, 61801

Strain effects in quantum wells have been intensively investigated for applications to semiconductor lasers, photodetectors and electronic devices such as pseudomorphic high electronic mobility transistors. High quantum efficiency, high power (70 mW CW and 180 mW pulsed operation), modulation-doped $In_{0.8}Ga_{0.2}As$ strained-layer (compression) quantum-well lasers emitting at 1.5 μm wavelength have been reported [1]. A record high power output (206 mW CW) strained-layer InGaAs/InP quantum-well laser emitting at 1.48 to 1.51 μm using the effects of tension strain has been demonstrated [2]. A very low threshold (92 A/cm^2) strained-layer quantum-well laser at 1.6 μm has also been obtained [3].

For an $In_{1-x}Ga_xAs$ layer grown on InGaAsP lattice matched to InP along the [001] direction, the strain effects modify the valence band structures considerably. In Fig. 1, we show the valence band structures along two principal axes (k_x and k_z) for three cases, (a) lattice matched, (b) compression and (c) tension strains. The constant energy contours for the heavy hole and light hole are on the right. For a lattice-matched material (x=0.468), the heavy-hole and the light-hole bands are degenerate at the zone center. For x smaller than 0.468, the biaxial compressive strain makes the heavy-hole $|3/2,\pm 3/2\rangle$ band possess a lighter effective mass and the light-hole $|3/2,\pm 1/2\rangle$ band possess a heavier effective mass in the transverse plane (k_x-k_y plane), and the heavy-hole band is shifted above the light-hole band. For this case, the gain of the TE polarization (optical field parallel to the x-y plane) is larger than that of the TM polarization. On the other hand, for x greater than 0.468, the strain is tensile and the light-hole band is shifted above the heavy-hole band. Accordingly, the gain of the TM polarization should be higher than that of the TE polarization, since the light-hole band will be populated before the heavy-hole band.

For a strained-layer quantum-well structure, the transition energies are determined by three factors: (1) the Ga composition x, which determines the energy gap $E_g(x)$ of the

92-22383

unstrained $In_{1-x}Ga_xAs$; (2) the strain effects due to the hydrostatic and the shear components, which depend on the amount of lattice mismatch between $In_{1-x}Ga_xAs$ and InP; and (3) the quantum-size effects due to the one-dimensional confinement and the mixing between the heavy hole and the light hole. The quantization energies are primarily determined by the effective masses in the growth direction, along which the effective mass of the heavy hole is still greater than that of the light hole. Therefore, in the case of a tensile strain ($x > 0.468$), there will be a competition between the light-hole band and the heavy-hole band. For a small tensile strain, the first heavy-hole subband is still above the light-hole subband since the quantization effect is dominant. However, for a large tensile strain, the first light-hole subband becomes higher than the heavy-hole subband due to the shear component of the strain. We have developed an efficient method to calculate the quantum-well valence band structures based on a two-by-two Hamiltonian approximation. This Hamiltonian is either the upper or lower block of the block-diagonalized matrix obtained from a unitary transformation on the four-by-four Luttinger-Kohn Hamiltonian. The eigenvalues and eigenvectors for the heavy hole and the light hole can be expressed in analytical forms. The general valence band structure is shown in Fig. 2 for an $In_{1-x}Ga_xAs$ quantum well with a width of 50 Å grown on InGaAsP (1.2 μm) lattice matched to InP for different gallium compositions. For the compression, Fig. 2(a), and lattice-matched cases, Fig. 2(b), the top subband is HH1. It is interesting to find that the top subband for the tension case at x=0.58 is still heavy hole in nature, but its effective mass becomes negative. When we increase the amount of tension strain to x=0.65, the top subband becomes LH1. The significance of the negative effective mass and its possible enhancement of the joint density of states for optical transitions will lead to interesting properties of the strained-layer quantum-well lasers.

Acknowledgement: This work was supported by the Office of Naval Research under the grant N00014-90-J-1821.

[1] P. J. A. Thijs and T. van Dongen, Electron. Lett. 25, 1735 (1989).

[2] T. Tanbun-Ek, R. A. Logan, N. A. Olsson, H. Temkin, A. M. Sergent, and K. W. Wecht, Appl. Phys. Lett. 57, 224 (1990).

[3] C. E. Zah, R. Bhat, K. W. Cheung, N. C. Andreadakis, F. J. Favire, S. G. Menocal, E. Yablonovitch, D. M. Hwang, M. Koza, T. J. Gmitter and T. P. Lee, Appl. Phys. Lett. 57, 1608 (1990).

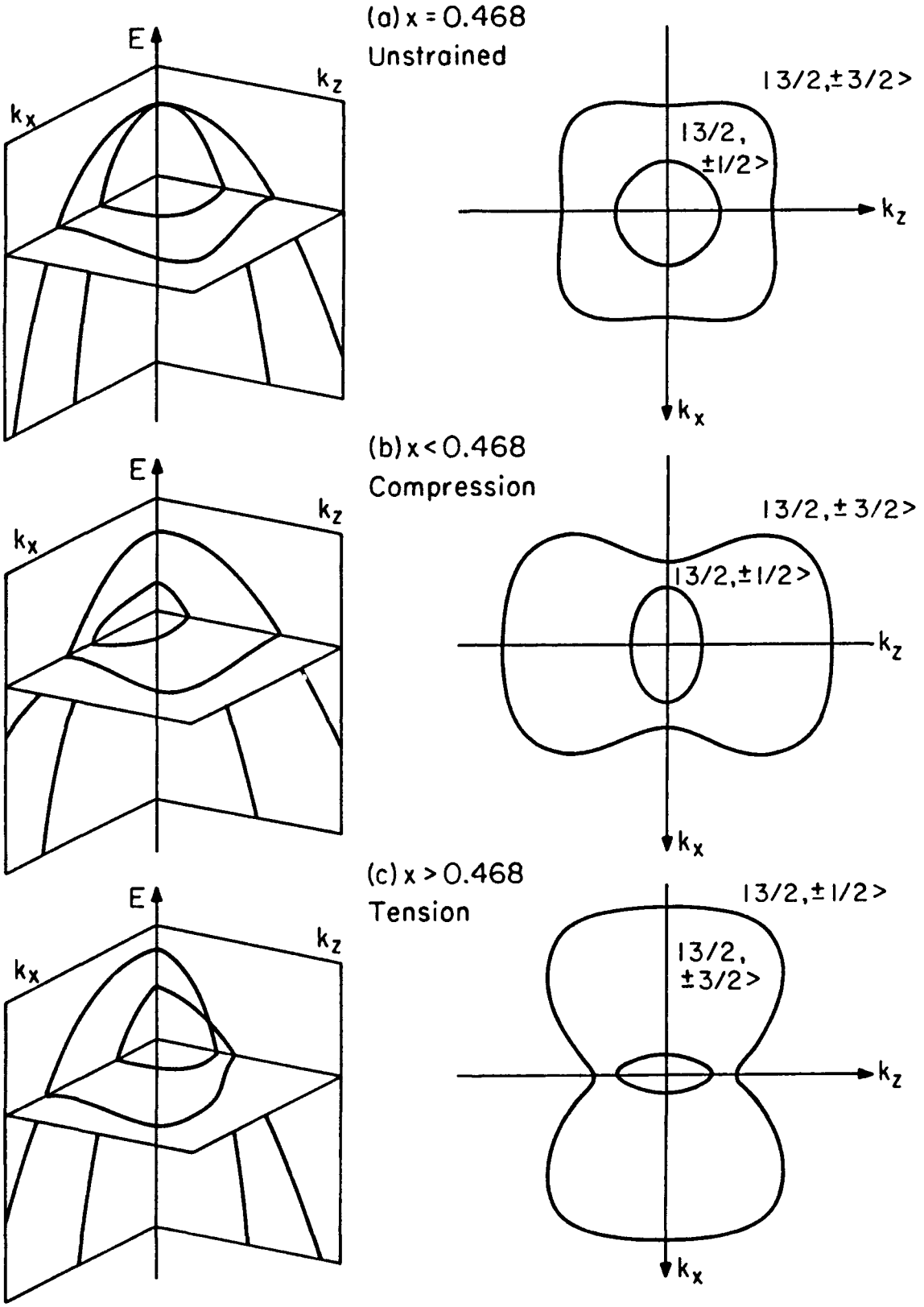


Fig.1: The valence band structures of $In_{1-x}Ga_xAs$ grown on InP and the constant energy contours for the (a) compression, (b) no strain and (c) tension cases.

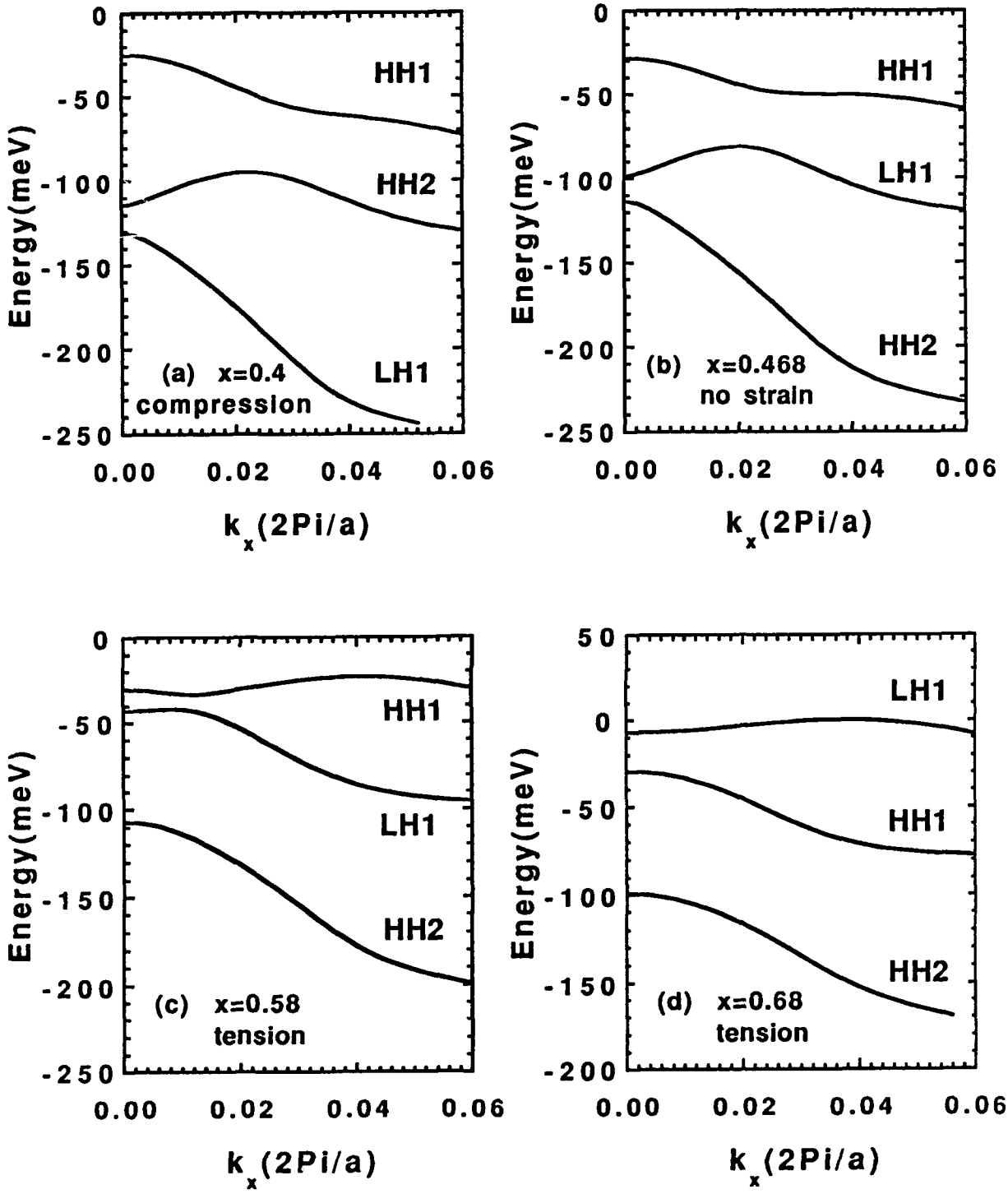


Fig.2: The subband structures of a 50 Å $In_xGa_{1-x}As$ quantum well grown on InGaAsP (1.2μm wavelength) for (a) x=0.40, (b) x=0.468, (c) x=0.58, and (d) x=0.65.

AD-P007 855

Coulomb enhancement of ultrafast nonlinearities in quantum well structures.

92-22384

J. Khurgin

Department of Electrical and Computer Engineering
The Johns Hopkins University
Baltimore, MD 21218

Recent works in the area of ultrafast nonlinearities due to virtual carriers in semiconductor heterostructures have generated significant interest among researchers. It has been shown[1] that excitons in QW's behave very much like conventional two-level atoms, to the extent that exciton-exciton interaction can be neglected. Therefore, fast coherent phenomena usually associated with two-level system may occur in excitonic QW transitions. Indeed, dynamic (AC) Stark effect in QW's have been demonstrated [2,3]. When semiconductor QW's were pumped *below* the absorption edge there were a strong "blue" shift of the exciton resonance, accompanied by a strong bleaching.

The effect of blue shift caused by the below absorption edge excitation can be understood very simply if one uses virtual carrier (or virtual exciton) concept[4]. The virtual carriers are excited by the nonresonant (below the bandedge) radiation. In the limit of long electric dipole relaxation time T_2 virtual carrier population pulsates with Rabi frequency $\Omega=\mu E/\hbar$ and amplitude proportional to the light intensity and inversely proportional to the square of detuning. Therefore, absorption is modulated with Rabi frequency, i.e. absorption sidebands appear at frequencies $\omega\pm\Omega$. This is called dynamic Stark effect[5]

In this work we discuss influence of Coulomb carrier-carrier or exciton-exciton interaction on the ultrafast nonlinear optical properties of QW's. Due to large differences in effective masses of electron and hole in III-V QW's electron and hole wavefunctions can be separated from each other by relatively large (tens of $\AA$) distances, as, for example, in stepped QW (symmetric or asymmetric) shown in Fig.1a. In this situation, interaction between virtual carriers can be treated in Hartree approximation, and can be expressed in the form of Coulomb potential V(t) (Fig.1d). Since the magnitude of this potential is proportional to the virtual

population, it pulsates with the Rabi frequency Ω. When treated as perturbation, this pulsating Coulomb potential leads to synchronous pulsations of the energy levels (shown in dashed lines in Fig.1e). In other words, introduction of Coulomb carrier-carrier or exciton-exciton interaction into the description of pump-probe experiment, results in a following situation: *saturation of upper state (phase state filling) and increase of the energy difference between ground and excited levels occur simultaneously and in phase with each other at the same frequency Ω. As a result, dynamic Stark effect is enhanced.* Similar enhancement occurs for the case of intersubband transitions, where spatial separation between ground and excited electron levels can be made quite large.

We present the results of calculations of the Coulomb enhancement of dynamic Stark effect in the QW's of different geometries, for the cases of excitonic, band-to-band and intersubband transitions. It is shown that by proper design of QW's, the dynamic Stark effect can be enhanced by as much as factor of 5 and for the intersubband transitions by a factor of two to four depending on modulation doping density. An interesting situation occurs for the bandedge transitions, where Coulomb enhancement is insignificant at low temperatures, but at room temperature it can be observable. We consider AC Stark effect using both bare states and dressed state approaches and we also present the treatment of the Coulomb-assisted third order nonlinear optical susceptibility using the concept of virtual carriers, as well as the results of the exact solution of the optical Bloch's equations with Coulomb interaction taken into account. We show that under certain conditions instability can result. We also consider potential applications of the effect in the ultrafast all-optical switching devices.

This work is supported by AFOSR.

References

[1] S. Schmitt-Rink and D. S. Chemla, Phys. Rev. Lett., **57**, 2752, (1986).
[2] A. Mysyrowcz, D. Hulin, A. Antonetti, and A. Migus, Phys. Rev. Lett., **56**, 2748, (1986).
[3] A. Von Lehmen, D. S. Chemla, J. E. Zucker, and J. P. Heritage, Opt. Lett., **11**, 609, (1986).
[4] E. Yablonovitch, J. P. Heritage, D. E. Aspnes, and Y. Yafet, Phys. Rev. Lett., **63**, 976, (1989).
[5] R. W. Boyd and M. Sargent III, J. Opt. Soc. Am. B, **5**, 99, (1988).

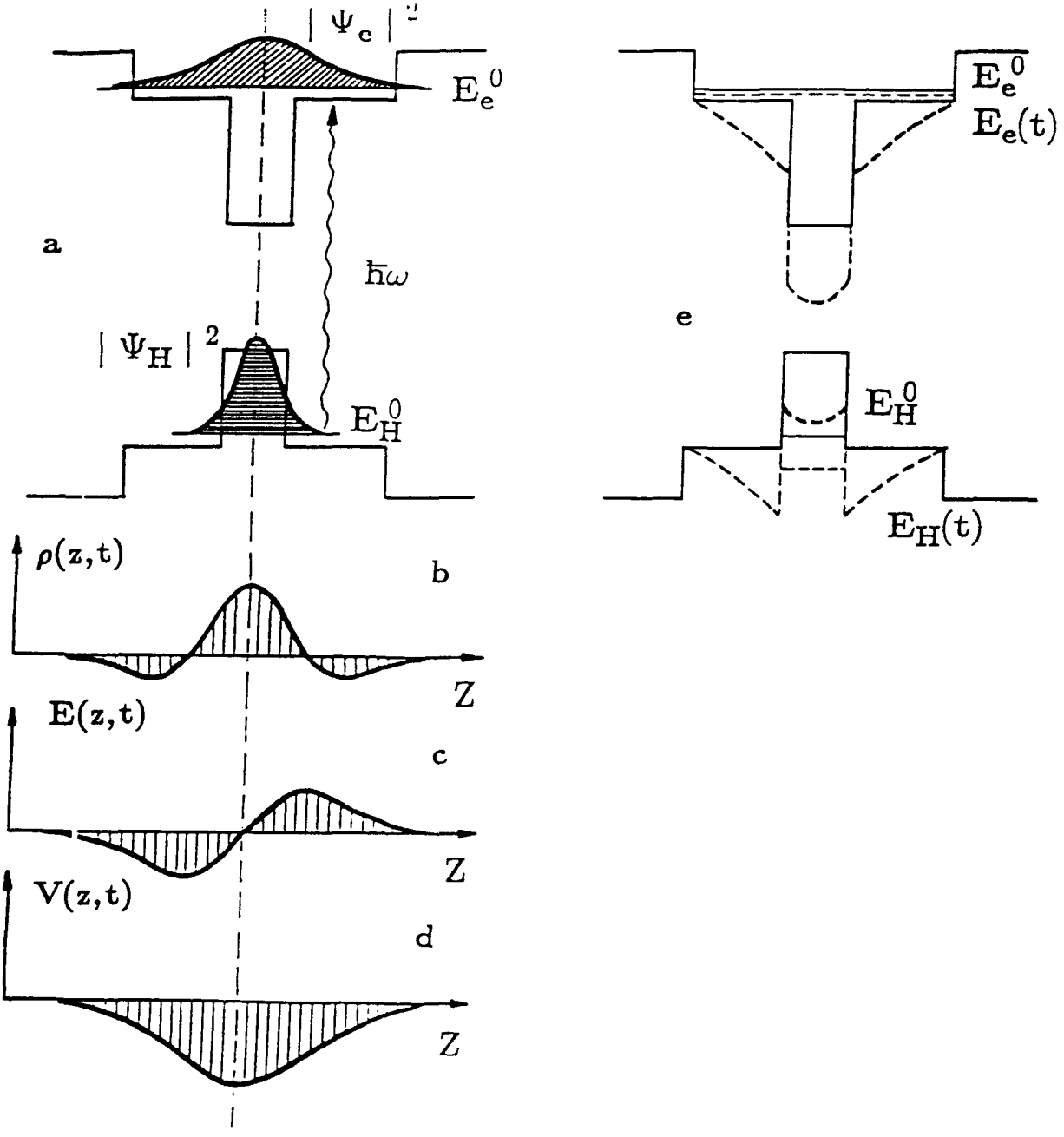


Fig.1. Coulomb-assisted energy level pulsations of excitonic transition in stepped quantum well.

a. geometry of the QW and the ground states energies and wavefunctions for conduction and valence bands.

b. pulsating virtual charge density $\rho(z,t)=\rho(z)e^{-i\Omega t}$

c. pulsating electric field $E(z,t)=E(z)e^{-i\Omega t}$

d. pulsating Coulomb potential $V(z,t)=V(z)\sim e^{-i\Omega t}$

e. pulsating energy levels for electron and hole $E_{e,h}(t)=E^0_{e,h}+\delta E_{e,h}e^{-i\Omega t}$

Cross-Well Charge Transfer Rates as a Function of Carrier Density in a GaAs/AlGaAs MQW pin Modulator

C.B. Park, P. LiKamWa, D. C. Hutchings, A. Miller

Center for Research in Electro-Optics and Lasers,

University of Central Florida,

Orlando, FL 32826

Tel: (407) 658 6800

AD-P007 856

92-22385

One of the most promising devices to emerge for optical logic applications is the quantum well self electro-optic effect device (SEED) which employs a shift of exciton absorption feature with electric field via the quantum confined Stark effect (QCSE). The ultrafast response of this device is important for high frequency operation and depends on the detailed nature of the cross well carrier transport mechanisms. Previous measurements have employed the excite-probe technique with picosecond pulses to monitor thermionic emission and tunneling via transmission changes caused by the carriers leaving the wells and moving towards the contact regions[1-3]. In the present work, we have extended the measurements to longer time delays and investigated the effects of higher carrier densities on the temporal response of the device. In this case, the response is significantly altered because of the space-charge field dynamically changing the absorption coefficient and the tunneling rates.

For these measurements we have employed 1 psec pulses from a cavity dumped and synchronously pumped Styryl 9 dye laser. The MQW device consisted of 60 GaAs wells of width

87Å and $Al_xGa_{1-x}As$ (x=0.3) 60Å thick barriers. Excite-probe measurements were used to determine the photoconductive risetime on picosecond timescale from the screening of the field due to charge separation and the resulting changes in absorption through the QCSE. The laser was tuned just below the exciton absorption feature to maximize this effect. At low excitation levels, the field dependent risetime varied from over 300 psec to 10psec as a function of applied voltage. The signal consisted of a rise due to charge separation screening the field and a subsequent fall in signal due to transverse diffusion of the carriers in the doped regions. This process occurs on timescales faster than the external bias circuitry can respond. By fitting the transmission rise and fall times taking account of the transverse diffusion process in the heavily doped p and n-type regions the rise times shown in figure 1 were determined. This gives a minimum at 5V bias under conditions of resonant tunneling between the n=1 level in one well and the n=2 level in the adjacent well.

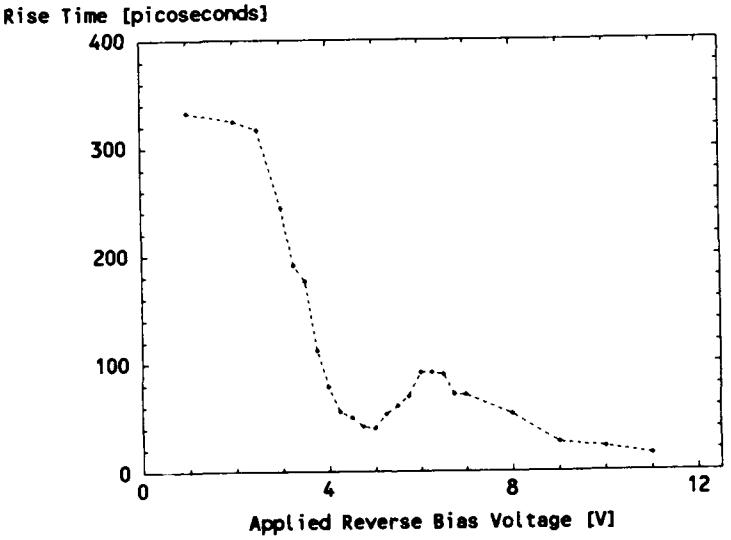


Figure 1

The temporal reponse of the SEED device at higher excitation levels is shown in figure 2. The measurements presented here were made under initial conditions of resonant tunneling. As the carrier density is increased, the response time gets longer. The transmission response will depend

on the form of the absorption feature, the locally induced space charge fields and the way the functional form of these parameters vary with applied electric field. We ascribe the observed temporal response to a slowing of carrier tunneling from the wells due to the larger space charge fields (and therefore lower net field) induced at higher carrier densities.

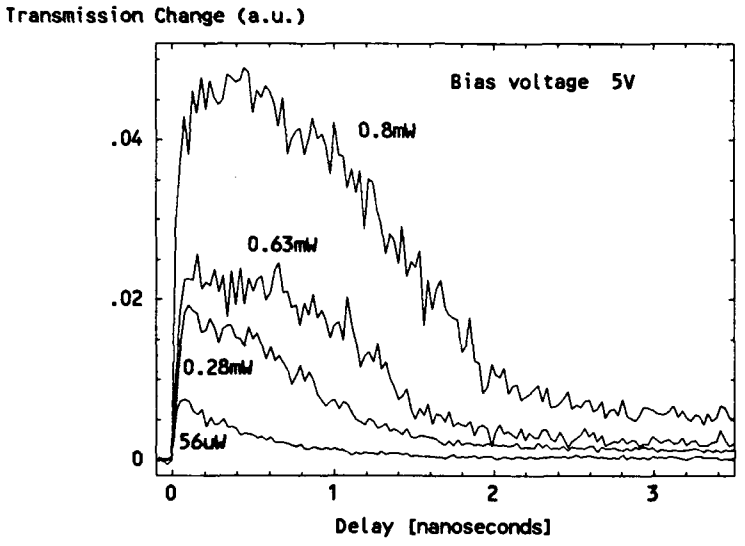


Figure 2

We have modeled the temporal response of the pin modulator numerically. This self-consistent model computes the spatial distribution of electrons within each well as a function of time after carrier generation by the excitation pulse. The evolution of the local field within each well is used to derive inter-well scattering rates, tunneling rates from the confined states within the wells to the continuum, and transit rates across the device. We also allow for the transverse diffusion of electrons in the contact region[2]. We find good agreement with the experiments in terms of response times and relative signal size which are determined by the different time constants of the charge motion.

This talk will present data on the charaterization of this effect for different applied voltages. The results apply to the response times of a number of MQW devices under conditions of higher excitation level, including SEED logic elements, photocunductive detectors and nonlinear optical devices employing cross-well carrier sweep-out.

References

1. R J Manning, P J Bradley, A Miller, J S Roberts, P Mistry, M Pate
Electron. Lett. **24** 854 (1988)

2. G Livescu, A M Fox, D A B Miller, T Sizer, W H Knox, A C Gossard, J H English Phys. Rev. Lett. **63** 438 (1989)

3. R J Manning, P J Bradley, A Miller, J S Roberts, P Mistry, M Pate
Electron. Lett. **25** 269 (1989)

OPTICAL LINE SHAPES OF QUANTUM WELLS AND QUANTUM WIRES

T. Ohtoshi and M. Yamanishi†

Central Research Laboratory, Hitachi, Ltd.
Kokubunji, Tokyo 185, Japan

† Faculty of Engineering, Hiroshima University
Saijyo, Higashi-Hiroshima 724, Japan

AD-P007 857

INTRODUCTION Optical line shapes, which represent homogeneous broadenings due to carrier collisions, play a crucial role in estimating the linear and nonlinear susceptibilities of low-dimensional semiconductors. So far, the Lorentzian function has been widely used to analyze the gain and the refractive index in quantum-well (QW) and quantum-wire lasers [1, 2]. However, these papers have not proven that it is truly possible to approximate the line shapes with the Lorentzian function.

In this paper, the authors theoretically derive the line shape functions of QW and quantum-wire structures based on a theory involving the non-Markovian relaxation processes [3]. The understanding of the line shapes at high-carrier densities is vital for predicting semiconductor laser properties. It is also important for estimating the line shape functions at low-carrier densities This is because line broadening must be minimized in order to lower the switching power of ultra-fast optical devices that utilize the virtual charge-induced optical nonlinearity (VCON) effect [4, 5] and the ac-Stark effect [6] under low real-excited carrier density conditions. Therefore, the carrier-density dependence of line shapes as well as the carrier-dimension dependence are presented in the present report.

THEORY The optical dipole moment $P(t)$, which decays owing to collisions, can be written as

$$P(t)=P(0)\exp(\mp i\omega_0 t)\exp\{-L(t)\}, \qquad (1)$$

where ω_0 is the resonant frequency. The line shape function $F(\hbar\omega)$ is given by the Fourier transform of $P(t)$. The phase damping factor $L(t)$ in Eq. (1) is defined as the decay rate of off-diagonal density matrix elements [3]. Included here are the non-Markovian relaxation processes, which cause $L(t)$ to have a non-

92-22386

linear time dependence. This gives rise to the crucial difference between the line shape of the present work and the Lorentzian line shape.

Carrier-carrier scattering and carrier-LO phonon scattering were considered to be responsible for the phase damping of dipoles. The formulation of Coulomb potentials and screening were done for pure 2-D and 1-D systems. The LO phonon modes were assumed to be confined to the wells. Evidence of localized LO phonon modes in QW structures has already been shown experimentally and theoretically [7].

RESULTS Calculated results for GaAs/$Ga_{0.6}Al_{0.4}As$ QW and quantum-wire structures are presented. Figure 1 shows the real part of $L(t)$ in 100Å QW and 100Åx100Å quantum-wire structures with an electron (hole) density of $2\times10^{18}cm^{-3}$. It was found that the values of $Re[L(t)]$ are proportional to t^2 in the early stage ($t \lesssim 10^{-15}$s) and are proportional to $t^{1.0}$ (bulk), $t^{1.3}$ (QW), and $t^{1.7}$ (wire) in the final stage ($t \gtrsim 10^{-13}$s). Thus, as the carrier dimension decreases, the line shape function is expected to become Gaussian-like since the line shape function is Gaussian if $Re[L(t)] \propto t^2$. This tendency can be understood as a result of the strong carrier-carrier coupling (the non-Markovian effect) in low-dimensional systems.

The line shape functions $F(\hbar\omega)$ at a high carrier density are shown in Fig. 2. The $F(\hbar\omega)$ of low-dimensional structures has stronger convergent characteristics at off-resonant energies. Most notably, the $F(\hbar\omega)$ of the quantum wire is very close to a Gaussian function, and has a wider spectral width than that of the QW.

The line shape functions in p-type modulation doped (MD) QW structures are presented in Fig. 3. The spectral width becomes narrow as the acceptor concentration in barriers N_A increases. This is because the high hole density enhances the screening effect influencing Coulomb interactions.

The damping factors at a low carrier density ($1\times10^{14}cm^{-3}$) can be seen in Fig. 4. In this case, the LO phonon scattering is dominant. It is obvious that the $Re[L(t)]$ depends linearly on time in $t \gtrsim 10^{-13}$s, even in low-dimensional systems. Thus, the relaxation time T_2 in the final stage can be estimated to be

0.1ps (bulk), 0.3ps (QW), and 0.7ps (wire). The longer T_2-time in the low-dimensional systems is caused by phonon localization.

The line shape functions at low carrier densities have stronger convergent characteristics than the Lorentzian function, as shown in Fig. 5. Moreover, the low-dimensional systems have smaller homogeneous broadening widths. Therefore, one can expect the switching power in devices using virtual optical transitions to be lower since the off-resonant energy can be reduced under low real-carrier density conditions.

CONCLUSION The optical line shapes in QW and quantum-wire structures have been theoretically presented taking the non-Markovian relaxation processes into account. The line shape functions in low-dimensional systems with high carrier densities have strong convergent characteristic. For low carrier densities, low-dimensional systems have smaller homogeneous broadening widths.

REFERENCES

[1] Y. Arakawa *et al.*, Appl. Phys. Lett., 45, 950(1984).
[2] M. Asada *et al.*, Jpn. J. Appl. Phys., 24, L95(1985).
[3] M. Yamanishi *et al.*, IEEE J. Quantum Electron., QE-23, 367(1987).
[4] M. Yamanishi, Phys. Rev. Lett., 59, 1014(1987).
[5] D. S. Chemla *et al.*, Phys. Rev. Lett., 59, 1018(1987).
[6] A. Mysyrowicz *et al.*, Phys. Rev. Lett., 56, 2748(1986).
[7] M. V. Klein, IEEE J. Quantum Electron., QE-22, 1760(1986).

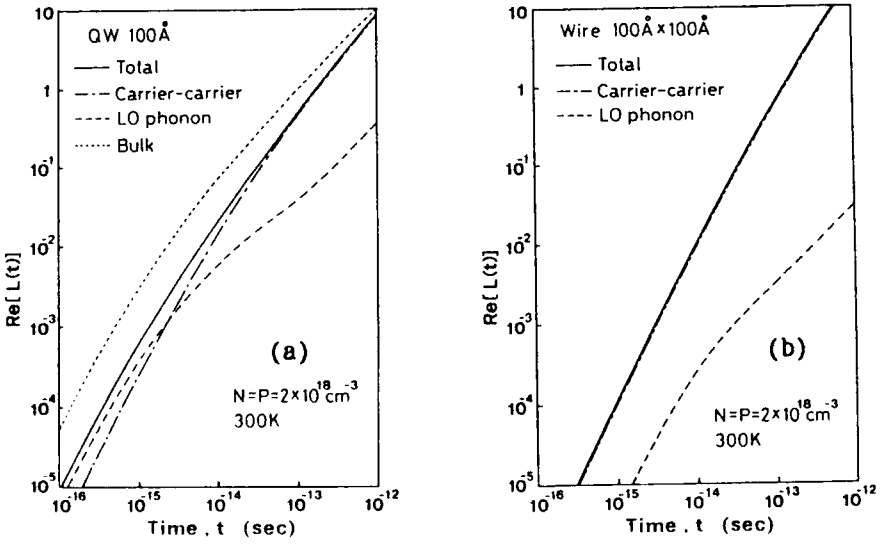


Fig. 1 Real part of phase damping factor $L(t)$ at carrier density of $2\times10^{18}\,cm^{-3}$. (a) 100Å QW, (b) 100Å×100Å quantum wire.

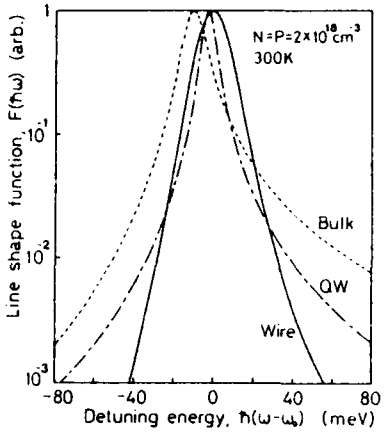


Fig. 2 Line shape functions at high carrier density.

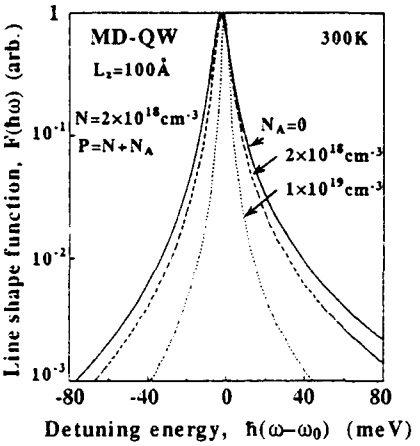
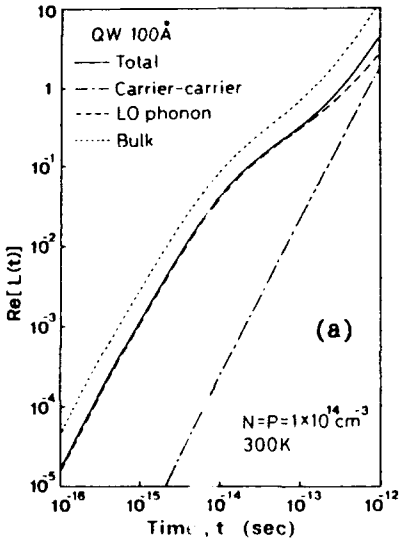


Fig. 3 Line shape functions of *p*-type modulation doped (MD) QW structures.



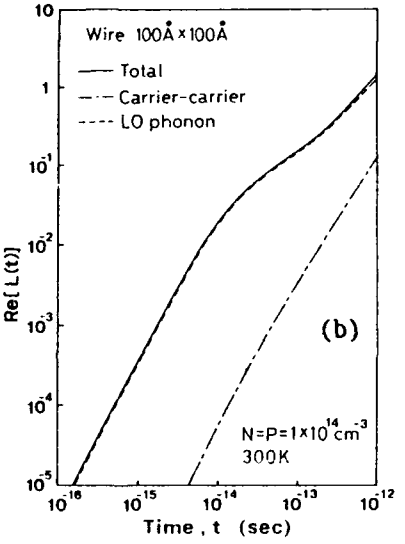


Fig. 4 Real part of phase damping factor $L(t)$ at carrier density of $1\times10^{14}\,cm^{-3}$. (a) 100Å QW, (b) 100Å×100Å quantum wire.

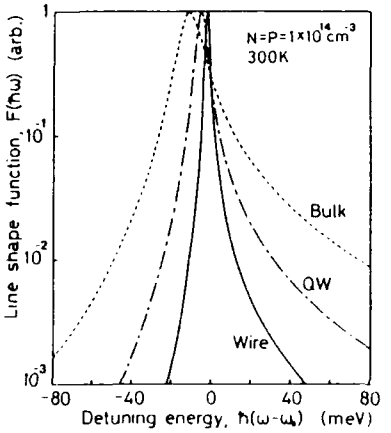


Fig. 5 Line shape functions at low carrier density.

AD-P007 858

92-22387

EFFECT OF LIGHT-INDUCED DRIFT IN CONFINED SEMICONDUCTOR HETEROSTRUCTURES

Mark I. Stockman†, *Lakshmi N. Pandey and Thomas F. George*

Departments of Chemistry and Physics & Astronomy, Center for Electronic and Electro-optic Materials, 239 Fronczak Hall, State University of New York at Buffalo Buffalo, New York 14260

†Internet address: nsmark@ubvms.cc.buffalo.edu. Phone: (716)636-3070. Also with: Institute of Automation and Electrometry, Siberian Branch of the USSR Academy of Sciences, 630090 Novosibirsk, USSR.

The effect of light-induced drift (LID) in gases, predicted by Gel'mukhanov and Shalagin[1] and observed later[2], is manifested in mechanical drift of the absorbing atoms (molecules) in response to optical excitation. The effect of LID takes place if the atom interaction with light is velocity-dependent (due to the Doppler effect), the spectrum of the exciting radiation is asymmetric with respect to the the absorption line, and the absorbing molecules experience collisions with a buffer gas, with the collision rate dependent upon their internal state.

The idea of LID is the following. Suppose for the sake of definiteness that the collision frequency of the absorbing molecules with the buffer is greater in the excited state and that the exciting light is red-shifted with respect to the absorption contour. Then due to the Doppler shift, the radiation interacts mainly with the counter-moving molecules, which undergo transitions into an excited state, in which their friction upon the buffer component is increased. Due to this increase, the counter-flying molecules are slowed down, while the molecules moving in the direction of light are not affected. The net effect is a drift of the absorbing component in the direction of light. The drift alternates its direction with the change of signs of either the detuning or the difference in the collision frequencies.

Later, a similar effect, surface LID, was predicted[3] and observed[4] to take place in a one-component gas whose scattering from the walls of the container is dependent on the molecule internal state. Also, it has been predicted[5,6] and observed[7] that there exists LID of electrons in semiconductors in the presence of a magnetic field. In this case the translational motion occurs along the field direction, and light excites transitions between Landau levels ("internal" states of the electron). If the electron translational relaxation depends on which of the Landau levels the electron occupies, LID takes place.

In this report we predict LID for quantum-confined electrons in semiconductor heterostructures: quantum wells, wires, and one- and two-dimensional superlattices. The heterostructures discussed are of great interest from the point of view of various applications in microelectronics and quantum optics (see, e.g., Ref. 8). The effect of LID manifests itself as the parallel (with respect to the heterostructure) current of the carriers with an antisymmetric dependence on the detuning of the exciting radiation from the transition between states in the well, which is characteristic of LID.

For definiteness, let us consider electrons in quantum wells. Straightforward generalization of the theory is possible to describe quantum wires as confined structures and also periodic quantum structures (superlattices). The quantum well is a flat layer in the semiconductor with different chemical composition. Electrons are confined within this layer, which can be considered as a one-dimensional (say, along the z-coordinate) potential well, while their (quasi)momentum $\mathbf{p}$ in the xy-plane is conserved. Light causes transitions between states in the well. The electrons in the quantum well can be considered as a two-dimensional gas of particles, whose internal state is the state in the well. The

electron translational relaxation can depend on this internal state (see below). If so, the conditions of the existence of LID are met. Note that a similar idea concerning thin films and inversion layers was mentioned in Ref. 6 but was not examined there.

Let us consider the transitions between two electron bands m and n, with energies at origin ε_a and dispersion laws $\epsilon_{\mathbf{p}}^{(a)}$, where $a = m,\ n$. The resonance condition is $\left|\varepsilon_n + \epsilon_{\mathbf{p}+\mathbf{q}}^{(n)} - \varepsilon_m - \epsilon_{\mathbf{p}}^{(n)} - \hbar\omega\right| \lesssim \hbar\Gamma$, where $\mathbf{q}$ and ω are the photon momentum and energy, and Γ is the transition homogeneous width. This condition should be met for a resonant momentum $\mathbf{p}_0$, but not for momenta $\mathbf{p}$ perpendicular to $\mathbf{p}_0$, which ensures the selectivity of excitation in the electron velocities and, consequently, existence of the drift. Let us suppose a non-degenerate electron gas and use the approximation $\epsilon_{\mathbf{p}}^{(a)} = p^2/2m_a^*$, where m_a^* is the corresponding effective mass. The magnitude of the drift velocity v_d is proportional to and limited by the thermal velocities of the electrons participating in the resonant transitions $v_0 \sim p_0/m^*$. From these arguments, the drift velocity can be shown to be maximum and on order of the thermal velocity in the case of intersubband transitions, where the efficient masses are equal, $m_n^* = m_m^* \equiv m^*$. Otherwise, in the case of interband transitions, $m_n^* \neq m_m^*$ and the velocity v_d is reduced by a small factor $q/p_t \sim \left(\varepsilon_{mn}/m^*c^2\right)^{1/2}$, where p_t is the mean thermal momentum of electrons, c is the velocity of light and $\varepsilon_{nm} \equiv \varepsilon_n - \varepsilon_m$. For the parameters typical for GaAs/AlGaAs wells, $m^* = 0.068m_e$, where m_e is the electron mass and ε_{nm}= 30 meV, it can be estimated $q/p_t \sim 10^{-3}$. Note that the maximum drift velocity induced by photon-drag (light-pressure) can be estimated as q/m^* and is by a factor q/p_t less than the LID velocity in the case of parallel bands, where $m_n^* = m_m^*$. Based on the above estimates, we shall now consider the intersubband (QWEST) transitions of the quantum-confined electrons. This ensures parallel bands and maximum drift velocity.

Using the techniques of the one-electron density matrix, for the non-degenerate electron gas in the well and small (non-saturating) light intensities we have obtained the expression for the magnitude of the LID-current density j (the vector $\mathbf{j}$ for isotropic semiconductors is directed parallel to the wave vector $\mathbf{k}$),

$$j = I|e_z|^2 \frac{8\pi^{3/2}e^3}{\hbar^2 c} \frac{z_{mn}^2 n}{kZ} \left(\nu_n^{-1} - \nu_m^{-1}\right) \left[\exp(-\varepsilon_n/T) - \exp(-\varepsilon_m/T)\right] C(\xi) \ . \qquad (1)$$

Here e is the elementary charge, k is the wave vector, I is the light intensity, e_z is the z-component of the light polarization vector, z_{mn} is the transition matrix elements of the electron z-coordinate between the states in the well, n is the two-dimensional electron density in the well, ν_m and ν_n are the collision frequencies of the electron in the corresponding states, T is the temperature, $Z = \sum_a \exp(-\varepsilon_a/T)$ is the statistical sum, and the real function C and its complex argument ξ are defined as $C(\xi) \equiv \mathrm{Re}\left\{\xi \exp(-\xi^2)\left[1 + \mathrm{erf}(\imath\xi)\right]\right\}$, $\xi \equiv \xi' + \imath\xi''$, $\xi' = (\omega - \omega_{nm})/kv_t$, $\xi'' = \Gamma/kv_t$, where $\omega_{nm} = \varepsilon_{nm}/\hbar$, $v_t = (2T/m^*)^{1/2}$. One can easily see from Eq. (1) that j alternates direction with the sign change of either the relative detuning ξ' or difference $\nu_n - \nu_m$, as expected for LID. The spectral dependence of LID is illustrated in Fig. 1. The current density j (1) has characteristic polarization dependence: it vanishes for polarization parallel to the well plane.

Let us estimate the maximum current j_{max} under conditions of optical saturation. In the most important case, where the homogeneous broadening is large compared to the Doppler broadening, $\Gamma \gg kv_t$, the saturation condition is $G_{mn}^2/\Gamma \sim \min(\nu_m, \nu_n)$. In this case, we get from Eq. (1) the estimate

$$j_{max} \sim enkv_t^2 \Gamma^{-1} (\nu_m - \nu_n) \left[\max(\nu_m, \nu_n)\right]^{-1} Z^{-1} \left[\exp(-\varepsilon_n/T) - \exp(-\varepsilon_m/T)\right] \ . \qquad (2)$$

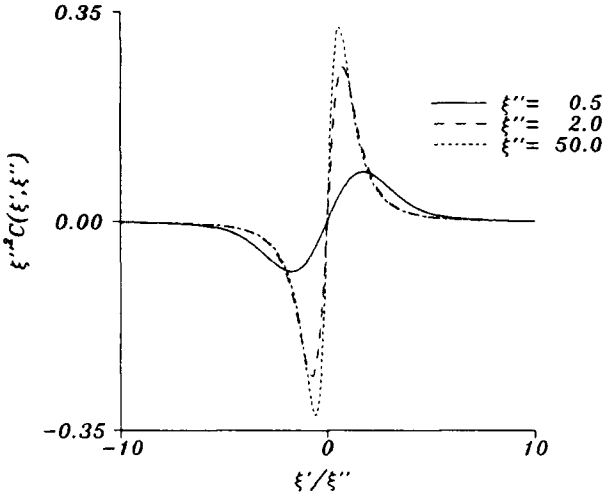


Fig. 1. Profile of the LID effect as a function of the relative detuning $\xi' = (\omega - \omega_{nm})/kv_t$ for the values of the relative width Γ/kv_t shown.

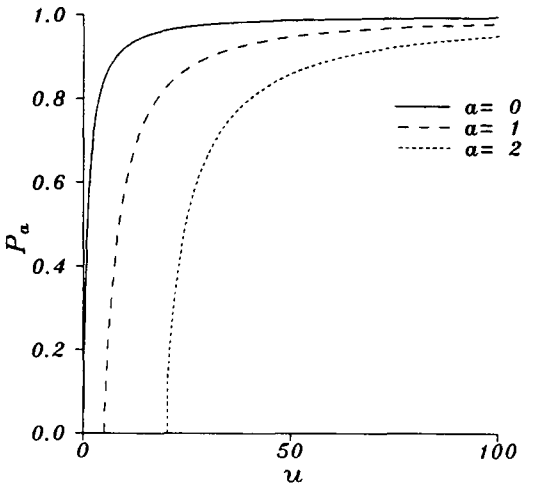


Fig. 2. Probability P_a as a function of the dimensionless parameter $u = U_0 m^* l^2/\hbar^2$, where U_0 is the potential well depth.

Let us discuss the physical situation in regard to an experimental examination of the effect suggested. We assume, as discussed above, intersubband (QWEST) transitions in GaAs/AlGaAs quantum wells, $T \sim \varepsilon_{nm} \approx 30$ meV, the latter corresponding to the well depth $l \approx 140$ Å. To have an appreciable concentration n of electrons in the conduction band inside the well, barrier or well regions should be doped with donor impurities. These impurities may simultaneously serve as the scatterers needed for LID (see also below). The concentrations usually achieved are $n = 10^9$ to 10^{12} cm^{-2}. At these concentrations, electron-electron scattering does not play a significant role in relaxation. We also note that the electron concentration may be controlled by normal electric field or incoherent optical pumping. The energies and temperatures assumed are below the spectral gap of optical phonons, which are therefore unlikely to contribute significantly to the electron relaxation. The role of acoustic phonons for the processes under consideration is not very important. Thus, under the present conditions, the main origin of the polarization relaxation is the broadening of the transition due to the variation Δl of plus or minus one atomic monolayer of the depth l of the well. This brings about the relative width $\hbar\Gamma/\varepsilon_{nm} \approx 2\Delta l/l \approx 0.04$, which is adopted below. This value is in fairly good agreement with the line widths experimentally observed[9,10] at both 60 K and 2 K (the absence of a temperature effect confirms the non-phonon broadening mechanism).

In the case under consideration, the dependence $j_{max}(T)$ is that explicitly shown in Eq. (2), and it levels off for $T \gtrsim \varepsilon_{nm}$, i.e., for temperatures in the liquid nitrogen range. Adopting for definiteness $T = 77$ K, we get $kv_t/\Gamma \approx 0.015$, which corresponds to the case of weak Doppler broadening. Assuming a large difference in the collision frequencies and, as an example, adopting the width L of the well (in the xy-plane) to be 1 mm, from (7) for $n \sim 10^9$ to 10^{12} we obtain the estimate for the saturated current $J_{max} = Lj_{max} \sim 1$ μA to 1 mA, which is more than sufficient to observe the effect and also promises the possibility

of applications.

The difference $\nu_m - \nu_n$ originates from the fact that the distributions of both scatterers and confined electrons depend upon z, with the latter being state dependent. To illustrate this, consider a realistic model in which the translational relaxation is due to scattering by a potential of impurities with concentrations n_i and n_o inside and outside the well. Applying Fermi's golden rule, and assuming that scattering from impurities is inelastic (i.e. causing the transitions $m \leftrightarrow n$) and the well is rectangular, we obtain for the relaxation frequencies the expression with clear physical meaning

$$\nu_a = f\left[(n_i - n_o)P_a + n_o\right] \quad , \quad P_a = \int_0^l |\phi_a(z)|^2 \mathrm{d}z \quad , \tag{3}$$

where P_a is the probability for an electron in the state $a = m, n$ to be inside the well (ϕ_a is the corresponding wave function), and f is a state-independent parameter determined by the interaction. The dependence of P_a on the state is illustrated in Fig. 2 for the three lowest levels in the well ($a = 0, 1, 2$). For realistic parameters of the well, one obtains $P_a \approx 1$. It then follows from (3) that a favorable condition for LID is $n_o \gg n_i$, which can be achieved by doping the external (barrier) regions of the well.

To summarize, we predict a new effect, LID of electrons in quantum-confined semiconductor heterostructures. This effect differs from photon drag and some other optoelectric phenomena in semiconductors by its magnitude and the characteristic spectral and polarization dependences.

We are grateful to B. D. McCombe and W. J. Li for useful discussions. This research was supported in part by the Office of Naval Research.

References

1. F. Kh. Gel'mukhanov and A. M. Shalagin, Pis'ma Zh. Eksp. Teor. Fiz. **29**, 773 (1979) [Translation: JETP Lett. **29**, 711 (1979)].
2. V. D. Antsygin, S. N. Atutov, F. Kh. Gel'mukhnov, G. G. Telegin and A. M. Shalagin, Pis'ma Zh. Eksp. Teor. Fiz. **30**, 262 (1979) [Translation: JETP Lett. **30**, 243 (1979)].
3. A. V. Ghiner, M. I. Stockman and V. A. Vaksman, Phys. Lett. A **96**, 79 (1983).
4. R. W. M. Hoogeven, R. J. C. Spreeuw, L. J. F. Hermans, Phys. Rev. Lett. **59**, 447 (1987).
5. E. M. Skok and A. M. Shalagin, Pis'ma Zh. Eksp. Teor. Fiz. **32**, 201 (1980) [Translation: JETP Lett. **30**, 184 (1980)].
6. A. M. Dykhne, V. A. Roslyakov and A. N. Starostin, Dokl. Akad. Nauk SSSR **254**, 599 (1980) [Translation: Sov. Phys. Dokl. **25**, 741 (1980)].
7. A. V. Kravchenko, A. M. Pakin, V. N. Sozinov, O. A. Shegai, Pis'ma Zh. Eksp. Teor. Fiz. **38**, 328 (1983). [Translation: JETP Lett. **38**, 393 (1983)].
8. Gerald Bastard, *Wave Mechanics Applied to Semiconductor Heterostructures* (Les Editions de Physique, Les Ulis, France, 1988).
9. W. J. Li, B. D. McCombe, F. A. Chambers, G. P. Devane, J. Ralston and G. Wicks, Surf. Sci. **228**, 164 (1990).
10. A. Lorke, U. Merkt, F. Malcher, G. Weimann and W. Schlapp, Phys. Rev. B **42**, 1321 (1990).

92-22388

AD-P007 859

High-Contrast Electron-Transfer GaAs/AlGaAs Multiple Quantum Well Waveguide Modulator

*O. Blum**, *J. E. Zucker* , *T. Y. Chang, N. J. Sauer, M. Divino,*

*K. L. Jones, T. K. Gustafson**

AT&T Bell Laboratories, Holmdel, NJ 07733

* Department of EECS, University of California, Berkeley, CA 94720

Phone: (415) 643-9862, Fax: (415) 643-8426

In this paper, we present the first demonstration of the barrier reservoir and quantum well electron transfer structure (BRAQWETS) concept in the GaAs/AlGaAs material system. The BRAQWETS uses an applied voltage (V_{app}) to transfer electrons from the highly doped reservoir region to a quantum well, blue shifting the absorption edge in the quantum well due to bandfilling. Waveguide modulators with a 5 BRAQWETS active core exhibit contrast ratios as high as 75:1 in a 490 μm-long device. We show how the operation and performance of the device can be understood in terms of the voltage-induced changes in the BRAQWETS energy band diagram and the corresponding photocurrent spectra.

The measured performance of waveguide modulators is shown in Fig 1a for TM polarized light and in Fig 1b for TE polarized light, where the ON/OFF ratio is plotted as a function of applied voltage for several wavelengths. Here, the OFF state is defined as the transmission at V_{app} = 10 V, where the optical output power is minimum. Large contrast ratios are obtained. For example, at λ = 864.5 nm and TM polarized light, the ON/OFF ratio is 75:1 (18.7 dB) for the voltage swing from -5 V to 10 V. Three distinct voltage ranges of operation can be distinguished for all wavelengths in Fig 1. In region I, from -10V to -5V, the transmission is increasing, reaching a maximum at -5 V. In region II, from -5V to +5V, there is a steep transmission decrease, while in region III, from +5V to +10V, the decrease in transmission is much more gradual. The most efficient operation occurs in region II, with an ON/OFF

ratio of 12:1 for a -5V to 5V voltage swing at λ = 864.5 nm for TM polarization. Furthermore, in this voltage range the decrease in transmission is most linear. We note that for both TE and TM polarizations, the optimum wavelength is 864.5 nm, with decreasing contrast ratios for both shorter and longer wavelengths. In the following, we will show how the voltage and wavelength dependences can be understood in terms of the BRAQWET band structure.

The field- and carrier-induced changes in absorption are conveniently monitored by measurements of photocurrent spectra in large-area mesas. Photocurrent spectra for voltage range II, shown in Fig 2a indicate a clear blue shift of the absorption edge as V_{app} is decreased from 5 V to -5 V. This shift can be understood in terms of the calculated band diagrams, shown in Figs 2b and 2c. At 5 V, the field across the QW is large, giving the red-shifted excitonic absorption associated with the QCSE. This corresponds to the observed decrease in transmission at +5V shown in Fig 1. Application of negative voltage to the right-hand side of the band diagram decreases the field as shown in Fig 2c allowing electrons to flow into the well from the reservoir and cause bandfilling. This is consistent with both the blue shift in the photocurrent spectra of Fig 2a as well as the high transmission at -5 V shown in Fig 1. In addition, the photocurrent spectra in Fig 2a show that the optimum wavelength of operation for the waveguide modulator is just above the absorption edge where the bandfilling effect is a maximum.

Fig 3a shows photocurrent for voltages in regions I and III. The absorption edge for +10V and -10V is in almost the same position, red shifted from its position at -5V. This indicates that at +10 and -10 V the QCSE is present. Calculated band diagrams in Figs 3b and 3c support this interpretation. The corresponding transmission is therefore low at +10 V, although this change in transmission associated with the QCSE alone is minor compared with that produced by bandfilling in voltage range II. At the other extreme, at -10 V a field of opposite polarity is established across the QW with the associated QCSE red shift. This accounts for the decrease of contrast ratio in voltage range I.

In conclusion, we have demonstrated the first GaAs/AlGaAs BRAQWETS modulator with ON/OFF ratios of 75:1 in a 490 μm long device. The wavelength of operation is well suited to modu-

lation of high power AlGaAs lasers, currently the preferred optical source in applications from optical data storage to pumping miniature Nd:YAG lasers. We successfully interpret the voltage and wavelength behavior of the modulator in terms of its energy band diagram and observe the transitions at high field from bandfilling to the quantum confined Stark effect. It is interesting to compare the present device with a 5 BRAQWETS waveguide in the InGaAs/InAlAs system, where the voltage-length product for a 75:1 contrast ratio was 5.9 V-mm. We obtain comparable performance, 7.3 V-mm. However, since the depth of the conduction band potential well in InGaAs/InGaAlAs is larger than that of the present structure, we see that device performance in GaAs/AlGaAs BRAQWETS could be improved by increasing the Al concentration in the AlGaAs reservoir and barrier regions. Another feature of the GaAs/AlGaAs system is that the QW excitonic peak absorption is larger than in InGaAs-based QWs, providing potentially greater intensity modulation.

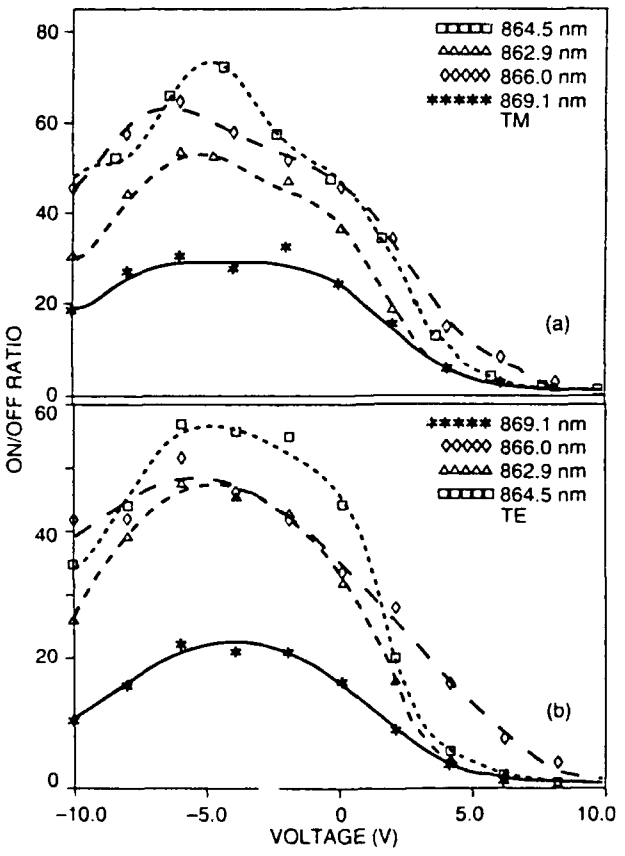


Fig. (1) ON/OFF ratio as a function of voltage at several wavelengths for (a) TM polarized light (b) TE polarized light. Lines indicate polynomial fits to the data and every tenth data point is shown with symbol.

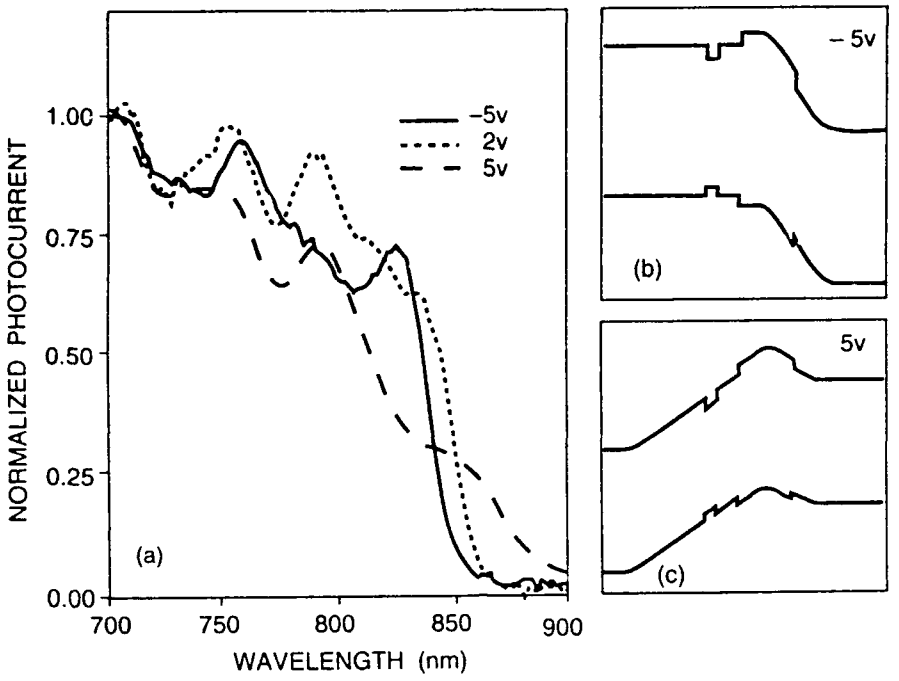


Fig. (2) (a) Photocurrent spectra for $-V_{app}$ = -5V, 2V and 5V, normalized to the value at short wavelength. Calculated energy band diagrams for (b) V_{app} = -5V, (c) V_{app} = 5V.

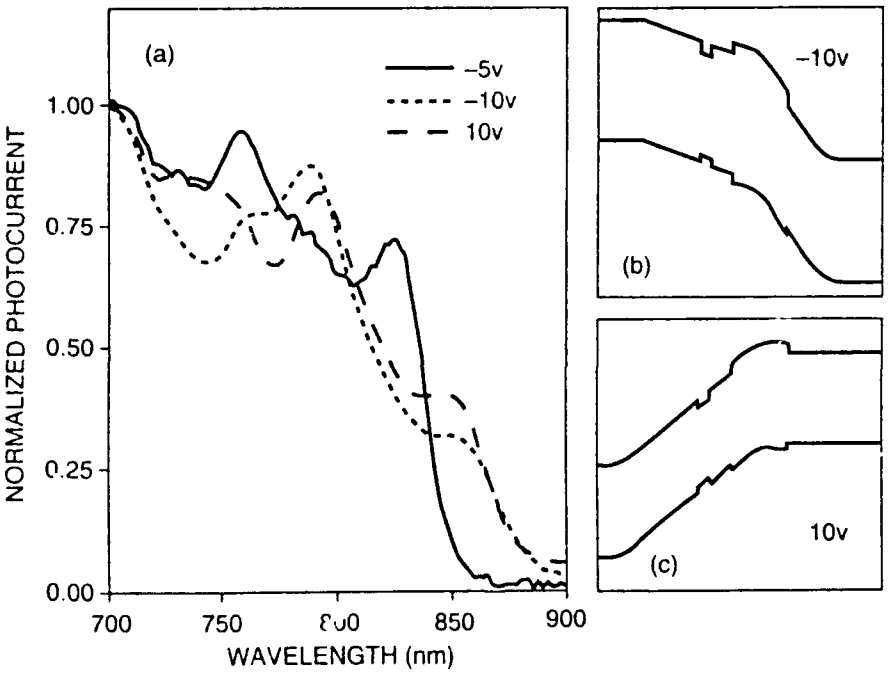


Fig. (3) (a) Normalized photocurrent spectrum for $-V_{app}$ = -10V, -5V and 10V. Calculated energy band diagrams for (b) V_{app} = -10V, (c) for V_{app} = 10V.

AD-P007 860

92-22389

Growth of Ultra-Thin $Ga_xIn_{1-x}As$/InP Quantum Wells with Modulation Doping and Strained Structure

Toshi K. Uchida, N. Yokouchi, T. Uchida, T. Miyamoto,
F. Koyama and K. Iga

Tokyo Institute of Technology
4259 Nagatsuta, Midori-ku, Yokohama 227 Japan

Lattice-matched GaInAs to InP is being avidly investigated for increasing device applications in optoelectronics. Recent advancements of epitaxial growth techniques have made these applications possible using sophisticated multilayer heterostructures such as quantum wells (QWs) and modulation doping.[1,2] Progress in this area has also made it possible to coherently grow an entire range of $Ga_xIn_{1-x}As$ ($0 \leq x \leq 1$) on to InP while keeping these layers less than a critical thickness.[3,4] These pseudomorphic materials have drawn an increasing attention for optical and electronic devices.[5,6] Although these devices have been successfully fabricated and demonstrated promising performance, some fundamental characteristics of unstrained and strained materials still need to be explored. We have grown modulation doped ($4 \times 10^{19} cm^{-3}$) $Ga_{0.47}In_{0.53}As$ QWs and biaxially strained QWs using $Ga_xIn_{1-x}As$/InP ($0 \leq x \leq 0.32$, compressive mode) on InP and optically characterized.

An all-gas source chemical beam epitaxial system manufactured by RIBER was used for this experiment. For group V sources, pure arsine and phosphine were used and precracked at 900°C by our originally designed cracking cell. Trimethylindium (TMI) and triethylgallium (TEG) were used as group III sources with hydrogen carrier-gas. Solid Be and Si were used as p-type and n-type dopants. Ten $Ga_xIn_{1-x}As$ QWs were grown on (100)-oriented InP substrates (prepared by Nippon Mining Co.) between InP barriers. By optimizing valve sequence and growth interruption,

single-peaked photoluminescence (PL) spectra were obtained for all strained samples.

Modulation doped QWs were prepared by doping Be in 150Å thick InP barriers. In bulk InP, Be was successfully doped up to $4x10^{19}cm^{-3}$. In Fig. 1, relative PL intensity and PL linewidth of modulation doped quantum wells are shown for different impurity levels. Intensity increased with increasing doping levels up to $2x10^{19}cm^{-3}$. Above this level, intensity became saturated and linewidth broadened. The results show the possibility of improvements in laser device performance using QWs with appropriate doping structures.

$Ga_xIn_{1-x}As$ (x=0, 0.2, 0.32) strained QWs were grown between 240Å InP barriers. Emission wavelengths of these samples for various well widths at 300K are shown in Fig. 2. Solid lines represent theoretical estimates using 50% of the total band offset for the conduction band offset and the effective mass approximation. As can be seen in the figure, wavelength can be estimated reasonably well. It is important to be able to select desired wavelength for device applications. In Fig. 3, PL linewidths of strained samples (x=0.2, 0.32) at 300K and 77K are plotted. Linewidths rapidly increase for well widths of less than 20Å due to layer fluctuations. The PL intensity of strained samples (x=0, 0.2, 0.32) relative to the maximum intensity obtained for $Ga_{0.2}In_{0.8}As$ samples are shown in Fig. 4. Intensity increases until well width of around 20Å due to the quantum size effect. However, intensity decreases below this width due probably to layer fluctuations as seen in Fig. 3. PL intensities of strained samples were usually much higher than those of unstrained QW samples. Strained QWs of appropriate well width and composition are extremely useful for optical device applications. Currently, we are investigating effects of barrier thickness for

strained QWs. These is a critical thickness for barriers to keep a coherent growth.

Our results show some possibilities of improving device performances using this growth technique. We are now growing laser devices with these structures including vertical cavity surface emitting lasers.

The authors wish to acknowledge Prof. Y. Suematsu, the President of Tokyo Institute of Technology, for his constant encouragement on this work. This work was supported by the Scientific Research Grant-in-Aid 61065002 from the Japan Ministry of Education, Science and Culture.

References

1. H. Temkin, T. Tanbun-Ek, R.A. Logan, J.A. Lewis, and N.K. Dutta, Appl. Phys. Lett. 56 (1990) 1222.
2. K. Uomi, T. Mishima, and N. Chinone, Appl. Phy. Lett. 51 (1987) 78.
3. D. Gershoni, H. Temkin, J.M. Vandenberg, S.N.G. Chu, R.A. Humm, and M.B. Panish, Phys. Rev. Lett. 60 (1988) 448.
4. T.Y. Wang and G.B. Stringfellow, J. Appl. Phys. 67 (1990) 344.
5. P.J.A. Thiji, J.J.M. Binsma, G.L.A. v.d. Hofstad, and L.F. Tiemeyer, 12th Int. Semiconductor Laser Conf., Davos, Switzerland (1990) Post Deadline Paper PD-1.
6. S. Sasa, N. Nakata, Y. Sugiyama, T. Fujii, and E. Miyauchi, J. Cryst. Grwoth 95 (1989) 189.

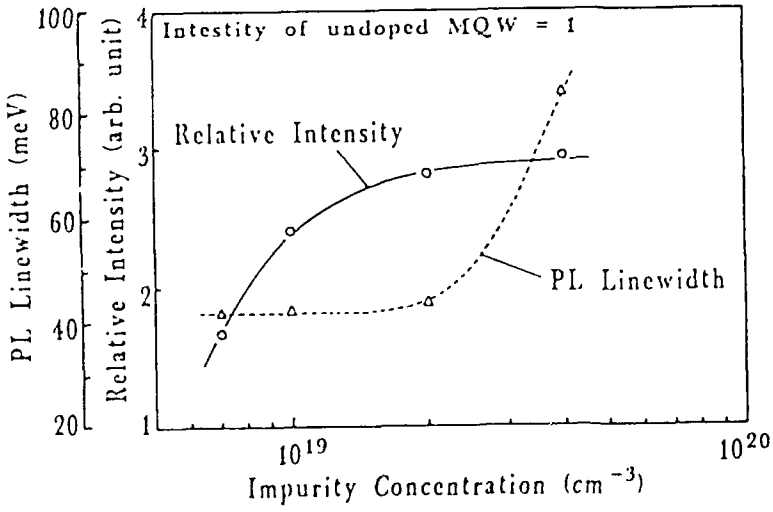


Fig. 1 PL intensity and linewidth of modulation doped QWs vs impurity level in InP barriers at room temperature. Well width was about 80Å and intensities were relative to an undoped QW of the same structure.

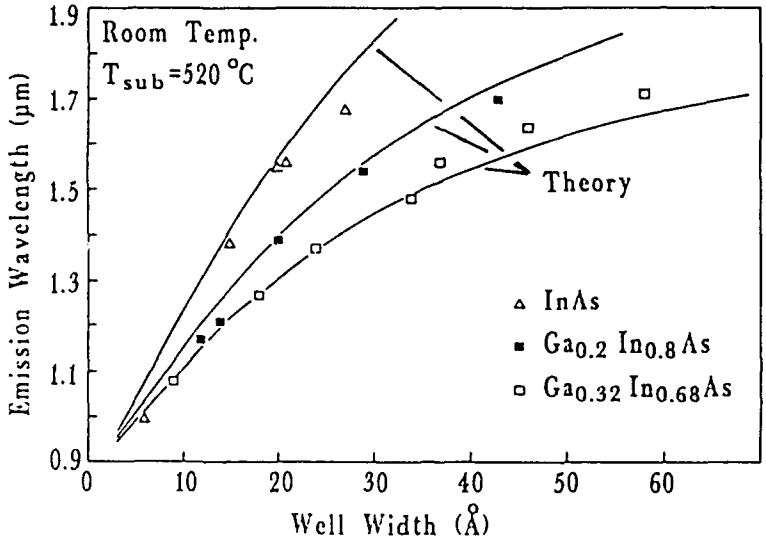


Fig. 2 Room temperature emission wavelength vs well width of strained QWs. Solid lines represent theoretical estimations (see ref.4).

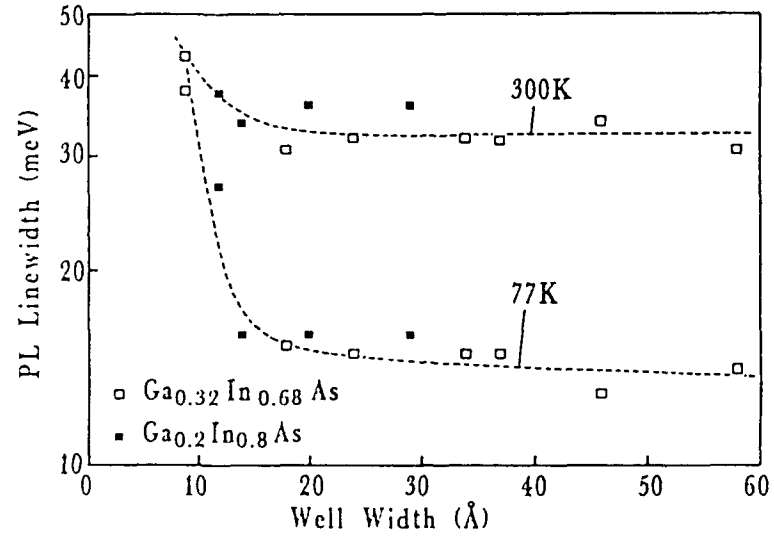


Fig. 3 PL linewidth vs well width of strained QWs at 300K and 77K. At 77K, around 15meV of linewidths were obtained for well widths of above 20Å and less than 60Å. For well width less than 20Å, linewidth increased due probably to layer fluctuations.

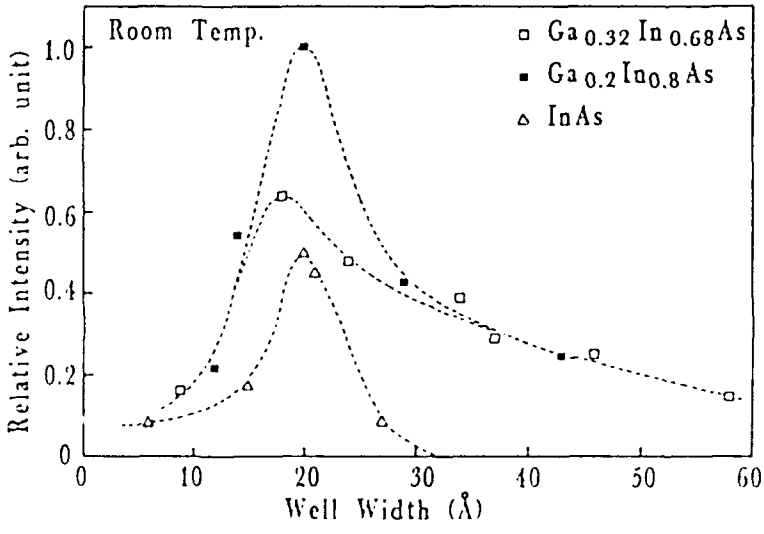


Fig. 4 Room temperature relative PL intensity vs well width of strained QWs. Intensity increased from well width of 60Å to 20Å, but decreased rapidly after 20Å. It was probably due to layer fluctuations.

AD-P007 861

A high contrast, low insertion loss asymmetric Fabry Perot modulator operating at 4.1Volts.

P. Zouganeli, M. Whitehead*, P.J. Stevens, A. Rivers and G. Parry,
Department of Electronic &Electrical Engineering, University College London, Torrington Place, London WC1E 7JE, U.K.
**Department of Electrical & Computer Engineering, University of California, Santa Barbara, CA 93106, USA.*
J.S. Roberts,
Department of Electronic & Electrical Engineering, University of Sheffield, Sheffield S1 3JD, U.K.

A very high contrast (>20dB), low insertion loss (~3.3dB) GaAs/AlGaAs multiple quantum well (MQW) reflection modulator with an operating voltage of ~9V reverse bias has recently been demonstrated [1]. The device was electrically a p-i-n diode with the MQW in the intrinsic region, and optically an asymmetric Fabry-Perot (FP) cavity. The back mirror of the FP cavity was formed using an integrated quarter wave reflector stack and exhibited a reflectivity of >95%. The front mirror was the natural air-semiconductor interface with a reflectivity of ~30%. A reduction of the operating voltage, aiming at a high contrast, low insertion loss modulator is addressed in this paper.

For an asymmetric Fabry-Perot modulator (AFPM), the operating wavelength is set at the FP resonance. That wavelength is (for a "normally-on" device) at a wavelength longer than that of the e1-hh1 (heavy hole) exciton peak for zero bias. The red shift of the exciton absorption peaks under an applied field (Quantum Confined Stark Effect [2]) induces absorption at the operating wavelength, which effectively reduces the reflectivity of the back mirror equalising it to that of the front. The cavity is thus balanced and the overall reflectivity zero.

At the FP resonance, the reflectivity R of the structure is strongly dependent upon the absorber present in the cavity and is given by[3]

$$R = \frac{R_f \cdot \left(1 - R_\alpha / R_f\right)^2}{\left(1 - R_\alpha\right)^2} \qquad (1)$$

92-22390

$$R_\alpha = \sqrt{R_f \cdot R_b} \cdot e^{-\alpha d}$$

where R_f and R_b the front and back reflectivities, α the absorption coefficient of the MQW region, and d the thickness of the MQW region.

A reduction of the operating voltage to less than 5V is strongly desirable for compatibility of the optoelectronic device with CMOS driving electronics. At the same time, an insertion loss much higher than ~3dB may impose constraints on the fan-out, or prohibiting total optical power requirements for a practical system. For a given quantum well system (well material and width, barrier material and width), the operating voltage will be reduced if the thickness of the intrinsic region is reduced. The critical amount of absorber $[\alpha d]_c$ needed to zero the reflectivity is given by

$$[\alpha d]_c = \ln \sqrt{\frac{R_b}{R_f}} \qquad (2)$$

An increase of R_f or a decrease of R_b both result in a decrease of $[\alpha d]_c$ and consequently of the operating voltage. The above are made clear in Figure 1. For the same $[\alpha d]_c$, a decreased R_b leads to an enormous reduction of the reflectivity of the "on" state (increase of the insertion loss). Therefore the increased R_f and consequently higher finesse case has to be chosen. Generally, the back mirror effectively provides the reflectivity of the "on" state and it should thus be made as highly reflective as possible.

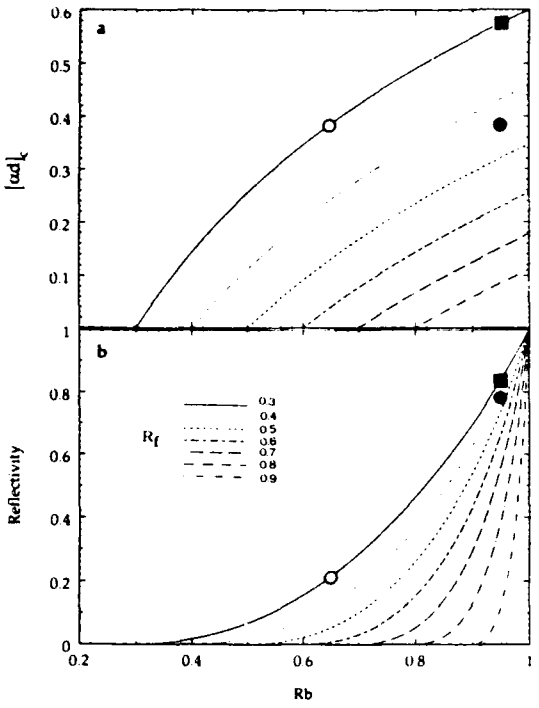


Figure 1.a) *The critical amount of absorber* $[\alpha d]_c$ *required to zero the overall reflectivity and*
b) *reflectivity of a cavity with no absorption, as a function of the reflectivity of the back mirror* Rb, *for different front reflectivities* Rf.
■ *device in ref[1].*
● *present device.*
○ *alternative low back reflectivity case.*

An AFPM structure with a front reflectivity of ~43% has been grown by atmospheric pressure MOVPE[4]. The detailed epitaxial structure of the device is shown in Figure 2. The MQW region consists of 32 GaAs wells with a nominal thickness of 94Å and 31 nominally 60Å-wide $Al_{0.3}Ga_{0.7}As$ barriers. The integrated mirrors were formed by subsequent pairs of alternating high (H) and low (L) refractive index quarter wave thick dielectric layers, namely 609Å $Al_{0.1}Ga_{0.9}As$ (H) and 724Å AlAs (L). The front mirror consists of 1.5 such pairs (HLH) and the back mirror of 12.5 (HLHL...H). The top $Al_{0.1}Ga_{0.9}As$ layer of the bottom reflector was unintentionally doped to act as an i-region buffer. A 100Å n^+ GaAs layer is used as a capping layer. 400μmX400μm optical window devices were fabricated by standard photolithographic techniques. Reflectivity spectra were obtained on an optical multichannel analyser system with white light at normal incidence. The reflected spectra were normalised to that of a freshly deposited Au film.

Reflectivity spectra obtained in this manner are shown in Figure 3 for the unbiased (0V) and the

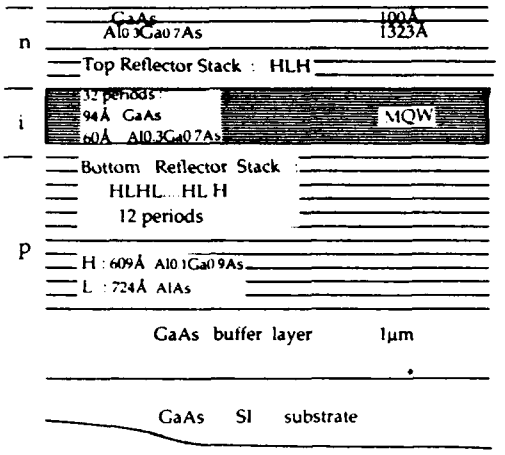


Figure 2. *The epitaxial structure of the* AFPM *device.*

maximum-contrast case. Maximum contrast was obtained under ~4.1V reverse bias. Contrast of ~14dB has been achieved, the operating wavelength being ~857nm and the insertion loss at that wavelength ~3dB (Figure 4).

The advantages of the AFPM have been the large optical bandwidth[1] and the relative insensitivity to temperature[5]. An increased finesse cavity has been thought to result in an elimination of the above advantages as has also been indicated by the results of Yan et al [6], together with an increased sensitivity to cavity thickness fluctuations. The appropriate parameter of merit is in fact the width of the FP resonance, which directly sets the optical bandwidth but also in turn determines the modulator's tolerances to temperature (as far as contrast is concerned). An increase of the coefficient of finesse F results in a "sharper" resonance according to

$$\beta = 4 \cdot \sin^{-1}\left(1/\sqrt{F}\right) \qquad (3)$$

where β the FWHM of the resonance in phase terms. In wavelength terms though, the FWHM is given by

$$\delta\lambda = \frac{\lambda^2 \beta}{4\pi L n} \qquad (4)$$

where n the mean refractive index of the cavity, λ the resonant wavelength, and L the cavity thickness. In other words, an increase of the cavity finesse does not necessarily lead to a narrower FP resonance, δλ being inversely proportional to L.

In this structure we have kept the cavity as thin

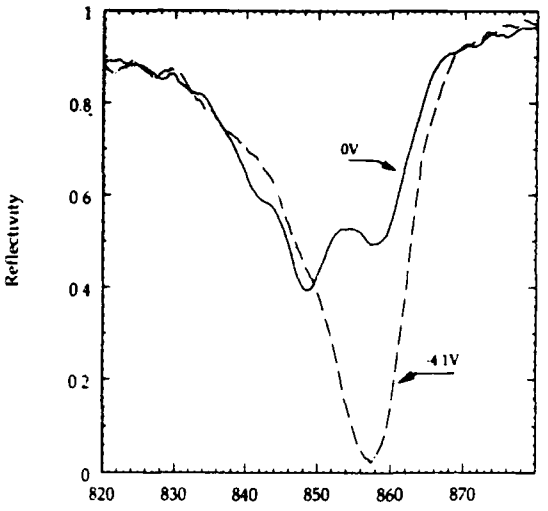


Figure 3. *Reflectivity spectra for the unbiased (0V) and the maximum contrast case (4.1V reverse bias).*

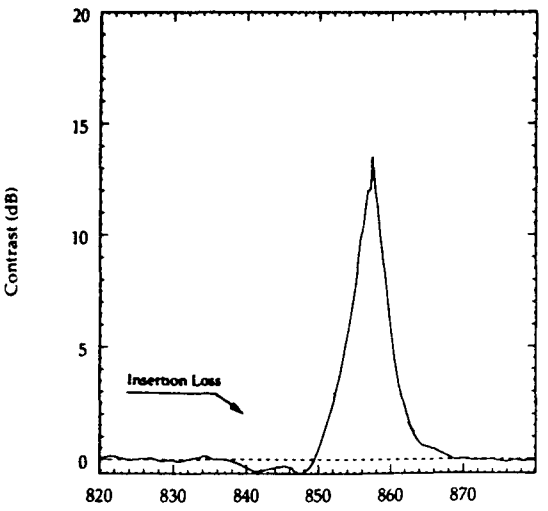


Figure 4. *Contrast (R(0V)/R(-4.1V)) (——) and insertion loss ( ) vs wavelength.*

as possible. At the same time, the increase of the finesse resulted in a reduction of the i-region thickness, allowing for a further reduction of the cavity thickness. Although a direct comparison with the device of ref 1. cannot be made since a "zero" off-reflectivity has not been achieved here, it is important to note that the FP resonance is indeed broader for the present device, in agreement with our previous analysis. When a very high contrast modulator is "off", the front and the effective back reflectivities are equal. The effective finesse would be ~3.6 for the present device leading to a FWHM of the resonance of ~36nm (equation 4). The corresponding figures for ref[1] are ~2.45 and ~26nm respectively. The above do not take into account the fact that the absorption is wavelength dependent, but do allow us to compare the two structures. The broader resonance of the present device implies improved fabrication tolerances, and indicates a possible improvement of the temperature sensitivity as far as the contrast is concerned. Additionally, it is worth noting that the shift of the FP resonant wavelength due to growth variations (dL/L , L the cavity thickness) or due to changes of the mean refractive index is not dependent upon the cavity finesse.

The direct increase (ignoring the contribution of absorption) of the insertion loss when the front reflectivity is increased from 30% to 43% is only minimal (~6%), as can be evaluated from Figure 1, while, if we focus on structures incorporating the critical amount of absorber, the insertion loss due to absorption is not critically dependent upon the finesse, determined mainly by the relative position of the heavy hole exciton peak to the FP resonance (for a given well/barrier system). The higher finesse cavity may be making "better use" of the absorber, but simultaneously the amount of absorber is accordingly scaled down. The built-in field is higher (roughly double) for the higher finesse structure, since the intrinsic region thickness is reduced, but the consequent broadening of the zero bias exciton peaks is estimated to be negligible. Note that a broadened zero bias exciton is undesirable since it would impose a higher insertion loss.

A further increase of the front reflectivity to 50%-60% can be attempted without a great penalty on the insertion loss, further lowering the operating voltage. Alternatively, a decrease of the insertion loss can be accomplished if the zero bias wavelength separation of the heavy hole peak and the FP resonance are increased. An increased MQW region will be required to account for the reduction of the absorption coefficient at the operating wavelength, thus the insertion loss will be decreased at the expense of the operating voltage. Generally, the optimum combination of the above two options would be determined by the specific application requirements.

In summary, we have demonstrated a considerably improved asymmetric Fabry-Perot modulator by increasing the front reflectivity to ~43%. The operating voltage has been reduced to ~4.1V, making the device compatible with CMOS technology, while the insertion loss has been ~3dB for a high contrast (14dB) device.

At the same time, the device's tolerances to fabrication and environmental factors are expected to have been improved.

Acknowledgements

P. Zouganeli is sponsored by the Greek State Scholarships Foundation and by the U.K SERC. The project support was provided by the U.K. SERC.

References.

1 WHITEHEAD, M., RIVERS, A., PARRY, G., ROBERTS, J.S., and BUTTON, C. :"Low voltage Multiple Quantum Well reflection Modulator with on:off ratio >100:1",Electron. Lett., 1989, 25, pp. 984-985.

2 MILLER, D.A.B., CHEMLA, D.S., DAMEN, T.C., GOSSARD, A.C., WIEGMANN, W., WOOD, T.H., and BURRUS, C.A.: "Electric field dependence of optical absorption near the band-gap of quantum well structures", Phys. Rev. B, 1985, 32, pp. 1043-1060.

3 WHITEHEAD, M., PARRY, G., and WHEATLEY, P. : "Investigation of etalon effects in GaAs/AlGaAs multiple quantum well modulators", IEEE Proceed. J., 136(1), 1989, pp. 52-58.

4 ROBERTS, J.S., PATE, M.A., MISTRY, P., DAVID, J.P.R., FRANKS, R.B., WHITEHEAD, M, and PARRY, G. : "MOVPE grown MQW p-i-n diodes for electro-optic modulators and photodiodes with enhanced electron ionisation coefficient", J. Crystal Growth, 1988, 93, pp. 877-884.

5 ZOUGANELI, P., WHITEHEAD, M., STEVENS P.J., RIVERS, A., PARRY, G., ROBERTS, J.S., BUTTON, C. : "Temperature sensitivity of asymmetric Fabry-Perot modulators", Electr. Lett. 1990, 26, pp. 1384-1386.

6 YAN, R.N., SIMES, R.J., COLDREN, L.A. : "Extremely low-voltage Fabry-Perot reflection modulators", IEEE Photon. Technol. Lett., 1990, vol 2, pp 118-119.

92-22391

LO Phonons in CdS_xSe_{1-x} Semiconductor Microcrystallites

P007 862

Takayoshi Kobayashi and Shintaro Nomura
University of Tokyo, 7-3-1 Hongo, Bunkyo-ku, Tokyo 113, Japan
Phone 81-3-812-2111, ex. 4228
Fax. 81-3-818-7812

1. INTRODUCTION

It is of interest and importance to study semiconductor microcrystallites[1,2] as three dimensionally confined system in conjecture with one dimensionally confined quantum well systems. Because the oscillator strengths are concentrated on several discrete states, microcrystallites are expected to have large optical nonlinearities. To accomplish this large optical nonlinearities, however, the spectral width play a major role.[3] The intrinsic width is introduced by exciton-phonon coupling rather than an inhomogeneous width which originates from the distribution in the size of microcrystallites. Recently, couplings to longitudinal optical (LO) phonons were investigated by various groups and it was suggested that a microcrystallite of smaller radius exhibits larger coupling to LO phonons because of the increase in couplings to shorter wavelength phonons by the confinement of the exciton wave functions in real space.

In the former part of this paper, the temperature dependence of the exciton energy and the width is investigated by the modulation spectroscopy of the absorption.[4] In the latter part, the exciton-LO phonon coupling constant (Huang-Rhys parameter) is investigated theoretically.

2. EXPERIMENTAL

The samples used in this experiments were CdS_xSe_{1-x} ($x=0.12\pm0.05$) microcrystallites. The details of the experiments are in cur previous paper.[4] The average radii of the microcrystallites were between 50.5 Å and 17.5 Å. The sample temperature was varied in the range of 15–293 K. The increase in the temperature of the samples due to absorption of the probe light from an incandescent lamp passed through a monochromator was estimated to be negligibly small. The transmittance change of the samples induced by an external electric field was measured with a lock-in amplifier.

3. EXPERIMENTAL RESULTS

The electroabsorption was utilized to determine the width and the energy of the excitons. The obtained temperature dependence of the exciton energy is shown in Fig. 1. The bulk band gap from Ref. 5 is also depicted. The temperature dependence of the exciton energy is similar to that of the band gap of bulk diatomic semiconductors, which suggests the involvement of the optical phonons. The first derivatives of the exciton energy by the temperature above 70 K are

$dE/dT = -3.1 \times 10^{-4}$ eV K^{-1} (70 K – 290 K, $R = 50.5$ Å) and (1)

$dE/dT = -2.6 \times 10^{-4}$ eV K^{-1} (70 K – 293 K, $R = 17.5$ Å). (2)

The decrease in dE/dT as the radius becomes smaller is the one of the evidences of the quantum confinement effects. In Fig. 2, the temperature dependence of the full width at half maximum of the exciton is shown. The solid curve is the best fitted curve assuming the LO phonon energy of 28 meV.

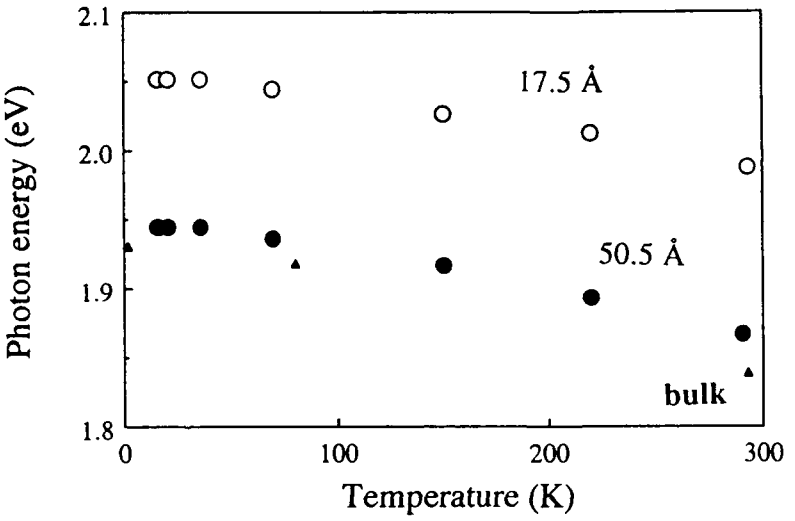


FIG. 1 The temperature dependence of the exciton energy of microcrystallites of radius of 17.5 Å (open circles) and 50.5 Å (closed circles), respectively. The bulk band gap is also depicted[5] (triangles).

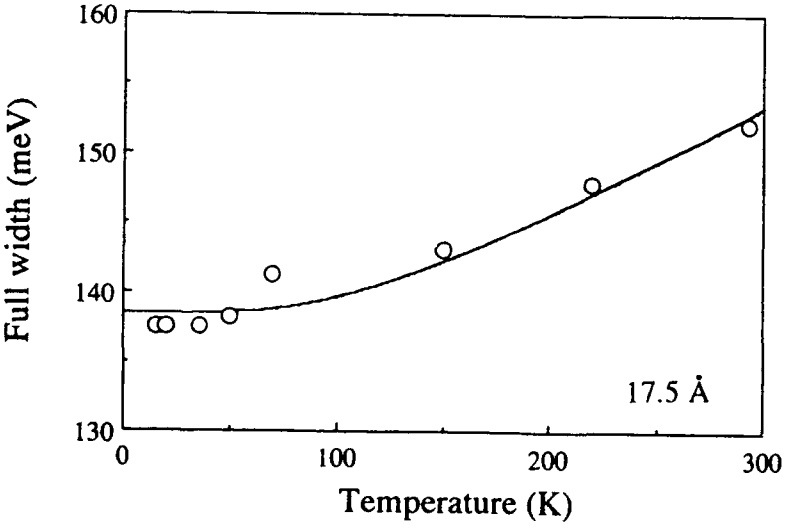


FIG. 2 The temperature dependence of the width of the exciton in 17.5 Å microcrystallites. The solid curve is the best fitted curve.

4. THEORY AND DISCUSSION

There are several factors to be considered to explain the temperature dependence, the change in the dielectric constants, the lattice constants, and the effective masses. The contribution of them to the exciton energy is found to be small, and the dominant effect is the change in the self energy due to the couplings to LO phonons as in the bulk semiconductors.[6]

By the fits, the width divided by the Bose distribution function, *i.e.*, $\Gamma_{LO}/n(T)$ is obtained to be 30 and 29 meV for 50.5 and 17.5 Å microcrystallites, respectively. $\Gamma_{LO}/n(T)$ of bulk CdSe is 106 meV. Clearly, this reduction in the exciton width by the quantization of the electron states in microcrystallites is observed. Although the width by LO phonons is much reduced, it is still essentially important for the temperature dependence higher than 70 K.

Both the temperature dependence of the exciton energy and the width suggest the couplings to LO phonons. However, the interaction with the LO phonons in the microcrystallites differs from the bulk in that all the states in the microcrystallites are discrete. In the bulk, there is a continuum state as a final state for scatterings, but in the microcrystallites, there is no such a state for excitons to be scattered. Here, the interaction Hamiltonian is

$$H_{\text{ex-ph}} = \sum_{\substack{\mathbf{q} \\ \lambda\mu}} \frac{1}{\sqrt{V}} \frac{f}{q} v_{\lambda\mu}(\mathbf{q}) B_\lambda^\dagger B_\mu [a(\mathbf{q}) + a^\dagger(-\mathbf{q})] \tag{3}$$

and the Huang-Rhys parameter (g) is obtained by

$$g_\lambda = \frac{f^2}{(2\pi)^3} \int d^3\mathbf{k} \frac{1}{k^2} \frac{|v_{\lambda\lambda}(\mathbf{k})|^2}{(\hbar\omega_{LO})^2} \tag{4}$$

where f is the Fröhlich interaction constant, $B^\dagger$ and $a^\dagger$ are the exciton and phonon creation operators, respectively, λ, μ are indices for excitons, and $\mathbf{r}_{12}$ is the relative coordinate of an electron and a hole. Here, the displacement harmonic oscillator model is considered. This model is valid in the case where the phonon energy ($\hbar\omega_{LO}$) is smaller than the energy separations of electronic (excitons) states and the electronic states are not changed by phonons, *i.e.*, λ equals to μ. In a moderate or weak confinement region, the difference in the effective mass is important. The wave function of a hole has larger amplitude at the center of a microcrystallite than an electron, while that of an electron is more extended to the outside the potential. This effects are taken into account by using a five-parameter variational wave functions. The wave functions also reflect the penetration of an electron and a hole through a finite potential barrier, which is assumed to be 2.5 eV. The results are

shown in Fig. 3. It is seen that as the confinement becomes stronger, the coupling of the exciton to LO phonons becomes stronger. This agrees with the experimental results that the lowest exciton state in smaller microcrystallites has larger width.

In comparison with the bulk semiconductor, microcrystallites have smaller couplings to LO-phonons because of the small number of the transitions which can be coupled. Although the contribution of each state becomes smaller as the system approaches to the bulk limit as shown in Fig. 3, the total couplings to LO-phonons become stronger in the bulk semiconductor.

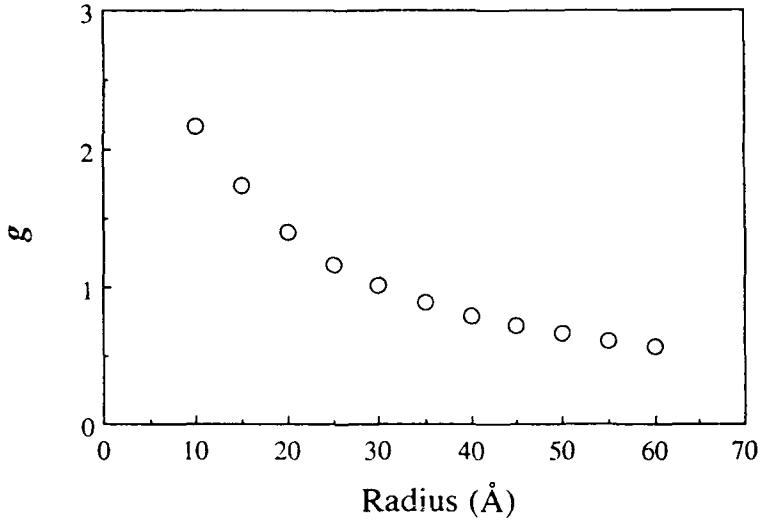


FIG. 3 The calculated size dependence of the Huang-Rhys parameter, g.

5. CONCLUSION

In this paper, the exciton-LO phonon couplings are shown to be important in semiconductor microcrystallites both experimentally and theoretically. By utilizing the electroabsorption method, the temperature dependence of the width and the energy of the lowest exciton are determined. The exciton-LO phonon coupling constant, the Huang-Rhys parameter, is obtained with a five-parameter variational function and is found to be larger for smaller microcrystallites.

REFERENCES

[1]Al. L. Efros and A. L. Efros, Sov. Phys. Semicond. **16**, 772 (1982).
[2]L. E. Brus, IEEE J. Quantum Electron. **22**, 1909 (1986).
[3]S. Schmitt-Rink, D. A. B. Miller, and D. S. Chemla, Phys. Rev. B **35**, 8113 (1987).
[4]S. Nomura and T. Kobayashi, Solid State Commun. **73**, 425 (1990).
[5]*Landolt-Börnstein Numerical Data and Functional Relationship in Science and Technology*, edited by K. H. Hellwege (Springer, Berlin, 1982) *New Series* Vol. **17b**.
[6]H. Y. Fan, Phys. Rev. **82**, 900 (1951).

Broadband GaAs/$Al_xGa_{1-x}As$ Multi-Quantum Well LED

A.J. Moseley, D.J. Robbins, C. Meaton[1], R.M.Ash, R. Nicklin, P. Bromley, R.R. Bradley, A.C. Carter, C.S. Hong* and L. Figueroa*.

Plessey Research Caswell, Towcester Northants, NN12 8EQ. UK.

* Boeing Electronics, High Technology Centre Seattle Washington 98124-2499 USA

92-22392

AD-P007 863

Introduction

A high power LED source has been designed and fabricated which allows broad band emission to be achieved over the wavelength range 700-900nm with low spectral ripple. The design is based on a GaAs/$Al_xGa_{1-x}As$ multi-quantum wells active region where each well is designed to emit at a different peak wavelength. The superposition of the emission spectra of the individual wells produces a broad band spectrum with many times the spectral width of a bulk device with a single active composition, which is typically 40nm. This is a candidate source for sensor applications such as analogue spectral filtering [1], in which broadband emission over ~100-200nm is typically required.

Device design.

The active region, shown schematically in figure 1, typically contains eight to ten $Al_xGa_{1-x}As$ quantum wells ($0<x<0.3$) with $Al_{0.4}Ga_{0.6}As$ barriers located within a graded composition, $Al_{0.4}Ga_{0.6}As$ to $Al_{0.6}Ga_{0.4}As$, carrier confinement region for efficient electrical injection. A variation of either well width, over the range 30-300Å, or well composition ($0<x<0.3$) has been used to tailor the well emission wavelength, with the well emission energies spaced by ~kT for minimal spectral ripple. In practice, variations

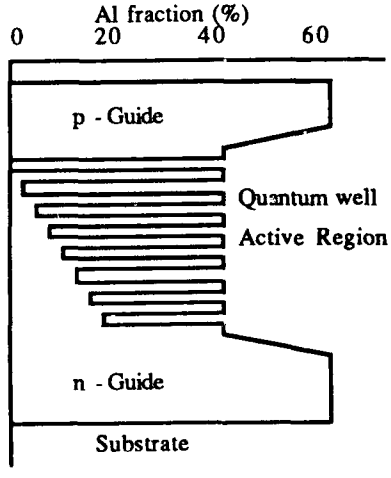


Figure 1. Typical layer structure for a broad band surface emitting LED.

[1] Present address: Epitaxial Products International, Cypess Drive, St Mellons, Cardiff CF3 OEG, U.K.

in well composition were preferred to variations in well thickness to ensure uniform carrier capture into each well, which to first order is proportional to the well thickness. The device design was therefore based on 100Å wells with the aluminium content varying over the range 0% to 22% with increments of 2-3% in Al content between adjacent wells. Additional 150Å GaAs wells were used to enhance the long wavelength end of the spectrum. Simulated emission spectra were obtained by the superposition of calculated spontaneous emission spectra of a series of wells of different composition. Under conditions of high carrier injection, ~$2x10^{18}cm^{-3}$, these showed broad band emission for wells spaced ~30meV apart with a significant contribution to spectral broadening from emission from higher subbands. The uniform distribution of carriers across the wells in the active region is important to achieve uniform emission across the spectral range, and heavy p-doping of the wells and barriers was used to minimise the effects of non-uniform hole injection. In operation the electrical pumping is then dominated by the electron injection and capture by the large hole concentration in the wells. Figure 2 shows the simulated carrier distribution for high and low injection levels into a series of eight 100Å wells, where the well number indicates the position of the well in the active region. This calculation was based on a rate equation model for the steady state carrier densities which is similar in concept to an analysis of carrier capture effects in MQW InGaAs lasers reported in [2]. At low carrier injection levels the excitation was described by an exponential carrier capture coefficient analagous to optical absoption with a decay length of α_0^{-1}.

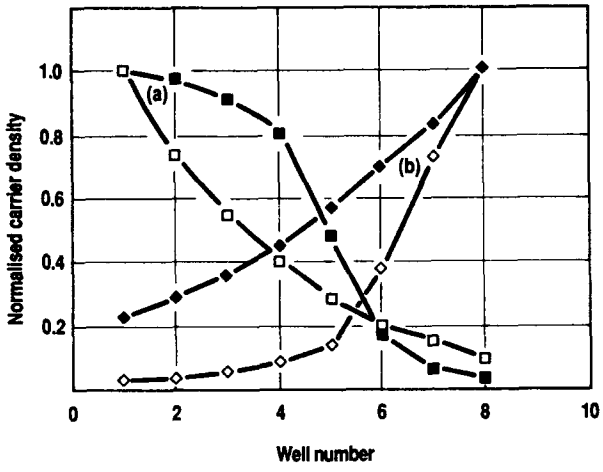


Figure 2.Modelled carrier distribution across a series of 100Å wells, a-electrons, b-holes. Solid points - high injection, open points -low injection.

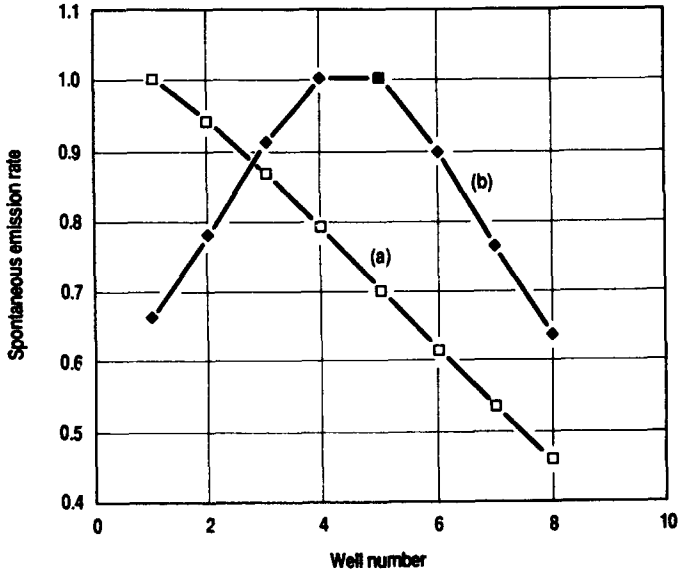


Figure 3. Simulated spontaneous emission rates for a series of 100Å wells. a - low injection, b - high injection.

Carrier recombination by radiative and non-radiative processes was included within the wells, and loss in the barriers ignored. Values of radiative rate of $2x10^{-10}cm^3s^{-1}$, and non radiative lifetimes of 2.5ns were used together with a value of $\alpha_o=4x10^5cm^{-1}$, established by analysis of the broadband spectra in the low injection regime. Under high injection the effects of well filling and emission of carriers from the wells becomes important. Thermionic emission between adjacent wells was included in the model but well filling limiting the density of available states, and thereby decreasing the effective capture coefficient, was found to be the more important process in determining the carrier distribution. The corresponding spontaneous emission rates are plotted in figure 3 for the cases of high and low injection. Clearly if each of the wells has a different Al content such plot gives an indication of the combined spectral emission obtained, and this was later confirmed by a full calculation of the combined spontaneous emission spectrum.

Device fabrication and characteristics.

Material for the devices was grown by atmospheric pressure MOCVD using a rapid switching radial manifold system to realize abrupt herero-interfaces, described previously in [4]. Direct pumping of the wells in room temperature photoluminescence showed broad band emission with the contribution from each well identifiable. Under high power optical injection the absolute efficiency of the quantum wells was found to be in the range 50-100%. The low temperature luminescence shown in figure 4 indicates clearly the emission from each well, and coupled with TEM measurements of well thicknesses, confirms the well compositions. To obtain high power output this active section of the device was contained within a conventional surface emitting LED structure with wide band gap, $Al_{0.6}Ga_{0.4}As$, cladding and buffer layers. The light from the active region was coupled out of the device through the transparant $Al_{0.6}Ga_{0.4}As$ buffer layer, and a

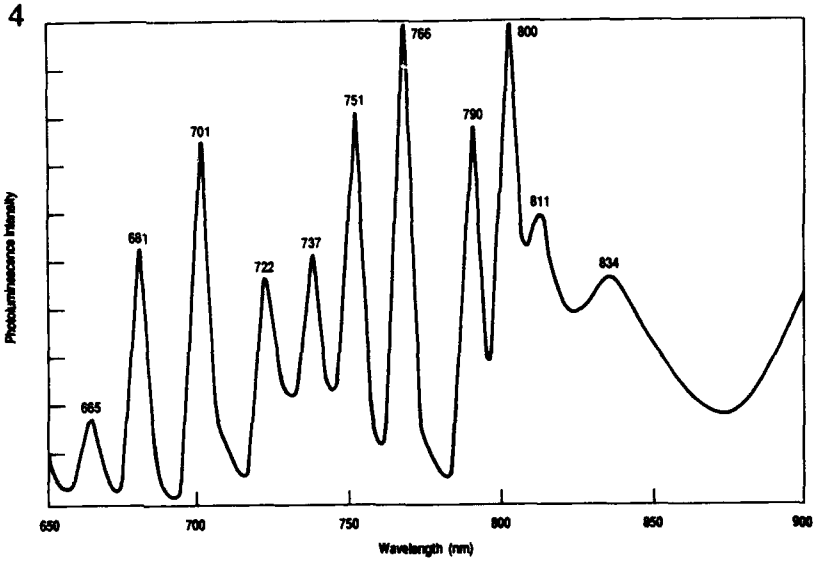


Figure 4. Photoluminescence spectrum at 10K showing the emission from each of the ten wells in the active region.

well etched through the GaAs substrate, into a fibre via a microlens.

Broad band electroluminescence was obtained from these devices with a linewidth in excess of 100nm for an injction current density above 1kA/cm^2. At very low injection, 10-100A/cm^2, the emission spectrum is dominated by the penetration depth of the electrons into the p-doped active region as shown in the simulation, figure 3. At very high carrier levels injection effects became very much less marked, but the total thickness of quantum wells which can be electrically pumped was shown to be limited to ~1000Å-1500Å. This limits the number of wells that can be used in the active region, and hence the achievable spectral range. This active region thickness corresponds to a carrier decay length α_o^{-1} of the order of 250Å. Assuming that the capture of carriers into the wells is dominated by the LO phonon emission so that the capture time is ~1ps this leads to an effective velocity of the carriers ~2.5x10^{6}cm/s across the multiple well system which is not unreasonable. Time resolved luminescence spectroscopy of InGaAs/InP quantum wells [3] has shown an effective capture time of ~2-3ps for electrons and holes.

Broadband emission has been obtained in the spectral range 700-900nm with a FWHM up to 144nm and less that 25% ripple. With this geometry the total emitted power over the spectral range was 2.8mW at a drive current of 150mA indicating an internal efficiency approaching 100%. Operation over a wide temperature range shows a thermal derating of the output of ~0.3%/°C upto an ambient temperature of 200°C. A band width in excess of 120nm was maintained over thetemperature range -55°C to +125°C when packaged in a DIL style package with internal thermocooler.

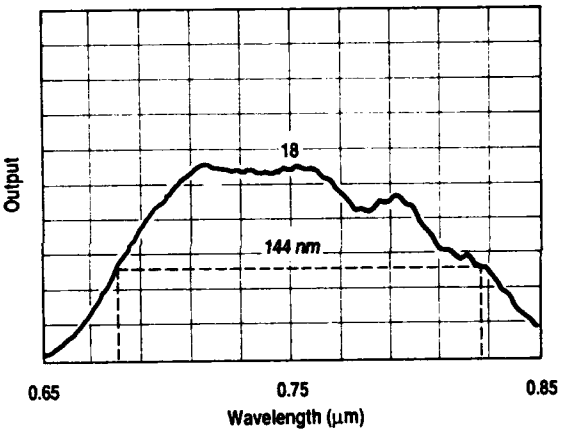


Figure 5. Electroluminescence spectrum from broadband SLED at room temperature.

References

[1]. Batchellor C R, Pearce D A J, Dakin J P.' Fibre Optic sensors for aerospace applications' OE/Fibre 87 San Diego, Aug. 87 SPIE Vol. **838.**

[2] Williams P J, Robbins D J , Cush R, Scott M D, Davies J I , Marshall A C, Riffat J, and Carter A C. 'Effect of barrier width of the performance of long wavelength InGaAs/InP Multiple-quantum well Lasers' (1988) Electron Lett **24** 859-860.

[3] Deveaud B, Shah J, Damen T C., and Tsang W T Appl. Phys. Lett. **52**, (1988) 1886-1888.

[4] Jones M W and Forbes N 'MOCVD growth of GaAs/AlGaAs Epitaxial Layers for Monolithic Optoelectronic Devices' J Cryst Growth **68** (1986) 466-473.

AD-P007 864

Optically Encoded Second-Harmonic Generation in Semiconductor Microcrystallite Doped Glasses

by R. L. MacDonald and N. M. Lawandy, Brown University, Department of Physics box 1843, Providence, RI 02912

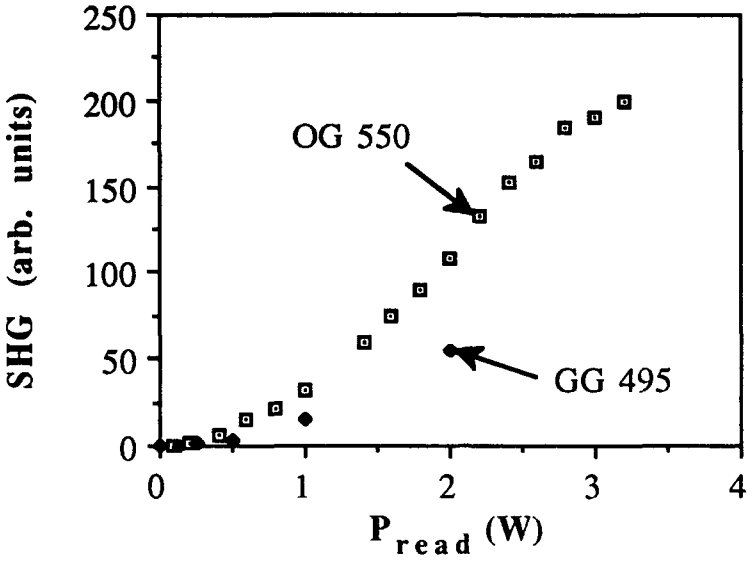
Since the discovery of second-harmonic generation (SHG) in germanosilicate fibers no other materials have been found which exhibit optically organized $\chi^{(2)}$ gratings.[1,2] We have discovered that CdS_xSe_{1-x} semiconductor doped glasses can be prepared for efficient SHG when the glass is simultaneously exposed to 532 nm and 1.06 μm radiation from a Q-switched and modelocked laser.[3] Using 5 cm path length in a 530 nm bandgap filter we have observed a 10^{-6} conversion efficiency, which resulted in a green spot visible in room lights. The effect is permanent in some glasses and is a strong function of the position of the microcrystallite bandgap. The phenomenon poses a test to our basic understanding of electronic processes in nanocrystals and heterogeneous glasses and opens a door to new materials for frequency doubling laser sources.

The experimental set-up consisted of a modelocked, Q-switched and frequency doubled Nd:YAG laser, two polarizers, a 10 cm focussing lens, and a phase sensitive detection system capable of detecting 10^{-14} W of average power. The laser produced pulses which were 110 psec and 80psec long at 1.06 μm and 532 nm, respectively, with a 76 MHz modelocking rate and a Q-switching rate of 1 kHz.

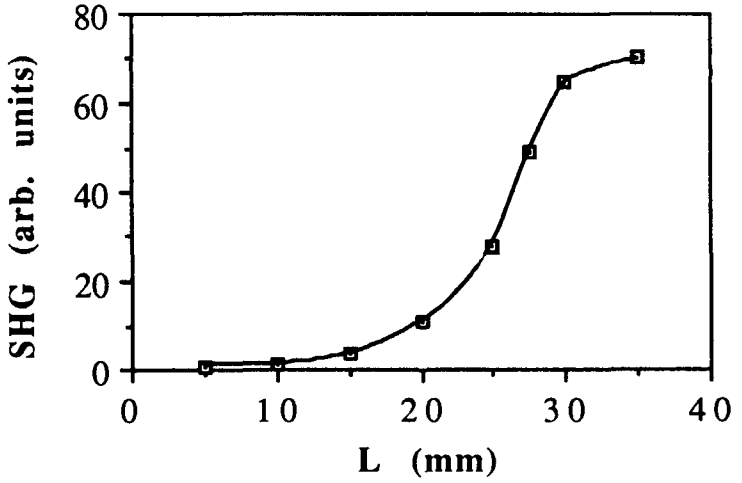
Experiments were performed on Schott Glass filters ranging from GG 495 to RG 630 and with a variety of thicknesses (1 mm to 5 cm). In addition to the semiconductor doped glasses we tested a single crystal sample of CdS. This sample exhibited a preparation induced increase in SHG of a factor of two. The result serves to demonstrate that the observed increase of several orders of magnitude of SHG in the colloidal filters is unique to the microcrystallite guest-glass host system.

In order to verify that a second order process was indeed responsible for the signals, we determined the dependence of the SHG signal on input power. The results are shown below for the OG 550 and GG 495 filters. The GG 495 filter has negligible absorption at 532 nm ($\alpha \approx 0.03$ cm^{-1}) and is expected to be less sensitive to pumping and readout induced index changes from carrier excitation and thermally induced shrinkage of the energy gap.[4] The dependence of SHG on IR power for the GG 495 filter was determined from a least squares fit to a log-log plot of the data. The results indicate that the process is dependent on $I(\omega)^{1.98}$ with a correlation greater than 0.99. Based on these results it is clear that an effective $\chi^{(2)}$ has been induced in these materials.

92-22393



To test that a phase matched process is occurring in the semiconductor doped glasses we examined the scattered sidelight at 532 nm from the GG 495 filter prepared along 5 cm . The growth of the second-harmonic beam along the propagation axis of the filter is shown below.



Although the dependence on length is not perfectly quadratic, the data serves to illustrate that phase matching has occurred. The second-harmonic conversion efficiency of this filter after nine hours of preparation was found to be 5×10^{-7}. A similar preparation in the GG 495 filter resulted in 10^{-6} conversion efficiency. This value, along with the input beam parameters results in a $\chi^{(2)}L$ product of 10^{-17} m^2/V and an effective value of $\chi^{(2)}$ of the order of 10^{-16} m/V.

In addition to the two filters discussed so far we tested other filters to determine the role of resonance on the process. Nine colloidally doped filters with bandgaps ranging from 400 nm to 590 nm were prepared

under identical conditions. The resulting SHG was sharply peaked around 532 nm, indicating that resonance strongly enhances the effect.

Some of the earliest work on second-harmonic generation in germanosilicate glasses proposed that phase matching occurs by a periodic $\chi^{(2)}$, whose period is the coherence length between the fundamental and the second-harmonic.[5] This process, referred to as quasi-phase matching, leads to

$$\chi^{(2)} \sim \chi^{(3)}(0;\omega,\omega,-2\omega)E_{dc}\cos(\Delta kz+\varphi),$$

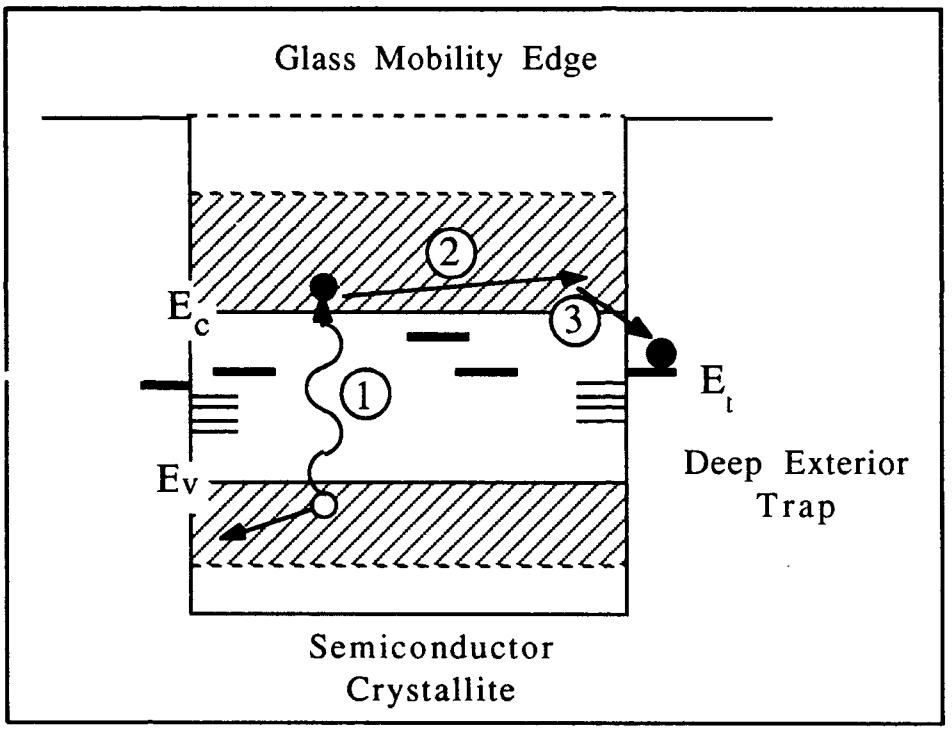
where $\chi^{(3)}$ is the third order susceptibility tensor for the composite crystallite glass material, and E_{dc} is the amplitude of the internal field encoded by the writing beams. Thus symmetry can be broken and quasi-phasematching can occur if the optical encoding process leaves behind a permanent periodic electric field. The data on the response of glasses doped with varying relative concentrations of S and Se, to tune the crystallite bandgap, reveal a preparation resonance around 550 nm. The increase of SHG as the bandgap moves closer into resonance from the long wavelength side indicates that carrier excitation may be required. The decrease in SHG after the resonance may be a consequence of absorption in the writing and readout process.

The microscopic mechanisms which result in a periodic frozen in field are considerably more speculative at this point. The small $\chi^{(3)}(0;\omega,\omega,-2\omega)$ of silica results in weak encoding fields ($\sim 10^3$ V/m), suggesting that the writing process does not occur by optical rectification in the medium surrounding the microcrystallites. The situation is quite different in the semiconductor crystallites since $\chi^{(3)}_{mc}$ is greatly enhanced for near bandgap excitation (10^3 times the off-resonance value and about 10^5 times larger than that of silica).[6] Thus if we turn our attention to electron dynamics within the microcrystallites, we can expect internal optical rectification fields as large as 10^7 V/m (which includes the static dielectric constant of CdS, $\varepsilon_r \sim 8.9$ [7]) for above gap excitation.

A possible scenario for the encoding process is shown below. The primary optical encoding steps are believed to be: 1) optical excitation of the electron to the conduction band; 2) motion of the electron under the influence of the internal optical rectification field, establishing a wavefunction pinned against one side of the crystallite; and 3) trapping in an "exterior" deep trap of energy E_t. The trap site is most likely an S or Se vacancy with Cd orbitals dangling away from the crystallite surface and towards the glass. This trap is expected to be at nearly the same energy as luminescent traps, which may be S or Se vacancies one or two atomic planes from the crystallite surface.

The model presented results in expected effective $\chi^{(2)} \sim 10^{-16}$ m/V of the composite system, consistent with our experimental findings. The

value of $\chi^{(2)}_{mc}$ is estimated assuming one electron is trapped at the surface of each crystallite, and the composite $\chi^{(2)}$ is scaled by the volume fraction of the crystallites.



Many possibilities exist for extending this discovery to microcrystallites in the quantum dot regime, where quantum confinement results in larger nonlinearities, and to other semiconductors, such as PbS and CuCl.

References

1. Y. Sasaki and Y. Ohmori, Appl. Phys. Lett. **39**, 466 (1981).
2. U. Osterberg and W. Margulis, Opt. Lett. **11**, 516 (1986).
3. N. M. Lawandy and R. L. MacDonald, submitted to JOSA B, August (1990).
4. J. I. Pankove, Optical Processes in Semiconductors, Dover Publications, Inc., New York (1971), p. 27.
5. R. H. Stolen and H. W. K. Tom, Opt. Lett. **12**, 585 (1987).
6. R. C. Miller, D. A. Kleinman and A. Savage, Phys. Rev. Lett. **11**, 146 (1963).
7. J. I. Pankove, Optical Processes in Semiconductors, Dover Publications, Inc., New York (1971), appendix II.

Nonlinear and Dynamical Effects in Heterostructures

WA 8:30am–10:00am
Salon F

D. A. B. Miller, *Presider*
AT&T Bell Laboratories



Fast response of the excitonic optical nonlinearity in type–II $Al_xGa_{1-x}As$ / AlAs multiple quantum–wells

J. Feldmann* and E. Göbel
Fachbereich Physik, Philipps–Universität, Renthof 5, 3550 Marburg, FRG
**present address: AT&T Bell Laboratories, Holmdel, NJ 07733, USA*

In type–II $Al_xGa_{1-x}As$ / AlAs multiple quantum–wells (MQW) the lowest lying electronic states in the conduction band are X–related states confined in the AlAs layers.[1] However, the absorption spectrum is governed by the direct optical transitions at higher energies, involving the Γ valence band and Γ conduction band states of the $Al_xGa_{1-x}As$. As a consequence of this type–II band alignment, electrons photocreated in the Γ–states confined in the $Al_xGa_{1-x}As$ layer scatter to the lower lying X–states located in the adjacent AlAs layer.[2] We demonstrate that the associated change of the dielectric constant leads to a complete recovery of the initially bleached absorption, if the laser photon energy is at the low–energy side of the direct heavy–hole excitonic transition. The response time of this large excitonic nonlinearity is thus given by the Γ–X transfer time, which is on a picosecond or even subpicosecond time–scale.[3]

We performed optical pump and probe experiments using optical pulses of 1–2 ps from a cavity–dumped hybridly mode–locked dye laser with a repetition rate of 500 kHz. The temporal development of the differential transmission (DT), which is the difference in transmission of the probe beam with and without the pump beam, is depicted in Fig.1 for the type–II $(GaAs)_{11}(AlAs)_{24}$ sample at room–temperature (m=11 and n=24 stand for the number of monolayers GaAs and AlAs, respectively). The absorption spectrum at the lowest lying direct heavy–hole exciton is depicted as an inset. The arrows in the insets labeled A–C indicate the respective laser photon energies, where the transient DT spectra are performed. The fast increase of the bleaching at t=0 for each photon energy is followed by a decrease to a quasi–constant value, whose magnitude drastically decreases, when the laser photon energy is tuned to the low–energy part of the heavy–hole excitonic resonance. At the energetic position labelled C in Fig.1 the optical nonlinearity even changes from bleached to induced absorption with increasing time–delay. The initial recovery of the bleached absorption can be ascribed to a change in the dielectric constant, when electrons scatter from the Γ–related states of the $Al_xGa_{1-x}As$ layer to the X–related states of the AlAs layer.[2,3] However, the laser pulses are not short enough to resolve the Γ–X transfer, which takes place with a time–constant of about 0.65 ps for this type–II sample.[2,3]

For times larger than the Γ–X transfer time electrons occupy the X–related states of the AlAs spatially separated from the heavy–holes in the Γ–related states of the $Al_xGa_{1-x}As$. Consequently, after the Γ–X transfer only the heavy–holes contribute to the bleaching of the excitonic transition by phase space filling. The loss in state filling due to the Γ–X transfer of electrons causes a partial recovery of the bleached absorption as observed at the peak–position of the heavy–hole exciton.

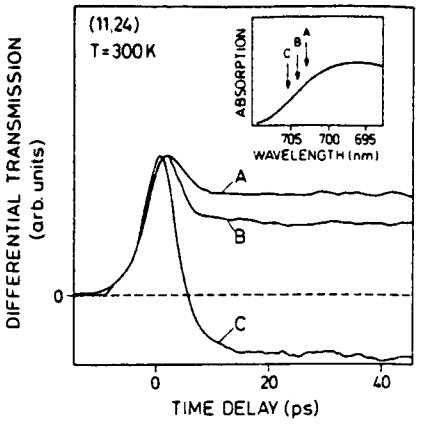


Fig.1 Differential transmission vs time delay between pump and probe pulses for the type–II $(GaAs)_{11}(AlAs)_{24}$ MQW.

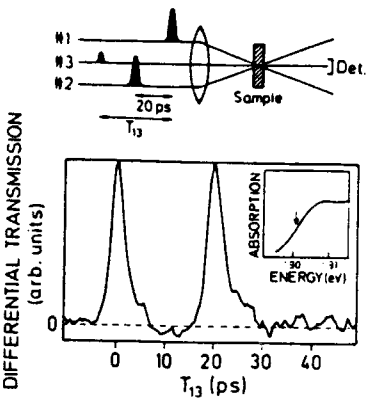


Fig.2 Pump and probe experiment of the type–II $(Al_{0.37}Ga_{0.63}As)_{68}$ $(AlAs)_{36}$ sample using two pump pulses separated by 20 ps.

Since the contribution of X–electrons located in the AlAs layers to screening of the direct excitons in the $Al_xGa_{1-x}As$ layer should be negligible, the loss in screening of the excitonic enhancement due to the Γ–X transfer of electrons also causes a partial recovery of the bleached absorption. However, the transition from bleached to induced absorption during the spatial Γ–X transfer for photon energies in the low–energy part of the excitonic resonance implies that also a red–shift or/and a broadening of the excitonic transition occurs after the Γ–X transfer of electrons.

An energy shift of the type–I Γ–Γ transition is expected because of the spatial separation of charges leading to band bending effects. We can estimate the amount of this shift in the following way: We have calculated the envelope wavefunctions for the lowest heavy–hole state confined in the $Al_xGa_{1-x}As$ layer and for the lowest X–electron state confined in the AlAs layer according to the Kronig–Penney model. Assuming that the concentration of the respective carriers in these lowest quantized states is N, we can integrate Poisson's equation. The energetic shift of the type–I transition is then calculated using first–order perturbation theory. For $N = 1 \cdot 10^{12}$ cm^{-2}, which is an upper limit for the photoinduced carrier densities in the pump and probe experiments depicted in Fig.1, we find a blue–shift of only 0.6 meV for the type–I transition of the $(GaAs)_{11}(AlAs)_{24}$ MQW. Consequently, the band bending effects cannot account for the experimentally observed induced absorption at the low–energy part of the heavy–hole excitonic resonance.

A possible explanation for our findings could be that the red–shift of the type–I transition due to band gap renormalization, which after the Γ–X transfer is mainly caused by heavy–holes, overcompensates the blue–shifts caused by state–filling and screening due to heavy–holes as well as the small blue–shift caused by band bending.

An alternative explanation could be that the induced absorption is due to

collision broadening of the type–I excitonic resonance. After the Γ–X transfer of electrons the broadening should mainly be determined by scattering with bare heavy–holes in the $Al_xGa_{1-x}As$ layer. Since exciton – free carrier scattering is about 8 times more efficient than exciton–exciton scattering[4], the broadening should drastically increase during the spatial Γ–X transfer leading to the observed dependence of the nonlinear excitonic response on photon energy.

For possible applications of this fast nonlinearity it is important to know, whether the response of the optical nonlinearity is repeatable after a short cycle time.[5] In particular, this requirement has to be considered for type–II samples, since the fast response is not due to recombination but to relaxation of photocreated carriers. As illustrated in the upper part of Fig.2, we have performed a pump and probe experiment with two subsequent pump pulses separated by 20 ps. The temporal evolution of the DT at room–temperature for a type–II $(Al_{0.37}Ga_{0.63}As)_{68}$ $(AlAs)_{36}$ sample is depicted in Fig.2 for the spectral position indicated by the arrow in the inset. Obviously, the responses to the two successive pump pulses are virtually identical, demonstrating that the long carrier lifetimes, as characteristic of these type–II samples, does not prevent fast switching at extremely high repetition rates.

We would like to point out that the room–temperature optical nonlinearity in the low–energy part of the heavy–hole exciton not only has a fast response but is also very large. For zero time–delay the relative change in the absorption coefficient $\Delta\alpha / \alpha$ at the spectral position indicated in the inset of Fig.2, where the complete recovery is observed with a time–constant of 2 ps, amounts to about 15 % at pump energies of 0.04 pJ/cm^2 per pulse. This is comparable in size to the optical nonlinearities of type–I $GaAs/Al_xGa_{1-y}As$ quantum–wells.[6]

In particular, the nonlinear optical response illustrated in Fig.2 shows that type–II MQW's fulfill the requirements for fast saturable absorbers, which can be used for laser mode–locking.[7] They should provide loss for both the leading and the trailing edge of a mode–locked laser–pulse and they should allow operation at high repetition rates. In order to check the application for mode–locking at high repetition rate we replaced the organic saturable absorber DQTCI in the hybridly mode–locked Coherent 702 dye–laser with DCM as the gain medium by the type–II $(Al_{0.37}Ga_{0.63}As)_{68}(AlAs)_{36}$ sample as schematically depicted in Fig.3. A frequency–doubled actively mode–locked Nd:YAG laser is used for synchronous pumping (80 ps pulse width, 76 MHz repetition rate). A 1–plate birefringent filter allows for tuning of the laser emission wavelength. The optical spectrum as well as the intensity autocorrelation (AC) using phase–matched second harmonic generation are measured for characterization of the dye laser pulses.

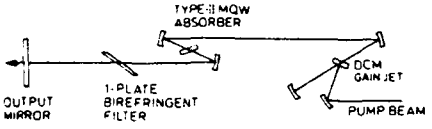


Fig.3 Setup for mode–locking experiment

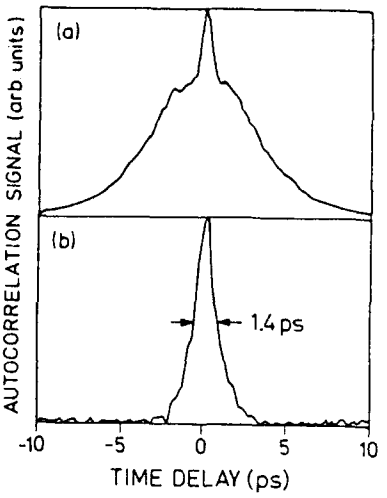


Fig.4 Intensity autocorrelation traces of the dye–laser output without (a) and with (b) the type–II absorber installed.

The AC traces of the DCM laser output without and with the type–II saturable absorber in the resonator are depicted in Fig.4a and b, respectively. Indeed, with the type–II absorber installed the pulse–width reduces from $\tau_p = 4.9$ ps to $\tau_p = 0.9$ ps and the time–bandwidth product reduces from $\tau_p \cdot \Delta\nu = 8.9$ to $\tau_p \cdot \Delta\nu = 0.57$, when the dye–laser is tuned to the low–energy part of the direct excitonic transition. By using type–II GaAs/AlAs short–period superlattices with subpicosecond Γ–X transfer times as short as 100 fs[3] as fast saturable absorbers it should be possible to produce even shorter pulses.

We would like to thank K. Ploog for the high quality sample. The excellent assistance of M. Preis is also gratefully achnowledged. This work has been supported by the Deutsche Forschungsgemeinschaft.

[1] K.J. Moore, G. Duggan, P. Dawson, and C.T. Foxon, Phys. Rev. **B38**, 5535 (1988).
[2] J. Feldmann, R. Sattmann, E. Göbel, J. Kuhl, J. Hebling, K. Ploog, R. Muralidharan, P. Dawson, and C.T. Foxon, Phys. Rev. Lett. **62**, 1892 (1989).
[3] J. Feldmann, J. Nunnenkamp, G. Peter, E. Göbel, J. Kuhl, K. Ploog, P. Dawson, and C.T. Foxon, Phys. Rev. **B42**, 5809 (1990).
[4] A. Honold, L. Schultheis, J.Kuhl, and C.W. Tu, Phys. Rev. **B40**, 6442 (1989).
[5] Y.H. Lee, H.M. Gibbs, J.L. Jewell, J.F. Duffy, T. Venkatesan, A.C. Gossard, W. Wiegmann, and J.H. English, Appl. Phys. Lett. **49**, 486 (1986).
[6] J.L. Jewell, Y.H. Lee, M. Warren, H.M. Gibbs, N. Peyghambarian, A.C. Gossard, W. Wiegmann, Appl. Phys. Lett. **46**, 918 (1985).
[7] H.A. Haus, J. Appl. Phys. **46**, 3049 (1975).

AD-P007 866

Dynamics of Excitons in Quantum Wells

M. Zachau, J.A. Kash and W.T. Masselink
IBM Research Division , T.J. Watson Research Center
P.O. Box 218, Yorktown Heights, New York 10598, USA

We measure the time dependence of the excitonic photoluminescence (PL) in quantum wells (QWs) with well width L_z ranging from 25Å to 50Å. The samples are $Al_{0.2}Ga_{0.8}As/GaAs$ multiple QWs with 30 periods with decoupled wells and were grown by molecular beam epitaxy (MBE). QWs grown with and without growth interruption at the interfaces are investigated. The excitation is provided by 5 psec pulses from a synchronously pumped tunable dye laser. The PL spectrum is detected by an imaging (i.e. multichannel) photomultiplier with a spectral resolution of 0.5 meV and time resolution (FWHM) of 120 psec.

A typical time-resolved PL spectrum is shown in Fig. 1. The decay is always non-exponential. Both the rise and especially the decay of the PL depend on both the excitation energy E_L and the detection energy E_{det}. The characteristic decay time τ_{PL} of the PL (obtained from the full time dependence of the PL as indicated in Fig. 1) is

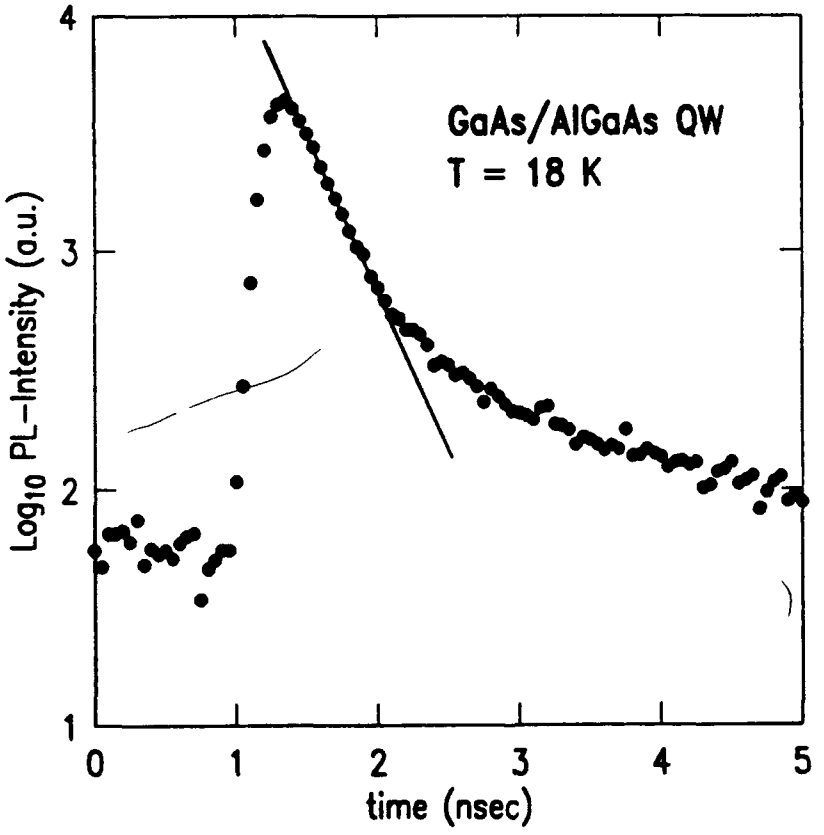


FIG. 1. Photoluminescence intensity as a function of time for a nominally 25Å thick GaAs/AlGaAs quantum well. The excitation energy E_L = 1666.2 meV, the detection energy E_{det} = 1662.8 meV. The straight line indicates how τ_{PL} is obtained from the inverse of the steepest slope.

92-22395

plotted in Fig. 2 as a function of E_L for three different detection energies. The most important experimental observations are:

1. τ_{PL} is shortest for resonant excitation. This shortest time is almost independent of E_{det}.
2. In the low-E_L regime (i.e. E_L near E_{det}), τ_{PL} increases rapidly with E_L up to some maximum. For further increases in E_L, the high-E_L regime, τ_{PL} stays approximately constant.
3. For lower E_{det}, the slope of τ_{PL} with E_L is steeper and τ_{PL} approaches a higher final value.

We want to stress how different the dynamics in the low-E_L and high-E_L regimes are. To our knowledge these are the first time-resolved measurements in the low-E_L regime. It will become clear that the low-E_L measurements are essential for establishing our model for the relaxation of excitons in quantum wells.

We first postulate that the fluctuations of L_z in the QW plane are correlated so that L_z varies relatively smoothly (mainly in steps of one monolayer). This assumption seems reasonable considering that the MBE-growth occurs predominantly two-dimensionally.

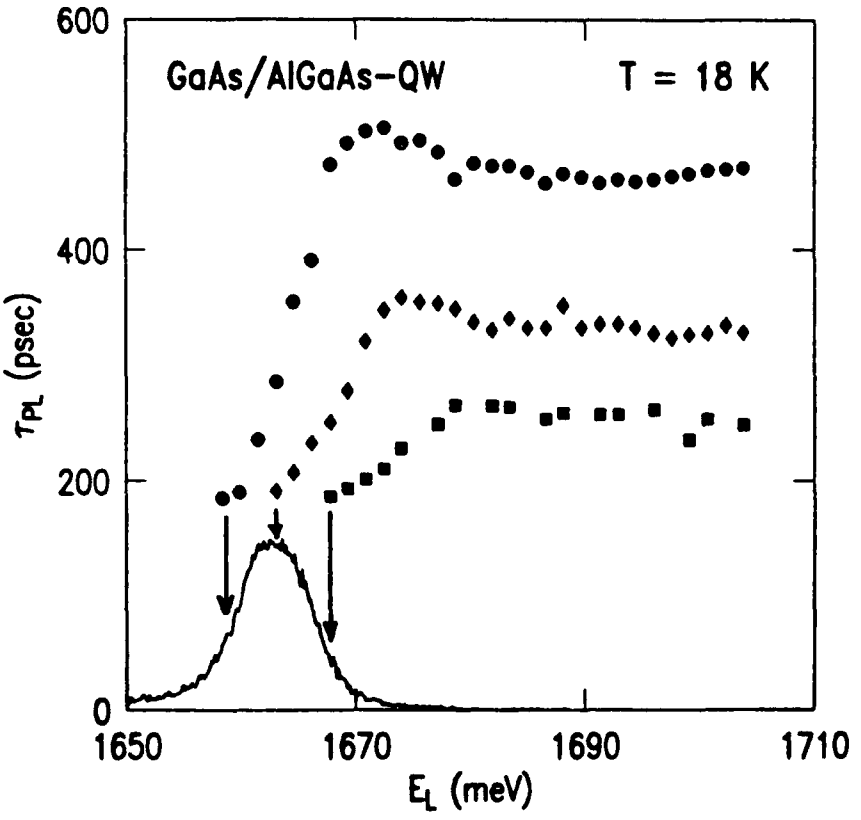


FIG. 2. Photoluminescence decay times vs. excitation energy for three different detection energies given by the arrows. The time-integrated photoluminescence spectrum is shown for comparison. The experimental conditions are the same as in FIG. 1.

We also point out beforehand that the measured decay time τ_{PL} is usually not the lifetime of the excitons (either radiative or non-radiative), but is determined to great extent by how fast excitons move from the place and energy of creation to the place and energy of recombination. While travelling, the excitons may also decay radiatively with a rate $1/\tau_{rad}$. It is a crucial point here that moving to lower energies means moving to more localized places with a smaller homogeneous linewidth /1/ and a shorter radiative lifetime τ_{rad} /2/. As the exciton moves, τ_{rad} decreases and therefore the average radiative lifetime $<\tau_{rad}>$ of all excitons decreases with time.

In the low-E_L regime excitons are created inhomogeneously only at those places within the QW plane where L_z corresponds to E_L. At any point in the QW plane, the local thermodynamic equilibrium within the excitonic branch is established rapidly compared to our time scale (mainly by scattering with acoustic phonons). There is, however, no global equilibrium. Therefore the excitons start to move within the QW plane toward the places of widest well width which are local energy minima. The exciton movement is determined by drift and diffusion and is understood in analogy to the Haynes-Shockley experiment /4/. In the original Haynes-Shockley experiment, a sheet of carriers excited by a light pulse at one spot moves along the sample driven by an external electric field,

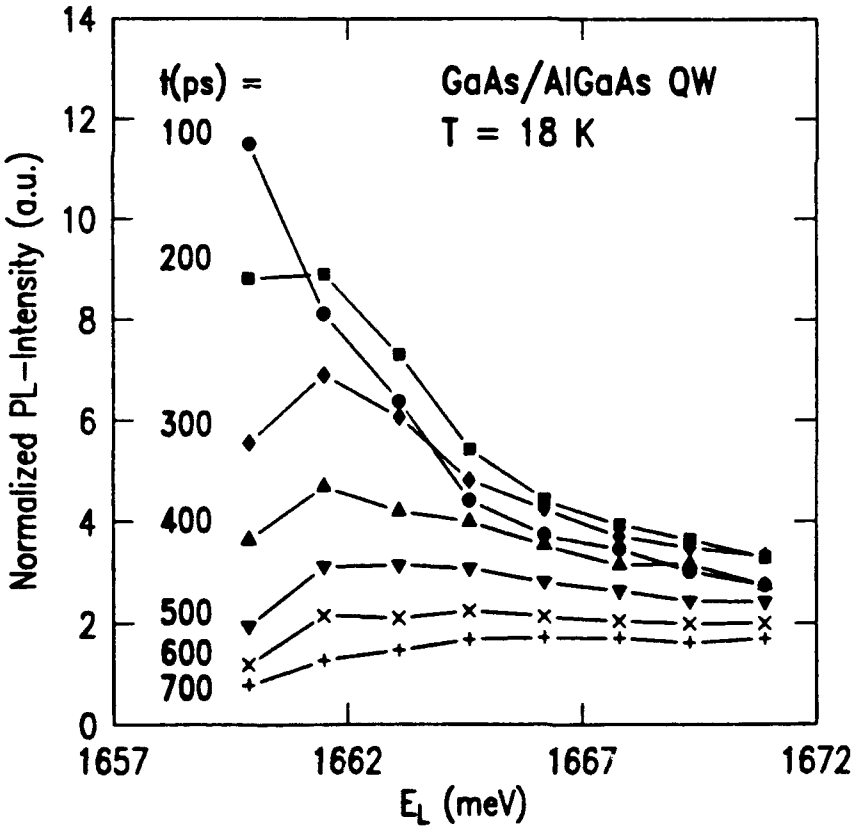


FIG. 3. Normalized photoluminescence intensity vs. excitation energy for various discrete times. The detection energy E_{det} = 1658.3 meV. The experimental conditions are the same as in FIG. 1.

simultaneously spreading out due to diffusion. In our case the detection energy E_{det} defines regions of local energy minima in the QW plane. The excitons move from the place of creation to the place of detection. Because of our assumption on the interface roughness, the distance the excitons travel (and therefore the time before they are detected) increases as $|E_L - E_{det}|$ increases.

Fig 3 shows for various discrete times the PL intensity as a function of E_L while E_{det} is kept at a fixed value in the low-energy shoulder of the PL spectrum. The PL intensity has been divided by the time-integrated PLE spectrum to correct for the different number of carriers created at each excitation energy. The values of E_L shown here all are in the low-E_L regime. In the Haynes-Shockley picture each curve represents the number of excitons arriving at the place of detection as a function of the distance they have travelled. It is evident that the excitons come from farther and farther away as time moves on. At the same time the pattern spreads out due to diffusion.

For high E_L, electron-hole pairs are created. The relaxation of the free carriers to the bottom of their subbands, the formation of the excitons, and the relaxation of the excitons to $K_{cm} \cong 0$ within the excitonic branch (K_{cm} is the wave vector of the center of mass motion of the exciton) are again fast compared to our time scale. This explains why τ_{PL} is approximately constant in the high-E_L regime (in agreement with /3/). Therefore at $t \cong 0$ we find $K_{cm} \cong 0$ excitons distributed with a homogeneous density everywhere. Although the excitons move in the same way as they do in the low-E_L regime, the drift-diffusion motion is obscured by this averaging over all excitons within the inhomogeneous line. That is the reason why previous measurements which used only excitation in the high-E_L regime could not see the drift-diffusion motion. It is exactly this process, however, which determines the measured τ_{PL}.

The QWs with growth-interrupted interfaces show a similar overall behaviour. However, the time-integrated PL spectrum shows the well-known peak splitting due to islands with L_z differing by multiples of one monolayer. In this case the intra- and inter- island transfer can be studied separately.

References

1. J. Hegarty, L. Goldner, and M.D. Sturge, Phys. Rev. B 30, 7346 (1984)
2. J.Feldmann, G. Peter, E.O. Goebel, P. Dawson, K. Moore, C. Foxon, and R.J. Elliot, Phys. Rev. Lett. 59, 2337 (1987)
3. T.C. Damen, J. Shah, D.Y. Oberli, D.S. Chemla, J.E. Cunningham, and J.M. Kuo, J. Lumin. 45, 181 (1990)
4. J.R. Haynes and W. Shockley, Phys. Rev. 81, 835 (1951), and S.M. Sze, "Physics of Semiconductor Devices", J. Wiley & Sons, 2nd edition, p. 54 (1981).

Optical Nonlinearity Through Internal Field Screening in Intrinsic Stark Effect Strained-Layer Superlattices

D. E. Watkins, I. Sela, B. K. Laurich, and D. L. Smith
Los Alamos National Laboratory, MEE-11, MS D429
P.O. Box 1663, Los Alamos, NM 87545

S. Subbanna* and H. Kroemer
ECE, Univeristy of California, Santa Barbara, CA 93106
*Present address: IBM East Fishkill, Hopewell Junction, NY 12533

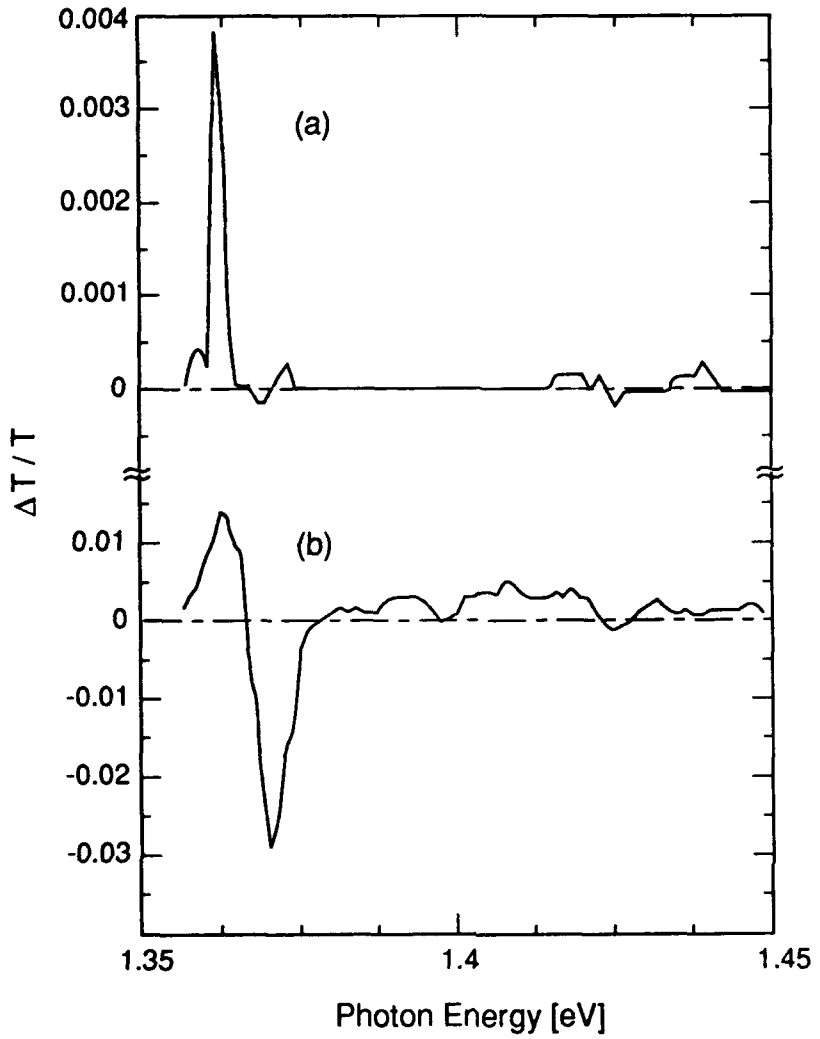
A strong nonlinear optical effect has been predicted for strained-layer superlattices (SL's) grown with III-V semiconductors along axes other than [100].[1,2] These materials have been denoted "intrinsic Stark-effect superlattices" (ISES) because the strain generates an electric field through the piezoelectric effect, and this field shifts the exciton resonance to lower energy and decreases the optical matrix element. Fields in excess of 10^5 V/cm have been theoretically predicted. In contrast SL's grown along the [100] axis should not exhibit any piezoelectric effect. Free carriers excited optically are expected to screen the internal field, shifting the exciton resonance to the blue and increasing the absorption cross section.[2,3] A blue shift in the exciton resonance frequency has been observed recently by applying a reverse bias to a PIN diode with a [111] $Ga_{1-x}In_xAs$ -GaAs SL structure in the intrinsic region.[4] We report the first observation of optical nonlinearities due to free carrier screening of the intrinsic Stark effect fields in $Ga_{1-x}In_xAs$ - GaAs strained-layer superlattices. The strength of the nonlinearity due to this internal field screening (IFS) mechanism is compared to that due to exciton saturation by the phase space filling (PSF) mechanism,[5] and we show that the former is much stronger.

The two SL samples studied were grown simultaneously to obtain nearly identical structures, one along the [211]B crystal axis[6] and the other along the [100] axis. The SL's were grown by molecular beam epitaxy on n^+-type Si-doped GaAs substrates with 2500 Å intrinsic GaAs buffer layers. The SL's have 10 periods, each consisting of 70 Å $Ga_{0.85}In_{0.15}As$ wells and 140 Å GaAs barriers (so the SL is well below the critical thickness). The SL is capped with a 2500 Å intrinsic GaAs layer and a 2500 Å p^+-type Be-doped GaAs layer. Examination of the samples by high resolution electron microscopy in cross section shows

uniform 10 period SL's with a limited number of dislocations. Free carrier lifetime was measured in the samples by using a picosecond optical (532 nm) excitation source to generate carriers and monitoring the change in sample transmission at the exciton resonance using a 912 nm probe and a fast photodiode. In both samples the change in transmission had a decay constant of about 2 ns.

The nonlinear absorption coefficient was obtained by measuring differential transmission as a function of wavelength in a pump-probe experiment[7] using a cw Ti:sapphire laser pumped by an Ar^+-ion laser. The Ti:sapphire laser beam was split into a pump beam with intensity I_p and a probe or test beam with intensity I_t for the differential transmission measurements. The two beams were focused onto the same spot on the sample (spatial overlap was verified visually using a microscope and an infrared viewer), and the test beam spot size was kept smaller than the pump beam spot size. The pump beam was chopped and the resulting modulation of the test beam transmission was measured using a photodiode and lockin amplifier.

Results of the differential transmission measurements for the [100] and [211] samples are shown in the figure. The two measurements were made under similar excitation conditions, with $I_p >> I_t$. The total intensity was kept in a regime where the change in absorption with pump intensity was linear, that is $\alpha(I) = \alpha_0 - \alpha_2 I$. (The total intensity was much less than the PSF saturation intensity for the [100] sample or the IFS saturation intensity for the [211] sample.) The change in transmission in the [100] sample clearly shows a decrease in absorption across the entire excitonic resonance, as expected for the PSF mechanism.[7] In contrast the differential transmission of the [211] sample shows a change in sign as the photon energy is increased, indicating that the absorption decreases to the red of the low intensity exciton resonance and increases to the blue of the exciton resonance. This behavior results from the blue shift in exciton resonance as the internal field is screened through free carriers generated by the modulated pump beam. The relative strength of the negative part of the signal compared to the positive part indicates that the exciton absorption is increasing due to the screening. These observations are in agreement with the predicted differential transmission for the IFS mechanism.[2,3] Comparing the magnitudes of the signals from the two samples clearly shows that the optical nonlinearity in the [211] sample is much greater than that in the [100] sample. The estimated maximum value of the nonlinear absorption index, $|\alpha_2|$, is 6.9 cm/W in the [100] sample and 54 cm/W in the [211] sample. The corresponding values for $|\mathrm{Im}\,\chi^3|$ are 0.042 esu and 0.33



Differential transmission spectra for (a) the (100) sample and (b) the (211) sample. Both sets of data were taken with I_p = 26 W/cm^2 and I_t = 2.9 W/cm^2 in the samples.

esu respectively.[8] For comparison, ref. 7 gives $|\alpha_2|$ = 39 cm/W for a GaAlAs-GaAs SL at room temperature. However, the carrier recovery time in the GaAlAs-GaAs SL (20 ns) was much longer than that in our samples (2 ns). The longer carrier recovery time of the GaAlAs-GaAs SL is entirely responsible for the larger value of α_2 in that sample compared with the [100] SL studied here, since, all other things being equal, α_2 increases linearly with increasing carrier recovery time. Even though the GaAlAs-GaAs SL studied in Ref. 7 has an order of magnitude larger carrier recovery time than that of the [211] SL studied here,

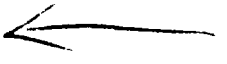
the [211] SL has the larger value of α_2. It is desirable to have both strong optical nonlinearities and short response times in order to achieve both high sensitivity and high speed response.

Intrinsic Stark effect strained layer superlattices have been shown to be novel and promising optically nonlinear materials. We have observed a strong blue shift of the exciton resonance energy and an increase in absorption with increasing light intensity, resulting directly from the screening of the internal field by photoexcited carriers. The combination of the blue shift with both a strong optical nonlinearity and a fast response time makes these materials excellent candidates for applications such as all-optical switching and modulation.

We acknowledge the invaluable work of T. E. Mitchell and O. Unal on the electron microscope measurements. The work of S. S. and H. K. was supported by the Office of Naval Research.

References

1. D. L. Smith and C. Mailhiot, *J. Vac. Sci. Technol.* A5, 2060 (1987).
2. D. L. Smith and C. Mailhiot, *Phy. Rev. Lett.* 58, 1264 (1987).
3. C. Mailhiot and D. L. Smith, *J. Vac. Sci. Technol.* A7, 609 (1989).
4. K. W. Goossen, E. A. Caridi, T. Y. Chang, J. B. Stark, D. A. B. Miller, and R. A. Morgan, *Appl. Phys. Lett.* 56, 715 (1990).
5. S. Schmitt-Rink, D. S. Chemla, and D. A. B. Miller, *Advances in Physics* 38, 89 (1989) and references therein.
6. S. Subbanna, H. Kroemer, and J. L. Merz, *J. Appl. Phys.* 59, 498 (1986).
7. D. S. Chemla, D. A. B. Miller, P. W. Smith, A. L. Gossard, and W. Wiegman, *IEEE J. Quantum Electron.* QE-20, 265-275 (1984).
8. We define χ^3 as in S. S. Jha and N. Bloembergen, *Phys. Rev.* 171, 891 (1968).



Optical Nonlinearities of Type-II Quantum Wells

G. R. Olbright, W. S. Fu†, A. Owyoung, and J. Klem
Sandia National Laboratories††, Albuquerque, NM 87185

R. Binder and S. W. Koch
Optical Sciences Center and Physics Department, University of Arizona, Tucson, AZ 85721

In this paper we describe a detailed study of the complete time evolution of the optical nonlinearites of type-II GaAs/AlAs quantum wells using nanosecond and femtosecond pump/probe spectroscopy. We explain these nonlinearities by solving the generalized Wannier equation for the case of a type-II quantum-well structure. In contrast to the usual type-I quantum-wells, we observe different shifts and saturations of light- and heavy-hole excitons as well as the abscence of gain. The dominant effects are a blue shift and saturation of the heavy-hole (HH) exciton.

In the quasi-steady state we observe a large blue shift and saturation of the HH exciton in several type-II samples. The blue shift is a consequence of the separation of electrons and holes and has been previously reported for type-II quantum wells.[1,2] Time-resolved spectra show a small blue shift and saturation which occurs after 300 fs pump/probe delay, which requires several hundred picoseconds to evolve into the full quasi-steady state blue shift. We explain the delayed onset and full development of the magnitude of the blue-shift in the time-resolved measurements through thermalization of the electrons and holes by acoustic phonon emission. Consistent with this interpretation, computed spectra show that the blue shift is strongly dependent upon the plasma temperature. We find that only a small blue shift can be observed for a plasma temperature of 300 K (corresponding to a pump/probe delay of ~500 fs) and that the large blue shift appears when the plasma temperature has cooled to ~30 K (corresponding to a pump/probe delay of ~100 ps).

After optical excitation of a type-II quantum well electron/hole space-charge separation occurs on sub-ps timescales[3] leading to an electron plasma at the X-point in the AlAs layers and a hole plasma at the Γ-point in the GaAs layers. In Fig. 1 we present quasi-steady state nonlinear absorption spectra obtained on three type-II quantum-well structures; 11/30, 11/18, and 11/11 that show the effects of this space-charge separation (n/m implies n monolayers of GaAs and m monolayers of AlAs). In Fig. 1 we observe a strong bleaching of the heavy-hole (HH) exciton resonance accompanied by a pronounced blue shift. Simultaneously the light-hole (LH) exciton exhibits a small red shift which is caused by screening due to the HH plasma.

In a separate set of experiments, we examined the time-dependent behavior of the pump-induced absorption changes. We used 100-fs-duration pump pulses and time-correlated white-light continuum probe pulses obtained from a colliding pulse mode-locked ring dye laser amplified in a copper-vapor-laser-pumped dye cell. In Fig. 2 we show time-resolved spectra of the 11/30 structure. We observe a small blue shift (≃4 meV) of the heavy-hole exciton for pump/probe time delays after several hundred femtoseconds which then develops into the large blue shift (>15 meV) as the quasi-equilibrium state is approached (notice the strong similarity between the 100 ps curve in Fig. 2 and the 110 μW curve in Fig. 1a.). The observed nonlinearities are caused by the excited hole- and electron plasmas which separate on a sub-ps time scale with respect to both spatial and momentum coordinates. The cooling of the plasmas occurs on a ~100-ps timescale, so that the quasi-steady state condition is that of a cold e-plasma located at the X-point of the Brillouin zone in the AlAs layer and a cold HH-plasma at the Γ-point in the GaAs layer.

The spatially separated plasmas in type-II structures lead to a significant difference of the probe-absorption spectra compared to those of bulk or usual type-I quantum well structures. To explain these differences one should realize that gain cannot occur in an ideal type-II system and, hence the gain-part of a type-I absorption spectrum is replaced by a zero-absorption region in type-II structures. In type-II quantum wells, the quasi-chemical potential coincides with the onset of

absorption. In bulk or type-I structures, however, increasing excitation first leads to a pure bleaching of the exciton without any significant shift until, at high densities, a gain region occurs. In this latter case, the cross-over point from gain to absorption (i.e. the quasi-chemical potential of the electron-hole plasma) shifts to higher energies with increasing density since the band-gap shrinkage due to the plasma is always less than the increase of the chemical potential. Because of the absence of a spectral region with optical gain in a highly-excited low-temperature type-II system, the Coulomb-enhanced resonance above the quasi-chemical potential appears as a blue shifted HH exciton.

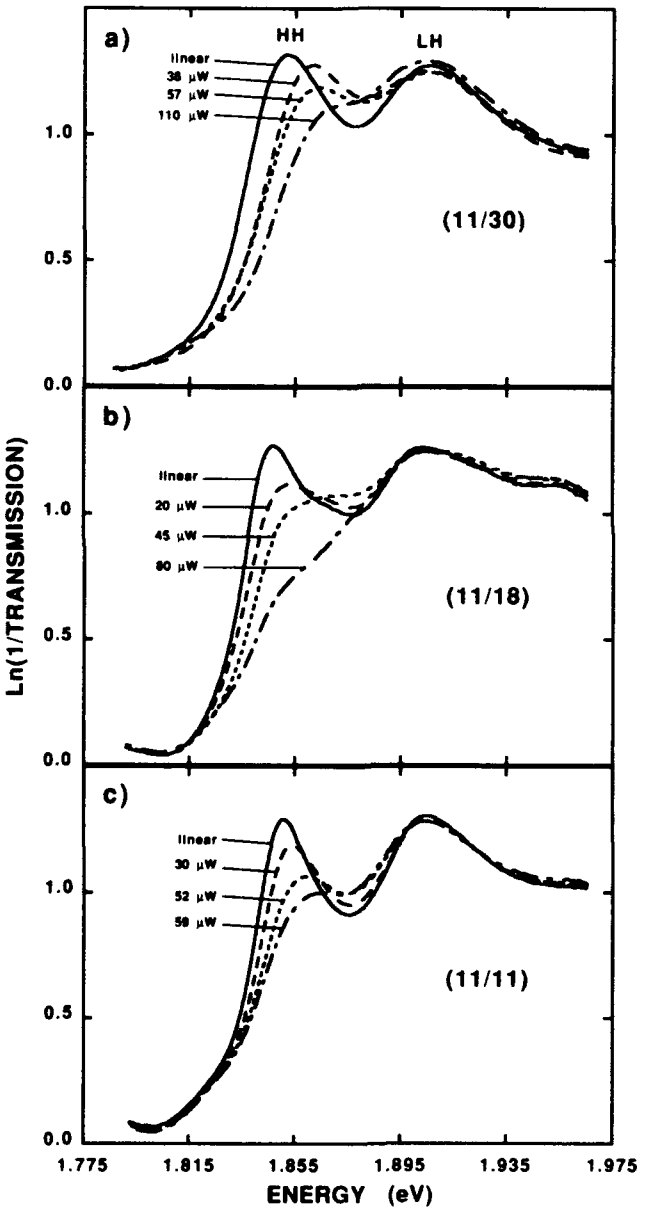


Figure 1. Nonlinear absorption spectra of structure a) 11/30, b) 11/18, and c) 11/11. T = 15 K, E_{exc} = 2.14 eV, f = 8.2 kHz, τ_{pulse} = 20 ns.

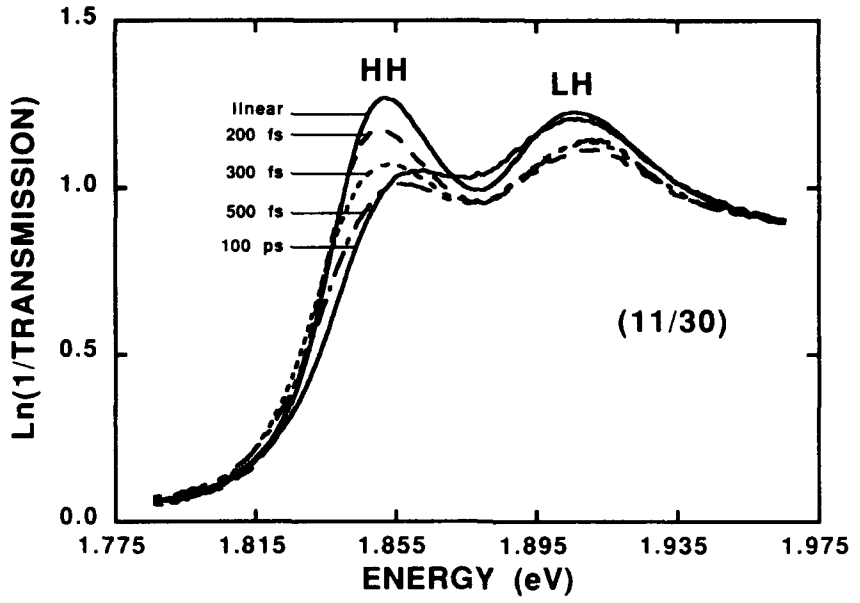


Figure 2. Femtosecond time-resolved absorption spectra for the (11/30) structure. P_{exc} = 8.5 μW, E_{exc} = 1.96 eV, T = 15 K.

In order to compute the discussed nonlinearities, we assume perfect electron-hole charge separation. The LH band is virtually unoccupied for the situations investigated and only the Γ-point holes contribute to phase-space filling of the GaAs heavy-hole exciton state. For this case we numerically solve the equations for the interband polarization for LH- and HH-transitions and include the relevant exchange and dynamic screening effects. The total homogeneous absorption is obtained by summing the HH and LH contributions, where the relative dipole strengths are chosen for the case of circularly polarized light. Since the experimentally obtained resonances contain significant inhomogeneous broadening due to well-width fluctuations we include these fluctuations in our calculations by averaging the spectra using a Gaussian distribution of well thicknesses. The amount of broadening needed to reproduce the experimental zero-density spectrum corresponds to well-width fluctuations of $\simeq$ half monolayer.[4]

The computed absorption spectra are shown in Fig. 3 for parameters corresponding to our 11/30 sample discussed above. In Fig. 3 we show the linear spectrum and spectra for 30 Kelvin and 300 Kelvin plasma temperatures. These spectra compare well with the curves labeled "linear" and "110 μW" in Fig. 1a, as well as with the curves labeled "linear" and "100 ps" in Fig. 2, respectively. The comparison between the computed spectra reveals that the HH-exciton blue shift at low temperatures disappears at higher plasma temperatures. The computed 300 K spectrum compares well with the 300 fs spectrum in Fig. 2. We explain the delayed onset and full development of the magnitude of the blue-shift in the femtosecond measurements through thermalization of holes. Initially electrons and holes are injected into the conduction and valence bands with considerable excess energy. After the initial cooling by LO-phonon emission, complete thermalization to the lattice temperature occurs on a time scale of hundreds of picoseconds via acoustic phonon emission. Hence, for a hot plasma, there is little blue shift of the exciton resonance due to phase-space filling since the carriers have not yet relaxed to the band minimum.

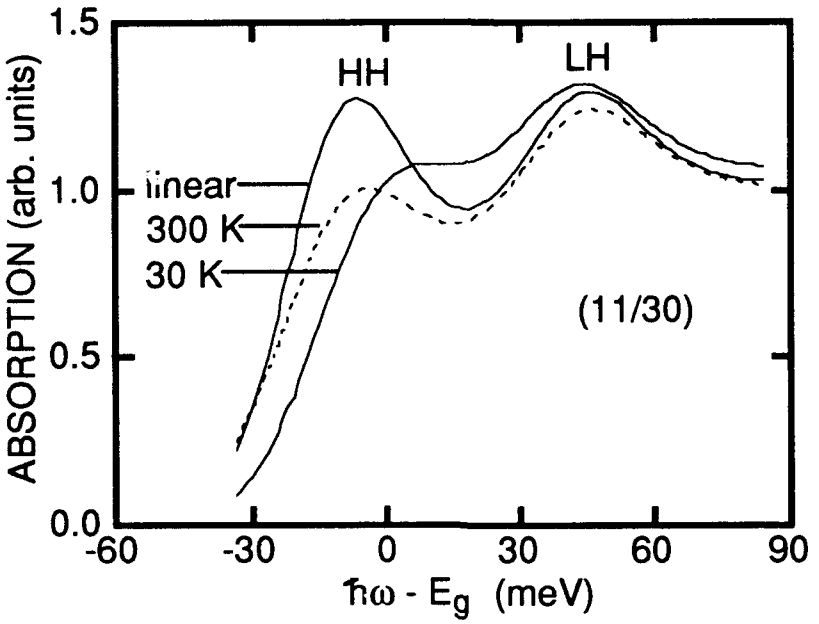


Figure 3. Calculated carrier-density-dependent absorption spectra computed for an 11/30 GaAs type-II quantum well including inhomogeneous broadening. Linear ($N \simeq 0$) spectrum, and spectra for the carrier density of 0.4 a_B^{-2} at plasma temperatures of 30 K and 300 K, respectively. E_g^{hh} is the heavy-hole energy gap and where a_B is the bulk-exciton Bohr radius.

In conclusion we have presented experimental and theoretical details of large optical nonlinearities in type-II multiple quantum wells. The primary effect is a shift of the heavy-hole exciton to higher energy on a ps-time scale which is explained by the many-body effects associated with the presence of a HH-plasma in the GaAs layer. The good agreement of the calculated absorption changes with the experimental spectra shows that our theoretical model contains the necessary physics to describe the large nonlinearities observed.

Arizona research is supported by NSF, SNL, OCC, and the Pittsburgh Supercomputer Center.

† Solid State Electronics Laboratories, Stanford University, Stanford, CA 94305.

†† SNL research is supported by DOE contract No. DE-ACO4-76DP00789.

References

1. G. R. Olbright, W. S. Fu, J. Klem, T. E. Zipperian, R. Binder, and S. W. Koch, Submitted.
2. G. R. Olbright, J. Klem, A. Owyoung, and T. M. Brennan, J. Opt. Soc. Am. B *7*, 1473 (1990)
3. J. Feldmann, R. Sattmann, E. O. Göbel, J. Kuhl, J. Hebling, K. Ploog, R. Muralidharan, P. Dawson, and C. T. Foxon, Phys. Rev. Lett. *62*, 1892 (1989).
4. W. S. Fu, G. R. Olbright, A. Owyoung, J. F. Klem, R. M. Biefeld, and G. R. Hadley, Appl. Phys. Lett. (14), 1 October 1990.

Low Power Optical Nonlinearities Produced by Spatially Separated Electron/Hole Plasmas

P Dawson, I Galbraith and C T Foxon

Philips Research Laboratories, Cross Oak Lane, Redhill, Surrey, U.K.

AD-P007 869

92-22398

Quantum well structures have received a great deal of interest as nonlinear elements in a variety of optical systems. In the absence of non-radiative recombination the dominant factor which controls the density of the electron/hole plasma (which mediates the nonlinearity) is the radiative lifetime. Thus if we wish to reduce the required optical power density in such systems we must maximise the radiative lifetime. In type I quantum wells the radiative lifetime (T=10K) is of the order of 500 ps[1] which leads to critical power densities of ~kW/cm^2. This lifetime is governed by the strong spatial overlap of the electron and hole wavefunctions. In type II quantum wells, by definition, the electron hole wavefunction overlap is greatly reduced leading to increased radiative lifetimes and hence low power optical nonlinearities.

It is already well established[2] that by choice of appropriate sample parameters it is possible to produce a type II band alignment in the GaAs/AlAs materials system. This occurs for GaAs layer thicknesses less than 35Å with AlAs thickness greater than 16Å, so that the lowest confined electron state of the GaAs is pushed above the X minima of the AlAs (see Fig.1(a)). Typically the radiative lifetime (T=10K) in such structures is in the μs regime. As has already been observed[3] this results in optical nonlinear phenomena being observed at power densities of ~W/cm^2.

The purpose of this paper is to describe the results of an investigation of the nonlinear optical properties of so-called mixed type I/II structures. The arrangement of a typical mixed type I/II structure is shown in Fig. 1(b). In these structures electrons which are created in the 25Å

GaAs layer rapidly scatter (via the AlAs X minima) down to the lowest confined state of the 50Å quantum well. On the other hand heavy holes which are created in the 25Å quantum well are prevented from tunnelling into the 50Å quantum well by the thick (80Å) AlAs barrier. These effects allow us to create an electron/hole plasma whose lifetime is governed by the heavy hole tunnelling time or the cross well recombination time.

As shown in Fig. 2 this mixed type I/II configuration allows us to investigate the bleaching of the 50Å quantum well transitions at power densities $\sim W/cm^2$. A numerical solution of the appropriate Bethe Salpeter equation for this structure is in good agreement with these spectra. In this paper we will report on the extension of these initial studies to samples where the width of the collector quantum well width is increased to allow us to study the bleaching phenomena in spectra where the inhomogeneous broadening is greatly reduced. We shall also report on the dynamics of the scattering and tunnelling processes which determine the time response of the mixed type I/II structures.

References:

(1) J Feldman, G Peter, E Gobel, P Dawson, K Moore, C Foxon and R J Elliott, Phys. Rev. Lett. 59 (1978) 2337.

(2) P Dawson, Optical and Quantum Electronics, 22 (1990) 5231.

(3) P Dawson, I Galbraith, A I Kucharska and C T Foxon. Proc. SPIE Physical Concepts of Materials for Novel Optoelectronic Device Applications, Aachen, 1990, (to be published).

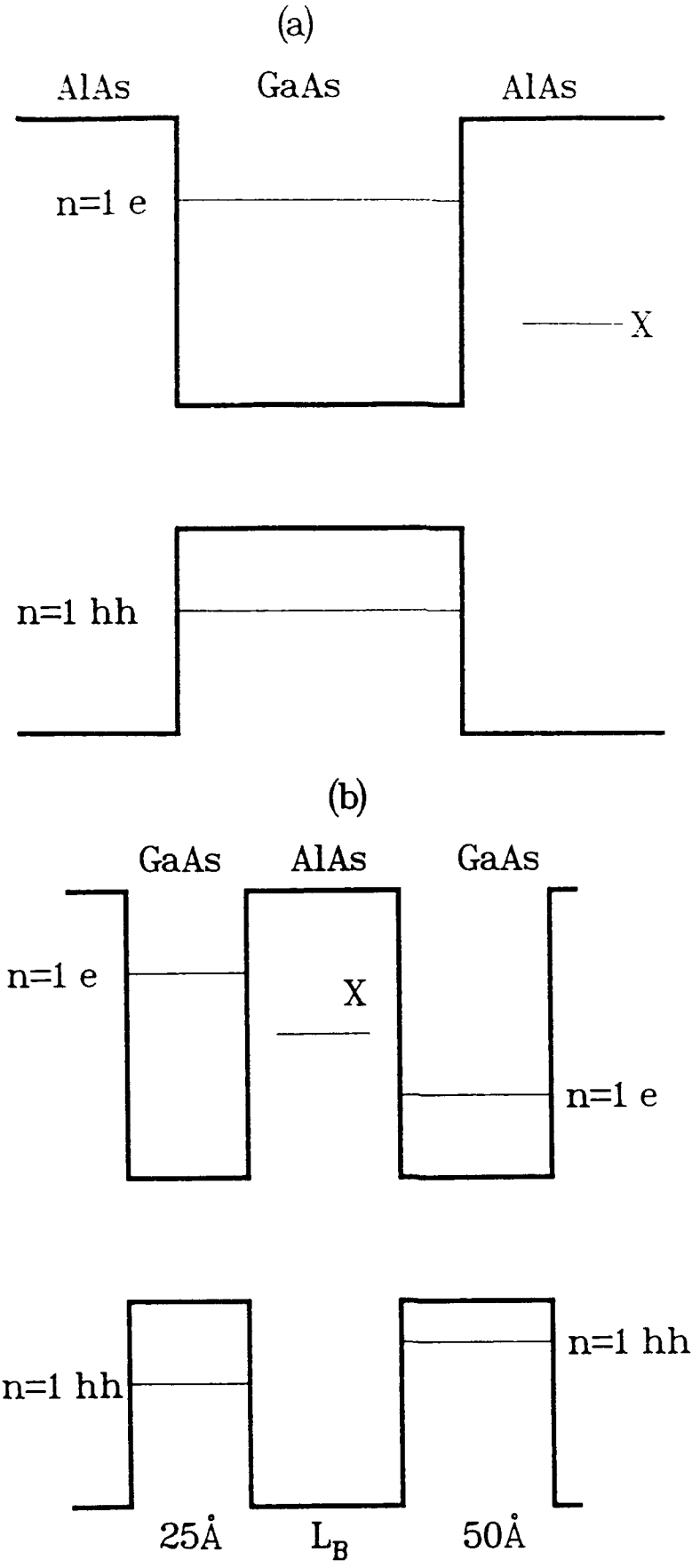


Figure 1: (a) conventional type II band alignment heterostructure
(b) mixed type I/type II band structure

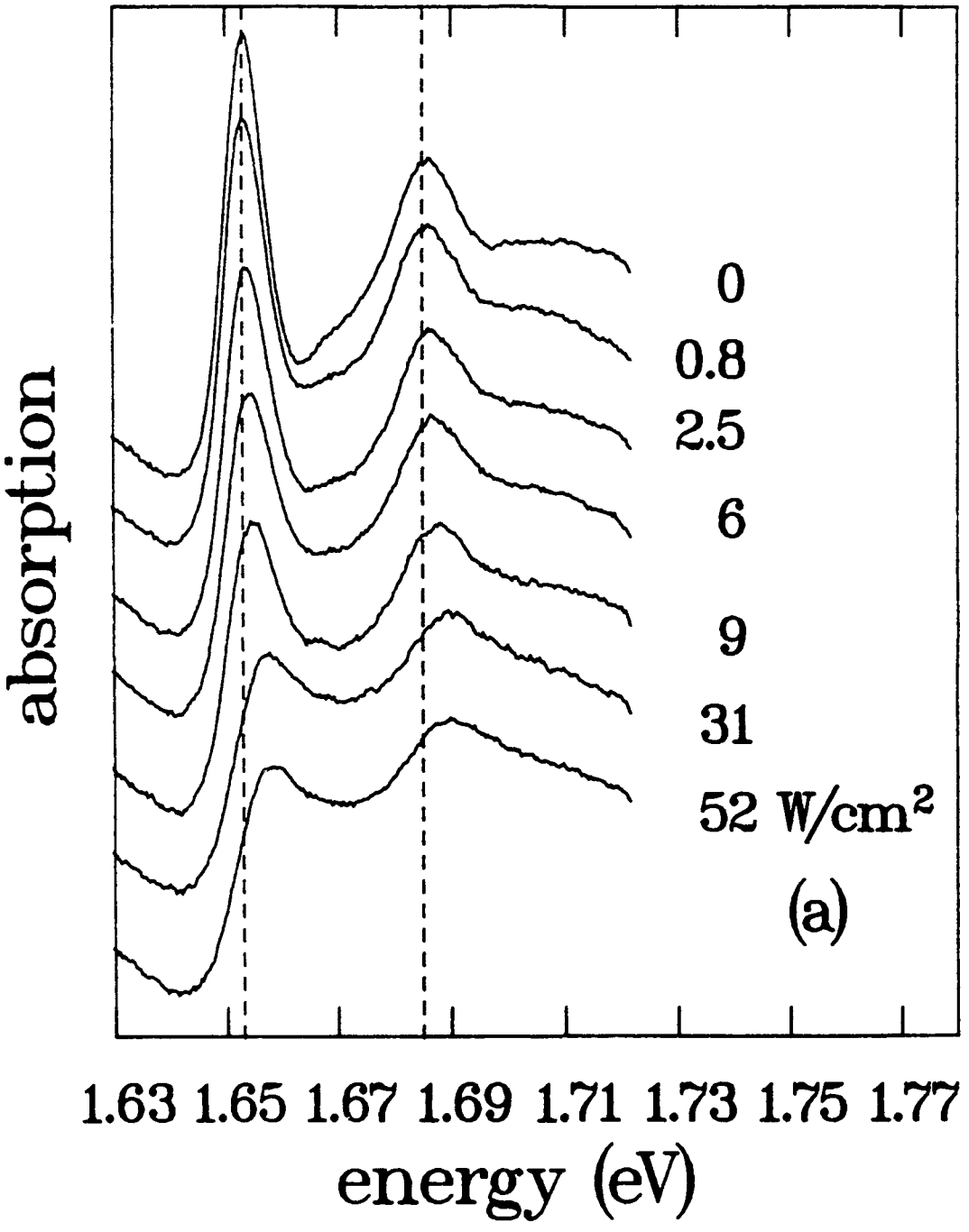
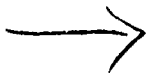


Figure 2: Nonlinear absorption spectra for the mixed type I/II samples having the 80Å barrier around the 50Å band edge. Annotated numbers indicate the cw power density



Fast State Filling Optical Nonlinearities with Charge Carrier Transport

AD-P007 870



Jeff White, Alan Kost, Tom Hasenberg, and George Valley

Hughes Research Laboratories

3011 Malibu Canyon Road, Malibu, CA 90265

Elsa Garmire

National Center for Integrated Photonic Technology and Center for Laser Studies

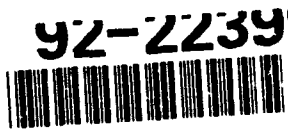
University of Southern California, Los Angeles, CA 90089-1112

The effects of exciton saturation and state filling on the transmission of quantum wells can be extremely large and their onset is limited only by optical pulse length[1]. On the other hand, recovery time is usually determined by the rate of electron-hole recombination, so that in high quality samples recovery may take tens of nanoseconds or longer. We have previously demonstrated that absorption saturation in quantum wells can be achieved at lower intensities by putting the quantum wells in the i-region of a hetero n-i-p-i structure[2]. Here it is shown that the built-in fields of a hetero n-i-p-i can be used to sweep photocarriers out of quantum wells and reduce recovery times to the picosecond regime. This approach has advantages over methods to increase recombination rates such as the use of surface recombination which is not effective with quantum wells and ion bombardment which has a detrimental effect on excitons.

Fig. 1 shows the structure of the sample grown by molecular beam epitaxy. Each intrinsic region contains 12 coupled GaAs wells. The two wells in a pair (each 48 Å) are separated by a thin (36 Å) $Al_{0.3}Ga_{0.7}As$ barrier. A thicker 100 Å barrier of $Al_{0.3}Ga_{0.7}As$ separates two pair. The n and p regions are nominally doped to 2×10^{18}. A total of 5 intrinsic regions were grown.

The linear transmission of the sample is shown in Fig. 2a with the corresponding absorption in Fig. 2b. Because the coupling between wells is small, the transitions which are most

92-22399



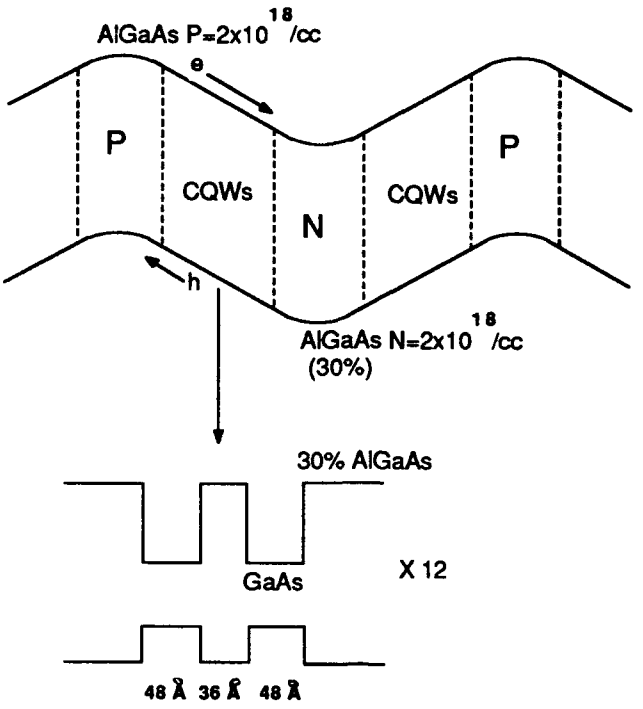


Fig 1. The energy band diagram for a multiple quantum well hetero n-i-p-i structure with coupled quantum wells.

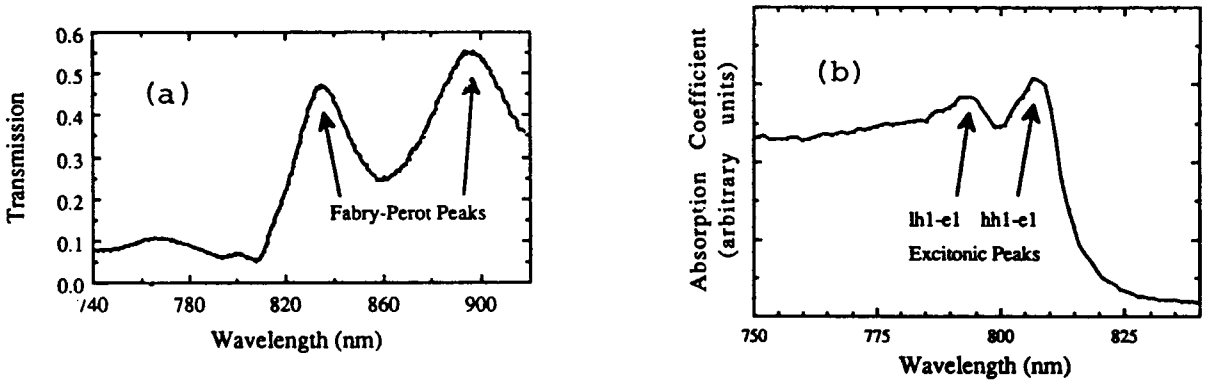


Fig. 2 (a) The transmission of the hetero n-i-p-i. Fabry-Perot oscillations due to multiple reflections from the sample surfaces are indicated. (b) The absorption coefficient deduced from (a). The n=1 heavy (hh1-e1) and light (lh1-e1) hole excitons of the weakly coupled wells are at the same wavelengths as for isolated 48 Å wells.

easily observed in these spectra are the same as those for isolated 48 Å wells. For weak excitation this sample exhibits very interesting nonlinearities arising from a small coupling between wells[3].

The saturation effects studied here, on the other hand, can occur in a n-i-p-i sample with an arbitrary type of quantum well.

Figure 3 shows the transmission of a probe beam as a function of delay relative to a pump with fluence 2.9 mJ/cm^2. Both the pump and probe are at 820 nm, well below the heavy hole exciton, and have autocorrelation widths of 6 psec full width at have maximum. Pump to probe ratio is ≈ 20:1. The rapid increase in transmission near zero delay we attribute to a combination of effects. First, the pump fills the quantum wells with > 10^{12} electron-hole pairs/cm^2/well so that the absorption of the wells is saturated[4]. Second, there is a shift of the Fabry-Perot resonance near 835 nm to shorter wavelengths due to the decrease in the refractive index below the absorption edge which accompanies the decrease in absorption above the edge[5]. What is striking in Fig. 3 is the speed at which the absorption recovers. A 40% increase in transmission is reduced to 10% in 100 psec. This recovery is too fast to be attributed to electron-hole recombination. It appears, instead that absorption recovers when photocarriers are swept from quantum wells by built-in electric fields.

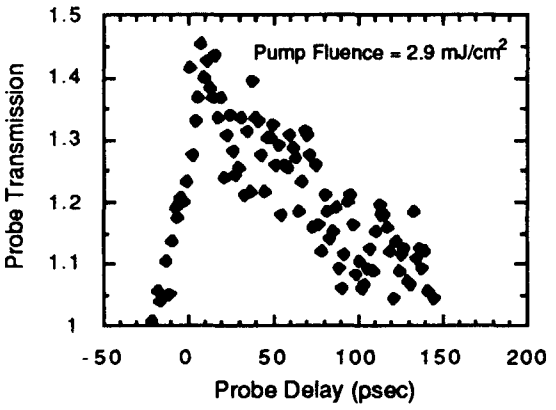


Fig. 3. Saturating absorption in multiple quantum wells. The transmission, at 820 nm, recovers quickly as built-in fields sweep carriers from the wells.

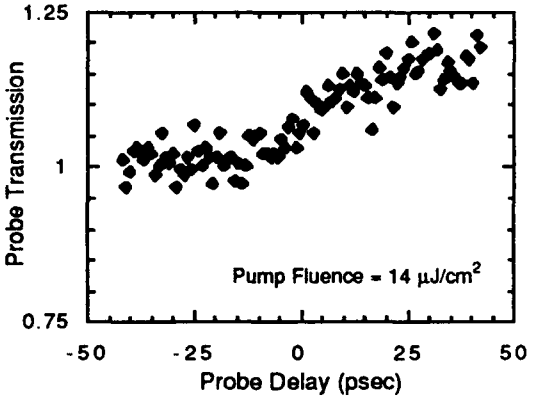


Fig. 4. At low fluences, a persistent change in transmission can be seen at 809 nm as photocarriers swept to doped layers screen the built-in fields.

Differential transmission at smaller fluences (Fig. 4) confirms our interpretation of the data presented in Fig. 3. With a pump fluence of 14 $\mu J/cm^2$, the density of electrons and holes deposited in the quantum wells (~ 5 x $10^{11}/cm^2$/well) is insufficient to cause a large change in the transmission of the probe through exciton saturation or state filling. On the other hand, if photocarriers are swept to the doped regions of the n-i-p-i, there is a sufficient number to modify the transmission by screening the built-in field. The transmission of an 809 nm probe, as a function of probe delay, is shown in Fig. 4 for the case of a weak pump The transmission increases roughly as $\Delta T = \Delta T_{max} (1-e^{-t/\tau})$ with a time constant t ≈ 15 psec, characteristic of field-induced emission from quantum wells[6]. Note that at ≈ 50 psec the transmission has leveled off at a value corresponding to an increase of ≈ 20 %. Measurements at longer delays show that the transmission remains constant for at least 200 psec. There is no sign of the fast recovery which is so prominent in Fig. 3 and none is expected since the transmission change at low fluences is due to photocarriers which have already been swept out of quantum wells.

[1]D. S. Chemla, D. A. B. Miller, and S. Schmitt-Rink, *Optical Nonlinearities and Instabilities in Semiconductors*, Harmut Haug, Editor (Academic Press, San Diego, 1988) pp. 83-120.

[2]Alan Kost, Mike Jupina, Elsa Garmire, and Tom Hasenberg, Optical Society of America Annual Meeting 1990, paper WJ1.

[3]Alan Kost, Elsa Garmire, and Tom Hasenberg, *Nonlinear Optical Properties of Materials*, Howard R. Schlossberg, Raymond V. Wick, Editors, Proc. SPIE 1148, 144 (1990).

[4]Hsing-Chung Lee, A. Kost, M. Kawase, A. Hariz, P. Daniel Dapkus, and Elsa M. Garmire, IEEE J. of Quantum Electron. **QE-24**, 1581 (1988).

[5]Y. H. Lee, A. Chavez-Pirson, S. W. Kock, H. M. Gibbs, S. H. Park, J. Morhange, A. Jeffery, N. Peyghambarian, L. Banyai, A. C. Gossard, and W. Wiegmann, Phys. Rev. Lett. **57**, 2446 (1986).

[6]Anders Larsson, Peter A. Andrekson, Sverre T. Eng, and Amnon Yariv, IEEE J. Quantum Electron. **QE-24**, 787 (1988).

Quantum-Well Devices

WB 10:30am–12:00m
Salon F

J. Harris, *Presider*
Stanford University



AD-P007 871

92-22400

Structure Dependence of Carrier Replenishment in Multiple Quantum Well Optical Amplifiers

J. M. Wiesenfeld, S. Weiss[a], D. S. Chemla[a], G. Eisenstein[b]
U. Koren, G. Raybon, G. Sucha[a], and M. Wegener[c]

AT&T Bell Laboratories, Holmdel, NJ 07733

In forward biased quantum well structures, such as lasers and optical amplifiers, electrons and holes must flow through the barrier regions before they are captured by the quantum wells. This capture process, which concerns the scattering of a three-dimensional barrier state into a two-dimensional state in the quantum well, is of fundamental interest [1]. It is also significant for devices, because it relates to the efficiency and modulation performance of quantum well lasers, as well as to the gain recovery time and, hence, gain saturation characteristics of quantum well optical amplifiers.

In previous work [2-5, for example] carrier capture by quantum wells has been studied by time-resolved photoluminescence experiments. In these works, carriers are injected into the quantum well structure by photoexcitation using a short optical pulse. The carrier capture process is then observed as the rise time of the photoluminescence from the quantum wells or as the fall time of the photoluminescence from the barrier regions. Photoexcitation creates free carriers in the absence of preexisting free carriers, with a distribution that reflects the photoexcitation process. Thus, these experiments measure the capture of individual carriers which evolve under the initially unscreened Coulomb potential of the quantum well structure. By contrast, forward biased devices operate under conditions of a high-density electron-hole plasma, in which many-body effects, such as screening of the Coulomb interaction and carrier-carrier scattering, are significant. We study the carrier capture process under such conditions in the present work, by measuring the recovery of the gain, following removal of carriers by an ultrashort optical pulse, in optical amplifiers made from multiple quantum well laser diodes. By comparing the results for several structures, carrier diffusion in the barrier regions is shown to be the rate-limiting step.

Gain recovery is measured by a pump-probe experiment, using 0.4 ps pulses derived from an additive pulse modelocked (APM) color center laser, which is tunable between 1.47 and 1.52 μm. [6,7] Time-delayed pump and probe pulses from the APM laser are combined in a fiber directional coupler and then coupled into the optical amplifier using a fiber microlens. The gain of the TE polarized probe pulse is measured as a function of delay following the TM polarized pump pulse. Typically, the probe pulse is 50 - 100 times less intense than the pump pulse. The pump pulse depletes the gain of the amplifier by stimulated emission by up to 6 - 8 dB. Optical amplifiers were fabricated by applying SiO_x anti-reflection coatings to both facets of laser diodes. Amplifiers fabricated from three diode structures were studied. The active region of the first device (multiple quantum well: MQW) consisted of four 8.0 nm wide InGaAs quantum wells

---

a *Present address: Lawrence Berkeley Laboratory and Department of Physics, University of California, Berkeley, CA 94720*

b *Present address: Department of Electrical Engineering, Technion, Haifa, 32000, Israel.*

c *Present address: Fachbereich Physik, Universitat Dortmund, Dortmund, Germany.*

separated by 10 nm wide 1.3 μm-InGaAsP (0.95 eV bandgap) barriers and clad on both sides by 100 nm InGaAsP barriers. The active region of the second device (strained-layer (SL) MQW) contained four 2.5 nm wide strained InGaAs quantum wells, separated by 9.0 nm wide InGaAsP barriers and clad on both sides by a separate confinement heterostructure (SCH) consisting of a 60 nm wide 1.3 μm-InGaAsP layer followed by a 90 nm wided 1.1 μm-InGaAsP layer. Finally, the third device was a conventional channelled substrate buried heterostructure (CSBH or V-groove) device, with a 150 nm wide 1.55 μm-InGaAsP active region, clad on both sides by InP. Because the devices have anti-reflection coatings on both facets, high bias levels could be used and carrier densities in the wells and barriers as large as 6×10^{18} cm^{-3} were achieved.

The optical amplifiers are studied under conditions of high bias current, so that the quasi-Fermi levels extend into the barrier regions for the MQW and SL MQW devices. After removal of carriers from the quantum wells by stimulated emission, the gain of the amplifier is reduced. Carriers are replenished in the quantum wells by diffusion and capture of carriers stored in the barrier regions, which serve as carrier storage reservoirs for the MQW and SLMQW devices. The CSBH device has no such reservoirs. On a time scale determined by the nonradiative (Auger) recombination time in the devices, carriers are resupplied tc the barriers from the external bias current source to the amplifier. Figure 1 shows the gain recovery dynamics for the MQW amplifier. [7] The data is plotted on a semilogarithmic scale of gain compression in dB. The data can be fit as a sum of two exponentials, with time constants 0.7 ± 0.1 ps and 7 ± 1 ps. The shorter time constant is assigned, by analogy to other pump-probe experiments on optical amplifiers, as carrier cooling. [6] The longer time constant is a diffusion time for carriers across the 100 nm wide cladding regions, which is given by $\tau \approx L^2/D$, where L is the diffusion distance (50 nm for the MQW device) and $D = 4$ cm^2/sec is the diffusion constant for 1.3 μm-InGaAsP. [7] From the above numbers, $\tau \approx 6$ ps, in agreement with the data.

The gain recovery dynamics for the SLMQW amplifier are shown in Fig. 2, also as a semilogarithmic plot of gain compression in dB. The data are again fit with two time constants, with values 0.6 ± 0.1 ps and 2.5 ± 0.5 ps. The time constants are assigned, as above, to carrier cooling and diffusion across the 1.3 μm-InGaAsP cladding region. In the SLMQW device, the width of 1.3 μm-InGaAsP cladding is 60 nm, so for $L \approx 30$ nm, the calculated diffusion time would be 2 ps, in close agreement to the data. Finally, the gain recovery dynamics for the bulk CSBH amplifier are shown in Fig. 3 as time-resolved transmission changes. There is a fast, partial recovery, followed by a very slow recovery (infinite on a 20 ps time scale). The fast recovery, which is fit by a time constant of 0.9 ± 0.2 ps is assigned to carrier cooling. [6] Because the CSBH amplifier has no barrier regions to serve as carrier storage reservoirs, the carriers removed by stimulated emission must be replaced from the external current source. This replenishment occurs on the time scale of Auger recombination [7], which is greater than 200 ps for the CSBH device.

Comparison of the results shown in Figs. 1 - 3 demonstrates the effect of the different device structures on the gain recovery process. In all devices a subpicosecond time constant, caused by carrier cooling, is present. This is a material-dependent process. A subsequent gain recovery process, with a time constant between 2 and 7 ps, is present in the quantum well devices. This process is gain replenishment by carriers stored in the barrier regions, which act as carrier storage reservoirs. The time constant scales with length and in magnitude consistently with carrier diffusion in the barrier regions. Thus, the rate-limiting step for carrier replenishment in high-density electron-hole plasmas in forward biased quantum well devices is carrier diffusion.

References:

1. J. A. Brum and G. Bastard, Phys. Rev. B, 33, 1420 (1986).
2. E. O. Gobel, H. Jung, J. Kuhl, and K. Ploog, Phys. Rev. Lett., 51, 1588 (1983).
3. B. Devaud, J. Shah, T. C. Damen, and W. T. Tsang, Appl. Phys. Lett., 52, 1886 (1988).
4. A. Weller, P. Thomas, J. Feldmann, G. Peter, and E. O. Gobel, Appl. Phys., A48, 509 (1989).
5. P. W. M. Blom, R. F. Mols, J. E. M. Haverkort, M. R. Leys, and J. H. Wolter, Superlattices and Microstructures, to be published.
6. K. L. Hall, J. Mark, E. P. Ippen, and G. Eisenstein, Appl. Phys. Lett., 56, 1740 (1990).
7. G. Eisenstein, J. M. Wiesenfeld, M. Wegener, G. Sucha, D. S. Chemla, S. Weiss, G. Raybon, and U. Koren, Appl. Phys. Lett., to be published.

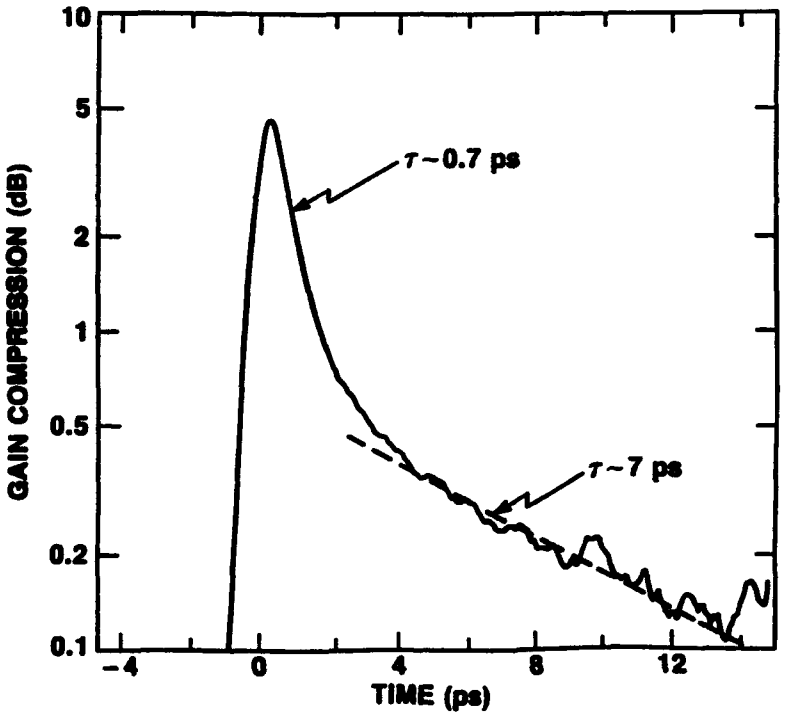


Figure 1: Gain recovery of the MQW amplifier, measured at 1.47 μm with 150 mA bias.

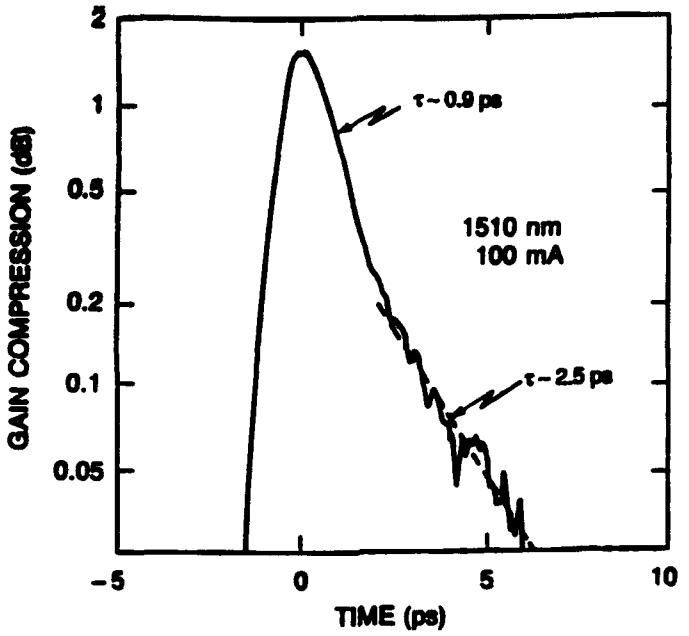


Figure 2: Gain recovery of the SLMQW amplifier, measured at 1.51 μm and 100 mA bias.

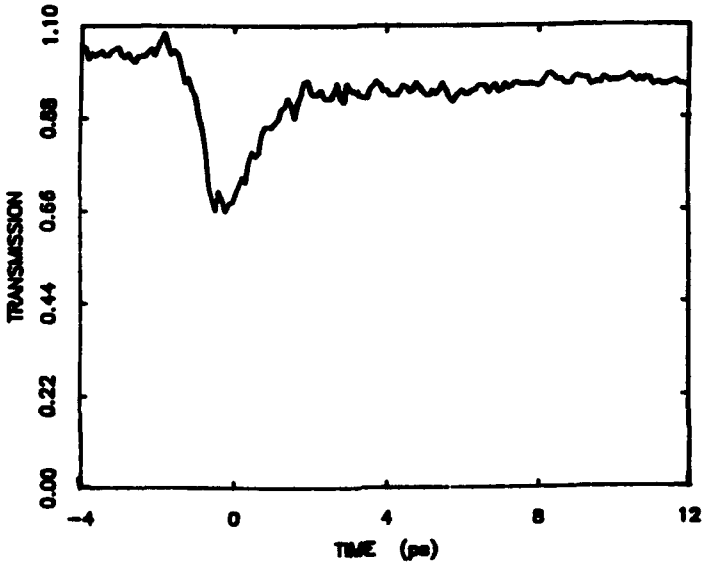


Figure 3: Gain recovery of the CSBH amplifier, measured at 1.52 μm and 40 mA bias. The data here is presented as time-resolved transmission.

AD-P007 872

Coupled-Cavity Modelocking of Solid-State Lasers using Quantum Wells

U. Keller, G. W. 't Hooft, W. H. Knox, and T. K. Woodward*

AT&T Bell Laboratories, Crawfords Corner Road, Holmdel, NJ 07733

**Philips Research Laboratories, Prof. Holstlaan, 5600 JA Eindhoven, The Netherlands*

The ultrafast physics of MQW samples have been studied extensively [1,2]. We used this to passively modelock solid-state lasers with small gain cross section such as Ti:Sapphire and Nd:YLF lasers [3,4,5]. Figure 1 shows the laser cavity design which is called coupled cavity resonant passive modelocking (RPM) - "resonant" because of the near-resonant nonlinearity in the coupled cavity. The excitation level of the MQW reflector is high with an average intensity of > 20 kW/cm^2 and a peak intensity of > 20 MW/cm^2 at 250 MHz repetition rate. The modelocking disappears at lower excitation levels. Using the RPM Ti:Sapphire laser with its picosecond tunable pulses, we performed some pump-probe measurements on a separate piece of the same p-i-n MQW reflective modulator structure which modelocks the Ti:Sapphire laser. We measure a fast reflectivity modulation with a time constant determined by the pump and probe pulse width superimposed on a long time transient due to carrier recombination, heating and screening of the built-in field.

The RPM laser is made by adding to a cw solid-state laser an external cavity with a nonlinear resonant reflector (Fig. 1). In the case of the RPM Ti:Sapphire laser, we generate stable picosecond pulses and demonstrate wavelength tuning over several tens of nanometers using a single GaAs/AlGaAs quantum well reflector without dispersion compensation and active stabilization of the external cavity [3,4]. The Ti:Sapphire laser is a Spectra Physics #3900 laser pumped by a cw argon ion laser. The nonlinear reflector for the Ti:Sapphire laser is an AR coated conventional p-i-n GaAs/GaAlAs quantum well modulator structure that incorporates a AlAs/AlGaAs dielectric mirror centered around 850 nm. The undoped MQW region consists of 75 periods of 95 Å wide GaAs quantum wells and 45 Å wide $GaAl_{0.3}As_{0.7}$ barriers. In case of the

RPM Nd:YLF laser, we use an InGaAs/GaAs strained layer quantum well reflector with a bandgap near 1.047 μm [Sample D of 6] and generate 4 ps pulses with nJ pulse energy with only 1.5 W pump power at 798 nm. Figure 2 shows a real-time autocorrelation trace of a 4.2 ps long pulse (FWHM assuming $sech^2$ pulse shape) at 1.047 μm wavelength at 250 MHz repetition rate using C_1= 3% and C_2 = 48% (Fig. 1). We are able to detune the external cavity length over millimeters and still obtain modelocked pulses, however, the pulse width increases with increased cavity length detuning. At exact cavity length matching the laser strongly fluctuates and no stable modelocking is observed.

We believe that the resonant nonlinearity in coupled cavity modelocking yields a new mode of operation. The laser operates in stable modelocked pulse trains by self-adjusting its optical frequency in response to phase shifts caused by external cavity length fluctuations, which is a basic property of a linear Fabry-Perot coupled cavity [4,7]. Self-stabilized operation is not obtained with a Kerr medium in the external cavity, because the frequency corresponding to maximum power is not the same frequency corresponding to maximum nonlinear reflectivity [7]. Because the gain saturation in these lasers is small, we believe that the main pulse forming mechanism is due to a fast reflectivity modulation from the semiconductor reflector. We used the tunable RPM Ti:Sapphire laser to perform non-collinear pump-probe measurements on another piece of the MQW reflector. Some results are shown in Figure 3. In order to achieve pump intensities on the reflector of ≈ 20 kW/cm^2, which are the intensity levels incident onto the nonlinear reflector inside the laser, we use a a shorter focusing lens (≈ 15 mm) in the pump-probe experiment and ≈ 50% output coupler (C_2 in Fig. 1) which does not correspond to the optimal laser operation in terms of pulse width and tunability. Figure 3a gives the pump and probe pulse duration as a function of wavelength and the the probe reflectivity with blocked pump beam which was used in the absolute calibration of the measurements shown in Fig. 3b. The laser was tunable over the wavelength range from ≈ 848 nm to ≈ 861 nm, for which we observe a fast reflectivity transient with a time constant determined by the excitation pulse width (Fig. 3b). As soon as either the fast rise or the fast fall of the reflectivity transient becomes very small it also becomes very difficult to modelock

the laser. The shortest pulses are achieved around 856 nm where the rapid reflectivity modulation is the largest. This is in agreement with H. A. Haus's theory [7]. The fundamental process of this reflectivity transient with ultrafast intrinsic response for wavelengths above the absorption edge is possibly due to exciton ionization, and below the absorption edge due to a.c. Stark effect. We will also discuss different samples.

Especially the work on the RPM Nd:YLF laser is strongly motivated by the need for high-power high-repetition-rate pulsed laser sources with pulse energies ranging from 1 pJ to 1 nJ, for potential communication and computing applications. Presently, high speed photonic switching elements require switching energies of the order of 1 pJ [8,9]. Using high power diode laser arrays as efficient pump sources, solid state lasers such as Nd:YLF, Nd:glass etc are high-power laser sources with clean spatial and spectral mode properties. Most difficulties center around practical high-repetition rate modelocking techniques for which our new RPM technique may offer a solution.

The authors like to acknowledge K. W. Goossen, J. E. Cunningham, and W. Y. Jan for the GaAs/AlGaAs quantum well reflector sample and D. L. Sivco and A. Y. Cho for the InGaAs/GaAs sample; G. Raybon for the AR coating of the 1.06 μm sample; K. J. Weingarten of Lightwave Electronics Corp. for the Nd:YLF crystal; and H. A. Haus and E. P. Ippen at MIT for helpful discussions.

---

[1] W. H. Knox, R. L. Fork, M. C. Downer, D. A. B. Miller, D. S. Chemla, and C. V. Shank, Phys. Rev. Lett. 54, 1306, 1985; W. H. Knox, C. Hirlimann, D. A. B. Miller, J. Shah, D. S. Chemla, and C. V. Shank, Phys. Rev. Lett., 56, 1191,1986

[2] J. L. Oudar, D. Hulin, A. Migus, A. Antonetti, and F. Alexandre, Phys. Rev. Lett. 55, 2074, 1985

[3] U. Keller, W. H. Knox, and H. Roskos, in Digest of *Ultrafast Phenomena VII* (Springer Verlag, 1990) p. 69

[4] U. Keller, W. H. Knox, and H. Roskos, to be published in *Optics Lett.* Dec. 1, 1990

[5] U. Keller, T. K. Woodward, D. L. Sivco, and A. Y. Cho, *Optics Lett.*, submitted

[6] T. K. Woodward, T. Sizer II, D. L. Sivco, and A. Y. Cho, *Appl. Phys. Lett.* **57**, 548, 1990

[7] H. A. Haus, U. Keller, W. H. Knox, "A Theory of Coupled-Cavity Modelocking with a Resonant Nonlinearity," *JOSA B*, submitted

[8] M. N. Islam, C. E. Soccolich, and D. A. B. Miller, *Optics Lett.* 15, 909, 1990

[9] D. A. B. Miller, *Optical and Quantum Electronics* 22, S61, 1990

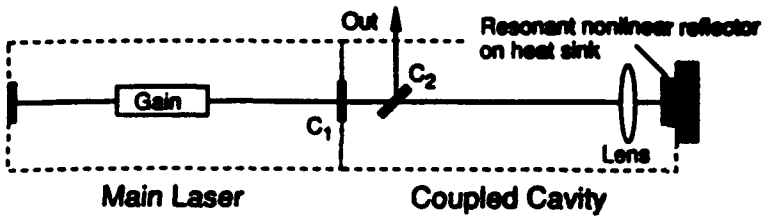


Fig. 1: RPM Laser

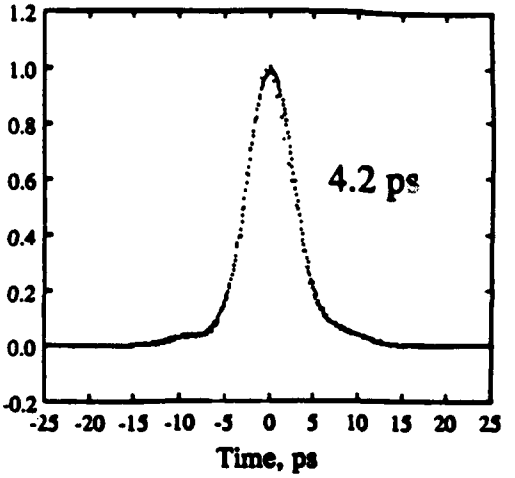


Fig. 2: RPM Nd:YLF autocorrelation

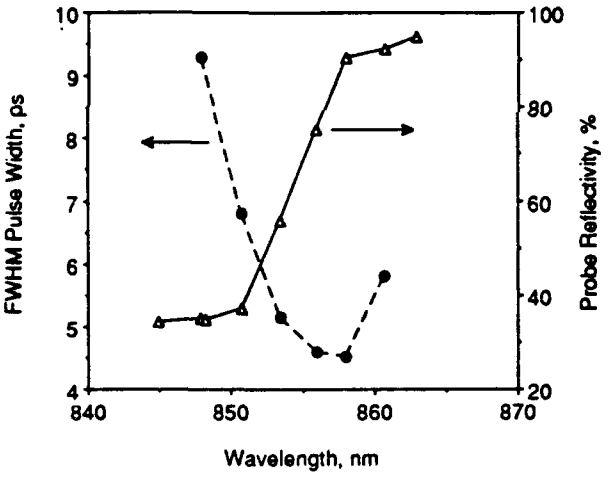


Fig. 3a: Parameters for pump-probe experiment

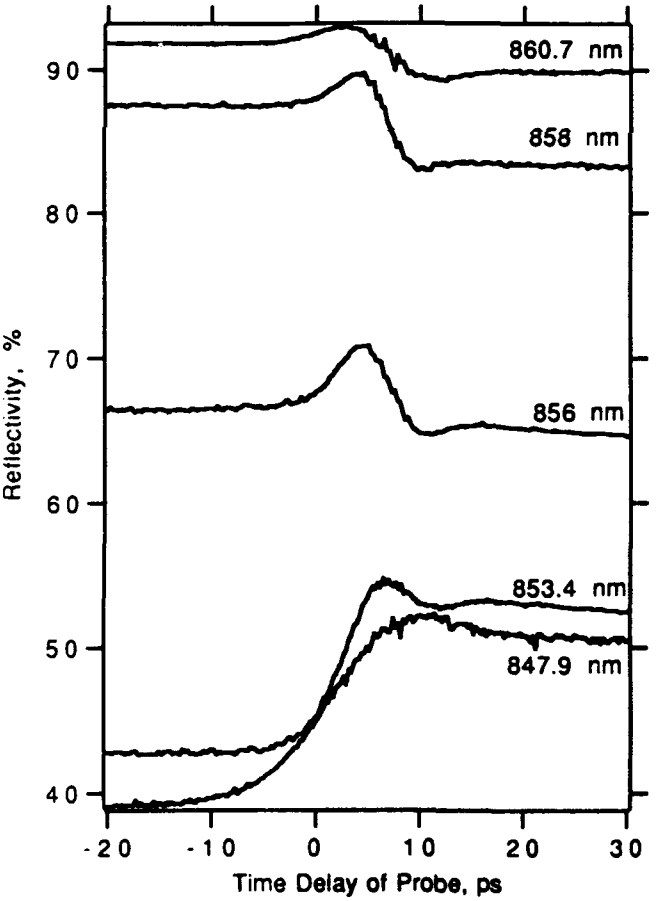


Fig. 3b: Pump-probe experiment on the GaAs/GaAlAs resonant reflector

AD-P007 873
92-22402

External-Cavity Surface-Emitting InGaAs/InP MQW Laser: High Powers and Subpicosecond Pulses

W. B. Jiang*, S. R. Friberg,
NTT Basic Research Laboratories
3-9-11, Midori-Cho, Musashino-shi, Tokyo 180 Japan
Ph: 81-422-59-4349, Fax: 81-422-59-3285

H. Iwamura,
NTT Optoelectronics Laboratories
Mori-no-Sato, Atsugi-shi, Kanagawa, 243-01 Japan
Ph: 81-462-40-3213, Fax: 81-462-40-4305

and

Y. Yamamoto
NTT Basic Research Laboratories
3-9-11, Midori-Cho, Musashino-shi, Tokyo 180 Japan
Ph: 81-422-59-2334, Fax: 81-422-59-3285

We have demonstrated an external-cavity surface-emitting semiconductor laser (EX-SEL), obtaining pulses as short as 710 fsec and peak powers as high as 64 W (after compression). A surface-emitting semiconductor laser (SEL) lacks the beam quality problems associated with cleaved-cavity lasers, and can be used to generate high output powers. Previous work with a SEL has produced 120 mW of CW power [1]. Gain-switching of a SEL has yielded 3.9 psec pulses [2]. To produce shorter pulses, mode-locking in an external cavity has been proved to be advantageous. For example, an external-cavity edge-emitting laser produced 580 fsec pulses at average powers of ~1.4 mW [3]. Hybrid mode-locking techniques combined with amplification and pulse-compression have resulted in 560 fsec pulses, average powers of 6.5 mW, and peak powers of 38 W [4]. This paper describes mode-locking of an SEL in an external cavity.

Figure 1 diagrams our EX-SEL. The gain medium is InGaAs in an MBE-grown InGaAs/InP MQW consisting of 200 periods of InGaAs (150 Å) separated by InP (50 Å). The InGaAs has a room temperature excitonic absorption peak at

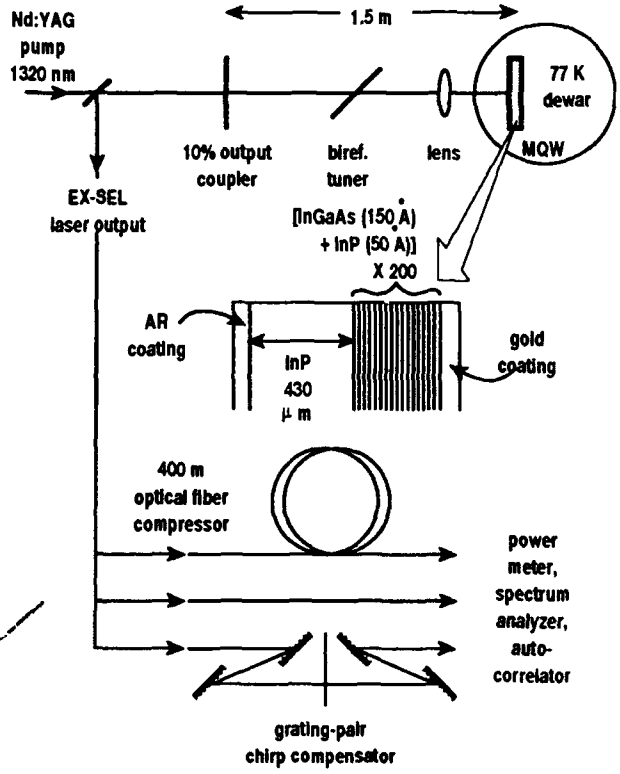


Figure 1: External-cavity surface emitting semiconductor laser (EX-SEL). A 1.5 m cavity is formed by a 10% output coupler and a gold-coated InGaAs/InP MQW at 77 K.

1.589 μm and the room temperature luminescence spectrum is shown in Fig. 2a (CW excitation at 1.06 μm). At laser operating temperatures of 77 K, the excitonic absorption peak moves to below 1.50 μm, and the luminescence spectrum is that shown in Fig. 2b. We gold-coated the epitaxial side of the substrate as a mirror (and as a heat-sink), and AR-coated the substrate side. Nonradiative Auger recombination losses are large at room-temperatures [5], thus 77 K operation. The lasing cavity consists of the MQW sample with integral end-mirror, an AR-coated lenses focused on the MQW sample, a 1 mm thick quartz birefringent tuning element (bandwidth of 30 nm), and a 10% output coupler. A dichroic steering-mirror couples in pump light from a 1.32 μm Nd:YAG laser, and couples out laser light at 1.5 μm.

CW operation of our EX-SEL laser gave large output powers. Figure 3a shows output powers as a function of pump power. Peak powers were 190 mW at 1.3 W pump powers, the lasing threshold was at 40 mW pumping. These power levels are comparable to those of color-center lasers at this wavelength. The absolute quantum efficiency of conversion from pump photons to lasing photons was as high as 18%, and the maximum differential quantum efficiency is 23%. Figure 3b shows the center wavelength of the laser at peak powers, which shifts from 1.495 μm at threshold to 1.518 μm. Thermal loading, due to inadequate thermal contact of the MQW to the cryostat cold finger helped to prevent further increases of output power. The laser could be tuned from 1.44 μm to 1.53 μm with the birefringent tuning element, as shown in Fig. 4.

Synchronous pumping at 100 MHz with 110 psec pulses from the 1.32 μm Nd:YAG gave 100 psec pulses and average output powers nearly identical to the CW results, but with a reduced threshold pump power of 20 mW. Synchronous pumping pulses compressed to 6 psec (maximum average power, 250 mW) gave average output powers that followed the CW curve up to a maximum output power of 15 mW. The (averaged) autocorrelator trace of the resulting pulse is shown in Fig. 4a. Assuming a hyperbolic secant profile, the pulse has a full-width half-

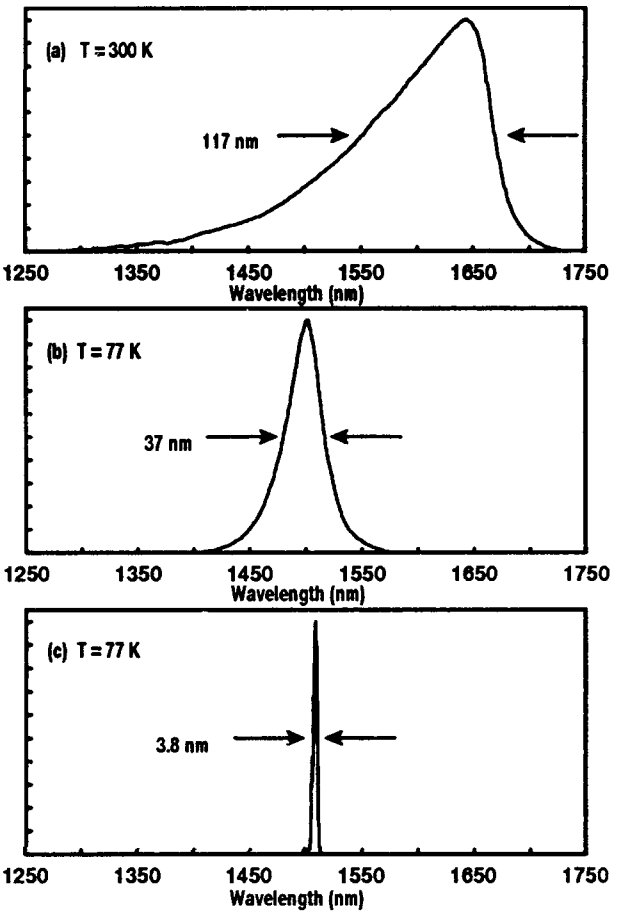


Figure 2: InGaAs/InP MQW luminescence spectra at 300 K (a) and 77 K (b), EX-SEL lasing spectrum at 77 K (c).

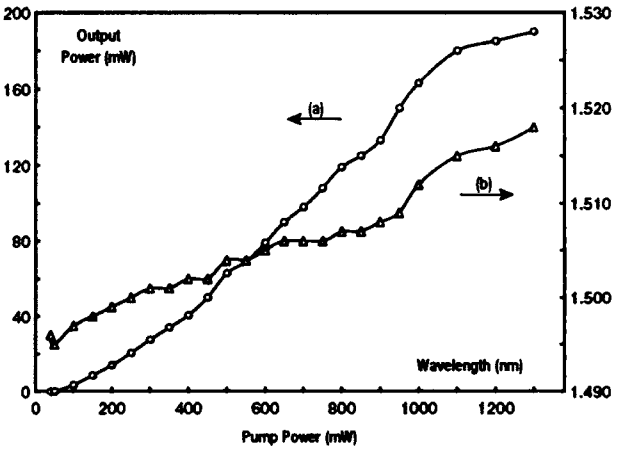


Figure 3: EX-SEL CW output power (a) and center-frequency (b) as a function of pump power (1.32 μm CW Nd:YAG).

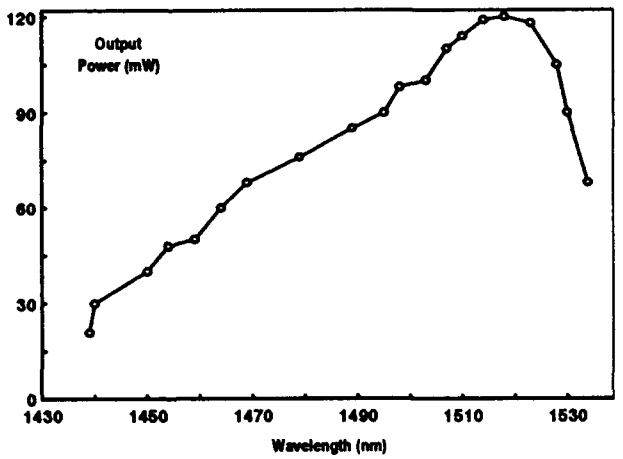


Figure 4: EX-SEL peak lasing power as a function of wavelength. Operating temperature is fixed at 77 K.

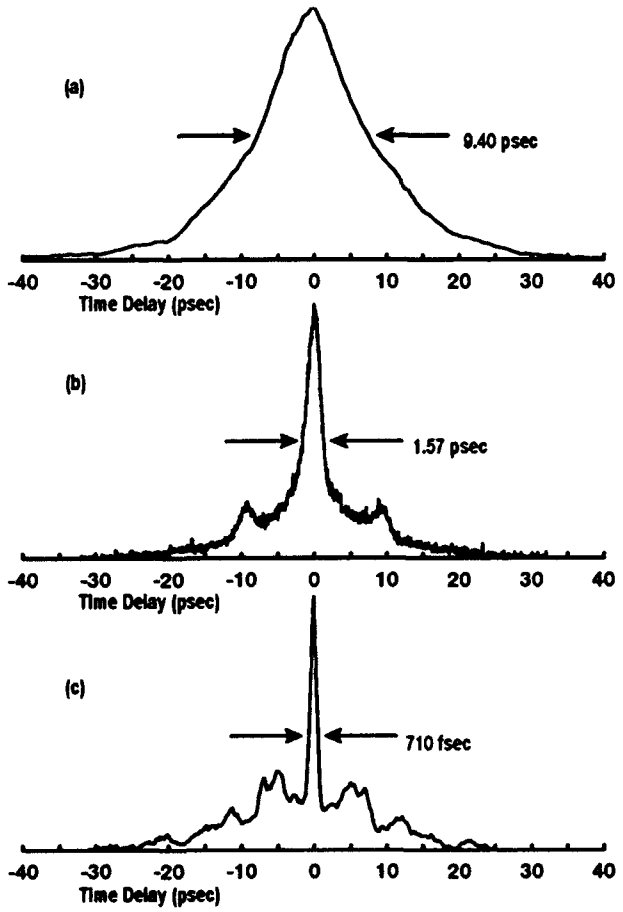


Figure 5: EX-SEL autocorrelation traces. FWHM pulse widths are (a) 9.4 psec directly, (b) 1.57 psec when compressed by a grating-pair, and (c) 710 fsec when compressed by a fiber.

maximum (FWHM) width τ of 9.4 psec. Single traces without averaging show pulses as short as 7.7 psec. The output spectrum, with a deconvoluted FWHM width of 2.8 nm (2.5 nm resolution of the spectrometer), is shown in Fig. 2c. The time-bandwidth product $\delta\lambda\delta\nu$ (assuming 7.7 psec pulses) is 2.8, or roughly 9 times the transform limit, indicating that the pulses are strongly chirped.

We further shortened the pulses by grating-pair chirp-compensation and negative-GVD fiber compression. Grating-pair compression was accomplished with two 600 line/mm diffraction gratings spaced 36 cm apart. The resulting autocorrelation traces are shown in Fig. 4b. Pulse durations were 1.57 psec (averaged), or 1.1 psec single-shot, the discrepancy due to sweep-to-sweep jitter in our rotating-mirror autocorrelator. The spectral width (FWHM) of the pulse is reduced to 2.0 nm. We saw a small subsidiary pulse about 9.5 psec from the main pulse, implying a slight etalon effect in the ~ 430 μm thick sample. Average powers were 7 mW, corresponding to peak powers of ~ 64 W. Using negative group velocity dispersion in a 400 meter length of single-mode optical fiber (GVD of negative 16 psec/km-nm), we were able to produce pulses as short as 710 fsec, with average powers of 10 mW emerging from the fiber. As shown in Fig. 4c, the results include a sizeable pedestal, so we can not accurately estimate peak powers.

Certain of the advantages of an external-cavity surface-emitting semiconductor laser are evident in our results. The observed output power of 190 mW is probably limited by heating effects which can be reduced by improved heat sinking techniques, etc, or by pumping electrically. The observed short pulses and high peak powers are in part due to the use of an external cavity, which allows us to use active mode-locking methods. Good beam quality allows coupling into fibers and other optical devices. This means that a wide range of both passive and active mode-locking techniques can be applied, perhaps in conjunction with intra-cavity chirp compensation techniques, to directly produce subpicosecond pulses with large peak powers. Figure 2a and Fig. 2b show that our MQW samples exhibit a fluorescence spectral

width of 117 nm at 300 K and 30 nm at 77 K. This implies the possibility of transform limited pulses as short as 20 fsec (80 fsec at 77 K).

There are other advantages of EX-SEL lasers that we have not demonstrated here. Semiconductor materials can be tailored to provide a wide range of bandgaps, so that EX-SEL laser systems can be operated at many different wavelengths, including the important ranges centered at 800 nm, 1300 nm, and 1500 nm. Electrical pumping would allow the elimination of pump lasers.

* Present Address: Department of Electrical and Computer Engineering; University of California, Santa Barbara; Santa Barbara, CA 93106.

References:

1. L. M. Zinkiewicz, T. J. Toth, L. J. Mawst, D. Tran, and D. Botez, Appl. Phys. Lett. **54**, 1959 (1989).
2. J. R. Karin, L. E. Melcer, J. E. Bowers, S. W. Corzine, R.S. Geels, L. A. Coldren, CLEO 1990, Paper FC2, Anaheim, CA, 1990.
3. H. Yokoyama, H. Ito, and H. Inaba, Appl. Phys. Lett., **40**, 105 (1982).
4. P. J. Delfyett, C. H. Lee, L. Florez, N. Stoffel, N. Andreadakis, T. Gmitter, G. A. Alphonse, and J. C. Connolly, 1990 Topical Meeting on Ultrafast Phenomena, Postdeadline Paper PD12-1, Montreal, CA, 1990.
5. G. H. B. Thompson and G. D. Henshall, Electron. Lett., **16**, 42 (1980).

AD-P007 874
92-22403

Nonlinear Device for Optical Image Processing Based on Semi-insulating CdZnTe/ZnTe Multiple Quantum Wells

Afshin Partovi, Alastair M. Glass, Don H. Olson, George J. Zydzik
AT&T Bell Laboratories, 600 Mountain Ave., Murray Hill, NJ 07974

Robert D. Feldman and Richard F. Austin
AT&T Bell Laboratories, Crawfords Corner Road, Holmdel, NJ 07733

For optical information processing applications, devices with high contrast ratio, speed, resolution and sensitivity are desirable. Devices based on charge transport nonlinearities can provide these requirements at low intensities. In particular, the SEED device takes advantage of the large excitonic nonlinearities in multiple quantum wells (MQWs) together with charge transport processes to achieve large electro-optic effects at small interaction lengths.[1] Another example of charge transport nonlinear devices is the Pockels Readout Optical Modulator (PROM) which consists of a semi-insulating electro-optic material placed between two dielectric layers and transparent electrodes. The electro-optic material serves as both a photoconductor and the nonlinear medium.[2] We report on a device based on the PROM concept using ion-implanted semi-insulating II-VI MQWs as the nonlinear medium. Ion implantation of MQWs provides diffraction limited resolution without need for pixellation of the device.[3] Very large and sensitive nonlinearities can be achieved in this device.

Recently, progress in the growth of II-VI multilayer structures by Molecular Beam Epitaxy (MBE) has resulted in high quality MQWs with well defined room temperature excitonic absorption [4]. These structures are potentially attractive for electro-optic applications because of their high excitonic oscillator strength and their high exciton saturation intensity [4]. Furthermore, the exciton absorption peak in these structures is in the visible. Use of the shorter wavelength of light corresponds to a smaller pixel size and higher information packing density.

We report on the first room temperature measurements of the excitonic electroabsorption in CdZnTe/ZnTe MQWs. Figure 1 shows the QCSE for different applied fields. The structure used consisted of 50 periods of 67Å $Cd_{0.33}Zn_{0.67}Te$ wells and 77Å ZnTe barriers grown on a 1.7μm thick $Cd_{0.15}Zn_{0.85}Te$ buffer layer on top of a 1.2μm ZnTe layer grown on an undoped semi-insulating GaAs substrate. A 0.72μm thick $Cd_{0.15}Zn_{0.85}Te$ cap layer is then grown on top of the MQWs. The thick $Cd_{0.15}Zn_{0.85}Te$ buffer layers are designed to minimize strain in the lattice mismatched MQW. To conduct measurements of the quantum confined stark effect (QCSE), the sample was sandwiched between two thin transparent electrodes. In order to apply these fields, the sample resistivity has been increased through proton bombardment. No change in the exciton absorption peak with bombardment with 10^{12} cm^{-2} dose of 200-keV protons has been observed.

An electro-optic device has been fabricated by placing the proton implanted MQW structure between two evaporated 2000Å thick dielectric layers of Vicor. The transparent electrodes are then evaporated on the dielectric layers. The MQW structure used in this device did not have a cap layer and had an exciton peak at 604nm. Figure 2 shows the QCSE in this structure as a function of an ac square wave voltage of 15V (peak to zero) for several different frequencies of the voltage with very low probe light intensity (~μW/cm^2). The dielectric relaxation time of the semi-insulating MQW structure is give by

$$\tau_d = \frac{\varepsilon}{(\sigma_d + \sigma_p)}, \qquad (1)$$

where ε is the permitivity of the material and σ_d and σ_p are respectively the dark conductivity and

photoconductivity.

For an ac field with period longer than τ_d, the carriers in the MQW structure have sufficient time to accumulate at the dielectric barriers and screen the applied field. Figure 3 shows the magnitude of the QCSE at $\lambda=604$nm as a function of the frequency of the applied voltage for different light intensities. With increasing light intensity the frequency of the voltage necessary to observe the full QCSE increases as expected from Eq. (1). At the lowest incident intensity, the QCSE saturates for frequencies higher than 1kHz. This is consistent with the dark dielectric relaxation time obtained with the dark resistivity of $\sim 10^9 \Omega$–cm of the sample.

As can be seen from Fig. 3, at a voltage frequency of for example 100 Hz, the QCSE (and therefore the absorption of the sample) can then be easily controlled with the incident intensity. We have obtained changes in the QCSE value by as much as $\Delta\alpha=7000\text{cm}^{-1}$ at 150V applied voltage by illuminating the sample with 1mW of power. We have recorded a grating in this device by intersecting two beams from a dye laser at the device. The response of the device to the interference pattern of the beams results in an absorption and corresponding index grating which causes self-diffraction of the two beams. In preliminary measurements, a diffraction efficiency of 0.2% has been obtained. With optimization of parameters we expect diffraction efficiencies of 10% to be achieved with this device. Such a device would be of interest for many image processing applications.

References

1. For a recent review of devices, see D. A. B. Miller, Int. J. High Speed Electronics, *1*, 19 (1990).
2. B. A. Horwitz and F. J. Corbett, Opt. Engin., *17*, 353 (1978).
3. A. M. Glass, D. D. Nolte, D. H. Olson, G. E. Doran, D. S. Chemla, and W. H. Knox, Opt. Lett., *15*, 264 (1990).
4. D. Lee, J. E. Zucker, A. M. Johnson, R. D. Feldman, and R. F. Austin, Appl. Phys. Lett., *57*, 1132 (1990).

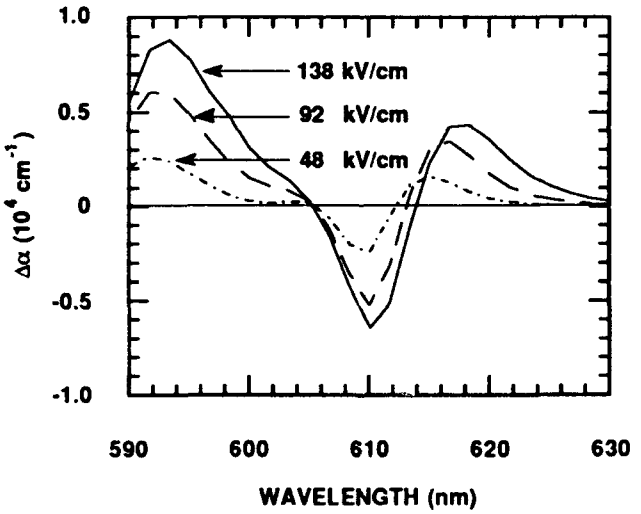


Figure 1. Change in the absorption coefficient due to the quantum confined stark effect in II-VI multiple quantum wells for several different applied fields.

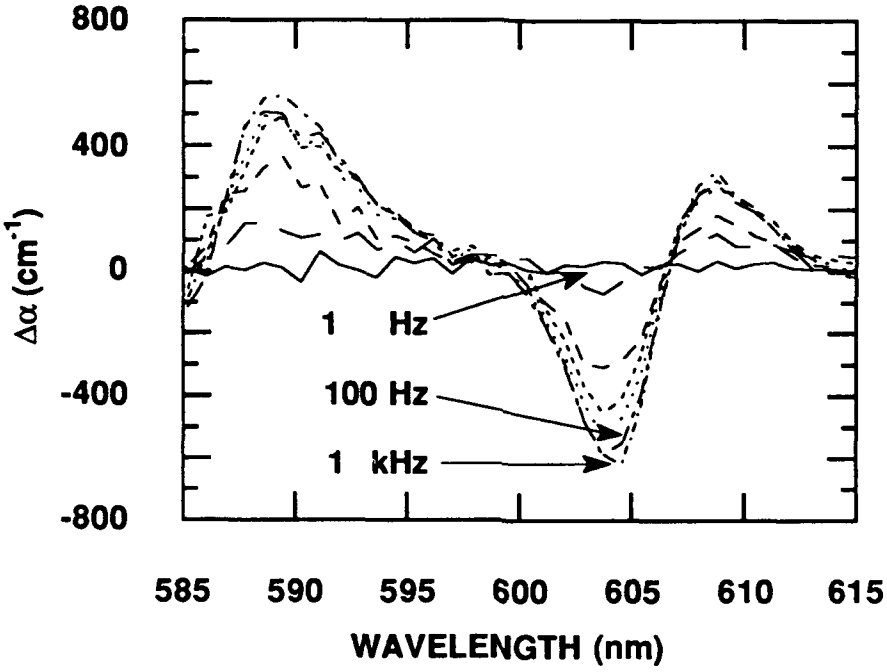


Figure 2. Change in the absorption coefficient as a function of the frequency of the applied ac field for a multiple quantum well sandwiched between dielectric layers.

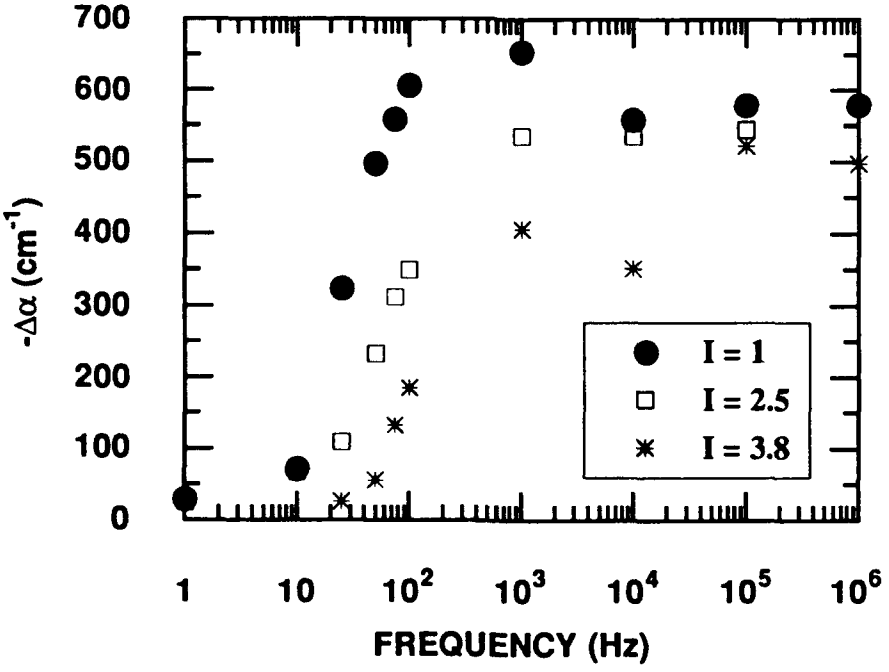


Figure 3. Electroabsorption due to the quantum confined stark effect at λ=604 nm as a function of frequency of the applied ac field for several incident light intensities.

92-22404

APPLICATION OF MINIBANDS TO InAlAs/InGaAs SUPERLATTICE AVALANCHE PHOTODIODES

S. Hanatani, H. Nakamura, S. Tanaka, C. Notsu*, K. Ishida

Central Research Laboratory, Hitachi Ltd.,
Kokubunji, Tokyo 185, Japan
* Hitachi Device Engineering Co., Ltd.
Mobara, Chiba 297, Japan

D-P007 875

INTRODUCTION

An InAlAs/InGaAs superlattice Avalanche Photodiode (SL-APD) is of great interest for 10-Gb/s lightwave transmission, because it is expected to operate with a high gain-bandwidth product and a low multiplication noise [1]. Recently, using the SL-APD, the receiver sensitivity of -24 dBm at 10 Gb/s was achieved [2]. This is higher than that obtained using the conventional InP/InGaAs APDs. For the improvement of the 10-Gb/s receiver sensitivity, the SL structure must be optimized, because the characteristics of SL-APDs depend on it. From this point of view, we proposed a novel SL-APD structure with thin-width wells [3], however the effect of thin wells on high speed operation has not been sufficiently considered.

This paper proposes an application of minibands to hetero-interfaces of a SL-APD to make wells thinner for high-speed and low-noise operation. High-speed electron transport through minibands is also discussed and demonstrated in a PIN-photodiode (PD) with minibands.

DEVICE CONCEPT

As shown in Fig.1(a), since an electron must gain energy in an InGaAs well to get smoothly out of it after an impact ionization, carrier pile-up will occur when the well width gets thinner. For high-speed operation, the band edge step must be reduced or eliminated to make wells thinner. In conventional InP/InGaAs APDs, multi-InGaAsP layers with mid-gap energies have been used to solve this problem. F. Capasso et al. proposed introducing AlInGaAs layers into the InAlAs/InGaAs SL-APD [4]. However, these layers requires fine controlling of crystal growth both for their compositions and thickness.

Here, we propose a novel structure to reduce or/and remove the band edge step using tunneling coupling. As the barrier width in the superlattice (SL) becomes thinner than 30 Å, tunneling coupling between wells forms minibands, through which electrons can transit.

The minibands in the SL can be controlled by the thickness of wells and barriers, which is easily realized by MBE. This minibands SL has a total thickness of about 100-300 Å, which is thinner than the 600-1200 Å graded gap SL proposed by F. Capasso [5]. It is suitable for an SL-APD with many hetero-interfaces. With these minibands at the hetero-interfaces in the SL-APD, as shown in Fig.1(b), after an impact ionization an electron doesn't "see" the band edge step and can get smoothly out of a well through the minibands. It is therefore possible to get the well-width thin enough for impact ionization to be able to occur. A hole, also, doesn't "see" the energy step when it arrives in a well from a barrier, so its ionization rate is reduced compared with the conventional SL-APD. This leads to very different ionization rates for electrons and holes, and lower-noise operation of the SL-APD is expected.

It is, however, desirable to transport electrons through the minibands for operations at such high speed as 10 Gb/s. To demonstrate high-speed minibands transport, we fabricated PIN-PDs with this minibands.

EXPERIMENTAL RESULTS

Figure 2(a) shows a cross-sectional view of a minibands-PIN-PD with a mesa structure (minibands PIN). It is fabricated in the following steps. On an n^+-InP substrate, 7 layers (n^+-InAlAs, undoped-InAlAs, an undoped-InAlAs/InGaAs superlattice layer, undoped-InGaAs, p-InGaAs, p^+-InAlAs, and p^+-InGaAs) are successively grown by MBE. The SL layer consists of 7 periods with chirped well-widths. The InGaAs-well-layer thickness is linearly decreased from 35 to 5 Å, while the InAlAs-barrier layers keep their 10 Å thickness constant as shown in Fig. 2(b). This SL layer is designed to form minibands with electric fields above 100 kV/cm. A mesa structure is formed by Br+HBr+H_2O chemical etching. A polyimide layer is used for surface passivation, antireflection, and reduction of stray capacitance.

For comparison, we prepared other two types of PIN-PDs with the same mesa structure as the minibands PIN; one in which the i-region consists only of an undoped-InGaAs absorption layer (InGaAs PIN); and another type consisting of undoped InGaAs and InAlAs layers just like the minibands PIN, without the SL layer (hetero PIN).

The frequency reponses of these three PDs are measured, using with a 1.55-μm DFB-LD with a 3dB-bandwidth of 16 GHz [6], a signal generator, and a spectrum analyzer controlled by a computer. Figure 3(a) shows the measured frequency response of the InGaAs PIN as well as the result calculated from an equivalent circuit model. The 3dB bandwidth of the InGaAs PIN is about 10 GHz. The small peaking around 6 GHz is caused by the resonance of the photodiode capacitance and the

bond-wire inductance. The good agreement with the calculation shows that the frequency response of the InGaAs PIN is limited by the CR time constant. Figure 3(b) shows the frequency responses of the hetero PIN measured at electric fields of 40 and 80 kV/cm. Electron pile-up at the hetero-interface occurs below 40 kV/cm and it is negligible above 80 kV/cm. The frequency responses of the minibands PIN below 40 kV/cm is similar to that of the hetero PIN, and above 100 kV/cm, high-speed carrier transport through the minibands is obtained.

Figure 4 shows the reverse bias dependence of the 3dB bandwidth for the three PIN-PDs. The frequency responses of all three PIN-PDs are limited by the CR time constant, and the degradation of the 3dB bandwidth of the minibands PD at electric fields below 100 kV/cm is due to formation of incomplete minibands.

CONCLUSION

A novel structure applying minibands to SL-APDs is proposed to reduce well width and improve performance for 10-Gb/s systems. High-speed carrier transport through the proposed minibands, up to 10 GHz, is demonstrated.

ACKNOWLEDGMENT

The authors would like to thank Dr. M. Maeda and Dr. N. Chinone for continued encouragement.

REFERENCES

[1] T. Kagawa, et al., :"A Low-Noise and Wide-Bandwidth InGaAs/InAlAs Superlattice APD," Proc. of IEDM 89-725

[2] T. Kagawa, et al.,:"Superlattice Avalanche Photodiode for High Bit Rate Optical Transmission Systems," Proc. of 3rd OEC 13A2-7 (1990) Y. Miyamoto, et al., Nat'l. Conv. Rec. IEICE Japan B-776 (1990)

[3] H. Nakamura, et al., :"A Novel Structure for InAlAs/InGaAs Super-lattice Avalanche Photo Diode for 10 Gb/s Lightwave Transmission Systems," Proc. of ECOC '90-261

[4] F. Capasso, et al., :"Staircase Solid-State Photomultipliers and Avalanche Photodiodes Enhanced Ionization Rate Ratio," IEEE Trans. ED-30, 38 (1983)

[5] F. Capasso, et al., :"Pseudo-quaternary GaInAsP semiconductors : A new GaInAs/InP Graded Gap Superlattice and its applications to avalanche photodiodes," Appl. Phys. Lett., 45, 1193 (1984)

[6] K. Uomi, et al.,:"Ultralow Chirp and High-Speed 1.55 μm Multi-quantum Well λ/4–shifted DFB Lasers," IEEE PTL-2, 229 (1990)

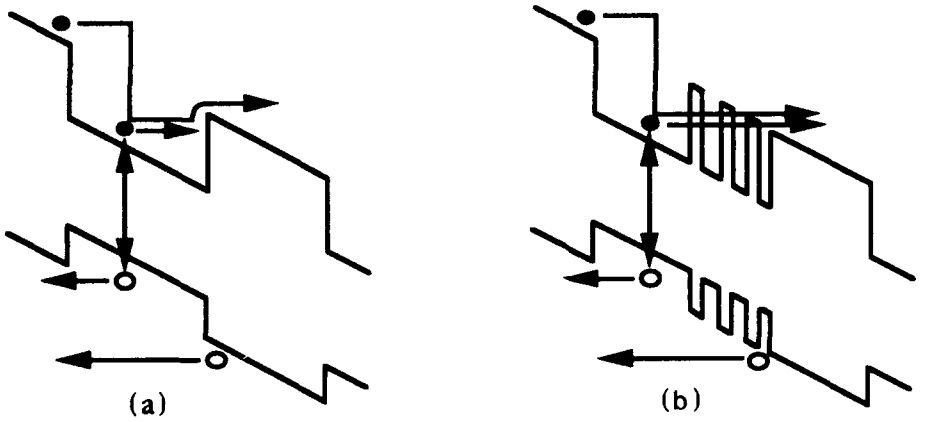


Fig.1 Energy diagrams of a conventional SL-APD (a) and a miniband SL-APD (b)

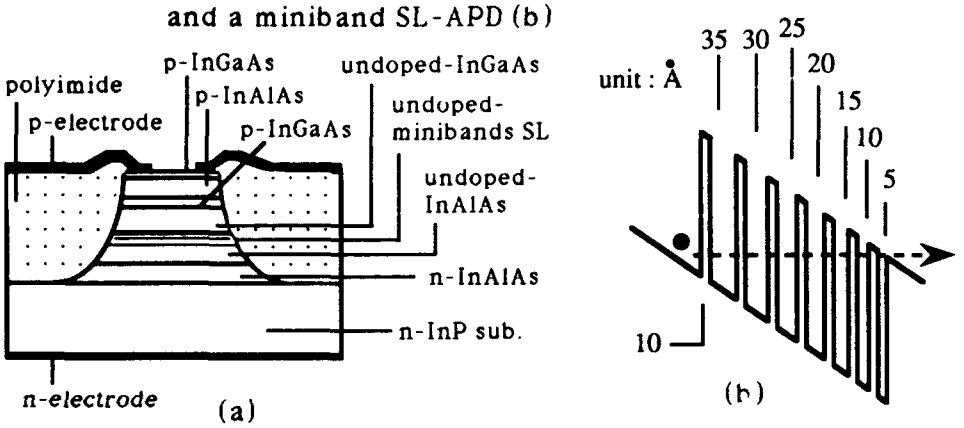


Fig.2 Cross-section of a miniband-PIN (a) and energy diagram of the fabricated minibands (b)

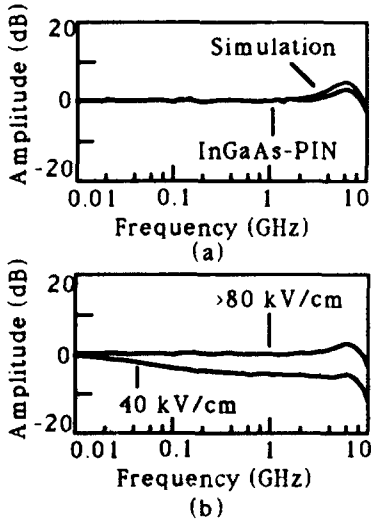


Fig. 3 Frequency responses of an InGaAs-PIN (a) and a hetero-PIN (b)

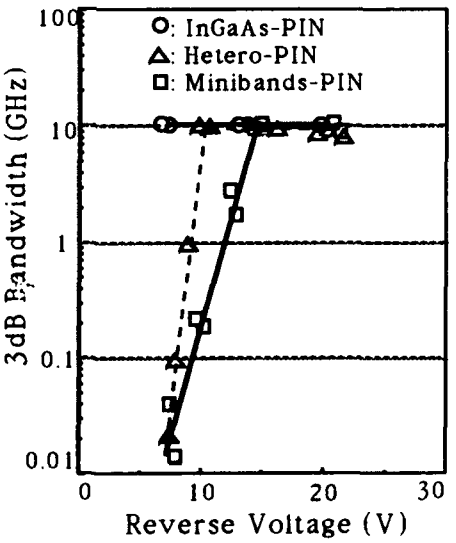


Fig.4 Bias dependence of frequency responses of the three PINs

Investigation of carrier transport in photorefractive superlattices by time-correlated photon counting

Andrea Lacaita [a], Stephen E. Ralph [b], Federico Capasso, and Roger J. Malik

AT&T Bell Laboratories, Murray Hill, NJ 07974

Recently a new class of photorefractive structures has been demonstrated.[1,2] These devices rely on the spatial separation of photogenerated electrons and holes to produce a large refractive index modulation via the electro-optic effect and might have potential for all optical switching applications. One of these devices consists of an asymmetric δ-doped superlattice which is optically excited by a picosecond laser source.[2] The resulting space charge field produced by charge separation creates a refractive index change of 3.8×10^{-4} at a pump energy density of 40 fJ/μm^2. In this paper we report the first time-resolved studies of the carrier relaxation in these structures. The measurements were performed by a Time Correlated Photon Counting (TCPC) technique.[3,4]

The twenty periods asymmetric GaAs superlattice was grown between two $Al_{0.4}Ga_{0.6}As$ window layers on semi-insulating GaAs substrates. The dopant planes of each dipole, a few monolayers thick, were separated by 50Å and each identical dipole pair was separated from the next pair by 500Å.[5] A secondary ion mass spectroscopy analysis verified the p-type dopant density to be 8×10^{12} cm^{-2} and the n-type dopant concentration to be nearly 50% higher. The luminescence was excited by a picosecond dye laser, analyzed with a monochromator, and detected by a Microchannel Plate Photomultiplier Tube (MCP-PMT) or a standard PMT with an S1 photoresponse, depending on the luminescence wavelength. The measured instrument response with the MCP was 35ps Full Width at Half Maximum (FWHM) and 3ns with the PMT. All the data were taken at a sample temperature of 5K and are shown normalized to the system spectral response.

Figure 1a depicts the calculated energy band diagram of the sawtooth structure at equilibrium. Due to the unbalanced dopant sheets the superlattice contains excess electrons which accumulate in the triangular wells. Electrons and holes are photogenerated throughout the structure using a pump wavelength of 620nm (2.00eV). In a few picoseconds the carrier plasma reaches an equilibrium temperature by carrier-carrier scattering.[6,7]

a) On leave from Centro di Elettronica Quantistica e Strumentazione Elettronica - CNR. Piazza L. da Vinci 32, 20133 Milano (Italy)
b) Present address: IBM Thomas J.Watson Research Center, Yorktown Heights, New York 10598

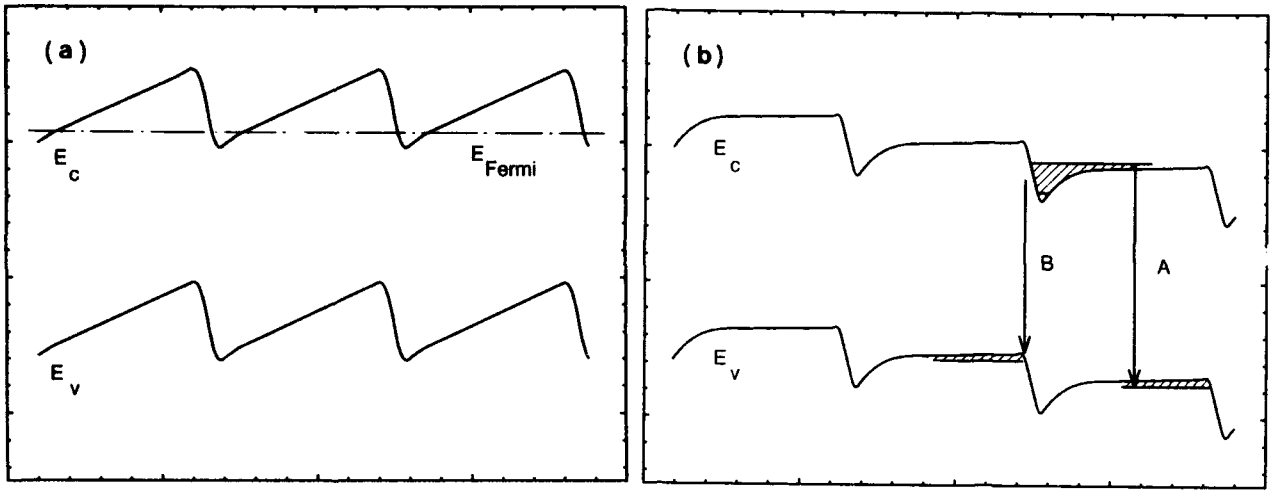


Fig. 1 - Three periods of the calculated energy band diagram of the δ-doped superlattice. a) Structure at equilibrium. b) Band diagram after photogeneration of $5x10^{12}$ cm^{-2} electron-hole pairs in each well. Carriers recombine in flat band regions (A) and via tunneling assisted recombination (B).

Under the influence of the internal fields the carriers move in opposite directions to the corresponding minima of the V-shaped wells resulting in a space-charge field which opposes the field of the ionized dopants. Fig. 1b shows the band diagram calculated for a photogenerated carrier density of $5x10^{12}$ cm^{-2}, comparable to the dipole charge density. Due to the two dimensional density of states, a triangular well, ~0.25eV deep, remains in the band structure. while other regions approach a flat band condition.

The simultaneous presence of flat band regions and potential wells is confirmed by the time-resolved luminescence shown in Fig. 2. The data clearly show luminescence at short times (50-500ps), originating from both above bandedge transitions (1.59-1.55eV) and subband transitions (1.46-1.31eV). The above bandedge luminescence originates mostly from the flat band regions of the structure. The observed rise times of the high energy signals are system limited. The deconvolved lifetime of the 1.59 eV (780nm) luminescence is of 50ps. When the average carrier energy falls below the optical phonon energy, the luminescence time constant significantly increases. The 1.55eV (800nm) luminescence decays with a 100ps time constant consistent with the cooling rate of photoexcited carriers in GaAs.[6,7]

The fast rise times of the luminescence ranging from 1.46eV (850nm) to 1.31eV (950nm) confirm that potential wells, at least 0.20eV deep, remain in the structure in spite of the large free carrier concentration. If the photogenerated carriers were able to establish, by screening of the internal field a quasi flat band condition everywhere in the

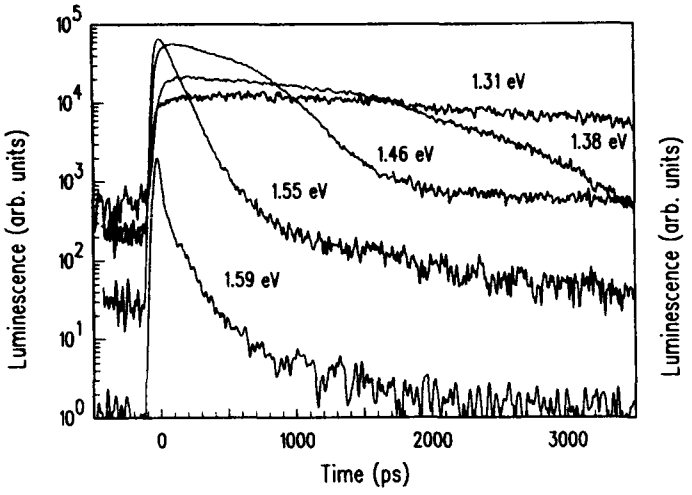


Fig. 2 - Luminescence of the δ-doped superlattice photoexcited with $5x10^{12}$ cm^{-2} electron-hole pairs. Time dependence of above bandgap luminescence (1.59-1.55eV) and sub bandedge luminescence (1.46-1.31eV) on a short time scale.

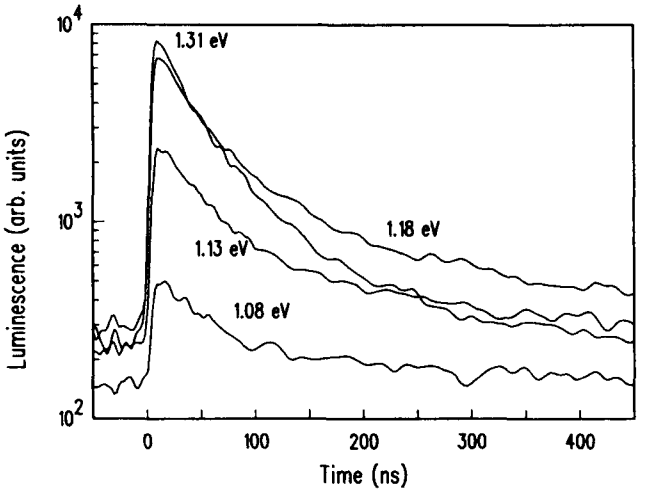


Fig. 3 - Time resolved luminescence for emission energies from 1.08eV to 1.31eV showing the slow nonexponential decay of the low energy transitions.

structure, the emission of photons with sub-bandgap energy would be precluded at short times.

Another notable feature of the luminescence is shown in Fig. 2. Nearly 1ns after excitation the luminescence decay rate of the 1.46eV signal increases and the intensity falls to less than 1% of its initial value. The increase in the decay rate occurs when the difference between the quasi Fermi levels for electrons and holes falls below the photon energy of the luminescence signal. The luminescence at 1.38eV and 1.31eV each show similar behavior with longer time constants associated with increased electron-hole separation in the lower energy states.

Figure 3 shows the luminescence for energies ranging from 1.08eV (1.2μm) to 1.31eV (950nm). The luminescence decays are nonexponential because as carriers recombine the modulation depth of the structure increases. The carrier states become more confined and the recombination lifetime is increased. The increase of the decay rate observed in Fig. 2 does not occur for the low energy luminescence since the electron quasi Fermi level remains more than 100meV above the "V" minima as a result of the residual n-type doping.

We have estimated the order of magnitude for the recombination lifetimes based on the energy band diagram at equilibrium (Fig. 1a) and the corresponding subband levels. We note that the transition rate for interband recombination, $1/\tau_i$, can be approximated as the product of the bulk recombination rate, $1/\tau_{bulk}$, and the overlap

integral of the two states involved in the transition.[8] Taking for τ_{bulk} a value of 1-2ns, we calculated the lifetimes for the first four subband levels which account for transition energies from 0.95eV to 1.13eV obtaining for the lowest energy transition (0.95eV) an estimated lifetime of 650ns-1.3μs and for the 1.13eV transition a lifetime of 140-280ns, in agreement with the decay lifetimes in Fig. 3.

In conclusion we have directly measured the tunneling-assisted recombination in δ-doped structures. We have also shown that a modulation of the band structure remains in spite of intense photogeneration of excess carriers.

References

1 S.E. Ralph, F. Capasso, and R.J.Malik, Phys. Rev. Lett. **63**,2272 (1989).

2 S.E.Ralph, F.Capasso, and R.J.Malik, Appl. Phys. Lett. **57**, 626 (1990).

3 D. V. O'Connor and D. Phillips, *Time Correlated Single Photon Counting* (Academic Press, New York 1983).

4 A. Lacaita, S. E. Ralph, F.Capasso, and R. J. Malik. Appl. Phys. Lett. in press.

5 E.F. Shubert, Opt.Quantum Electron. **22**, S141 (1990) and references therein.

6 J. Shah, IEEE J. Quantum Electron. **QE-22**, 1728 (1986).

7 D. von der Linde, and R. Lambrich, Phys. Rev. Lett. **42**, 1090 (1979).

8 G. H. Dohler and K. Ploog in *Synthetic Modulated Structures* ed. by L. L. Chang and B. C. Giessen (Academic Press, Orlando, 1985).

Joint Session on Tunneling: I

WC 1:30pm–2:45pm
Salon F

Arto V. Nurmikko, *Presider*
Brown University

AD-P007 877

Electron Transport in Double Barrier Diodes Studied by Differential Absorption Spectroscopy

T. K. Woodward[1], D. S. Chemla[1], I. Bar-Joseph[2], D. L. Sivco[3], A. Y. Cho[3]
[1] AT&T Bell Laboratories, Holmdel NJ 07733
[2] Weizmann Institute of Science, Rehovot 76100, Israel
[3] AT&T Bell Laboratories, Murray Hill, NJ 07974

Double barrier tunneling heterostructures are part of an emerging class of devices that rely on quantum-mechanical effects for their operation. A deeper understanding of these devices is possible when diagnostic methods that augment electrical measurements are employed. In our project, we have used differential absorption spectroscopy (DAS) to investigate the operation of the double barrier diode (DBD). This technique, whose experimental realization is detailed in Fig. 1, relies on measurements of normalized changes in optical transmission, $\Delta T/T = [T(V) - T(V_0)]/T(V_0)$ where $T(x)$ is the transmission at voltage x, arising from electrical modulation imposed upon the device.[1,2] For small signals $\Delta T/T = l\Delta\alpha$, where $\Delta\alpha = \alpha(V_0) - \alpha(V)$ is the change in absorption and l is the length over which the change occurs. Lock-in signal extraction allows the observation of $\Delta T/T$ signals as small as $\sim 10^{-4}$, permitting observation of events on length scales ~ 10Åwith low probe intensities (we use an incandescent lamp). DBD depletion and accumulation regions can be seen, as can signals originating in the QW. This signal can be calibrated to obtain the QW stored charge Q. Other workers have reported measurements of Q using photoluminescence,[3] excitation spectroscopy in conjunction with photoluminescence,[4] as well as methods involving magnetic fields.[5] Since we can use low light intensities and rely on optical absorption–a technique allowing *absolute calibration*–we believe DAS to be both a significantly more accurate[3] and a much less invasive method of determining Q. In addition, we can determine the energy distribution of the electrons stored inside the QW, without the confusion caused by creating large numbers of highly excited electron-hole pairs in the measurement process. All samples were grown by MBE on conducting InP substates and show profound negative differential resistance (NDR). Geometries are similar to that illustrated in Fig. 2, with variable barrier thicknesses.[1] The barrier material is $In_{0.52}Al_{0.48}As$, with QW and electrodes being $In_{0.53}Ga_{0.47}As$. Measurements were performed on 150 μm^2 mesas at 10K.

Representative 10 K DAS data are shown in Fig. 2. The three $\Delta T/T = [T(V) - T(0)]/T(0)$ spectra were obtained for modulation between zero and points indicated on the I–V curve: low voltage prior to the onset of tunneling (smallest curve), at the peak of the NDR, and at the valley of the NDR (dotted curve). The major features of the data are a negative going signal peaked at $\sim$ 0.83 eV due to the formation of a depletion layer, a positive feature at $\sim$ 0.9 eV due to the formation of an accumulation region, and a set of signals near 1 eV coming from the QW. In the accumulation layer, increases in carrier density relative to zero bias increase the number of occupied states at $E > E_g + E_f$ (E_g is the bandgap and E_f is the zero bias fermi energy), preventing absorption from taking place and making the sample slightly more transparent in this energy range. This causes a positive $\Delta T/T$ signal. Similarly, depletion of carriers from beyond the collector barrier enhances absorption for $E_g < E < E_g + E_f$ and causes a negative peak.

QW signals have two distinct lineshapes, which is helpful in identifying device activity. Differential (two-signed) signals are due to field induced shifts of the exciton resonance, and arise from the quantum confined stark effect. These signals are indicative of a mainly empty QW. As electrons populate the QW, they bleach the excitonic absorption through the Pauli exclusion principle, and cause a strictly positive spectral feature. Thus, we can see the filling and emptying of the QW during transport. At low voltages, prior to the onset of tunneling, the QW signal is small and differential, consistent with the empty state of the QW resonance. At the peak of the NDR, the signal is strong and positive, indicating charge accumulation. At the valley of the NDR, the signal becomes abruptly differential in nature, consistent with a mostly empty QW.

Bleaching signals obtained for current densities ranging from the onset of tunneling to the peak of the NDR can be calibrated to obtain the QW stored charge to an accuracy of roughly 50 percent. Calibration is achieved by knowing the amount of exciton bleaching induced by a known population of electrons. We get this information by measurements of a 50 period multiple QW sample having 45 Å $In_{0.53}Ga_{0.47}As$ wells and 70 Å $In_{0.52}Al_{0.48}As$ barriers. In this sample we can measure the absolute exciton absorption strength, binding energy, and saturation density. Relations between absorption bleaching and carrier population for various levels of carrier density then allow us to obtain the QW stored charge.[1,2,6,7] The most basic of these relationships, valid in the small signal regime, is $\Delta\alpha/\alpha = -N/N_s^e$, where α refers to the exciton absorption and N_s^e is the exciton saturation density for electrons.[8] In Fig. 3 we summarize the results of these studies with tabulation of Q and Q/J as a function of J for various samples.

There are a number of important implications to the results presented in Figs. 2 and 3. Observe that the NDR peak bleaching signal in Fig. 2 is that of a carrier population localized near the bottom of the band, in that no evidence of absorption bleaching is observed at higher energies. At the peak of the NDR, the resonance level aligns with the conduction band edge of the injecting electrode. Tunneling electrons therefore have essentially zero momentum directed perpendicular to the barriers and a wide range of energies $E_{||} = (\hbar k_{||})^2/(2m)$ associated with $k_{||}$, the momentum directed parallel to the barriers: $0 < E_{||} < E_f$.[9] $E_f \geq 55$ meV in our samples. We conclude that the carriers have relaxed via intra-subband scattering from an initial distribution of $0 < E_{||} < E_f$ to one of $0 < E_{||} < E_b$, where $E_b \simeq 9$ meV is the exciton binding energy in this sample. This relaxation is observed in all our samples and demonstrates the inelastic nature of the resonant tunneling process in them.

This result is not particularly surprising when the time scales over which carriers reside in the QW are considered. Q/J provides such a time scale and is plotted in Fig. 3(b). Of particular interest is the Q/J behavior of our asymmetric sample consisting of a thin 55 Å front barrier (denoted by l and transmission probability T_l) and a thicker 80 Å collector barrier (denoted by r and T_r). For electron flow from l to r, we measure a large Q relative to similar symmetric samples, and Q/J shows a clear decrease with bias. This decrease is consistent with the theoretical form for Q/J that we have found, $Q/J = \hbar\pi/(T_r E_1)$, where E_1 is the energy of the quasibound QW resonance. However, it is inconsistent with the bias dependence of the coherent state lifetime $\hbar/\Delta E$, where ΔE is the half width of the total transmission resonance. We find $\hbar/\Delta E \simeq \hbar\pi/[(T_r + T_l)E_1]$, and the two theoretical forms are not equal. The asymmetry of this particular sample causes $\hbar/\Delta E$ to increase with bias, while Q/J shows a decrease. Thus, we establish both theoretically and experimentally that $Q/J \neq \hbar/\Delta E$, contrary to commonly held assumptions.[1,3,4,10] Intuitively, this follows because the state lifetime measures the escape of carriers from both barriers, whereas Q/J is sensitive to the current carrying electrons and so depends only on the collector barrier.

Evidence for inter-subband scattering can be found by studying a sample containing two confined states and having two NDR regions.[5] This sample has 70 Å barriers and a 100 Å QW and is doped in the electrodes to $1.5 \times 10^{17}\,cm^{-3}$. Biasing to voltages approaching the second NDR region injects carriers into the second QW level. In Fig. 4, we present data for the two-resonance sample, specifically the DAS signals arising from the second QW level, obtained at various modulation voltages. The I-V curve is also shown, with intersections denoting the electrical state of the device. The DAS signal from the second QW level is differential in shape at all voltages, indicating *no significant accumulation of charge in the second QW level.* This establishes the tunneling process here as being sequential in nature, in that electrons relax from the second level to the first before tunneling out of the structure.

We have been able to reach several conclusions about DBD transport from our DAS studies. We can observe the formation of depletion and accumulation regions as well as the character of

the QW behavior. We can quantify Q, the QW stored charge, and through our studies obtain information about the energy distribution of tunneling carriers that presents direct evidence of both inter- and intra-subband scattering. Finally, we have shown that Q/J is *not* equal to the coherent state lifetime $\hbar/\Delta E$. These studies demonstrate the value of DAS as a diagnostic tool.

We would like to acknowledge the contributions of H. U. Baranger, H. A. Fertig, Y. Gedalyahu, D. A. B. Miller, G. Sucha, M. Weggener, S. Weiss, and A. Yacoby.

References

[1] I. Bar-Joseph, T. K. Woodward, D. S. Chemla, D. Sivco, A. Y. Cho, *Phys. Rev. B* **41**, 3264 (1990).

[2] D. S. Chemla, I. Bar-Joseph, J. M. Kuo, T. Y. Chang, C. Klingshirn, G. Livescu, and D. A. B. Miller, *IEEE J. Quant. Electron.* **24**, 1664 (1988).

[3] Jeff F. Young, B. M. Wood, G. C. Aers, R. L. S. Devine, H. C. Liu, D. Landheer, B. Buchanan, A. J. SpringThorpe, P. Madeville, *Phys. Rev. Lett.* **60**, 2085 (1988). and a comment about this work, W. R. Frensley, M. A. Reed, J. H. Luscombe, *Phys. Rev. Lett.* **62**, 1207 (1989).

[4] Hisao Yoshimura, Joel N. Schulman, Hiroyuki Sakaki, *Phys. Rev. Lett* **64**, 2422 (1990).

[5] M. S. Skolnick, D. G. Hayes, P. E. Simmonds, A. W. Higgs, G. W. Smith, H. J. Hutchinson, C. R. Whitehouse, L. Eaves, M. Henini, O. H. Hughes, M. L. Leadbeater, D. L. Halliday, *Phys. Rev. B* **41**, 10754, (1990).

[6] S. Schmitt-Rink, D. S. Chemla, and D. A. B. Miller, *Phys. Rev. B* **32**, 6601 (1985).

[7] S. Schmitt-Rink, C. Ell, *Jnl. of Luminescence* **30**, 585 (1985) and H. Haug, S. Schmitt-Rink, *Progress in Quantum Mechanics* **9**, 3 (1984).

[8] Measurements of the saturation density in the calibration multiple QW sample yield N_s^{eh}, the saturation density for electron hole pairs. For $N < 2 \times 10^{11}\,\mathrm{cm}^{-2}$ we find $N_s^e = 1.6 N_s^{eh} = 1.16 \times 10^{11}\,\mathrm{cm}^{-2}$. This differs from that published previously in [1] of $2.7 \times 10^{11}\,\mathrm{cm}^{-2}$. Charge densities appearing there should be *reduced* by the ratio of 1.16/2.7 to reflect this new information.

[9] Serge Luryi, *Appl. Phys. Lett* **47**, 490 (1985).

[10] R. Ricco and M. Ya. Azbel, *Phys. Rev. B* **29**, 1970 (1984). and P. J. Price, *Phys. Rev. B* **36**, 1314 (1987). and E. E. Mendez, in *NATO ASI Series, Series B: Physics, Vol 170*, E. E. Mendez and K. von Klitzing, editors, Plenum Press, NY pp. 159-188 (1987).

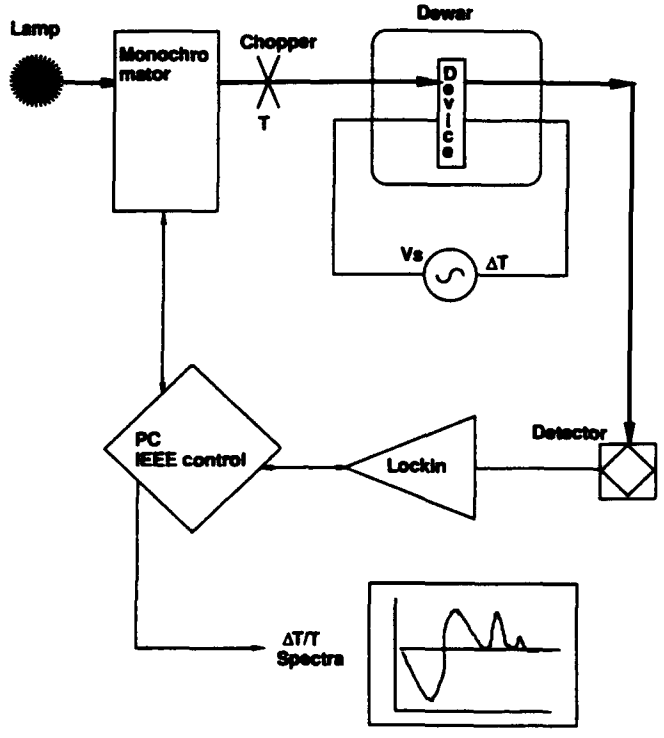


FIG. 1. Experimental setup

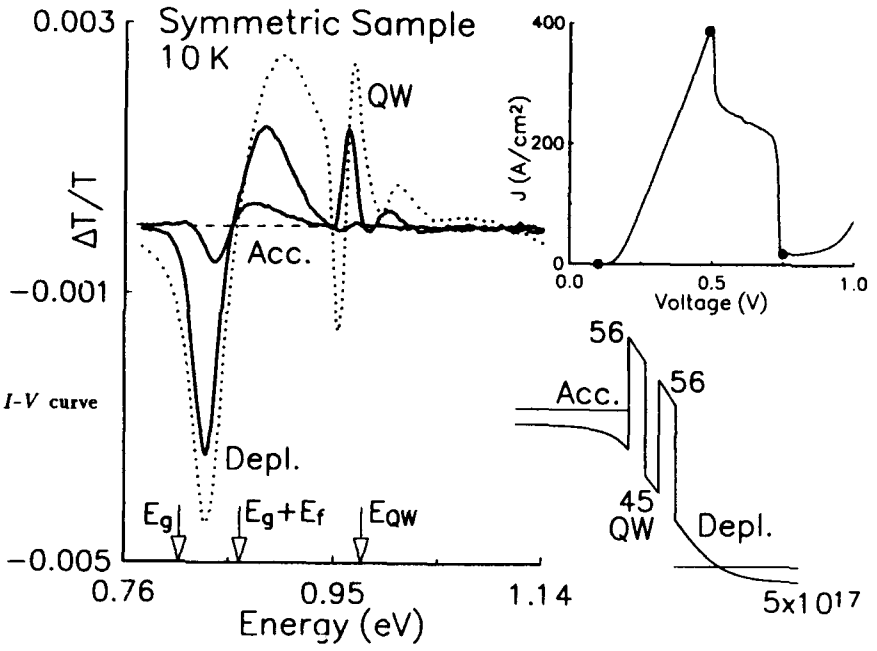


FIG. 2. Representative DAS spectra and *I-V* curve at 10K, with sample geometry.

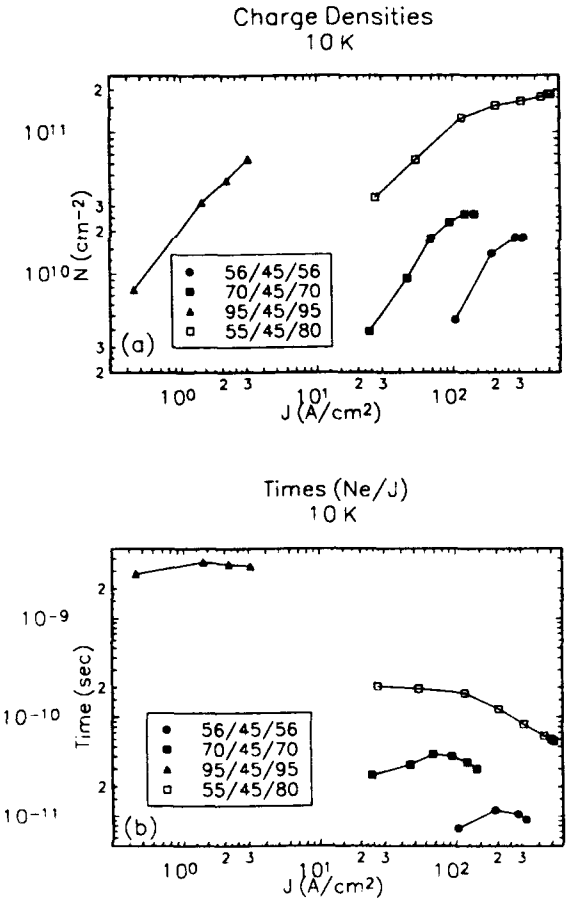


FIG. 3. (a) N vs. J for all samples. (b) Q/J vs. J for all samples

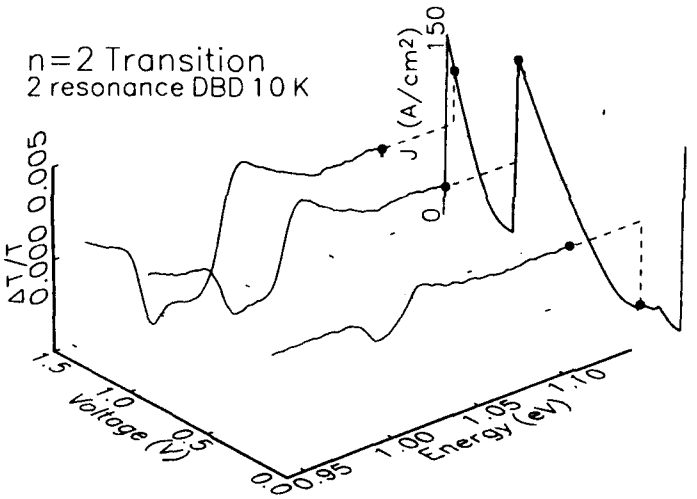


FIG. 4. DAS spectra for a two resonance sample at various modulation voltages for photon energies corresponding to the second QW resonance.

AD-P007 878

Photon-Assisted Resonant Tunneling Through a GaAs/AlGaAs Multiple Quantum Well Structure

92-22407

Bjorn Jonsson and Ingemar Andersson
Department of Optoelectronics and Electrical Measurements
Chalmers University of Technology
S – 412 96 Goteborg, SWEDEN

Anders Larsson
Center for Space Microelectronics Technology
Jet Propulsion Laboratory / California Institute of Technology
4800 Oak Grove Drive, Pasadena, CA 91109, USA

Thorwald Andersson and Johan Westin
Department of Physics
Chalmers University of Technology
S - 412 96 Goteborg, SWEDEN

Introduction

The use of bandgap engineering techniques to tailor the perpendicular transport characteristics of layered semiconductor structures has resulted in a variety of new phenomena and devices concepts [1]. In particular the coherent interaction of electron waves reflected at interfaces gives rise to resonant tunneling effects which filter electrons of certain energy through the structure. A structure specifically designed for electron energy filtering is the variably spaced superlattice energy filter (VSSEF) in which the quantized states in adjacent quantum wells become aligned under appropriate bias conditions [2].

Device structure

The photoconductive device discussed here is based on intersubband absorption in a $GaAs/Al_xGa_{1-x}As$ multiple quantum well (MQW) structure. The epitaxial structure is shown in Figure 1. The device consists of a total of 30 quantum wells, 78 Å wide, separated by a 190 Å wide VSSEF-structure. From the schematic of the conduction band shown in Figure 2 the principle of operation can easily be understood. Electrons are excited from the ground state energy level E_1 to the second level E_2 by infra-red (IR) radiation. When an appropriate bias voltage is applied to the structure the energy levels in the VSSEF are aligned with the energy level E_2, and the electrons can tunnel out through the structure. The measured photocurrent will hence employ a resonance peak at an appropriate applied electric field (≈ 50 kV/cm).

The MQW-structure used in the experiments was grown by molecular beam epitaxy (MBE) on n-doped GaAs (100). The growth rate of the quantum wells were calibrated by reflection high energy electron diffraction (RHEED) oscillations and the four quantum wells in each VSSEF were 17, 14,

11, and 9 Å wide, respectively. The $Al_xGa_{1-x}As$ barriers (x = 0.4) were all 28 Å wide. Typical growth rates were 0.8 μm/h for GaAs. In the center of each of the 78 Å wide quantum wells, a 58 Å thick part was doped with Si.

For measurement purposes, individual detector elements were formed by etching mesas, 90 μm in diameter and 2 μm high. The detector chip was cemented to a copper block and the whole assembly was mounted in a cryostat for low temperature measurements. Figure 3 shows a single device and the electrical connections for the experimental set-up. Conventional bonding techniques were used to connect the device to the bias voltage and the load resistance. This type of intersubband absorption is only sensitive to light with the electric field polarized parallel to the growth direction. In order to maximize both the component of the light with the right polarization incident on the device and the illuminated detector area, the substrate was lapped to an angle of 45°, as indicated in Figure 3.

Experimental results

Measurements were performed on these detector elements, using a CO_2-laser, with a total output power of approximately 300 mW. The light intensity was attenuated to give approximately 5 mW incident on the area of the device. In order to obtain good sensitivity, the load resistance, R_L was set to 1 kΩ. To avoid excessive dark currents the bias voltage V_b was adjusted to give detector voltages V_d below 7 V. An optical chopper and lock-in amplifier were used to monitor the changes in the photo-current by measuring the voltage across the load resistance.

The photocurrent versus bias voltage characteristics recorded at two different temperatures are shown in Figure 4. For these measurements the CO_2-laser was tuned to a wavelength of 9.53 μm. Measurements were also performed for several wavelengths in the interval 9.5 – 10.6 μm. For wavelengths longer than 10.0 μm, corresponding to the separation between the energy levels E_1 and E_2, the photocurrent response drops rapidly. The curves in Figure 4 show a clear peak at a detector bias voltage V_d of approximately 5.7 V. This peak is believed to be due to alignment of the energy levels in the VSSEF. At higher detector voltages the responsivity drops rapidly indicating a high negative differential resistance. This is a unique feature of the VSSEF device not observed in commonly used photo-detectors. At temperatures of 50 K or less the resonance peak is easily observed. For higher temperatures the peak is, however, smeared out.

Conclusions

We have observed photon-assisted resonant tunneling in a GaAs/AlGaAs VSSEF-structure. Electrons confined in the quantum wells are excited to the second state by intersubband absorption of incident IR radiation. At an appropriate applied electric field the electrons can then tunnel through the VSSEF. This is manifested by the measured peak in the photo-current at a detector voltage of 5.7 V. To our knowledge this is the first time this effect has been observed and it could prove useful for IR-detector applications.

Acknowledgements

This work was supported by the National Swedish Board for Technical Development (STU).

References

[1] B. F. Levine et al., "GaAs/AlGaAs quantum well long-wavelength infra-red (LWIR) detector with a detectivity comparable to HgCdTe", *Electron. Lett.*, vol 24, No 12, pp 747 – 748, 1988.

[2] C. J. Summers and K. F. Brennan, "Variably spaced superlattice energy filter, a new device design concept for high-energy electron injection", *Appl. Phys. Lett.*, vol 48, No 12, pp 806 – 808, 1986.

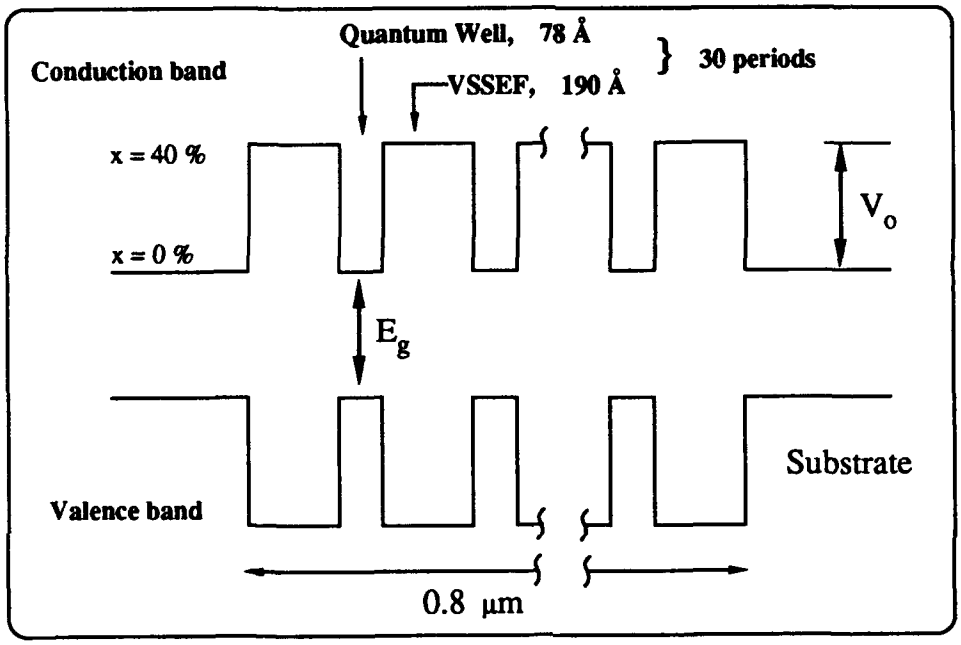


Figure 1. Band diagram showing the epitaxial structure of the detector.

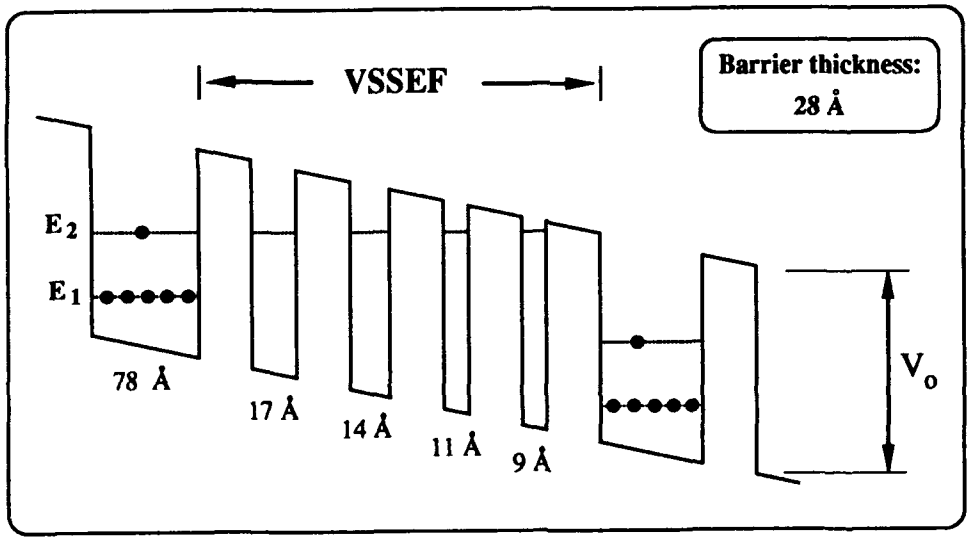


Figure 2. Schematic diagram of the conduction band potential profile with an applied external bias voltage. The location of the energy levels in the quantum wells and the alignment of the energy levels in the VSSEF are illustrated.

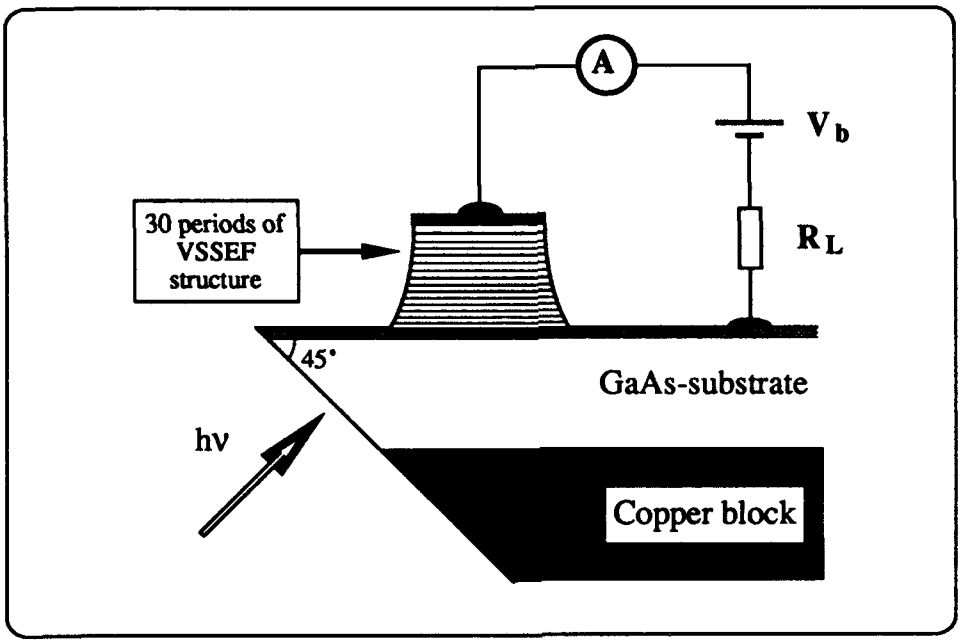


Figure 3. Experimental setup and illumination principle.

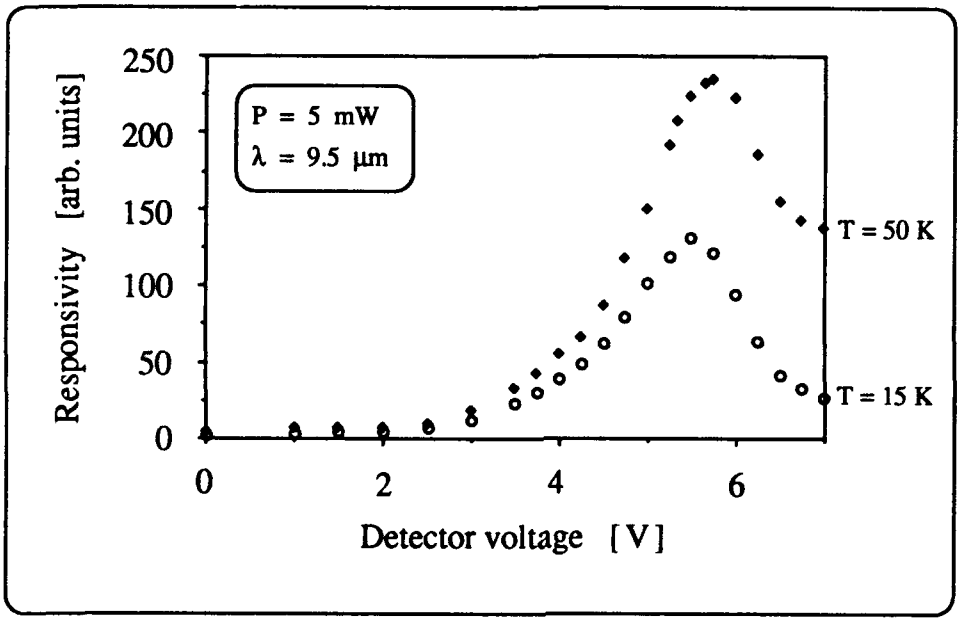


Figure 4. Detector responsivity as a function of detector voltage, measured at temperatures of 15 K and 50 K.

CARRIER SWEEP-OUT FROM QUANTUM WELLS IN AN ELECTRIC FIELD

A.M.Fox[a], D.A.B. Miller, G.Livescu[b], J.E. Cunningham, and W.Y. Jan

AT&T Bell Laboratories
Crawfords Corner Road, Holmdel, NJ 07733

AD-P007 879

The physics of carrier escape from quantum wells in an electric field is important for improving the quantum well electroabsorptive devices such as the Self Electrooptic Effect Device (SEED) [1]. The carrier lifetime is important not only because it puts a lower limit on the switching time [2], but also because it affects other properties such as the electroabsorption and the exciton saturation intensity [3]. This latter point in fact proves to be very significant for SEED systems, because these systems tend to run at intensity levels much greater than that required to switch a single device. (Sufficient energy must be passed to the next device in the system to switch it after allowing for the system losses.) At these high power levels, the exciton absorption saturates, which puts an upper limit on the intensity which can be used. We have recently shown how the saturation intensity is strongly affected by the design of the quantum well structure, most likely because of the changes in carrier sweep-out times which accompanied the change in design [3].

In this paper we report measurements of the field- and temperature-dependent sweep-out times in three carefully designed GaAs/$Al_xGa_{1-x}As$ quantum well p-i-n structures. The principal variable between the samples is the height and thickness of the AlGaAs barriers: the reference sample had x = 0.3 and a barrier thickness (L_b) of ~60Å; the second sample had the same x-value, but L_b was reduced to 35Å, and the third sample had approximately the same L_b as the reference, but had x reduced to 0.2 . Since the barrier height is determined by the x-value, these samples allow us to study the variation of the sweep-out time against the barrier height at constant barrier thickness, and vice versa.

Carrier Sweep-out Measurements

We measured the sweep-out times by the technique of time-resolved electroabsorption [4]. In Fig. 1 we show our results for the three samples. (The sample details are given in the figure caption.) Measurements were performed between 10K and room temperature.

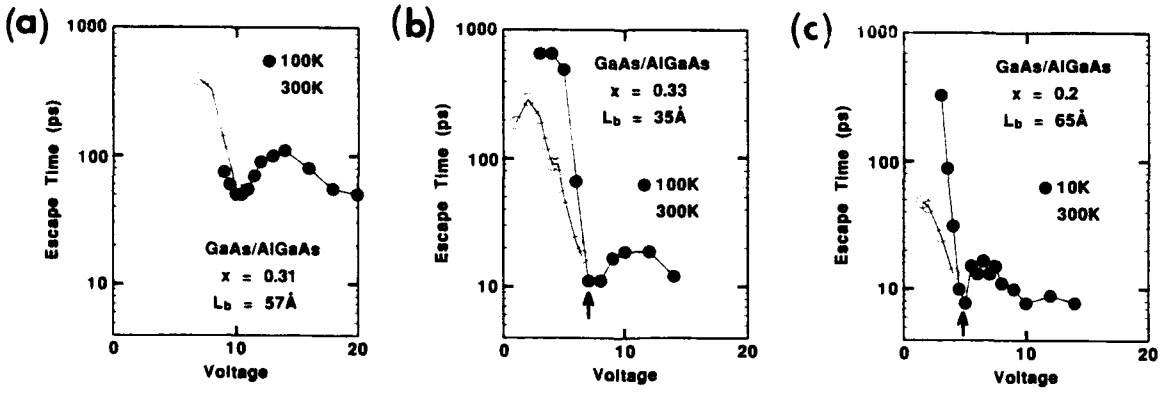


Figure 1 Measured sweep-out times for our GaAs/$Al_xGa_{1-x}As$ p-i-n quantum well structures against reverse bias and temperature. The sample details are as follows: (a) 75 periods with L_w=65Å, L_b=57Å, x= 0.31 ; (b) 80 periods with L_w=95Å, L_b=35Å, x= 0.33 ; (c) 65 periods with L_w=95Å, L_b=65Å, x= 0.20 . The arrows in (b) and (c) indicate the resonant tunneling voltage determined from photocurrent spectroscopy.

On comparing the results for the three samples, we note that:

- The sweep-out times tend to decrease as the field is increased.
- All three samples show a minimum in the escape time at the voltage for resonant tunneling of electrons. The position of the minima agree well with the resonant voltage found from careful spectroscopic studies [5].
- Escape times decrease on reducing x or L_b.
- Below the resonant voltage the escape time decreases strongly with temperature, but above resonance, the sweep-out time is practically independent of temperature. (The absence of 100K data points in Fig.1(a) for voltages below 9V indicates a very long lifetime).

The results clearly show the importance of the barrier design in determining the sweep-out time.

Discussion

The carrier lifetime in a quantum well in an electric field F can be written as:

$$\frac{1}{\tau_i} \simeq \frac{1}{\tau_R} + \left[\frac{k_B T}{2\pi m_i L_w^2}\right]^{1/2} \exp -\left[\frac{H_i(F)}{k_B T}\right] + \frac{n\hbar\pi}{2L_w^2 m_i} \exp -\left[\frac{2L_b\sqrt{2m_{bi}H'_i(F)}}{\hbar}\right] \quad (1)$$

The three terms refer to recombination, thermionic emission and tunneling respectively. The subscript i refers to electrons or holes, and allows for the fact that the sweep-out rate of the two particle types may differ. τ_R is the recombination lifetime, T is the temperature, m_i and m_{bi} are the effective masses in the well and barrier respectively. L_w is the well width, L_b is the barrier width, and n is the quantization number of the sub-level, $H_i(F)$ and $H'_i(F)$ are the effective barrier heights for thermal emission or tunneling respectively. $H_i(F)$ may be written approximately as:

$$H_i(F) = Q_i \Delta E_g - E^{(n)}_i - |e| F L_w/2 \quad (2)$$

where Q_e/Q_h is the ratio of conduction to valence band discontinuities, $(Q_e + Q_h = 1)$, ΔE_g is the difference in band gaps between the well and barrier material, and $E^{(n)}_i$ is the n^{th} subband energy relative to the center of the well. $H'_i(F)$ would be given by a similar expression, but with $L_w/2$ replaced by the position of the weighted mean potential of the tilted barrier. The thermal emission term in Eq.(1) is taken from Schneider and von Klitzing [6], but with the simplification that thermal emission against the field is neglected. The tunneling term is a simplified version taken from Larsson *et al* [7], where tunneling through just one barrier is considered. Eq.(1) is not expected to be rigorously accurate, but should correctly predict the physical trends.

Our experimental results compare favorably with the predictions of Eq.(1). The changes in τ brought about by varying F, x and L_b are well explained by the variation of the thermionic emission and tunneling times. The fact that τ is insensitive to temperature at high fields indicates that the dominant high field escape mechanism is tunneling. The sensitivity of τ to T at low fields clearly points to the importance of thermal emission.

To examine the thermal emission process in more detail, we show in Fig.(2) the thermal emission time of the sample with x=0.2 as a function of 1 / T at 3.0V and 3.5V. We observed that the sweep-out times were practically independent of the temperature up to 100K, but decreased strongly with T above this point. The low temperature limit of τ tells us the tunneling time τ_T , and thus we can determine the thermionic emission time τ_E from Eq.(1) by subtracting $1/\tau_T$ from $1/\tau$. (τ_R is assumed to be negligible). The linear variation on the logarithmic τ axis enables us to deduce an activation energy of ~ 48±15 meV. This activation energy is consistent with three possible escape mechanisms:

(a) Thermal emission of holes from the n = 1 heavy hole sub-level over the top of the AlGaAs confining barrier.

(b) Thermal activation of electrons to the minimum energy at which they have to tunnel through just one barrier.

(c) Phonon-assisted tunneling of electrons or holes [8,9].

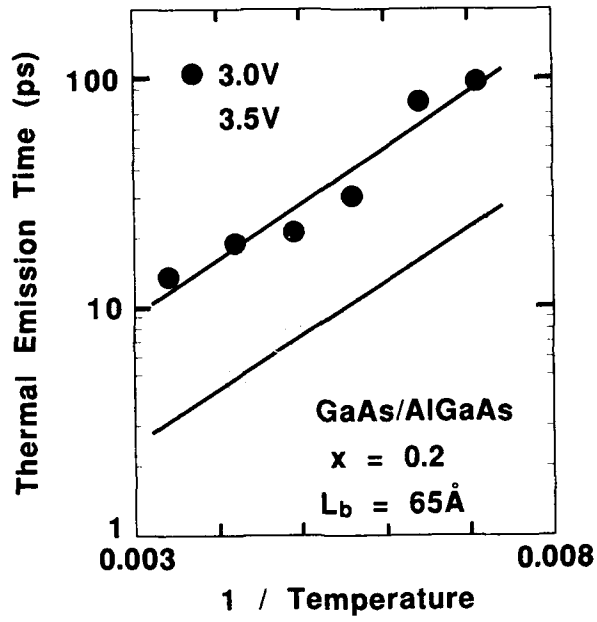


Figure 2 Thermal emission time for the sample of Fig. 1(c) against 1 / T at 3.0V and 3.5V . The straight lines are fits assuming an activation energy of 49meV at 3.0 V and 47meV at 3.5V .

Since the low field escape time is also very sensitive to barrier thickness, it seems likely that the dominant mechanism is in fact a thermally-assisted tunneling process such as (b) or (c). Our results do not seem to be consistent with pure thermal emission of electrons over the top of their confining barrier, nor with the proposed escape mechanism of thermal population of higher sublevels followed by rapid tunneling [7].

Conclusions

We have demonstrated the importance of thermal emission of carriers as an escape mechanism at low fields, and of tunneling at high fields. The precise mechanism of the thermal emission is still not fully resolved, and is worthy of further study. An improved understanding of the sweep-out physics should lead to further technological advances such as the recently demonstrated 33ps SEED switch [2].

Acknowledgements

We would like to acknowledge the work of J.E. Henry and M.M. Becker in processing the samples.

(a) Present address: Clarendon Laboratory, Parks Road, Oxford OX1 3PU, UK
(b) Present address: AT&T Bell Laboratories, Solid State Technology Center, Breinigsville, PA 18031

References

[1] For a recent review see D.A.B. Miller, Optical and Quantum Electronics **22**, S61 (1990)

[2] G.D. Boyd, A.M. Fox, D.A.B. Miller, L.M.F. Chirovsky, L.A.D'Asaro, J.M. Kuo, R.F. Kopf and A.L.Lentine, Appl. Phys. Lett. **57**, 1843 (1990)

[3] A.M. Fox, D.A.B. Miller, G. Livescu, J.E. Cunningham, J.E. Henry and W.Y. Jan, Appl. Phys. Lett. (to be published November 1990)

[4] G. Livescu, A.M. Fox, D.A.B. Miller, T. Sizer, W.H. Knox, J.E. Cunningham, A.C. Gossard and J.H. English, Semicond. Sci. and Technol. **5**, 549 (1990)

[5] A.M. Fox, D.A.B. Miller, G. Livescu, J.E. Cunningham, J.E. Henry and W.Y. Jan, Phys. Rev. B **42**, 1841 (1990) ; *Quantum-Well and Superlattice Physics III*, G.H. Dohler, E.S. Koteles and J.N. Schulman, Eds., Proc. SPIE 1283, 164 (1990)

[6] H. Schneider and K. v. Klitzing, Phys. Rev. B **38**, 6160 (1988)

[7] A. Larsson, P.A. Andrekson, S.T. Eng and A. Yariv, IEEE J. Quantum Electron. **QE-24**, 787 (1988)

[8] D.Y. Oberli, J. Shah, T.C. Damen, J.M. Kuo, J.E. Henry, J. Lary and S.M. Goodnick, Appl. Phys. Lett. **56**, 1239 (1990)

[9] M.G. Shorthose, J.F. Ryan and A. Moseley, Solid State Electron. **32**, 1449 (1989)

AD-P007 880

The Temperature Dependence of the Resonant Tunneling Process

I. Bar-Joseph, Y. Gedalyahu, A. Yacoby
Department of Physics, Weizmann Institute of Science, Rehovot, Israel
J.K. Woodward, D.S. Chemla, D.L. Sivco and A.Y. Cho
AT&T Bell Laboratories, NJ, USA

92-22409

The nature of a resonant tunneling process that involves inelastic scattering events is of a wide interest lately[1-3]. In this paper, we investigate the influence of inelastic scattering by measuring the tunneling characteristics at various temperatures. We show that the stored charge and the transit time are not sensitive to a large temperature change.

We used a symmetric double barrier diode under electric bias to study the electrons tunneling process. Our sample was composed of two 70Å InAlAs barriers and a 45Å InGaAs well between them. The zero bias Fermi energy in the emitter and collector was 55 meV. A more detailed description of the sample is given at ref(4). The experimental method we used is differential absorption spectroscopy (DAS): We modulated the charge density in the well by modulating the voltage applied to the diode. This in turn caused a modulation of the absorption coefficient α of the well material. The absorption coefficient is related to the electrons density N, primarily due to Pauli exclusion principle, which inhibits transitions into states filled by electrons. This mechanism, often referred as phase-space-filling, affect both the excitonic and the continuum band-to-band spectra. At low density, $\alpha_c(\hbar\omega) = \alpha_c^0(\hbar\omega)[1 - f_e]$ where α_c and α_c^0 are the continuum contribution to the absorption coefficients when the QW is filled (α_c) or empty (α_c^0), and f_e is the electrons normalized distribution function. In the excitonic case it is common to define a characteristic saturation density N_s, such that $\Delta\alpha/\alpha = N/N_s$. Low carriers density produces small changes in the absorption coefficient, and then $\Delta T/T = -\Delta\alpha l$, where T is the transmitted light through the sample and l is the well thickness. Hence, by modulating the voltage on the diode between $V = 0$ and V, and measuring ΔT using a lock-in technique, one can calculate the change in the electrons density in the quantum well, if N_s and α are known. In our measurements V is the voltage that corresponds to maximal current, and is denoted V_{peak}.

Figure 1 shows 4 DAS measurements taken at T=10K, 90K, 170K and 290K. The largest positive peak is due to bleaching of the heavy-hole (hh) exciton, and it is accompanied by a small positive peak (higher in energy), which is due to bleaching of the light-hole (lh) exciton. The lower energy features originated from the contact layers, and will not be discussed here. The absorption bleaching at all temperatures is concentrated at the bottom of the band, although hot electrons are also injected to the well from the emitter, where the Fermi energy is about 55meV. This is an evidence to electrons thermalization through phonons emission. At high temperatures, when the typical time between collisions is much smaller then the transit time, phonon absorption becomes the dominant process, and a tail toward the high energies appears in the DAS.

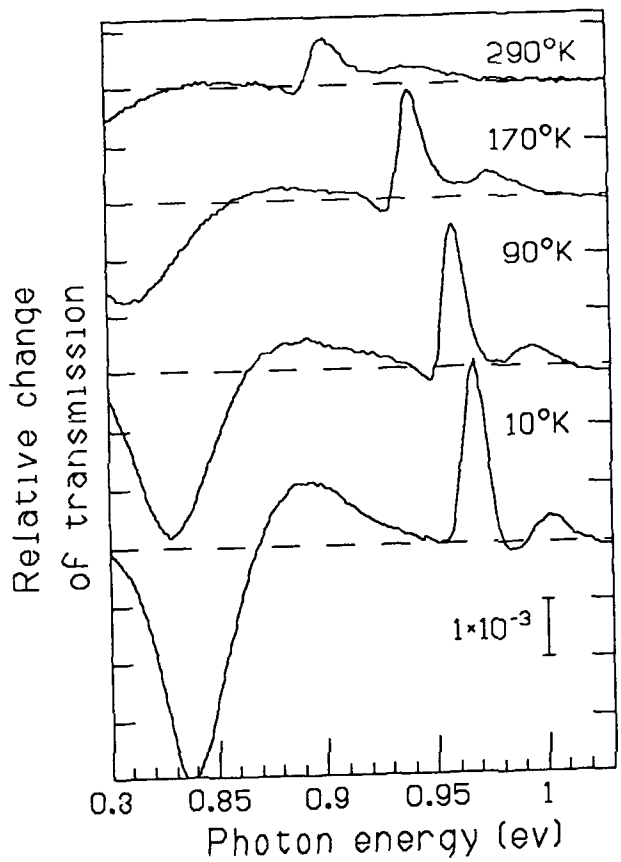


Fig. 1. Differential absorption spectra at 4 different temperatures measured at V_{peak}.

To analyze the measurements, we performed a careful fit of the DAS at each temperature, to a curve which is a sum of differential signals from the hh and lh excitons and the continuum. The excitons were assumed to have a gaussian line shape and the continuum was described by a temperature broadened step function multiplied by the Sommerfeld enhancement. We included both the bleaching due to phase space filling and the small contribution due to a Stark shift of the QW energy level. Figure 2 shows the *relative integrated change* of the area under the hh exciton, Δ_{hh}/A_{hh}, as a function of temperature, where $\Delta_{hh} = \int \Delta\alpha_{hh}(\hbar\omega)d(\hbar\omega)$ and $A_{hh} = \int \alpha_{hh}(\hbar\omega)d(\hbar\omega)$. $A_{hh}(T)$

was obtained by measuring the absorption spectra of a 50 QW's calibration sample with identical well and barriers width. Measurements were done at various temperatures, although A_{hh} is essentially temperature independent.

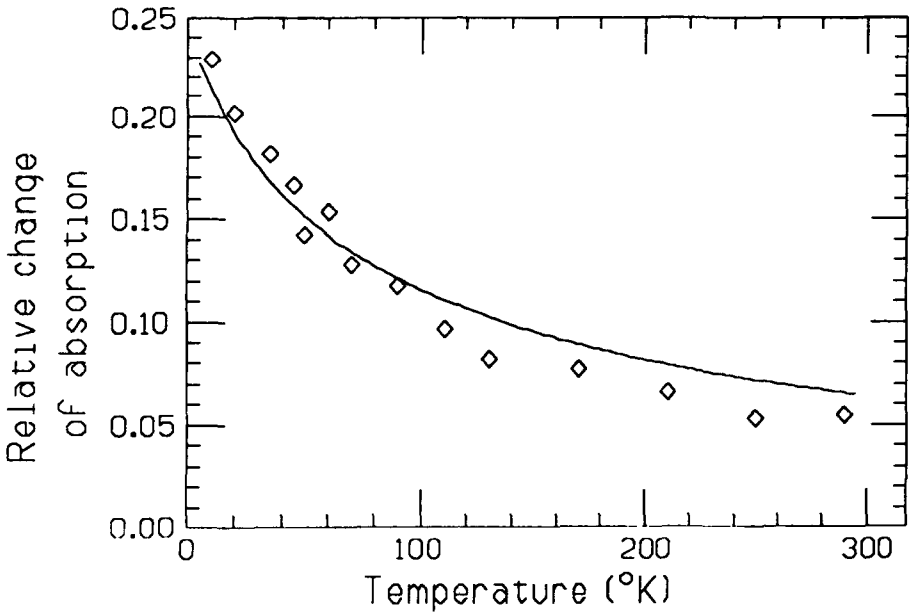


Fig. 2. The relative change of the heavy hole exciton area as a function of temperature. The solid line is the calculated $N/N_s^e(T)$ for $N = 2.5 \times 10^{10} cm^{-2}$.

As mentioned above, one has to know the saturation density N_s at each temperature, in order to find the electrons density N. We derived the temperature dependence of $N_s^e(T)$ and $N_s^{e-h}(T)$, the exciton saturation density in the presence of electrons and in the presence of electron-hole pairs, respectively[5]. This allowed us to determine $N_s^e(T)$ from optical measurements[4] of N_s^{e-h} at 10K. The solid line in Fig. 2 shows N/N_s^e as a function of temperature for the calculated $N_s^e(T)$ and for a constant N. It can be seen that the decrease in Δ_{hh} is consistent with the expected increase of the saturation density N_s^e over that temperature range. We can thus conclude that the temperature dependence of Δ_{hh} is due to that of N_s^e and that the electron density in the QW is essentially independent of the temperature. The resulting value for the constant electrons density is $2.8 \times 10^{10} \mathrm{cm}^{-2}$.

The current density J was also measured at each temperature, and found to be

almost constant over the entire temperature range: $J_{peak} \approx 60A/cm^{-2}$. Dividing the accumulated charge Q by the current density J we can get the transit time through the structure $\tau = Q/J \approx 65$ps, in a reasonable agreement with a transfer matrix calculation. Since J and τ are temperature independent, so are the total transmission probability and the escape rate from the well. This is in agreement with the quantum mechanical description of the tunneling process given in Ref(3).

We also note, that the intrinsic (elastic) width of the resonance, Γ_{el}, depends only on the decay rates through the barriers, which are temperature independent. When temperature is increased, the *inelastic* width Γ_{in} increases. At room temperature, although $\Gamma_{in} \gg \Gamma_{el}$, the process characteristics changes only slightly, due to conservation of the *integrated* transmission probability. It follows that resonant tunneling *can* be observed even when $\Gamma_{in} \gg \Gamma_{el}$, in a contradiction to Ref(2).

To summarize, inelastic scattering processes involving the tunneling electrons were shown to occur in the well, such that the electrons distribution is thermalized with the lattice at all temperatures. Nevertheless, the three major physical quantities which characterize the tunneling process, the current density, the stored charge and the transit time, are insensitive to a large temperature change. We demonstrated that resonant tunneling *can* be observed even when its inelastic width is grater than the elastic one, and that the electron transmission probability through the structure is modified by inelastic scattering in such a way that the integrated probability remains constant.

references:

1. M. Buttiker. IBM J. Res. and Develop. **32**, 63 (1988)
2. A.D.Stone and P.A.Lee, Phys. Rev. Lett. **54**, 1196 (1985).
3. N.S. Wingreen, K.W. Jacobsen, and J.W. Wilkins Phys.Rev. **B40**, 11834 (1989), and Phys.Rev.Lett **61**, 1396 (1988).
4. I. Bar-Joseph, T.K. Woodward, D.S. Chemla, D. Sivco, and A.Y. Cho, Phys. Rev. **B41**, 3264 (1990).
5. S. Schmitt-Rink, D.S. Chemla, and D.A.B. Miller, Phys. Rev. **B32**, 6601 (1985).

Joint Session on Tunneling: II

WD 3:15pm–4:30pm
Salon F

Gerhard Sollner, *Presider*
MIT Lincoln Laboratory

Coherent Oscillations of a Wavepacket in a Semiconductor Double Quantum Well Structure

Karl Leo, Jagdeep Shah, Ernst O. Göbel[a], and T.C. Damen

AT&T Bell Laboratories, Room 4D-417, Holmdel, NJ 07733, U.S.A.

Stefan Schmitt–Rink and Wilfried Schäfer[b]

AT&T Bell Laboratories, Murray Hill, NJ 7974, U.S.A.

AD-P007 881



Klaus Köhler

Fraunhofer-IAF, D-7800 Freiburg, Germany

Advances in the growth of ultrathin semiconductor layers have allowed to realize structures showing novel physical effects and device applications. One of the most exciting developments was the ability to grow heterostructures with barrier layers thin enough that *tunneling* becomes important. One particular structure which has recently found much interest is an asymmetric double quantum well structure (a-DQW), which is related to double well potentials important in many other fields of physics.[1] Figure 1 depicts schematically an a-DQW structure: Out of resonance (left), the electronic wavefunctions are localized in the respective well; at resonance (right), the levels anticross, and the wavefunctions are *delocalized over both wells*. If one excites resonantly the WW with a short pulse having a spectrum which covers transitions to both electronic levels, a *wavepacket* localized in the WW is created. This wavepacket will subsequently oscillate between the wells with a time constant T_{osc} inversely proportional to the splitting between the levels:[2]

$$T_{osc} = h/\Delta E\,. \qquad (1)$$

Such oscillations are a pure quantum-mechanical process without classical analog.[1] Half of the oscillation time can be considered as the tunneling time of an *ideal coherent tunneling process.*

We report here the first observation of coherent wavepacket oscillations in a solid.[3,4] The oscillation is traced in the time domain by by pump-and-probe (PP) as well as degenerate four-wave mixing (DFWM) spectroscopy. The subpicosecond tunneling time is in good agreement with the coherent model. By varying the alignment of the levels, the properties of the wavepacket and its dynamics are strongly influenced.

The results presented here were obtained in a ten-period structure consisting of a 170 Å GaAs quantum well, followed by a 17 Å $Al_{0.35}Ga_{0.65}As$ barrier, and a 120 Å GaAs quantum well. Figure 2 shows the transmission spectra of the sample in the vicinity of the first heavy-hole (hh) and light-hole (lh) transition, taken at low density with a cw

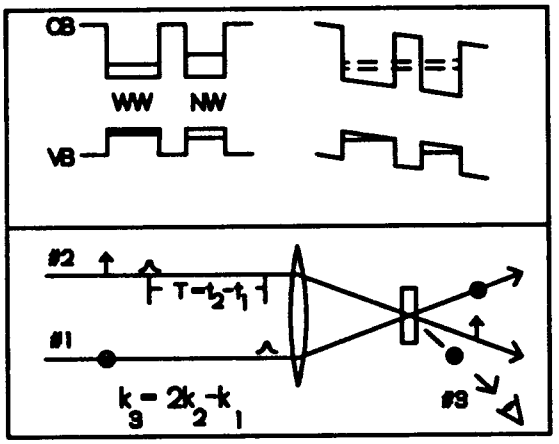


Figure 1: Top: schematic of the double well structure at resonance, for fields where the electronic levels are out of (left) and in resonance (right). Bottom: geometry of the experiment.

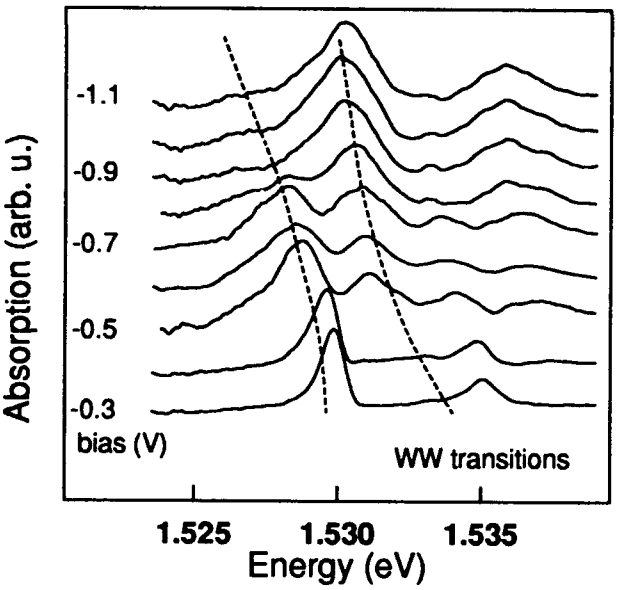


Figure 2: Transmission spectra for different bias fields. The dashed lines are guides for the eye to indicate the two transitions.

laser. For low electric field (-0.3V), the spectrum shows the first hh and lh exciton transitions of the WW. As the field is increased, a new peak appears above the hh exciton peak (-0.5V). This peak gains strength and the original hh exciton peak loses strength until have about equal intensity at resonance (-0.6V). The splitting between the peaks is about 3meV. With further increase in field, the lower energy peak rapidly moves to lower energy and loses strength, while the higher energy peak moves slowly and acquires the strength of the original hh exciton peak. The spectra reflect the eigenstate probability distribution in the wells: At electronic resonance, both states are delocalized and have nearly equal probability in both wells; out of resonance, the delocalization gradually disappears, and only the transitions within a well are important.

The oscillation of the wavepacket is observed in a PP transmission experiment. The "pump" pulse (direction $\mathbf{k}_1$) with a duration of about 500fs creates the wavepacket; the sample transmission is probed with a weak "probe" pulse ($\mathbf{k}_2$) as a function of delay time, T (Fig. 1, bottom). Figure 3 shows the change in transmitted probe intensity versus delay time. The excitation is chosen resonantly to the WW transition, thereby creating an excitonic wavepacket in this well. Temperature (5K) and density ($\approx 5\times10^8 cm^{-2}$) are kept low to avoid fast dephasing of the transition due to carrier-phonon or carrier-carrier scattering. The trace for a bias of -1.3V represents the case of nonresonant conduction electron levels: The signal has a step-like onset due to the bleaching of the absorption by the carriers and decays subsequently. The trace for electronic resonance of the wells (-0.6V) clearly shows an oscillatory modulation, with a period of about 1.3 ps. This oscillation period agrees well with that expected from the measured splitting $\Delta E \approx 3$ meV

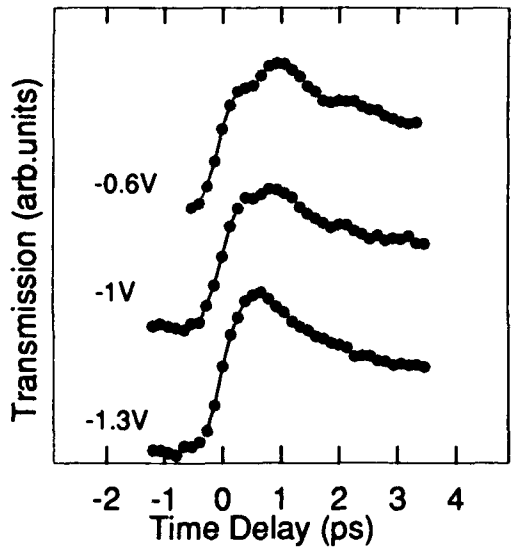


Figure 3: Transmission versus delay time for different bias fields.

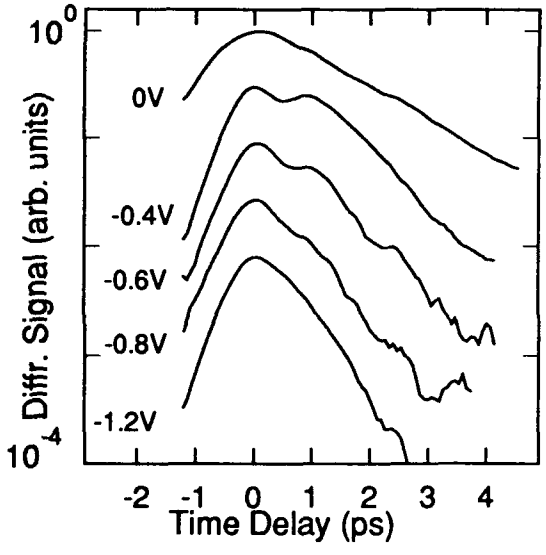


Figure 4: Diffracted signal in the DFWM experiment for various electric fields.

in the linear absorption spectrum at resonance (Fig. 3). Since the oscillation is significantly damped we observe only one pronounced peak and a weak second oscillation. If the conduction electron levels are detuned (-1V) , the modulation becomes weaker and the period shorter, as expected due to the increased splitting between the levels and an increased localization of the wavefunctions.

These results are confirmed by a time-resolved self-diffracted DFWM experiment. Here, two incoming beams with the directions $\mathbf{k}_1$ and $\mathbf{k}_2$ form an excitonic grating, and a probe signal is diffracted from this grating into the background-free direction $2\mathbf{k}_2-\mathbf{k}_1$ (Fig.1, bottom). This time-integrated diffracted signal is measured as a function of the delay time T between the incoming pulses and gives information about the exciton dynamics. The DFWM signal versus the delay time for our a-DQW is shown in Fig.4 for various applied voltages. If the electric field is above (0V) or below (-1.2V) the field where the electronic levels are in resonance, the signal is exponential and reflects the free decay of the polarization, i.e., the loss of phase coherence of the excitons due to scattering processes. The decay shows a periodic modulation, if the conduction electron levels are tuned in resonance (-0.6V). The modulation of the DFWM signal reflects the oscillatory behavior of the wavepacket, which was photoexcited in the WW. The modulation period agrees with the period observed in the PP experiment. If we tune the conduction electron levels slightly out of resonance (-0.4V and -0.8V), the modulation becomes weaker due to the increasing localization of the eigenstates in the wells.

The dynamics of the oscillation is well described by a theoretical model describing the coupled wells as a three-level-like system. It turns out that the oscillation in the PP

experiment is damped because of the dephasing of the transition between the coupled levels and the DFWM signal because of the dephasing of the transition above the bandgap. This reflects their different physical origin (polarization effects in the former case and population effects in the latter). A preliminary analysis of the data shows that the thermalization time between the extended levels is short (≈1ps) leading to a strongly damped wavepacket motion.

Our results are closely related to the recent luminescence studies of tunneling in a-DQW.[5-8] Oberli et al.[5] have first shown that the electron tunneling time has a pronounced resonance when the electron levels are aligned. Leo et al.[8] have shown that the hole tunneling time shows similar resonances when the heavy-hole levels are aligned. However, the observed tunneling times were in both cases much longer than the expected *coherent* tunneling time. These experiments correspond to the case of an overdamped oscillation, which leads to much longer transfer time, in agreement with theory.[8]

We are indebted to J.P. Gordon for fruitful discussions. We thank E. Ippen, S. [illegible]vi, and D.A.B. Miller for useful discussions, and P. Ganser for assistance in the GaAs MBE growth. The work of K.L. was partially supported by the Max-Planck-Gesellschaft zur Förderung der Wissenschaften e.V.

(a) permanent address: Philipps-Universität, D-3550 Marburg, Germany
(b) permanent address: Forschungszentrum Jülich, HLRZ, D-5170 Jülich, Germany

[1] A.J. Leggett et al., Rev. Mod. Phys. **59**, 1 (1987).
[2] S. Luryi, Solid State Commun. **65**, 787 (1988).
[3] K. Leo, J. Shah, E.O. Göbel, T.C. Damen, S. Schmitt-Rink, W. Schäfer, K. Köhler, submitted for publication.
[4] K. Leo, E.O. Göbel, T.C. Damen, J. Shah, S. Schmitt-Rink, W. Schäfer, C. Stafford, J.F. Müller, K. Köhler, and P. Ganser, Proc. *Ultrafast Phenomena VII*, eds. C.B. Harris, E.P. Ippen, G.A. Mourou, and A.H. Zewail (Springer Verlag Berlin Heidelberg New York 1990), pp. 250-253.
[5] D.Y. Oberli, J. Shah, T.C. Damen, C.W. Tu, T.Y. Chang, D.A.B. Miller, J.E. Henry, R.F. Kopf, N. Sauer, and A.E. DiGiovanni, Phys. Rev. B **40**, 3028 (1989).
[6] B. Deveaud, F. Clerot, A. Chomette, A. Regreny, R. Ferreira, G. Bastard, and B. Sermage, Europhysics Letters **11**, 367 (1990).
[7] M.G.W. Alexander, M. Nido, W.W. Rühle, and K. Köhler, Phys. Rev. **B41**, 12296 (1990).
[8] K. Leo, J. Shah, J.P. Gordon, T.C. Damen, D.A.B. Miller, C.W. Tu, and J.E. Cunningham, Phys. Rev. **B42**, 7065 (1990).

AD-P007 882

Terahertz absorption between split subbands in coupled quantum wells

Hartmut Roskos, Martin C. Nuss, Jagdeep Shah, Ben Tell, and Jack Cunningham

AT&T Bell Laboratories, Crawfords Corner Rd., Holmdel NJ 07733
Tel. (201) 949-4925; Fax: (201) 949-6010

Two quantum systems with energy levels in resonance with each other experience a splitting of these levels when the wavefunctions of the systems overlap. In semiconductor structures consisting of pairs of closely spaced quantum wells the wavefunction overlap of charge carriers in the wells leads to a novel kind of intersubband transition. To date, this transition has been studied by interband absorption and luminescence and, most recently, by four-wave-mixing experiments [Leo, 1990]. Here, we report of the first direct absorption measurements of the split-subband transition in coupled quantum wells.

The sample used in this experiment consists of 50 periods of pairs of identical square potential quantum wells grown by gas-source molecular-beam-epitaxy. Each pair is formed by two 80 Å thick GaAs layers separated by a 31 Å (11 monolayers) wide $Al_{0.3}Ga_{0.7}As$ barrier. 200 Å thick $Al_{0.3}Ga_{0.7}As$ buffer layers isolate the double quantum wells from each other. The buffer layers are n-doped providing modulation-doping ($n_{wells} = 1.2 \times 10^{17}$ cm^{-3}) to the quantum wells. The whole stack of quantum wells is sandwiched between 500 Å thick layers of undoped $Al_{0.3}Ga_{0.7}As$. 5000 Å thick n-doped $Al_{0.3}Ga_{0.7}As$ layers ($n = 1.5 \times 10^{17}$ cm^{-3}) on the top and the bottom of the stack prevent the formation of a depletion zone in the well region ensuring flatband conditions.

The amount of splitting of the resonant levels can be estimated by solving the eigenvalue equation for coupled square wells. For the parameters of our sample we calculate a design splitting of 5 meV (corresponding to a frequency of 1.2 THz).

We measure the absorption spectrum of the split-subband transition by time-domain spectroscopy. Information about the dispersion and absorption properties of the sample is extracted by Fourier analysis from the change of the shape of an ultrashort light pulse propagating through the sample.

The far-infrared pulses needed for our experiment are generated in a photo-conducting dipole antenna [Smith, 1988]. The dipole consists of a 50 μm long, 5 μm wide and 0.25 μm thick gold strip on a sapphire wafer. A 5 μm wide gap in the middle of the strip is centered on a 0.6 μm thick photoconducting silicon mesa that has been radiation damaged with 350 keV silicon ions at a dose of 5×10^{14} cm^{-2}. The antenna is biased with 9 V across the gap. Optical generation of carriers in the photoconductor with 100 fs long light pulses from a balanced colliding pulse mode-locked (CPM) dye laser produces an ultrashort pulse of electrical current in the antenna which radiates off a terahertz bandwidth electromagnetic pulse. Most of the power is directed into the sapphire substrate. This part of the beam is collimated by a hyper-hemispherical silicon lens, glued on the backside of the substrate, and radiated onto the sample. A second, identically built, antenna is used to measure the waveform of the transmitted light via

photoconductive sampling. Both the emitter and the receiver antenna are mounted inside a cryostat but are not in thermal contact with the cold finger.

A schematic representation of the experimental setup in the cryostat is shown in the upper part of Fig.1. A special sample geometry has to be chosen because of the prediction that only light polarized parallel to the growth direction of the quantum wells is absorbed in the intersubband transition. Our experiments corroborate this: we do not observe intersubband excitations with far-infrared light polarized perpendicularly to the growth direction. To maximize the absorption signal the sample was ground to a trapezoidal form with the far-infrared light entering and leaving through the side walls. Experimental results are presented here for a sample with the side walls tilted by 25°. In this case, the angle of incidence of the far-infrared light on the quantum wells is 19°. The sample was prepared from a 600 μm thick wafer. After grinding and polishing, the sample consists of a 1.8 mm wide and about 1 cm long stripe that is mounted on the cold finger of the cryostat. An aperture made of aluminum foil that is glued on the top and the bottom of the sample blocks all radiation passing around the sample.

In Fig. 1 waveforms of terahertz bandwidth far-infrared pulses after propagation through the sample are shown for sample temperatures of 300 K (solid line) and 7 K (dashed line), respectively. At 300 K, the electrons populate the lower and the higher subband nearly equally. The far-infrared pulse suffers hardly any attenuation because intersubband absorption is compensated to a great extent (theoretically about 95 %) by stimulated emission. At 7 K, we observe a reduced amplitude of the transmitted far-infrared pulse accompanied by a phase shift. Both are attributed to the intersubband excitation of electrons that now occupy nearly exclusively states in the lower subband.

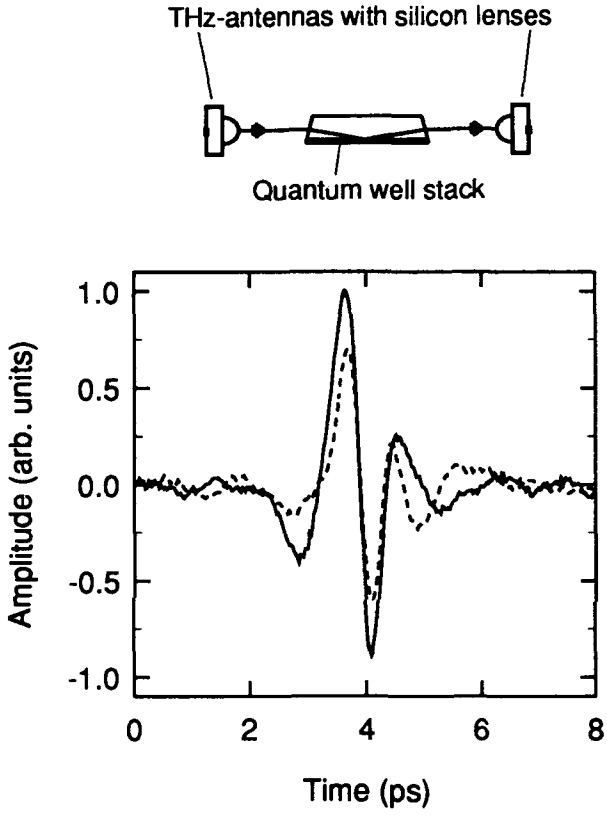


FIG. 1: *Time dependence of the detected amplitude of the far-infrared light pulse after propagation through the sample. Sample temperatures: 300 K (solid line) and 7 K (dashed line). The experimental setup is shown schematically in the upper part of the figure.*

The Fourier transforms of the electrical pulses reveal the effect of the absorption more clearly (see Fig. 2). For a sample temperature of 7 K, the spectrum of the far-infrared pulses shows a strong dip around 750 GHz, that is not observed at a sample temperature of 300 K. Subtracting the spectra for 300 K and 7 K from each other yields the dotted curve in Fig. 2. The peak position and the shape of this curve change only slightly

when it is divided by the correlation function of the emitter and receiver antennas to eliminate the frequency dependence of the detection scheme. The corrected absorption line has a full width at half maximum of 450 GHz (1.8 meV). The shoulder at the low frequency side of the absorption line is probably an artifact of the Fourier transform technique.

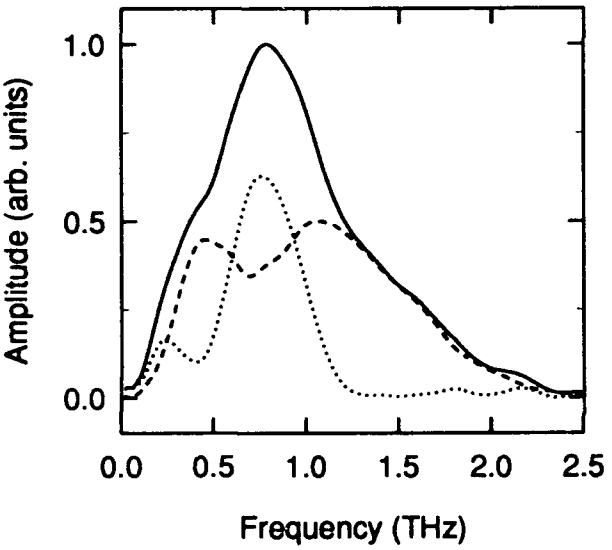


Fig. 2: *Fourier spectra of the far-infrared pulses of Fig. 1 for sample temperatures of 300 K (solid line) and 7 K (dashed line). The dotted line shows the difference between the two spectra.*

To simulate the absorption process we perform model calculations for a system of absorbers with two energy levels. The temporal shape of the electrical pulse is assumed to be given by a cosine function at a frequency of 700 GHz multiplied with the second derivative of the antenna current response function.[1] To obtain the temporal shape of the transmitted pulse the Fourier transform of the incident pulse is multiplied with a propagation factor containing the complex dielectric function of the absorber material [Yariv, 1967]. The detection process is modeled by convolving the temporal shape of the transmitted pulse with the antenna current response.

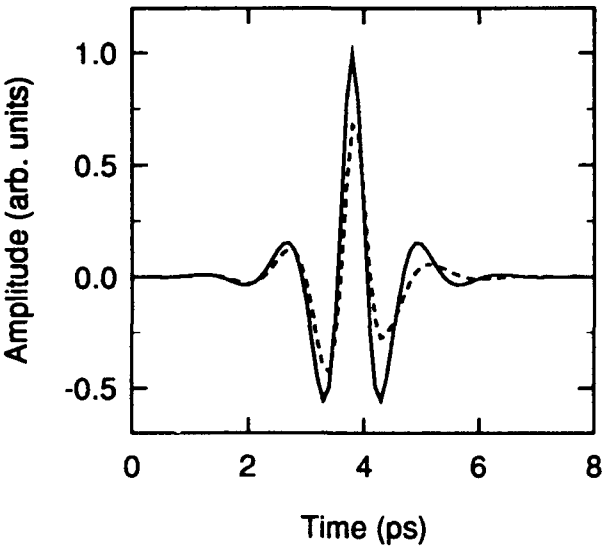


Fig. 3: *Calculated temporal shape of a detected far-infrared pulse without (solid line) and with (dashed line) absorption.*

Figure 3 shows results of the model calculations in the time domain. The solid line of Fig. 3 represents the temporal shape of the incident pulse as detected by the receiver antenna. The dashed line depicts the detected temporal shape of a pulse transmitted through the model sample. It was assumed that the absorption line is predominantly homogeneously broadened (FWHM of the Lorentzian absorption line: 450 GHz, corresponding to a relaxation time of 700 fs). The inhomogeneous broadening is assumed to be small (50 GHz width of the Gaussian frequency distribution). Fig. 3 shows that a more than 450 GHz wide absorption line probed by a terahertz bandwidth electrical pulse reveals itself only by frequency and phase shifts within the pulsewidth and does not produce a ringing signal that trails the original pulse as should be observed with a narrower line. It should be mentioned that model calculations for a predominantly inhomogeneously broadened

line produce a similar temporal shape like the one shown in Fig. 3. As a consequence we are not able to decide which type of line broadening prevails in our experiment. Considering the homogeneous linewidth derived from the four-wave-mixing results of Leo et al., it seems plausible that inhomogeneous line broadening should be dominant in our case. This is not surprising, taking into account that the microwave beam in our experiment probes a rather large area (in the order of 1 mm^2) of the sample and averages over areas with different transition energies. This assumption is supported by the fact that we observe a considerable variation of the strength and center frequency of the absorption when the beam is scanned over the samples we have tested so far.

We assume a dipole matrix element $e\langle z\rangle$ of 35 eÅ in our calculation to obtain a comparable attenuation of the far-infrared pulse at 750 GHz as in the experiment. This value for the dipole moment is considerably higher than the dipole moment of about 20 eÅ found for the intersubband transition in single quantum wells [West, 1985, Lobentanzer, 1988]. From calculations with model wavefunctions for our coupled quantum well system we have expected to find an even higher value than 35 eÅ for $e\langle z\rangle$ because of the strong delocalization of the electrons. That we do not observe a stronger dipole moment may be a consequence of sample inhomogeneities. The resonance of the energy levels in the two wells is very sensitive to small fluctuations in the thickness of the two wells and the barrier height. The delocalization and hence the dipole moment of electrons in sample regions with disturbed resonance of the levels is strongly reduced. A smaller dipole moment may also result from the fact that the actual intersubband splitting (3 meV) in our sample is not as big as the design value (5 meV). At low temperatures, the Fermi level of the electrons (about 3.5 meV) is already above the band edge of the upper subband. As a consequence not all electrons can be excited from the lower to the higher subband. In this case the true dipole matrix element is larger than the one obtained by fitting the model to the experimental data because the model assumes contribution of all electrons to the polarization in the sample.

In summary, we have performed the first direct absorption measurements on the split subband transition in coupled quantum wells by time domain spectroscopy with a beam of far-infrared pulses. This novel kind of intersubband transition at a transition energy of only 3 meV exhibits a huge dipole moment of at least 35 eÅ. The linewidth is about 1.8 meV with a probably strong contribution by inhomogeneous line broadening. To reduce this contribution experiments with a focussed beam of far-infrared pulses are under way allowing to sample over a smaller area.

[1] The antenna current response is assumed to be of the form $(1 - (1 + \exp(t/100fs))^{-1}) \times \exp(-t/500\ fs)$.

REFERENCES:

Leo, K., Göbel, E. O., Damen, T. C., Shah, J., Schmitt-Rink, S., Schäfer, W., Müller, J. F., Köhler, K., and Ganser, P. (1990), in Ultrafast Phenomena VII (eds. Harris, C. B., Ippen, E. P., Mourou, G. A., and Zewail, A. H.), Springer, Berlin, p. 250-252.

Lobentanzer, H., König, W., Stolz, W., Ploog, K., Elsässer, T., and Bäuerle, R. J. (1988), Appl. Phys. Lett. 53, 571-573.

Smith, P., Auston, D. H., and Nuss, M. C. (1988), IEEE J. Quantum Electron. QE-24, 255-260.

West, L. C., and Eglash, S. J. (1985), Appl. Phys. Lett. 46, 1156-1158.

Yariv, A. (1967), Quantum Electronics, Wiley, New York, 153.

TUNNELLING AND RELAXATION IN COUPLED QUANTUM WELLS

B. Deveaud, A. Chomette, F. Clérot, A. Regreny
C.N.E.T (LAB/OCM) 22301 Lannion (FRANCE)
and
S. Gurvitz, I. Bar Joseph
Weizmann Institute, Rehovot (ISRAEL)

AD-P007 883



92-22412



In a double barrier resonant tunnelling diode, the lifetime of the electrons in the well is governed by the coupling of the confined states to the continuum of states outside the barriers. The well states are broadened by the interaction with the continuum on each side of the structure and are thus metastable, even without any relaxation mechanism such as phonon emission. If an electron is injected into the structure as in the experiment of Tsuchyia et al [1], it will leak out with a time constant given only by the barrier thickness.

In a system of coupled quantum wells (CQW) on the contrary, we are dealing with eigenstates of the system. Even at resonance, when one level of the narrow well (NW) is at the energy of a level of the wide well (WW), finite lifetimes are only observed because of additional perturbations to the system. In the absence of such perturbations, electrons would stay forever on the coupled levels (we are dealing here with a system prepared in a "classical mixture" i.e. with electrons equally distributed in the two wells). The strongest perturbation, in the case where the coupled levels are separated from the ground state by more than one optical phonon, is the coupling to LO phonons [2].

In the simple picture of perfect alignment of the levels in the two wells, coupling by a thin barrier gives rise to the well-known bonding and anti-bonding states split by an energy d which is exponentially varying with the barrier thickness. The eigenfunctions $|\Phi_{\pm}>$ would then read:

$$|\Phi_{\pm}> = 1/\sqrt{2}\,(|\phi_{1n}> \pm |\phi_{2w}>) \qquad (1)$$

where $|\phi_{1n}>$ and $|\phi_{2w}>$ are the wavefunctions of the first and second levels of the isolated NW and WW respectively. In this very simple picture, where perfect resonance is achieved and where phonon emission is treated as a small perturbation to the system, the coupling to phonons leads to a scattering time equal to exactly twice the time in one isolated quantum well, independantly of the barrier thickness. More precise calculations only show a change in time for very narrow barrier when the splitting between the coupled levels cannot be neglected and results in a difference in the q vector of the emitted LO phonon [3].

CQWs have been studied by time resolved luminescence in order to get information on the dynamics of the system : the parameter of importance is the time constant of the NW luminescence decay. Resonance has been obtained by applying an electric field [4,5]. This has the great advantage of tunability: it allows to go through the resonance with only one sample.

We have chosen to study the resonance by a proper adjustment of the growth parameters [6] : resonance is achieved by growing a series of samples, only changing one parameter (in our case the width of the WW or of the tunneling barrier). This method necessitates of course the growth of more samples, but it has a number of advantages. First it allows to work on several CQW periods without any problem with the field inhomegeneity. Second our samples have been p-doped in order to:

-Increase the cooling rate of the electrons, which interact with the background holes,

-Increase the luminescence efficiency (proportional to the number of holes),

-Select electron effects as the possible movement of photocreated holes has a negligible effect on the observed dynamics in the low density regime.

The first two effects are of great importance as we want to study very short transients. Our samples are grown in the GaAs/AlGaAs system by molecular beam epitaxy. The width and Al content (around 26 %) of the different layers are carefully checked by using x-ray diffraction together with a simulation program of the different diffracted intensities [3]. We study the dynamics of the different luminescence transitions with subpicosecond resolution by upconversion of the luminescence signal [7]. Resolution of our system is basically limited by the width of the laser pulses which can be as short as 120 fs. The measurements are carried out with 600 to 800 fs pedestal free pulses with an energy of 2.04 eV.

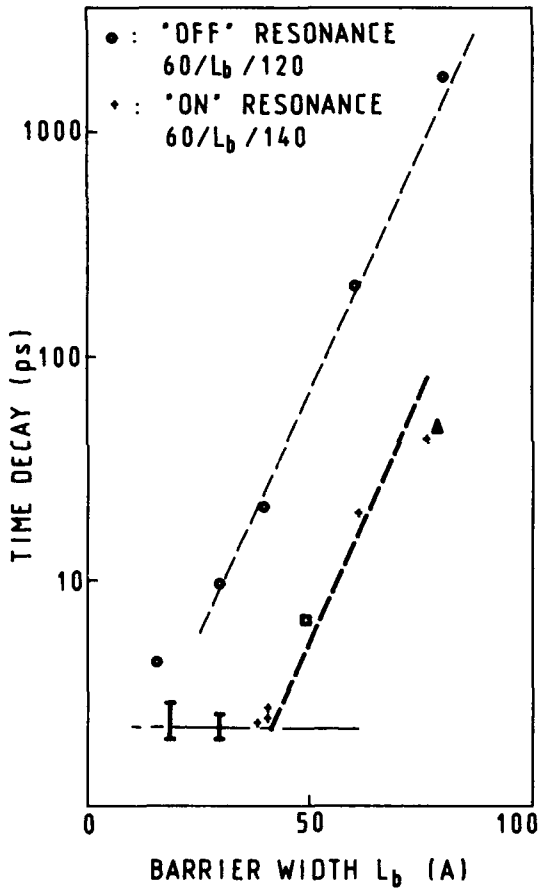


Fig.1: Decay time of the NW luminescence as a function of the barrier thickness for two series of samples: (o) "off resonance", and (+) on resonance". On resonance decay times observed by Oberli et al [3] (▫) and by Alexander et al [4] (▲) are also plotted.

We show on Fig.1 the results obtained on two series of samples: one grown to be "on resonance", and the other to be "off resonance". On this figure, we have plotted the NW luminescence decay time as a function of L_b, the thickness of the tunnelling barrier. On the same figure, we have also reported the results of the studies by Oberli et al [3] and Alexander et al [4]. For these 3 studies the samples are in fact quite similar as made out of GaAs/AlGaAs with comparable Al content in the barriers. Note that all "on resonance" experimental results follow the same trend.

The decay times for the "on resonance" samples show two well defined regions : one corresponding to barrier thicknesses larger than 40 Å where the variation of the decay time with the barrier thickness is exponential (note that the slope in that case is exactly the same as for the "off resonance" samples). In the second region, below 40 Å, the decay time stays approximately constant (between 1.7 and 2.5 ps, taking into account the uncertainties in the measurement) for the seven different samples studied (whose barrier thicknesses range from 42 Å to 22 Å).

One possible interpretation of this behaviour is the following. For barrier thicknesses below 40 Å, it is indeed possible to grow samples where $|\phi_{1n}>$ and $|\phi_{2w}>$ are resonantly coupled. By "resonantly coupled" we mean that the wavefunctions of the bonding and antibonding states $|\Phi_+>$ and $|\Phi_->$ both extend over the two wells, with approximately equal probabilities. The situation of resonant coupling is rather easy to obtain for very narrow barriers, even if the resonance condition is not perfect. On the

contrary, when the barrier becomes large, the resonance condition is much more stringent. In a simplified picture, the wavefunctions of the two coupled levels would read :

$$| \Phi_+ > = (1-\varepsilon/2\delta) | \phi_{1n} > + \varepsilon/2\delta | \phi_{2w} >) \quad (2)$$

$$| \Phi_- > = \varepsilon/2\delta | \phi_{1n} > + (1-\varepsilon/2\delta) | \phi_{2w} >) \quad (3)$$

where ε is the energy mismatch between the two levels and δ the strength of the coupling. It is easy to see that for small coupling, $| \Phi_+ >$ is localized in the NW and $| \Phi_- >$ in the WW.

Since the ground state of the system is almost entirely localized in the WW, relaxation of $| \Phi_+ >$ to the ground state is governed by the small lobe of the wavefunction still extending into the large well. Due to the exponential variation of δ with the barrier thickness, the relaxation of $| \Phi_+ >$ to the ground state will also vary exponentially, as experimentally observed. The same interpretation exactly holds for the case of purposely "off resonance" samples: the small part of the wavefunction $(\varepsilon/2\delta) | \phi_{2w} >$ extending in the WW still governs the relaxation of the NW.

Thus the observed behaviour in the different experiments is quite well reproduced by the very simple calculations exposed here. More detailed calculations using the envelope function formalism are exposed in ref. 2, they lead to the same qualitative tendencies, the quantitative agreement is also quite satisfactory. The main limitation of our description is not in the region of narrow barriers but in the case of large barriers where our way of treating the coupling to phonons as a small perturbation to the energy levels of the system is not adequate anymore close to the resonance. This is then especially true for the experiments of Oberli et al [4], and Alexander et al [5] where it may be though that they come closer to resonance than in our adjustment of the growth parameters.

In order to improve over these calculations, it is necessary to perform a calculation treating on a equal footing the coupling between the two wells and the phonon scattering. This can be performed in the framework proposed in [8]. The result of such a calculation will only be briefly exposed here. The decay time T of the population in the coupled levels can be written as:

$$T = 2/\Gamma_0 + (1+n_3)(4\varepsilon^2+\delta^2)/(2\Gamma_0\delta^2) + \delta(2\varepsilon n_1 + \Gamma_0 n_2)/(\Gamma_0\delta^2) \quad (4)$$

where Γ_0 is the strength of the phonon scattering, and $n_{1,2,3}$ describe the initial carrier distribution. In our experiments, it is reasonable to assume that we start with a classical mixture : the initial distribution is equally distributed over the two wells. Then, $n_3=n_1=n_2=0$ and the above equation reduces to :

$$T = 2/\Gamma_0 + (4\varepsilon^2+\Gamma_0^2)/(2\Gamma_0\delta^2) \quad (5)$$

This equation describes the main features of the observed phenomena. For a strong mismatch ($\varepsilon > \delta$), it gives :

$$T = 2\varepsilon^2 / \Gamma_0\delta^2 \quad (6)$$

Owing to δ^2, T varies exponentially with the barrier thickness, which explains the exponential variation of the observed times, for both the "off resonance" samples and the "on resonance" ones with large barriers, in a way exactly similar to the simple description of eq. 2 and 3.

If on the contrary we assume a negligible detuning, then we have two main regimes: the first where the electronic coupling d is strong enough ($\delta >> \Gamma_0$, i.e. narrow enough barriers), then :

$$T = 2/\Gamma_0 \tag{7}$$

and we find the same result than in the preceeding description : the decay time should be twice the scattering time in an equivalent isolated quantum well. If on the contrary the coupling is small (compared to Γ_0) the time should follow :

$$T = 2/\Gamma_0 + \Gamma_0/\delta^2 \tag{8}$$

T should show a non monotonic behaviour as a function of Γ_0. Numerical estimates for the case of refs. 4 and 5 improve the quantitative agreement, but do not explain totally the observed times. The largest change would be observed for the experiment of Alexander et al [5], where the barrier is quite large (80 Å), eq.8 would predict a decay time of the order of 5 ps at resonance significantly longer than the 2 ps calculated in the previous model, but still shorter than the experimental time of 50 ps. The rest of the descrepancy at resonance (50 ps versus 5ps) must be due to residual interface roughness effects which have been neglected up to now.

Aknowledgments:

We would like to acknowledge numerous discussions with M.G.W. Alexander, G. Bastard, R. Ferreira, W.W. Rühle. We are greateful to P. Auvray for his determination of the sample parameters.

References:

[1] M. Tsuchyia, T. Matsutsue, H. Sakaki, *Phys. Rev. Lett*, **59**, 2359 (1987)
[2] R. Ferreira, G. Bastard, *Phys. Rev.* **B40**, 1074 (1989)
[3] B. Deveaud, A. Chomette, F. Clérot, P. Auvray, A. Regreny, R. Ferreira, G. Bastard, to be published in *Phys. Rev.* B (1990)
[4] D.Y. Oberli, J. Shah, T.C. Damen, C.W. Tu, D.A.B. Miller, J.E. Miller, R.F. Kopf, N. Sauer, A. di Giovanni, *Phys. Rev.* **B40**, 3028 (1989)
[5] M.G.W. Alexander, Nido, W.W. Rühle, *Phys. Rev.* B, (1990) to be published
[6] B. Deveaud, F. Clérot, A. Chomette A. Regreny, R. Ferreira, G. Bastard, *Europhys. Lett.*, **11**, 367 (1990)
[7] J. Shah, T.C. Damen, B. Deveaud, D. Block, *Appl. Phys. Lett.*, **50**, 1307 (1987)
[8] S. Gurvitz, I. Bar Joseph, B. Deveaud, to be published

Competition Between Tunneling and Exciton Formation of Photoexcited Carriers in Asymmetric Double Quantum Wells

AD-P007 884

J. Kuhl, R. Strobel* and R. Eccleston
Max-Planck-Institut für Festkörperforschung
Heisenbergstr. 1, 7000 Stuttgart 80, FRG
Tel. (711) 6860-590 FAX: (0049) 711 687 3371

K. Köhler
Fraunhofer-Institut für Angewandte Festkörperphysik
7800 Freiburg, FRG

92-22413

Time-resolved photoluminescence (TRPL) spectroscopy has been utilized by various groups to determine resonant and nonresonant tunneling times of electrons as well as of holes in asymmetric double quantum well (ADWQ) structures /1-4/. The main disadvantage of the TRPL method arises from the fact that it is impossible to measure electron and hole tunneling times simultaneously or to determine hole tunneling times directly in the absence of an electric field. These drawbacks are inherent to the linear TRPL technique since the photoluminescence (PL) decay time of the narrow quantum well (QW_n) depends only on the tunneling time of the carrier type which tunnels faster.

In this paper we show that the nonlinear photoluminescence cross-correlation technique /5/ renders possible simultaneous determination of both the electron and hole tunneling time in ADQW's in a single experiment. Photoluminescence cross-correlation measurements performed at 80 K on similar ADQW's have been applied in Ref. /7,8/ to determine electron tunneling times. Here we demonstrate that the full potential of this technique has not been utilized in these previous experiments. We demonstrate the nonlinear dependence of the photoluminescence intensity on the excitonic transition of the ADQW's on the excitation intensity. This behavior contrasts the situation in an isolated single quantum well where the PL intensity increases linearly with excitation density. The difference is explained by the competition between exciton formation in the narrow QW and tunneling of elecrons from the narrow to the wide QW. Thus, the nonlinear signal from a double pulse TRPL experiment can be used to determine not only the electron and hole tunneling times, but also the time required to form excitons from photo-excited free carriers.

The samples under investigation were 3 GaAs-$Al_xGa_{1-x}As$ ADQW's grown on a Si-doped n^+ GaAs (100) substrate. The sample structures consisted of a buffer layer (600 nm GaAs, 20nm $Al_{0.35}Ga_{0.65}As$, 1nm GaAs, 10nm $Al_{0.35}Ga_{0.65}As$, five periods of a 2nm GaAs/3nm $Al_{0.35}Ga_{0.65}As$ superlattice), 100 nm $Al_{0.35}Ga_{0.65}As$, 10 nm wide quantum well (QW_w), $Al_{0.35}Ga_{0.65}As$ tunneling barrier of various thicknesses, 5nm narrow GaAs quantum well (QW_n), 100 nm $Al_{0.35}Ga_{0.65}As$ and a 4 nm GaAs cap. The barrier thicknesses were 3 nm in sample 3, 4 nm in sample 4, and 20 nm in sample 20. Sample 20 was used as a reference structure since tunneling is negligible for a barrier of this width

The experimental arrangement for the nonlinear PL cross-correlation technique is shown schematically in Fig. 1. A hybrid mode-locked Pyridine 1 dye laser generates pulses of around 700 fs (FWHM autocorrelation function) at 715 nm. The output is divided equally between the two beams which are sent through the two arms of an optical delay line, chopped at different frequencies and then superimposed on the same spot of the sample maintained at 8K in a helium cryostat. The photoluminescence is dispersed by a 1/2 m spectrometer and detected at

the sum frequency using a cooled GaAs photomultiplier. The beams are perpendicularly polarized by means of a $\lambda/2$ plate to suppress any coherence artifact in the detected signal /5/. By varying the delay between the two pulses, the decay of the nonlinear change in PL output generated by the two pulses may be measured. The excitation density n_{ex} was always kept < 2 $x10^{10}$ cm^{-2} in order to avoid space charge effects so that the tunneling times remained independent of n_{ex} .

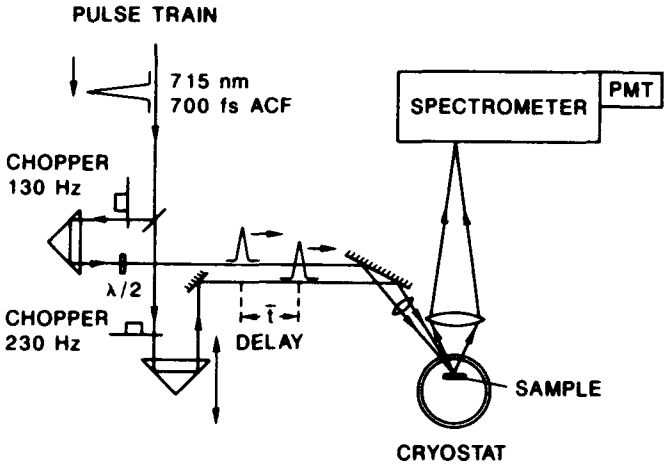


Fig. 1

Schematic of the nonlinear cross-correlation measurement. (ACF-auto-correlation function, PMT-photomultiplier tube)

The origin of the nonlinear effect is the *bimolecular* nature of the exciton formation process, i.e. the exciton formation rate is proportional to the product of the free electron and free hole densities. The formation rate is then a strong function of n_{ex}. At low n_{ex}, such that the free electron tunneling time τ_e is much smaller than the exciton formation time τ_{ex}, exciton formation, and consequently excitonic luminescence, is relatively unlikely. As n_{ex} is increased, the exciton formation rate increases but the tunneling rate (independent of n_{ex}) remains constant. The probability of a photocreated carrier contributing to excitonic luminescence therefore is increased, and a nonlinear change in the excitonic luminescence from the narrow well of such structures is expected as n_{ex} is varied. For QW_n of sample 4, the tunneling out of the well is efficient and a strong nonlinear variation of the integrated luminescence signal is observed, the gradient of 2 on a log-log scale indicating a square law dependence at low excitation. This square law variation is in exact agreement with the variation expected for the low excitation case where $\tau_e < \tau_{ex}$. This result excludes the possibility of a geminate contribution /9/ to the exciton formation rate because the square law variation is in exact agreement with that predicted for bimolecular formation (geminate formation would generate a linear dependence). Thus our experiment proves that for excitation densities above 10^8 cm^{-2}, excitons are formed purely nongeminately. Such a conclusion is perhaps not surprising since the carriers are photoexcited with large excess energy. Several LO-phonons are immediately emitted and separation of the geminate pair is likely to be a very efficient process. By contrast, the PL from QW_w of sample 4 and QW_n of sample 20, where tunneling out of the well is absent, exhibits no measurable nonlinear variation in the excitation density. We therefore conclude that the nonlinearity is related to tunneling.

This nonlinearity may be calculated for the PL cross-correlation measurement by modeling the carrier dynamics in the narrow well of the ADQW after photoexcitation by two short pulses using a system of three rate equations describing the population of free electrons (n), free holes (h) and excitons (N) as a function of time. This model considers generation of free electrons and holes in QW_n via absorption of the two excitation pulses, tunneling of electrons and holes from the narrow to the wide QW with tunneling times τ_e and τ_h, respectively, exciton formation (rate $C \cdot n \cdot p$, where C is the bimolecular exciton formation coefficient) and decay of the excitons with a lifetime τ_{LT}. We assumed that no difference exists between the tunneling rates of free electrons (or holes) and electrons (or holes) bound in an exciton in accordance with

recent TRPL measurements /10/. Our theoretical analysis took into account that tunneling of electrons and holes bound in excitons does not only decrease the density of excitons, but also gives a positive contribution to the free hole and free electron densities, respectively.

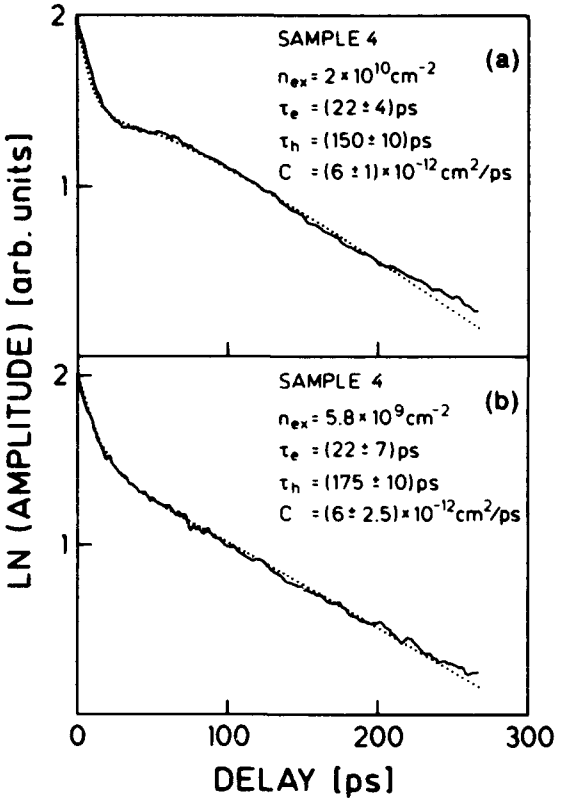


Fig. 2

PL cross-correlation signal vs. delay from QW_n/ sample 4 at (a) $n_{ex} = 2x10^{10}cm^{-2}$ and (b) $n_{ex} = 5.8 \times 10^9 cm^{-2}$. Also shown is the theoretical fit to the data and the fit parameters used.

Figure 2 shows typical nonlinear PL curves from sample 4 at two different excitation densities. The dashed line represents the best fit to the data using the rate equation model. In the case of low excitation ($\tau_e < \tau_{ex}$) the signal closely approximates to two exponential decays with time constants given by τ_e and τ_h. The higher excitation curve (Fig. 2a) shows a nonexponential shoulder region expected for the case $\tau_e > \tau_{ex}$. For this condition the initial decay becomes faster owing to efficient exciton formation between electrons and holes excited by the first pulse. If the electrons bound in these excitons start to tunnel to the wide well, the holes left behind can form new exitons with electrons from the second pulse. Their radiative decay contributes to the nonlinear signal and is the origin of the shoulder. The subsequent exponential decay of the signal reflects tunneling of the holes generated by pulse 1. The exciton formation coefficient C is determined most accurately from the curve for high excitation density. The fit yields $C = 6 \times 10^{-12}$ cm^2/ps which corresponds to $\tau_{ex} = 14.4$ ps at the excitation density of $2x10^{10}$ cm^{-2}. This value is consistent with the upper limit of 20 ps obtained in Ref. /9/. It should be noted that the current measurement is not influenced by the exciton cooling time. This time complicates any determination of the exciton formation time from conventional TRPL measurements, because the rise time of the excitonic luminescence is determined by both the exciton formation time and the exciton cooling time. The tunneling times for the electrons (22ps) and holes (150ps and 175ps, determined from the fit of Fig. 2a and 2b, respectively) agree fairly well with values estimated by TRPL measurements on the same samples. Shorter tunneling times ($\tau_e = 7 \pm 2$ps and $\tau_h = 66 \pm 3$ps) but the same value of C are obtained on a sample with a thinner (3mm) barrier.

In conclusion, we have reported on the nonlinear variation of PL output with excitation density on the exciton transition in the narrow well of two ADQW structures. The close agreement between experiment and a theory based on a rate equation model demonstrates the bimolecular nature of exciton formation. A value of $6x10^{-12}$ cm^2/ps is obtained for the bimolecular exciton

formation coefficient. The nonresonant electron and hole tunneling times are also measured simultaneously.

Acknowledgments

We would like to thank M.G.W. Alexander and W.W. Rühle for stimulating discussions.

References

*On leave from Friedrich Schiller Universität, Jena (FRG)

1. M. Tsuchiya, T. Matsusue, and H. Sakaki, *Phys. Rev. Lett.* **59**, 2359 (1987).
2. M. Nido, M.G.W. Alexander, W.W. Rühle, T. Schweizer, and K. Köhler, *Appl. Phys. Lett.* **56**, 355 (1990).
3. D.Y. Oberli, J. Shah, T.C. Damen, C.W. Tu, T.Y. Chang, D.A.B. Miller, J.E. Henry, R.F. Kopf, N. Sauer, and A.E. DiGiovanni, *Phys. Rev.* **B40**, 3028 (1989).
4. M.G.W. Alexander, M. Nido, W.W. Rühle, and K. Köhler, *Phys. Rev.* **B41**, 12295 (1990).
5. D. von der Linde, J. Kuhl, and E. Rosengart, *J. Luminescence* **24/25**, 675 (1981).
6. A detailed analysis of our studies will be published in: R. Strobel, R. Eccleston, J. Kuhl and K. Köhler, "Measurement of the Exciton Formation Time and the Electron and Hole Tunneling Times in a Double Quantum Well Structure", submitted to *Phys. Rev. B.*
7. M.K. Jackson, M.B. Johnson, D.H. Chow, T.C. McGill and C.W. Nieh, *Appl. Phys. Lett.* **54**, 552 (1989).
8. N. Sawaki, R.A. Höpfel, E. Gornik and H. Kano, *Appl. Phys. Lett.* **55**, 1996 (1989).
9. T.C. Damen, J. Shah, D.Y. Oberli, D.S. Chemla, J.E. Cunningham and J.M. Kuo, *J. Luminescence* **45**, 181 (1990).
10. M.G.W. Alexander, private communications.

Ackett, Gerard – TuC1
Allawadi, N. K. – MB3
Alphonse, G. A. – TuC4
Amano, Chikara – MB2
Andersson, Ingemar – WC2
Andersson, Thorwald – WC2
Arakawa, Y. – TuA2, TuC
Ash, R. M. – TuD12
Austin, Richard F. – MC5, WB4

Bacher, G. – TuD1
Bar-Ad, S. – MC3
Bar-Joseph, I. – MC3, WC1, WC4, WD3
Binder, R. – TuC5, WA4
Björk, Gunnar – TuA1
Blum, O. – TuD8
Boggess, Thomas F. – MC4
Bradley, R. R. – TuD12
Bromley, P. – TuD12
Bryan, R. P. – TuC5
Burrus, Charles A., Jr. – MD4

Capasso, Federico – WB6
Carter, A. C. – TuD12
Chang, Tao Y. – MD4, TuD8
Chao, Calvin Y. P. – TuD3
Chemla, Daniel S. – MA, TuB3, WB1, WC1, WC4
Chen, W. – TuB1
Chirovsky, L. M. F. – MB5
Chiu, T. H. – MD3
Cho, A. Y. – MD3, WC1, WC4
Chomette, A. – WD3
Chuang, Shun-Lien – TuD3
Cingolani, R. – TuB2, TuB5
Claisse, P. – MD2
Clerot, F. – TuC2, WD3
Coldren, Larry A. – MA3, MB1, MD, MD6
Cooke, P. – MD2
Cundiff, S. T. – MC2
Cunningham, J. E. – MB3, MB5, WC3, WD2

Dagli, Nadir – MA3
Damen, T. C. – WD1
Dawson, Martin D. – MC4
Dawson, P. – WA5
Delfyett, P. J. – TuC4
Deveaud, B. – TuC2, WD3
Ding, J. – MA2, TuC3
Ding, Y. J. – MD6
Divino, M. – TuD8

Eccleston, R. – WD4
Eisenstein, G. – WB1

Feldman, Robert D. – WB4, MC5
Feldmann, J. – WA1
Figueroa, L. – TuD12
Fox, A. M. – MB3, WC3
Foxon, C. T. – WA5
Friberg, S. R. – WB3
Fritze, M. – TuB1
Fu, W. S. – TuC5, WA4
Fujiwara, K. – TuC2
Fukuzawa, T. – MA4
Furdyna, J. – MA2, TuC3

Göbel, Ernst – WA1, WD1
Galbraith, I. – WA5
Garmire, Elsa – WA6
Gedalyahu, Y. – WC4
George, Thomas F. – TuD7
Glass, Alastair M. – WB4
Goossen, K. W. – MB3, MB5
Guo, C. L. – MD6
Gurvitz, S. – WD3
Gustafson, T. K. – TuD8

Hanatani, Shoichi – MD1, WB5
Harris, James S., Jr. – MB4, TuC5, WB
Hasenberg, Tom C. – MC4, WA6
Heitmann, D. – MA1
Honda, Y. – TuA5
Hong, C. S. – TuD12
Hooft, G. W. 't – WB2
Horowicz, Ricardo – TuA1
Huang, X. R. – MC4
Hulin, Danièle – MD5
Hutchings, D. C. – TuD5

Iga, K. – TuD9
Inoue, Hiroaki – MD1
Ishida, Koji – MD1, WB5
Ishihara, T. – TuC3
Iwamura, H. – WB3

Jan, W. Y. – MB3, MB5, WC3
Jeon, H. – TuC3
Jiang, M. – MC2
Jiang, W. B. – WB3
Johnson, A. M. – MC5
Johnson, Bart C. – MD4
Jones, K. L. – TuD8
Jonsson, Bjorn – WC2

Köhler, Klaus – WD1, WD4
Kalt, H. – TuB5
Kaplan, A. E. – MD6
Kasahara, K. – TuA4
Kash, J. A. – WA2
Keller, U. – WB2
Kern, K. – TuB2
Khurgin, J. B. – MD6, TuD4
Klem, J. F. – WA4, TuC5
Knox, W. H. – TuB3, WB2
Kobayashi, Takayoshi – TuD11
Koch, S. W. – TuC5, WA4

Koren, U. – WB1
Kosaka, H. – TuA4
Kost, Alan – WA6
Kovac, J. – TuD1
Koyama, F. – TuD9
Kroemer, H. – WA3
Kuhl, J. – WD4
Kurokawa, Takashi – MB2

Lösch, R. – TuD1
Lacalta, Andrea – WB6
Larsson, Anders – WC2
Laurich, B. K. – WA3
Law, C. T. – MD6
Law, K. -K. – MD6
Lawandy, N. M. – TuD13
Lee, D. – MC5
Lehr, G. – TuD2
Lentine, A. L. – MB3
Leo, Karl – WD1
Li, S. – MD6
LiKam Wa, P. – TuD5
Livescu, G. – WC3
Luo, H. – MA2, TuC3

Maan, J. C. – TuB2, TuB5
MacDonald, R. L. – TuD13
Machida, Susumu – TuA1
Malik, Roger J. – WB6
Masselink, W. T. – WA2
Matsuo, Shinji – MB2
Mayer, G. – TuD2
McCallum, D. S. – MC4
Meaton, C. – TuD12
Meier, H. P. – TuD2
Mendez, Emilio – MB
Merkt, Ulrich – MC1
Miller, A. – TuD5
Miller, D. A. B. – MB3, WA, WC3
Miyamoto, T. – TuD9
Morgan, R. A. – MB5
Morin, S. – TuC2
Moseley, A. J. – TuD12

Nakamura Hitoshi – WB5
Nickel, H. – TuD1
Nicklin, R. – TuD12
Nishioka, M. – TuA2
Nomura, Shintaro – TuD11
Notsu, Chiaki – WB5
Numai, T. – TuA4
Nurmikko, A. V. – MA2, TuB1, TuC3, WC
Nuss, Martin C. – WD2

Ochi, N. – TuA5
Ogura, I. – TuA4
Ohtoshi, T. – TuD6
Olbright, G. R. – TuC5, WA4
Olson, Don. H. – WB4
Owyoung, A. – WA4

Pandey, Lakshmi N. – TuD7
Park, C. B. – TuD5
Parry, G. – TuD10
Partovi, Afshin – WB4
Pastalan, John Z. – MD4
Paul, A. – TuC5
Paye, Jérome – MD5
Pelekanos, N. – MA2
Pezeshki, Bardia – MB4
Ploog, K. – TuB2, TuB5
Poirier, G. E. – TuC5
Potemski, M. – TuB2, TuB5

Ralph, Stephen E. – WB6
Raybon, G. – WB1
Regreny, A. – WD3
Richardson, Wayne H. – TuA1
Rivers, A. – TuD10
Robbins, D. J. – TuD12
Roberts, J. S. – TuD10
Roskos, Harmut – WD2

Samarth, N. – MA2, TuC3
Sano, Hirohisa – MD1
Sargood, S. – MD2
Sauer, Nicholas J. – MD4, TuD8
Schäfer, Wilfried – WD1
Schlapp, W. – TuD1
Schmitt-Rink, Stefan – TuB3, WD1
Schweizer, H. – TuD1, TuD2
Sela, I. – WA3
Shah, Jagdeep – WD1, WD2
Shiotani, T. – TuA5
Silberberg, Y. – TuC4
Simes, Robert J. – MB1
Sivco, D. L. – MD3, WC1, WC4
Sizer, Theodore, II – MD3
Smirl, Arthur L. – MC4
Smith, D. L. – WA3
Soliner, Gerhard – WD
Stark, J. B. – TuB3
Steel, Duncan G. – MC2, TuA
Stellato, J. – MD6
Stevens, P. J. – TuD10
Stockman, Mark I. – TuD7
Strobel, R. – WD4
Subbanna, S. – WA3
Sucha, G. – WB1
Suemune, I. – TuA5
Sugimoto, M. – TuA4

Tanaka, Shigehisa – MD1, WB5
Taylor, G. W. – MD2
Tell, Ben – WD2
Thomas, Dominique – MB4

Uchida, T. – TuD9
Uchida, Toshi K. – TuD9

Valley, George – WA6
Valster, Ad – TuC1
Vang, T. – MD2

Wang, Hailin – MC2
Watkins, D. E. – WA3
Webb, M. D. – MC2
Wegener, M. – WB1
Weiss, S. – WB1
Westin, Johan – WC2
White, Jeff – WA6
Whitehead, M. – TuD10
Wiesenfeld, J. M. – WB1
Wood, Thomas H. – MD4
Woodward, T. K. – MD3, WB2, WC1, WC4

Yacoby, A. – WC4
Yamamoto, Yoshihisa – TuA1, TuA3, WB3
Yamanishi, Masamichi – TuA3, TuA5, TuB, TuD6
Yamauchi, T. – TuA2
Yan, Ran-Hong – MB1
Yi, Jong Chang – MA3
Yokouchi, N. – TuD9

Zachau, M. – WA2
Zhang, Y. H. – TuB2
Zimmerman, R. – MC, TuB4
Zouganeli, P. – TuD10
Zucker, J. E. – TuD8, MC5
Zydzik, George J. – WB4

92-22414 AD-P007 885

Strong Photo-Optic Effects in Periodically δ-Doped InGaAs/GaAs Multiple Quantum Well Structures

A. Larsson and J. Maserjian
Center for Space Microelectronics Technology
Jet Propulsion Laboratory / California Institute of Technology
4800 Oak Grove Drive, Pasadena, CA 91109

1. Introduction

Semiconductor materials exhibiting strong photo-optic effects are attractive for devices intended for parallel all-optical computing and signal processing [1]. The use of quantum well (QW) structures in combination with periodic doping has provided large changes in the optical absorption and refractive index with weak excitation intensities [2-7]. The periodic doping spatially separates photogenerated electrons and holes leading to long recombination lifetimes and consequently large free carrier concentrations [8]. Depending on the structure design, these free carriers can be used for exciton quenching and band filling [2-4] or Stark shifts of the excitonic resonance in the QWs [2,5-7].

For array devices, operating with the light incident normal to the surface of the wafer, strong effects per unit length of the epitaxial material are desired to limit the total thickness of the structure to reasonable values. Periodically doped structures with short periods are therefore needed. However, as the thickness of the doped layers approaches the mean distance between the dopants, fluctuations in the modulation depth of the conduction and valence band potentials occur which reduces the carrier lifetimes. Here we show that strong photo-optic effects can be achieved in short period structures through the use of periodic δ-doping. By localizing the dopants in planes the statistical spread of the doping atoms is reduced leading to a deeper and more uniform modulation of the conduction and valence band potentials [9]. This reduces the probability for tunneling as well as for thermally assisted recombination.

2. Principals of operation

The energy band diagrams of the periodically δ-doped InGaAs/GaAs MQW structures under consideration are shown in fig.1. The sample in fig.1a., denoted sample A, is designed for optically induced absorption modulation through exciton quenching and band filling by placing the QWs in the conduction band minima of the periodically doped structure. Photogenerated electrons thermalize rapidly into the lowest subband of the QWs while the holes escape into the p-δ-doped GaAs layers

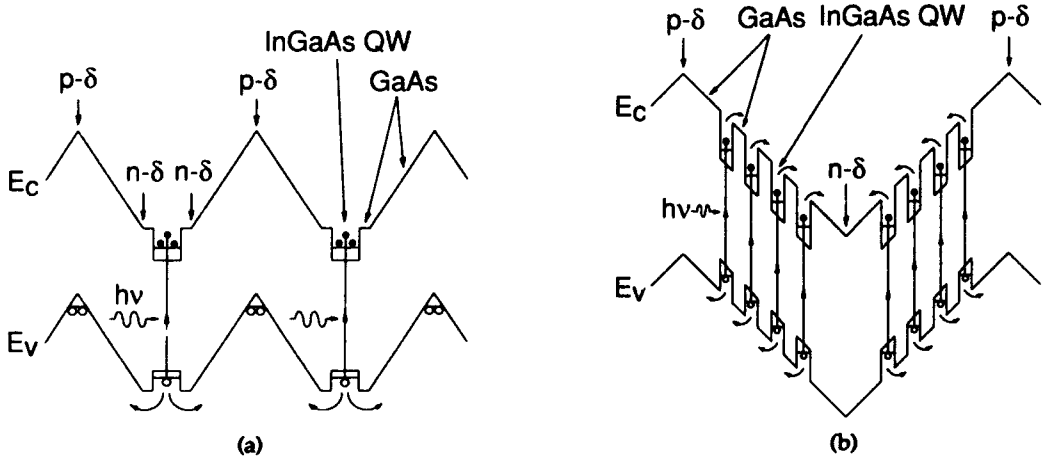


Fig.1. Energy band diagrams of (a) sample A and (b) sample B.

through thermal excitation over the barriers. The excess electron density in the QWs modulates the near band edge absorption through exciton quenching and band filling.

The sample in fig.1b., denoted sample B, is designed for optically induced excitonic electroabsorption by placing the QWs in the electric field regions between the doping planes. At thermal equilibrium, the internal electric fields produced by the periodic δ-doping shift the excitonic resonance of the QWs to longer wavelengths through the quantum confined Stark effect [10]. Under optical excitation, photogenerated electrons and holes escape the QWs through thermal excitation over the barriers and are spatially separated by the internal fields into the n and p-doping planes, respectively. This reduces the internal space charge fields, thus shifting the excitonic resonance to shorter wavelengths and resulting in large changes in the QW optical absorption near the band edge.

In both samples, the spatial separation of the photogenerated carriers increases the recombination lifetime, allowing strong effects with low optical excitation intensities. Excitation below the GaAs bandgap but above the fundamental bandgap of the QWs ensures uniform excitation throughout the structures. In addition, the use of an InGaAs/GaAs MQW structure allow the optical signals to be coupled through the transparent GaAs substrate.

3. Fabrication

The two structures in fig.1 were grown by molecular beam epitaxy on undoped GaAs (100). Sample A consists of 44 $In_{0.20}Ga_{0.80}As$ QWs, each 65 Å thick, separated by 780 Å thick GaAs barriers. In the center of each GaAs barrier a Be-doping plane with a sheet concentration of 9.0 10^{12} cm^{-2} was inserted. On both sides of each QW, using 100 Å spacer layers, Si-doping planes with a sheet concentration of 3.0 10^{12} cm^{-2} were inserted. In sample B, the distance between the doping planes is 1000 Å and the sheet doping concentrations are 6.0 10^{12} cm^{-2} in both planes. Four $In_{0.23}Ga_{0.77}As$ QWs, each 65 Å thick, separated by 100 Å thick GaAs barriers were centered between each pair of doping planes. The structure consists of six periods. Both structures were capped with 1000 Å GaAs.

4. Measurements

Room temperature absorption spectra were recorded using a monochromatic light source with 1 nm resolution as a tunable narrow band probe signal. The probe signal was focused on samples with an area of 0.1 cm^2 and the power of the probe beam was kept below 100 nW. A strained layer InGaAs/AlGaAs single quantum well laser with an emission wavelength of 925 nm was used to pump the sample for absorption modulation measurements. The long carrier lifetimes (in the ms-range) and the large associated lateral carrier diffusion lengths ensure uniform carrier densities over the entire sample [4,7].

5. Results

Absorption spectra of the periodically δ-doped samples, with and without optical excitation, are shown in fig.2. In sample A (fig.2a), strong absorption modulation is achieved at the excitonic resonance. A maximum change in QW absorption of 9000 cm^{-1} was measured with an excitation intensity of 100 mW/cm^2 (the lowest curve in fig.2a) which corresponds to a differential QW absorption change of 58%. The spectral QW absorption changes for the various excitation levels are shown in fig.3. We have also calculated the associated change in QW refractive index from the QW absorption change data using the Kramers-Kronig relation. The results from these calculations are shown in fig.4. For sample A (fig.4a), a maximum change in the refractive index as high as 0.07 is achieved close to the excitonic resonance and a value of 0.03 just below the bandgap were the material is transparent.

In sample B, a clear shift of the excitonic resonance to shorter wavelengths is seen with increased excitation (fig.2b). With an excitation intensity of 10 mW/cm^2 we have measured a maximum QW absorption change of 7000 cm^{-1} (fig.3b), corresponding to a differential QW absorption change as high as 80%. A maximum QW refractive index change of 0.04 is achieved close to the excitonic resonance (fig.4b).

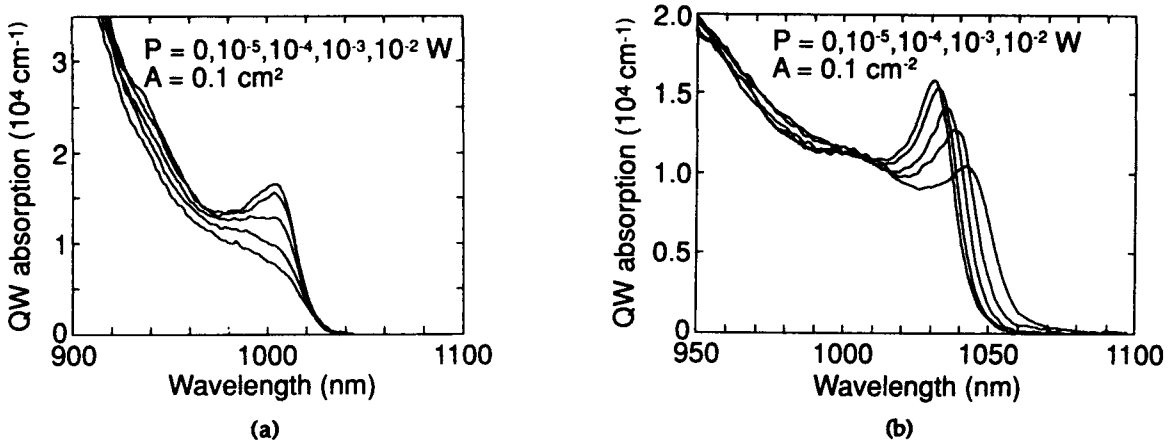


Fig.2. Optical QW absorption spectra of (a) sample A and (b) sample B recorded with various excitation intensities.

6. Discussion

In sample A, the absorption modulation is mainly due to exciton quenching through screening of the Coulomb interaction by the photogenerated electrons. We find an essentially logarithmic dependence of the optically induced carrier density on the excitation intensity. This is a consequence of the excitation dependent lifetime of the spatially separated carriers in the periodically doped structure. The measured absorption modulation is more than an order of magnitude higher than that achievable in conventional doping superlattices with similar excitation intensities [11]. However, the reduction in carrier lifetime with excitation intensity limits the attainable carrier density leading to an incomplete quenching of the excitonic resonance. The relatively high residual absorption would translate into a high insertion loss in an optical modulator.

In sample B, the observed behavior of the optical QW absorption is consistent with an optically induced excitonic electroabsorption [10]. From the logarithmic dependence of the photogenerated carrier density on excitation intensity and the quadratic dependence of the Stark shift on the electric field [10] combined with the linear dependence of the electric field on carrier density we expect the optically induced excitonic electroabsorption to saturate with increasing pump intensity, consistent with the observed behavior (fig.2b). The measured saturation pump intensity is about 100 mW/cm^2. To

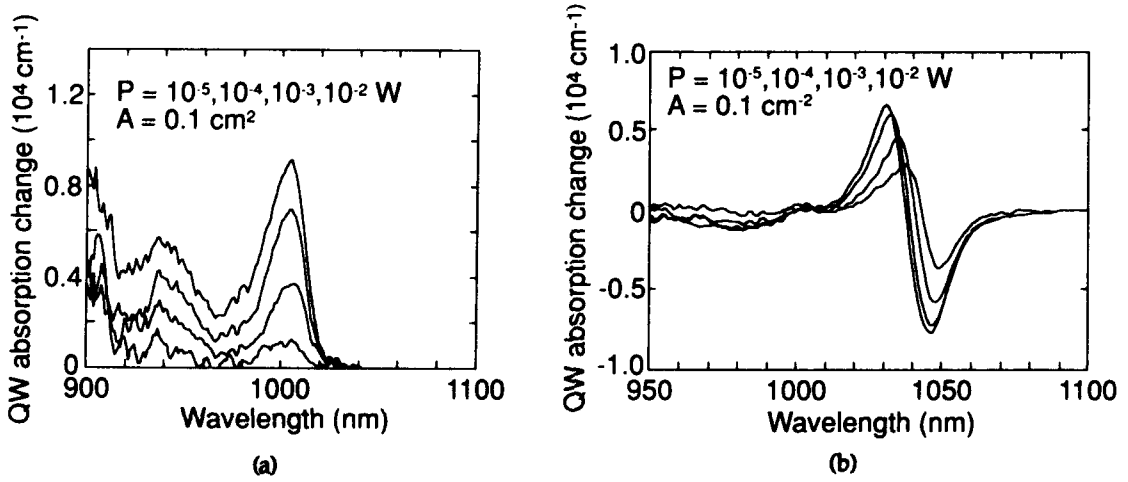


Fig.3. Spectral QW absorption change calculated from the results in fig.2. (a) Sample A, (b) Sample B.

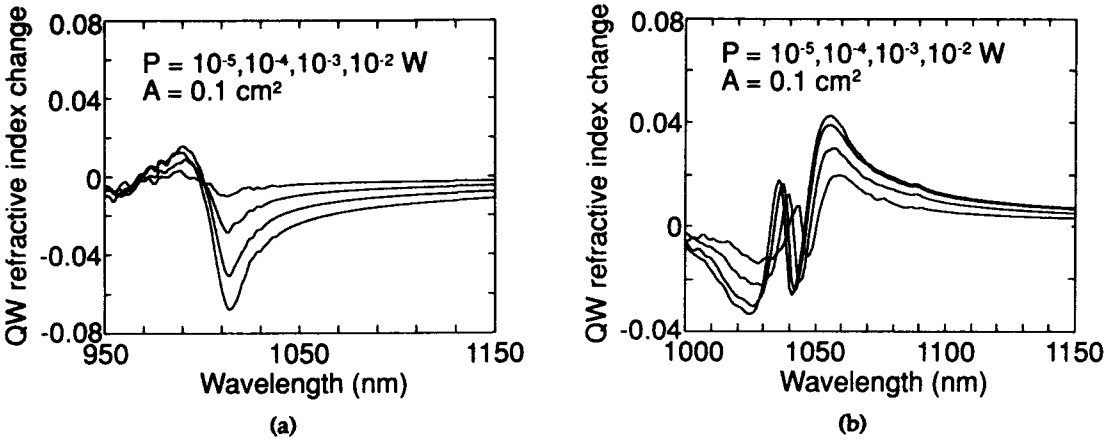


Fig.4. Spectral QW refractive index change calculated from fig.3. (a) Sample A, (b) Sample B.

achieve large changes in the optical QW absorption the structure has to operate in the high field regime because of the quadratic dependence of the shift of the excitonic resonance on the electric field. This implies a short distance (~1000 Å) between the n and p-doping planes. The use of δ-doping allows this to be achieved while maintaining a large number of QWs and consequently strong effects per unit length of the epitaxial material. The changes in QW absorption reported here are about a factor of two higher than those previously reported using conventional homogeneous doping and similar excitation intensities [7]. It is more than an order of magnitude higher than that measured in conventional doping superlattices (without QWs) utilizing the Franz-Keldysh effect alone [11]. Compared to sample A, this structure provides considerably lower residual absorption at the saturation pumping intensity and is therefore more suitable for optical modulators based on absorption modulation.

7. Conclusion

In conclusion, we have fabricated periodically δ-doped InGaAs/GaAs MQW structures which exhibit strong photo-optic effects for excitation levels compatible with low power semiconductor lasers. This material is promising for parallel all-optical computing and signal processing.

8. Acknowledgment

The research described in this paper was performed by the Center for Space Microelectronics Technology, Jet Propulsion Laboratory, California Institute of Technology, and was sponsored by the Strategic Defense Initiative Organization, Innovative Science and Technology Office, through an agreement with the National Aeronautics and Space Administration.

9. References

1. A.R. Tanguay, Jr., Opt. Eng. 24, 2, 1985.
2. J. Maserjian, P.O. Andersson, B.R. Hancock, J.M. Ianelli, S.T. Eng, F.J. Grunthaner, K.K. Law, P.O. Holtz, R.J. Simes, L.A. Coldren, A.C. Gossard, and J.L. Merz, Appl. Opt. 28, 4801, 1989.
3. G.H. Dohler, J.N. Miller, R.A. Street, and P.P. Ruden, Surface Sci. 174, 240, 1986.
4. J.M. Ianelli, J. Maserjian, B.R. Hancock, P.O. Andersson, and F.J. Grunthaner, Appl. Phys. Lett. 54, 301, 1989.
5. A. Kost, E. Garmire, A. Danner, and P.D. Dapkus, Appl. Phys. Lett. 52, 637, 1988.
6. K.K. Law, J. Maserjian, R.J. Simes, L.A. Coldren, A.C. Gossard, and J.L. Merz, Opt. Lett. 14, 230, 1989.
7. H. Ando, H. Iwamura, H. Oohashi, and H. Kanbe, IEEE J. Quantum Electron. 25, 2135, 1989.
8. G.H. Dohler, IEEE J. Quantum Electron. 22, 1682, 1986.
9. E.F. Shubert, Surface Sci. 228, 240, 1990.
10. D.A.B. Miller, D.S. Chemla, T.C. Damen, A.C. Gossard, W. Wiegmann, T.H. Wood, and C.A. Burrus, Phys. Rev. B 32, 1043, 1985.
11. A.D. Danner, P.D. Dapkus, A. Kost, and E. Garmire, J. Appl. Phys. 64, 5206, 1988.

AD-P007 886

NORMALLY-ON AND NORMALLY-OFF ASYMMETRIC FABRY-PEROT REFLECTION MODULATORS PRODUCED BY IMPURITY FREE DISORDERING

M.GHISONI and G.PARRY,
Department of Electronic and Electrical Engineering, University of London IRC for Semiconductor Materials, University College London, London WC1E 7JE, United Kingdom

M.PATE, G.HILL and J.S.ROBERTS
Department of Electronic and Electrical Engineering, University of Sheffield, Sheffield S1 3JD, U.K.

Abstract:- We demonstrate that controllable intermixing of GaAs/AlGaAs multiple quantum well stuctures can be applied to the post-growth production of normal incidence devices.

Introduction

In this paper we demonstrate, for the first time, that impurity free vacancy diffusion (IFVD)[1,2] can be applied to the post-growth fabrication of normal incidence devices, specifically asymmetric Fabry-Perot reflection modulators (AFPM)[3,4] made from GaAs/AlGaAs multiple quantum well (MQW) material. From the same wafer we have successfully produced both normally-off[5] and normally-on[3] devices, by achieving blue shifts of up to 52meV (30nm) and maintaining clearly resolved heavy and light hole excitons. The results are significant for optoelectronic integrated circuit (OEIC) applications, where monolithic integration of devices performing different functions will be required.

IFVD is distinct from impurity induced layer disordering (IILD) where recent work has focussed on providing lateral control over the optoelectronic properties, by spatially selective intermixing of the MQW region. Here impurities are diffused or implanted selectively into the MQW structure to enhance intermixing on subsequent annealing at elevated temperatures. It has proved possible, using the resulting blue shift of the absorption edge and the associated change in refractive index, to use the technique to provide lateral confinement in laser structures[6] and to fabricate passive waveguide sections.[7] IFVD can also produce enhanced intermixing of the well/barrier interface but has considerable advantages over IILD, since it is possible to produce a blue shift of the bandedge while still retaining both clearly resolved room temperature excitons and the quantum confined Stark effect (QCSE).[8] The technique uses native gallium vacancies, produced using a dielectric encapsulant, instead of the impurities used in IILD. Attention has so far focussed on its application to planar waveguide configurations[9], in this paper we focus on its use for normal incidence devices.

Experiment

The structure was originally designed for operation as a normally-off AFPM at a wavelength of 862nm. In this operating mode the hh exciton coincides with the FP resonance at zero bias, causing absorption in the cavity and a minimum in the reflected signal. As a field is applied the exciton moves out of the resonance, resulting in a drop in absorption and an increase in reflectivity. Thus both the well width and the cavity thickness are calculated to coincide in wavelength so that this should occur. The wafer was grown as a p-i-n structure by metallo-organic chemical vapour deposition (MOCVD) on a semi-insulating GaAs substrate. The layers were grown as follows ; a 2μm p^+ doped GaAs buffer layer, followed by a p^+ doped 15 period Bragg reflector stack consisting of alternating 609Å $Al_{0.1}Ga_{0.9}As$ and 723Å AlAs layers. The stack was grown to provide the back mirror of the FP cavity, and gave reflectivities of >95%. The top layer of the stack (AlGaAs layer) was left nominally intrinsic. On top of the stack was grown the MQW region which consisted of thirty 150Å GaAs wells seperated by 60Å $Al_{0.3}Ga_{0.7}As$ barriers, the MQW region was nominally intrinsic. A 1.08μm n^+ $Al_{0.3}Ga_{0.7}As$ layer was then grown, the structure was completed with a 50Å p^+ GaAs capping layer for contact purposes. The air\semiconductor interface provided the top mirror, with a reflectivity of ≈30%.

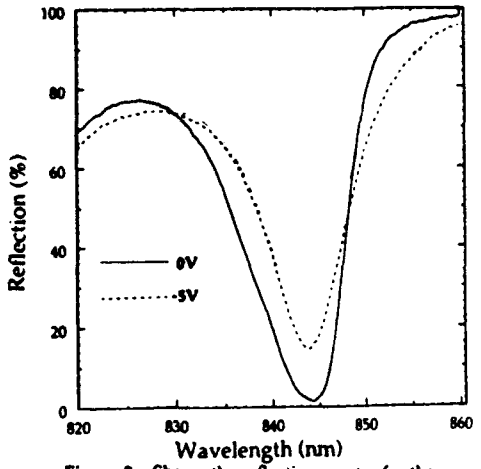


Figure 2 :- Shows the reflection spectra for the sample annealed at 930°C for 120s for different biases. We can clearly see that the heavy hole has been blue-shifted by 31meV into the resonance to enable normally-off operation of the device.

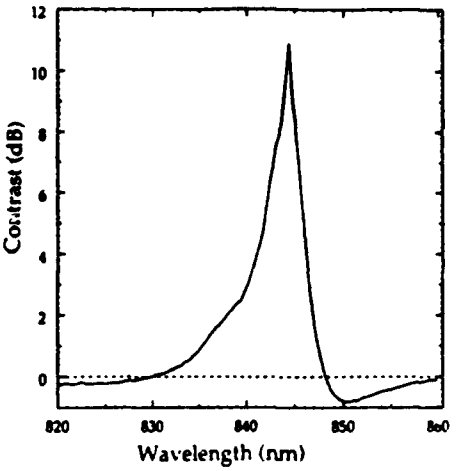


Figure 3 :- Displayed is the reflection contrast in dB of the normally-off device in Fig.2, for a voltage swing of 0V to -5V.

Figure 4 shows the photocurrent spectra of the sample annealed for 180s, for a variety of reverse biases. This displays some extremely clear features, especially resolvable, in the 0V spectra, are the heavy and light hole excitons. The hh exciton is situated at 832nm, and has thus been blue shifted by 52meV (30nm) from its original position. This is to our knowledge the largest reported blue shift where a heavy and light hole have still been clearly resolvable. In Fig.4 we can also see the FP resonance position at ≈847nm. As we apply a reverse bias the exciton is again red shifted, this time into the resonance. This results in an increase in absorption and hence a rapid increase in photocurrent, as can clearly be seen. The effect this has on the reflection spectra is shown in Fig.5. In the 0V spectra we can clearly see the hh exciton at 832nm and the FP resonance at 847nm. As a bias is applied, and the exciton red shifts, the increase in absorption at the resonant wavelength results in a drop in reflectivity from 79% to 48% for -8V. Such a reflectivity change from high to low, due to the electroabsorptive changes within the cavity, is characteristic of a normally-on AFPM. Thus we have successfully produced, from the same wafer, AFPM devices with distinctly different operating characteristics. For a normally-on device, one would expect the reflectivity to drop to near zero on application of a field. This does not occur here, because the structure was designed for normally-off operation. Hence the number of wells in the MQW region do not provide the absorption required to enable the reflectivity to drop to near zero when operating in a normally-on mode. With proper design modification, however, this could be rectified, so that the structure could operate as both an as-grown normally-off AFPM, and after intermixing could then be operated with equal efficiency in the normally-on mode.

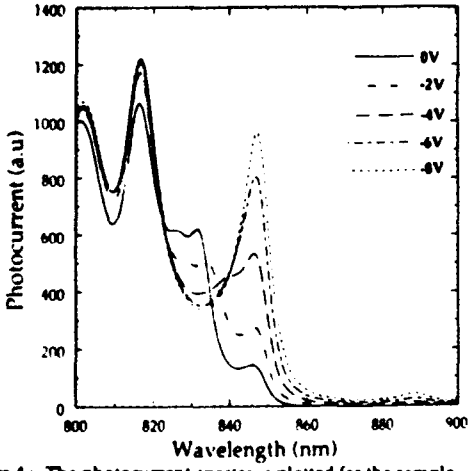


Figure 4 :- The photocurrent spectra is plotted for the sample annealed at 930°C for 180s. The heavy and light hole can both be resolved at 832nm and 827nm respectively. This means the heavy hole has been blue shifted by 52meV.

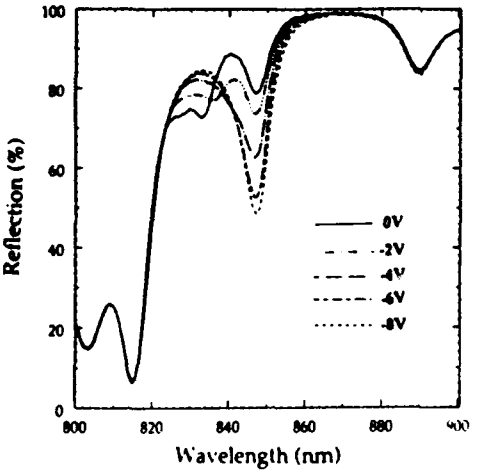


Figure 5 :- This shows the reflectivity spectra for the device of Fig 4. We can clearly see, that as a bias is applied it behaves as a normally-on AFPM.

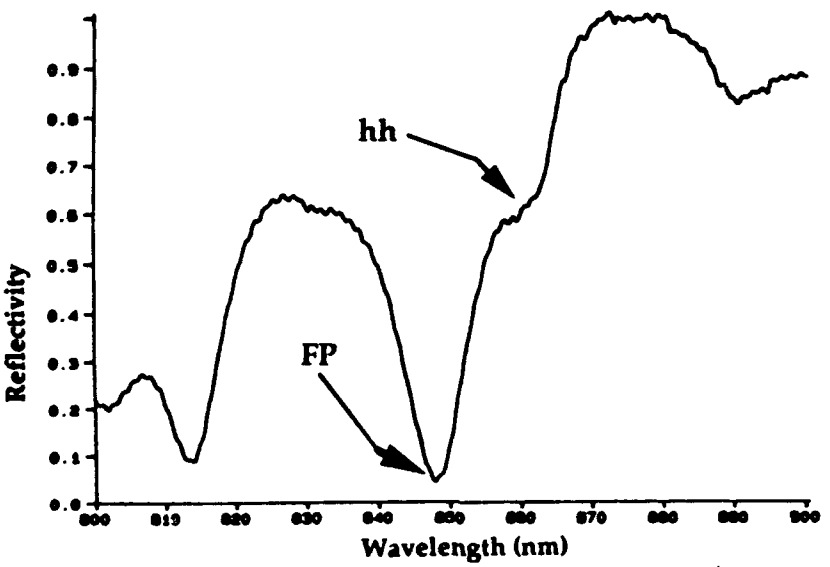


Figure 1 :- This shows a typical 0V reflection spectra for the original wafer. The heavy hole (hh) exciton is at 862nm while the Fabry-Perot resonance has clearly been misplaced to 848nm. Thus the hh is to the wrong side to permit modulation.

After growth the real time reflection spectra of the wafer was mapped using an EG & G optical spectrometer. The hh position proved to be uniformly situated at 862nm across the wafer. However the FP resonance position, though fairly uniform, was unfortunately to the short wavelength side of the desired value. This is due to its sensitivity to the thickness of the cavity. Figure 1 shows a typical reflection spectra from the wafer. The hh position can clearly be seen at 862nm as can the misplaced FP resonance at 848nm. Thus it was decided to utilise the IFVD technique to blue shift the excitonic position in order that it should coincide with the resonance.

A 3500Å layer of SiO_2 was deposited on the surface of the structure using plasma enhanced chemical vapour deposition. Rapid thermal annealing at 930°C was carried out using an AST SHS100_MA rapid thermal processor, with the temperature determined via a fast extended range pyrometer, on samples for times of 120s and 180s respectively. The samples, having had the SiO_2 removed with hydrofluoric acid, were then fabricated into standard photodiodes by mesa etching. Room temperature photocurrent and reflection spectra were obtained, using a 0.25m monochromator with automated lock-in detection.

Results

Figure 2 shows the reflection spectra (normalised to freshly deposited gold film) for the 120s annealed sample for biases of 0V, -5V and -10V. As can be seen from the 0V spectra the hh exciton and the FP resonance now coincide at ≈844nm. Thus the heavy hole has been blue shifted by 31meV (18nm) from its original position. The shift is attributed to the out-diffusion of gallium atoms into the SiO_2 encapsulant, which creates group III vacancies at the surface. These then diffuse through the structure and on reaching the MQW enhance the intermixing of the well\barrier interface. Essentially aluminium diffuses from the barrier into the well resulting in a change of profile from a square to an error function shape.1 This gives rise to an increase in the confined energy levels of the electron and holes and hence an increase in the transition energy, ie. a blue shift. From Fig.2, we can see that the shifting of the excitonic absorption to the resonant wavelength results in a reflectivity of ≈1% at 0V. As the bias is increased the exciton, due to the QCSE, red shifts out of the resonance, whereupon the absorption drops and hence the reflectivity increases. Thus we have produced a normally-off AFPM device.

In Fig.3 we have plotted the contrast in dB for a voltage swing of 0V to -5V. The device exhibits a contrast ratio of >10dB, but has the penalty of a high insertion loss of ≈8dB. The latter is inherent to the structure as originally designed and is not associatedwith the interdiffusion process.

Conclusions

We have demonstrated that IFVD disordering can retain full excitonic and electrical characteristics while producing blue shifts of up to 52meV in AFPM MQW structures. By using these blue shifts we have shown that we can produce normally-off devices (10dB contrast for -5V) from areas of a wafer which were previously unusuable. Furthermore the production, from the same wafer, of a normally-on device (>30% reflection change for -8V), using IFVD, has also been demonstrated. In both cases the reflectivity of the back Bragg reflector stack appeared to be unchanged by the intermixing process.

The technique opens up possibilities for increased device yield from a wafer, and importantly, the monolithic integration of different reflection modulators to perform switching and logic functions in optical interconnection systems.

Acknowledgements

The authors wish to thank R.Grindle and P.Zouganeli for useful discussion on AFPM operation, and for the help provided by K.Lee and A.W.Rivers in device fabrication. This work was funded by the U.K Science and Engineering Research Council (SERC).

References

1) J. D. Ralston, S. O'Brien, G. W. Wicks and L. F. Eastman: Appl. Phys. Lett. 52 (1988) 1511.
2) M. Ghisoni, M. Gibson, A. Rivers, I. W. Boyd, G. Parry and J. S. Roberts: Electron. Lett. 26 (1990) 1058.
3) R. H. Yan, R. J. Simes and L. A. Coldren: IEEE Photon. Technol. Lett. 2 (1990) 118.
4) M. Whitehead, A. Rivers, G. Parry, J. S. Roberts and C. Button: Electron. Lett. 25 1989) 984.
5) M. Whitehead, A. Rivers, G. Parry and J. S. Roberts: Electron. Lett. 26 (1990) 1589.
6) R. L. Thornton, W. J. Mosby, R. M. Donaldson and T. L. Paoli: Appl. Phys. Lett. 56 (1990) 1623.
7) J. Werner, T. P. Lee, E. Kapon, E. Colas, N. G. Stoffel, S. A. Schwarz, C. L. Schwartz and N. Andreadakis: Appl. Phys. Lett. 57 (1990) 810.
8) D. A. B. Miller, D. S. Chemla, T. C. Damen, A. C. Gossard, W. Wiegmann, T. H. Wood and C. A. Burrus: Phys. Rev. B 32 (1985) 1043.
9) T. Miyazawa, T. Kagawa, H. Iwamura, O. Mikami and M. Naganuma: Appl. Phys. Lett. 55 (1989) 828.

AD-P007 887

LASING IN SUB-MICRON WIDE VERTICAL CAVITY MICROLASERS BY PICOSECOND OPTICAL PUMPING

J.L. Jewell[a], A. Scherer[b], B. Van der Gaag[b], S.L. McCall[c],

J.P. Harbison[b], L.T. Florez[b], and L.M. Schiavone[b]

(a) AT&T Bell Laboratories, Rm. 4G-520, Holmdel, NJ 07733 USA

(b) Bellcore, Red Bank, NJ 07701 USA

(c) AT&T Bell Laboratories, Murray Hill, NJ 07974 USA

92-22416

Microcavity lasers potentially will have ultra-low thresholds in the μA range or even lower [1-4]. We have begun to investigate lasing in GaAs/AlAs microresonators as small as ~0.4 μm wide (less than half the free-space wavelength) and in various rectangular shapes. The smallest devices, ~0.4X0.4 μm had the lowest threshold which was only 2 pJ *incident*. This low threshold, achieved despite ~10 ps carrier lifetimes, an estimated 5 % absorption efficiency in the cavity spacer, and probably low coupling efficiency of the pump beam, is encouraging for the long range development of microcavity lasers.

The design for the structure, grown by molecular beam epitaxy, is shown in Fig. 1. The spacer contains a single quantum well (SQW) of InGaAs designed to lase at ~960 nm wavelength. Small-diameter microresonators are known to exhibit size-dependent waveguide dispersion which blue-shifts the cavity resonances. Therefore the cavity was designed for a longer wavelength than that of the gain peak, and the thicknesses in the top and bottom mirrors were deliberately varied with the same gradient direction. This provided resonant wavelengths of about 1000 +/-50 nm which varied with position on the wafer. Both mirrors were designed for well over 99.9 % reflectivity, resulting in a 8-μm total thickness.

Various rectangular shapes were patterned onto a bilevel resist/mask using electron beam lithography with the dimensions indicated in Fig. 2. This provide square devices of width 1.5, 1.0, 0.7, 0.6, 0.5, 0.4, and 0.3 μm down the diagonal of the overall pattern, and rectangles of various apect ratios and orientations in the rest. Chemically assisted ion beam etching formed the microresonator structures [5]. To maximize the straightness of the sidewalls, the gas pressure and ion beam current were varied during the etch to compensate for unavoidable rising temperature. A scanning electron micrograph (SEM) of some microresonators is shown in Fig. 3. The SEM's revealed the actual device sizes to be about 0.1 μm wider than the lithographic pattern, thus the smallest device size is ~0.4X0.4 μm.

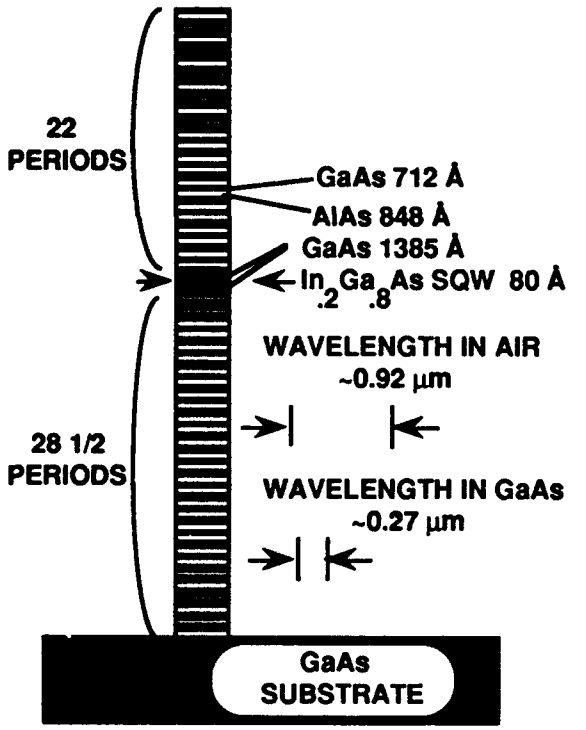


Fig. 1. Scale diagram of a 0.5 μm wide microresonator showing the MBE layer design.

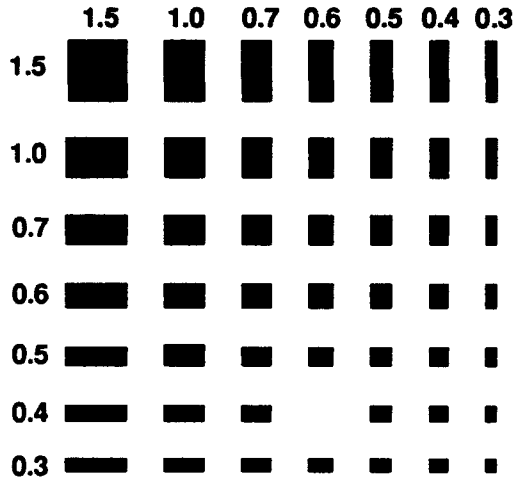


Fig. 2. Dimensions patterned by electron beam lithography. Actual device spacing was 3 μm center-to-center.



Fig. 3. SEM of the microresonators as seen from the corner with the smallest sizes.

Optical measurements were carried out using ~10 ps, 800 nm pump pulses and the same high-numerical-aperture focusing system we used previously [6] to investigate microresonator gates of ~0.5 μm diameter. Fig. 4 shows the setup with half-wave plates HW1, HW2, HW3, polarization beam splitters PBS1, PBS2, and the $SrTiO_3$ hemisphere HEMI. The hemisphere has a refractive index about 2.4 which, in conjunction with the LENS, allows us to focus the pump beam to a spot with a full width at half maximum of ~0.4 μm. Rotating HW2 revealed the polarization of the microlaser outputs. The spectrometer was an optical multichannel analyzer which displayed the output spectrum. An acousto-optic modulator (not shown) modulated the 82 MHz mode-locked pulse train in 250 ns envelopes with a 5 μs period (5% duty cycle) to reduce heating effects.

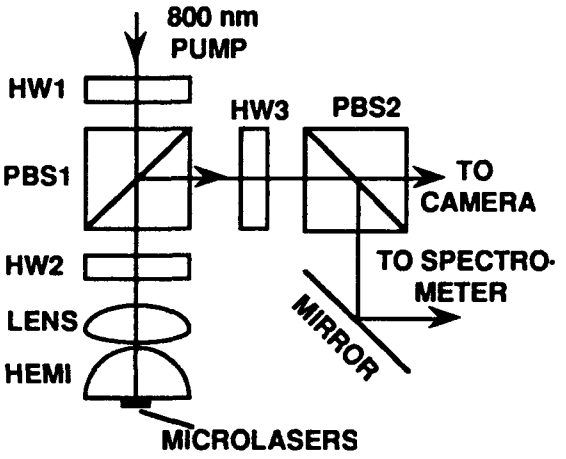


Fig. 4. Schematic of the experimental setup.

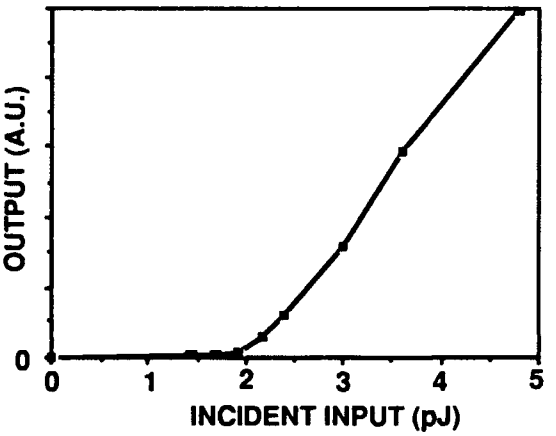


Fig. 5. Output at 865 nm vs. incident input energy for a 0.4X0.4 μm microlaser.

Large unetched regions of the wafer showed lasing in the 950-1002 nm region, and provided calibration of the local thicknesses. The etched devices always lased at shorter wavelengths, ranging from 850 to 965 nm. If in the etched devices, only the lowest order transverse mode were lasing, there would be a clear trend of smaller widths emitting at shorter wavelengths due to the waveguide dispersion. Although this trend was sometimes observed, more often even the largest devices (1.5 μm square) showed very large wavelength shifts, >100 nm, from the large area laser. Since the lasing wavelength was typically in the region of 880 nm, it is clearly due to the GaAs spacer material and a higher order mode. Laser emission in the 900-910 nm region in small devices make it difficult to interpret either the nature of the cavity mode or the active material responsible for the lasing. At this stage of the investigation we will not attempt to do so. Polarization was often observed in the outputs, sometimes along the long axis and sometimes along the short one. It appears that selection of a cavity mode whose resonance best matches the material gain is more important than slight differences in loss for the two polarizations. A few devices showed two emission lines of opposite

polarizations. For example a ~0.6X0.7 μm ("real" size) device emitted at 888 nm polarized along the long axis and at 899 nm along the short one.

The lowest threshold recorded was for the smallest device of our set, ~0.4X0.4 μm, and Fig. 5 shows its output/input characteristic. The threshold was 2 pJ with an emitted wavelength of 865 nm. Transition of the output from unpolarized below threshold to polarized above threshold verified that the device was indeed lasing. The fraction of pump light absorbed in the spacer region is estimated to be ~5% based on a constant 10^4 cm^{-1} absorption coefficient for the GaAs layers in the top mirror and the spacer. Based on more extensive determinations of the cavity absorption efficiency in a similar structure [4], we feel the estimate is accurate to within a factor less than two. This value yields an energy absorbed in the spacer is ~100 fJ, and the carrier density was ~10^{19} cm^{-3},or about 5 times the density required for transparency in GaAs. Since the coupling efficency into the microresonator should not be particularly high, the energy and carrier density should be even smaller. The expected carrier lifetime in such a small structure is ~10 ps based on our earlier gating experiments. Since the pump pulses are about 10 ps also, significant carrier reduction occured during the pumping pulse. Considering all these photon and carrier losses. it seems clear that the carrier density was not much above that required for transparency.

References

[1] E. Yablonovitch, T.J. Gmitter, and R. Bhatt, Phys. Rev. Lett. **61**, 2546 (1988).

[2] Y. Yamamoto, S. Machida, K. Igeto and Y. Horikoshi, Proc of the 6th Rochester Conf. on Coherence and Quantum Optics (ed. by J. H. Eberly, L. Mandel, and E. Wolf, Plenum Press, NY 1989) p. 1249.

[3] H. Yokoyama, S.D. Brorson, E.P. Ippen, K. Nishi and T. Anan, Proc. of IQEC 1990, p. 136 (1990).

[4] J.L. Jewell, K.F. Huang, K. Tai, Y.H. Lee, R.J. Fischer, S.L. McCall, and A.Y. Cho, Appl. Phys. Lett. **55**, 424 (1989).

[5] A. Scherer, J.L. Jewell, J.P. Harbison, L.T. Florez, Y.H. Lee, and C.J. Sandroff, Appl. Phys. Lett. **55**, 2724 (1989).

[6] J.L. Jewell, S.L. McCall, A. Scherer, H.H. Houh, N.A. Whitaker, A.C. Gossard, and J.H. English, Appl. Phys. Lett. **55**, 22 (1989).

AD-P007 888

FAST ESCAPE OF PHOTOCREATED CARRIERS OUT OF SHALLOW QUANTUM WELLS

J.Feldmann, K.W.Goossen, D.A.B.Miller, A.M.Fox[a], J.E.Cunningham, W.Y.Jan

AT&T Bell Laboratories
Crawfords Corner Road, Holmdel, NJ 07733

94-27411

Recently, strong and well-resolved excitons have been observed in the room-temperature absorption spectra of shallow GaAs/$Al_xGa_{1-x}As$ quantum wells for values of x as low as 0.02.[1] In addition, these shallow quantum wells exhibit strong electroabsorption at low electric fields applied perpendicular to the layers. This pronounced electroabsorption effect at low biases is caused by both the red-shift of the exciton as observed for deeper quantum wells[2] and the fact that the low $Al_xGa_{1-x}As$ barriers cannot prevent the field-ionization of the exciton,[1] hence giving field-induced broadening.

From a practical point of view, both strong electroabsorption and fast sweep-out of carriers from the quantum wells in the intrinsic region of the p-i-n structure are desirable, since the sweep-out rate is the key parameter to improve the switching speed of self electrooptic effect devices (SEED)[3]. It has been found that for deep ($x > 0.2$) quantum wells the carrier sweep-out rates increase with decreasing barrier height but decrease with decreasing electric field.[5,6] To improve the speed performance of SEEDs by using shallow quantum wells it is important to know how fast the carrier sweep-out becomes for small x-values at low electric fields.

In this paper, we demonstrate that at room-temperature the sweep-out times of photo-generated carriers out of the intrinsic shallow quantum well region of a p-i-n structure is as fast as for pure GaAs of the same thickness, if the Al-concentration in the barriers does not exceed 0.04. Even at forward-bias carriers are swept out with the saturated drift velocity of GaAs. Consequently, the switching speed of SEEDs could be increased by using shallow quantum wells. To understand the physical carrier escape mechanism out of the shallow quantum wells we have also performed temperature-dependent measurements of the escape times. The results are in agreement with a phonon-assisted tunneling model.[7] According to this model, the reason for the fast escape of carriers out of the shallow quantum wells is given by the fact that carriers can be efficiently scattered to unconfined continuum states by absorption of an LO-phonon, if the effective barrier height for the carriers is less than the LO-phonon energy.

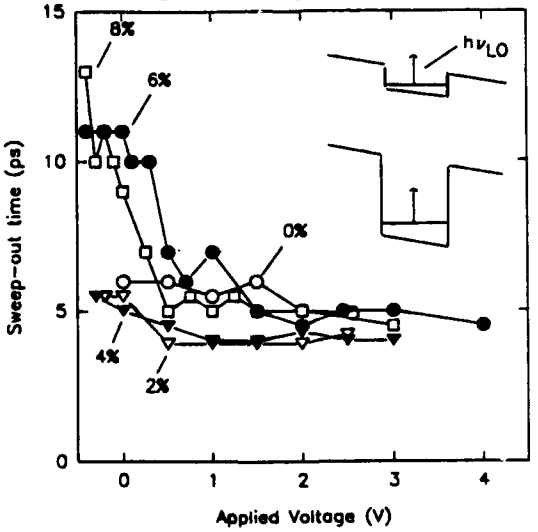


Fig.1: Experimentally determined sweep-out times versus applied reverse bias voltage for all 5 shallow quantum well samples at room-temperature. As an inset we schematically illustrate the situations when the effective barrier height is smaller or larger than the LO-phonon energy.

Four shallow GaAs/$Al_xGa_{1-x}As$ multiple quantum well samples with x = 0.02, 0.04, 0.06 and 0.08 were prepared by molecular beam epitaxy, each consisting of 50 periods of 10 nm GaAs quantum wells and 10 nm $Al_xGa_{1-x}As$ barriers. The multiple quantum well structure forms the intrinsic region of a p-i-n diode[8] so that the internal electric field can be controlled by applying a voltage to the diode. In addition, an x = 0 "shallow quantum well" sample was grown, i.e. the intrinsic region consists of pure GaAs having the same total thickness (1μm) as the x > 0 multiple quantum well structures. All samples were processed into 200 μm x 200 μm mesas and gold top contacts were deposited. The samples were mounted on sapphire and we removed the n^+ GaAs substrate by selective chemical etching for the optical transmission experiments.

To determine the sweep-out times we performed optical pump and probe experiments in transmission using laser pulses of about 0.7 ps duration at a repetition rate of 80 MHz. The laser photon energy is tuned to the lowest n = 1 heavy-hole exciton and the light intensity is set to create carrier densities of about $5 \cdot 10^9 cm^{-2}$ per pulse. For these low densities the nonlinear optical signal at positive time-delays is caused by the field-induced separation of photocreated electrons and holes partly screening the field within the intrinsic region of the p-i-n diode and thus changing the optical properties of the quantum well structure due to the electroabsorptive effect.[6,9,10] Within the accuracy of the experimental data a single exponential function $(1 - \exp\frac{-t}{\tau_{so}})$ can be fitted to the temporal rise of the nonlinear electroabsorptive signal. The experimentally determined values for the sweep-out times τ_{so} are shown in Fig.1 versus the applied reverse bias voltage for all 5 samples at room-temperature. First of all, Fig.1 shows that the sweep-out times for the sample with an intrinsic GaAs layer (x = 0) are virtually constant for the voltage range investigated and amount to about 5.5 ps. Assuming that on an average the carriers have to travel half of the total thickness of the intrinsic region in order to reach the contact layers we estimate the carrier drift velocity to be 10^7 cm/sec. This value corresponds to the saturated drift velocity of GaAs for electric fields larger than 10^4 V/cm.

In the case of the x > 0 shallow quantum wells we find the remarkable result that the carrier sweep-out rate for the x = 2% and x = 4% samples is still determined by the saturated drift velocity even at small forward bias voltages. This means that for these low $Al_xGa_{1-x}As$ barriers the carrier escape out of the shallow quantum wells is not a limiting factor for their sweep-out out of the intrinsic region. As can be seen in Fig.1, this statement does not hold for the x = 6% and x = 8% shallow quantum well samples, since their sweep-out times increase for lower applied voltages. We can conclude that shallow GaAs/$Al_xGa_{1-x}As$ quantum wells with $x \leq 4\%$ not only show strong electroabsorption but also have the shortest possible sweep-out times at low voltages and thus are well-suited to improve the speed of SEEDs.

We argue that at low electric fields the fast carrier escape out of shallow quantum wells with $x \leq 0.04$ is due to the fact that electrons in the conduction-band as well as holes in the valence-band are effectively scattered to unbound continuum states by absorption of an LO phonon. Since the effective barrier heights are definetely not larger than the LO phonon energy of 36 meV, continuum states with a pronounced probability of being in the well region become available as possible final states for the scattering of carriers out of the bound quantum well state. Once in these continuum states the carriers rapidly move away from the well region. This phonon-assisted tunneling model[7] can explain the fact that the sweep-out rates are limited by the saturated drift velocity even at low electric fields. In the case of deeper quantum wells the leakage of the continuum wavefunctions, which are available as final scattering states, into the quantum well is reduced leading to smaller matrix elements, i.e. longer scattering times. In accordance with our experimental findings shown in Fig.1 the low-field sweep-out times for deeper wells ($x \geq 0.06$) are limited not only by the transit time through the intrinsic region but also by the LO phonon scattering time. We thus find a simple qualitative explanation for the experimental fact that for low applied voltages the room-temperature sweep-out rate is extremely high as long as the Al-concentration does not exceed $x \approx 0.04$. As schematically illustrated in the inset of Fig.1, the sweep-out rate crucially depends on whether the effective barrier height is less or more than the LO phonon energy.

In order to verify our assumption of LO phonon assisted tunneling we investigated the temperature dependence of the carrier sweep-out rate for the temperature range from T = 10 K up to T = 295 K. In Fig.2,

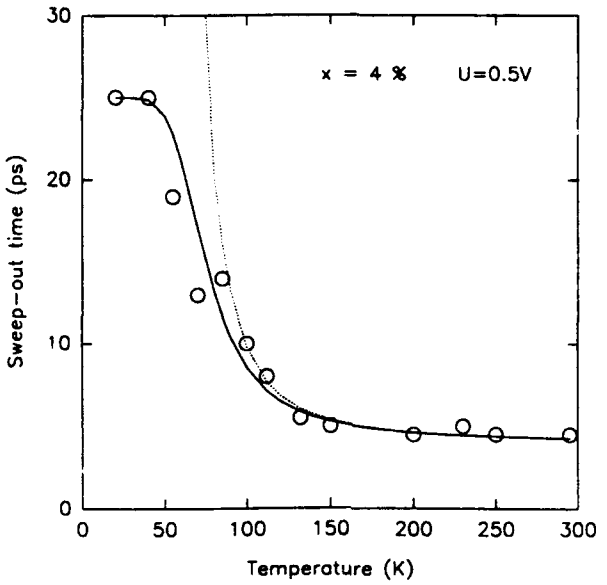


Fig.2: Temperature dependence of the sweep-out times for the x = 4% sample at an applied voltage of 0.5 Volt. The dotted and solid curves represent calculated sweep-out times τ_{so} according to our simple model (for details see text).

the experimentally determined time constants (circles) are shown versus the crystal temperature for the x = 0.04 shallow quantum well at U = 0.5 V. It is seen that for temperatures below 130 K the sweep-out time increases. At low voltages a decrease of the sweep-out rate with decreasing temperature is found for each x > 0 shallow quantum well structure. This definitely rules out the possibility that the fast room-temperature sweep-out times at low voltages are due to direct tunneling out of the quantum well, since the rate for direct tunneling should be independent of temperature. It is, however, reasonable to assume that the long sweep-out times at low temperature and low biases reflect the direct tunneling out of the shallow quantum wells.[6]

The dotted line in Fig.2 represents the result of a simple calculation. We assume that the sweep-out time τ_{so} is given by the sum of the time τ_{esc} it takes to escape out of the quantum wells and a constant transit time τ_{tr} to reach the contacts:

$$\tau_{so} = \tau_{esc} + \tau_{tr} \tag{1}$$

In a first approach, we merely consider scattering of carriers to the continuum states by absorption of an LO phonon as a possible escape mechanism:

$$\tau_{esc}^{-1} = \tau_{sc}^{-1} = \tau_0^{-1} \left[e^{\frac{h\nu_{LO}}{kT}} - 1 \right]^{-1} \tag{2}$$

It was recently reported[12] for a shallow quantum well structure with 3% depth that at zero electric field the excitons are ionized with a time-constant of about 0.3 ps leading to 3-dimensional carriers in the continuum states above the barrier. For our calculation the value for τ_0 is chosen to obtain an LO phonon scattering time τ_{sc} of 0.3 ps at T = 295 K ($h\nu_{LO}$ = 36 meV). Assuming a transit time τ_{tr} of 4 ps, which is in accordance with the saturated drift velocity, we end up with the dotted curve of Fig.2. For T > 100 K the experimental data are well described by Eq.(1) and (2) supporting our assumption that the fast room-temperature carrier escape mechanism out of shallow quantum wells is due to LO phonon assisted tunneling. Below 100 K the LO phonon scattering becomes very weak and a different escape mechanism dominates. Probably, direct tunneling of carriers out of the wells determines the sweep-out rate at low temperature. We can extend Eq.(2) by introducing a temperature independent escape time τ_{tun} as a fitting parameter:

$$\tau_{esc}^{-1} = \tau_{sc}^{-1} + \tau_{tun}^{-1} = \tau_0^{-1} \left[e^{\frac{h\nu_{LO}}{kT}} - 1 \right]^{-1} + \tau_{tun}^{-1} \quad (3)$$

For τ_{tun} = 21 ps the solid curve in Fig.2 is obtained for the sweep-out times τ_{so}, which is in very good agreement with the experimentally determined temperature dependence.

In summary, we have shown that the room-temperature low-field carrier escape out of the intrinsic $GaAs/Al_xGa_{1-x}As$ shallow quantum well region is as fast as for pure GaAs of the same thickness provided x does not exceed 0.04. This result has important implications for the improvement of the switching speeds of self electrooptic effect devices. In addition, we have demonstrated that an LO phonon-assisted tunneling model consistently explains our experimental findings. In conclusion, shallow quantum wells show strong electroabsorption and fastest possible sweep-out times at low reverse bias if the barrier heights for the carriers are less than the LO phonon energy.

We would like to thank W.H. Knox for helpful discussions.

(a) Present address: Clarendon Laboratory, Parks Road, Oxford OX1 3PU, UK

REFERENCES

[1] K.W.Goossen, J.E.Cunningham, and W.Y.Jan, Appl. Phys. Lett. **57**, 2582 (1990).

[2] D.A.B.Miller, D.S.Chemla, T.C.Damen, A.C.Gossard, W.Wiegmann, T.H.Wood, and C.A.Burrus, Phys. Rev. **B32** 1043 (1985).

[3] For a recent review see D.A.B.Miller, Optical and Quantum Electr. *22, 61 (1990).*

[4] G.D.Boyd, A.M.Fox, D.A.B.Miller, L.M.F.Chirovsky, L.A.D.'Asaro, J.M.Kuo, R.F.Kopf, and A.L.Lentine, Appl. Phys. Lett. **57**, 1843 (1990).

[5] A.M.Fox, D.A.B.Miller, G.Livescu, J.E.Cunningham, J.E.Henry, and W.Y.Jan, Appl. Phys. Lett. **57**, 2315 (1990).

[6] A.M.Fox, D.A.B.Miller, G.Livescu, J.E.Cunningham, and W.Y.Jan, submitted to IEEE J. Quantum Electron.

[7] M.G.Shorthose, J.F.Ryan, and A.Moseley, Sol. State Electr. **32**, 1449 (1989).

[8] The detailled sample design can be found in Ref.1.

[9] R.J.Manning, P.J.Bradley, A.Miller, J.S.Roberts, P.Mistry, and M.Pate, Electron. Lett. **24**, 854 (1988).

[10] G.Livescu, D.A.B.Miller, T.Sizer, D.J.Burrows, J.E.Cunningham, A.C.Gossard, and J.H.English, Appl. Phys. Lett. **54**, 748 (1989).

[11] A.Larsson, P.A.Andrekson, S.T.Eng, and A.Yariv, IEEE J. Quantum Electron. **QE-24**, 787 (1988).

[12] W.H.Knox, K.W.Goossen, G.E.Doran, D.A.B.Miller, J.Cunningham, and W.Y.Jan, submitted to CLEO, Baltimore 1991.

AD-P007 889

Femtosecond Time-Resolved Studies of High-Field Parallel Transport in GaAs Quantum Wells

W. Sha and T.B. Norris, *Ultrafast Science Laboratory, University of Michigan, 2200 Bonisteel, Ann Arbor, MI 48109-2099*
W.J. Schaff, *The School of Electrical Engineering, Cornell University, Ithaca, NY 14850*
K.E. Meyer, *Cavendish Laboratory, University of Cambridge, Cambridge, UK*

92-22418

I. INTRODUCTION

Ballistic transport of electrons in semiconductors has recently been a topic of great interest. These studies are important because ballistic transport is expected to play a role in the operation of a number of state-of-the-art semiconductor devices [1]. Ballistic drift in a field-free region of electrons launched across a heterojunction has been observed. In this paper we describe experiments that apply optical spectroscopy to time-resolve the distribution functions of electrons in the presence of a strong electric field applied in the plane of a MQW structure. The carriers are injected with zero initial kinetic energy by a short laser pulse. The exciton field-ionization, electron quasi-ballistic acceleration, field-induced heating, and real-space transfer of electrons into the barrier region of the MQW are observed by monitoring the carrier distribution function using femtosecond-pump continuum-probe techniques.

II. EXPERIMENT

The sample used for these experiments consists of 40 GaAs quantum wells of 50 Å width separated by 150 Å $Al_{0.3}Ga_{0.7}As$ barriers. The MQW structure is situated in the depletion region of a horizontal p-i-n diode, so that electric fields of up to 20 kV/cm can be applied in the plane of the wells. The separation between the p and n contacts is 50 μm.

The laser source used to perform the experiments produces 100-fs 620-nm pulses with 10 μJ energy at a 2-kHz repetition rate. These pulses are used to generate a white-light continuum, from which the pump (830 +/– 5 nm) and probe (varying over 840-680 nm) beams are selected. The pump beam is amplified to give up to 2 nJ incident on the sample. Dispersion in the probe beam was compensated by prisms so that the absorption spectrum could be obtained with sub-100-fs resolution. Differential spectra were acquired on an OMA (optical multichannel analyzer). A selection of the data is shown in Fig.1. All experiments were performed at room temperature.

II. RESULTS

The pump beam was tuned so that only n=1 heavy-hole excitons were generated. Thus the initial carrier distribution has an effective temperature of 0 K, with the chemical potential at the exciton energy [2]. The absorption spectrum in the spectral region of -20 to

+200 meV relative to the band edge was monitored, showing saturation of the n=1 heavy and light hole excitons due to both excitons and free carriers, and saturation of the band-to-band continuum transitions due to free carriers. The experimental absorption coefficients were fitted to these three components (heavy and light hole excitons and the continuum). While the electron distribution function is directly given by the differential transmission spectra for energies above the exciton transitions, the fitting procedure requires an assumption of the functional form of the distribution within 50 meV of the band edge. Thus we fitted the data assuming a Fermi-Dirac distribution near the band edge. Even with this assumption we found it was always possible to achieve a good fit to the data, which indicates that the distribution near the band edge is always thermal, and thus carrier-carrier scattering is very strong at these densities (2-3 x 10^{11} cm^{-2}). An example of the fitted absorption coefficient is shown in Fig.2. From the distribution functions we computed the average energy per carrier; this is shown in Fig. 4 for fields of 0 and 16 kV/cm.

With no electric field, the heavy-hole excitons ionize (due to phonon absorption) in about 300 fs, and the electron distribution heats up to room temperature in about 1.5ps. With a 16 kV/cm field, the exciton ionization occurs in approximately 50 fs. The electric field then rapidly accelerates the electrons to higher energy. The distribution functions are shown in Fig. 3. We observe that for a short time (about 150 fs) after the pump pulse, the absorption can be fitted well by a thermal distribution near the band edge, but at higher energies the distribution is nonthermal. The average energy per carrier shows a rapid rise to about 40 meV, which is approximately the energy expected for ballistic acceleration. (This corresponds to a maximum velocity of 4.5 x 10^7 cm/s, and a ballistic transport distance of 250 Å.) As the high energy tail disappears, only the remaining thermalized electrons remain near the band edge; these heat up to a temperature slightly above room temperature in about 0.5ps. The overshoot in the average energy per carrier is directly associated with the growth and disappearance of the nonthermal component of the distribution.

Finally, we have probed the absorption spectrum in the vicinity of the barrier band edge, and have observed the buildup of a population there. Thus we have time-resolved real-space transfer of electrons into the barrier (continuum) states.

REFERENCES

1. See, for example, J.R. Hayes and A.F.J. Levi, *IEEE J. Quantum Electron.* **QE-22**, 1744 (1986), and references therein.

2. W.H. Knox, *et al., Phys. Rev. Lett.* **54**, 1306 (1985).

ACKNOWLEDGEMENT

This work was supported by the AFOSR under grant URI-090-0214.

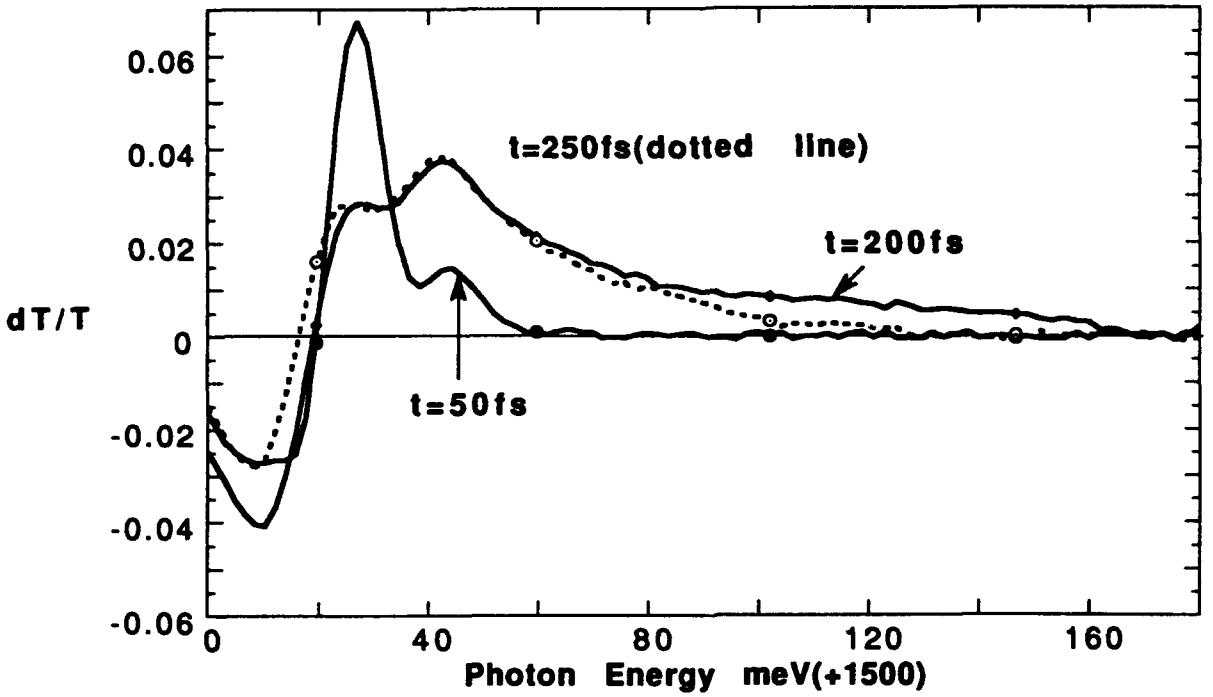


Fig.1 Differential transmission spectra, $(T_E-T)/T$ where T_E is transmissivity with E=16kV/cm, T iswithout the field. Pump is always on.

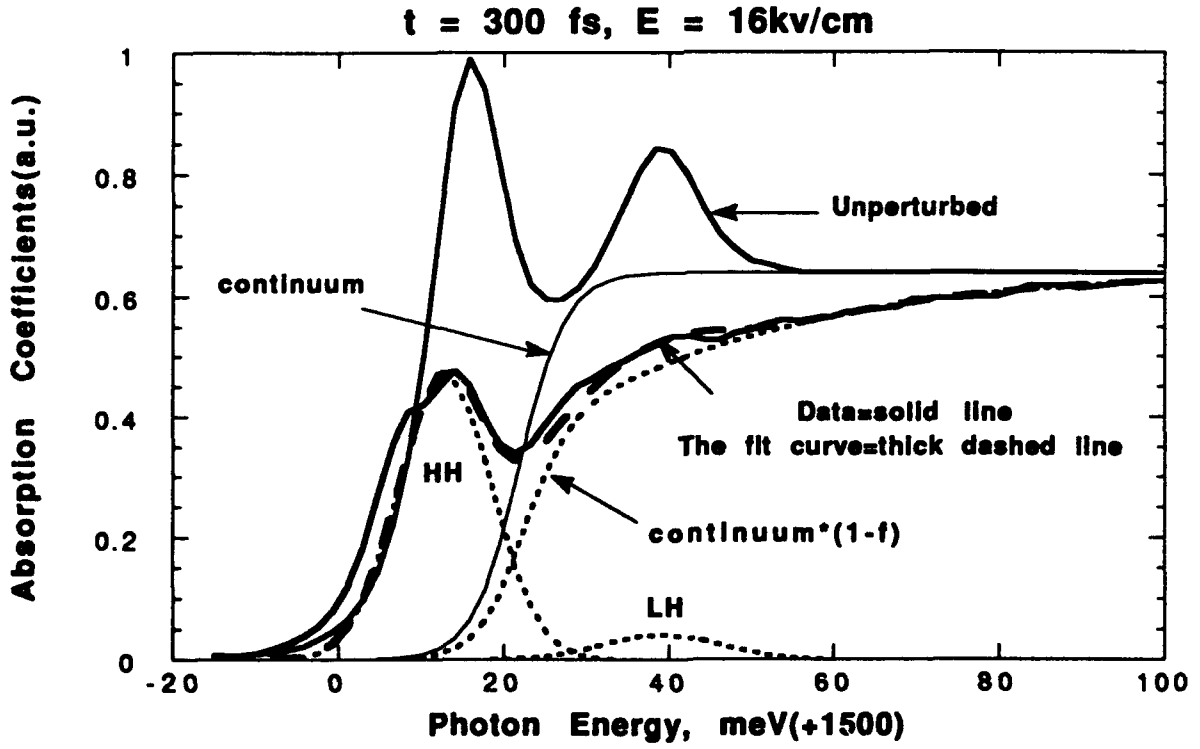
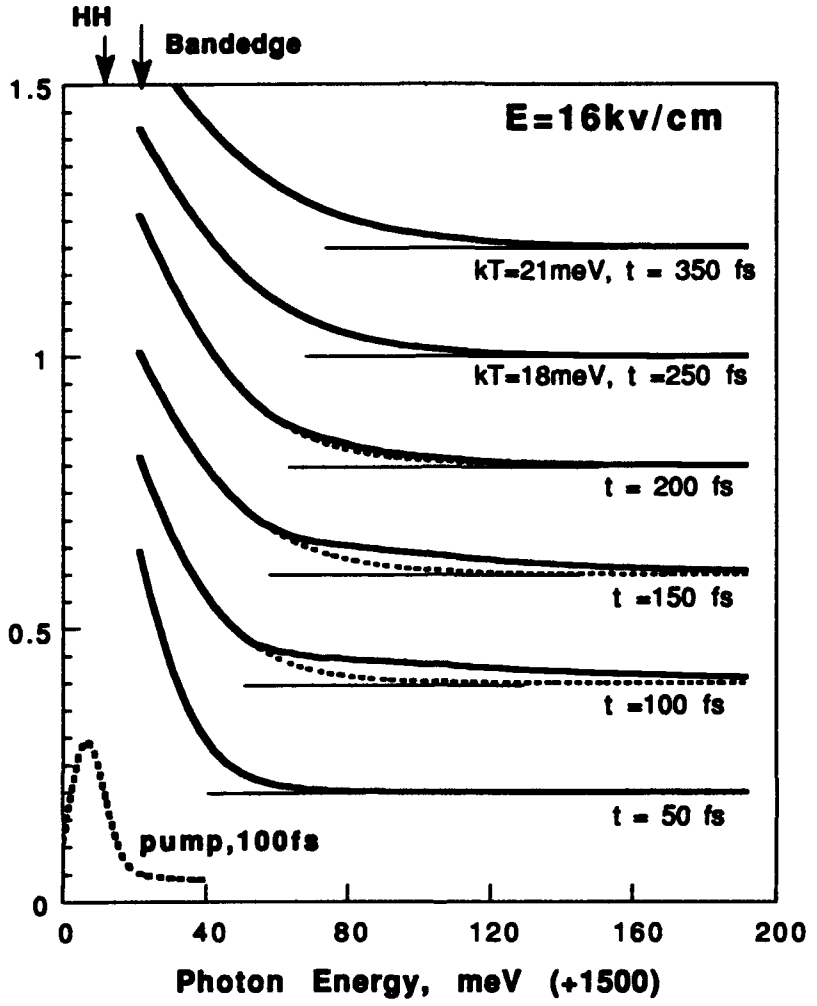


Fig.2 Fitted absorption coefficient showing the three components.

Fig.3 Distribution Functions extracted from the experiment by fitting



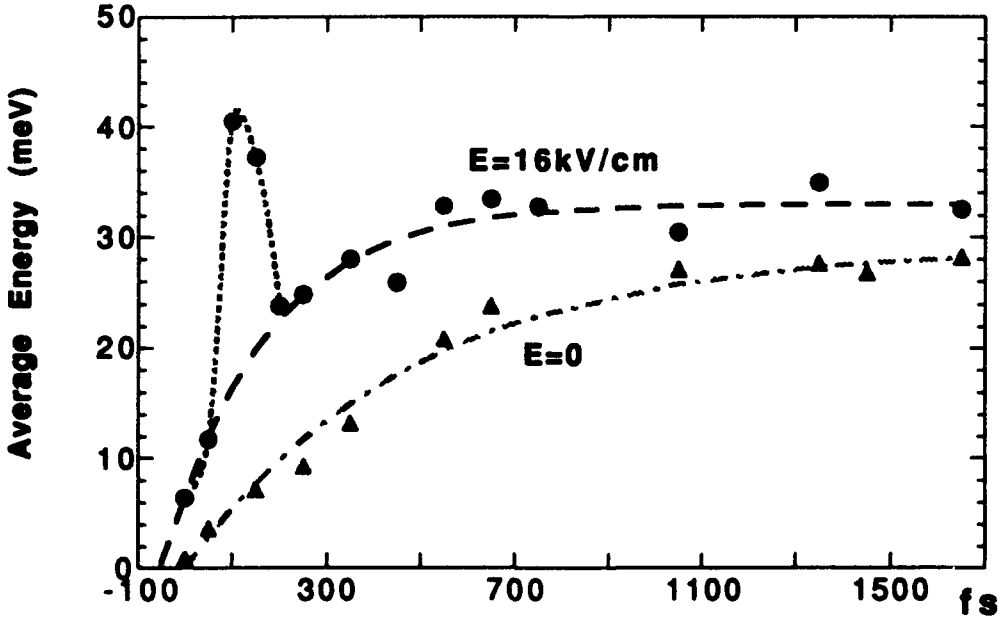


Fig.4 Average energy vs.delay time after the excitation

KEY TO AUTHORS
POSTDEADLINE PAPERS

Cunningham, J. E.	PDP4, 307
Feldmann, J.	PDP4, 307
Florez, L. T.	PDP3, 303
Fox, A. M.	PDP4, 307
Ghisoni, M.	PDP2, 299
Goossen, K. W.	PDP4, 307
Harbison, J. P.	PDP3, 303
Hill, G.	PDP2, 299
Jan, W. Y.	PDP4, 307
Jewell, J. L.	PDP3, 303
Larsson, A.	PDP1, 295
Maserjian, J.	PDP1, 295
McCall, S. L.	PDP3, 303
Miller, D. A. B.	PDP4, 307
Meyer, K. E.	PDP5, 311
Norris, T. B.	PDP5, 311
Parry, G.	PDP2, 299
Pate, M.	PDP2, 299
Roberts, J. S.	PDP2, 299
Sha, W.	PDP5, 311
Schaff, W. J.	PDP5, 311
Scherer, A.	PDP3, 303
Schiavone, L. M.	PDP3, 303
Van der Gaag, B.	PDP3, 303